



# **Mineral Potential Modelling of Gold and Silver Mineralization in the Nevada Great Basin**



## **A GIS-Based Analysis Using Weights of Evidence**

By:

Mark J. Mihalasky<sup>1</sup>

Open-File Report: 01-291

This report is preliminary and has not been reviewed for conformity with U.S. Geological Survey editorial standards or with the North American Stratigraphic Code. Any use of trade, product, or firm names is for descriptive purposes only and does not imply endorsement by the U.S. Government.

---

**U.S. DEPARTMENT OF THE INTERIOR  
U.S. GEOLOGICAL SURVEY**

<sup>1</sup> Formerly at: U.S. Geological Survey, Reno Field Office, Mackay School of Mines, MS-176, University of Nevada, Reno, Nevada, 89557. Currently at: Richard Stockton College, Faculty of Natural Sciences and Mathematics, PO Box 195, Pomona, New Jersey, 08240.

## ABSTRACT

The distribution of 2,690 gold-silver-bearing occurrences in the Nevada Great Basin was examined in terms of spatial association with various geological phenomena. Analysis of these relationships, using GIS and *weights of evidence* modelling techniques, has predicted areas of high mineral potential where little or no mining activity exists. Mineral potential maps for sedimentary (“disseminated”) and volcanic (“epithermal”) rock-hosted gold-silver mineralization revealed two distinct patterns that highlight two sets of crustal-scale geologic features that likely control the regional distribution of these deposit types.

The weights of evidence method is a probability-based technique for mapping mineral potential using the spatial distribution of known mineral occurrences. Mineral potential maps predicting the distribution of gold-silver-bearing occurrences were generated from structural, geochemical, geomagnetic, gravimetric, lithologic, and lithotectonic-related deposit-indicator factors. The maps successfully predicted nearly 70% of the total number of known occurrences, including ~83% of sedimentary and ~60% of volcanic rock-hosted types. Sedimentary and volcanic rock-hosted mineral potential maps showed high spatial correlation (an area cross-tabulation agreement of 85% and 73%, respectively) with expert-delineated mineral permissive tracts. In blind tests, the sedimentary and volcanic rock-hosted mineral potential maps predicted 10 out of 12 and 5 out of 5 occurrences, respectively. The key mineral predictor factors, in order of importance, were determined to be: geology (including lithology, structure, and lithotectonic terrane), geochemistry (indication of alteration), and geophysics.

Areas of elevated sedimentary rock-hosted mineral potential are generally confined to central, north-central, and north-eastern Nevada. These areas form a conspicuous “V”-shape pattern that is coincident with the Battle Mountain-Eureka (Cortez) and Carlin mineral trends and a segment of the Roberts Mountain thrust front, which bridges the southern ends of the trends. This pattern appears to delineate two well-defined, sub-parallel, northwest–southeast-trending crustal-scale structural zones. These features, here termed the “*Carlin*” and “*Cortez*” structural zones, are believed to control the regional-scale distribution of the sedimentary rock-hosted occurrences. Mineralizing processes were focused along these structural zones and significant ore deposits exist where they intersect other tectonic zones, favorable host rock-types, and (or) where appropriate physio-chemical conditions were present. The origin and age of the Carlin and Cortez structural zones are not well constrained, however, they are considered to be transcurrent features representing a long-lived, deep-crustal or mantle-rooted zone of weakness.

Areas of elevated volcanic rock-hosted mineral potential are principally distributed along two broad and diffuse belts that trend (1) northwest-southeast across southwestern Nevada, parallel to the Sierra Nevada, and (2) northeast-southwest across northern Nevada, extending diagonally from the Sierra Nevada to southern Idaho. The first belt corresponds to the Walker Lane shear zone, a wide region of complex strike-slip faulting. The second, here termed the “*Humboldt shear(?) zone*”, may represent a structural zone of transcurrent movement. Together, the Walker Lane and Humboldt shear(?) zones are believed to control the regional-scale distribution of volcanic rock-hosted occurrences. Volcanic rock-hosted mineralization was closely tied to the southward and westward migration of Tertiary magmatism across the region (which may have been mantle plume-driven). Both magmatic and mineralizing processes were localized and concentrated along these structural zones. The Humboldt shear(?) zone may have also affected



the distribution of sedimentary rock-hosted mineralization along the Battle Mountain–Eureka (Cortez) and Carlin mineral trends. The Getchell trend and Independence group deposits are believed to be the northeastward-displaced northern extensions of these mineral trends (respectively). Displacement was achieved by post-mineralization right-lateral movement along crustal segments within the Humboldt shear(?) zone. Latest movement along the Humboldt shear(?) zone is constrained between ~42–30 Ma (sedimentary rock-hosted mineralization) and ~17–14 Ma (most recent igneous activity along the northern Nevada rift zone). However, this structure likely has origins relating to the mid-Proterozoic assembly of the Laurentian protocraton and/or late Proterozoic rifting.

# TABLE OF CONTENTS

<b>1. Introduction</b>	<b>1</b>
1.1 Overview	1
1.2 Study Area	1
1.3 Purpose and Objectives	2
1.4 Methodology	2
1.5 Spatial Datasets	4
1.6 Similar Studies	5
1.7 Layout	6
<b>2. Geology of the Great Basin</b>	<b>8</b>
2.1 Introduction	8
2.2 Physiographic Setting	8
2.3 Tectonic Setting and Geologic History	9
2.4 Craton Development	11
2.4.1 Assembly and Margin Formation	11
2.4.2 Western Edge and Crustal Provinces	12
2.5 Cenozoic Extensional Tectonism	13
2.5.1 Early Stage (Mid-Eocene to Late-Lower Miocene)	14
2.5.1.1 Magmatic Activity—Distribution, Age, and Composition	16
2.5.1.2 Extensional Activity—Distribution, Age, Character, Magnitude	18
2.5.2 Late Stage (Late-Lower Miocene to Present)	18
2.5.2.1 Magmatic Activity—Distribution, Age, and Composition	18
2.5.2.2 Extensional Activity—Distribution, Age, Character, Magnitude	19
2.6 Strike-Slip and Related Features	21
2.7 Characteristics of the Present-Day Crust	24
2.7.1 Lithotectonic Framework and Tectonostratigraphy	25
2.7.2 Crustal Thickness	26
2.7.3 Gravity Anomaly and Crustal Structure	27
2.7.4 Geomagnetic Anomaly and Crustal-Scale Structures	28
2.7.5 Heat Flow and Crustal Fluid Circulation	29
2.7.6 Electrical Conductivity and Crustal Permeability	29
2.7.7 Seismicity and Seismic Velocities	30
<b>3. Characteristics and Distribution of Sedimentary and Volcanic Rock-Hosted Deposits</b>	<b>31</b>
3.1 Introduction	31
3.2 Sedimentary Rock-Hosted Gold Deposits	32
3.2.1 Characteristics	32
3.2.2 Distribution	32
3.3 Volcanic Rock-Hosted Gold-Silver Deposits	34
3.3.1 Characteristics	34

3.3.2	Distribution	35
3.4	Regional-Scale Distribution with Respect to Mineral Trends and Belts	37
3.5	Regional-Scale Distribution with Respect to Crustal Terranes	40
3.6	Quantitative Studies on Mineral Trends and Crustal Terranes	42
<b>4.</b>	<b>Analysis and Modelling Techniques</b>	<b>44</b>
4.1	Introduction	44
4.2	Preliminary Spatial Data Analysis	44
4.3	Weights of Evidence Mineral Potential Modelling	44
4.3.1	Introduction	44
4.3.2	Theoretical Framework	45
4.3.3	Conditional Independence	47
4.3.4	Posterior Probability Uncertainty	48
4.3.5	Practical Implementation of the Modelling Procedures	48
<b>5.</b>	<b>Spatial Datasets</b>	<b>49</b>
5.1	Introduction	49
5.2	GIS Study Area Parameters	49
5.2.1	Projection	49
5.2.2	Extents	50
5.2.3	Resolution	50
5.3	Spatial Datasets—Selection Criteria and Terminology	50
5.3.1	Data Sources	50
5.3.2	Gold-Silver-Bearing Mineral Occurrences (Training Datasets)	53
5.3.3	Mineral Potential Modelling Evidence Maps	54
5.4	Error, Data Accuracy and Limitations	56
5.4.1	Error Sources	56
5.4.2	Data Limitations	57
<b>6.</b>	<b>Single Map Analysis, Interpretation, and Mineral Predictor Map Generation</b>	<b>58</b>
6.1	Introduction	58
6.2	Gold-Silver-Bearing Occurrences	59
6.2.1	Introduction and Summary of Findings	59
6.2.2	Distribution of Gold-Silver-Bearing Occurrences	59
6.2.3	Correlations and Interpretive Synthesis	61
6.3	Lithology	63
6.3.1	Introduction and Summary of Findings	63
6.3.2	Distribution and Spatial Association of Gold-Silver-Bearing Occurrences	64
6.3.3	Correlations and Interpretive Synthesis	66
6.4	Lithologic Diversity and Lithotectonic Terranes	69
6.4.1	Introduction and Summary of Findings	69
6.4.2	Distribution and Spatial Association of Gold-Silver-Bearing Occurrences	70
6.4.3	Correlations and Interpretive Synthesis	71

6.5	Distance Buffers Around Plutons and Faults	74
6.5.1	Introduction and Summary of Findings	74
6.5.2	Distribution and Spatial Association of Gold-Silver-Bearing Occurrences	75
6.5.3	Correlations and Interpretive Synthesis	77
6.6	Geophysics—Geomagnetic and Gravity Anomalies	78
6.6.1	Introduction and Summary of Findings	78
6.6.2	Distribution and Spatial Association of Gold-Silver-Bearing Occurrences	79
6.6.3	Correlations and Interpretive Synthesis	81
6.6.3.1	Sedimentary Rock-Hosted Occurrences: Geomagnetic Lows—Isostatic Gravity Highs	81
6.6.3.2	Volcanic Rock-Hosted Occurrences: Geomagnetic Highs—Isostatic Gravity Lows	83
6.7	Geochemistry—K/Na and Ba/Na Anomalies	85
6.7.1	Introduction and Summary of Findings	85
6.7.2	Distribution and Spatial Association of Gold-Silver-Bearing Occurrences	87
6.7.3	Correlations and Interpretive Synthesis	88
<b>7.</b>	<b>Multi-Map Modelling and Gold-Silver Mineral Potential</b>	<b>90</b>
7.1	Introduction	90
7.2	Combination of Mineral Potential Evidence	91
7.2.1	Introduction	91
7.2.2	Combination Weighting Factors	91
7.3	Sedimentary and Volcanic Rock-Hosted Mineral Potential Maps	92
7.3.1	Introduction	92
7.3.2	Favorability for Sedimentary Rock-Hosted Occurrences	92
7.3.3	Favorability for Volcanic Rock-Hosted Occurrences	93
7.4	Validation of Mineral Potential Models	93
7.4.1	Introduction	93
7.4.2	Conditional Independence and Uncertainty of the Mineral Potential Maps	94
7.4.3	Favorability at Known Gold-Silver-Bearing Occurrence Areas	95
7.4.4	Comparison to Expert-Delineated Mineral Potential Areas	96
7.4.5	Blind Test of Mineral Potential Model Predictability	97
7.5	Geologic Characterization and Delineation of Regional-Scale Sedimentary and Volcanic Rock-Hosted Occurrence Exploration Targets	98
7.5.1	Introduction	98
7.5.2	Sedimentary Rock-Hosted Mineral Potential Regions	100
7.5.3	Volcanic Rock-Hosted Mineral Potential Regions	103
<b>8.</b>	<b>Controls on Sedimentary and Volcanic Rock-Hosted Occurrence Distribution</b>	<b>107</b>
8.1	Introduction	107
8.2	Mineral Potential Evidence Associated with the Gold-Silver-Bearing Occurrences	107
8.2.1	Sedimentary-Rock Hosted Occurrences	107
8.2.2	Volcanic Rock-Hosted Occurrences	108

8.3	Delineation of the Regional-Scale Control Structures .....	110
8.3.1	Sedimentary Rock-Hosted Mineralization .....	110
8.3.2	Volcanic Rock-Hosted Mineralization .....	110
8.4	The Humboldt Shear(?) Zone .....	112
8.4.1	Geologic and Other Evidence .....	112
8.4.2	Topographic Expression .....	112
8.4.3	Origin, Age, and Character of the Humboldt Shear(?) Zone .....	113
8.5	The Carlin and Cortez Structural Zones .....	116
8.5.1	Geophysical and Geochemical Evidence .....	116
8.5.2	Age and Origin of the Carlin and Cortez Structural Zones .....	118
8.5.3	Transcurrent Movement .....	120
8.5.4	Truncation of the Battle Mountain–Eureka (Cortez) and Carlin Mineral Trends by the Humboldt Shear(?) Zone .....	121
8.6	A Mantle Plume .....	124
	<b>References</b> .....	126
	<b>Appendix A</b> Stratigraphy and Description of Lithologic Units. ....	A1
	<b>Appendix B</b> Weights of Evidence Mineral Potential Modelling Theory, Implementation, and FORTRAN Utilities .....	B1
	<b>Appendix C</b> Mineral Potential Map Generation, Conditional Independence, and Uncertainty .....	C1
	<b>Appendix D</b> Mineral Potential at Known Mineral Occurrence Areas .....	D1

## LIST OF TABLES

<b>Table 1.1</b>	Types of Models Used in the Geosciences . . . . .	180
<b>Table 1.2</b>	Types of Mineral Potential Models . . . . .	181
<b>Table 1.3</b>	Gold-Silver-Bearing Occurrences Examined in this Study . . . . .	182
<b>Table 3.1</b>	Sedimentary Rock-Hosted Deposit-Type Synoptic Model . . . . .	183
<b>Table 3.2</b>	Volcanic Rock-Hosted Deposit-Type Synoptic Model . . . . .	186
<b>Table 5.1</b>	Geoscience Datasets Composing the Navada and Great Basin GIS Database . . . . .	190
<b>Table 5.2</b>	Total Number of Observations in All Gold-Silver-Bearing Occurrence-type Samples. . . . .	199
<b>Table 7.1</b>	Weights of Spatial Association and Related Data for the Primary, Sedimentary, and Volcanic Rock-Hosted Occurrence-Type Mineral Potential Models . . . . .	200
<b>Table A.1</b>	Correlation Chart of Geological Map Units with Accompanying Table of Unit Descriptions . . . . .	A2
<b>Table A.2</b>	Key to GIS Geological Map Legend and Lithologic Unit Abbreviations Appearing on Digital Maps . . . . .	A15
<b>Table A.3</b>	Key to Lithologic Units Composing Assemblage Map Units . . . . .	A17
<b>Table B.1</b>	Example of an Attribute Table Used for Map Reclassification . . . . .	B26
<b>Table B.2</b>	Example of a Unique Conditions Map Attribute Output from SPANS GIS . . . . .	B27
<b>Table B.3</b>	Map Area Analysis Table Output from SPANS GIS . . . . .	B28
<b>Table B.4</b>	Point-in-Polygon Analysis Table Output from SPANS GIS . . . . .	B29
<b>Table B.5</b>	Contingency Table for Testing Conditional Independence, Based on Cells Containing Only Deposits . . . . .	B15
<b>Table B.6</b>	Output from the FORTRAN Utility <i>WTS.EXE</i> for the Weights of Spatial Association Estimation Component of Weights of Evidence Mineral Potential Modelling . . . . .	B30
<b>Table B.7</b>	Example of Weights of Evidence Bayesian Map Overlay Modelling Equation Implemented in SPANS GIS . . . . .	B31
<b>Table B.8</b>	Output from the FORTRAN Utility <i>PREDICT.EXE</i> for the Bayesian Multi-Map Overlay Component of Weights of Evidence Mineral Potential Modelling . . . . .	B32
<b>Table B.9</b>	Output from FORTRAN Utility <i>CI.EXE</i> for the Error Analysis Component of Weights of Evidence Mineral Potential Modelling . . . . .	B33
<b>Table C.1</b>	Pairwise Conditional Independence (CI) test $\chi^2$ Scores for the Primary Occurrence-type Model . . . . .	C10
<b>Table C.2</b>	Pairwise Conditional Independence (CI) test $\chi^2$ Scores for the Sedimentary Rock-Hosted Occurrence-type Model . . . . .	C11
<b>Table C.3</b>	Pairwise Conditional Independence (CI) test $\chi^2$ Scores for the Volcanic Rock-Hosted Occurrence-type Model . . . . .	C12
<b>Table C.4</b>	Summary Information for the Overall Conditional Independence Test for the Various Mineral Potential Models . . . . .	C13
<b>Table C.5</b>	Comparison of Expected Versus Observed	

	Occurrences for the Weights of Evidence (WOE) and Weighted Logistic Regression (WLR) Methods of Evidence Combination . . . . .	C14
<b>Table D.1</b>	Primary Gold-silver-bearing Occurrences of All Sizes and Types Having Posterior Probabilities $\geq 0.1000$ , as Determined with the Primary 7-layer Mineral Potential Model . . . . .	D4
<b>Table D.2</b>	Posterior Probabilities Associated with Gold-silver-bearing Sedimentary Rock-hosted Occurrences of All Sizes, as Determined with the Sedimentary Rock-hosted 8-layer Mineral Potential Model . . . . .	D12
<b>Table D.3</b>	Posterior Probabilities Associated with Gold-silver-bearing Volcanic Rock-hosted Occurrences of All Sizes, as Determined with the Volcanic Rock-hosted 7-layer Mineral Potential Model . . . . .	D14

## LIST OF FIGURES

<b>Figure 1.1</b>	Great Basin Physiographic Province, Southwestern United States . . . . .	202
<b>Figure 1.2</b>	“Basin and Range” Topography . . . . .	203
<b>Figure 1.3</b>	Principal Metallogenic Features of the Great Basin . . . . .	204
<b>Figure 2.1</b>	Cordilleran Orogenic Belt, North America . . . . .	205
<b>Figure 2.2</b>	The Great Basin and Environs . . . . .	206
<b>Figure 2.3</b>	Plate Tectonic Setting and Selected Tectonomagmatic Elements of the Western United States . . . . .	207
<b>Figure 2.4</b>	Primary Tectonic Subdivisions of the Central Cordilleran Orogen . . . . .	208
<b>Figure 2.5</b>	Major Orogenic Belts and Thrusts of the Central Cordilleran Interior . . . . .	210
<b>Figure 2.6</b>	Time Chart of Orogenic Events Affecting the Great Basin . . . . .	211
<b>Figure 2.7</b>	Phases of the Cordilleran Orogeny— Space-Time Relationships . . . . .	212
<b>Figure 2.8</b>	Geologic Events Affecting the Great Basin and Environs During the Cenozoic . . . . .	213
<b>Figure 2.9</b>	Depositional Framework of the Cordilleran Geosyncline . . . . .	214
<b>Figure 2.10</b>	The Western Edge of Precambrian North America . . . . .	215
<b>Figure 2.11</b>	Crustal Formation Provinces of the Western United States . . . . .	216
<b>Figure 2.12</b>	Variability of Selected Geologic Attributes across the Southern Great Basin . . . . .	217
<b>Figure 2.13</b>	Phanerozoic Tectonostratigraphy of the Great Basin . . . . .	218
<b>Figure 3.1</b>	Distribution of Sedimentary Rock-Hosted and Volcanic Rock- Hosted Gold-Silver Deposits . . . . .	219
<b>Figure 3.2</b>	Sedimentary and Volcanic Rock-Hosted Deposit Age Boundary . . . . .	220
<b>Figure 3.3</b>	Mineral Trends and Belts of Nevada . . . . .	221
<b>Figure 4.1</b>	Weights of Evidence Mineral Potential Modelling Method . . . . .	222
<b>Figure 6.1</b>	Distribution of Gold-Silver-Bearing Occurrences in the Nevada Great Basin . . . . .	223
<b>Figure 6.2</b>	Distribution of Sedimentary Rock-Hosted and Volcanic Rock- Hosted Gold-Silver-Bearing Occurrences in the Nevada Great Basin . . . . .	224
<b>Figure 6.3</b>	Density Map of Gold-Silver-Bearing Occurrences and All Metallic Mineral Occurrences . . . . .	225
<b>Figure 6.4</b>	Time-Slice Maps of Cenozoic Igneous Rocks in Nevada . . . . .	226
<b>Figure 6.5</b>	Map Patterns of Various Datasets Reflecting the “U-Shaped” or “Horse-Shoe Shaped” Distribution Pattern of the Precious and Non-Precious Metal Occurrences in Nevada . . . . .	227
<b>Figure 6.6</b>	Shaded-Relief Image of Topography in the Southwestern United States Highlighting Regional-Scale Linear Trends and Features . . . . .	228
<b>Figure 6.7</b>	Geological Map of Nevada . . . . .	229
<b>Figure 6.8</b>	Lithologic Assemblage Map of Nevada . . . . .	230
<b>Figure 6.9</b>	Frequency of Primary Occurrences by Lithologic Assemblage . . . . .	231
<b>Figure 6.10</b>	Lithologic Units Hosting Over 90% of Primary Occurrences . . . . .	232
<b>Figure 6.11</b>	Lithologic Units Having a Strong Spatial Association with Primary	



	Occurrences .....	233
<b>Figure 6.12</b>	Frequency of Sedimentary Rock-Hosted Occurrences by Lithologic Assemblage .....	234
<b>Figure 6.13</b>	Lithologic Units Hosting 100% of Sedimentary Rock-Hosted Occurrences .....	235
<b>Figure 6.14</b>	Lithologic Units Having a Strong Spatial Association with Sedimentary Rock-Hosted Occurrences .....	236
<b>Figure 6.15</b>	Frequency Volcanic Rock-Hosted Occurrences by Lithologic Assemblage .....	237
<b>Figure 6.16</b>	Lithologic Units Hosting 100% of Volcanic Rock-Hosted Occurrences .....	238
<b>Figure 6.17</b>	Lithologic Units Having a Strong Spatial Association with Volcanic Roc-Hosted Occurrences .....	239
<b>Figure 6.18</b>	Lithology Ternary-Class Predictor Map for Gold-Silver-Bearing Occurrences of all sizes and deposit types .....	240
<b>Figure 6.19</b>	Lithology Binary-Class Predictor Maps for Sedimentary and Volcanic Rock-Hosted Gold-Silver-Bearing Occurrences .....	241
<b>Figure 6.20</b>	Lithologic Units Reclassified by Posterior Probability of Hosting Small, Medium, and Large Primary-Commodity Gold-Silver-Bearing Occurrences .....	242
<b>Figure 6.21</b>	Lithologic Units Having Elevated Posterior Probabilities for Hosting Small, Medium, and Large Primary-Commodity Gold-Silver-Bearing Occurrences .....	243
<b>Figure 6.22</b>	Lithologic Units Having Elevated Posterior Probabilities for Hosting Small and Big Primary-Commodity Gold-Silver-Bearing Occurrences .....	244
<b>Figure 6.23</b>	Comparison Between the Extent and Trend of the Cordilleran Geosyncline “Transitional Assemblage” and Lithologic Units Having Elevated Posterior Probability for Hosting Small Size Gold-Silver-Bearing Occurrences .....	245
<b>Figure 6.24</b>	Lithologic Units Having Elevated Posterior Probabilities for Hosting Sedimentary Rock-Hosted or Volcanic Rock-Hosted Gold-Silver-Bearing Occurrences .....	246
<b>Figure 6.25</b>	Lithologic Units Having “Substantial” Posterior Probabilities for Hosting Volcanic Rock-Hosted Gold-Silver-Bearing Occurrences, Compared to a Map Illustrating the Space-Time Distribution of Volcanic Rocks in Nevada .....	247
<b>Figure 6.26</b>	Diversity of Lithology and Diagrammatic Representation of the Diversity Neighborhood .....	248
<b>Figure 6.27</b>	Lithotectonic Terranes of Nevada .....	249
<b>Figure 6.28</b>	Frequency of Primary Occurrences by Lithologic Diversity Unit .....	250
<b>Figure 6.29</b>	Frequency of Sedimentary and Volcanic Rock-Hosted Occurrences by Lithologic Diversity Unit .....	251
<b>Figure 6.30</b>	Strength of Spatial Association Between Primary Occurrences and Lithologic Diversity Units .....	252
<b>Figure 6.31</b>	Frequency of Primary Occurrences by Lithologic Terranes .....	253
<b>Figure 6.32</b>	Frequency of Sedimentary and Volcanic Rock-Hosted Occurrences	

	by Lithologic Terranes . . . . .	254
<b>Figure 6.33</b>	Strength of Spatial Association Between Primary Occurrences and Lithotectonic Terranes . . . . .	255
<b>Figure 6.34</b>	Diversity of Lithology Map and Diversity Binary-Class Predictor Map for Gold-Silver-Bearing Occurrences of All Sizes and Types, Sedimentary Rock-Hosted Occurrences, and Volcanic Rock-Hosted Occurrences . . . . .	256
<b>Figure 6.35</b>	Lithotectonic Terranes Binary-Class Predictor Maps for Gold-Silver-Bearing Occurrences of All Sizes and Types, Sedimentary Rock-Hosted Occurrences, and Volcanic Rock-Hosted Occurrences . . . . .	257
<b>Figure 6.36</b>	Plutonic Rocks of Nevada, Buffered Plutons, Pluton Density, and the Density of All Gold-Silver-Bearing Occurrences . . . . .	258
<b>Figure 6.37</b>	Faults from the Geological Map of Nevada, Faults Distance Buffers, and Density of Faults . . . . .	259
<b>Figure 6.38</b>	Frequency of Primary Occurrences Within Buffer Zones Surrounding Plutonic Bodies . . . . .	260
<b>Figure 6.39</b>	Frequency of Sedimentary and Volcanic Rock-Hosted Occurrences Within Buffer Zones Surrounding Plutonic Bodies . . . . .	261
<b>Figure 6.40</b>	Variation of Contrast with Successive Area-Cumulative Distance Intervals from Plutonic Bodies for Primary Occurrences . . . . .	262
<b>Figure 6.41</b>	Frequency of Primary Occurrences Within Buffer Zones Surrounding Faults . . . . .	263
<b>Figure 6.42</b>	Frequency of Sedimentary and Volcanic Rock-Hosted Occurrences Within Buffer Zones Surrounding Faults . . . . .	264
<b>Figure 6.43</b>	Variation of Contrast with Successive Area-Cumulative Distance Intervals from Faults for Gold-Silver-Bearing Occurrences . . . . .	265
<b>Figure 6.44</b>	Pluton Buffer and Fault Buffer Binary-Class Predictor Maps for Primary, Sedimentary and Volcanic Rock-Hosted Gold-Silver-Bearing occurrences . . . . .	266
<b>Figure 6.45</b>	The Total Residual Field Geomagnetic Anomaly, the Isostatic Residual Gravity Anomaly, and the Bouguer Gravity Anomaly of Nevada . . . . .	267
<b>Figure 6.46</b>	Frequency of Primary Occurrences Relative to the Strength of the Total Residual Field Geomagnetic Anomaly . . . . .	268
<b>Figure 6.47</b>	Frequency of Sedimentary and Volcanic Rock-Hosted Occurrences Relative to the Strength of Total Residual Geomagnetic Anomaly . . . . .	269
<b>Figure 6.48</b>	Variation in Contrast with Successive Area-Cumulative Total Residual Field Geomagnetic Anomaly Values for Primary Occurrences . . . . .	270
<b>Figure 6.49</b>	Frequency of Primary Occurrences Relative to Strength of Isostatic Gravity Anomaly . . . . .	271
<b>Figure 6.50</b>	Frequency of Sedimentary and Volcanic Rock-Hosted Occurrences Relative to Strength of Isostatic Residual Gravity Anomaly . . . . .	272
<b>Figure 6.51</b>	Variation in Contrast with Successive Area-Cumulative Isostatic Residual Gravity Anomaly Intervals for Primary Occurrences . . . . .	273
<b>Figure 6.52</b>	Geophysical Binary-Class Predictor Maps, Derived from Total	

	Field Geomagnetic and Isostatic Gravity Geophysical Anomaly Data .....	274
<b>Figure 6.53</b>	The Total Residual Field Geomagnetic Anomaly Intervals Determined to Have a Strong Spatial Association with Sedimentary and Volcanic Rock-Hosted Occurrences .....	275
<b>Figure 6.54</b>	The Isostatic Residual Gravity Anomaly Intervals that are Spatially Associated with Sedimentary and Volcanic Rock-Hosted Occurrences .....	276
<b>Figure 6.55</b>	Composition-Slice Maps of Cenozoic Igneous Rocks in Nevada .....	277
<b>Figure 6.56</b>	Sedimentary Rocks and Cenozoic Volcanic, Subvolcanic, and Related Intrusive Rocks of Nevada .....	278
<b>Figure 6.57</b>	K/Na and Ba/Na Geochemical Ratio Maps derived from National Uranium Resource Evaluation Program Data .....	279
<b>Figure 6.58</b>	Frequency of Primary Occurrences Relative to K/Na Anomaly .....	280
<b>Figure 6.59</b>	Frequency of Primary Occurrences Relative to Ba/Na Anomaly .....	281
<b>Figure 6.60</b>	Frequency of Sedimentary and Volcanic Rock-Hosted Occurrences Relative to K/Na Anomaly .....	282
<b>Figure 6.61</b>	Frequency of Sedimentary and Volcanic Rock-Hosted Occurrences Relative to Ba/Na Anomaly .....	283
<b>Figure 6.62</b>	Variation in Contrast Across Successive Area-Cumulative K/Na Anomaly Intervals for Primary Occurrences .....	284
<b>Figure 6.63</b>	Variation in Contrast Across Successive Area-Cumulative Ba/Na Anomaly Intervals for Primary Occurrences .....	285
<b>Figure 6.64</b>	Geochemical Binary-Class Predictor Maps Derived from K/Na and Ba/Na Geochemical Anomaly Data for Primary, Sedimentary and Volcanic Rock-Hosted Occurrences .....	286
<b>Figure 6.65</b>	Spatial Distribution of the K/Na and Ba/Na Geochemical Anomalies Relative to the Distribution of the Sedimentary Rock-Hosted Occurrences Along the Battle Mountain–Eureka (Cortez) and Carlin Mineral Trends .....	287
<b>Figure 7.1</b>	Relative Influence of Evidence: Primary Mineral Potential Models .....	288
<b>Figure 7.2</b>	Relative Influence of Evidence: Sedimentary Rock-Hosted Mineral Potential Models .....	289
<b>Figure 7.3</b>	Relative Influence of Evidence: Volcanic Rock-Hosted Mineral Potential Models .....	290
<b>Figure 7.4</b>	Sedimentary Rock-Hosted Occurrence-Type Posterior Probability Map .....	291
<b>Figure 7.5</b>	Volcanic Rock-Hosted Occurrence-Type Posterior Probability Map .....	292
<b>Figure 7.6</b>	Difference Between Mineral Potential Maps .....	293
<b>Figure 7.7</b>	Sedimentary Rock-Hosted Occurrence-Type Mineral Potential Model Results .....	294
<b>Figure 7.8</b>	Volcanic Rock-Hosted Occurrence-Type Mineral Potential Model Results .....	295
<b>Figure 7.9</b>	Uncertainty of Posterior Probabilities Used to Generate the Sedimentary Rock-Hosted Occurrence-Type 8-Layer Mineral Potential Map .....	296
<b>Figure 7.10</b>	Uncertainty of Posterior Probabilities Used to Generate the	

	Volcanic Rock-Hosted Occurrence-Type 8-Layer Mineral Potential Map .....	297
<b>Figure 7.11</b>	Posterior Probabilities Appended to Sedimentary Rock-Hosted Gold-Silver-Bearing Occurrences .....	298
<b>Figure 7.12</b>	Posterior Probabilities Appended to Volcanic Rock-Hosted Gold-Silver-Bearing Occurrences .....	299
<b>Figure 7.13</b>	Sedimentary Rock-Hosted Occurrence-Type 8-Layer Mineral Potential Model—The Distribution of Elevated Favorability Mineral Potential Areas in Comparison to the Distribution of Known Sedimentary Rock-Hosted Occurrences .....	300
<b>Figure 7.14</b>	Volcanic Rock-Hosted Occurrence-Type 7-Layer Mineral Potential Model—The Distribution of Elevated Favorability Mineral Potential Areas in Comparison to the Distribution of Known Volcanic Rock-Hosted Occurrences .....	301
<b>Figure 7.15</b>	Comparison Between Sedimentary Rock-Hosted Mineral Potential Areas Delineated in This Study and Tracts Permissible for Carlin-Style Sediment-Hosted Gold Mineralization as Delineated by Teams of Experts .....	302
<b>Figure 7.16</b>	Comparison Between Volcanic Rock-Hosted Mineral Potential Areas Delineated in This Study and Tracts Permissible for Epithermal Gold-Silver Mineralization as Delineated by Teams of Experts .....	303
<b>Figure 7.17</b>	Blind Test of the Weights of Evidence Sedimentary Rock-Hosted 8-Layer Mineral Potential Model .....	304
<b>Figure 7.18</b>	Blind Test of the Weights of Evidence Volcanic Rock-Hosted 7-Layer Mineral Potential Model .....	305
<b>Figure 7.19</b>	Regional-Scale Exploration Target Areas for Sedimentary Rock-Hosted Occurrence-Types, as Predicted by the Weights of Evidence 8-Layer Mineral Potential Model .....	306
<b>Figure 7.20</b>	Sedimentary Rock-Hosted Occurrence-Type Regional Exploration Target Areas #1 and #2 .....	307
<b>Figure 7.21</b>	Sedimentary Rock-Hosted Occurrence-Type Regional Exploration Target Areas #3 and #4 .....	308
<b>Figure 7.22</b>	Sedimentary Rock-Hosted Occurrence-Type Regional Exploration Target Area #5 .....	309
<b>Figure 7.23</b>	Regional-Scale Exploration Target Areas for Volcanic Rock-Hosted Occurrence-Types, as Predicted by the Weights of Evidence 7-Layer Mineral Potential Model .....	310
<b>Figure 7.24</b>	Volcanic Rock-Hosted Occurrence-Type Regional Exploration Target Area #1 .....	311
<b>Figure 7.25</b>	Volcanic Rock-Hosted Occurrence-Type Regional Exploration Target Areas #2 and #3 .....	312
<b>Figure 7.26</b>	Volcanic Rock-Hosted Occurrence-Type Regional Exploration Target Area #4 .....	313
<b>Figure 7.27</b>	Volcanic Rock-Hosted Occurrence-Type Regional Exploration Target Area #5 .....	314
<b>Figure 8.1</b>	Linear Trends Highlighting Possible Regional-Scale Crustal	

	Structures that May Have Been Important to the Localization of Sedimentary Rock-hosted Occurrences . . . . .	315
<b>Figure 8.2</b>	Broad Regional Crustal Structures that May Have Been Important to the Localization of Volcanic Rock-Hosted Occurrences . . . . .	316
<b>Figure 8.3</b>	Spatial Distribution Relationships Among All Gold-Silver-Bearing Occurrences, K/Na Geochemical Anomaly, Geomagnetic Anomaly, K/Na Anomaly Layered on Shaded Relief of Geomagnetic Anomaly, Isostatic Gravity Anomaly, and Bouguer Gravity Anomaly . . . . .	317
<b>Figure 8.4</b>	Kriged Surface Map of RADB Radiometric Age Dates for Cenozoic Igneous Rocks in the Great Basin Region . . . . .	318
<b>Figure A.1</b>	Stratigraphy of Nevada: Correlation of Geological Map Units . . . . .	A3
<b>Figure B.1</b>	Standard and Quadtree Raster Data Structures . . . . .	B34
<b>Figure B.2</b>	Two- and Multi-Map Overlay and Combination Methods . . . . .	B35
<b>Figure B.3</b>	Entity and Unique Conditions Map Overlays and Linked Attribute Tables . . . . .	B36
<b>Figure B.4</b>	Weights of Evidence Multi-Map Overlay Modelling Method . . . . .	B38
<b>Figure B.5</b>	Spatial Overlap Relationships . . . . .	B39
<b>Figure B.6</b>	Graph of Area-Cumulative Contrast Versus Buffer Zone Distances or Anomaly Intensity Values . . . . .	B22
<b>Figure C.1</b>	Primary Occurrence-Type Mineral Potential Model Results . . . . .	C15
<b>Figure C.2</b>	Sedimentary Rock-Hosted Occurrence-Type Mineral Potential Model Results . . . . .	C16
<b>Figure C.3</b>	Volcanic Rock-Hosted Occurrence-Type Mineral Potential Model Results . . . . .	C17
<b>Figure C.4</b>	Overall Goodness-of-Fit Test for All Size and Type Occurrences, Using the K-S Statistic: Primary 11-Layer Model; Primary 7-Layer Model . . . . .	C18
<b>Figure C.5</b>	Overall Goodness-of-Fit Test for All Size and Type Occurrences, Using the K-S Statistic: Sedimentary Rock-Hosted 9-Layer Model; Sedimentary Rock-Hosted 8-Layer Model . . . . .	C19
<b>Figure C.6</b>	Overall Goodness-of-Fit Test for All Size and Type Occurrences, Using the K-S Statistic: Volcanic Rock-Hosted 9-Layer Model; Volcanic Rock-Hosted 7-Layer Model . . . . .	C20
<b>Figure C.7</b>	Difference Between Mineral Potential Favorability Maps . . . . .	C21
<b>Figure C.8</b>	Posterior Probability Estimates Derived from WOE and WLR Methods for the Primary 11-Layer Mineral Potential Model . . . . .	C22
<b>Figure C.9</b>	Posterior Probability Estimates Derived from WOE and WLR Methods for the Sedimentary Rock-Hosted 9-Layer Mineral Potential Model . . . . .	C23
<b>Figure C.10</b>	Posterior Probability Estimates Derived from WOE and WLR Methods for the Volcanic Rock-Hosted 9-Layer Mineral Potential Model . . . . .	C24
<b>Figure C.11</b>	Examples of the Various Sources and Types of Uncertainty in the Posterior Probability Estimates Used to Generate the Primary Occurrence-Type 11-Layer Mineral Potential Map . . . . .	C25
<b>Figure C.12</b>	Uncertainty of Posterior Probabilities Used to Generate the Primary Occurrence-Type 7-Layer Mineral Potential Map . . . . .	C26

<b>Figure C.13</b>	Uncertainty of Posterior Probabilities Used to Generate the Sedimentary Rock-Hosted Occurrence-Type 8-Layer Mineral Potential Map .....	C27
<b>Figure C.14</b>	Uncertainty of Posterior Probabilities Used to Generate the Volcanic Rock-Hosted Occurrence-Type 8-Layer Mineral Potential Map .....	C28
<b>Figure C.15</b>	Three-Dimensional Rendering of Relative Uncertainty of Posterior Probabilities Used to Generate the Sedimentary Rock-Hosted Occurrence-Type 8-Layer Mineral Potential Map .....	C29
<b>Figure D.1</b>	Distribution of Posterior Probabilities associated with Big (Large and Medium), Small, and Unknown Size Primary Occurrences .....	D23
<b>Figure D.2</b>	Primary Occurrence-Type 7-Layer Mineral Potential Model—The Distribution of Elevated Favorability Mineral Potential Areas in Comparison to the Distribution of Known Primary Gold-Silver-Bearing Occurrences .....	D24
<b>Figure D.3</b>	Distribution of Posterior Probabilities associated with Big (Large and Medium), Small, and Unknown Size Sedimentary Rock-Hosted Occurrences .....	D25
<b>Figure D.4</b>	Sedimentary Rock-Hosted Occurrence-Type 8-Layer Mineral Potential Model—The Distribution of Elevated Favorability Mineral Potential Areas in Comparison to the Distribution of Known Sedimentary Rock-Hosted Occurrences .....	D26
<b>Figure D.5</b>	Distribution of Posterior Probabilities associated with Big (Large and Medium), Small, and Unknown Size Volcanic Rock-Hosted Occurrences .....	D27
<b>Figure D.6</b>	Volcanic Rock-Hosted Occurrence-Type 7-Layer Mineral Potential Model—The Distribution of Elevated Favorability Mineral Potential Areas in Comparison to the Distribution of Known Volcanic Rock-Hosted Occurrences .....	D28

## ACKNOWLEDGEMENTS

This open file report is based on dissertation research, which was supervised and supported by Dr. Eion M. Cameron (Geological Survey of Canada, primary advisor), Dr. Graeme F. Bonham-Carter (Geological Survey of Canada), and Dr. Anthony D. Fowler (University of Ottawa). Dr. Gary L. Raines (U.S. Geological Survey, Reno Field Station, Reno, Nevada) contributed much in the way of resources, encouragement, and discussion. Numerous scientists and staff at the USGS Reno Field Station and the MacKay School of Mines (University of Nevada) also contributed to my understanding of Great Basin geology. Dr. Leigh A. Readdy (President, GAEA Consulting) provided valuable insights and support. Reviews by Byron R. Berger (U.S. Geological Survey, Denver) contributed to a much more focused manuscript.

Assistance with technical and statistical matters was provided by Qiuming Cheng (York University), Bahram Daneshfar, Brian Eddy, Brad Sim, Kevin Telmer (University of Victoria), and Danny Wright (Geological Survey of Canada). TYDAC Technologies Inc. and Newmont Exploration Ltd. provided summer employment and assistance with various technical and geological matters.

Special acknowledgements are given to the numerous workers in the Great Basin who have contributed data, both public-domain and private (the citations in Table 5.1 should be read as an extended acknowledgement). Data and assistance were also provided by scientists and staff at the Geological Survey of Canada in Ottawa, NOAA National Geophysical Data Center in Denver, the U.S. Bureau of Mines in Spokane (now, unfortunately, defunct), U.S. Geological Survey Office of Mineral Resources in Washington D.C., and the U.S. Geological Survey EROS Data Center in Sioux Falls.



# Chapter 1. Introduction

## 1.1 Overview

The Great Basin is a “classic” modern extensional tectonic regime located in the central Cordilleran interior of the southwestern United States. It has a long and complex geologic history of crustal rifting, shortening, and accretion that can be traced back to the Archean. The Great Basin is host to a large number and a variety of base- and precious-metal deposits. In recent years, it has emerged as one of the more important gold-producing areas in the world, especially since the start-up of the Carlin open-pit mine in 1965 and the rise in gold price to more than \$200US per ounce in 1978 (Mohide, 1981; Coope, 1991). The greater and richest part of the Great Basin lies within the State of Nevada, and it is here that the well-known precious-metal deposits occur. These include low-grade–high-tonnage sedimentary rock-hosted (Carlin-type) deposits, such as Carlin and Getchell, and high-grade–low-tonnage volcanic rock-hosted (epithermal) deposits, such as Comstock and Goldfield.

A high level of economic interest has stimulated much research into the genesis of precious-metal mineralization in Nevada. As a result, a comprehensive collection of geological, geophysical, and geochemical spatial data has been generated. In the mid-1980's, Babcock (1984) and Cook (1986) predicted that the search for new gold environments would likely accelerate with emphasis on more sophisticated application of databases and conceptual models, such as inference networks (artificial intelligence programs) used for computer assisted prospecting. Since the early 1990's, computer-based *Geographical Information Systems* (GIS) applications have become an integral part of many mineral resource exploration programs. A GIS is an integrated system of hardware, software, and methodologies for the management of spatial (georeferenced) data. It facilitates data compilation and synthesis, and permits exploratory data analysis and modelling. Evaluation of geoscience data with GIS can provide support for various geological investigations and aid decision making processes, such as determining successful and cost-effective exploration or management strategies.

The use of GIS-based techniques to explore geoscientific data may reveal insights not readily obtained by more traditional means of data analysis or representation. In this study, quantitative mineral potential modelling with a GIS has been used to investigate the regional-scale distribution of precious-metal mineralization in the Nevada Great Basin. *Weights of evidence*, a recently developed mineral potential modelling method, has been applied to this task. *Weights of evidence* is a data-driven, discrete multivariate statistical method that uses conditional probabilities to determine the relative importance of mineralization “evidence” and Bayesian principles for integrating multiple “layers of evidence”.

## 1.2 Study Area

The area of interest in the Great Basin is confined to the State of Nevada ([Fig. 1.1](#)). Nevada, situated near the geographic center of the Great Basin, contains most of the basin's area and precious-metal mineral occurrences. The political constraints of the study area extent is due to the digital geological data available at the commencement of this study. A sound geology base



map is essential to a study of this type, and at the time, Nevada was the only region within the confines of the Great Basin for which digital geology of suitable resolution and accuracy was publicly available.

Basin-range structure is wide-spread and highly-developed across the region, and consists of roughly north–south-trending, evenly spaced parallel mountain ranges with intervening broad, flat, alluviated desert basins (Fig. 1.2). On a regional-scale, the Great Basin is characterized by:

- *Uplift and extension*—mean elevation of ~ 1.5 km and with an average extension of 100%, in excess of 300-400 % in some areas (Stewart, 1978; Dewey, 1988; Wernicke, 1992; also see Harry et al., 1993).
- *Thinned crust*—less than 30 km over much of the region, in comparison to 40-50 km for surrounding regions (Allenby and Schnetzler, 1983; Allmendinger et al., 1987; also see Harry et al., 1993).
- *Anomalous upper mantle*—regional Bouguer gravity low (Eaton et al., 1978), low seismic mantle velocities (Stewart, 1978; Dewey, 1988; Smith et al., 1989; also see Harry et al., 1993), high heat flow (“*reduced*” HFU values 50 to 100% and up to 300% greater than in stable regions) (Blackwell, 1978; Morgan and Gosnold, 1989).
- *Modern seismic activity*—seismicity is concentrated around the margins of the region (Christiansen and Yeats, 1992).

The Great Basin region has a long and complex geologic history, involving major episodes of crustal accretion, sedimentation, igneous activity, compressional deformation, and continental rifting (Stewart, 1980). This includes at least three orogenies in the Precambrian, two compressional orogenies in the Paleozoic, three compressional orogenic phases in the Mesozoic (to earliest Cenozoic), two extensional events in the middle and late Cenozoic, and the present-day continued basin-range development (Stewart, 1980; Hoffman, 1989; Berger and Bonham, 1990; Burchfiel et al., 1992; Miller et al., 1992). The longevity, diversity, and intensity of tectonomagmatic activity in this region has resulted in the formation of a distinctly unique and rich geologic-metallogenic province.

## 1.3 Purpose and Objectives

The purpose of this study was to produce maps of mineral potential that predict the distribution of sedimentary and volcanic rock-hosted gold-silver-bearing occurrences across Nevada. Mineral potential modelling was carried out using weights of evidence method (Bonham-Carter et al., 1989). The objectives were to:

- Determine and evaluate the spatial associations between the gold-silver-bearing occurrences and a variety of regional-scale geoscientific data.
- Produce predictive maps of mineral potential (favorability) for sedimentary and volcanic rock-hosted occurrences, which include analyses of error and uncertainty associated with the mineral potential maps.
- Delineate promising regional-scale exploration targets for sedimentary and volcanic rock-hosted occurrences, and determine the important mineral potential evidence in these areas.
- Determine the first-order geologic factors controlling the regional-scale spatial distribution of the sedimentary and volcanic rock-hosted occurrences.

## 1.4 Methodology

An important goal of mineral potential modelling is to discover new deposits. As such, mineral

potential mapping involves the use of *predictive* models, as opposed to *prescriptive* models, which are based on a set of criteria that represent sound engineering practices, and/or some blend of economic or social factors (Bonham-Carter, 1994a).

In the geosciences, models can be classified into three types based upon the kinds of relationships they represent: (1) theoretical, (2) hybrid, and (3) empirical (Table 1.1). Mineral potential models based on statistical or heuristic relationships, such as weights of evidence, are empirical models. Such models are usually augmented or constrained by relationships formulated as conceptual models, as the geologic conditions and processes that lead to the formation of mineral deposits is too complex to express mathematically (Bonham-Carter, 1994a).

Empirical mineral potential models can be further subdivided on the basis of how the relative importance of a deposit-indicator (or predictor) map pattern is determined: (1) data-driven or (2) expert-driven (Table 1.2). Weights of evidence is data-driven. In weights of evidence, mineral potential is calculated by weighting and combining multiple sources of evidence, which typically includes multi-class “evidence maps” of geologic, geochemical, geophysical, or other geoscientific phenomena. The estimation of mineral potential consists of two main procedures: (1) the application of conditional probabilities to measure the spatial associations between known mineral occurrences and various evidence maps; and (2) the use of Bayesian updating techniques to combine the evidence and produce a posterior probability map. In the first step, multi-class evidence maps are typically reduced to binary-class deposit-indicator or “predictor maps” (the “*layers of evidence*”) in order to maximize the spatial association (the weights) between the evidence and mineral occurrences and to simplify map combination carried out in step two. Weights of evidence attempts to explain the spatial distribution of mineral occurrences in terms of the spatial distribution of evidence map patterns. The ultimate intent is to produce a map of mineral potential that accurately models mineral occurrence distribution. Ideally, the mineral potential map will highlight areas of yet undiscovered mineral occurrences.

In general, model building consists of three main stages (Chatfield, 1988):

1. Model formulation or specification.
2. Parameter estimation, or model fitting.
3. Model validation.

As applied to weights of evidence mineral potential modelling conducted in this study, these stages involved:

1. (a) Establishing and measuring the spatial associations between the gold-silver-bearing occurrences and multi-class mineralization “evidence maps”.  
 (b) Determining the significance of these relationships.  
 (c) The creation of binary-class mineral “predictor maps” from the mineralization-favorable units composing multi-class evidence maps.
2. Generating mineral potential maps for sedimentary and volcanic rock-hosted occurrences by combining the predictor maps in a multi-map overlay using a loglinear formulation of Bayes’ Rule.
3. Validation of the models, including testing for conditional independence among the evidence layers, analysis of mineral potential estimation uncertainty, mineral favorability at known occurrence locations, and blind tests.

## 1.5 Spatial Datasets

The geoscientific spatial data compiled for this study include:

1. *Mineral deposits*—various metallic mineral occurrence datasets, and mineral belts and trends.
2. *Regional geology*—bedrock and surficial geology, metamorphic rocks and core complex locations, volcanic centers and cinder cone locations, Mesozoic pluton distribution, geosyncline facies boundaries, regions of strong upper crustal extension, numerous fault and thrust fronts datasets, deep-seated fracture zones, lithotectonic terranes, and Tertiary rock attitudes.
3. *Physical geography*—30 arc-second and 5 arc-minute gridded elevation, mountain peak heights, generalized and detailed Great Basin physiographic province boundaries.
4. *Geophysical*—various gravity anomaly data (observed, isostatic, Bouguer, free air), geomagnetism, geothermal heat flow, geothermal conductivity, geothermal heat production, geothermal well/hot spring temperatures, and paleothermal anomaly.
5. *Seismic*—depth to reflection Moho, earthquake depth and magnitude, and crustal stress data.
6. *Geochemical*—igneous rock radiometric age dates, base- and precious-metal mineralization radiometric age dates,  $^{87}\text{Sr}/^{86}\text{Sr}$  initial values and  $I_{\text{Sr}}=0.706$  and  $0.708$  isopleths, and major and minor element data.
7. *Remote sensing imagery*—LANDSAT linear features, AVHRR, and SLAR radar.
8. *Hydrology*—drainage divides, streams and water bodies.
9. *Human/cultural-features*—major cities, administrative boundaries, roads, highways, and railways.

A series of mineral potential evidence maps was prepared from these datasets. Some were used for weights of evidence analysis and modelling while others served as supplementary material for interpretation, exemplification, and referencing (see [section 5.3.3](#)).

The *Mineral Resource Data System* mineral occurrence database (MRDS; U.S. Geological Survey, 1993) was used to model the distribution of precious-metal mineralization in Nevada. From a population of 5572 metallic and semi-metal mineral occurrences listed in MRDS, 2690 gold-silver-bearing occurrences (containing gold and/or silver as the primary commodity listed in MRDS) were selected and subdivided into samples as indicated in [Table 1.3](#):

The mineral occurrences in MRDS are classified according to the scheme of Cox and Singer (1986). Occurrence size designation is based on precious-metal content (production plus reserves), and is derived from the *Metallogenic Map of North America* (Guild, 1968). Modelling was carried out using the three principal occurrence-type samples (training datasets). In some instances, analysis and modelling was also performed using the large, medium, and/or small size sub-samples.

The sedimentary rock-hosted occurrences, which include “Carlin-type”, “carbonate-hosted”, or “disseminated” deposit types, are largely situated in north-central and north-eastern Nevada. The most important and greatest number are distributed along two regional-scale deposit alignments known as the Carlin and the Battle Mountain–Eureka (Cortez) mineral trends ([Fig. 1.3](#)), which are both oriented at acute angles to the regional structural grain (compare [Figs. 1.3](#) and [1.2](#)). Sedimentary rock-hosted deposits are typically low-grade–high-tonnage open-pit operations, and generally defined as stratiform occurrences of sub-microscopic to microscopic gold coating disseminated sulfide minerals in carbonaceous calcareous sedimentary rocks (Bagby and Berger, 1985; Cox and Singer, 1986). The age of these deposits was poorly constrained until recently, with ages ranging between 8–35 to ~120 Ma (see Arehart et al., 1993, 1995; Christensen, 1995;

Kuehn, 1989), but new research suggests that they formed between Late Eocene and Early Oligocene time (42-30 Ma) (Maher et al., 1993; Emsbo et al., 1996; Groff et al., 1997; Hall et al., 1997; Hofstra, 1997).

Most of the volcanic rock-hosted occurrences, which include “epithermal”, “hot springs”, “vein/stockworks  $\pm$  disseminations” deposit types, are located in southwestern and western Nevada, and occur within a broad belt that parallels the Nevada-California border (Fig. 1.3). This belt, known as the Walker Lane, is a zone of strike-slip movement that trends northwest at an acute angle to the regional structural grain of the central Great Basin (compare Figs. 1.3 and 1.2). Volcanic rock-hosted deposits are usually high-grade–low-tonnage underground operations (open-pit in the case of some disseminated mineralization). They are generally defined as “volcanic centered” vein and/or disseminated occurrences (often co-occurring) of gold $\pm$ silver-bearing minerals in, or associated with, a variety of brittle deformation structures hosted by volcanic and associated rock types (Cox and Singer, 1986; Panteleyev, 1986; Berger and Henley, 1989; Hedenquist et al., 1996). The volcanic rock-hosted deposits appear to be Upper Oligocene, to Early to Middle Miocene and younger in age (most forming between 27 and 5 Ma, making them about 20 to 100 Ma younger than the sedimentary rock-hosted deposits) (Dreier, 1984; Cox et al., 1991; Hutchinson and Albers, 1992; Ludington et al., 1993).

## 1.6 Similar Studies and Original Contribution

The application of GIS to minerals exploration, specifically mineral potential modelling, is gaining an increasing amount of attention and has been shown to yield favorable results (see Bonham-Carter et al., 1988; Bonham-Carter et al., 1989; George and Bonham-Carter, 1989; Watson and Rencz, 1989; Agterberg et al., 1990; Braux et al., 1990; Moon, 1990; An et al., 1991; Bonham-Carter, 1994a; Cheng et al., 1994). Much of this work was done in Canada, and until recently, GIS-based quantitative mineral potential modelling studies in the United States, specifically data-driven statistical approaches, have been limited in number. As of September 1997, nothing had been published on mineral potential modelling in the Great Basin, however, the U.S. Geological Survey and various mining companies and private consultants are now actively engaged in such research.

Gary L. Raines, of the U.S. Geological Survey, Reno Field Office, began weights of evidence modelling in 1991. He produced a posterior probability mineral potential map for hot spring-related gold, based upon proximity to volcanic rocks and vents, hydrothermal alteration, placer deposits, faults, linear features, and anomalous U, Ag, As, Mn, Se and aeromagnetic values. Dr Raines used expert-delineated maps of hot spring mineral permissibility to validate his model, which showed a high degree of agreement (74%).

Dean D. Turner, a private consultant from Reno and former employee of the Newmont and FMC gold companies, began working on an M.Sc. thesis at the Colorado School of Mines in 1991 (a paper summarizing his results, Turner, 1997, was presented at the *Exploration '97* symposium in Toronto, which was held in October of 1997). Mr. Turner produced a gold favorability map, based on weights of spatial association with non-placer gold-bearing occurrences, using buffered host-rock lithology and granitoid pluton domains, structural domains (lineament intensity, based on interpretation of topography and aeromagnetic, isostatic gravity, and radiometric anomalies),

and geochemical domains (based on As-Sb-Zn-Ag-W and Cr-V-Fe-Co-Sc pathfinder element groupings). The model was validated using 52 major sediment-hosted gold deposits, 88.5% of which were identified by his favorability map.

The study undertaken here differs substantially from, and extends beyond, those conducted by Raines and Turner. A fully-implemented application of weights of evidence mineral potential modelling was undertaken, complete with weights of spatial association analysis and assessment, generation of posterior probability maps of mineral potential (favorability), analyses of modelling error and uncertainty, and blind testing of the models. Also, this study is broader in scope, dealing not only with hot spring-related deposits and non-placer gold-bearing occurrences in north-central Nevada, but also with other epithermal mineralization (collectively modelled as “volcanic rock-hosted”), sedimentary rock-hosted occurrences State-wide, and with gold-silver-bearing occurrences in general. For the mineral potential models produced here, the training datasets and combinations of mineralization evidence are substantially different from those used by Dr. Raines and Mr. Turner (as well as having been utilized and processed differently). In addition, a large number of supplementary datasets were used in this study for interpreting the output of the models.

The original contribution of this research to the study of economic geology in the Nevada Great Basin includes:

- Predictive maps of mineral potential favorability for sedimentary and volcanic-rock hosted mineralization, which highlight areas of elevated potential but no known deposits. Associated maps of error and uncertainty.
- Maps delineating regional-scale exploration targets for sedimentary and volcanic rock-hosted occurrences, including a review of the important mineral potential evidence within the target area and a listing of specific high mineral potential sites (at the mountain-range-scale) for further investigation.
- New, revised, and supporting hypotheses regarding the regional-scale controls over the distribution of sedimentary and volcanic rock-hosted mineralization. It has been demonstrated that a data-driven approach to mineral potential mapping can illuminate the understanding of mineral deposit distribution.

In addition, the work carried out here identifies new, potentially mineral-rich, regions for research opportunity, as well as demonstrating the capacity to facilitate mineral resource assessment in the Great Basin.

## 1.7 Layout

This study is subdivided into eight chapters and five appendices. The appendices are provided as digital files on a CD-ROM located in the back cover pocket, and are available in Adobe Acrobat (.pdf) version 4.

<i>Chapter</i>	<i>Contents</i>
<b>1.</b>	<b><i>Introduction</i></b> —An overview and of this study. Includes the purpose, scope, and objectives, as well as a review of the datasets and the analysis and modelling techniques.
<b>2.</b>	<b><i>Geology of the Great Basin</i></b> —An overview of the geology of the Great Basin and its environs, with emphasis placed on the features and time periods pertinent to the interpretation of the sedimentary and volcanic rock-hosted weights of evidence mineral potential maps. This is a background chapter that represents a summary literature review.

3. ***Characteristics and Distribution of Sedimentary and Volcanic Rock-Hosted Deposits***—An overview of sedimentary and volcanic rock-hosted deposit types, with emphasis placed on their spatial distribution. This is a background chapter that represents a summary literature review.
4. ***Analysis and Modelling Techniques***—An overview of preliminary GIS spatial data analysis techniques and weights of evidence mineral potential modelling (an extended and detailed discussion is given in Appendix B). This is a background chapter that represents a summary literature review.
5. ***Spatial Datasets***—An overview of the GIS study area, training datasets, and mineral potential evidence. Included is a discussion on gold-silver-bearing mineral occurrence selection criteria, evidence map selection, and reviews on data coverage, collection, accuracy, and error issues.
6. ***Single Map Analysis, Interpretation, and Mineral Predictor Map Generation***—Analysis of mineral potential evidence. Each evidence map is examined in relation to the distribution of gold-silver-bearing occurrences (this chapter represents the first of two procedures that constitute the weights of evidence modelling method; see Chapter 4). The distribution and basic statistical nature of the datasets are described, and the spatial associations between the occurrences and the evidence maps are measured. The significance of the spatial relationships is determined and an interpretive synthesis in light of geology and metallogeny is given. Also discussed are generation of binary-class mineral predictor maps and various assumptions, definitions, and selection criteria for the gold-silver-bearing occurrences.
7. ***Multi-Map Modelling and Gold-Silver Mineral Potential***—Summary and discussion of the results and output of mineral potential modelling. The mineral predictor maps are combined to produce the mineral potential maps (this chapter represents the second of two procedures which constitute the weights of evidence method; see Chapter 4). Analyses of mineral potential model conditional independence, error, and uncertainty are reviewed. Validation of the models, including mineral favorability at known occurrence locations and blind tests are discussed. Regional-scale sedimentary and volcanic rock-hosted occurrence exploration targets are delineated.
8. ***Controls on Sedimentary and Volcanic Rock-Hosted Occurrence Distribution***—Discussion and summary of the geologic and metallogenic interpretation of the mineral potential maps. Important mineral potential evidence within each target region is reviewed. Possible factors controlling the regional-scale distribution of sedimentary and volcanic rock-hosted occurrences are delineated and discussed.

## ***Appendix***

## ***Contents***

- 
- A. ***Stratigraphy and Description of Lithologic Units***—A correlation chart of geological map units with an accompanying table of unit descriptions.
  - B. ***Weights of Evidence Mineral Potential Modelling Theory, Implementation, and FORTRAN Utilities***—A detailed theoretical discussion of the weights of evidence modelling procedure, implementation of the procedure, and DOS and OS/2 executable and source code for the stand-alone command-line FORTRAN utilities (used to calculate the spatial weights of association, the posterior probabilities, and the weights errors and uncertainty factors). Also included is a review of various GIS spatial analysis techniques and tools. The DOS and OS/2 utilities are included on this CD-ROM in the \appd\_b folder.
  - C. ***Mineral Potential Map Generation, Conditional Independence, and Uncertainty***—A detailed account and analysis of mineral potential maps generation, conditional independence testing, interpretation and mitigation and of conditional dependence, and mineral potential map uncertainty.
  - D. ***Mineral Potential at Known Mineral Occurrence Areas***—A detailed examination of how well the mineral potential models predict data from which they were built. Includes three tables containing the posterior probability value associated with each of the occurrences.



## Chapter 2. Geology of the Great Basin

### 2.1 Introduction

The Great Basin is one of the most intensely studied regions on Earth. This chapter presents a review of the geology of the Great Basin and its environs, with emphasis placed on the features and time periods pertinent to the interpretation of the sedimentary and volcanic rock-hosted weights of evidence mineral potential maps. An overview of physiographic and tectonic setting and an outline of the geologic history are given in [sections 2.2 and 2.3](#). The Precambrian and Cenozoic time periods are reviewed in greater detail in [sections 2.4 and 2.5](#). Strike-slip tectonism and related regional-scale crustal features are discussed in [section 2.6](#). The characteristics and structure of the present-day crust are reviewed in [section 2.7](#).

Comprehensive reviews of the geologic, tectonic, magmatic, and geophysical nature of Great Basin can be found in Atwater (1970, 1989), Axen et al. (1993), Bally and Palmer (1989), Best and Christiansen (1991), Burchfiel et al., (1992), Coward et al., (1987), Crittenden et al. (1980), Eaton (1982), Ernst (1988), Pakiser and Mooney (1989), Raines et al. (1991), Smith and Eaton (1978), Stewart (1980), and Zoback et al. (1981).

### 2.2 Physiographic Setting

The Basin and Range Province of the southwestern United States and northern Mexico is an extensional tectonic regime set in the southern North American Cordillera, part of the larger Cordilleran orogenic belt that stretches from southwestern Alaska in North America to Chile and Argentina at the southern tip of South America ([Fig. 2.1](#)). It is part of a region known as the “continental interior” of the Cordilleran orogen (Christiansen and Yeats, 1992), also referred to as the Intermontane System (Anderson, 1989). The Intermontane System covers a vast region in the western United States—it extends from the United States-Mexico border northward to southeastern Oregon and southern Idaho; it is bound to the east by the Rocky Mountain System and to the west by the Pacific Mountain System; and it encompasses the Basin and Range Province, the Colorado Plateaus, and the high lava plains of the Snake River Plateau (Anderson, 1989; Thelin and Pike, 1991) ([Fig. 2.2](#)). The Cordilleran orogen in the western United States is unusually wide, measuring approximately 1,500 km across (Guild, 1985), as compared to the modern-day Andean orogen with a width of 400-800 km (Dickinson and Snyder, 1978).

The Basin and Range Province of the southwestern United States may be subdivided into northern, central, and southern regions, based upon contrasting geologic histories and structural styles (Wernicke, 1992), and is composed of five individual physiographic sub-provinces ([Fig. 2.2](#)) (Thelin and Pike, 1991):

1. Great Basin
2. Sonoran Desert, or the Mojave Block (Wilkins, 1984)
3. Salton Trough
4. Mexican Highland (which includes the Rio Grande Rift zone), or the Porphyry Copper Block (Wilkins, 1984)
5. Sacramento section

The Great Basin, coincident in name and in expanse with the northern Basin and Range Province, is the largest of the five physiographic provinces, covering ~452,000 km<sup>2</sup> (as circumscribed by Thelin and Pike, 1991) and varying from 500 to 1000 km in width (see Harry et al., 1993). It occupies nearly all of the State of Nevada (~95%), much of western Utah, small parts of southern Idaho and Oregon, and California east of the Sierra Nevada Range. The Great Basin is not a basin proper, but rather is a collection of over 200 small basins that form a large region of interior drainage that is bound to the east (Wasatch front, Utah) and to the west (Sierra Nevada, California) by marginal highlands rising 2-3 km above SML, approximately one kilometer above the surrounding regions (Eaton et al., 1978; Mayer, 1986; Hendricks and Plescia, 1991; Sherrod and Tosdal, 1991; Christiansen and Yeats, 1992; Wernicke, 1992). The area within the Great Basin is uniformly above one kilometer SML and has an average elevation of 1.5 km, comparable to that of the Colorado Plateau (Christiansen and Yeats, 1992; also see Wilkins, 1984; Harry et al., 1993). Basin–range-style topography is characteristic of the Basin and Range Province as a whole, but is best developed in the Great Basin sub-province (Fig. 1.2).

## 2.3 Tectonic Setting and Geologic History

The Cordilleran orogen is one of the longest-lived and extensive orogenic belts in the world (Burchfiel et al., 1992). The major tectonic elements within and surrounding the Great Basin date from the Archean through the present, and with the exception of the Precambrian elements, are products of the interaction between the Pacific oceanic and the North American continental tectonic plates (Atwater, 1970, 1989; Mutschler et al., 1987). The tectonic environments of the western United States and the Great Basin are illustrated in Figures 2.3 and 2.4, respectively. The major orogenic belts in the Great Basin are shown in Figure 2.5.

The geologic history of the Great Basin region is complex, spanning at least 600 to >800 Ma, and involving major episodes of crustal accretion, sedimentation, igneous activity, compressional deformation, and continental rifting and extension. This history includes at least three orogenies in the Precambrian (Yavapai-Mazatzal, episodic Middle Proterozoic intracontinental rifting, polyphase Late Proterozoic marginal rifting; Burchfiel et al., 1992; Hoffman, 1989), two in the Paleozoic (Antler and Sonoma; three if the “Humboldt event” is included, see Stewart, 1980; Miller et al., 1992), three in the Mesozoic (Nevadan-Elko, Sevier, and start of the Laramide; or one, if considered as three pulses of the “Cordilleran orogeny”, see Miller et al., 1992), one in the Cenozoic (initial local crustal extension and basin-range development; Laramide activity wanes), and the present-day continued basin and range development (Stewart, 1980; Berger and Bonham, 1990). The current stage of basin-range development represents only about 5% of its total evolution (Stewart, 1980). Precambrian and Phanerozoic orogenic history are illustrated in Figure 2.6, mid-Mesozoic through early Cenozoic in Figure 2.7, and latest Cretaceous through present in Figure 2.8.

In broadest terms, the Phanerozoic geologic setting and history of the Great Basin region can be summarized in terms of three contrasting regimes:

1. *Latest Proterozoic to late Devonian passive margin regime*—A tectonically quiescent stable Precambrian continental passive margin along which a two-fold northerly-trending miogeoclinal-eugeoclinal depositional regime developed (Stewart, 1980; Suppe, 1985).
2. *Late Devonian to early Tertiary accretionary and compressional regime*—Island-arc and oceanic terranes



were accreted to the western edge of the continental margin. Eastward-directed compressional orogenic events emplaced areally-extensive thrust sheets along and east of the margin, resulting in large-magnitude crustal shortening and the juxtaposition of the coeval but contrasting miogeoclinal and eugeoclinal sequences. Geosynclinal sedimentation was terminated in the Early Triassic. By Late Triassic or Early Jurassic an “*Andean-type*” continental-margin subduction regime was established. Widespread plutonism and upper crustal thrusting followed, resulting in the development of a regionally extensive magmatic arc, foreland fold and thrust belt and associated hinterland (Coney, 1978; Stewart, 1978, 1980; Suppe, 1985; Mutschler et al., 1987; Berger and Bonham, 1990; Thorman et al., 1991).

3. *Early Tertiary to Present extensional regime*—The modern-day Great Basin developed east of a waning Mesozoic magmatic arc in an intra-arc and back-arc setting within thrust belts formed from Paleozoic miogeoclinal and accreted terranes. A transition from compressional to extensional tectonics occurred around 45-40 Ma, and after about 36 Ma, widespread volcanism and crustal extension prevailed (Stewart, 1978, 1980; Eaton, 1983; Lipman, 1983; Wernicke et al., 1987; Hamilton, 1988; Berger and Bonham, 1990).

The geologic events that shaped these three regimes, as well as the pre-Cordilleran settings, may be subdivided into seven stages:

1. *Archean to Latest Proterozoic*—Nucleation and configuration of the core of the North American crystalline craton, including numerous episodes of collisional and extensional deformation; polyphase rifting gives rise to approximate shape of present-day North American continent and truncates Precambrian tectonic grain.
2. *Latest Proterozoic to Late Devonian*—Passive-divergent subsiding margin and sedimentation; inception and main-stage deposition of the Cordilleran geosyncline; depositional framework consisted of a western siliceous assemblage (the eugeosynclinal facies) and the eastern carbonate assemblage (the miogeoclinal facies), separated by a transitional zone (the transitional facies).
3. *Late Devonian to Late Triassic*—Passive, sub-island arc subduction, accretionary margin; addition of crust to the western margin of the Precambrian crystalline craton core; initial deformation of the Cordilleran geosyncline; two island-arc system's and their associated accretionary prism sequence's are welded to the craton in two separate episodes during the Antler and Sonoma orogenies (emplacement of the Roberts Mountain and Golconda allochthons, respectively); sedimentation in the Cordilleran geosyncline is terminated at the start of the Sonoma orogeny in the Early Triassic; global plate reorganization and tectonic truncation of Paleozoic orogenic grain by Late Triassic; arc polarity reversal.
4. *Late Triassic to Upper Cretaceous*—Active margin sub-continental subduction (“*Andean-type*” steep angle plate descent mode); passive-to-active margin transition, and initiation of sub-continental subduction; crustal thickening and compressional deformation; development of continental magmatic arc (Nevadan-Elko phase) and “*thin-skinned*” fold and thrust belt and associated hinterland (Sevier phase); region of present-day Great Basin undergoes contraction between a continental arc on the west and the craton in central Utah to the east.
5. *Upper Cretaceous to Mid-Eocene*—Active margin sub-continental subduction (shallow angle plate descent mode, high rate of plate convergence); Cordilleran geosyncline depositional environment is wiped out; intraplate deformation; compressional orogenesis migrates inland toward the craton during Laramide activity; arc magmatism shifts progressively eastward and wanes; transition from compressional to extensional orogenesis occurs as active margin sub-continental subduction wanes.
6. *Mid-Eocene to Late-Lower Miocene*—Active margin sub-continental subduction rapidly ending (steep angle subduction plate roll-backs from east to west, decreasing plate convergence rate); Pacific oceanic plate closes on North American continental plate; large-magnitude, pre-basin-range-style extension (early extensional phase, ~36-17 Ma), characterized by low angle shallow listric and detachment faulting in the upper crust and in some places the emergence of mid-crustal metamorphic core complexes; regional uplift; magmatism resumes and sweeps generally west and southward (predominantly felsic-intermediate calc-alkaline volcanic flows and silicic ash-flow tuffs); inception and growth of San Andreas transform system; cessation of active margin sub-continental subduction and transition to passive transform margin.
7. *Late-Lower Miocene to Present*—Transform margin between North American continental plate and Pacific oceanic plate develops as Mendocino triple junction migrates north; earlier extensional period wanes and is superseded by wide-spread basin-range-style extension (later extensional phase, 17-6 Ma), characterized by high angle deep-penetrating block faulting that produces the modern Basin and Range Province structural grain and topography; brief lull in felsic-intermediate and silicic calc-alkaline magmatism (20-17 Ma)

followed by transition to bimodal rhyolite-basalt volcanism which is characterized by increasing proportions of basalt; intensity of silicic volcanism progressively decreased during last 10 m.y.

These seven stages are based upon plate boundary interactions and orogenic styles, and reflect coherent periods in the development of the Great Basin region and its environs. They are not meant to suggest any implicit genetic relationship between the events within any one stage, though in many instances this may be the case.

## 2.4 Craton Development

The Precambrian terrain of the western Cordillera of the United States is a poorly understood collage of collided oceanic island arcs, overprinted by continental magmatic arcs, complicated by rifts, and perhaps affected by anorogenic magmatism (Hamilton, 1987). For the most part, the evolution and tectonic activity of the Precambrian have not been delineated in detail (Dickinson, 1981), but recent work by Hoffman (1989) has added greatly to the understanding of this era in North America.

### 2.4.1 Assembly and Margin Formation

The evolutionary stages of the North American craton overlap in time, but can be roughly outlined as: (1) 1.98-1.83 Ga initial assembly of the Archean core of the Laurentian protocraton; (2) 1.91-1.65 Ga growth of the Laurentian protocraton by accretion of mainly proterozoic material; (3) 1.65- 0.8 Ga Laurentian supercontinental tectonic environment; and (4) 0.8-0.5 Ga marginal rifting of Laurentia (ages generalized from Hoffman, 1989). The fourth stage was particularly important. During this stage, the edges of Laurentia were carved away, forming the crystalline cratonic core of North America and establishing the cratonic margin in the southwestern United States (Stewart, 1980; Hoffman, 1989). This episode of continental margin rifting was to have far reaching effects on the orientation, location, and style of subsequent Phanerozoic orogenic elements that developed in the southwestern Cordillera and northern Basin and Range Province.

The initial assembly of Laurentian protocraton took place in the Early Proterozoic (1.98-1.83 Ga) when seven former microcontinents were welded together during collisional orogenesis, which was characterized by deformed passive margin and foredeep sedimentary prisms, “*Andean-type*” magmatic arcs, hinterlands with compression-related fault tectonism, and foreland thrust-fold belts (Hoffman, 1989). These microcontinents (or crustal provinces, in post-accretionary parlance) are Late Archean crustal aggregates that contain variable proportions of Early and/or Middle Archean rocks, and include the Superior, Wyoming, Slave, Nain, Hearne, Rae, and Burwell provinces (Hoffman, 1989). In the Early Proterozoic, growth continued as crust containing little or no Archean material was accreted along the western, southern, and southeastern margins of the Archean core of the protocraton between about 1.91 and 1.65 Ga (Hoffman, 1989). Along the southern and southwestern United States, more than 1,200 km of juvenile crust was accreted between 1.80 and 1.65 Ga during the Central Plains and Yavapai-Mazatzal orogenies, respectively (Hoffman, 1989). The construction of the Laurentian supercontinent, within which the North American craton was embedded, was coherent by 1.7 Ga and assembled by 1.65 Ga (Dickinson, 1981; Hoffman, 1989; Burchfiel et al., 1992).

In the late Middle Proterozoic, sedimentary rocks now within the Cordilleran orogen were

probably deposited during at least three pre-Cordilleran intracontinental extensional events that took place around 1.5-1.3 Ga, 1.15-1.07 Ga, and 0.9-0.8 Ga, the first being the most extreme of the three (Burchfiel et al., 1992). Between 0.8 and 0.5 Ga, polyphase rifting took place along the margins of Laurentia, giving rise to the approximate shape of present-day North American craton (Hoffman, 1989). Rifting along the present-day western margin of North America was accompanied by wide-spread mafic igneous activity and sedimentation, and marked the initiation of the throughgoing Cordilleran geosyncline, which was considered by Burchfiel et al. (1992) to be the inception of the Cordillera orogen. Main-stage deposition of the Cordilleran geosyncline dominated geologic activity from latest Precambrian through mid-Paleozoic. By about 650-600 Ma, major rifting had subsided and the western edge of the North American craton resembled a passive Atlantic-type margin (Stewart, 1980; Burchfiel et al., 1992). Strata were deposited along and inland from the continental margin, resting unconformably on structurally complex crystalline basement rocks consisting of gneiss, schist, quartzite, marble, greenstone, and granite ranging in age from about 2.5 to 1.41 Ga, and on younger supracrustal sedimentary and volcanic rocks ranging in age from about 1.45 to 0.9-0.8 Ga (Poole et al., 1992). The pattern of deposition that was to characterize the early Paleozoic was well defined in Nevada by latest Precambrian time (Stewart, 1980) (Fig. 2.9). Clastic shelf sedimentation continued through the Early Cambrian, but as the continent moved into lower latitudes, it was gradually superseded in the Middle Cambrian by younger shallow-water carbonate strata that transgressed farther inland onto the cratonic basement (Hamilton, 1987). These conditions continued with only minor changes in sedimentation patterns and with little disruption through the lower and middle Paleozoic until stable-margin sedimentation ended in the late Devonian-early Mississippian with the Antler compressional orogeny, during which the Roberts Mountain and Golconda allochthons were emplaced, respectively (Stewart, 1980; Dickinson, 1981; Speed, 1983; Suppe, 1985; Hamilton, 1987; Hutchinson and Albers, 1992).

## 2.4.2 Western Edge and Crustal Provinces

The western edge of the Precambrian craton in the western United States is commonly believed to correspond closely to an initial value of  $^{87}\text{Sr}/^{86}\text{Sr} = 0.706$  in Mesozoic and Tertiary granitoids (Fig. 2.10), a value considered to represent the boundary between magmas related to oceanic or continental lithosphere (Kistler and Peterman, 1973; Stewart, 1980). In the Great Basin, the  $^{87}\text{Sr}/^{86}\text{Sr} I_{\text{Sr}} = 0.706$  isopleth trends from the central Sierra Nevada to western Idaho in a variable north or northeast orientation, which is dependant upon the datasets and interpretations used to place the line (see Kistler and Peterman, 1973; Fleck and Criss, 1985; Kistler, 1990; Carlson et al., 1991). Burchfiel et al. (1992) noted that the  $^{87}\text{Sr}/^{86}\text{Sr} I_{\text{Sr}} = 0.706$  isopleth is a composite line with a location throughout the Cordillera controlled by different events of different ages. Strike-slip activity (late Paleozoic, mid- to late Mesozoic, and Cenozoic) has been the controlling factor in the position of the line from the Mexican border to the central Sierra Nevada (Burchfiel et al., 1992), hence the northwestward “spike” in the line along the California-Nevada border. In central Nevada, its location may be close to the original site of the latest Precambrian rifting, albeit modified by the effects of Paleozoic and Mesozoic shorting and Cenozoic extension (Burchfiel et al., 1992; see Levy and Christie-Blick, 1989, for a Pre-Mesozoic palinspastically restored  $^{87}\text{Sr}/^{86}\text{Sr} I_{\text{Sr}} = 0.706$  isopleth). An alternative to the  $^{87}\text{Sr}/^{86}\text{Sr} I_{\text{Sr}} = 0.706$  isopleth is the  $^{87}\text{Sr}/^{86}\text{Sr} I_{\text{Sr}} = 0.708$  ( $\epsilon_{\text{Nd}} = -7$ ) isopleth (Farmer and DePaolo, 1983), located as much as 100 km to the east of the  $^{87}\text{Sr}/^{86}\text{Sr} I_{\text{Sr}} = 0.706$  isopleth (Levy and Christie-Blick, 1989). The  $^{87}\text{Sr}/^{86}\text{Sr} I_{\text{Sr}} = 0.708$  ( $\epsilon_{\text{Nd}} = -7$ ) isopleth, however, appears to be inconsistent with the distribution of

Proterozoic and Lower Cambrian sedimentary rocks that occur near the  $^{87}\text{Sr}/^{86}\text{Sr}$   $I_{\text{Sr}} = 0.706$  isopleth (Levy and Christie-Blick, 1989). The western edge of the craton may also be delineated by a late Paleozoic-early Mesozoic regional paleothermal anomaly that trends roughly north-south across Nevada (Cunningham, 1988) (Fig. 2.10).

In addition to the craton edge, three or four Precambrian crustal formation provinces that underlie the Great Basin have been delineated using (1) initial Sr and Nd isotopic ratios in Late Proterozoic, Mesozoic, and Tertiary granitoids and mafic rocks, (2) Pb isotopic compositions of ores and Mesozoic and Cenozoic igneous rocks, and (3) granitoid crystallization ages (Zartman, 1974; Farmer, 1988; Livaccari and Perry, 1993; and especially Bennett and DePaolo, 1987, figures 3 and 6) (Fig. 2.11). These Precambrian crustal formation provinces trend roughly west-southwest—east-northeast, at a high angle to the western edge of the craton, and decrease in age from northwest to southeast, reflecting a basement structure which suggests successive accretion of increasingly younger Proterozoic-aged crust.

The tectonic grain of the Precambrian North American craton in the southwestern United States generally trends east-west to northeast-southwest, at a high angle to the generally north-south to northwest-southeast tectonic grain of Cordilleran orogen, and was most probably truncated by the Late Proterozoic (0.8-0.5 Ga) polyphase rifting event (Hamilton, 1987; Burchfiel et al., 1992). The youngest rocks having the older tectonic grain include the Belt Supergroup in the United States, and its Canadian correlative, the Purcell Supergroup. Estimates for the age of the Belt/Purcell rocks range from a low of 1.5-0.9 Ga to a high of 1.6-1.3 Ga, the better of the two ranges being the latter (Burchfiel et al., 1992). In Nevada, Precambrian basement rocks occur in the southernmost tip of the State and compose less than one-half of one percent (~0.4%) of the total unit area mapped on the geological map of Nevada (Stewart and Carlson, 1978; Stewart, 1980). These units include Precambrian Y (~1.5-1.4 Ga) granitic rocks and Precambrian X (~1.74-1.70 Ga) metamorphic rocks, and are part of a metamorphic terrain developed from stratified and volcanic geosynclinal rocks that is perforated by anorogenic porphyritic rapakivi granites (Stewart, 1980). The several known Precambrian tectonic events subsequent to the formation of the crystalline basement rocks in the western United States are not recognized in Nevada. Rocks that would show the effects of these events (i.e.—rocks equivalent in age to the Belt/Purcell Supergroup) do not crop out in the State (Stewart, 1980).

## 2.5 Cenozoic Extensional Tectonism

The end of the Laramide orogenesis in the Cordillera of the western United States marked a fundamental change in the style from compressional tectonism, which had dominated since the Late Triassic, to local and regional extension and local strike-slip tectonism, which dominated during the middle and late Cenozoic and is still ongoing today (Figs. 2.6, 2.7, and 2.8). Middle and late Cenozoic extensional orogenesis and associated magmatism are responsible for the present-day tectonomagmatic and structural configuration of the Great Basin, and developed in two main stages: (1) an earlier (middle Tertiary, ~36-17 Ma) stage of calc-alkaline-dominated magmatic activity, and rapid, extreme, and localized extension characterized by “thin-skinned-style” low-angle fault structures, including Cordilleran metamorphic core complexes; and (2) a later (late Tertiary, ~17-0 Ma) stage of predominantly basaltic magmatism, and slow, moderate, and more widespread extension characterized by high-angle block-fault structures (Zoback et al.,

1981; Eaton, 1982, 1984; Stewart, 1983; Wernicke, 1985; Rehrig, 1986; Hamilton, 1987; Patino-Douce and Humphreys, 1987). In the hinterland of the Sevier orogen, where the Great Basin was to develop, magmatism and extension were time-transgressive, migrating southward and westward across the region during the early through subsequent late stage of extensional tectonism (Armstrong et al., 1969; Stewart 1980; Silberman 1985; White 1985; Gans et al, 1989; Best and Christiansen, 1991; Seedorff, 1991).

### **2.5.1 Early Stage (Mid-Eocene to Late-Lower Miocene)**

The early stage of extensional orogenesis is characterized by: (1) the renewal of vigorous, predominantly silicic to intermediate calc-alkaline tuff and lava volcanism, which swept generally west and southward; and (2) crustal thinning in the form of discrete, relatively narrow and elongate, localized domains of large-magnitude extension in the ductile lower crust, which include low-angle shallow listric and detachment faults in the upper crust, and locally the exhumation of mid-crustal rocks in the form of metamorphic core complexes (Stewart, 1983; Wernicke et al., 1987; Gans et al., 1989; Best and Christiansen, 1991; Seedorff, 1991; Catchings, 1992; also see Harry et al., 1993). The end of this stage of extensional orogenesis is characterized by the waning of calc-alkaline magmatic activity, a decline in large-magnitude extension, and by the transition to a passive transform continental margin, brought about by the collision of the Pacific and North American plates in middle Oligocene and the initiation of San Andreas transform system.

#### **2.5.1.1 Magmatic Activity—Distribution, Age, and Composition**

The Sevier hinterland had been magmatically and tectonically quiescent throughout most of the late Paleocene and early Eocene. Arc magmatism in this region, which had thrived until about 80 Ma, had been extinguished, and a gap in the continuity of the arc created (Laramide magmatic gap) as Laramide magmatism and deformation migrated eastward well onto the craton in response to subhorizontal inboard subduction tectonics (Coney and Reynolds, 1977; Coney, 1978; Dickinson and Snyder, 1978; Keith, 1978; Dickinson, 1981; Berger and Bonham, 1990; Armstrong and Ward, 1991; Hutchinson and Albers, 1992). Magmatism resumed in Idaho and Montana north of the Sevier hinterland in earliest Eocene time, swept southward after 45 Ma narrowing the Laramide magmatic gap, and entered the northern part of the Sevier hinterland in Eocene time, about 43 Ma (Gans et al, 1989; Armstrong and Ward, 1991; Best and Christiansen, 1991). Magmatic activity continued a southward transgression during the Oligocene into a southern part of the region along an arcuate roughly east-west front that was at a high angle to the continental margin and on the order of hundred kilometers long (Elston, 1983; Wernicke et al., 1987; Best and Christiansen, 1991). Coeval with the southerly sweep of magmatism through Nevada and Utah, volcanism swept west and north out of southwest New Mexico across southern Arizona, and by the beginning of Miocene time (~22 Ma), the northern and southern magmatic fronts had merged, closing the Laramide magmatic gap, and a continuous arc trend extended once again along the flank of the whole western Cordillera (Dickinson, 1981; Dickinson and Snyder, 1978; Anderson, 1989; Armstrong and Ward, 1991). In southernmost Nevada, the landward portions of the southerly- and northerly-migrating volcanic fronts converged, but did not completely merge, resulting in an “amagmatic zone” extending from ~37° to ~36° latitude trending nearly east-west (McKee, 1971; Blakely and Jachens, 1991).

In the Sevier hinterland, magmatism was concentrated within the core and interior regions of the present-day Great Basin, first appearing in east-central Nevada, or the north-central part of the basin in Late Eocene to Early Oligocene time (~43-35 Ma) then generally swept south and westward toward the subduction zone (Armstrong et al., 1969; Noble, 1972; Stewart and Carlson, 1976; McKee, 1977; Smith, 1978; Tweto, 1979; Leeman and Fitton, 1989; Zoback et al., 1981; Elston, 1983; Stewart, 1983; Schermer, 1985; Best et al., 1989). The initial phases of magmatic activity overlapped the final period of waning subduction (Leeman, 1982; McKee, 1995) and increased in intensity throughout the latest Eocene and Oligocene (Berger and Bonham, 1990; Leeman and Harry, 1993) (Fig. 2.8). Magmatic activity peaked between 31-20 Ma (Best and Christiansen, 1991) in a regional event known as the “*great ignimbrite flareup*” (Noble, 1972), which was characterized by a widespread and dramatic increase in the volume of ash-flow tuffs and pyroclastics extruded (Best and Christiansen, 1991). During this interval, great thicknesses of volcanic materials erupted from nested calderas and formed northwest- to west-northwest-trending troughs or belts in central Nevada (Anderson, 1989). Magmatism waned after the ignimbrite flareup and a short lull in igneous activity was experienced in the Early Miocene (~20-17) (McKee, 1977; Wernicke et al., 1987).

Magmatism was predominantly intermediate calc-alkaline in chemistry (McKee, 1995), also referred to as silicic to intermediate in composition (Stewart and Carlson, 1978; Stewart, 1980; Wernicke et al., 1987; Glazer and Ussler III, 1989; Hamilton, 1989; Best and Christiansen, 1991; Leeman and Harry, 1993). Minor basaltic variants occurred locally (Leeman, 1982; Leeman and Harry, 1993). Stewart and Carlson (1976, 1978) and Stewart (1980) categorized the Cenozoic igneous rocks in Nevada into four broad temporal groups or “time-slices”:

- 43-34 Ma** Characterized by andesitic to rhyolitic lava flows and shallow intrusives, local voluminous silicic ash-flow tuffs, and granitic plutons. These rocks are distributed across the central, north-central, and east-central parts of the State. The 34 Ma lower boundary marks the approximate middle of the transition from dominantly andesitic and rhyolitic lavas of the 43-34 Ma time period to dominantly silicic tuffs of 34-17 Ma period (Stewart, 1980; Stewart and Carlson, 1976; Thorman and Christensen, 1991).
- 34-17 Ma** Characterized by voluminous quartz latitic to rhyolitic ash-flow tuffs, sparse basaltic lavas, and intermediate to granitic plutons. These rocks are distributed in a broad arc, trending east-west across southern Nevada (just north of the amagmatic zone) and southeast-northwest across central Nevada parallel to the northeastern margin of the Walker Lane. The 17 Ma lower boundary falls within a period of relatively little volcanic activity and marks a time of significant tectonic change that eventually led to the development present-day basin-range structure (Stewart, 1980; Stewart and Carlson, 1976; Thorman and Christensen, 1991).
- 17-6 Ma** Characterized by basalt, bimodal rhyolite-basalt, high silica rhyolite, and andesite volcanism and the emplacement of intermediate to granitic plutons. These rocks are distributed in a crescent-shaped pattern that surrounds central and east-central Nevada, trending east-west across southern Nevada (just north of the amagmatic zone), southeast-northwest along (within) the Walker Lane, and southwest-northeast in a broad belt across northern Nevada. The 6 Ma lower boundary marks the approximate end of widespread ash-flow activity (Stewart, 1980; Stewart and Carlson, 1976; Thorman and Christensen, 1991).
- 6-0 Ma** Characterized by scattered basaltic cinder cones and lava flows, and minor rhyolite and andesite flows (Stewart, 1980; Stewart and Carlson, 1976;

Thorman and Christensen, 1991). These rocks occur locally along the Walker Lane and in northwest, north-central, and south-central Nevada, but are primarily distributed outside the borders of Nevada, around the margins of the Great Basin (see Stewart and Carlson, 1976).

This scheme is based upon the gross composition, spatial distribution, and the time and tectonic environment in which the igneous rocks were emplaced or extruded (see Stewart, 1980). It is a useful way of representing the space-time and geologic aspects of these rocks in a GIS environment.

### **2.5.1.2 Extensional Activity—Distribution, Age, Character, Magnitude**

Extensional activity in the Cordillera began during the waning stages of the Laramide phase, well before Laramide calc-alkaline intermediate arc volcanism had ended (Eaton, 1983; Elston, 1986; Wernicke et al., 1987). Contemporaneous with the renewal of magmatism (Gans et al., 1989), or shortly thereafter (Best and Christiansen, 1991), a pattern of relatively localized tectonic extension began to develop throughout parts of the region in response to relaxation of Laramide contractional stresses (Mutschler et al., 1987; Dewey, 1988; Christiansen and Yeats, 1992). Extension began in the Pacific Northwest, and probably swept southward in the wake of the southern sweep of Eocene-Oligocene magmatism (Best et al., 1989) where it became best developed within four subregions, that include from north to south: (1) the Omineca extended belt in northeastern Washington State and southern British Columbia; (2) the Rocky Mountains Basin and Range in southwestern Montana, eastern Idaho, and northwestern Wyoming; (3) the northern and southern Basin and Range provinces; and (4) the Rio Grande rift zone, which extends north-south across central New Mexico north into Colorado (Wernicke, 1992, see figure 1).

Extension can be traced from early Eocene time in southern British Columbia as it migrated south into the northern Cordillera of Washington, Idaho, and Montana, and then as it continued through the central Cordillera and further south (Tweto, 1979; Zoback et al., 1981; Mutschler et al., 1987; Wernicke et al., 1987; Gans et al., 1989). Extensional tectonism is first evident in the geologic record at ~52 Ma in southern British Columbia, northern Washington, Idaho and Montana (Eaton, 1983, Wernicke et al., 1987). In the northern Basin and Range, extensional tectonism is recognized as early as the latest Eocene in southern Oregon and northern Nevada, between about 38-35 Ma in the Great Basin, and at 29 Ma in the Rio Grande Rift (Eaton, 1983; Gans and Mahood, 1987; Wernicke et al., 1987; Gans et al., 1989). Extension in the Sevier hinterland during the early stage of extension was concentrated within the core and interior regions of the present-day Great Basin. The initial phases started in the middle to late Eocene (~39 to 36 Ma) in east-central Nevada, or the north-central part of the present-day basin, and migrated southwestward and slightly eastward into western Utah and central Nevada in early Oligocene (Eaton, 1980, 1984; Rehrig, 1986; Wernicke et al., 1987; Gans et al., 1989; Hodges and Walker, 1992). Extensional activity appears to have proceeded in two phases that were separated by the great ignimbrite flareup, the period of peak volcanic activity that took place from about 31 to 22-20 Ma (Best and Christiansen, 1991).

Extension was not uniformly distributed, rather, it occurred in relatively localized, elongate, and narrow corridors or domains of high-magnitude rapid extension (Wernicke et al., 1987; Gans et al., 1989; Seedorff, 1991; Catchings, 1992; Christiansen and Yeats, 1992; Wernicke, 1992).



The domains are arranged in “patchwork pattern” of belts, trending roughly north to north-northeast (Axen et al., 1993; Wernicke, 1990, 1992), and formed initially in a restricted region within the Sevier fold-thrust belt, along the eastern margin of the then-developing Great Basin (Eaton, 1982; Elston, 1984; Hamilton, 1987; Wernicke et al., 1987; Hodges and Walker, 1992; Miller et al., 1992). Known extensional domains occur primarily in the eastern half of the present-day Great Basin, however, they are probably much more widespread than is generally accepted, especially in the north-central and western regions (Seedorff, 1991). The extensional domains at present are roughly 30-100 km wide (Seedorff, 1991), and are structurally complex, composed of fields of low-angle normal and listric faults, surficial detachment faults, and include, but are not limited to, Cordilleran metamorphic core complexes (Dickinson, 1981; Eaton, 1982; Stewart, 1983; Seedorff, 1991). Metamorphic core complexes are considered to be among the most extreme and visible effects of crustal attenuation, and may represent local sites where thermal weakening of the crust and an unusually shallow brittle-ductile transition, the result of intense magmatic activity and/or upwelling of subcrustal mafic material, allowed the middle and lower continental crust to be dragged out from beneath a fracturing, extending upper crust (Rehrig, 1986; Lister and Davis, 1989; Armstrong and Ward, 1991).

Widening of the Cordilleran orogen in the western United States, which had begun during Laramide- time when orogenic activity migrated east onto the craton, continued throughout the early and late stages of Cenozoic extensional orogenesis. Crustal extension occurred primarily in the Basin and Range and Rio Grande provinces (Elston, 1986). As a whole, the Basin and Range Province approximately doubling in width (Hamilton, 1989), with the most dramatic widening taking place in the Great Basin. Estimates of the average increase in width across the present-day Great Basin over that of the original width of the region prior to extension varies greatly: 10-35% (Stewart, 1978); 50% (Proffett, 1977); 55% (Smith et al., 1991); 50-85% (Hauser and Lundy, 1989); 65-75% (Oldow et al., 1989; Wernicke et al., 1982); and as great as 100% (Hamilton and Myers, 1966; Elston, 1986, 1987; Rehrig, 1986). An average amount of extension for the Great Basin as a whole, however, is difficult to determine because of the differences in extensional style between the early or late stage of Cenozoic extensional orogenesis (localized thin-skinned versus widespread brittle extensional structures), and because of complications created by the structural overprint of late Tertiary extension. Leeman and Harry (1993) noted that the amount of extension decreases from south to north, from about 100% at the latitude of Las Vegas, Nevada, to 75% in central Nevada, to probably less than 40% in southern Oregon. In domains of extreme extension (“hyperextended” regions), the amount of extension can be in excess of 250% to 300-400% (Hamilton, 1987; Gans et al., 1989; Oldow et al., 1989; Spencer and Chase, 1989; Wernicke, 1992). In absolute distance, the above estimates translate to extension at the surface ranging from a low of in excess of 10 km (Wernicke, 1990) to 50-100 km (Hamilton and Myers, 1966), and up to 250 km in hyperextended domains (Wernicke, 1992). Bogen and Schweickert (1985) estimated the total east-west extension across the Great Basin at 40° latitude to be  $178 \pm 33$  km.

Isolating the amount of extension in the Great Basin due specifically to either the early or late stage of Cenozoic extensional orogenesis is also problematic (for the same reasons as stated above). However, with the exception of the westernmost and southern Great Basin, the majority of extension probably took place prior to the middle Miocene, during earlier “*pre-basin and range*” extension, and was concentrated in local extensional domains, which include metamorphic core complexes (Zoback et al., 1981; Patino-Douce and Humphreys, 1987;



Seedorff, 1991). Total middle Tertiary extension is estimated to be from 50%-80% to 100% on average, and up to 200%, presumably in domains of hyperextension (Proffett, 1977; Wernicke, 1981; Zoback et al., 1981; Stewart, 1983; Speed et al., 1988). Speed et al. (1988) concluded that most of the extension in the Great Basin took place in the eastern half, estimating 0-20% extension for the western half of the basin, based upon an average elongation of 80%-100% for the eastern half reported by Wernicke (1981) and corroborated by Phillip B. Gans in a 1986 personal communication (see Speed et al., 1988).

Strain rates were extremely high, on the order of  $10^{-14}$ /s and locally higher (Zoback et al., 1981; Eaton, 1982; Gans et al., 1989). Maximum strain rates occurred at about 22-17 Ma and have declined exponentially through time since the Miocene, probably as a result of gravitational potential due to crustal thinning (Gans et al., 1989; Armstrong and Ward, 1991). The direction of strain was generally normal to Laramide or older Cordilleran structural trends (Dickinson, 1981). Data based on preferentially orientated dike swarms and fault slip vectors indicate a strikingly uniform west-southwest–east-northeast least principal stress orientation (the direction of extensional movement) during the early stage of extension (Zoback et al., 1981).

## 2.5.2 Late Stage (Late-Lower Miocene to Present)

The late stage of Cenozoic extensional orogenesis (17-0 Ma) affected a much broader area than did the earlier stage of orogenesis, developing over regions previously unaffected by extension (Eaton, 1982; Stewart, 1983; Wernicke et al., 1987). During this extensional stage, the present-day Great Basin region experienced further widening and modern basin-range rift topography (Fig. 1.2) was attained as the province was broken into blocks, generally 30 km across, where continental sediments collected in the intermontane graben structures (Stewart, 1980; Eaton, 1982; Elston, 1986; Hamilton, 1987; Wernicke et al., 1987). The late stage of extensional orogenesis is characterized by: (1) widespread and increasingly basalt-dominated bimodal rhyolite-basalt lava volcanism (magmatism overall, however, was on the decline); (2) continued regional uplift; and (3) crustal thinning in the form of upper crust brittle deformation by high-angle, deep-penetrating block faulting, having moderate heaves and occurring at relatively slow strain rates (Stewart, 1983, 1978; Zoback et al., 1981; Lipman, 1983; Eaton, 1982, 1984; Mutschler et al., 1987; Wernicke, 1985, 1987; Hamilton, 1988). High-angle structures were superimposed in part upon earlier low-angle extensional structures, strongly distorting, dismembering, and rotating many preexisting geologic features (Stewart, 1983; Wernicke et al., 1987; Hamilton, 1988; Seedorff, 1991). Large-magnitude low-angle thin-skinned faulting, though considered typical of the earlier stage of extensional orogenesis and not the later, was nonetheless not unusual (Proffett, 1977, 1989; Seedorff, 1991). Strike-slip faulting was locally, and possibly regionally, most active during the late Tertiary than at any other time in the Phanerozoic (see section 2.7 below) (Stewart, 1983; Stewart and Crowell, 1992). In the latter phase of this extensional stage, basalt-dominated volcanism became more prevalent, although magmatic activity as a whole declined to the point of magmatic quiescence. Extensional block-faulting continued, but at greatly reduced strain rates (Eaton, 1982; Wernicke et al., 1987).

### 2.5.2.1 Magmatic Activity—Distribution, Age, and Composition

In the early Miocene (~22 Ma) the Laramide magmatic gap, which had been a prominent feature in the central Cordillera since about 80-70 Ma, had closed as calc-alkaline arc activity was

renewed and volcanic fields to the north and south merged (Armstrong and Ward, 1991). Arc volcanism was short lived, however, as the Mendocino triple junction migrated north and the San Andreas transform evolved along the continental margin, progressively ending subduction tectonics and extinguishing arc activity inland (Dickinson, 1981). By the Middle Miocene, the northern and southern volcanic arcs were once again receding, as the southern end of the Cascades arc retreated northward and the northern end of the Mexican arc withdrew southward (Dickinson, 1981). At present, arc volcanism in the region of the central Cordillera is inactive, but continues to the north in the Cascades range of Oregon and Washington states, flanking the Juan de Fuca subduction trench, and to the south in the Trans-Mexico volcanic belt of the Sierra Madre Del Sur in the southern Cordillera of Mexico, stretching along the middle America subduction trench (Stewart, 1978; Dickinson, 1981).

Late Tertiary magmatism in the Great Basin was generally concentrated along the outer regions of the present-day basin, surrounding a core of more felsic-intermediate calc-alkaline volcanic rocks (Smith and Luedke, 1984; Wernicke et al., 1987). The transition to fundamentally basaltic and bimodal volcanism in the Great Basin took place between approximately 22-15 Ma (Mellott and Hart, 1987), beginning in the southeast, near the axis of the province in areas undergoing active extension, then moved northwest (Snyder et al., 1976; Wernicke et al., 1987). Widespread ash-flow volcanism had ceased by about 20 Ma throughout most of the Great Basin (Best and Christiansen, 1991), except in westernmost Nevada, where andesitic volcanism was voluminous (Stewart, 1980), and was followed by a brief lull in magmatic activity between about 20-17 Ma (McKee, 1977; Smith, 1978; Wernicke et al., 1987). By about 15 Ma volcanism had resumed, but with a distinct switch to bimodal basalt-rhyolite compositions, and marked bimodal tendencies after 14 Ma (McKee, 1977; Smith, 1978; Stewart, 1980; Elston, 1986, 1987; Wernicke et al., 1987; Axen et al., 1993). A well-developed bimodal compositional spectrum and “true basalt” (IUGS classification) did not appear, however, until after the latest Miocene, about 8-6 Ma (Best and Christiansen, 1991).

Late Tertiary magmatism in the western Cordillera was most intense during its initial phases, and was most profound in the Great Basin and its immediate environs, but relative to earlier middle Tertiary activity, magmatism as a whole was on the decline (Eaton, 1982, 1984; Mutschler et al., 1987; Armstrong and Ward, 1991; Leeman and Harry, 1993). During the last 10 m.y., the intensity of silicic volcanism progressively decreased (Armstrong et al., 1969), and since about 6-0 Ma, volcanic activity in general has fallen sharply (Seedorff, 1991). Quaternary and present day (1.5-0 Ma) magmatic activity is largely localized along the eastern and western edges of the Great Basin, and in a north-northeast-trending belt into central Nevada (Mutschler et al., 1987; Wernicke et al., 1987; Christiansen and Yeats, 1992). At the eastern edge of the basin, basaltic volcanism has migrated onto the margin of the Colorado Plateau (Christiansen and Yeats, 1992). Along the western margin of the basin, within the zone at the Sierran front, a long-lived volcanic field climaxed in the Pleistocene with voluminous rhyolitic ash flows to form the Long Valley caldera (Stewart, 1980; Christiansen and Yeats, 1992). In Nevada, only scattered volcanism has occurred, mainly as basaltic cinder cones and lava flows with many local sources (Stewart, 1980). The present-day Great Basin is by and large magmatically quiescent (Seedorff, 1991).

### **2.5.2.2 Extensional Activity—Distribution, Age, Character, Magnitude**

Basin-range block faulting began to develop during the earlier stage of localized large-magnitude

thin-skinned extensional activity when extension and uplift rates were at their maximum in the Great Basin (22-17 Ma), and continued as strain rates declined after 17 Ma (Eaton et al., 1978; Elston, 1986). Modern block-faulting first appeared around 22 Ma in the Rio Grande and Basin and Range provinces (Elston, 1986) and probably entered the Great Basin around 20-17 Ma (Eaton et al., 1978). Development of block-faulting in the Great Basin was erratic in space and time, and probably not abrupt (Christiansen and Lipman, 1972; Zoback et al., 1981). Locally, both large-magnitude low-angle thin-skinned faulting and high-angle block-faulting occurred concurrently, and it is uncertain as to what degree the two structural styles represent differences in, or a continuum of, middle through late Cenozoic crustal extension processes (Proffett, 1977, 1989; Zoback et al., 1981; Seedorff, 1991)

Basin-range block-faulting was largely confined to, and best developed in, the Great Basin (Hamilton, 1988). Extensional deformation spread over a much broader region than it had during middle Tertiary time, moving into regions that had not previously been affected by extension, and widening areas that had already undergone extension (Stewart, 1983; Wernicke et al., 1987). Basin-range-style faulting in the Great Basin began between 17-15 Ma with the creation of local basins in which erosional debris collected (Eaton, 1982; Wernicke et al., 1987; Best and Christiansen, 1991; Bohannon and Parsons, 1995). Block-faulting and regional uplift were most active from about 14-12 to 6-4 Ma (Eaton, 1986, 1987; Elston, 1986), but the present-day well-developed basin-range physiography and pronounced north-northeast-south-southwest structural and topographic grain (Fig. 1.2) was not attained before 10 Ma, at the earliest (Stewart, 1978; Zoback et al., 1981). Since about 6-5 Ma, faulting has proceeded at a much slower rate and continues to the present-day (Zoback et al., 1981; Christiansen and Yeats, 1992). Quaternary and present-day activity are largely localized along the eastern and western edges of the Great Basin, in positions corresponding to the Walker Lane tectonic belt of western Nevada and the Colorado Plateau transition zone (Smith, 1978; Mutschler et al., 1987; Wernicke et al., 1987; Gans et al., 1989). On the western edge of the basin, the youngest initiation of extension was westward from Death Valley to the Sierra Nevada front, where a Pliocene erosion surface is now broken by five major ranges (Christiansen and Yeats, 1992). The Great Basin may be expanding eastward and westward at the expense of the Colorado Plateau and the Sierra Nevada (Mutschler et al., 1987; Wernicke et al., 1987) into the thicker and gravitationally unstable crust (Gans et al., 1989).

Relative to the earlier middle Tertiary episode of extension, basin-range extension was much more uniform in its distribution and fault structure. Late Tertiary crustal extension broke the province into gently tilted blocks—horsts, grabens, and other tilted, rotated, and dismembered units, generally 30 km across—bounded by steeply-dipping normal faults (Stewart, 1978; Zoback et al., 1981). Block-faulting probably occurred in the upper 5-15 km of the crust (Eaton, 1980; Zoback et al., 1981; Wernicke, 1985; Hamilton, 1987; Fitton et al., 1988) and took place on a complex hierarchy of faults, including high-angle and listric faults (Zoback et al., 1981). Basin-range “mountain blocks” were created by the vertical movement of adjacent blocks along major high-angle faults on one or both sides of the block, but faulting was not confined only to the sides of mountain blocks, rather it was distributed throughout the mountain areas and in suballuvial rocks of the valleys as well (Stewart, 1983). Major crustal blocks are aggregate structural units, moving more or less in a uniform manner relative to adjacent structural units (Stewart, 1983). Fault blocks may also have developed in groups of blocks. Shawe (1965) observed that, surface faulting, related to seven major earthquakes in the past 60 years, is

distributed along a coherent arcuate linear zone known as the “*Churchill arc*”, located in west-central Nevada (see Shawe's figure 1). The Churchill arc transgresses several mountain ranges, demonstrating that the basin-range fault-block mountains in the Great Basin have probably not grown independently of one another (Shawe, 1965).

Most of the widening of the Great Basin region took place during the later episode of slower basin-range extension (Wernicke et al., 1987; Bohannon and Parsons, 1995), as opposed to crustal extension, the majority of which was achieved during earlier middle Tertiary rapid extension, and affected the whole of the Basin and Range Province (Zoback et al., 1981; Sedorff, 1991). The amount of extension in the Great Basin due to late Tertiary basin-range block-faulting has been difficult to determine because of the effects of earlier attenuation. Stewart (1980) explained that, estimates on the amount of extension necessary to produce basin-range structure are generally of order of 10 to 35 percent of the original width of the region, but varies considerably because of disagreements about the geometry of the high-angle normal faults at depth. If the structure is considered to be composed of relatively simple horsts and grabens, then estimates of the amount of extension suggest about 10- to 20-percent increase in the width of the region, whereas if the structure is considered to be composed of blocks tilted along downward-flattening faults, estimates range from 30 to 50 percent, to as much as 100 percent locally. In absolute ground distance, conservative estimates of extension range from 72 km (13%) to 50-100 km (8-18%) (Hamilton and Myers, 1966; Stewart, 1978).

The rate of strain at which time basin-range deformation developed was generally much lower than during the earlier stage of extensional orogenesis, and has been declining since the Miocene (Eaton, 1982; Armstrong and Ward, 1991). The regional stress field orientation in which basin-range strain initially took place (~17-15 Ma) was the same as that which had prevailed during earlier extension (west-southwest–east-northeast least principal stress orientation) (Zoback et al., 1981). By about 10 Ma, however, a 45° clockwise swing in the orientation of least principal stress to west-westnorthwest–east-eastsetheast occurred, at which point present-day “classic” basin-range block-faulting began and continues to develop (Zoback et al., 1981). The Late Miocene rotation of the regional stress field was most likely in response to the northward migration of the Pacific plate and growth of the San Andreas transform boundary along the western margin of the continent (Atwater, 1970, 1989; Zoback et al., 1981; Eaton, 1982; Ward, 1991).

## 2.6 Strike-Slip and Related Features

Wrench tectonism has been a major element in the development of the western Cordillera of the United States (Stewart and Crowell, 1992), and has probably played a significant role in the evolution of the Great Basin. Regional- and local-scale northwest-trending right-lateral and northeast-trending left-lateral strike-slip faults are common in certain parts of the Great Basin, and have offsets on individual faults as great as 80-100 km (Stewart and Crowell, 1992; also see Stewart, 1983). Dip-slip faulting appears to be the predominant mode of deformation in the Great Basin throughout the middle and late Tertiary stages of Cenozoic extensional orogenesis, and is relatively well mapped and understood. Strike-slip faulting, however, is neither well understood nor sufficiently mapped across the whole of the Great Basin (Stewart and Crowell, 1992).

Precambrian origins have been proposed for a number of regional-scale strike-slip tectonic zones in the western Cordillera (see Fig. 2.3), including the Great Falls tectonic zone (see Hoffman, 1989), the Louis and Clark zone (Marshak and Paulsen, 1996, see figure 3; also see Stewart and Crowell, 1992), the Snake River plain (Christiansen and Yeats, 1992; Poole et al., 1992), the Walker-Texas lineament (Brookfield, 1993; Marshak and Paulsen, 1996, see figure 3), the Mojave-Sonora megashear (Anderson, 1983; Dickinson, 1981; Marshak and Paulsen, 1996, see figure 3, also see Stewart and Crowell, 1992, p. 624), and the Colorado lineament (Warner, 1978). However, evidence for such ancestry is usually circumstantial and conjectural, with the possible exception of the Colorado lineament (Stewart and Crowell, 1992).

Paleozoic strike-slip systems in the western Cordillera are not well known, but those that have been proposed are mostly right-lateral northwest-trending faults that are likely inland effects of the collision of North America with South America-Africa during the Paleozoic Ouachita-Marathon orogeny (see Stewart and Crowell, 1992). In the Rocky Mountains, 200 km of left-lateral Paleozoic offset has been proposed on a fault along the trend of the Snake River plain in Idaho (see Fig. 2.3, however, Mesozoic displacement has also been suggested along the same trend by other workers (Poole et al., 1977; Poole and Sandberg, 1977).

In the Upper Paleozoic and Early Mesozoic, a regional-scale strike-slip system is thought to have been in operation along the western and southwestern margin of North America, which had formed in response to a change in global patterns of continental drift and seafloor spreading that accompanied the breakup of Pangea—the splitting of North America-Europe from South America-Africa, and the opening of the North Atlantic between Africa and North America and the Gulf of Mexico (Caribbean ocean basin) between North and South America (Dickinson, 1981; Suppe, 1985). The transition from Paleozoic sub-island arc compressional orogenesis (Antler and Sonoma orogenies) to sub-continental Andean-style compressional orogenesis (Cordilleran orogeny) is distinguished by the tectonic truncation of the Paleozoic structural and stratigraphic trends of the southwestern Cordillera against the newly developing Mesozoic continental arc (Saleeby and Busby-Spera, 1992; see Fig. 2.6). This second and last major tectonic truncation episode in the history of the Cordilleran region (the first being pre-Cordilleran, occurring between 0.8-0.5 Ga) is known as the “*Early Mesozoic truncation event*” (Hoffman, 1989; Suppe, 1985). This event represents the reorientation of continental margin deformation along a northwest-southeast trend that acutely crosscuts the roughly northeast-southwest Paleozoic orogenic grain, and marks the initiation Cordilleran tectonic activity that was dominated by continental margin volcanic and plutonic activity (Suppe, 1985). Paleozoic orogenic belts that might reasonably have been expected to continue on the western side (the Pacific side) of the Cordilleran orogenic belt are nowhere to be found. They are postulated to have been displaced southward across Mexico along the *Mojave-Sonora megashear* (Silver and Anderson, 1974), a controversial strike-slip system extending between southern California and the Gulf of Mexico, roughly along the U.S.-Mexican border (Dickinson, 1981, see figures 4 and 5; also see Saleeby and Busby-Spera, 1992; Suppe, 1985). Truncation, and presumably movement on the megashear, appears to have begun in Pennsylvanian time, when a northwest-trending left-lateral strike-slip zone formed across the Antler orogenic belt and adjacent miogeocline along east-central and southern California. Rocks of the Antler belt were displaced southward toward the Mojave region during Pennsylvanian-Permian time along a transcurrent zone that may have extended through the Mojave region and into Sonora, Mexico, where other miogeoclinal strata are suspected to have been displaced southward (see Saleeby and Busby-

Spera, 1992, figures 1 and 2). Movement of the megashear continued throughout mid-Early and mid-Late Jurassic time, and by the late Jurassic, truncation of the Paleozoic tectonic grain was well established (Dickinson, 1981; Suppe, 1985). Up to 800 km of left-lateral movement has been postulated along the Mojave-Sonora megashear (Burchfiel et al., 1992).

A few Mesozoic or early Cenozoic strike-slip systems have been recognized inland of the Mesozoic western margin of North American, the most significant in the Great Basin being the Wells fault of Nevada, along which 65 to 80 km of right-lateral offset has been proposed, and the Tintic Prince, Inez, and Leamington right-lateral faults in western Utah (see Stewart and Crowell, 1992). North of the Great Basin, the Olympic-Wallowa lineament (see Fig. 2.3), manifest as a zone of discontinuous northwest-trending faults and folds in the overlying late Cenozoic cover (i.e.—Columbia River Plateau basalts), may be early Mesozoic to early Cenozoic in age, although it might have genetic connections with a Proterozoic or Mesozoic cratonal margin (Mann and Meyer, 1993; also see Stewart and Crowell, 1992).

Most of the recognized strike-slip activity in the Great Basin appears to be late Cenozoic in age (see Stewart and Crowell, 1992). After about 20 Ma, the central Cordilleran region became progressively influenced by a right-lateral stress regime as the plate tectonic setting changed from a convergent margin to a complex margin characterized by convergence in its northern part and transform faulting along the San Andreas system in its southern part (Atwater, 1970, 1989; also see Stewart and Crowell, 1992). By 12.5-10 Ma, the old plate margin fell apart with the onset of major strike-slip faulting and the opening of the Basin and Range (Ward, 1991). Five late Cenozoic strike-slip systems have been recognized in the Great Basin (Stewart and Crowell, 1992, see references therein if not otherwise noted):

1. *Strike- or oblique-slip reactivation*—Inactive preexisting faults (or systems) that were reactivated with a strike-slip component in response to changes in the orientation of local or regional stress fields.
2. *Oblique-slip components on dip-slip faults*—Oblique-slip faulting related to variations in strike of extensional faults, producing normal movement on segments perpendicular to a regional extension directions and oblique-slip on segments oblique to extension direction.
3. *Strike-slip accommodation-zone systems*—Strike-slip faulting orientated parallel to extension direction that occurred along a boundary between areas that differ in the amount, rate, or sense of normal faulting. Such systems represent “zones of accommodation” between regions differing in kinematic behavior, and should typically be expected to form along transverse zones separating regions with different tilt directions of basin-range blocks.
4. *Walker Lane belt*—A northwest-trending structural zone 700 km long and from 100 to 300 km wide containing both right-lateral and left-lateral faults. Also known as the Walker Lane shear zone, this regional-scale strike-slip system is a complex zone composed of structural sections (large structural blocks as well as relatively narrow zones) that have undergone either right-lateral shear, left-lateral shear, or remained relatively undeformed by shear. The Walker Lane separates the Sierra Nevada region to the west from areas of typical basin-range topography on the east, and is far and away the largest and most significant known strike-slip feature in the Great Basin (see Fig. 2.3). The Walker Lane may have origins dating back to the Mesozoic (Stewart, 1988), perhaps related to the Mojave-Sonora megashear (see Saleeby and Busby-Spera, 1992, figures 1 and 2), or to the Precambrian, perhaps related to late Proterozoic rifting (Blakely and Jachens, 1991, also see section 2.4). It is currently active.
5. *Regional conjugate system*—A widespread system of conjugate north- to northwest-trending right-lateral faults and northeast-trending left-lateral faults. Most are in the western, southern, and eastern regions of the Great Basin, and, at least in southwestern Utah, the strike-slip faults are great in number, but generally short in length. This system of strike-slip faults may be related to the same stress field that has produced extensional basin-range structures, suggesting that normal faulting and strike-slip faulting are intermixed and



contemporaneous. Shawe (1965) proposed that this broad conjugate strike-slip system provides the fundamental structural framework of the Great Basin, and that these strike-slip structures in general probably lie within the upper mantle, penetrating clear through the crust, although some might be blind. When movement along these structures took place, near-surface rocks (the upper part of the crust) responded by faulting into horsts and grabens, en echelon to the underlying or nearby shears. The orientation of the crustal blocks were controlled by the established “grain” of northerly oriented folds and foliations, developed at deeper structural level during earlier periods of deformation (Shawe, 1965). Carey (1955, 1958, 1976, 1988) and Livaccari (1979) have made similar proposals from the perspective of regional-scale tectonism. A review of structural patterns and basin formation in relation to strike-slip faults by Christie-Blick and Biddle (1985) details how such a mechanism could produce basin-range structure as observed in the Great Basin. Putnam and Henriques (1991) have interpreted structural relationships observed in the Pinon Range in terms of strike-slip tectonism, and have extended this interpretation to the regional-scale suggesting the presence of northwest-oriented wrench-fault system in northeastern Nevada.

In addition to these five systems, the circumference of the Great Basin is bound by what appear to be late Cenozoic strike-slip zones that act to accommodate differential extension in a manner analogous to oceanic transform faults (Christiansen and Yeats, 1992). The faults composing these zones vary in trend and history, and their positioning may have been guided by older preexisting structures (Christiansen and Yeats, 1992). The northern boundary is wide, diffuse, and not well defined, and is mainly composed of structures related to the eastern Snake River plain volcanic trend and Brothers fault zone (Fitton et al., 1991; Christiansen and Yeats, 1992). Evidence for strike-slip movement on the fault, inferred to be under Miocene Snake River volcanic cover, can be demonstrated by offset of the Sevier thrust system, and indicates left- and right-lateral movements (Poole et al., 1977; Poole and Sandberg, 1977; Poole et al., 1992). The western strike-slip boundary of the Great Basin can be considered to be Walker Lane shear zone (Stewart and Crowell, 1992). The southern Great Basin is bound by left-lateral features that include the Lake Mead fault zone in Nevada and the Garlock fault in California, where the trace of the Garlock fault may in part follow an old rifted margin of Precambrian continental crust (Kistler and Peterman, 1978). The eastern margin of the Great Basin is not well delineated by strike-slip features, although a conjugate system composed of many short strike-slip faults does occur in southwestern Utah (Stewart and Crowell, 1992).

## 2.7 Characteristics of the Present-Day Crust

The crust in the Great Basin is a complex collage of sedimentary and tectonomagmatic provinces that were tectonically assembled, transformed, and molded together into a single geologic and physiologic entity by a nearly continuous cycle of orogenesis dating from the Archean through the Holocene. Virtually every type of sedimentary, igneous, and metamorphic rock is represented in the lithologic assemblages of crust in the Great Basin and its environs (King, 1969). The crust in Nevada and the Great Basin is relatively thin as compared to surrounding regions, and is characterized by (1) low regional Bouguer gravity anomaly, (2) a roughly even distribution of shallow- and deep-source magnetic anomalies, (3) high regional heat flow, (4) high regional electrical conductivity, (5) low seismic velocities in the crust and upper mantle, and (6) ongoing seismic activity (Blackwell, 1978; Eaton et al., 1978; Lachenbruch and Sass, 1978; Stewart, 1978; Eaton, 1982; Allmendinger et al., 1987; Dewey, 1988; Speed et al., 1988; Wernicke et al., 1988; Morgan and Gosnold, 1989; Blakely and Jachens, 1991; Christiansen and Yeats, 1992; Wernicke, 1992; also see Harry et al., 1993) ([Fig. 2.12](#)).



### 2.7.1 Lithotectonic Framework and Tectonostratigraphy

The Great Basin straddles the edge of the Precambrian craton, and as such, can be subdivided into two principal crustal provinces: (1) an eastern region of latest Proterozoic to Late Devonian and younger sequences that are underlain by older supracrustal rocks and North American Precambrian crystalline craton; and (2) a western Paleozoic and Mesozoic accretionary belt (Burchfiel et al., 1992; Poole et al., 1992) (Figs. 2.4 and 2.10).

In the eastern region of the Great Basin, the Precambrian basement consists of two main crustal blocks: (1) the Archean (>2.7 Ga) Wyoming province (a “core” province), underlying the northeasternmost part of the basin, and (2) juvenile 2.3-2.0 to 1.8-1.7 Ga accreted terranes of the Yavapai-Mazatzal orogen, underlying the most of the eastern, southeastern, and southern areas of the basin (Bennett and DePaolo, 1987; Hoffman, 1989) (Fig. 2.11). Precambrian basement in the Great Basin extends as far west as central Nevada. Supracrustal sedimentary and volcanic rocks ranging in age from about 1.4 to 0.9-0.8 Ga, presumably related in part to Middle-Late Proterozoic rifting that formed the western margin of the North American craton, occur locally, and unconformably overly the crystalline basement rocks (Poole et al., 1992, see figure 2). Latest Proterozoic to Late Devonian and younger miogeoclinal successions unconformably onlap both the supracrustal and basement rocks. In the Sevier hinterland and foreland fold-thrust belt of east-central Nevada and west-central Utah, mountain ranges are underlain mostly by an upper Precambrian to Triassic sequence of sandstones, shales, and carbonates, which include about 20 distinctive and regionally extensive formations with an aggregate thickness in excess of 13 km (Stewart and Poole, 1974; also see Poole et al., 1992, figure 2).

The western accretionary belt (Fig. 2.4) is composed of material that was successively obducted on and accreted to the Precambrian craton margin from the Late Devonian through Middle-Late Jurassic time, mainly during the Antler, Sonoma, and Nevadan orogenies (Fig. 2.5). This material includes eugeoclinal-miogeoclinal sequences flanking the continental margin, oceanic island arc terranes and related forearc sequences, scraps of oceanic basins with ophiolitic basement, fragments of continental margins (some with Precambrian basement), and other adjoining oceanic and continental environments (Silberling, 1991; Burchfiel et al., 1992; Jones et al., 1982). The terranes are mainly of oceanic affinity and most have somewhat uncertain origins (Burchfiel et al., 1992). A few western accreted terranes have been identified as “native” and can be tied directly to North America, while a small number of others appear to be “exotic” and have travelled far from other parts of the Pacific Basin (Burchfiel et al., 1992). These terranes were rafted into place, welded to the laterally expanding continental margin, modified during younger accretionary events, and reworked in nonaccretionary plate-boundary systems (Burchfiel et al., 1992).

The Foothills suture in the Sierra Nevada is a major accretionary structure that separates terranes that attached to the passive margin of North America before Middle-Late Triassic time (i.e.—Antler and Sonoma accretionary activity) from those that arrived during the later active margin phase (i.e.—Nevadan and later accretions) (see Speed, 1983; Speed et al., 1988). East of the foothills suture in the Great Basin, three major accretionary terranes are exposed (Speed, 1983):

1. *Roberts Mountains allochthon*—Accretionary prism of the Antler magmatic arc (formed as it converged on

North America); consists of a tectonic assemblage of pelagic, hemipelagic, turbiditic, and volcanic rocks of early Paleozoic age and probable oceanic derivation; laps over lower Paleozoic strata of the North American continental shelf at least 130 km from the sialic edge and was almost certainly emplaced from the west early in Mississippian time.

2. *Golconda allochthon*—Accretionary prism of the Sonomia magmatic arc (formed as it converged on North America); possesses similar rocks and architecture to the Roberts Mountains allochthon, except that the rocks are Mississippian to Permian age; emplaced in Early Triassic time at least 100 km inboard of the sialic edge and above the earlier Roberts Mountains allochthon and the late Paleozoic and Early Triassic cover to the Roberts Mountain.
3. *Sonomia*—Sonoma magmatic arc; believed to be a lithospheric fragment of Paleozoic arc-related lithotectonic units, surmounted by a Permian magmatic arc; collided with the edge of sialic North America early in the Triassic; the central regions of Sonomia are deeply buried below thick Triassic flysch and continental arc volcanics that succeeded Sonomia.

A cryptic fourth terrane (Antleria) has been postulated, but is nowhere exposed (Dickinson, 1981; Speed, 1983).

In the western Great Basin, between the Sierra Nevada and Nevada-Utah border, rocks at the surface can be assigned seven major lithotectonic units (Fig. 2.13), two of which are comprised by the Roberts Mountains and Golconda allochthons, and Sonomia (Speed et al., 1988):

1. *Precambrian crust plus parautochthonous cover*—Cover may be as young as Triassic in the eastern Great Basin; this unit has probably maintained near-coherency through Phanerozoic time although probably deformed by major extension in late Precambrian, contraction in Mesozoic, and extension in Cenozoic time.
2. *Displaced Paleozoic oceanic terranes*—Composed of the Roberts Mountains and Golconda allochthons; overlies the western ~150 km of Precambrian sialic North America; Early Triassic and older attachment.
3. *Displaced Paleozoic terranes*—Sonomia; probably of arc and oceanic origin; probable Early Triassic attachment to North America; overlain and intruded by Mesozoic arc rocks.
4. *Parautochthonous Mesozoic cover to and intrusions in displaced Paleozoic terranes*—Triassic and Jurassic strata of mainly basinal but locally shelfal affiliation; Mesozoic sedimentary and igneous rocks that were deposited or intruded near their present sites; magmatic rocks, including the Sierra Nevada batholith, of probably arc affinity and latest Triassic through Late Cretaceous ages; everywhere allochthonous with respect to North America on the Fencemaker and Luning thrusts.
5. *Mainly autochthonous Mesozoic cover to and intrusions in Precambrian sial, sial cover, and older displaced terranes*—Mainly autochthonous Mesozoic rocks that probably or certainly formed above or in the Precambrian crust or its parautochthonous cover; chiefly contains shelfal strata and rhyolite of Triassic ages that were deposited on the Golconda allochthon.
6. *Other displaced terranes*—Consists of displaced and suture-related terranes of Mesozoic melange or of arc affiliation; Late Triassic or younger attachment.
7. *Quaternary to upper Cretaceous cover*—Cover to all other units; consists of sedimentary and volcanic rocks that are as old as Late Cretaceous in California and Oregon, and Tertiary farther east.

The terranes of unit 6 are separated from those of units 1-5 by the Sierra Nevadan Foothills suture. The Sonoma magmatic arc terrane (lithotectonic unit 3) has recently been further subdivided by Silberling (1991) into six or more subterrane based on various temporal, compositional, depositional, deformational, and stratigraphic relationships (see Silberling, 1991, figure 1).

## 2.7.2 Crustal Thickness

The present-day thickness of the lithosphere (crust plus upper mantle) is at least 65 km (probably

closer to 80 to 100 km thick), as compared to 100-110 km thick beneath the Sierra Nevada and Colorado Plateau, and approximately 80 km thick beneath the Colorado Plateau margin transition zone (Thompson and Zoback, 1979; Eaton, 1980; Smith et al., 1989; Hendricks and Plescia, 1991; also see Leeman and Harry, 1993). At 40 Ma, prior to extension, the lithosphere may have been considerably thicker, possibly as thick as 115 to 175 km (assuming a uniform vertical strain distribution of a net 75% extension) (Leeman and Harry, 1993). The present-day crustal thickness in the Great Basin ranges from 25 to 35 km in thickness (Fig. 2.12), averaging 30 km, as compared to the 40-50 km thick crust beneath the adjacent Colorado Plateau and Sierra Nevada, and especially in comparison to its thickness in the Cretaceous, when the crust may have exceeded 60 km as a result of crustal shortening and thickening during Sevier and Laramide compressional orogenies (Allenby and Schnetzler, 1983; Allmendinger et al., 1987; Dewey, 1988; Benz et al., 1990; Catchings and Mooney, 1991).

The crust is thickest in the center of the Great Basin, where the reflection Moho is encountered at approximately 34 km (Allenby and Schnetzler, 1983; Allmendinger et al., 1987). Crustal thickness generally decreases away from the central Great Basin, thinning eastward to approximately 25 km at the Wasatch front in Utah (Allenby and Schnetzler, 1983), and westward to < 30 km at the eastern front of the Sierra Nevada (Allenby and Schnetzler, 1983; Allmendinger et al., 1987). The largest area of thin crust (~20-22 km) is in the northwestern Great Basin, in the region of the “Battle Mountain heat high anomaly” (see section 2.7.5), near the Carson Sink (Allenby and Schnetzler, 1983). Beyond the western and eastern margins of the Great Basin, crustal thickness increases rapidly to about 50 km under the Sierra Nevada and > 40 km under the Wasatch range (Allenby and Schnetzler, 1983; Allmendinger et al., 1987). Most recent data, however, indicates that the thin crust of the southern Great Basin in the region of the Sierra Nevada eastern front may actually extend under the eastern High Sierra as well, where it is estimated to be 30-40 km thick (Wernicke et al., 1996). North and northeast of the Great Basin the crust thickens to >40 km towards the Idaho Batholith. In the northwestern United States, an axis of crustal thinness (<30 or 25 km) extends roughly north from the Carson Sink area to central Washington State (Allenby and Schnetzler, 1983). The axis of crustal thinness also trends southeast from the Carson Sink area, following along the Walker Lane shear zone where the crust is <30 km, and extends into southernmost Nevada (just northwest of Las Vegas) where the crust may approach only ~20-22 km thick (Allenby and Schnetzler, 1983). The ~20-22 km thick area is relatively small in geographic extent and occurs in the “amagmatic zone” (see McKee, 1971; Blakely and Jachens, 1991).

### 2.7.3 Gravity Anomaly and Crustal Structure

The Great Basin is situated in a regional gravity low (Eaton et al., 1978) (Fig. 2.12). Regional Bouguer gravity at wavelengths greater than 1000 km indicate that the dominant, first-order feature in the Great Basin and adjacent regions to the east, is an enormous anomalous low (less than -200 mGals), and reflect sources within the pre-Tertiary basement (Kane and Godson, 1989, see plate in back pocket; Blakely and Jachens, 1991).

At residual Bouguer gravity wavelengths of less than 250 km, the Great Basin is characterized by predominantly northwest trending high-low-alternating anomalies, which extend roughly the length of the State of Nevada, and are approximately 100 km wide with an approximate amplitude of 200 km (Kane and Godson, 1989, see plate in back pocket). A series of four,

possibly four and a half or five, high-low anomaly pairs are visible as standing-wave-sets that “roll” across California, where they are very well defined, through Nevada, where they become increasingly less defined as the anomalies enter the Great Basin, and into Utah, where the anomalies break up and end abruptly against the Wasatch Range (eastern margin of the Great Basin). The progressive degradation in the definition of these anomalies across the Great Basin is probably due to late Lower Miocene basin-range extension, characterized by block-faulting, and may indicate that the anomalies were established at least before the onset of regional-scale block-faulting (~10 Ma). On the scale of Nevada, in the center of the Great Basin, one and a half cycles of the 250 km wavelength anomaly has been referred to as an “axis of bilateral symmetry” or “the butterfly”, reflecting higher topography and thicker crust in this region (Eaton et al., 1978).

Simple Bouguer gravity features in Nevada are bounded by an orthogonal system of mostly northeast- and northwest-trending lines, suggesting that major crustal blocks of differing density may be bounded by northeasterly and northwesterly structural zones. Some of these hypothetical structural zones are also visible in total field magnetic anomaly data in Nevada (Shawe, 1991, see figures 2 and 3). The major negative anomalies of the 250-km-filtered and 1000-km-filtered Bouguer gravity data suggest that these anomalies represent low density material at depths extending from the crust-mantle boundary to >125 km (Mutschler et al., 1992; Parsons et al., 1994).

#### **2.7.4 Geomagnetic Anomaly and Crustal-Scale Structures**

The magnetic character of the Great Basin is variable. On a continent-wide scale, the magnetic anomaly is relatively fine-grained to flat. There are no conspicuous anomalies in comparison to areas north (Cascades Range, Oregon Plateaus, Snake River Plain), west (Sierra Nevada), southeast (Colorado Plateau), or east (Laramide uplifts), with the exception of the Walker Lane anomaly(-ies), which range from about 400 to -100 nT (Kane and Godson, 1989, see plate in back pocket). On a regional-scale (Great Basin), the northern Nevada rift zone and the Walker Lane are the most prominent features.

The northern Nevada rift is visible as long, narrow, and well defined magnetic anomaly “splays” trending north-northwest, the longest of which (the Northern Nevada rift proper) extends at least 280 km through the north-central part of the State (see [Fig. 2.3](#)). The rift is characterized by a linear swarm of dikes and associated lavas (basalt and basaltic andesite) of 17 to 14 Ma age, by a fault-bounded trough, and by a northwest-southeast topographic grain (most visible in shaded relief) which cuts obliquely across the north-northeast–south-southwest basin-range structural grain (see [Fig. 1.2](#)) (Christiansen and McKee, 1978; Zoback and Thompson, 1978; and Zoback et al., 1994; also see Christiansen and Yeats, 1992). The anomaly source-depth of northern Nevada rift zone appears to be both shallow and deep, possibly extending as deep as 15 km (Blakely and Jachens, 1991; also see Christiansen and Yeats, 1992). Stewart et al. (1975) suggested that this feature might represent the southern extension of the Brothers fault zone (see [Fig. 2.3](#)), which is a 240 km long zone of short en echelon shears younger than 6 Ma (Stewart et al., 1975; Christiansen and Yeats, 1992). Together, they form the Oregon-Nevada lineament (or the Orvada rift), which has been interpreted to be the surface expression of a deep-seated fracture zone that may have had a complex history of strike-slip and transcurrent movement (Stewart et al., 1975; Smith, 1978; Livaccari, 1979). The northern Nevada rift, and the other

mega-scale linear features in the western Cordillera (see Fig. 2.3), may be the surface manifestations of deep crustal or mantle-rooted zones of weakness, and have been inferred by Carey (1976, 1988), Shawe (1965), and Livaccari (1979) to be shear-related features.

The Walker Lane is marked by arcuate, northwesterly-trending anomalies. The width of the anomaly pattern as a whole is considerably wider than that of the belt, and extends in some places over 150 km north-northeast of the Walker Lane into topography with north to northeast trends more typical of the Basin and Range province (Blakely and Jachens, 1991).

### 2.7.5 Heat Flow and Crustal Fluid Circulation

The Great Basin has anomalous heat flow (Fig. 2.12). The “reduced” heat flow values for the Great Basin (those for which radiogenic heat production in the crust has been accounted for) are greater than those for stable regions by as much as 50% to 100%, and in warmer regions of the basin, by as much as 300% (Eaton, 1982). An average for the whole of Basin and Range Province is given by Morgan and Gosnold (1989) as 2.7 HFU and is likely higher in the Great Basin when taken alone. Mean heat flow values in the Sierra Nevada (1.3 HFU) and the Colorado Plateau (1.6 HFU) provinces, which are marginal to the Great Basin (see Fig. 2.2), are more typical of stable continental lithosphere, indicating an unusually high geothermal gradient beneath the basin (Morgan and Sass, 1984; Morgan and Gosnold, 1989). These heat flow observations, together with the widespread and voluminous occurrence of Mesozoic and Cenozoic igneous rocks, suggests that elevated temperatures have persisted within the crust for at least 230 m.y. (Eaton, 1982; Elston, 1984). These conditions probably facilitated fluid circulation at many crustal levels in the Great Basin region, creating an environment favorable for wide-spread mineralization.

Much of the present-day anomalous heat is believed to have been transferred into the crust by convection from below (Eaton, 1982). Heat flow appears to be highest in north-central and west-central Nevada, in a region known as the “*Battle Mountain heat flow high*”, coincident with an area of thin ( $\leq 20$  km) crust. In northern regions, heat flow averages about 2.8 HFU as opposed to an average of approximately  $< 1.7$  HFU for the southeastern part of the State (Hittelman et al., 1990; David D. Blackwell, 1994, personal communication). The temperature of geothermal well and spring waters is also higher in the northern regions, averaging  $\geq 60^\circ\text{C}$ , as compared to an average of  $\leq 30^\circ\text{C}$  in the southeastern part of the State (Trexler et al., 1983).

### 2.7.6 Electrical Conductivity and Crustal Permeability

Electrical conductivity is anomalously high in the Basin and Range Province in contrast to regions east and west. The extent of a probable regional conductivity high is nearly centered on the Great Basin (see Keller, 1989, figure 35), and is coextensive with the Great Basin regional gravity low. Anomalously high values of conductivity are observed at depths as shallow as 10 km in the crust, and profound lateral changes in the electrical properties of the upper mantle (very strong anomalies) are present at depths as much as 350 km—the roots of the Rocky Mountains and the Wasatch Front in particular appear to be reflected by important electrical structures extending to more than a depth of 300 km (Keller, 1989). These conductive zones may be caused either by partial melting of crustal rocks in regions of high heat flow, or by the presence of significant amounts of fluid in fractured rock (Keller, 1989). Partial melting is

probable for the deep-source anomalies whereas deeply circulating fluid is likely for the shallow conductors in the crust. In the upper crust, permeability is relatively high and fluids are normally at or near hydrostatic pressure (McCaig, 1988). Calculations indicate that with permeabilities of  $10^{-17} \text{ m}^2$  or greater, fluids can freely circulate under a normal geothermal gradient, suggesting that fluid movement through upper crustal fault zones is common (Nesbitt and Muehlenbachs, 1989). Permeabilities on the order of  $10^{-16} \text{ m}^2$  have been observed to depths of 10 km in the Kola deep drill hole in the Soviet Union (Kozlovsky, 1987). Permeabilities in excess of  $10^{-17} \text{ m}^2$  are typical in the upper crust, especially in areas that have undergone even minor amounts of strain, such as the Great Basin (Brace, 1984). An increase in strain from 1% to 6% is capable of producing an increase in permeability of five orders of magnitude or more (Spiers and Peach, 1989), suggesting deep circulating fluids in the crust of the Great Basin are especially common place. This was probably critical to the metallogenic development of Great Basin.

### 2.7.7 Seismicity and Seismic Velocities

Seismic activity is ongoing in the Great Basin. It is generally restricted to the eastern and western margins of the basin, and to an arcuate linear zone known as the “*Churchill arc*” located in west-central Nevada (Shawe, 1965, see figure 1; Smith, 1978; Christiansen and Yeats, 1992). Seismic data compiled by Hittelman et al. (1990), detailing earthquake activity over the past century in the southwestern United States, indicate that the greatest amount of activity occurs along the southwestern border of the State, which corresponds to the Walker Lane shear zone. Although greatly concentrated, this activity is of relatively low magnitude (typically  $\leq 3.5$ -3.0 Richter magnitude) and shallow depth ( $\leq 8$  km). The higher magnitude ( $\geq 4.0$  Richter magnitude) and deeper ( $\geq 20$  km) earthquakes occur in the north-central and southeasternmost part of Nevada where activity is less frequent and not as concentrated (or data are sparse).

As a whole, the crust and upper mantle in the Great Basin are characterized by relatively low average seismic velocities as compared to the eastern and mid-continental U.S., the northwestern U.S., and the adjacent Sierra Nevada to the west (Beghoul and Barazangi, 1989; Braile et al., 1989, see figures 4 and 5; Iyer and Hitchcock, 1989; Benz et al., 1990; Catchings and Mooney, 1991; Hearn et al., 1991). Seismic velocities show strong dependencies on temperature, lithostatic pressure, and pore pressure (Christensen and Wepfer, 1989; Morgan and Gosnold, 1989). Velocities increase with increasing lithostatic pressure and decrease with increasing temperature, pore pressure, and porosity. The greatest increases occur over the first 100 MPa and are attributed to the closure of microcracks (Christensen, 1989; Christensen and Wepfer, 1989). Upper crustal seismic velocities are often lower than those predicted because the upper crust is penetrated by regional-scale fractures. Data from the Soviet deep Kola hole suggest that, at least locally, fractures and fluids may be pervasive throughout much of the upper crust, indicating that velocities through such regions will tend to be lower than theoretical velocities (Fountain and Christensen, 1989). As such, the low seismic velocities in the crust of the Great Basin (for example,  $\sim 7.5$  km/sec P-wave; Smith et al., 1989) may be due to pervasive fluid-filled fracture or shear systems at depth (see Catchings, 1992), which most likely are products of crustal extension.



## Chapter 3. Characteristics and Distribution of Sedimentary and Volcanic Rock-Hosted Deposits

### 3.1 Introduction

Nevada is known as the “Silver State”, but is a major contributor to world gold production. Nevada has a long and varied history of gold mining. Much of the early gold production (pre-1965) was related to volcanic rock-hosted “epithermal”, high-grade silver-gold vein deposits. Since 1965, sedimentary rock-hosted “Carlin-type”, bulk-mined, lower-grade disseminated deposits have become the principal gold producers. Nevada has a total historic gold production (1849-1996) of approximately 95.4 million Troy ounces (derived from Elevatorski, 1981, and Meeuwig, 1995, 1997). In 1995, the United States produced 10,170,000 troy ounces of gold, second only to South Africa, which produced 16,800,000 ounces (Anonymous, 1997). Nevada produced 6.8 million troy ounces of gold worth \$2.6 billion in 1995, which amounted to 65% of all gold produced in the United States and about 10% of all gold produced in the world (Meeuwig, 1996). Just over 56% of this gold came from a small number of sedimentary rock-hosted open-pit mines that occur along the well known Carlin mineral trend (see [Fig. 1.3](#)). Total published gold resources for Nevada, including mineable reserves and perhaps sub-economic deposits, totalled 144,000,000 ounces at the end of 1995 (Meeuwig, 1996).

The Great Basin is a Tertiary-age, sedimentary rock-hosted plus volcanic rock-hosted, precious-metal deposit-type metallogenic province (Wilkins, 1984). Precious metals are recovered from a wide variety of deposit-types that occur in nearly every rock type of any age (Koschmann and Bergendahl, 1968; Thorman and Christensen, 1991; Ludington et al., 1993). The greatest amount of gold and silver in Nevada is recovered as primary-products from sedimentary rock-hosted disseminated, volcanic rock-hosted disseminated and vein, and a number of other epithermal vein and breccia deposit-types. By-product gold and silver are principally recovered from porphyry-related, skarn- and mantos-related, and a few volcanogenic massive sulfide deposit types (Wilkins, 1984; Thorman and Christensen, 1991; Ludington et al., 1993). The age of mineralization ranges from about middle Mesozoic to late Tertiary, with the bulk of the primary- or co-product gold-silver mineralization having occurred in the Tertiary (Wilkins, 1984; Cox et al., 1991; Hutchinson and Albers, 1992; Ludington et al., 1993). The abundance of precious metal occurrences in the Great Basin is attributed to its complex pre-Tertiary tectonic history and unique Tertiary tectonomagmatic setting, both of which produced a variety of favorable sedimentary and volcanic host lithologies, a high degree of structural permeability, and widespread hydrothermal activity (Shawe and Stewart, 1976; Eaton, 1984; Barton, 1990; Berger and Bonham, 1990; Seedorff, 1991; Hutchinson and Albers, 1992).

This chapter presents a summary of the sedimentary “Carlin-type” and volcanic “epithermal” rock-hosted deposits, with emphasis placed on their spatial distribution. The characteristics and distribution of sedimentary and volcanic rock-hosted occurrences are given in [sections 3.2](#) and [3.3](#), respectively. The regional-scale distribution of mineral occurrences with respect to mineral trends and crustal terranes is reviewed in [sections 3.4](#) and [3.5](#), respectively. A number of quantitative studies dealing with regional-scale distribution of mineral occurrences in relation



to mineral trends and crustal terranes are summarized in [section 3.6](#).

Comprehensive reviews on mineral deposits and metallogenesis in the Great Basin can be found in Berger and Bethke (1985, and papers therein), Berger and Bonham (1990), Berger and Eimon (1982), Berger and Henley (1989), Cox et al. (1991), Cunningham (1988), Eaton (1984), Heald et al. (1987), Hedenquist et al. (1996), Hutchinson and Albers (1992), Ludington et al. (1993), Percival et al. (1988), Raines et al. (1991, and papers therein), Schafer et al. (1988, and papers therein), Seedorff (1991), Singer (1996), Tooker (1985, and papers therein), Vikre et al. (1997, and papers therein), and Wilkins (1984).

## 3.2 Sedimentary Rock-Hosted Gold Deposits

### 3.2.1 Characteristics

The sedimentary rock-hosted deposits are variable in character and not well understood, but can generally be defined as sub-microscopic or microscopic gold, generally much less than 1 micron in size, that occurs within the crystal structure of pyrite, which is disseminated in variably silicified, argillized, and decalcified thin-bedded, flaggy, mixed carbonate-siliciclastic rocks of Paleozoic age (Cox and Singer, 1986; Peters et al., 1996; Romberger, 1986; Tooker, 1985). Most deposits contain both unoxidized (primary) and oxidized ores. Primary ores are subdivided into five gradational sub-types and constitute the bulk of ore at most of the deposits (e.g.—Carlin, Jerriitt Canyon, Mercur, Getchell). Oxidized ores are economically more desirable than unoxidized ores and are mined at most deposits, but of principal importance at only a few deposits (e.g.—Alligator Ridge) (for more information on ore types, see Radtke et al., 1980; Bagby and Berger, 1985; Romberger, 1986; Percival et al., 1988). The salient geologic features of sedimentary rock-hosted deposits are summarized as a synoptic model presented in [Table 3.1](#).

### 3.2.2 Distribution

The sedimentary rock-hosted deposits are predominantly located in the northeastern quadrant of Nevada, and are distributed in a roughly equant circular or ovoid pattern ([Fig. 3.1](#)). They are conspicuously absent from the Walker Lane belt (see [Figs. 1.3](#) and [2.3](#)), which is host to many volcanic rock-hosted deposits, and from the southern, western, and easternmost regions of Nevada as well. As a deposit-type group, the sedimentary rock-hosted deposits form a distribution “core” that lies inward of a semicircular “crescent-shaped” distribution of various volcanic rock-hosted deposits, referred to by Ludington et al. (1993) as the “epithermal crescent” (compare distribution patterns in [Fig. 3.1](#)). As a group, the sedimentary rock-hosted deposits are generally considered to be older than the volcanic rock-hosted ([Fig. 3.2](#); Ludington et al., 1993).

Most of the sedimentary rock-hosted deposits in Nevada occur in six groups or trends: the Carlin trend, the Battle Mountain–Eureka (Cortez) trend, the Getchell trend, the Humboldt trend, the Independence group, and the Alligator group ([Fig. 3.3](#)) (Roberts, 1966; Shawe and Stewart, 1976; Percival et al., 1988; Thorman and Christensen, 1991). A small number of other deposits occur as isolated mineral concentrations. Well developed trends are geologically characterized by alignments of igneous rocks, geophysical anomalies (or boundaries), and various structural features (Bagby and Berger, 1985; Percival et al., 1988; Shawe, 1991). The two most prominent

trends are the Carlin and the Battle Mountain–Eureka (Cortez), which are defined by the greatest number and the largest deposits. These trends are oriented north-northwest, oblique to the northerly to north-northeasterly grain of Paleozoic, Mesozoic and Cenozoic structures (Fig. 3.3).

The Carlin trend is 75 km long, and marked by sedimentary rock-hosted deposits (the “Carlin” type deposits) (Fig. 3.3). It extends from the Dee deposit in the northwest to the Emigrant Springs, Gnome, and Trout Creek deposits in the southeast (Thorman and Christensen, 1991). The trend is geologically characterized by an alignment of (1) structural windows (or “fenster”) eroded through overlying allochthonous units, (2) intrusive rocks (although they are relatively sparse), (3) positive aeromagnetic anomalies, and (3) broad antiforms or synforms adjacent to some deposits (Bagby and Berger, 1985; Madrid and Bagby, 1986; Shawe, 1991).

The Battle Mountain–Eureka belt (Cortez trend) is 235 km long, and marked by gold skarn deposits associated with hypabyssal stocks, vein and stockwork deposits, and disseminated types (Fig. 3.3; Shawe, 1991). The trend was once identified by the alignment of the Gold Acres, Cortez, Horse Canyon, and Tonkin Springs deposits (Bagby and Berger, 1985), but now extends northwest to include the Lone Tree and Stonehouse deposits, and to the southeast to include the Easy Junior-Night Hawk and Green Springs deposits (Thorman and Christensen, 1991; Singer, 1996). The trend was originally identified by Roberts (1966) as part of the Battle Mountain–Eureka mineral belt. Its trace is highlighted by a distinct linear feature visible on LANDSAT imagery of north-central Nevada, and it is geologically characterized by an alignment of (1) several sets of northwest-striking en echelon high-angle faults, (2) structural windows in the Roberts Mountain allochthon, (3) Mesozoic and Tertiary intrusive rocks, (4) aeromagnetic anomalies, and (4) northwest-directed regional folds at a number of deposits (Bagby and Berger, 1985; Shawe and Stewart, 1976; also see Percival et al., 1988). The Battle Mountain–Eureka (Cortez) trend is also subparallel to a long, narrow, and well-defined geomagnetic anomaly high that is believed to delineate the regional-scale northern Nevada rift zone (see Blakely and Jachens, 1991; Christiansen and Yeats, 1992; also see section 2.7.4; Fig. 2.3).

The Getchell trend is 50 km long, but unlike the Carlin and Battle Mountain–Eureka (Cortez) trends, it is oriented northeast-southwest, approximately parallel to the structural grain of the Great Basin (Fig. 3.3). It is largely localized along the eastern margin of the Osgood Mountains and marked by disseminated and vein gold deposits. It was originally defined by the alignment of Getchell, Pinson, and Preble deposits (Bagby and Berger, 1985), but now extends to the northeast to include the Twin Creeks (Chimney Creek and Rabbit Creek) deposit, and to the southwest to include the Kramer Hill deposit (Thorman and Christensen, 1991). The southwestern end of the trend coincides with northwestern end of the Battle Mountain–Eureka (Cortez) trend, at approximately the Marigold and Kramer Hill deposits. The deposits along the trend are characterized by intrusive rocks, and north–northeast-trending faults and anti- and synforms (Bagby and Berger, 1985; Kretschmer, 1991; Hall et al., 1997; also see Tooker, 1985 Percival et al., 1988).

The Humboldt “trend” is 35 km long, and is delineated by the Standard and Relief Canyon sedimentary rock-hosted deposits (Percival et al., 1988; Percival also included the Florida Canyon deposit just north of the Standard deposit (Fig. 3.3). In the version of MRDS used in this study, Florida Canyon is classified as a sedimentary rock-hosted deposit, but Singer et al., 1996, classify it as a hot spring deposit in pre-Tertiary sedimentary rocks). If the Fondaway Canyon

deposits to the south in the Stillwater Range are included, the length of the trend increases to 80 km. Percival et al. (1988) commented that the Humboldt trend is neither a well defined nor a recognized linear feature, but is a convenient way to refer to the deposits that occur along the Humboldt Range. The trend is characterized by thrusting, and antiformal structures occur at some deposits, both of which are controls at a number of the deposits (Percival et al., 1988). In addition, the Humboldt Range is dissected by numerous, predominantly north-trending, high-angle faults, which are significant structural features with respect to the localization of mineralization (Percival et al., 1988).

The Independence group is 40 km long, and marked by sedimentary rock-hosted deposits (Daly et al., 1991) occurring throughout the Independence Mountains (Fig. 3.3). The group is defined by the rough alignment of deposits extending from the Jerri Canyon (Saval Canyon) and Burns Basin deposits in the southern part of the range to the Wood Gulch deposit in the northern part of the range (Thorman and Christensen, 1991). East–west- through north–south-trending faults, the Roberts Mountain thrust fault, and regional east-west trending antiforms occur at some deposits (Bagby and Berger, 1985). The deposits do not appear to have an obvious linear controlling structure (Seedorff, 1991), and there are not enough data to determine how, or if, they are related (Thorman and Christensen, 1991). It has been suggested by Clark et al. (1985) that the late Eocene Bull Run normal fault may extend under the Independence range.

The Alligator group is a broad region of sedimentary rock-hosted deposits that extends 60 km northeast-southwest from the Bald Mountain district in the north to the Illipah district in the south, and extends even further (up to 90) if the group overlaps with the deposits at the southeastern end of the Battle Mountain–Eureka (Cortez) trend (Fig. 3.3; Thorman and Christensen, 1991). There is no known or apparent structure that collectively controls the distribution of these deposits. However, some of these deposits, particularly the Alligator Ridge deposit, are associated with gentle north–northwest-trending antiformal structures and strike-slip faults (Romberger, 1986; Nutt, 1997; also see Percival et al., 1988). Plutonic rocks occur in the Bald Mountain district (Hitchborn et al., 1996; Nutt, 1997).

## 3.3 Volcanic Rock-Hosted Gold-Silver Deposits

### 3.3.1 Characteristics

Volcanic rock-hosted deposits have been extensively studied and are generally better understood in comparison to sedimentary rock-hosted deposits (e.g.—Buchanan, 1981; Berger and Eimon, 1982; Dreier, 1984; Berger and Bethke, 1985, and papers therein; Hayba et al., 1985; Tooker, 1985, and papers therein; Mosier et al., 1986; Panteleyev, 1986; Bonham, 1988; Berger and Henley, 1989; Berger and Bonham, 1990; Hedenquist et al., 1996). These deposits can be generally defined as “volcanic centered” vein and/or disseminated gold-silver deposits that formed at relatively shallow (within ~1 km) crustal levels. Volcanic rock-hosted deposits can be broadly subdivided into two types: low-sulfidation (LS; “Adularia-sericite”) and high-sulfidation (HS; “Acid-sulfate”). Hedenquist et al. (1996) and Hedenquist and Lowenstern (1994) equate LS deposits to geothermal environments and HS to volcanic-hydrothermal. LS deposits significantly outnumber and are generally more important than the HS in Nevada. Examples of important LS deposits in Nevada include Comstock, Tonopah, and Round

Mountain; HS include Paradise Peak and Goldfield. The salient geologic features of volcanic rock-hosted deposits are summarized in [Table 3.2](#).

### 3.3.2 Distribution

The volcanic rock-hosted deposits are distributed across Nevada in a distinctive semi-circular “crescent-shaped” pattern, dubbed the “epithermal crescent” by Ludington et al. (1993), which encompasses the roughly circular distribution pattern of the sedimentary rock-hosted occurrences ([Fig. 3.1](#); Ludington et al., 1993). The “epithermal crescent” trends northeast–southwest across northern Nevada, arcs to the southeast in the vicinity of west-central Nevada, and extends northwest–southeast parallel to the southwestern boarder of Nevada. The majority of the volcanic rock-hosted deposits occur within the northwesterly-trending portion of the “epithermal crescent”, which is coincident with the Walker Lane shear zone (Blakely and Jachens, 1991; Cox et al., 1991; Hutchinson and Albers, 1992). The volcanic rock-hosted deposits are conspicuously absent from the roughly circular area in the northeast quadrant of Nevada that hosts nearly all of the sedimentary rock-hosted deposits, and, with a few notable exceptions in north-central and northeastern Nevada (i.e.—Getchell trend and Independence group deposits), the sedimentary rock-hosted deposits do not occur within the region of the volcanic rock-hosted deposit distribution pattern (Cox et al., 1991). As a group, the volcanic rock-hosted deposits are generally considered to be younger than the sedimentary rock-hosted ([Fig. 3.2](#); Ludington et al., 1993).

In contrast to the well-defined linear mineral trends formed by the sedimentary rock-hosted deposits, the volcanic rock-hosted deposits show only weak regional-scale continuous alignments, and have been grouped together into broad mineral belts ([Fig. 3.3](#); also see Roberts, 1966; Shawe and Stewart, 1976). These volcanic rock-hosted deposit mineral belts are generally not as clearly defined by geophysical, geochemical, or other geologic features as the sedimentary rock-hosted mineral trends. These belts commonly contain deposit types and districts other than volcanic rock-hosted (e.g.—polymetallic). With respect to mineral belts and trends in general, the best defined deposit alignments occur in eastern Nevada, and principally consist of sedimentary rock-hosted deposits, whereas the least well-defined are all farther west, and these are mainly defined by volcanic rock-hosted deposits (Shawe and Stewart, 1976). Like most of the sedimentary rock-hosted deposit trends, the volcanic rock-hosted deposit belts are oriented oblique to the structural grain of the Great Basin ([Fig. 3.3](#)). The main volcanic rock-hosted mineral belts include the Beatty-Searchlight, Aurora, Walker Lane (Virginia City-Tonopah), Fallon-Manhattan, Lovelock-Austin, and the northern extent of the Lynn-Railroad.

The Beatty-Searchlight belt is 325 km long, and marked by polymetallic-vein, Comstock-vein, and quartz-vein epithermal gold-silver-bearing deposits ([Fig. 3.3](#)). It extends from about the Tokop-Hornsilver district areas in the northwest to the Searchlight district in the southeast. The belt lies en echelon to, and is subparallel with, the Walker Lane shear zone and presumably follows a related fracture system (Roberts, 1966).

The Aurora belt is 75 km long, and marked by hot spring and Comstock-vein deposits ([Fig. 3.3](#)). It extends from the Borealis and Aurora district areas in the northwest to the Tip Top deposit in the southeast. The belt is situated in and parallels the structure of Walker Lane shear zone, and is associated with a northwest–southeast-trending alignment of geomagnetic highs.

The Walker Lane (Virginia City-Tonopah) belt is 350 km long, and is marked by quartz-alunite-vein, Comstock-vein, and hot spring deposits (Fig. 3.3). It extends from Peavine-Wedekind-Comstock district areas in the northwest, through the Camp Douglas and Gilbert districts, to the Tonopah, Divide, and Goldfield districts in the southeast (Fig. 3.1). This belt is rather broad, but it is one of the more productive and better defined volcanic rock-hosted deposit belts. The mineral belt lies within the Walker Lane shear zone, and it is collinear with a northwest-southeast alignment of geomagnetic highs, a broad isostatic gravity high, and a Bouguer gravity gradient “ridge”.

The Fallon-Manhattan belt is 200 km long, and is marked primarily by Comstock-vein deposits (Fig. 3.3). It extends from the Sandsprings-Fairview district areas in the northwest, through the Broken Hills district, to the Round Mountain, Manhattan, and Tybo districts in the southeast. The mineral belt is associated with a topographic discontinuity that coincides with the northeastern margin of the Walker Lane shear zone (Shawe and Stewart, 1976; see Fig. 3.3). Many of the ore deposits in this belt have been localized by west-northwest-trending faults, and regional aeromagnetic anomalies suggest the presence of west-northwest-oriented geologic trends (Shawe and Stewart, 1976).

The Lovelock-Austin belt is 230 km long, and is marked by Comstock-vein and low-sulfide quartz-gold-vein deposits to the north, and polymetallic-vein and sedimentary rock-hosted deposits to the south (Fig. 3.3). It extends from about the Rosebud and Sulfur districts in the northwest, past the Farrel, Seven Troughs, and Trinity districts, through the Rochester district, to the Reese River polymetallic district and the Birch Creek district in the southeast. The Birch Creek district is host to the Austin Gold Ventures sedimentary rock-hosted deposit. This mineral belt is sub-parallel with two long, narrow, and relatively well-defined geomagnetic anomaly highs that flank to the west the geomagnetic expression of the Northern Nevada rift zone (see Blakely and Jachens, 1991; Christiansen and Yeats, 1992; also see section 2.7.4; Fig. 2.3).

Lynn-Railroad belt is 200 km long, and is marked by the Comstock-vein and hot spring deposits to the north, and by the Carlin trend sedimentary rock-hosted deposits to the south (Fig. 3.3). It extends from about the National district in the northwest, through the Spring City, Gold Circle, and Hollister-Ivanhoe deposits, to the southeastern end of the Carlin trend deposits (Emigrant Springs-Gnome-Trout Creek area). The northern part of the belt is sub-parallel to a regional-scale northwest-southeast-trending Bouguer gravity gradient that separates an area of low gravity to the east from an area of higher gravity to the west. The southern portion of the Lynn-Railroad belt is addressed above in section 3.2.2 as the sedimentary rock-hosted deposit “Carlin trend”.

The Shoshone-Jarbidge and Tuscarora-Spruce Mountain mineral belts are very weak alignments based on few widespread deposits. The Shoshone-Jarbidge belt, which is the only mineral belt that trends roughly parallel to the structural grain of the Great Basin, is 220 km long, and extends from the Jarbidge Comstock-vein district in the northeast to the Shoshone Range southeast of the town of Battle Mountain, Nevada. This belt is host to major deposits of barite, and lies 15 km southeast of the northeast-striking Cambrian-Devonian Cordilleran geosynclinal depositional trend (as identified by Roberts, 1966, p. 50). The Shoshone-Jarbidge belt also hosts a number of deposits where it intersects other northwest-southeast-trending mineral belts—the northern Carlin trend deposits at the intersection of the Lynn-Railroad belt; the Lewis, Bullion, and Hill Top district deposits (various deposit-types) at the intersection of the Battle Mountain-Eureka



(Cortez) trend. The Tuscarora-Spruce Mountain mineral belt is 180 km long, and extends from the Good Hope and Tuscarora Comstock-vein districts in the northwest, through several silver and base-metal districts, to the Spruce Mountain polymetallic replacement deposit in the southeast (Roberts, 1966).

### 3.4 Regional-Scale Distribution with Respect to Mineral Trends and Belts

Mineral trends are commonly defined as district-scale linear alignments of similar type and age ore deposits, whereas mineral belts are broad regional-scale deposit alignments, which may include deposits of various types and ages (Seedorff, 1991; also see Roberts, 1966; Shawe and Stewart, 1976). In general, the sedimentary rock-hosted deposits are regarded in terms of trends whereas volcanic rock-hosted deposits occur in belts (see [section 3.2.2](#) and [3.3.2](#)). For sedimentary rock-hosted deposits, it is observed that:

- The mineral trends are generally well developed and defined, and are geologically characterized by alignments of igneous rocks, geophysical anomalies (or discontinuities), and various high- and low-angle dip-slip and strike-slip structural features.
- The deposits occur in six trends or groups: the Carlin trend, the Battle Mountain–Eureka (Cortez) trend, the Getchell trend, the Humboldt trend, the Independence group, and the Alligator group.
- The Carlin and the Battle Mountain–Eureka (Cortez) are the two most prominent trends, hosting the greatest number and the largest deposits.
- The Carlin and the Battle Mountain–Eureka (Cortez) trends are oriented north-northwest, oblique to the northerly to north-northeasterly grain of Paleozoic, Mesozoic and Cenozoic structures.

For volcanic rock-hosted deposits, it is observed that:

- The mineral belts are broad, show only weak regional-scale continuous linear alignments, and are generally lacking in distinct alignments of geologic and geophysical features (with the exception of the Walker Lane shear zone as a whole, which is characterized by northwest–southeast-trending strike-slip and normal faults, and by arcuate, northwesterly-trending aeromagnetic anomalies).
- The deposits occur mainly in seven belts: Beatty-Searchlight, Aurora, Walker Lane (Virginia City-Tonopah), Fallon-Manhattan, Lovelock-Austin, and Lynn-Railroad (northern extension).
- The principal deposits occur in the Walker Lane shear zone (a structural and magmatic belt), which comprises the Beatty-Searchlight, Aurora, Walker Lane (Virginia City-Tonopah), and Fallon-Manhattan mineral belts.
- Most of the mineral belts are oriented oblique to the structural grain of the Great Basin

The term “trend” will be used from here on as a general reference to alignments of any mineral deposit types.

The mineral trends are not well understood. Some hypotheses suggest that the trends follow zones of crustal weakness, such as deep-seated fracture, shear, or suture zones, which in some cases might be tectonically reactivated structures inherited from the underlying Precambrian basement (Roberts, 1966; Shawe and Stewart, 1976; Guild, 1985; Madrid and Bagby, 1986; Hutchinson and Albers, 1992; Arehart et al., 1993; Maher et al., 1993; Grauch et al., 1995; Rodriguez, 1997; Wooden et al., 1997). Others have speculated that deposit alignments parallel major lithotectonic and tectonomagmatic structures, such as terrane or facies boundaries and volcanic fronts (Roberts, 1966; Shawe and Stewart, 1976; Woodward, 1984; Bryant and Nichols, 1988; Hutchinson and Albers, 1992; Grauch et al., 1995). Wallace (1991) proposed that some

mineral trends in the Great Basin may be products of post-mineralization deformation. He suggested that the Getchell trend deposits, for example, may have originally formed along north–northwest-striking structures (parallel to the Battle Mountain-Eureka (Cortez) and Carlin trends), but that the present-day northeast-southwest distribution of the deposits reflects exposure by post-mineralization extension and movement along faults that strike oblique to the mineral trend.

Although there has been much interest in mineral trends, there has only recently been a concerted effort in northeastern Nevada to determine the physical nature of these apparent deposit alignments (see numerous papers in Vikre et al., 1997). The paucity of studies on the origins of mineral trends in the Great Basin, or a consensus as to what these features actually represent, has not discouraged continued speculation on the subject. Indeed, many researchers have argued for the existence of deep-seated regional-scale crustal features, and frequently include such structures as an integral part of their metallogenic models to explain the distribution and genesis of volcanic, and in particular, sedimentary rock-hosted deposits in the Nevada Great Basin.

Hutchinson and Albers (1992) noted that many latter Tertiary (22–0 Ma) gold and silver epithermal veins appear to be lineament-controlled by regional cryptic fracture systems, which is reflected by the linear alignment of numerous deposits or intrusions, often marked by parallel veins systems within individual deposits, and is strongly indicative of throughgoing fracture systems at the time of mineralization (also see Dreier, 1984; Berger and Bonham, 1990). This is probably especially true for mineralization within the Walker Lane belt, where Cox et al. (1991) suggested that mid-Tertiary and later shear zone deformation may have provided the tectonic conditions that permitted the formation of volcanic-hosted epithermal deposits.

The Carlin trend sedimentary rock-hosted deposits are coincident with alignments of igneous bodies and structural windows, and as a mineral trend, it transects the northerly trend of the Paleozoic tectonic fabric, suggesting that a regional, probably deep-seated, structural control was important for the formation and spatial distribution of these deposits (Madrid and Bagby, 1986; Shawe, 1991). Cunningham (1988) recognized that many of the major sedimentary rock-hosted deposits are located along the eastern margin of the older regional paleothermal anomaly, in close proximity to the western margin of the buried Precambrian craton and the Roberts Mountain Thrust (see Cunningham, 1988, figure 1, 2, and 4). In addition, the Carlin trend and the western limit of strongly extended domains in the Great Basin largely coincide with the western margin of the buried Precambrian craton, and Seedorff (1991) commented that many deposits, although lying outside of domains of extreme extension, are proximal to these areas.

Evidence for deep-crustal regional-scale structural control for the alignment of sedimentary rock-hosted and other types of deposits along the Battle Mountain-Eureka (Cortez) mineral trend appears to be much stronger than it is for the Carlin trend (Christensen, 1995; also see Maher et al., 1993; Grauch et al., 1995; Wooden et al., 1997). Percival et al. (1988) noted that, like the Carlin trend, the Battle Mountain-Eureka (Cortez) trend is in part defined by an alignment of structural windows developed within the Roberts Mountain allochthon and by Mesozoic and Tertiary intrusive rocks, but in addition, it is further defined by aeromagnetic anomalies, several sets of north–northwest-striking, en echelon, high-angle faults, which define a zone that obliquely transects the pervasive north-northeast Basin-Range structural fabric, and by a distinct linear feature that is visible in Landsat imagery of north-central Nevada. Furthermore, the Battle



Mountain-Eureka (Cortez) mineral trend lies near-parallel and in close proximity to the central northern Nevada Rift magnetic anomaly and to a gradient ridge (or a geophysical discontinuity) observed in the regional Bouguer and isostatic gravity anomalies (Shawe, 1991; Grauch et al., 1995; also see Blakely and Jachens, 1991; Christiansen and Yeats, 1992; [sections 2.7.3 and 2.7.4](#); [Fig. 2.3](#)). Collectively, these features have been interpreted to delineate a major crustal discontinuity—a fundamental regional-scale crustal structure—which controls the linear distribution of deposits along the trend (Shawe, 1991; Arehart et al., 1993; Grauch et al., 1995). Arehart et al. (1993) suggested that if such structures are responsible for the alignment of sedimentary rock-hosted deposits along the Battle Mountain–Eureka (Cortez) and Carlin mineral trends, then they must represent fairly long-lived and deep features in the crust (possibly related to the Precambrian craton margin) which controlled thermal and mineralizing processes on a regional scale through geological time (also see Roberts, 1966; Shawe, 1977; Speed, 1983; Woodward, 1984; Madrid and Bagby, 1986; Bryant and Nichols, 1988; Armstrong and Ward, 1991; Hutchinson and Albers, 1992).

Given the complex pre-Cenozoic tectonomagmatic history of the southwestern United States, the development of an extensional regime in the Cenozoic, and widespread occurrence of mineralizing processes that led to the formation of precious- and base- metal deposits across the province, it is not unreasonable to consider that the geometries and component structures of the Great Basin crust and its boundary regions may have had a bearing on the origin of the trends, or apparent trends (if the structures do indeed exist) (Shawe and Stewart, 1976; Cunningham, 1988; Seedorff, 1991; Hutchinson and Albers, 1992; Arehart et al., 1993). The presence of regional-scale crustal structures could facilitate ore deposit formation in a number of ways (see [sections 2.7.6 and 2.7.7](#)), some of which include:

- Increasing throughgoing fluid pathways, thereby promoting whole-crustal circulation of near-surface and deep fluids (increasing lower crust/upper mantle permeability and allowing the release and mixing of deep crustal fluids with upper crustal fluids).
- Assisting in the vertical and lateral transference of heat, whereby warmer lower crustal fluids and melts could more easily penetrate and migrate to higher crustal levels.
- Increasing the country-rock surface area on which circulating fluids could react and leach (scavenge) metals; occurs at many crustal levels.
- Contributing to shallow crustal ground preparation, whereby physical and chemical changes increase the suitability of potential host rock for mineralization (an increase in permeability, wallrock area, ore traps, etc.).
- Focusing, concentrating, and directing ore-bearing hydrothermal fluids, ultimately serving to control the localization of intrusions, volcanic fields, high-level thermal anomalies, meteoric hydrothermal cells, and individual deposits.

Shawe (1991) commented that the great linear extent of the Battle Mountain-Eureka (Cortez) and Carlin sedimentary rock-hosted mineral trends, the large number of deposits in each trend, and the evidence for a large vertical range of gold deposition, indicate that extremely large hydrothermal systems were concentrated along these trends (also see Thorman and Christensen, 1991). Shawe (1991) suggested that regional-scale (much larger than individual deposits), deeply-penetrating crustal structures controlled emplacement of magmas into the upper crust, guided dispersal of hydrothermal solutions and gases derived from the intrusions or formed from heated ground waters, and shattered upper crustal rocks along the extent of the trends, providing

local permeable zones favorable for solution flow and precipitation of gold ores (also see Cunningham, 1988; Berger and Henley, 1989; Arehart et al., 1993; Maher et al., 1993; Grauch et al., 1995). The same is probably also true with regard to the formation of volcanic rock-hosted deposits. Berger and Bonham (1990) noted that deeply rooted rifting is a key element in the genesis of epithermal systems within any volcanic terrane. In the western United States, they suggested that Mesozoic and Cenozoic epithermal deposits were formed in the near-surface zone above through-going, deep-seated fracture systems, which were formed or reactivated in an evolving plate tectonic framework, and that these fracture systems controlled the emplacement of magmas and served as conduits for magmatic and meteoric fluids. It has been suggested by Rowley (1996) that regional transverse zones of strike- and oblique-slip in the Great Basin controlled the localization of some Oligocene to Early Miocene calderas (e.g.—Caliente; also Big Ten Peak, Jefferson (Toquima), and Round Mountain; Byron R. Berger, 1998, personal communication), and in turn, the formation of epithermal gold districts (also see Shawe, 1995). In addition, it is likely that the role which such crustal structures may have played in controlling mineralizing processes and/or the distribution of ore deposits was enhanced by the Cenozoic extensional setting of the Great Basin (Guild, 1985).

### **3.5 Regional-Scale Distribution with Respect to Crustal Terranes**

Roberts (1966) subdivided the Great Basin into two metallogenic provinces, consisting of an eastern base-metal province, with peripheral gold-silver-bearing deposits, and a western precious-metal province, with primary precious-metal producing deposits (see [Fig. 1.3](#)). The east-west partiality observed in the distribution of precious- and base-metal deposits, which is defined best by the preference of primary-producing precious-metal deposits for the western half of the basin, may in part be related to the lithotectonic makeup of the crust, as well as differences in mantle composition (Roberts, 1966; Shawe and Stewart, 1976). The eastern base-metal sub-province coincides with the eastern carbonate assemblage (the miogeoclinal facies) of the Cordilleran Geosyncline, and overlies the western flank and margin of the Precambrian crystalline basement (see [Figs. 2.4, 2.9, 2.10, and 2.11](#)). The western precious-metal sub-province coincides with the western siliceous assemblage (the eugeoclinal facies), and is associated with predominantly Mesozoic basement crust composed of volcanic rocks and accreted arc and oceanic terranes (Roberts, 1966; also see Shawe and Stewart, 1976; Albers, 1983; Tooker, 1985; Titley, 1991). A transitional zone, trending approximately north-south, contains both base- and precious-metal occurrences, and roughly coincides with the Cordilleran geosyncline facies boundary (see [Fig. 2.9](#)).

The spatial correlation of broad kinds of ore deposit-types (e.g.—precious- versus base-metal) with crustal segments of grossly different lithotectonic composition, such as observed across the Great Basin metallogenic province, appears not to be merely coincidental. Indeed, Hodgson (1995) commented that it is very difficult to explain most metal provinces without evoking a control by chemical heterogeneity on the scale of the crust. Broad correlations between the metal contents of particular deposit types and the lithotectonic composition of the crust in which the deposits formed, as well as spatial clustering within particular crustal segments of deposits of differing ages and types that contain the same relative gold-silver content, suggest that the makeup of the crust at the mining district and regional scales may exercise a significant control

on the formation and distribution of specific metallic deposit types (Wilkins, 1984; Hodgson, 1995; also see Guild, 1985; Tooker, 1985; Hutchinson and Albers, 1992).

A number of studies have suggested that there is an association between mineral deposit metal content and upper crustal lithotectonic composition, and for the Cordilleran region of the western United States, these include Titley (1987, 1989, 1991), Albers (1981, 1983), and Campa and Coney (1983).

Titley (1987, 1989, 1991) documented the ratios of silver to gold produced from epigenetic ore districts in the southwestern United States and observed that, in general, ores relatively enriched in gold lie above, or within, a Proterozoic basement dominated by mafic-felsic volcanic (arc) successions (largely submarine volcanic and volcanoclastic strata, and devoid of Paleozoic strata), whereas ores relatively enriched in silver occur in terranes floored by thick Proterozoic clastic and Paleozoic marine successions (schists and metasedimentary rocks, formed from a protolith of mostly clastic sedimentary rocks). It was concluded that the metallogenic signatures of ore districts (regardless of the deposit type) are fundamentally related to the crust in which the ores occur, and do not appear to be related to subduction processes, wherein metals and magmas are directly derived from partial melting of a descending slab of oceanic rocks (Titley, 1987).

Albers (1981, 1983) examined the distribution of mineral deposits in the metallogenic provinces of California, and in accreted terranes and cratonal rocks of the western United States. Albers determined that: (1) most of the large deposits are in the craton (a few occur in accreted island-arc terranes); (2) miogeoclinal terranes underlain by craton are characterized by replacement and vein-type Pb-Zn-Ag, skarn W deposits, Mo, and Sn, and in Nevada by Carlin-type disseminated gold deposits; and (3) accreted terranes (mainly of Mesozoic age) contain all the known volcanogenic massive sulfide deposits, all chromite and chert-associated Mn, all the large gold quartz-vein deposits (except Goldfield, Nevada), and the greatest proportion of Hg and Sb deposits (Sb also forms important deposits in cratonal rocks). Hutchinson and Albers (1992), in a review of the metallogenic evolution of the Cordilleran region of the western United States, concluded that lode gold-producing mines and districts occur preferentially in accreted oceanic and island-arc terranes, whereas silver-rich deposits exhibit an even stronger preference for the craton, and that the terrane and cratonal rocks could have provided different suites of metals for the deposits they host.

Campa and Coney (1983) examined the distribution of the principal gold-silver and Pb-Zn producing mines in Mexico relative to the distribution of lithotectonic crustal terranes. They determined that the distribution of these two broad types of metallic ore deposits was a function of the distribution of basement terranes: (1) most of Mexico's important gold and silver mines (over 70%, perhaps up to 84%) are located within Late Jurassic (or older) to late middle Cretaceous accreted basement terranes, which consists of submarine to partly continental andesitic, and volcanic and associated volcanoclastic sequences of magmatic arc aspect; and (2) most of the productive mines for Pb and Zn (over 61%) occur in late Precambrian through Paleozoic age terranes, which are underlain by autochthonous Precambrian North American craton, and are composed of thick sequences of sandstones, shales, and limestones that appear to be correlative with miogeoclinal sequences in southwestern Nevada and southern California as well as well known sequences in Arizona and New Mexico. Overall, Campa and Coney (1983) concluded that the distribution pattern of gold-silver and Pb-Zn deposits in Mexico

appears to have a significant element of basement [terrane] control.

### 3.6 Quantitative Studies on Mineral Trends and Crustal Terranes

Few studies have used quantitative methods to specifically examine the spatial distribution of ore deposits with respect to mineral trends or crustal terranes, but the results of these suggest that regional-scale crustal structures and/or lithotectonic terranes do exercise some degree of control.

Carlson (1991) used fractal modelling techniques to examine the spatial distribution of 4,775 hydrothermal precious-metal deposits in the Great Basin. He observed that faults and fractures, and probably hydrothermal systems and igneous and tectonic heat sources as well, appear to be similar at many different scales, which suggests that the features and/or processes controlling mineral deposit distribution operate at scales other than those of a mining district. The spatial clustering of ore deposits was determined to be persistent at all scales between 1 and 1,000 km, reflecting geologically significant controls on mineralization acting at all of these scales (Carlson, 1991, p. 113 and 114). Carlson (1991) concluded that local-scale geologic controls, such as calderas, local faults, and the availability of ground water, are not sufficient to explain deposit clustering at the regional scale, and suggested that clustering on the scale of metallogenic provinces, lithotectonic terranes, or major zones of crustal weakness take on additional credibility (i.e.—major zones of crustal weakness, or regional scale crustal structures, may be in part responsible for the localization/distribution of deposits along mineral deposit trends; Carl A. Carlson, 1997, personal communication).

In the Indian Shield, Talapatra and Mukhopadhyay (1993) have performed a multi-variate cluster analysis on Cu-Pb-Zn base-metal sulfide deposits occurring along three mineral trends in order to locate undiscovered or concealed mineralization. They compiled between 20 to 23 variables relating to lithological, structural, and ore-mineral attributes for known deposits. These attributes were examined over a 10 by 10 km cell-size grid that was superimposed on the study areas, where each grid cell was evaluated for the “presence” or “absence” of each attribute. The analysis revealed that a number of barren cells (regions thought to be devoid of mineralization) clustered with control cells (regions containing known deposits) (see Talapatra and Mukhopadhyay’s figures 3, 5, and 7). The barren cells that were predicted to have some mineral potential occurred within the trends, bridging gaps between spatial clusters of deposits, and at the ends of the trends, extending outward along trend (see Talapatra and Mukhopadhyay’s figures 2, 3, and 6; particularly figure 2). These results suggest that the lithological, structural, and ore-mineral attributes examined may exercise some control over the linear distribution of the deposits in these trends.

In the northwestern United States (Oregon and environs), Tooker (1983) used an areal-pattern recognition technique to investigate the spatial distribution relationships between lithotectonic terranes and important metal occurrences (Co, Cr, Cu, F, Au, Fe, Pb, Mn, Hg, Ni, Pt-group, Sn, Ti, V, Zn). He calculated and contoured the relative areal-abundance of metal districts, deposits, or subeconomic occurrences within a 15-minute quadrangle unit cell. Tooker found that (1) Pb, Zn, Sn, and W metals are concentrated locally in the boundary zones along the edge and in the interior of the craton, (2) Ni, Co, Cr, and the Pt-group metals predominate in accreted terranes,

and (3) Cu and Au appear to be abundant in both accreted and cratonic terranes (read *craton-underlain* terranes). He observed that the occurrence of metals on the regional-scale is not random. Metals tend to occur along broad, linear, persistent zones that trend at sub-normal angles to one another, parallel to the Cordilleran orogenic fabric and the fabric of the Precambrian craton (see [section 2.4](#); see Tooker, 1983, figure 1 and 2). West of the craton margin, the metal-distribution patterns trend roughly northwest–north and seem to parallel axes of accretion of lithotectonic terranes, with a notable correlation to Mesozoic terrane assemblages. East of the craton margin (on the craton), metal-distribution patterns trend northeast–southwest, which was interpreted by Tooker (1983) to coincide generally with boundaries between Archean and Proterozoic crustal terranes or structural zones (this interpretation is consistent with the orientation of a number of Precambrian tectonic zones and craton crustal province boundaries to the south; see [Fig. 2.11](#) and [section 2.4](#)). Highest metal occurrence density appears to be coincident with intersections between the craton basement features and prominent, east-west to northwest-trending, near-surface structural zones (e.g.—the Lewis and Clark line) or uplifts (e.g.—Uinta trend). Tooker (1983) concluded overall that the metal occurrence distribution patterns reflect primary sources of metals in the deep crust, and that the patterns are controlled by the location of fundamental channels (crustal flaws) which collected and distributed ore-bearing fluids into receptive lithosphere structural traps and lithologies where the metals were deposited in a variety of occurrence types.

The purpose of the above studies was to investigate the spatial distribution of ore deposits in terms of mineral trends and/or crustal terranes. The research conducted in this study also considers these relationships (among other geologic associations), but not in such a direct manner. The primary objective of weights of evidence mineral potential modelling is to generate a map that shows areas favorable for ore deposit formation. The favorability patterns on these maps carry a large amount of geological information, representing a synthesis or distillation of various geologic phenomena associated with known areas of mineralization. The utility of the mineral potential maps can be extended beyond just exploration target delineation by examining the spatial distribution of the favorability patterns for trends, and interpreting these trends with respect to regional-scale geologic and metallogenic features. The trends can be inspected more closely to determine the specific, or combination of geologic factors that contribute to the favorability pattern, which in turn can shed some light on whether the favorability trend is controlled by regional-scale structural zones or lithotectonic associations.

## Chapter 4. Analysis and Modelling Techniques

### 4.1 Introduction

A GIS can facilitate data analysis and interpretation by revealing spatial associations which might otherwise be obscure. Spatial data analysis can be preliminary in nature, involving non-statistical or summary statistical approaches (e.g.—visual pattern recognition and simple map reclassification, or, histogram generation and area analysis, respectively), or it can be more sophisticated, involving statistical approaches with probabilistic components (e.g.—regression analysis, weights of evidence).

This chapter presents a summary and overview of the preliminary and more sophisticated analysis methods that were used to identify and measure the spatial associations between the gold-silver-bearing occurrences and the various mineral potential evidence maps. Preliminary methods are briefly mentioned in [section 4.2](#). [Section 4.3](#) covers the basics of the weights of evidence mineral potential modelling method. The theoretical framework, the assumption of conditional independence, and error and uncertainty issues are reviewed. An extended and detailed discussion of preliminary data analysis techniques and weights of evidence, including equations and practical implementation of the method, is presented in [Appendix B](#).

### 4.2 Preliminary Spatial Data Analysis

The modelling conducted in this study made use of many spatial data manipulation and analysis tools available in a standard GIS environment. The preliminary spatial data manipulation and analysis techniques used here include: (1) map reclassification/generalization; (2) map overlay/combination; (3) spatial and topological modelling; and (4) visual pattern recognition and spatial query. All of these methods assist in clarifying and defining trends and patterns. A comprehensive examination of these tools is beyond the scope of this study. GIS spatial data manipulation and analysis methods are well known. For a thorough and detailed treatment of spatial modelling and GIS in general, see Bonham-Carter (1994a).

### 4.3 Weights of Evidence Mineral Potential Modelling

#### 4.3.1 Introduction

*Weights of evidence* (WOE) provides a measure of spatial association (a “weight”) between multi- and/or binary-class map patterns and known point or polygon objects, and uses a loglinear formulation of Bayes’ probability theorem to combine the map patterns to predict the distribution of the point or polygon objects. As applied to mineral potential modelling, the point objects represent known mineral deposits. The multi-class map patterns are typically maps of particular geologic phenomena, such as geology, geochemistry, geophysics, etc., which are likely to be useful mineral deposit predictors. These maps are referred to as “*evidence maps*”, representing geo-spatial evidence for the occurrence of mineralization. In order to facilitate combination, the evidence maps are usually reduced to deposit-indicator or mineral “*predictor maps*” of a few discrete states (typically binary) where the spatial association between mineralization-favorable

evidence and the occurrences is optimized. The mineral predictor maps collectively constitute the “*layers of evidence*” for the mineral potential model.

A layer of evidence need not completely cover the study area, as the WOE modelling method can easily accommodate missing data (incomplete coverage). This is an important and distinct advantage of this method. Other advantages include uncomplicated calculations, an objective procedure for weighting the evidence layers, relatively straightforward interpretation of the weights, direct user involvement with optimization of the evidence maps, which is an important inductive process that provides insight into the spatial data relationships, and the ability to model the error and uncertainty of the mineral potential map (Bonham-Carter, 1994a, 1994b).

### 4.3.2 Theoretical Framework

The weights of evidence mineral potential modelling method has been described by Agterberg (1989a), Agterberg et al. (1990), Bonham-Carter (1994a, 1994b), Bonham-Carter (1991), Bonham-Carter et al. (1988), Bonham-Carter et al. (1989), Wright and Bonham-Carter (1996), and Wright (1996). WOE is a *data-driven* method, requiring data about the distribution of known mineral deposits to estimate weights of spatial association for the mineralization evidence layers. It is a discrete, multivariate statistical method based on a technique originally developed in a non-spatial context for medical diagnosis (Spiegelhalter and Knill-Jones, 1984) and has been modified by Bonham-Carter et al. (1989) to deal with spatial prediction—“diagnosing” mineral deposits using the “symptoms” of various geologic phenomena (Bonham-Carter, 1994b). WOE evaluates the spatial distribution of known mineral deposits (the *response variable*) relative to multi- or binary-class map patterns (the *predictor variables*), calculates weights of spatial association ( $W^+$  and  $W^-$ ) for each pattern, and produces a multi-map signature for mineralization (Bonham-Carter et al., 1989). The evidence layers are combined using a loglinear formulation of Bayes’ Rule in a multi-map overlay operation where the *prior probability* of an occurrence—the probability of an occurrence given no information (random), equal to the average density of known occurrences in the study area, and held constant over the whole area—is updated by the addition of predictor variables and their weights to produce a single *posterior probability* map of occurrence (Bonham-Carter et al., 1989; Bonham-Carter, 1991). In this case, the posterior probability map is a map of mineral potential, which reflects the distribution of known occurrences and predicts the distribution of yet unidentified occurrences (Bonham-Carter et al., 1988). The whole process is similar to that of an exploration geologist manually integrating information and combining maps in order to delineate favorable areas of mineralization (Agterberg et al., 1990).

Weights of evidence mineral potential modelling can be subdivided into two main procedures, as illustrated in [Figure 4.1](#):

- i. Conditional probabilities that involve area proportions are used to calculate two weights of spatial association between the occurrences and each individual evidence map class:  $W^+$  for a particular map class present,  $W^-$  for not present (the occurrence points are not themselves classified or weighted, and each point is treated as equally important). Weights are relative, dimensionless values, which depend on the ratio of occurrences that fall on a particular map class to the total number of occurrences, against, the ratio of the particular map class area to the total map area. A positive correlation between occurrences and a map class is represented by  $W^+ > 0$  and  $W^- < 0$  (there are more occurrences in a particular map class than would be expected due to chance); a negative correlation by  $W^+ < 0$  and  $W^- > 0$ . Where no spatial association exists



(i.e.—the two ratios are equal), the weights are both zero. Where data are unknown or missing (incomplete evidence map coverage), the weights are assigned the value zero (Bonham-Carter, 1991). The weights can be combined into a single coefficient called the *contrast* ( $C = W^+ - W^-$ ), which provides a useful measure of the strength of the spatial association between the occurrences and a particular map class. The weights and  $C$  provide a guide for reducing the multi-class evidence map to a binary-class deposit-indicator (or predictor) map pattern. For each evidence map, an individual map class that is highly correlated (spatially) with the mineral occurrences may be selected as a deposit-indicator pattern, or multiple map classes may be grouped in such a way as to maximize the spatial association between the occurrences and the map (see [Appendix B](#) for additional details).

- ii. The binary-class mineral predictor maps (layers of evidence) are combined in a multi-map overlay operation where a loglinear formulation of Bayes' Rule (based on an assumption of conditional independence) is used to sum and update the weights associated with each of the predictor map classes that come into coincidence, producing a posterior probability mineral potential map which closely exhibits the distribution of known deposits and indicates areas where more deposits are expected than are observed. In summary, the prior probability of an occurrence for a unit area is successively “updated” by the addition of each new layer of evidence (information) to produce a posterior probability. The prior probability is equal to the probability of an occurrence within a unit area given no further information, which for this study is taken to be equal to the density of known occurrences in the study area (total number of occurrences divided by the total area of the study region, assuming a 1 km<sup>2</sup> unit area of measure and where an occurrence point is represented by one unit area). Bayes' Rule effectively revises the prior probability by incorporating the new evidence into the model (Mendenhall and Reinmuth, 1974). The posterior probability reflects both the prior and the new evidence, and with each subsequent addition of new evidence, the posterior is treated as the prior, thus providing a more efficient model for prediction (Mendenhall and Reinmuth, 1974; Bonham-Carter, 1994a). The posterior probability calculated after the addition of new evidence may be larger or smaller than the prior probability, depending on the overlap combination of predictor maps and their weights (i.e.—if evidence of factors favorable to mineralization are added, the posterior probability rises, and vice versa) (Agterberg, 1989a; Bonham-Carter et al, 1989). The mineral potential map is generated by grouping into intervals the calculated posterior probabilities according to a user-defined classification scheme (“density slicing”; often based on quantiles, an area-based percentiles classification where the posterior probability interval break-points are determined in such a way that each interval is roughly equal in area). See [Appendix B](#) for additional details.

In WOE modelling, no “training area<sup>1</sup>” is used to select mineralization evidence or to calculate “initial baseline” weights (i.e.—to establish the “initial conditions”). The “initial conditions” of the mineral potential model are established using the mineral predictor maps, as indicated above in procedure “i”. A model may be further calibrated using other factors such as mineral deposit size, where different schemes for weighting the layers of evidence are calculated for each deposit size subset (Wright and Bonham-Carter, 1996). The selection of evidence maps is largely guided by an accepted or proven deposit or exploration conceptual model (this is the standard mode of implementation; see Bonham-Carter et al., 1989; Bonham-Carter, 1994a; Wright, 1996; Wright and Bonham-Carter, 1996). The choice of evidence should reflect current understanding on the genesis of the particular deposit type being modelled as well as the geologic features believed to control its spatial distribution. An evidence map should ideally provide either universal coverage or coverage over the majority of the study area (Bonham-Carter et al., 1989).

---

<sup>1</sup> As used here, the term “training area” is defined as a sub-region of, or a region outside of, the study area that is designated an experimental control, where (1) the geologic conditions are similar to the prospecting region, (2) all the mineral deposits are known, *and no more are expected to be discovered*, (3) all of the mineralization evidence is present (i.e.—full evidence map coverage), and (4) the quantitative relationships (the spatial weights of association) between the mineral deposits and the evidence are established (Chung, 1995; Chung and Moon, 1990).

### 4.3.3 Conditional Independence

An important assumption made in WOE modelling is that the mineralization evidence layers included in a model be *conditionally independent* (CI) of one another with respect to the mineral deposits (see Bonham-Carter, 1994a, pp. 312-317). The mineral potential map is adversely affected if, at the locations of the known mineral occurrences, the presence of a mineralization-favorable map pattern in one layer of evidence is dependent on the presence of a mineralization-favorable map pattern in another layer of evidence. Violation of CI results in either the over-estimation or under-estimation of posterior probabilities during the combination of predictor maps, and the expected mineral deposit frequencies either notably exceed or fall short of the observed deposit frequencies in the most and least favorable areas of the mineral potential map (Agterberg et al., 1990). In practice, CI is probably always violated to some degree, and the possibility of the occurrence of CI generally increases with an increase in the number of evidence layers included in a model (Bonham-Carter, 1991; Bonham-Carter, 1994a). Because of the CI assumption, calculation of the spatial weights of association are carried out independently between the mineral deposits and each evidence layer, and as a result, WOE has the opportunity to examine bivariate relationships in some depth (Bonham-Carter, 1994b). The assumption of CI leads to a model that, like most models, does not fit the data perfectly, but provides a simplification that is useful for prediction when applied carefully, and gives insight into the relative contributions of the separate sources of evidence (Bonham-Carter, 1994a).

It is important to understand how serious the CI violation is so that the appropriate action can be taken to minimize the problem and so that proper judgments can be made when evaluating areas of high mineral potential. Conditional independence can be checked visually or tested for using *pairwise* and *overall* goodness-of-fit methods. If a predictor map is found to be in serious violation of the assumption of CI, it can then be (1) rejected from the model, (2) combined with another map in order to minimize the dependency, or (3) modified in some way to reduce the problem (see Agterberg, 1989; Agterberg et al., 1990; Bonham-Carter, 1994a).

Both the pairwise and overall CI tests make use of the observed versus the expected number of observations (mineral occurrences). The pairwise goodness-of-fit test measures conditional independence (CI) between all possible pairings of binary-class predictor maps (with respect to the mineral deposits) by calculating the  $\chi^2$  (chi-square) statistic for each map pair, and comparing the calculated value of  $\chi^2$  to the tabled value of  $\chi^2$  having one degree of freedom (Bonham-Carter, 1994a). CI may be present due to three-way or multi-way interactions, and testing for these cases is also possible, but for practical purposes, pairwise testing reveals the most serious CI violations (Bonham-Carter, 1994a). The results of the test are typically presented in the form of pairwise cross-tabulation tables. The overall goodness-of-fit test is a measure of the conditional independence (CI) among all of the layers of evidence in a model as a whole. The overall method is a simple procedure involving the relative comparison of predicted versus observed occurrences—if the total predicted number of occurrences is much larger than the total observed number (greater than ~10-15%), it suggests that CI is being violated, and may warrant a check of the pairwise tests and some sort of remedial action (Bonham-Carter, 1994a). The overall test can be evaluated using the Kolmogorov-Smirnov (K-S) statistic. The K-S test is based on the maximum deviation of the observed number of occurrences from the predicted number, and the results are typically presented in graphic form. See [Appendix B](#) for additional details.

### 4.3.4 Posterior Probability Uncertainty

An important aspect to interpreting a mineral potential map is recognizing and quantifying the uncertainty inherent to the posterior probabilities. The two primary sources of uncertainty are: (1) the uncertainty due to variances in weight estimates ( $W^+$  and  $W^-$ ); and (2) the uncertainty due to one or more of the binary-class predictor maps having incomplete coverage (i.e.—missing data) (Bonham-Carter et al., 1989). The uncertainties due to weights and due to missing data may be examined separately, or combined to produce a *total* uncertainty for a given unique overlap combination of binary-class predictor maps, which is calculated as the variance due to weights, plus, the sum of variances due to missing data (Bonham-Carter et al., 1989). The uncertainty due to the weights, which includes the uncertainty of the prior probability, is in general correlated to the posterior probability, and therefore maps of variance of weights have the same trends as the posterior probability maps.

In addition to the uncertainties due to weights variances and missing data, a *relative certainty* (variance) of the posterior probability can be determined by dividing the posterior probability by its standard deviation (i.e.—a “studentized” posterior probability), which, in effect, applies a student t-test (based on a normal distribution) to determine whether the posterior probability is greater than zero for a given level of statistical significance (i.e.—compared to a tabled t-value) (Bonham-Carter et al., 1989; Agterberg et al., 1993). The larger the t-value over the critical tabled t-value cut-off, 1.645 for a significance of 95% for example, the greater the certainty of the posterior probability. The relative certainty is often more useful than the weights variances or missing data uncertainties because it indicates the degree of confidence to which the posterior probabilities are “real”, as opposed to being an artifact of “chance” effects (or due to chance). As compared to the uncertainty due to the weights variances or missing data, relative certainty is generally not as highly correlated to the posterior probability.

Ideally, the four uncertainty factors (weight variances, missing data, total, and relative) may be used to create classified uncertainty maps for comparison to the posterior probability mineral potential map, or the uncertainty factors may be combined in various ways and reclassified to a binary-class map which can be used to “mask-out” areas of the mineral potential map that are deemed to be too uncertain (Bonham-Carter et al., 1989; Bonham-Carter, 1994a).

### 4.3.5 Practical Implementation of the Modelling Procedures

Weights of evidence modelling was implemented in a geographical information system (GIS) environment. SPANS GIS (TYDAC Technologies Inc., 1993) was used to compile, prepare, and manage the spatial datasets, as well as perform most of the spatial data analysis and modelling procedures. Preliminary procedures, such as visual appraisal and pattern recognition, distance calculation, map reclassification and overlay operations, summary statistical analysis (histograms), and spatial and topological modelling (point and line buffering, point-in-polygon, area, and other coincidence analysis, and surface contouring and interpolation) were carried out using tools commonly available in a GIS. The calculation of  $W^+$ ,  $W^-$ , weights variances, and posterior probabilities for weights of evidence modelling was performed external to the GIS using custom-made command-line FORTRAN utilities. The output of these utilities was imported into the GIS as reclassification templates and used to generate posterior probability mineral potential maps, as well as various maps of posterior probability uncertainty (error maps).

## Chapter 5. Spatial Datasets

### 5.1 Introduction

The initial steps in developing any GIS database involve data collection and input. This phase typically accounts for 70% to 80% of the time spent on a project. The data used for this study are diverse, and characterize the nature of the lithosphere in the Nevada Great Basin from the earth's surface to the upper mantle. The data are subdivided according to regional geology, physical geography, geophysics, seismology, geochemistry, remote sensing imagery, economic geology, hydrology, and human features. They are listed in [Table 5.1](#), at the end of this chapter.

This chapter provides an overview of the GIS study area, training datasets, and mineral potential evidence. The GIS study area parameters are given in [section 5.2](#). In [section 5.3.2](#), the criteria used to select the gold-silver-bearing occurrences from the *Mineral Resource Data System* (MRDS) database are reviewed. Definitions for “*gold-silver-bearing occurrence*” and various occurrence-type samples and sub-samples (i.e.—“*small*”, “*medium*”, “*large*”, and “*sedimentary rock-hosted occurrences*” and “*volcanic rock-hosted occurrences*”) are also given. The initial examination and selection of the evidence maps is reviewed in [section 5.3.3](#). An overview of data accuracy, limitations, and error issues is given in [section 5.4](#).

### 5.2 GIS Study Area Parameters

#### 5.2.1 Projection

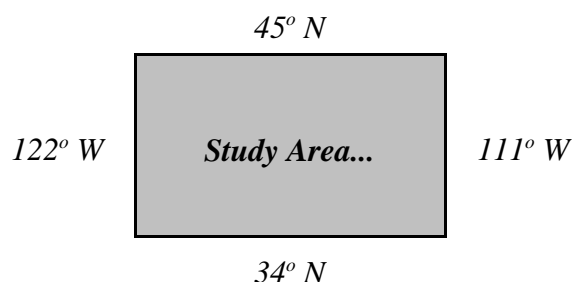
The projection was adopted from Stewart and Carlson’s (1978) geological map of Nevada:

<i>Projection:</i>	Lambert Conformal Conic
<i>Ellipsoid:</i>	Clarke 1866
<i>First Parallel:</i>	33.0°
<i>Second Parallel:</i>	45.0°
<i>Longitude of Origin:</i>	-117.0°
<i>Latitude of Origin:</i>	38.5°
<i>X-Coordinate False Origin:</i>	0.0
<i>Y-Coordinate False Origin:</i>	0.0

Coordinates west of the prime meridian (the Greenwich meridian) and south of the equator are represented as negative values.

### 5.2.2 Extents

The geographical coverage of the study area includes the region of the Great Basin and environs:



### 5.2.3 Resolution

The geological map of Nevada (Stewart and Carlson, 1978), which is the geological “base map” layer for this study, was compiled at a scale of 1:500,000. The effective resolution of a 1:500,000 scale map is 250 m (~820.2 ft.), assuming a 0.5 mm line thickness (a conservative thickness estimate) (Goodchild, 1995). The line width of the geological contacts on the geological map of Nevada (Stewart and Carlson, 1978) is nearer 0.2 mm, yielding an effective paper map resolution of 100 m (~328.1 ft.) for the position of the unit boundaries.

The resolution of the SPANS GIS study area for this analysis is 83.4 m (~273.6 ft.). In the southwestern United States this translates to longitude-latitude positional accuracy of approximately 3 seconds of arc, or 0.0008 decimal degrees. This therefore, is the theoretical limit of positional accuracy for this study, although as stated above, the practical effective limit to the accuracy of positional data ranges between ~4 and ~9 arc-seconds of longitude (~97-219 m) or latitude (~123-277 m), assuming that spatial objects were located and/or digitized in a reliable manner.

## 5.3 Spatial Datasets—Selection Criteria and Terminology

### 5.3.1 Data Sources

Public domain data comprises nearly all of the information compiled here and comes from the U.S. Geological Survey (USGS), the National Oceanic and Atmospheric Administration (NOAA), or “*the literature*”. Many of the digital datasets were obtained from the USGS and NOAA while a significant portion of the analog data, especially point and attribute data, were compiled from published documents. Most of the digital data and the analog data in map form are available from the USGS *Earth Science Information Centers (ESIC)*, the USGS *EROS Data Center*, and the NOAA *National Geophysical Data Center (NGDC)*. A small number of the digital datasets obtained from the USGS and other academic institutions are currently in preparation and are not yet available for general public consumption. These datasets were acquired through personal communications with the authors and were provided for the purposes of academic research.

### 5.3.2 Gold-Silver-Bearing Mineral Occurrences (Training Datasets)

A “*gold-silver-bearing occurrence*” is a mineral concentration having particular attributes that allow it to be classified as a specific deposit type, or can be said to have an anomalous concentration of gold or silver (Ludington et al., 1993). Specifically, for the purposes of this investigation, a gold-silver-bearing occurrence is any *lode* metallic ore mineral, in any concentration or deposit type, that is recorded in the *Mineral Resource Data System* mineral occurrences database (MRDS, 1993 download) and meets with any one of the following criteria:

- Gold or silver is the primary commodity produced or that is in reserve (i.e.—the first listed in the “commodities” field of the database).
- Gold or silver is a secondary commodity, where the primary commodity is a platinum group element, such as Pt or Pd.
- Gold or silver is a secondary commodity, where the primary commodity is a known precious-metal mineralization “*path-finder*” element (e.g.—Sb or As).
- Gold or silver is a secondary commodity, where the primary commodity is a non-metal, such as gem-quality semi-precious stones.

From a population of 5572 metallic and semi-metal mineral occurrences listed in MRDS, 2690 gold-silver-bearing occurrences were selected. Duplicate points (spatially the same) and redundant points deemed to represent the same occurrence were discarded (e.g.—a district having one large mine, but represented as a district point and a mine point). However, a large deposit, geologically and areally speaking, may be represented by one or more mines (points).

The occurrences matching the above criteria include past-producing mines, currently producing mines, and ore in reserve associated with producing mines, as well as lean or sub-economic mineral “showings”. Woodall (1984) has suggested that the geologic conditions and processes responsible for the formation of large economic ore deposits may differ substantially from those that produce lean ore deposits and sub-economic mineral occurrences. The implication is that not much emphasis should be placed on the lean and sub-economic occurrences. However, it has been recommended by Skinner (1979, p. 1) that exploration should be equally concerned with the occurrence and genesis of sub-economic mineralization as with economic deposits. The rationale being that sub-economic mineralization indicates where deposit-forming processes, albeit not economic ore-forming processes, have taken place (Ludington et al., 1993), and that *any* precious-metal concentration therefore provides valuable spatial information useful for delineating and refining mineral occurrence distribution patterns. The recognition of these distribution patterns, the identification of geologic features associated with the patterns, and the investigation into what factors might control them, can provide guidance in delineating exploration targets for economically viable deposits.

Of the 2690 gold-silver-bearing occurrences selected, 1106 had a Cox and Singer (1986) or Bliss (1992) deposit type classification designation. The occurrences were subdivided by deposit type into three “*occurrence-type samples*” according to the following criteria:



- *Gold-Silver-Bearing Occurrences of All Types*—Any type of mineralization that has gold and/or silver as its primary commodity (or as defined above). Includes 1584 unclassified deposits and 1106 deposits that include the following Cox and Singer (1986) and Bliss (1992) deposit types:

Deposit Model Name	Model Number	Count
W skarn	14a	7
Porphyry Cu	17	1
Cu skarn	18b	12
Zn-Pb skarn	18c	4
Au skarn	18f	2
Polymetallic replacement	19a	62
Replacement Mn	19b	5
Distal disseminated Ag-Au	19c	9
Porphyry Cu-Mo	21a	3
Porphyry Mo, low-F	21b	2
Polymetallic veins	22c	253
Besshi massive sulfide	24b	1
Hot spring Au-Ag	25a	49
Comstock epithermal veins	25c	328
Sado epithermal veins	25d	2
Epithermal quartz-alunite Au	25e	25
Epithermal Mn	25g	3
Sediment-hosted Au-Ag	26a	89
Hot spring Hg	27a	4
Simple Sb	27d	16
Kuroko massive sulfide	28a	2
Low-sulfide Au-quartz veins	36a	221
Au on flat faults	37b	4
Quartzite-hosted Au	37c	2

- *Sedimentary Rock-Hosted Occurrences*—Disseminated mineralization hosted by carbonate and/or clastic sedimentary rocks, commonly referred to as “Carlin-type” or “distal disseminated” deposits. Members of this group include the following Cox and Singer (1986) and Bliss (1992) deposit types:

Deposit Model Name	Model Number	Count
Distal disseminated Ag-Au	19c	9
Sediment-hosted Au-Ag	26a	89

The “*distal-disseminated*” type deposits were not well documented or understood at the commencement of this research, and were included under the general category of “sedimentary rock-hosted” deposit type. Present understanding may possibly warrant the separation of these two deposit types, but based upon the expertise of the mine geologists at the Cove deposit, this is unclear. The Cove deposit, the largest known distal disseminated type deposit in Nevada, is located along the Battle Mountain-Eureka mineral trend in the Battle Mountain area. Currently operated by Echo Bay Minerals, the McCoy-Cove exploration geologists believe that the distal-disseminated-style mineralization at Cove may be Carlin-style mineralization overprinted on preexisting skarn/porphyry base-metal mineralization (Dave McLean, 1997, personal communication). Such a scenario could account for some of the important geochemical traits typically associated with distal-disseminated type deposits: (1) the high variability (Cox, 1992) or generally higher (Singer, 1996) Ag-Au ratio as compared to the Carlin-type deposits; and (2) Mn, Zn, Pb, As, Sb trace

element geochemistry for distal-disseminated-type versus As, Sb, Hg, Zn for Carlin-type (Cox, 1992; Singer, 1996). With regard to mineral potential modelling, the inclusion of distal disseminated occurrences in the sedimentary rock-hosted training sample, what is being considered is the combined affect of the deposit types. Removal of the distal disseminated occurrences has negligible to inconsequential affects on the model: the difference in posterior probability values between a model trained with just “sediment-hosted Au-Ag” and a model including “Distal disseminated Ag-Au” is less than the prior probability (i.e.—indistinguishable from background noise and representing a probability of occurrence no more than that due to chance).

- *Volcanic Rock-Hosted Occurrences*—Vein or disseminated epithermal mineralization hosted primarily by volcanic rocks and less commonly by proximal volcanoclastic and sedimentary rocks. Members of this group include the following Cox and Singer (1986) deposit types:

Deposit Model Name	Model Number	Count
Hot spring Au-Ag	25a	44
Comstock epithermal veins	25c	333*
Sado epithermal veins	25d	2
Epithermal quartz-alunite Au	25e	25
Epithermal Mn	25g	3
Hot spring Hg	27a	4
Au on flat faults	37b	4

\* Note: Five occurrences in this category are also classified in part as 25a.

The occurrences were further broken down into a number of size categories (or “*sub-samples*”) based upon primary commodity (gold or silver) metal content:

- *Large*
  - Greater than 500 tonnes (16,075,373 Troy ounces) Au content (production plus reserves).
  - Greater than 10,000 tonnes (321,507,465 Troy ounces) Ag content (production plus reserves).
- *Medium*
  - 500-25 tonnes (16,075,373 to 803,768 Troy ounces) Au content (production plus reserves).
  - 10,000-500 tonnes (321,507,465 to 16,075,375 Troy ounces) Ag content (production plus reserves).
- *Small*
  - Less than 25 tonnes (803,768 Troy ounces) Au content (production plus reserves).
  - Less than 500 tonnes (16,075,375 Troy ounces) Ag content (production plus reserves).
- *Big*
  - Large and medium size occurrences.
- *Unknown*
  - Deposit size reported as “unknown” or not specified.

The size designations of large, medium, and small are coded into MRDS for 2,421 of the occurrences, and are derived from Guild's (1968) *Metallogenic Map of North America*.

The gold-silver-bearing occurrences as subdivided above are summarized in [Table 5.2](#):

The occurrence-type samples are referred to using the following terminology:

- *Primary occurrences*—Includes *all* occurrences of *any* size or *any* type (i.e.—all 2,690 occurrences examined in this study), unless otherwise noted. Also referred to as "*gold-silver-bearing occurrences*" or just "*occurrences*" if no reference to either sedimentary or volcanic rock-hosted mineralization is made.
- *Sedimentary rock-hosted occurrences*—A subgroup of the primary occurrences. Includes all sedimentary rock-hosted occurrence sizes, unless otherwise noted.
- *Volcanic rock-hosted occurrences*—A subgroup of the primary occurrences. Includes all volcanic rock-hosted occurrence sizes, unless otherwise noted.

Occurrence size—big, large, medium, small, unknown—is usually explicitly stated. If it is not stated, then occurrences of all sizes should be assumed (as indicated in the points above).

### 5.3.3 Mineral Potential Modelling Evidence Maps

The following evidence maps were considered for mineral potential modelling:

1. *Lithologic:*
  - Lithologic units (all 101 units considered separately; see [Appendix A](#)).
  - Diversity of map lithologic units (per 2.5 km by 2.5 km neighborhood grid cell).
  - Lithologic assemblage units (101 units grouped into 20 as per general rock-type and age; see [Appendix A](#)).
  - Cenozoic igneous rock unit distance buffers.
  - Cenozoic igneous rock time-slices.
  - Cenozoic igneous rock composition-slices.
  - Mesozoic pluton distance buffers.
  - Mesozoic pluton density.
  - Clastic and carbonate rock units.
  - Clastic and carbonate rock unit distance buffers.
2. *Structural/tectonic:*
  - Cenozoic fault distance buffers.
  - Cenozoic fault density.
  - Thrust-front distance buffers (Luning-Fencemaker, Golconda, Roberts Mountain, Sevier).
  - Strike-slip fault distance buffers.
  - LANDSAT linear-features distance buffers
  - LANDSAT linear-features density
  - Highly extended upper crustal terrain.
  - Deep-seated basement fracture system buffers.
  - Lithotectonic terrane.
  - Crustal thickness.
  - Tertiary rock dip angle and direction.
  - Late-Paleozoic–early Mesozoic paleothermal anomaly.
3. *Geophysical:*
  - Bouguer gravity anomaly.
  - Isostatic residual gravity anomaly.

- Total residual field geomagnetic anomaly.
  - Geothermal conductivity.
  - Geothermal gradient.
  - Crustal heat flow.
  - Geothermal wells and springs temperature.
4. *Geochemical (and related)*:
    - K/Na, Ba/Na, U/Th, Fe/Al, La/K, Sc/Fe, Sc/V, K, Al, As, geochemical anomalies (NURE data).
    - Igneous rock major element analyses (PETROS).
    - Igneous rock radiometric age dates (RADB data).
    - Mineralization (metallic deposits) radiometric age dates.
  5. *Geographic*:
    - Topographic elevation.
    - Shaded relief of topography.
    - Degree of topographic slope.

The suitability of each map as mineralization evidence was determined in two steps. In the first, initial evaluation was carried out using standard GIS analysis techniques, such as point-in-polygon analysis, interactive query and visual map inspection. In some instances, multi-map area cross-tabulation overlays and histogram generation were performed to investigate spatial associations in greater detail (see Bonham-Carter, 1994a, p. 238-264, for a discussion of these techniques). In the second step, the evidence maps that were found to be promising deposit indicators in the first step were measured for their spatial associations with respect to the occurrences (as described in [chapter 4](#) and detailed in [Appendix B](#)). The maps that displayed clear and strong spatial associations were selected for formal analysis and modelling, and include:

- Lithologic.
- Diversity of lithologic units.
- Lithotectonic terrane.
- Mesozoic pluton distance buffers.
- Cenozoic fault distance buffers.
- Isostatic residual gravity anomaly.
- Total residual field geomagnetic anomaly.
- K/Na geochemical anomaly.
- Ba/Na geochemical anomaly.

The maps that were found unsuitable for weights of evidence mineral potential modelling were rejected for one or more reasons:

1. Spatial correlations with the occurrences were either nonexistent (or not evident), poorly developed, or not readily interpreted. Many maps were consequently rejected, including the LANDSAT linear-features maps, the highly-extended terrains map, the deep-seated basement fracture system distance buffer map, the thrust-front distance buffer maps, and the Bouguer gravity anomaly map. Distance buffers around certain lithologic units seemed a logical choice for modelling, but most of these maps had poorly developed or ambiguous spatial correlations.

2. Some layers of evidence carried broadly similar types of deposit predictor/indicator information. These include the igneous composition-slice and time-slice maps, the Mesozoic pluton density map, the mineralization radiometric age date map, and the topographic slope map (which interestingly is spatially correlated with the fault distance buffer and lithologic diversity maps).
3. The spatial data density was insufficient or the distribution too irregular to produce a well-constrained evidence map. In such instances, it was not possible to determine if the inadequate data distribution was due to sampling bias or some other unknown controls. Much of the geophysical data were rejected on this basis, in particular the heat flow and other maps of geothermal measure, and the crustal thickness map. The PETROS major element igneous rock geochemical data were also rejected because, while being fairly uniform in distribution for the western United States, were not nearly dense enough.
4. Integrity problems with the source data. Most of the NURE geochemical data were unuseable or rejected on this basis (see [footnotes for section 6.7.1](#)).

The evidence maps considered unsuitable for formal analysis and modelling provided essential support for interpreting model output, developing metallogenic hypotheses, and illustrating various geologic spatial associations. In particular, the shaded relief topographic map played a critical role in delineating the crustal structures proposed in chapter 8 to control the regional-scale distribution of sedimentary and volcanic rock-hosted occurrences in the Nevada Great Basin.

## 5.4 Error, Data Accuracy and Limitations

### 5.4.1 Error Sources

Uncertainty of various types are inherent to spatial data, as well as its accompanying attribute data. Error associated with spatial data may be subdivided into two broad categories: (1) cartographic or positional error, and; (2) thematic or attribute error (Veregin, 1989; Chrisman, 1991). Aronoff (1989) cited six common sources of error encountered in using a GIS:

1. *Data collection*—errors in field data collection, in existing maps used as source data, and in the analysis of remotely sensed data.
2. *Data input*—inaccuracies in digitizing, and fuzziness inherent in the edges of geographic features.
3. *Data storage*—insufficient numerical precision and spatial precision.
4. *Data manipulation*—inappropriate class intervals, boundary errors, error propagation as multiple overlays are combined, and slivers due to polygon edge-matching problems.
5. *Data output*—scaling inaccuracies, error caused by inaccuracy of the output device and caused in medium instability.
6. *Use of results*—the information may be incorrectly understood or inappropriately used.

Thematic, or attribute data are complementary to positional data, and describe something about the spatial object or characterize some phenomena occurring at that location (i.e.—an anomaly in the geomagnetic field). These data may be discrete or continuous in nature (Aronoff, 1989). Error associated with attribute data can include (1) the misclassification of nominal data such as a geological unit, (2) incorrectly ranked ordinal data such as metamorphic grade, (3)

incorrectly determined ratio data such as the length of a fault, (4) or the misrepresentation of continuous data by imposing a classification scheme having too many intervals, thereby giving the impression that the data are more numerous, well distributed, or robust than they might be (Flowerdew, 1991). Many errors of this type may result from logical inconsistencies, such as in the misclassification of a geological unit by a field mapper, or from interpolation and estimation processes (Chrisman, 1991). For example, Morgan and Gosnold (1989) pointed out that making geophysical heat flow determinations is not a routine procedure. Many local factors can affect a measurement, such as topography, variations in ground-surface temperature, lateral variations in thermal conductivity and conductivity anisotropy, ground-water flow in the measurement interval, and a host of other conditions. With regard to gold-silver content of mineral deposits, Wilkins (1984) indicated that the past methods and practices of determining and recording production and reserves impact significantly on the accuracy of the figures.

### **5.4.2 Data Limitations**

Data quality and accuracy problems of the nature outlined above are not unusual to many of the datasets compiled for this study. Quality and accuracy metadata of some form should exist for every GIS dataset, but, unfortunately, not every dataset compiled for this analysis was accompanied with metadata. A good deal of caution was exercised when collecting datasets. Error detection and correction was performed throughout all aspects of assembling and compiling both digital and analog data. Where necessary, hard copy of the data or the dataset author was consulted. The consequences of mismatch between point and polygon locational accuracy were also assessed (e.g.—the proportion of volcanic or sedimentary rock-hosted occurrences not falling within their respective rock-type map units; see discussion at the bottom of [section 6.4.3](#)). It was not practical or possible to test the integrity of every aspect of every dataset to the fullest extent. At some point in the quality control process, the data had to be trusted and its overall quality understood. Despite such limitations and inherent errors, these datasets present a reasonable representation of the various geologic characteristics of this region.



# Chapter 6. Single Map Analysis, Interpretation, and Mineral Predictor Map Generation

## 6.1 Introduction

Chapter 6 is an analysis of the mineral potential evidence. It represents the first of three stages of model building, the *model formulation or specification* stage (Chatfield, 1988; see [section 1.4](#)). The material reviewed in this chapter constitutes the first of two procedures that compose the weights of evidence mineral potential modelling method, graphically illustrated in [Figure 4.1](#) as procedure “*i*”. The spatial associations between the gold-silver-bearing occurrences and the multi-class mineralization evidence maps were established and measured, and the significance of the relationships was determined. Binary-class mineral predictor maps (“*layers of evidence*”) were created from the mineralization-favorable units composing the multi-class evidence maps. The second and third stages of model building, *parameter estimation or model fitting* and *model validation*, are addressed in [chapter 7](#), where, in procedure “*ii*” of weights of evidence modelling, the predictor maps were combined in a multi-map overlay using a loglinear formulation of Bayes’ Rule to generate various mineral potential maps. In [chapter 8](#), the results of the modelling exercises carried out in [chapters 6 and 7](#) are discussed and interpreted with respect to geology and metallogenesis.

Most of the material presented in chapter 6 follows a standardized format. Datasets of like character are grouped together and discussed in tandem. The general distribution of the gold-silver-bearing occurrences is examined in [section 6.2](#). In [sections 6.3](#) through [6.7](#), the distribution of the occurrences is analysed with respect to lithology, lithologic diversity and lithotectonic terranes, proximity to faults and plutons, and geophysical and geochemical anomalies. With the exception of 6.2, each section consists of:

1. *Introduction*
  - Summary overview of the dataset(s), its relevance to gold-silver-bearing occurrence genesis and/or distribution.
  - A short statement highlighting the main points of the analysis carried out in that section.
2. *Distribution and Spatial Association of gold-silver-bearing Occurrences*
  - Examination and analysis of occurrence distribution with respect to the evidence maps.
  - Examination and analysis of the spatial associations between the occurrences and the evidence maps.
  - Reclassification of multi-class evidence map to binary-class mineral potential predictor map.
3. *Interpretive Synthesis*
  - Results from the previous section are interpreted and discussed in context of regional- and local-scale geology, tectonism, and magmatism.
  - Significance of the evidence as a mineral occurrence predictor is assessed.

Under each of these headings, analysis and discussion usually proceeds sequentially—firstly from “*primary occurrences*” (all sizes and types, as a group), secondly to “*sedimentary rock-hosted occurrences*”, and thirdly to “*volcanic rock-hosted occurrences*”.

The overall conclusion of the analyses carried out in this chapter is that the gold-silver-bearing occurrences in Nevada can be subdivided into two broad mineral deposit types—sedimentary and volcanic rock-hosted—as demonstrated by very different behavior in terms of their spatial distributions and geologic associations. Collectively, the geologic features spatially associated with the occurrences suggest that their respective regional-scale distributions are controlled in large part by two separate and distinct fundamental crustal-scale structures (or sets of structures). These structures—the Walker Lane shear zone and presumed northeast–southwest-trending regional-scale structures in northern Nevada (appearing to control the distribution of volcanic rock-hosted occurrences) and presumed northwest–southeast-trending regional-scale structures in central–north-central Nevada (appearing to control the distribution of sedimentary rock-hosted occurrences)—are introduced in this chapter. In [chapter 8](#), these are further developed into first-order constraints on the distribution of sedimentary and volcanic rock-hosted occurrences.

## 6.2 Gold-Silver-Bearing Occurrences

### 6.2.1 Introduction and Summary of Findings

[Section 6.2](#) serves as a general introduction to the regional-scale distribution of the gold-silver-bearing occurrences in space. No formal analyses or comparisons are made with respect to mineral potential evidence.

The principal findings of the analyses carried out in this section include: (1) gold-silver-bearing occurrences in general have an affinity for the western half of the Great Basin (the central and western portions of Nevada); (2) the distribution of volcanic rock-hosted occurrences forms a semi-circular pattern which stretches across northern, northwestern, western, and southwestern Nevada; and (3) the sedimentary rock-hosted occurrences form a roughly ovoid distribution pattern in the central and east-central region of northern Nevada, which “*cores*” the semi-circular distribution pattern of the volcanic rock-hosted occurrences. In addition, spatial density maps of the precious and base metal occurrences, as well as map patterns of a number of other geological datasets, show an overall “*U*”-shaped pattern to the distribution of precious metal mineralization. Distributions (2), (3), and the “*U*”-shaped pattern may reflect regional-scale lithotectonic features and/or crustal structural zones.

### 6.2.2 Distribution of Gold-Silver-Bearing Occurrences

The spatial point distribution of the primary occurrences is shown in [Figure 6.1](#). The point distributions of the sedimentary and volcanic rock-hosted occurrences are shown in [Figure 6.2](#). The occurrences appear to be preferentially concentrated in the western half of the Great Basin (western and central Nevada), especially the large and medium size occurrences. The volcanic rock-hosted occurrences form a semi-circular distribution pattern along the northern, western, and southwestern borders of Nevada. The distribution of the sedimentary rock-hosted occurrences forms a roughly ovoid pattern, which, by and large, is encompassed by the volcanic rock-hosted occurrences, forming a sedimentary rock-hosted occurrence “*core*” region in relation to the semi-circular volcanic rock-hosted occurrence distribution. Sedimentary rock-hosted occurrences are also notably scarce in the region of the Walker Lane shear zone (see [Figs. 1.3](#) and [6.2](#)), where volcanic rock-hosted occurrences tend to be concentrated.

The density of gold-silver-bearing occurrences is compared and contrasted to the density of all types of metallic mineral occurrences in Figure 6.3. The first-order density distribution pattern confirms the affinity of the occurrences for the western half of the Great Basin (central and western Nevada), as observed in Figures 6.1 and 6.3. Many of the occurrences appearing in the eastern half of the Great Basin (eastern Nevada and western Utah), in particular those in the southeast along the border of Utah, represent base-metal deposits (e.g.—Pb-Zn polymetallic replacements) that are silver-rich, having “Ag” listed as their primary commodity in MRDS. If these were removed from the gold-silver-bearing occurrences density map, the western affinity would be even stronger. A western affinity is also recognized for occurrences having:

- “*Lighter metals*” listed as the primary commodity—“lighter” defined here as having a density generally much less than 7 g/cm<sup>3</sup>, and “metal” as classified on the periodic table of elements. These include (in ascending order of density in g/cm<sup>3</sup>): Li, Na, Mg, Be, Al, Ba, Ti, As (a semi-metal), V, and Sb.
- Mo or W listed as the primary commodity.
- U or Th listed as the primary commodity (although this association does not appear to be particularly strong).

The eastern half of the state is dominated by occurrences having base metals, in particular Pb and Zn, as the primary listed commodity. The occurrences include polymetallic replacements, which have a strong eastern affinity, and Pb-Zn skarns, which as a deposit type are not well represented, but appear to have a weak eastern affinity as well. While it appears that occurrences having base metals listed as their primary commodity may be more common in the eastern half of the Great Basin (eastern Nevada and western Utah) than those having precious or “lighter” metals listed as primary commodities, the density map for all metallic mineral occurrences (Fig. 6.3) indicates that, in general, the western half of the Great Basin (central and western Nevada) is host to a greater number.

Second-order density distribution patterns show that gold-silver-bearing occurrences are noticeably concentrated in the central part of the Walker Lane shear zone region, and in a region in the northwestern quadrant of Nevada known as the “Battle Mountain heat high” (Fig. 6.3; see sections 2.6 and 2.7). Based on the distributions of occurrences in Figure 6.3, the elevated density in the Walker Lane region probably represents a concentration of predominantly volcanic rock-hosted occurrences, while sedimentary rock-hosted occurrences contribute more to the higher density regions in northern Nevada (Fig. 6.2). Hot-spring-type Au-Ag and Hg mineral occurrences have strong affinity for the “heat high” region. Gold-silver-bearing occurrences are distinctly lacking along an axis trending northwest-southeast through the central part of the state, extending from a most conspicuous region in southernmost Nevada known as the “*amagmatic zone*” (Fig. 6.4), a feature which is related to the closure of the “*Laramide magmatic gap*” around 22 Ma and represents the southern termination of the southwestward sweep of Tertiary magmatism in the Great Basin (McKee, 1971; Blakely and Jachens, 1991; also see section 2.5.1). This axis of occurrence-scarcity is better resolved in the density map of all metallic mineral occurrences. The metallic occurrences form somewhat of a “U”-shaped or “*horse-shoe-shaped*” distribution around this axis, as illustrated in the inset in Figure 6.3, entitled “*Generalized Distribution*”.

### 6.2.3 Correlations and Interpretive Synthesis

The most prevalent occurrence distribution patterns that emerge from the observations above are: (1) the eastern versus western affinity for Au-Ag primary commodity (western) and base-metal primary commodity (eastern) occurrences, and sedimentary rock-hosted (eastern) and volcanic rock-hosted (western) occurrences; (2) the roughly ovoid sedimentary rock-hosted occurrence distribution that “*cores*” a semi-circular volcanic rock-hosted occurrence distribution, and; (3) the generally “U”-shaped or “*horse-shoe-shaped*” overall distribution pattern of occurrences (includes all types of mineralization).

The east-west distribution character observed in the precious-metal-bearing and non-precious-metal occurrences is consistent with the observations of Roberts (1966), that Nevada contains two distinct metallogenic provinces—an eastern base-metal province and a western precious-metal province (see Fig. 1.3). The eastern province is characterized by deposits of Pb-Zn and peripheral by-product precious metal producers, whereas the western province hosts W, Hg, Sb, and primary precious metal producing deposits (Roberts, 1966, Shawe and Stewart, 1976). This regional east-west distribution has generally been ascribed to the compositional makeup of the crust—the eastern base-metal sub-province coincides with the eastern carbonate assemblage (the miogeoclinal facies) of the Cordilleran Geosyncline, and may also be related to the presence of Precambrian crystalline basement; the gold-silver occurrences of the western precious-metal sub-province are located in the western siliceous assemblage (the eugeosynclinal facies), and may be related to crust composed of volcanic rocks and accreted arc and oceanic terranes (Roberts, 1966, Shawe and Stewart, 1976) (see section 3.5). In regional-scale investigations conducted by Albers (1981, 1983) and Hutchinson and Albers (1992), it was found that non-placer gold-producing mines and districts in the Cordillera occur preferentially in accreted oceanic and island-arc terranes, whereas silver-rich deposits exhibit an even stronger preference for the craton, with the exception of northwestern Nevada, where deposits of both metals are common. Tooker (1983, 1985) and Hutchinson and Albers (1992) concluded that the marked east-west regional terrane preference of the precious-metal (Au) and base-metal (including Ag) deposits is due to different source rock which provide different metals for the two deposit-type suites (for additional information, see sections 3.5 and 3.6).

The sedimentary rock-hosted and volcanic rock-hosted occurrence point distributions observed here (Fig. 6.2) are the same as those described by Cox et al. (1991) and Ludington et al. (1993) (see Figs. 3.1 and 3.2). Ludington et al. (1993) referred to the semi-circular distribution of the volcanic rock-hosted occurrences as the “*epithermal crescent*”, and noted that the sedimentary rock-hosted occurrences are distributed in a roughly ovoid area inward from the crescent, forming a circular “*core*” of sedimentary rock-hosted deposits in north-central to eastern Nevada. This arrangement, wrote Cox et al. (1991), suggests that the tectonic environment in which the volcanic rock-hosted occurrences formed appears to preclude the simultaneous or subsequent formation of the sedimentary rock-hosted occurrences, irrespective of the presence of suitable host rocks. This observation led Cox et al. (1991) and Ludington et al. (1993) to conclude that the sedimentary rock-hosted occurrences, as a group, are probably older than the volcanic rock-hosted occurrences (>27 Ma versus <27 Ma for the volcanic rock-hosted; see Fig. 3.2).

The “U”-shaped or “*horse-shoe-shaped*” distribution of the metallic occurrences (Fig. 6.3)

represents the superpositioning of sedimentary and volcanic rock-hosted distribution patterns. The southwestern limb of the “U” is delineated by occurrences in the Walker Lane belt. The northeastern limb is delineated by occurrences that lie primarily along the Battle Mountain-Eureka (Cortez) and Carlin trends (sedimentary rock-hosted occurrences). The “hinge” region of the “U” is delineated by occurrences that cluster around the region of the Battle Mountain heat high and extend northeastward across northern Nevada (volcanic rock-hosted occurrences; including sedimentary rock-hosted occurrences in north-central Nevada). The “U”-shaped occurrence distribution pattern could be due to sampling bias, or it may be an artefact of the techniques used to render the maps of the density distributions. However, this distribution resembles (to varying degrees) map patterns that appear in a number of other regional-scale geological datasets compiled for this study (Fig. 6.5), suggesting that the distribution may be related to regional-scale lithotectonic and/or crustal features.

The “U”-shaped occurrence distribution appears to follow prominent northwest-southeast and northeast-southwest structural trends visible in shaded relief of topography (Fig. 6.6; also see Fig. 1.2). The “hinge” region occurrences coincide with the intersection of these trends (compare Figs. 6.3, 6.5, and 6.6). Given these general observations, it is not unreasonable to consider that the sedimentary rock-hosted occurrences may be controlled by regional-scale structural zones that parallel the Battle Mountain-Eureka (Cortez) and Carlin mineral trends in north-central Nevada, whereas the volcanic rock-hosted occurrences could be controlled by the northwest–southeast-trending Walker Lane shear zone in western Nevada and possible regional-scale structures trending northeast-southwest across northern Nevada. Similar proposals, particularly for the control of mineralization along the Battle Mountain-Eureka (Cortez) and Carlin trends, have been made in various studies, as reviewed in chapter 3 (section 3.4 and 3.6). The control of the Walker Lane shear zone over the distribution of volcanic rock-hosted occurrences is well recognized (see Cox et al., 1991). Of special interest is the northeast–southwest-trending distribution of volcanic rock-hosted occurrences across northern Nevada. No structural zone is commonly cited or recognized as a control over this distribution. The presence of a regional-scale structural feature may be reflected in the metallic mineral occurrence density maps (see Fig. 6.3), where a broad but clearly linear distribution of occurrences extends northeastward and southwestward away from the region of the Battle Mountain heat high (compare Fig. 6.3 to 6.5g and 6.5h). Along this trend, in a belt similar in width to the Walker Lane shear zone, sub-parallel linear features are visible in shaded relief of topography (Figs. 6.6 and 1.2). The most readily recognized feature of comparable position, orientation, and dimension is the “Humboldt gravity zone”, a broad and diffuse Bouguer and isostatic gravity anomaly high (Mabey et al., 1983). The origin of this zone, or what it represents, is controversial and uncertain (literature on this feature is sparse). If the Humboldt zone marks some type of broad crustal structure, it might exercise some degree of control over the regional-scale distribution of mineral occurrences in northern Nevada. The Humboldt zone, and other possible controls over the regional-scale distribution sedimentary and volcanic rock-hosted mineralization, are investigated in greater detail in subsequent sections in this chapter, and chapters 7 and 8, where the occurrences are analysed with respect to various geologic phenomena.



## 6.3 Lithology

### 6.3.1 Introduction and Summary of Findings

The distribution and spatial association of the gold-silver-bearing occurrences in relation to lithology is examined in this section.

Lithology is represented in two maps, the geological map of Nevada (Stewart and Carlson, 1978; Turner and Bawiec, 1991; [Fig. 6.7](#)) and a lithologic assemblage map ([Fig. 6.8](#)). The geological map of Nevada contains 101 lithologic units. The assemblage map contains 20 units and is generalized from the geological map (see [Appendix A](#)). Special treatment was given to the lithology map. Single-layer-of-evidence (i.e.—lithology) mineral potential maps, highlighting the lithologic units that have the highest posterior probability of hosting occurrences of various sizes and types, were prepared to facilitate interpretation and illustrate the geographic component of the distribution of the occurrences. Maps showing only the high-potential lithologic units were created as well.

The principal results of the analyses conducted in this section indicate that: (1) most of the gold-silver-bearing occurrences are hosted by marine and/or shelf carbonates of late Precambrian to late Paleozoic age, or by felsic to intermediate and intermediate to mafic extrusive and intrusive rocks of early Mesozoic to late Cenozoic age; (2) most of the medium and large size sedimentary rock-hosted occurrences are hosted by early to mid-Paleozoic marine and shelf assemblages, whereas most of the medium and large size volcanic rock-hosted occurrences are hosted by late Cenozoic felsic to intermediate extrusive and intrusive assemblages; (3) sedimentary rock-type lithologies display a stronger spatial association with occurrences of all sizes and types than do volcanic rock-type lithologies, whereas for large and medium size occurrences of any type, sedimentary and volcanic rock-type lithologies have about the same degree of spatial association with the occurrences; (4) most of the units composing the facies transitional between the eastern carbonate assemblage and western siliceous assemblage (specifically units St, Ot, Ct, CZS, Zw, and OCt) have strong spatial associations with the occurrences; (5) the sedimentary rock-hosted occurrences have the strongest spatial association with lithologic units composing the western siliceous and transitional assemblages (specifically units Os, Ch, Osv, St, and Ct); (6) the volcanic rock units composing the 6-17 Ma time-slice of Stewart and Carlson (1976) are strongly correlated with the volcanic rock-hosted occurrences, and these units are broadly distributed along the Walker Lane shear zone and Humboldt zone; (7) the volcanic unit Tmi (Tertiary intrusive rocks of intermediate to mafic composition) has the strongest weight of spatial association with volcanic rock-hosted occurrences; (8) lithologic units strongly correlated with small size occurrences of any type are generally more widely distributed across Nevada, and are located in the eastern (carbonate) assemblage and western (siliceous) assemblage, in the Walker Lane shear belt, and along the trend of the transitional assemblage; (9) lithologic units strongly correlated with large size occurrences of any type are generally less widely distributed across Nevada, and are located in the eastern (carbonate) assemblage, and particularly, in the Walker Lane shear zone belt; (10) the distribution of lithologic units strongly correlated with medium size occurrences of any type is weakly gradational between the distributions observed for units correlated with small and large size occurrences, but bears slightly more similarity to the distribution of the units correlated with large size occurrences; (11) spatial correlations suggest that small size occurrences of all types are hosted by a wider variety of lithologies than big size



occurrences, and overall, that big size occurrences in general should form in units that show a different geographic distribution, and to some degree, a different composition than those units that would host small size occurrences.

The most important result of this investigation with respect to training datasets and the analyses carried out in the remainder of this chapter, is that (1) the large and medium size occurrences exhibit similar lithologic affinities and map patterns and, therefore, may be treated as a group (the sample of “big” occurrences), rather than as two separate samples, and (2) the sedimentary rock-hosted and volcanic rock-hosted samples are better treated as two single samples composed of all sizes of their respective occurrences, rather than being subdivided into their respective large, medium, and small sub-samples (in part because of the low number of occurrences making up both the large or medium samples).

### 6.3.2 Distribution and Spatial Association of Gold-Silver-Bearing Occurrences

The review of occurrence distribution presented below excludes occurrences that are apparently “hosted” by unconsolidated or semi-consolidated Quaternary cover units (valley fill), such as Qa (alluvium), Qp (playa, etc.), Qls (landslide), Qm (moraine), and QToa (older alluvium) (see [Appendix A](#) for a description of these units). The relatively high number of occurrences falling within Quaternary cover units is discussed in the interpretations section below.

The most common group of like-lithologic assemblages hosting all sizes and types of occurrences are the marine and/or shelf carbonates of late Precambrian to late Paleozoic age ([Fig. 6.9](#), dashed box). Approximately 34% of all occurrences, and ~29 % of the medium and large size occurrences, fall within these four assemblage units. Of these four units, the greatest number of large and medium size occurrences (~20%) are hosted by the early to mid-Paleozoic marine and shelf assemblage. The single lithologic assemblage unit with the greatest number of occurrences is the late Cenozoic felsic to intermediate extrusive and intrusive assemblage unit, hosting nearly 15% of all and nearly 32% of the large and medium size. The rank of individual lithologies relative to the number of occurrences hosted is shown in [Figure 6.10](#). Unit Tt2 (Tertiary silicic ash-flow tuffs) has the greatest number of occurrences, hosting over 11%. Most of the large and medium size occurrences (almost 20%) are hosted by unit Ta3 (Tertiary andesite and intermediate volcanic rocks). The lithologic unit having the highest spatial association with the occurrences is Pzsp<sup>1</sup> (Paleozoic serpentinite), due to the fact that it covers only 6 km<sup>2</sup> but, hosts 8 occurrences (2 small, 2 medium, 4 of unreported size in the Candelaria district within the Walker Lane shear zone; occurrence locations are believed to be accurate) ([Fig. 6.11](#)). The majority of lithologic units with higher  $W^+$  values (10th percentile and greater  $W^+$  values; i.e.— $W^+$  values ranging from ~0.5 to 5) for spatial association with the occurrences are

---

<sup>1</sup> Very limited and local occurrences of serpentinite (unit Pzsp) occur within the Walker Lane belt and in northern Nevada within the region of the Humboldt zone (as indicated on the 1:500,000 scale geological map of Stewart and Carlson, 1978). The limited presence of serpentinite may be genetically significant, possibly indicating mantle uplift and upward thrusting of mantle slices that were structurally emplaced at shallow crustal levels as a result of alternating compressional-extensional transcurrent movement along the Walker Lane shear zone (see Vielzeuf and Kornprobst, 1984; Cameron, 1993). Because of Pzsp's small areal coverage, however, it is recognized as a highly rated unit but treated as an outlier.

predominantly sedimentary-type (~40% sedimentary; ~32% volcanic), and is even more so if the units of “mixed” rock type are included (~56% sedimentary; 38% volcanic). The top five highest rated units, excluding of Pzsp<sup>1</sup>, consist of mainly sedimentary rock-type units. For large and medium occurrences as a group, more volcanic lithologies have strong W<sup>+</sup> and the lithologies are split nearly 50%-50% between sedimentary units and volcanic units.

The most common group of like-lithologic assemblages hosting the sedimentary rock-hosted occurrence types are the marine and/or shelf carbonates of late Precambrian to late Paleozoic age (Fig. 6.12, dashed box). Approximately 51% of all sedimentary rock-hosted occurrences and ~58 % of the medium and large size fall within these four assemblage units. Of these four units, as well as any of the assemblage units, the greatest number of large and medium size sedimentary rock-hosted occurrences are hosted by the early to mid-Paleozoic marine and shelf assemblage (50%). The single lithologic assemblage unit having the greatest number of sedimentary rock-hosted occurrences is the early to mid-Paleozoic marine and shelf assemblage, hosting nearly 34% of all and 50% of the large and medium size. The rank of individual lithologies relative to the number of sedimentary rock-hosted occurrences hosted is shown in Figure 6.13. Units Os (Ordovician clastics, metamorphics, carbonates) and St (Silurian limestone, limy clastics, cherts) have the greatest number of sedimentary rock-hosted occurrences, hosting over 29%. The lithologic unit having the highest weight of spatial association with sedimentary rock-hosted occurrences is St (Silurian limestone, limy clastics, cherts) (Fig. 6.14), part of the facies transitional between the eastern carbonate assemblage and western siliceous assemblage (see Fig. 2.9). Most of the other units composing the transitional assemblage (i.e.—Ot, Ct, CZs, Zw, and OCt) also have strong associations with the gold-silver-bearing occurrences in general (see Fig. 6.11).

The most common group of like-lithologic assemblages hosting the volcanic rock-hosted occurrences are the felsic to intermediate and intermediate to mafic extrusive and intrusive rocks of early Mesozoic to late Cenozoic age (Fig. 6.15, dashed box). Approximately 49% of all volcanic rock-hosted occurrences and ~66 % of the medium and large size fall within these three assemblage units. Of these three units, as well as any of the assemblage units, the greatest number of large and medium size volcanic rock-hosted occurrences is hosted by the late Cenozoic felsic to intermediate extrusive and intrusive assemblage (~60%). The single lithologic assemblage having the greatest number of volcanic rock-hosted occurrences is the late Cenozoic felsic to intermediate extrusive and intrusive assemblage, hosting 40% of all and over 60% of the large and medium size. The rank of individual lithologies relative to the number of volcanic rock-hosted occurrences hosted is shown in Figure 6.16. Units Tt2 (Tertiary silicic ash-flow tuffs), Ta3 (Tertiary andesite, intermediate rocks), and Tr3 (Tertiary rhyolite flows and shallow intrusives) have the greatest number of volcanic rock-hosted occurrences, hosting approximately 50% of all and over 50% of the large and medium size. The lithologic unit having the highest weight of spatial association with volcanic rock-hosted occurrences is Tmi (Tertiary intrusive rocks of intermediate to mafic composition) (Fig. 6.17). Other related intrusive rocks (Tri and Ti) also have relatively strong associations with all occurrences, as well as some plutonic rocks of Triassic (Tgr and TJgr) and upper Cretaceous age (Jgr, KJd, Mzgr, and Kgr).

Based on the above relationships, three lithology mineral potential predictor maps were produced: (1) a ternary-class map composed of low, medium, and high units of favorability for hosting primary occurrences (Fig. 6.18); (2) a binary-class map of favorable units for hosting

sedimentary rock-hosted occurrences (Fig. 6.19); and, (3) a binary-class map of favorable units for hosting volcanic rock-hosted occurrences (Fig. 6.19). The high number of units composing the lithology map (101), and the minuscule area covered by the most favorable units (e.g.—the four highest rated units cover 202 km<sup>2</sup>, ~0.07 % the area of Nevada), necessitated the combination of groups of high favorability lithologic units (typically 7-15 units) into single favorability units for the predictor maps.

### 6.3.3 Correlations and Interpretive Synthesis

The spatial associations for the occurrence samples discussed above were used to create posterior probability maps for the small, medium, and large size occurrences, and are presented in Figure 6.20. These maps highlight in bulk lithologic units that are most highly correlated with the occurrences, and those units which host more occurrences than would be expected due to chance (that chance being the prior probability, see chapter 4 for more information). These single-layer-of-evidence posterior probability maps are used to detail and interpret the geographic component of the distribution of the spatial association data with regard to the lithologic units, which is lacking in the histograms presented above. The maps subdivide the lithologic unit posterior probabilities into six intervals—the lower values into larger and roughly equal areas (white and grey), and the higher values into smaller and roughly equal areas (blue, green, yellow, and red)—so as to highlight the distribution of those units with higher potential.

The distribution of lithologies having high posterior probabilities of hosting small, medium, and large size occurrences forms a continuum in map pattern between the small and large occurrence end members (Figs. 6.20a and 6.20c). Relative to the medium and large size occurrence posterior probability maps, the lithologies having a high posterior probability of hosting small size occurrences (Fig. 6.20a) are in general more widely distributed across the region, and displays a posterior probability high (red) which is both smaller in area coverage and different in geographical extent than the highs of the medium and large maps (Figs. 6.20b and 6.20c). The small occurrences map highlights units of the eastern (carbonate) assemblage and western (siliceous) assemblage, units in the Walker Lane shear belt, and especially units that parallel the trend of the transitional assemblage (see Figs. 1.3, 2.3, and 2.9). Lithologies having a high posterior probability of hosting large size occurrences (Fig. 6.20c) are generally less widespread compared to the small occurrences map, and are preferentially located in the Walker Lane and eastern (carbonate) assemblage. Lithologic units in the Walker Lane shear zone have particularly high (red) posterior probabilities for hosting large size occurrences. The distribution of lithologies having a high posterior probability of hosting medium size occurrences (Fig. 6.20b) is weakly gradational between the distributions of the small and large occurrences maps (Figs. 6.20a and 6.20c), displaying highs in the Walker Lane (similar to large occurrences map), as well as more highs in central and northwestern Nevada than does the large occurrences map (similar to the small occurrences map). Overall, however, the medium occurrences posterior probability map shares more characteristics with the large occurrences map than it does with the small. All three small, medium, and large occurrence maps taken together, the lithologic units having the highest posterior probabilities (red and yellow) are roughly coincident to the aforementioned “U”-shaped distribution (see section 6.2) of the occurrences—the highest posterior probability lithologic units in the medium and large occurrences map delineating the southwestern limb of the “U”, the second highest (yellow) posterior probability lithologic units in the large and (especially) and medium occurrences map delineating the northeastern limb, and the “hinge”

region of the “U” delineated by the high posterior probability (red and yellow) units in the small occurrences map (compare Fig. 6.20 to Figs. 6.3 and 6.6).

The specific lithologies making up the higher posterior probability units for the small, medium, and large size occurrences are shown in Figure 6.21. These lithologic units represent those having an “elevated” posterior probability.<sup>2</sup> These maps show essentially the same distribution patterns as the posterior probability maps above (Fig. 6.20), except that they highlight the lithologies with the highest posterior probabilities. As a result, the lithologies shown in these maps correspond with those having the highest posterior probability (red) on the posterior probability maps (Fig. 6.20), but are probably more representative of the units having anomalous or significant spatial associations with the occurrences. The elevated posterior probability lithologic unit maps (Fig. 6.21) suggest that the small size occurrences would tend to occur in a greater number of lithologies (a wider variety) than the medium or larger deposits, but this observation, though it may be true, is in part seen because of the far greater number of small (n=2269) occurrences as compared to the medium (n=118) or large (n=59) occurrences. Therefore, because of their greater number and wider distribution, the small size occurrences would be expected to be hosted by a greater number (variety) of lithologies. One point which is of interest is the relative proportion of sedimentary rock-type lithologies versus igneous rock-type lithologies making up the respective small-medium-large elevated posterior probability units. The number of sedimentary rock-type lithologies units composing the elevated posterior probability units hosting small occurrences is greater than the number of igneous rock-type units (10 to 7), as opposed to the medium and large occurrence elevated posterior probability lithology maps which have a greater number of igneous rock-type units (5 to 4 and 5 to 3, respectively; these counts include unit Pzsp, serpentinite). This is probably due in part to the greater number of large and medium occurrences represented in the volcanic rock-hosted sample as compared to the sedimentary rock-hosted sample.

The distribution patterns for medium and large size occurrences displayed by both the posterior probability (Fig. 6.20) and elevated posterior probability lithology (Fig. 6.21) maps suggest that these two occurrence samples may be treated as one sample—the sample of “big” occurrences. All subsequent analyses were carried out on this one big sample, rather than the two separate medium and large samples. In addition the lower cutoff for medium-sized occurrences, ~803,768 Troy ounces Au content (and/or ~16,075,375 Troy ounces Ag content), is close to the informal demarcation for “giant” “million ounce” gold camps. The lithologies having elevated posterior probabilities for hosting big occurrences is compared to those having elevated posterior probabilities for hosting small occurrences in Figure 6.22. The distribution of lithologies between these two samples is noticeably different. For the units having an elevated posterior probability of hosting small size occurrences, the number of sedimentary versus igneous rock-type lithologies is 10 to 7 (respectively; ~60% versus ~40% of the total number of lithologies), whereas for the units having an elevated posterior probability of hosting big size occurrences, the proportions are equal (5 sedimentary and 5 igneous lithologies). Only four elevated posterior probability lithologies are shared between the small and big occurrence samples (Tmi, Trk, Zw,

---

<sup>2</sup> For a given occurrence type or size sample, an elevated posterior probability is defined as those values which are greater than (and equal to) the value at the most pronounced upward inflection point on a sorted frequency distribution curve of the posterior probabilities. If more than one inflection point was prominent, the value closest to the upper ~20-25% fraction of the data sample was chosen.

and Pzsp; all less than 420 km<sup>2</sup> in area, and together totalling ~700 km<sup>2</sup>, or <0.25% of the total area of Nevada). The lithologies having elevated posterior probability of hosting small occurrences form a pattern trending roughly north-northeast, and correspond to the trend and some of the lithologies of the transitional assemblage (Fig. 6.23). Note also that the lithologies and the trend correspond to the general north-south occurrence density trend, which is positioned along the border separating the eastern base metal metallogenic province from the western precious metal metallogenic province (see Figs. 1.3, 6.1, and 6.3). The distribution of lithologic units having an elevated posterior probability for hosting big occurrences is correlative to regions known to host larger deposits, such as the Carlin and Battle Mountain-Eureka trends, and in the Independence group in northeastern and north central Nevada, and along the Walker Lane (Virginia City-Tonopah), Aurora, and Beatty-Search Light trends (see Fig. 3.3). Overall, the elevated posterior probability lithology maps suggest that the lithologies that host big occurrences are different in their geographic distribution, and possibly in their composition, than those that host smaller size occurrences.

The particular lithologies having elevated posterior probabilities for hosting sedimentary rock- and volcanic rock-hosted occurrences are shown in Figure 6.24. The distribution patterns for both of these elevated posterior probability lithologic unit maps reflect the distribution pattern of the occurrences (compare Fig. 6.2) and represent suitable host-rocks. For the sedimentary rock-hosted occurrences, the lithologic units of elevated posterior probability (Fig. 6.24a) are composed of nearly equal proportions of western (siliceous) and eastern (carbonate) assemblage lithologies (~45% and ~48% respectively; compare Fig. 6.24a to 6.23a). However, as indicated above in section 6.3.2, the sedimentary rock-hosted occurrences have the strongest spatial association with lithologic units composing the western siliceous and transitional assemblages (specifically units Os, Ch, Osv, St, and Ct). The western and transitional assemblages are coincident with the western edge of the Precambrian craton and the Roberts Mountain and Golconda thrust fronts, which are regional-scale crustal features that may have served to focus and concentrate mineralizing processes, and is further discussed in sections 6.4.3, 6.5.3, 6.6.3, and 6.7.3.

For the volcanic rock-hosted occurrences, the lithologic units of elevated posterior probability (Fig. 6.24b) are particularly correlative to the volcanic units making up the 34-17 Ma and 17-6 Ma age units in Stewart and Carlson's (1976) time-slice maps, as compared in Figure 6.25. The elevated posterior probability lithologies map for volcanic rock-hosted occurrences presented in Figure 6.25a is modified (lower threshold  $W^+$  value decreased) to include more volcanic units. This was done for the purpose of highlighting the correlation, but even without this modification, Figure 6.24b can still be seen to correlate well with the 17-6 Ma time-slice volcanic unit of Figure 6.25b (also see Fig. 6.4). This correlation indicates that the volcanic rock-hosted occurrences were closely tied to the space-time migration of magmatism across Nevada (as depicted in time-slice maps of Stewart and Carlson, 1976; Fig. 6.4). The regional distribution trend of the 17-6 Ma time-slice volcanic units parallel the Walker Lane shear zone and the Humboldt zone (compare Fig. 6.4 to 1.3 and 6.6). As indicated above and in section 6.2, the Walker Lane belt and the region of the Humboldt zone region are host to a large number of important volcanic rock-hosted occurrences (see Figs. 1.3, 3.3, and 6.2). Cox et al. (1991) suggested that Walker Lane-style (strike-slip) deformation provided the tectonic conditions that permitted the formation of volcanic rock-hosted deposits. In the Humboldt zone, the broad, linear distribution of volcanic rocks and their associated mineral occurrences suggests that



similar conditions and regional-scale structures may have focused magmatic and mineralizing activity. The high degree of spatial association between the volcanic rock-hosted occurrences and the volcanic units of the 34-17 Ma and 17-6 Ma time-slice implies that mineralization along the Walker Lane belt and Humboldt zone took place between 34-6 Ma, with the possibility that many (most?) formed between 17-6 Ma. The age of volcanic rock-hosted mineralization is generally within one to several million years of that of the host rocks (see Hutchinson and Albers, 1992) or less (possibly as little as 50,000 years at Round Mountain; see Henry et al., 1997).

The Quaternary cover units, especially unit Qa, were “apparently” host to a significant number of occurrences<sup>3</sup>. Because of the relatively large areal coverage of these units (139,103 km<sup>2</sup> combined, or ~49% of the total area of Nevada), they (particularly Qa) were rated as having a low spatial association with the occurrences (with the exception of those cover units having relatively small areas, such as the landslide or moraine units). Occurrences hosted by Quaternary cover or by units other than expected (e.g.—volcanic rock-hosted mineralization in sedimentary rocks, or vice versa) can be explained by (1) mineralization in pediments that are covered by Quaternary erosional materials, the real host rock possibly being that which lies range-ward of the valley-fill sequence, (2) mineralization in sedimentary host-rocks that were later covered by volcanic sequences (e.g.—a mineralized sedimentary unit is stratigraphically below a post-mineralization volcanic unit, or vice versa), or (3) volcanic rock-hosted mineralization in sediments or gravels associated with the geothermal environment (see [Table 3.2](#)). Alternatively, the occurrence points and/or the mapped unit boundaries might be misplotted.

## 6.4 Lithologic Diversity and Lithotectonic Terranes

### 6.4.1 Introduction and Summary of Findings

The distribution and spatial association of the gold-silver-bearing occurrences in relation to the diversity of lithology ([Fig. 6.26](#)) and lithotectonic terranes ([Fig. 6.27](#)) is reviewed in this section. The diversity map measures the spatial complexity of lithology, and was prepared from the geological map of Nevada (Stewart and Carlson, 1978). The lithotectonic terranes map is a representation of tectonically juxtaposed accreted terranes, and was prepared primarily from the maps of Silberling et al. (1987) and Silberling (1991).

In the Great Basin, lithologic complexity, at least in the plan view of a map, is in part a product of the structural, stratigraphic, and intrusive relationships within a given neighborhood area of measurement. For example, faults distort, dismember, and rotate structural blocks, disrupt the continuity of units, juxtapose unrelated rocks, and expose, end-up, once-horizontal stratigraphic units. The greater the number and more intricate these relationships, the more spatially complex an area should appear. The purpose of creating a lithologic diversity map is to determine the degree of spatial association between mineral occurrences and such areas, the rationale being that structure, stratigraphy, and intrusive activity are important factors controlling mineralization

---

<sup>3</sup> A total of 226 occurrences, including 5 large and 10 medium size occurrences. Of the total number of sedimentary rock-hosted deposits, ~13% fall in alluvium and 8% in igneous rock types. Of the total number of volcanic rock-hosted occurrences, ~9% fall in alluvium and 13% in sedimentary rock types.



and/or exposing ore bodies (see [sections 3.4](#) and [3.6](#)). It is likely, therefore, that lithologically diverse regions should show a high degree of spatial association with the occurrences. This proposition is supported by the research of Griffiths and Smith (1992), where it is demonstrated that there is a simple linear relationship between geologic diversity and the mineral-resource diversity. They found that sample units with relatively high diversity are favorable hosts for metallic ores, as demonstrated by most of the counties in Nevada (12 of 17) which have a high diversity and are prolific producers of base- and precious-metals. Geologically, Griffiths and Smith (1992) interpreted this as “reflecting the complex mixture of igneous, metamorphic, and sedimentary rocks that accompany metallic ores which, in turn, serves to emphasize the complexity of processes necessary to provide a good potential for metallic ores and a high geologic diversity.”

The lithotectonic terranes in Nevada are composed of Paleozoic and lower Mesozoic rocks, and each have a distinctive geologic history (see Silberling, 1991). The Mesozoic rocks represent fringing-arc, back-arc basin, and shelf environments with respect to North America (see [Fig. 2.4](#)). The Paleozoic rocks are incorporated and remobilized in the Mesozoic terranes, some of these having pre-Mesozoic emplacement histories (i.e.—Roberts Mountain and Golconda allochthons) (Silberling, 1991). The terranes are fault-bounded, and the present-day map pattern is primarily the result of Middle Jurassic to Early Cretaceous thrust and strike-slip faulting, further modified by faulting, rotation, and tilting in response to Cenozoic extensional tectonics (Silberling, 1991). See [Figure 6.27](#) for more information.

The principal results of the analyses conducted in this section indicate that occurrences in Nevada have a strong spatial association with: (1) areas of moderate lithologic complexity, where the strength of the spatial association generally *increases* with *increasing* lithologic diversity, but declines sharply in areas of moderately-high to high lithologic complexity (an effect related to lack of occurrences in very small areas of high complexity); and (2) accreted lithotectonic terranes that may possibly have an intrinsically high gold content (i.e.—potential gold source rocks) and that may also be proximal to possible deep-seated regional-scale crustal tectonic zones, which could have facilitated the movement of mineralizing fluids and formation of ore deposits (e.g.—the Walker Lane shear zone, the north–northeast-trending mid-Paleozoic to mid-Mesozoic overthrust zones of the Roberts Mountain, Golconda, and Luning-Fencemaker allochthons, and the western margin of the North American Precambrian craton).

#### **6.4.2 Distribution and Spatial Association of Gold-Silver-Bearing Occurrences**

Diversity units #2, #3, and #4 contain the most occurrences (76.5%), and the greatest number of sedimentary rock-hosted occurrences (nearly 83%) and volcanic rock-hosted occurrences (over 80%) ([Figs. 6.28](#) and [6.29](#)). This is because they collectively represent 65% of the total area of Nevada (see solid and dashed lines in [Figs. 6.28](#) and [6.29](#)). Of these three units, #3 contains the greatest number of primary occurrences (nearly 31%) and the largest number of big occurrences (nearly 33%). Unit #4 contains the greatest number of sedimentary rock-hosted occurrences (nearly 32%). Units #2 and #3 contain most of the volcanic-rock-hosted occurrences (32% each). Overall, sedimentary rock-hosted occurrences tend toward areas of slightly greater lithologic diversity than do the big, small, or volcanic rock-hosted occurrences. The spatial association between occurrences and lithologic diversity *increases* with *increasing* diversity.

Figure 6.30 shows the strength of spatial association (contrast of  $W^+$  and  $W^-$ ) between all occurrences and successive (non-area-cumulative) units of lithologic diversity. Collectively, diversity units #4-#7 account for ~40% of all occurrences, ~35% of big occurrences, ~44% of sedimentary rock-hosted occurrences, and ~26% of volcanic rock-hosted occurrences, but have a combined area of *only* ~15% of the total area of Nevada. At higher degrees of lithologic diversity, units #8 to #11, the strength in spatial association between the occurrences and lithologic diversity tapers off quickly, which is probably due to the fact that these diversity units, representing ~0.06% of the total area of Nevada, are highly scattered and account for only 3 occurrences (see Figs. 6.26 and 6.28).

The *North American miogeocline* (NA) lithotectonic terrane contains the greatest number of occurrences (35%), primarily by virtue of its large extent (~48% of the total area of Nevada), followed by the *Roberts Mountain allochthon* (RM) hosting 16%, and the Jungo (JO, includes the Fencemaker allochthon) and the *Golconda allochthon* (GC), which collectively host about 10% of the occurrences each (Fig. 6.31). Most of the big size occurrences are hosted by the NA (~27%) and RM (~26%) terranes, RM consisting of only ~11% of the total area of Nevada. The largest number of sedimentary rock-hosted occurrences is hosted by the RM terrane (~62%) and by NA (~23.5%) (Fig. 6.32). The largest number of volcanic rock-hosted occurrences are hosted by the *Cenozoic cover deposits* (Cz), JO, and NA terranes, containing each about 20% of the occurrences (Fig. 6.32). The lithotectonic units having the overall greatest spatial association with the primary occurrences sample are the *Paradise* (PD), *Pine Nut* (PN), RM, and *Sand Springs* (SS) terranes (Fig. 6.33). Big size occurrences show a strong spatial association for SS and RM, and in particular the PN terrane (accounting of ~13%). The RM terrane shows the strongest spatial association for sedimentary rock-hosted occurrences, hosting ~62%, while volcanic rock-hosted occurrences are most strongly associated with the JO (~19%), PN (~14%), and SS (~8%) terranes.

Based on the above relationships, four binary mineral potential predictor maps were produced; one from the diversity of lithology map, and three from the lithotectonic terranes map (Figs. 6.34 and 6.35). The lithologic diversity binary predictor map is composed of diversity units #4-#11, representing units favorable for hosting primary occurrences, sedimentary rock-hosted occurrences, and volcanic rock-hosted occurrences. The lithotectonic terranes map was reclassified into three separate binary predictor maps, one for each of the three occurrence samples (primary, sedimentary rock-hosted, and volcanic rock-hosted). All three of the maps are combinations of two or more lithotectonic terranes.

### 6.4.3 Correlations and Interpretive Synthesis

The increase in spatial association between occurrences and lithologic diversity with increasing diversity may reflect a higher density of structures that are thought to control, focus, localize, or expose mineralization (as expressed at the present-day erosional surface). If the proposition stated in the introduction to section 6.4 is reasonable—that the lithologic diversity of a map is dependent on the degree to which various structural, stratigraphic, and intrusive features are present at the surface within a region—then areas of higher lithologic diversity should represent (1) areas of post-mineralization exposure, where faulting and other tectonic activity have revealed crustal sections which host mineral occurrences, and/or (2) regions of “structurally prepared” host rocks that might facilitate ore formation if mineralizing processes have taken

place. The degree to which either one (or a combination) of these possibilities is responsible for the positive spatial association between lithologic diversity and mineral occurrences would likely be contingent on the age of mineralization relative to the features or events resulting in higher diversities. Where mineralization post- (or syn-) dates the events and features responsible for lithologic diversity, a higher density of faults and intrusives could provide “plumbing” for mineralizing fluids. If the faults (fault zones?) are presumed to continue at depth, they might promote upper crust permeability, acting as conduits and pathways for ascending deep-crustal fluids and magmas, which could contribute heat, metals, and/or agents for gold complexing and transport (also see [sections 2.7.6, 2.7.7, and 3.4](#)). Regions of “structurally prepared” ground might also expose geochemically favorable stratigraphic units. If mineralization pre-dates diversity, then the spatial correlation might largely exist by virtue of exposure and exhumation of ore-bearing units (see for example Wallace, 1991).

In the western United States and Mexico, a number of studies have found correlations between the lithotectonic composition of the crust and ore deposit type and metal content (see Roberts, 1966; Albers, 1981, 1983; Campa and Coney, 1983; Tooker, 1983; Titley, 1987, 1989, 1991; Hutchinson and Albers, 1992; see reviews in [sections 3.5 and 3.6](#)). In summary, these studies indicate that base-metal, silver, and ferro-alloy mineralization is more commonly related to crust composed of, or underlain by, Precambrian craton, whereas precious-metal mineralization (particularly gold) is more often associated with geosynclinal terranes accreted to the craton. In Nevada, the lithotectonic terranes that have stronger spatial associations with the occurrences may be composed of country-rocks that could have gold content above that of typical “background” values. Country-rocks (and rocks at depth) with higher than normal gold content may be potential source rocks for gold and other ore fluid components, and include mafic extrusive and intrusive igneous rocks and, in particular, pelitic geosynclinal sequences. This is investigated below.

The RM, GC, and JO terranes (spatially associated with the sedimentary rock-hosted occurrences) are composed of deep oceanic pelitic (RM and GC) and terrigenous-clastic (JO) sedimentary sequences (Silberling, 1991). The gold content of unaltered (sulfide-free or sulfide-poor) sedimentary rocks is reported to be restricted to a relatively narrow range, rarely exceeding 5 ppb and generally below 2 ppb (see Korobeynikov and Goncharenko, 1986; Krauskopf, 1979; Rose et al., 1979; Govett, 1983; Korobeynikov, 1985). In a geosynclinal depositional environment, however, pelitic rocks and terrigenous sequences that have undergone *any* alteration, even if only diagenetic, may have comparatively higher gold contents, and could potentially be a source for gold, especially if any degree of pyritization has taken place. Korobeynikov (1985) determined that the gold content of miogeoclinal-eugeoclinal carbonaceous black-shales, with respect to associated carbonate, clastic, and volcanic sequences, is elevated by a factor of 5-10 (6.7-65 ppb), having an estimated average gold content of 14.7 ppb. Pyrite was found to be the main concentrator of gold in carbonaceous shales and other pelitic rocks, containing 27-1360 ppb gold (Korobeynikov, 1985). Aureoles of elevated gold content were controlled by jointing zones, which allowed for influx of diagenetic and other solutions. Given the depositional and deformational history of the Cordilleran geosyncline, it is not unreasonable that assume that the geosynclinal sequences, especially those at greater depths, were affected by a certain amount of alteration, even if only diagenesis (in central Nevada, these units have attained great thickness, perhaps as much as 15 km at time of deposition; Stewart, 1980; Dickinson, 1981; also see [Fig. 2.9](#)). In Nevada, Nelson (1991) observed that many Carlin-type

deposits are spatially associated with rock units reported to contain metalliferous marine black shales, particularly the Vinini, Valmy, Woodruff, and Comus formations. In this study, three of these units—Vinini (Os), Valmy (Osv), and Chainman (MDs)—are found to host ~30% of the sedimentary rock-hosted occurrences (Fig. 6.13) and have especially strong weights of spatial association (Fig. 6.14; also see legend in Fig. 6.24a). The Vinini formation (Os), in particular, is highly correlated with the sedimentary rock-hosted occurrences. The pelitic rocks of the Cordilleran geosyncline may constitute potential pre-enriched source rocks from which, with the aid of induced permeability (i.e.—faults, fractures, stockworks, breccias), gold and other metals were scavenged. This is consistent with the findings of Hofstra (1997) and Hofstra et al. (1991), where new and existing sulfur isotope data from various Carlin-type gold deposits were examined (deposits include Jerritt Canyon, Getchell and Twin Creeks, Carlin, Post-Betze, Alligator Ridge, Gold Pick, Chert Cliff, Mercur, Melco, and the Lone Tree distal-disseminated deposit). Hofstra (1997) concluded that the bulk of  $\delta^{34}\text{S}$  values indicate that  $\text{H}_2\text{S}$  in the ore fluids was derived from a variety of sedimentary sources (values from Jerritt Canyon, Carlin, and Gold Pick are high enough to effectively exclude a magmatic source). Gold and sulfur may have been scavenged from the Cordilleran geosyncline sedimentary pile by deeply circulating meteoric fluids (Hofstra, 1994, 1997; Ilchik and Barton, 1997) or from ascending fluids derived from metamorphic devolatilization at depth (Seedorff, 1991).

The PD, SS, and PN terranes (associated with the volcanic rock-hosted occurrences) are all mainly volcanogenic, with varying degrees of intermediate-mafic rocks and basinal strata (Silberling, 1991). Tilling et al. (1973) reported that unaltered igneous rocks, particularly rocks of intermediate or silicic composition, have a rather restricted range in gold content, rarely exceeding 10 ppb and generally well below 5 ppb, but that mafic rocks tend to have more gold than felsic and intermediate rocks in both plutonic and volcanic suites (also see Gottfried et al., 1972; Korobeynikov, 1986; Korobeynikov and Goncharenko, 1986). The presence of basalt or gabbro might have acted as a pre-enriched source rock, from which circulating hydrothermal fluids could have scavenged gold. However, Tilling et al. (1973) concluded that the concentration of gold in a potential source rock is a trivial factor, and that the differences in gold content among common rock types is too small to consider any particular rock type a more favorable source of gold than another (also see Keays and Scott, 1976).

The lithotectonic terranes that have stronger spatial associations with the occurrences are also coincident with deep-seated regional-scale crustal tectonic zones. As previously discussed in chapter 3 (section 3.4) and earlier in this section, zones of structural deformation could facilitate vertical and lateral fluid movement, as well as promote fluid-wall rock interactions. The RM, GC, and JO terranes represent north–northeast-trending mid-Paleozoic to mid-Mesozoic allochthons, emplaced along the Roberts Mountain, Golconda, and Luning-Fencemaker thrust faults, respectively (see Figs. 2.4, 2.5, and 2.13; section 2.7.1; also see Hardyman and Oldow, 1991; Silberling, 1991). The orientation and location of the overthrusts coincide with the Late Proterozoic rifted margin of the North American craton, as delineated by  $^{87}\text{Sr}/^{86}\text{Sr} \text{ } I_{\text{Sr}} = 0.706$  and a late Paleozoic or early Mesozoic regional-scale paleothermal anomaly (Figs. 2.10 and 2.11). The rifted craton margin, a zone of crustal weakness and a suture along which terrane accretion took place, could have focused and localized mineralizing processes (see Cunningham, 1988; also see sections 2.4 and 3.4). The PD, SS, and PN terranes are located within the Walker Lane shear zone (see section 2.6). The Walker Lane crosscuts the older northeast-southwest Paleozoic orogenic grain that is tectonically truncated against the younger northwest-southeast Mesozoic

orogenic grain, and may be related to rifting and/or translational activity which took place during the early Mesozoic (the “*Early Mesozoic truncation event*”; Silver and Anderson, 1974; Dickinson, 1981; Suppe, 1985; also see [section 2.6](#)). The Walker Lane also has an extensive history of Cenozoic strike-slip movement (see Stewart and Crowell, 1992) and may coincide with a possible major crustal flaw zone, perhaps dating back to the Precambrian (Blakely and Jachens, 1991). As noted above, such a regional-scale structure could have focused and localized mineralizing processes and provided the tectonic conditions that permitted the formation of volcanic rock-hosted deposits (Cox et al., 1991).

From the spatial analyses carried out in this section, it is not possible to isolate exactly why lithotectonic terranes are important to the formation of gold-silver-bearing occurrences in Nevada. However, it would seem that an association with lithotectonic terranes composed of pre-enriched source rock could be a significant factor for sedimentary rock-hosted mineralization, whereas it may not be critical for the formation of volcanic rock-hosted occurrences. Ore depositing fluids in volcanic rock-hosted mineralizing systems appear to have important magmatic-derived components (see Rock and Groves, 1988; Rock et al., 1989; Giggenbach, 1992a, 1992b, 1992c; Muffler et al., 1992; Hedenquist and Lowenstern, 1994; Hedenquist et al., 1996; Taylor, 1996; Norman et al., 1996). For both sedimentary and volcanic rock-hosted mineralization, it seems that proximity to regional-scale structural features could facilitate mineralization. Perhaps of more importance to the formation of gold-silver-bearing occurrences in Nevada is the focusing of mineralizing processes by crustal structures associated with the lithotectonic terranes, which serve only to provide physiochemically suitable host rocks rather than pre-enriched source rocks.

## 6.5 Distance Buffers Around Plutons and Faults

### 6.5.1 Introduction and Summary of Findings

The distribution and spatial association of the gold-silver-bearing occurrences in relation to distance from plutonic bodies ([Fig. 6.36](#)) and faults ([Fig. 6.37](#)) are reviewed in this section. Maps of distance buffers from plutonic bodies ([Fig. 6.36b](#)) and faults ([Fig. 6.37b](#)) were prepared using data from the geological map of Nevada (Stewart and Carlson, 1978).

The plutonic rocks examined here range in age from Late Triassic to Late Miocene, but with respect to total area covered, are predominantly Mesozoic ([Fig. 6.36a](#)). Strictly Mesozoic rocks (Mzgr, Kgr, KJd, Jgr, Trgr) make up ~81% of the total area of all the plutonic rocks combined, and range in composition from granitic to dioritic and quartz-monzonitic. Rocks transitional between Cretaceous and Tertiary age include only one unit, TJgr, which makes up less than 3.6% of the combined total area, and is granitic in composition. The Cenozoic rocks (Tgr, Tri, Tmi, Ti) are Tertiary (~43-6 Ma) intrusions, ranging in composition from felsic to intermediate, with some mafic units, and make up nearly 20% of the combined total area. Conventional wisdom indicates that, for whatever the reason, genetic or otherwise, metallic mineralization is often found proximal to plutonic and intrusive igneous rocks. A map of relative spatial-density of plutons was constructed for Nevada ([Fig. 6.36c](#)), and the density distribution map pattern was found to bear a close resemblance to the map pattern for the density distribution of occurrences ([Fig. 6.36d](#)) (even more so to the density distribution map pattern for precious and base metal



mineralization; compare to [Fig. 6.3](#)). It is therefore reasonable to investigate the spatial association between occurrences and plutonic rocks in the Great Basin. Plutonic and intrusive bodies were buffered at intervals of 0.0–0.5, 0.5–1.0, 1.0–1.5, 1.5–2.5, 2.5–5.0, and 5.0–10.0 km.

The faults examined here are those which appear on the geological map of Nevada (Stewart and Carlson, 1978) ([Fig. 6.37a](#)), and include faults that are mapped as solid lines, dashed lines, dotted lines, or otherwise inferred (see Turner and Bawiec, 1991). The faults are of all ages, but predominantly Cenozoic, and include thrust, strike-slip, normal and reverse. No differentiation was made between fault type, age, or orientation<sup>4</sup>. On the deposit and district level, faults are known to be important ore controls and conduits for mineralizing fluids, and play a large part in “ground preparation”, which make the potential host rocks more receptive or more reactive to ore-bearing solutions (Guilbert and Park, 1986). Berger (1996) indicated that, empirically, it may be inferred that epithermal orebodies form preferentially in constraining structural environments within active faults. Fluid flow systems always show coupled mechanical, thermal, and hydraulic phenomena (Byron R. Berger, 1998, personal communication). The rate of change of synhydrothermal deformation may be a key aspect of focusing fluids and establishing environments favorable to efficient ore-depositing processes (Berger, 1996). Given the tectonic history of the Great Basin, it would therefore seem probable that a spatial relationship between faults and occurrences should exist, and the coupling of stress and fluid flow is the plausible argument (Byron R. Berger, 1998, personal communication). An analysis of fault distance buffers with respect to the location of mineral occurrences is one manner by which this relationship can be quantified in order to help predict precious metal mineralization. The fault dataset was buffered at intervals of 0.0–0.5, 0.5–1.0, 1.0–1.5, 1.5–2.5, 2.5–5.0, and 5.0–10.0 km ([Fig. 6.37b](#)). The relative concentration of faults per unit area is shown in [Figure 6.37c](#).

The most significant results of the analyses carried out in this section suggest that gold-silver-bearing occurrences in Nevada have a strong spatial association with areas of close to moderate proximity (1.0–2.5 km) to plutons, and close proximity (1.0–1.5 km) to faults. Sedimentary rock-hosted occurrences also show a moderate spatial association with distance (2.5–5.0 km to 5.0–10.0 km) from plutonic and intrusive bodies. These results indicate that fault zones and structural deformation related to regional-scale plutonism may have facilitated formation of the gold-silver-bearing occurrences.

### **6.5.2 Distribution and Spatial Association of Gold-Silver-Bearing Occurrences**

The distribution of occurrences, relative to pluton buffers, indicates that a nearly equal number fall within 0.5 km of (or in) plutonic bodies (22.2%) as do outside the outermost buffer zone (>10.0 km, 23.7%) ([Fig. 6.38](#)). However, only ~12% of the big occurrences fall within 0.5 km

---

<sup>4</sup> Azimuthal filtering of the fault dataset by the application of a binomial probability distribution technique (Donald L. Sawatzky, 1994, personal communication) determined that statistically significant fault orientations lie between N35W and N29E, forming an envelope of approximately 30° either side of north. A comparison of the strength of spatial correlation (contrast, C) between the occurrences and the azimuthally filtered datasets was found to be not as strong as the spatial relationship between the occurrences and the unfiltered dataset, hence the filtered fault dataset was not used for this analysis.

of (or in) plutonic bodies, the majority (48.6%) lie 5-10 km (19.2%) and >10 km (29.4%) away. Approximately 45% of all occurrences fall in or within 2.5 km of plutons, and just over 50% of the big deposits lie in or within 5 km of plutonic bodies. The volcanic rock-hosted occurrences have a distribution trend across the buffer zones that is somewhat similar to the primary occurrences, however, the greatest number of occurrences (~41%) fall 5-10 km (~20%) and >10 km (~21%) away from plutonic bodies, whereas only ~11% occur in or within 0.5 km of a pluton (Fig. 6.39). Approximately 60% of all volcanic rock-hosted occurrences lie in or within 5 km of a pluton. The distribution of sedimentary rock-hosted occurrences differs substantially from the distribution trends of both the primary occurrences and the volcanic rock-hosted occurrences. The highest number of sedimentary rock-hosted occurrences are located at a distance from plutonic bodies (Fig. 6.39). Approximately 23.5% of all occurrences lie in or within 2.5 km of plutonic bodies, whereas ~76.5% lie further than 2.5 km away from a pluton, the greatest number of occurrences (nearly 37%) lying >10 km away. The spatial association between occurrences and the proximity to plutonic bodies is strongest for primary occurrences within 1 km, strongest for sedimentary rock-hosted occurrences within 1.5 km, and strongest for big size and volcanic rock-hosted occurrences within 2.5 km of a plutonic or intrusive body (Fig. 6.40).

Approximately half of all the occurrences, of any of the occurrence type or big or small size samples, fall within 1 km of a fault (or fault zone)—greater than 50% of the primary occurrences, >64% of the big size occurrences, ~57% of the sedimentary rock-hosted occurrences, and >49% of the volcanic rock-hosted occurrences (Fig. 6.41 and 6.42). The 1 km buffer for all of the faults collectively represents ~27% of the total area of Nevada. The majority of occurrences in each of the occurrence-type or size samples fall within 0.5 km of a fault—just over 32% of the primary occurrences, >41% of the big size occurrences, >28% of the sedimentary rock-hosted occurrences, and ~31% of the volcanic rock-hosted occurrences. The 0.5 km buffer for all of the faults collectively represents ~16% of the total area of Nevada. There are also a relatively large proportion of occurrences beyond 2.5 km of a fault (~10% for any occurrence-type or size sample) and a significant number (about 8% for any occurrence-type or size sample) farther than 5 km from a fault. Outside of 10 km, only about 1% of the small size and volcanic rock-hosted occurrences are found, but none of the big size or sedimentary rock-hosted occurrences. The distribution of sedimentary versus volcanic rock-hosted occurrences shown in Figure 6.42 suggests that sedimentary rock-hosted occurrences (as a group) may be somewhat more closely distributed around faults than are volcanic rock-hosted occurrences. The spatial association between occurrences and the proximity to faults is strongest for primary occurrences within 5 km, strongest for big size, sedimentary and volcanic rock-hosted occurrences within 1.5 km (Fig. 6.43).

Based on the above relationships, two binary mineral potential predictor maps were produced, one from the pluton buffer map and a second from the faults buffer map (Fig. 6.44). Both maps are a combination of distance buffers that have high spatial associations with primary occurrences, sedimentary rock-hosted occurrences, and volcanic rock-hosted occurrences. The binary predictor map based on distance buffers from plutonic and intrusive bodies is a combination of buffer zones 1 and 2 (0.0-0.5 and 0.5-1.0 km), a 1.0 km threshold. The binary predictor map based on distance buffers from faults is a combination of buffer zones 1 and 2 (0.0-0.5 and 0.5-1.0 km), a 1.0 km threshold.



### 6.5.3 Correlations and Interpretive Synthesis

The strong spatial correlation between the occurrences and the plutonic and intrusive rocks may be related to structural modifications made to the country rocks during emplacement, which may have affected the crust at deeper levels and on a regional scale, and could be a product of older pre-Cenozoic events. Most of the plutonic rocks in western Nevada were emplaced in the Mesozoic during the Nevada-Elko phase of the Cordilleran orogeny when the continental magmatic arc was developing. This was well before most of the sedimentary and volcanic rock-hosted occurrences formed, 42-30 Ma (Hofstra, 1997) and 27-5 Ma (Ludington et al., 1993), respectively (see [Fig. 3.2](#)).

The emplacement of plutonic rocks is often accompanied by a high degree of structural modification to the surrounding country rocks (see Billings, 1972, chapter 17). At intermediate crustal depths, surrounding material is heated and compressed and transported laterally away from the zone of emplacement (Gastil, 1979; also see Paterson and Fowler, 1993). Upper crustal rocks respond by undergoing lateral extension along brittle high- and low-angle and strike-slip structures, while lower crustal rocks are thought to move laterally by ductile flow (Gastil, 1979; also see Christie-Blick and Biddle, 1985; Sonder and England, 1986; Gans et al., 1989; Thompson et al., 1989; Armstrong and Ward, 1991; Buck, 1991). Shearing at depth may also act to accommodate mid-crustal mass transfer (see Allmendinger et al., 1987; Hauge et al., 1987; Potter et al., 1987; Kusznir and Matthews, 1988; Malavieille and Taboada, 1991; Snyder et al., 1997). Strain related to pluton emplacement can result in an overall increase in permeability at both the upper and lower crustal levels (an increase in strain from 1% to 6% is capable of producing a five order of magnitude or greater increase in permeability; Spiers and Peach, 1989; see discussion in [sections 2.7.6, 2.7.7, and 3.4](#)). Hence, ductile flow and shear structures at depth could facilitate the transfer of heat and fluids from the lower crust and increase fluid-wall rock reaction-surface areas from which circulating fluids could scavenge metals. Brittle structures in the shallow crust could promote near-surface fluid circulation, focusing and localizing mineralizing processes, as well as creating favorable environments for mineral deposition (e.g.—structural traps). Cenozoic magmas and deeply circulating ore fluids may have taken advantage of the structural pathways and reaction-surface areas that the Mesozoic plutons could have provided, thus perhaps explaining in part the strong spatial association between the plutons and the occurrences.

The high degree of spatial association between the occurrences and close proximity to faults is not unexpected. Fault and shear zones have long been recognized as important conduits for the movement of fluids within the crust. This is well established from geochemical studies of alteration and mineralization in ancient structures and from contemporary observations related to seismic events (Kerrick, 1986). Crustal fluids play mechanical and chemical roles in a host of geologic phenomena which include faulting and shearing, magma generation, metamorphism, hydrocarbon migration, and transport of minerals (Kerrick, 1986; Oliver, 1986; Sibson, 1987). In the North American Cordillera, Eaton (1984) suggested that the circulation of hydrothermal fluids through extensional structures was the most important process responsible for Cenozoic ore formation. Similar associations are observed in Precambrian mid-crustal mesothermal deposits within compressional shear zones, such as those of the Canadian greenstone metamorphic belts (e.g.—Yellowknife, Larder Lake, Timmins, and many other shear zone hosted gold deposits). The degree and extent of mineralization associated with highly faulted and

sheared regions demonstrates how important these structures are to focusing fluid movement.

In the Great Basin, faults, fault zones, rift zones, and related structures are important to precious metal mineralization at the province-wide, regional, and local levels. At the province-wide scale (deep crustal), structural zones could provide throughgoing lower-crust–upper-mantle permeability, promoting whole-crust fluid circulation, and assisting in the transference of heat by allowing warmer lower-crustal fluids and melts to more easily penetrate and migrate to higher crustal levels. At the regional scale (shallow crustal and mineral belt), structures may control localization of intrusions, volcanic fields, high-level thermal anomalies, meteoric hydrothermal convection cells, and individual gold deposits (see Rowley, 1996, for example; also see [section 3.4](#)). Linear alignments of igneous features and possible basement flaws are believed to be present at several Cretaceous and Cenozoic gold deposits (see Bagby and Berger, 1985; Madrid and Bagby, 1986; Berger and Bonham, 1990; Shawe, 1991; Rodriguez, 1997; also see [sections 3.2.2](#), [3.3.2](#), and [3.4](#)). In many volcanic rock-hosted and pluton-centered deposits, intrusions acted as heat engines driving hydrothermal convection. Brittle faulting of upper crust provides “plumbing”, which promotes permeability and facilitates near surface and deep fluid circulation. Regional-scale shear and fault zones form fluid pathways that serve to concentrate and direct hydrothermal gold-bearing solutions (Bagby and Berger, 1985), as well as “structurally prepare” potential source rocks by effectively increasing the fluid-wall rock reaction-surface area, enhancing the leaching of metals from the rocks. At the local scale (deposit and ore body), faults may control the loci of mineral deposition, as well as determine the orientation of various fault-related structural traps, such as veins, fractures, stockworks, breccia pipes, and shatter zones. Faults and related secondary permeability structures facilitate physiochemical reactions that may induce mineral precipitation (e.g.—“fluid throttling”), and expose geochemically favorable environments to precious metal-bearing fluids where mineral precipitation may take place. Along the Carlin-trend, for example, sedimentary rock-hosted deposits and ore bodies are localized within favorable stratigraphic intervals near controlling local faults (see Bagby and Berger, 1985; Bakken and Einaudi, 1986; Percival et al., 1988).

## 6.6 Geophysics—Geomagnetic and Gravity Anomalies

### 6.6.1 Introduction and Summary of Findings

The distribution and spatial association of the gold-silver-bearing occurrences in relation to the total residual field geomagnetic and isostatic residual gravity anomalies are reviewed in this section ([Fig. 6.45](#)). The maps were prepared from data obtained from the National Oceanic and Atmospheric Administration.

Gravity and geomagnetic studies are complementary methods that are very valuable to mineral exploration (for comprehensive reviews, see Overstreet and Marsh, 1981; Blakely and Connard, 1989; Simpson and Jachens, 1989). They provide information about local- and regional-scale subsurface crustal structures and igneous rocks important to mineralization and ore formation, and contribute to the delineation and interpretation of the geologic development of a region. Geomagnetic anomalies are produced by contrasts in the magnetic properties of various rock types (primarily at shallow crustal levels, and in particular, igneous rocks). Magnetite ( $\text{Fe}_3\text{O}_4$ ) and its solid solutions with ulvöspinel ( $\text{Fe}_2\text{TiO}_4$ ), and in some situations a few other Fe-bearing minerals and compounds (usually hematite and pyrrhotite), are the most important magnetic

minerals, hence basalts and their intrusive equivalents are usually more magnetic than rhyolites and their equivalents (Mabey, 1983; Blakely and Connard, 1989). Anomalies originating from shallow (<1 km) sources (local) are higher in amplitude and shorter in wavelength, and appear “sharp” and well-defined, whereas anomalies originating from deeper sources (regional) are generally lower in amplitude and longer in wavelength, and appear broad and “smoother” (Blakely and Jachens, 1991; Saltus, 1988). Gravity anomalies (Bouguer or isostatic) are the result of lateral and vertical variations in rock density. Bouguer gravity anomaly maps emphasize regional signatures, originating as deep as the lower crust and upper mantle, whereas isostatic anomaly maps, the data being corrected for the regional effect of topographic compensation, isolate and emphasize small but broad intracrustal gravity anomalies, more clearly reflecting the shallow density distributions of the upper crust (Mabey et al., 1983; Saltus, 1988; Blakely and Jachens, 1991). Some of the more prominent magnetic and gravity anomaly features in Nevada are listed in [Figure 6.45](#).

The analysis in this section focuses on the total residual field geomagnetic and isostatic residual gravity anomalies, both of which emphasize somewhat different geologic structures and features in the shallow and upper crust. The Bouguer anomaly map is used to facilitate interpretations and for visual comparisons. Initial trials using the Bouguer and isostatic gravity datasets revealed that the isostatic gravity anomaly possessed a significantly better overall spatial correlation with the occurrences than did the Bouguer anomaly. In addition, the isostatic gravity dataset is a derivation of the Bouguer dataset, and as such, displays spatial patterns similar to those of the Bouguer anomaly.

The most significant results of the analyses carried out in this section suggest that sedimentary rock-hosted occurrences tend to occur in regions of lower intensity geomagnetic anomalies (0 nT and less) and higher intensity isostatic gravity anomalies (0 mG and greater), whereas volcanic rock-hosted occurrences tend to occur in regions of higher intensity geomagnetic anomalies (greater than 50 nT) and lower intensity gravity anomalies (-10 mG and less). On a regional scale, the geophysical character of these two deposit types suggest that: (1) sedimentary rock-hosted occurrences are associated with tectonically over-thickened crust, which is predominantly sedimentary in nature, generally lacking in late Cenozoic volcanism, and proximal to possible deep-seated structural features (e.g.—northern Nevada rift zone); and (2) volcanic rock-hosted occurrences are associated with crustal segments that lie along (or within) broad and diffuse structural zones, which have been subjected to wide-spread felsic volcanic activity and intruded by mafic and intermediate magmas (e.g.—Walker Lane belt; Humboldt zone). The occurrences are associated with contrasts in magnetic and gravity anomaly intensities, which are transitional between high and low values, suggesting a close spatial relationship to structural features that might act to facilitate fluid movement and/or host ore deposits.

### **6.6.2 Distribution and Spatial Association of Gold-Silver-Bearing Occurrences**

The frequency of occurrences display a fairly normal distribution across the magnetic intensity spectrum ([Fig. 6.46](#)), centered slightly to the negative side of the zero value, and correlate closely with the map area represented by each anomaly interval. Most of the occurrences (~39%) fall between -75 to +25 nanoteslas (nT), representing ~38% of the total area of Nevada, with the greatest number of occurrences (~11%) falling in the -50 to -25 nT range, representing ~11% of

the total area of the Nevada. The sedimentary and volcanic rock-hosted occurrences also show near-normal distributions (Fig. 6.47), but the distribution peaks of the occurrence samples are significantly offset—the distribution peak of the volcanic rock-hosted occurrences is offset toward the positive anomaly values (centered on 0 to +25 nT), whereas the sedimentary rock-hosted occurrence sample is offset more toward the negative anomaly values (centered on -75 to -50). The volcanic rock-hosted occurrences are also found over a broader range of magnetic anomaly values. This relationship indicates that sedimentary rock-hosted occurrences are preferentially located in areas of generally lower intensity magnetic anomalies, while volcanic rock-hosted occurrences are located in regions having generally higher values. The spatial association between the occurrences and the magnetic anomaly reaches its maximum strength in the low positive anomaly values (peaking at 0 nT) for the primary and volcanic rock-hosted occurrences. The >+450 to -200 nT intensity range accounts for about 55% of the volcanic rock-hosted and ~42.5% of the primary occurrences, and for both occurrence samples represents ~29% of the total area of Nevada. The big size and sedimentary rock-hosted occurrences reach maximum strength of spatial association with the magnetic anomaly in the middle range of anomaly intensity (peaking at -200 and -175 nT, respectively) (Fig. 6.48). The >+450 – -175 to -200 nT intensity range accounts for virtually all (>98%) of the big size and sedimentary rock-hosted occurrences, and represents nearly 95% of the total area of Nevada. The sedimentary rock-hosted occurrences have a strong spatial association (non-area-cumulative) with a relatively narrow range of lower intensity magnetic anomalies (-100 to 0 nT), as shown in Figure 6.48 by the heavy black line segment of the non-area-cumulative contrast (C) curve.

The distribution of primary occurrences is near normal across the isostatic gravity intensity spectrum (Fig. 6.49), the peak slightly offset toward the negative values (centered on -10 to 0 milligals), and correlates to the area of each anomaly interval. Most of the occurrences (~34%) fall in the -10 to 0 milligal (mG) interval, representing ~28% of the total area of Nevada, with the greatest number (nearly 29%) falling in the 0 to +10 mG interval, representing ~18% of the total area of Nevada. The distributions of the sedimentary and volcanic rock-hosted occurrences are skewed—the sedimentary rock-hosted occurrence toward positive values, and the volcanic rock-hosted occurrences toward negative values (Fig. 6.50, see trend lines). Sedimentary rock-hosted occurrences clearly have a preference for regions having higher isostatic gravity levels, whereas the volcanic rock-hosted occurrences tend toward regions of lower isostatic gravity. The non-area-cumulative C curves for the isostatic gravity anomaly (Fig. 6.51) indicate that the big size and sedimentary rock-hosted occurrences have positive spatial associations with 0 to >+10 mG intensities, cumulatively representing ~25% of the total area of Nevada, and accounting for ~43.5% of the big size and ~69% of the sedimentary rock-hosted occurrences. The sedimentary rock-hosted occurrences show an especially strong association with the highest isostatic gravity anomaly intensity interval (>10 mG), representing ~7% of the total area of Nevada, but accounting for nearly 41% of the occurrences—a rather notable correlation. The volcanic rock-hosted occurrences show the highest degree of spatial association with anomaly intensity values of -20 to -10, representing ~26% of the total area of Nevada and ~36% of these occurrences. Once again, the volcanic rock-hosted occurrences display a partiality for the lower end of the isostatic gravity anomaly spectrum, while the sedimentary rock-hosted occurrences show a bias for the higher end of the spectrum.

Based on the above relationships, two sets of three binary-class mineral potential predictor maps were produced from the magnetic and isostatic gravity geophysical anomaly maps, one for each

of the three occurrence samples (primary occurrences, sedimentary rock-hosted occurrences, and volcanic rock-hosted occurrences) (Fig. 6.52). For the magnetic anomaly map, the 19 highest intensity intervals were combined for the primary occurrences binary predictor map, and the 17 highest intervals were combined for the volcanic rock-hosted occurrence binary predictor map. In both cases, the threshold intensity interval was determined using the area-cumulative contrast (C) maximum. The volcanic rock-hosted occurrences binary predictor map excludes the two intensity intervals with the highest C values (hence combining 17 rather than 19 map successive classes) in order to emphasize the relation between the occurrences and the volcanic rocks that the anomalies represent. The sedimentary rock-hosted binary predictor map was produced by combining a group of four successive map classes that had the highest non-cumulative C values (Fig. 6.48, black segment of dashed curve). The magnetic binary predictor map for primary occurrences accounts for ~42.5% of the occurrences, and represents ~29% of the total area of Nevada. For the isostatic gravity anomaly map, the three highest intensity intervals were combined for the primary occurrences binary predictor map, and the highest intensity interval was used for the sedimentary rock-hosted occurrence binary predictor map. The volcanic rock-hosted occurrences binary predictor map is a combination of two successive map classes (intensity intervals 0 to -10 and -10 to -20) that, in combination, displayed the strongest weights of association with the occurrence, but especially important, yielded a more geologically meaningful binary map pattern than did other combinations of gravity map classes.

### 6.6.3 Correlations and Interpretive Synthesis

The gold-silver-bearing occurrences display two distinct frequency distribution trends with respect to the magnetic and isostatic gravity anomalies: (1) the sedimentary rock-hosted occurrence sample distribution mode is offset from zero toward negative magnetic anomaly values, and toward positive gravity anomaly values; and (2) the volcanic rock-hosted occurrence sample distribution mode is offset from zero toward positive magnetic anomaly values, and toward negative gravity anomaly values, an inverse relationship relative to the sedimentary rock-hosted occurrences sample (see Figs. 6.47 and 6.50).

The following two sections discuss the spatial relationship between various regional-scale crustal features interpreted from the geophysical data and the distribution of the sedimentary and volcanic rock-hosted occurrences. This material is expanded upon and the ideas further developed in [chapter 8](#).

#### 6.6.3.1 Sedimentary Rock-Hosted Occurrences: Geomagnetic Lows—Isostatic Gravity Highs

The frequency distributions for sedimentary rock-hosted occurrences, skewed toward negative magnetic values and positive isostatic gravity values, indicate that these occurrences tend to be found in regions characterized by less magnetic and higher density rocks (i.e.—regions having lower magnetic anomalies and higher isostatic gravity anomalies). [Figures 6.53a](#) and [6.54a](#) show the spatial distribution of magnetic and isostatic gravity anomalies associated with these occurrences. The geographic regions that these geophysical anomalies cover, especially the magnetic anomaly, are broadly correlative in extent with the circular-shape distribution pattern of the sedimentary rock-hosted occurrences, which form a “core” lying inward of the crescent-shape volcanic rock-hosted occurrences (compare to [Fig. 6.2](#)).



**Magnetic anomaly lows** in Nevada are generally associated with rhyolitic and related tuffaceous rocks, granitic rocks, and other non-igneous rock-types which are deficient (relative to mafic rocks) in magnetic minerals. The most prominent low-amplitude negative anomaly is the “magnetic quiet zone” (Figs. 6.45a, feature #3, and 6.53a). The magnetic quiet zone forms a north-trending zone along eastern Nevada that extends from a broad, low-amplitude, regional-scale magnetic low in the northeastern quadrant of Nevada to a smaller, circular region of very low magnetic intensity in southernmost Nevada, known as the “amagmatic zone.” The amagmatic zone marks the southern termination of the southwestward sweep of Tertiary volcanism (McKee, 1971; see Fig. 6.4), and may be non-magnetic simply because it was not affected by magmatism that occurred prior to 17 Ma (Blakely and Jachens, 1991). The broad portion of the magnetic quiet zone in northern Nevada corresponds to widespread coverage of thick sections of sedimentary rocks produced by late Paleozoic and Mesozoic overthrusting (Berger and Henley, 1989; see Figs. 2.4, 2.5, and 2.6), which may in part be responsible for the regional low (sedimentary rocks are commonly less magnetic than igneous rocks). The origin of magnetic quiet zone in northern Nevada may be quite complex, and is perhaps a product of regional-scale hydrothermal alteration, which effectively reduced the magnetic qualities of the quiet zone rocks, or is related to a belt of granitoids of low magnetic susceptibilities and remnant magnetizations, which are localized along the western edge of the craton margin (see Blakely, 1988, for full discussion).

**Isostatic gravity anomaly highs** in Nevada are related to rocks, or packages of rocks, of higher density. On a local level, gravity highs generally correlate with ranges where pre-Tertiary basement rocks are near the surface (Blakely and Jachens, 1991). On a much broader regional-scale, particularly in northern and northeastern Nevada, gravity highs correlate with the tectonically over-thickened crust (Berger and Henley, 1989; see Figs. 2.4, 2.5, and 2.6), which represents upward thrust emplacement of deeper-origin, *higher density* packages of rock (Blakely and Jachens, 1991; Saltus, 1988). The two isostatic gravity anomalies of principal concern in Nevada are a “gradient ridge” associated with the possible southern extension of the northern Nevada rift and the Humboldt zone gravity high (Figs. 6.45b, feature #1; 6.45b, feature #5; and 6.54a).

The Humboldt zone isostatic gravity high stretches northeast-southwest across northern Nevada, and is well distinguished in the northwestern quadrant of Nevada by a Bouguer gravity high, and, of particular interest, is correlative in broad extent with the magmatic quiet zone in the northeastern quadrant of Nevada (Figs. 6.45a, feature #3; 6.45b, feature #5; and 6.53a). As indicated above, the northeastern portion of this anomaly is coincident with tectonically over-thickened crust. The Humboldt zone is also correlative with a wide band of Cenozoic volcanism that trends northeast-southwest across northern Nevada (compare Figs. 6.45b and 6.4). The delineation, character, origin, and the relationship of the Humboldt zone to the distribution of the sedimentary and volcanic rock-hosted occurrences is further discussed in chapter 8.

The northern Nevada rift is most readily recognized by its geomagnetic signature (Fig. 6.45a, feature #1; also see section 2.7.4). Associated with the geomagnetic trace of the rift zone is a well-defined isostatic gravity “gradient-ridge”, which borders the magnetic anomaly on the west for ~250 km of its length, and continues south beyond the terminus of the magnetic anomaly, extending nearly as far as the amagmatic zone (see Figs. 6.45b, feature #1, and 6.54). The gravity gradient-ridge anomaly indicates that the northern Nevada rift may be at least 600 km

long in Nevada alone (Blakely, 1988; Blakely and Jachens, 1991). The origin of the anomaly may be related to, for example, the fault juxtaposition of low-density volcanic and sedimentary rocks filling down-thrown structures, and higher-density basement rocks composing up-thrown blocks. The gradient ridge may also reflect density increases or decreases related to complex structural features associated with the rift zone (e.g.—decreases in bulk rock density caused by wide-spread fracturing related to fault or shear zones, or increases in bulk rock density caused by igneous rocks that may have intruded along the rift zone). The isostatic gravity gradient ridge is also coincident with an axis of bilateral symmetry in the Bouguer gravity anomaly (Fig. 6.45c, axis of the “butterfly-shaped” low, centered just southeast under the number “1”), suggesting that the isostatic gravity anomaly associated with the rift may originate in the basement (Blakely and Jachens, 1991). The northern Nevada rift, including its southeastern extension as imaged by gravity anomaly, runs subparallel to the Battle Mountain–Eureka (Cortez) and Carlin sedimentary rock-hosted mineral trends, and is particularly well correlated to the southern half of the Battle Mountain–Eureka (Cortez) trend (compare Figs. 1.3 and 6.2 to Figs. 6.53 and 6.54). As indicated numerous times previously, proximity to a regional-scale structure may serve to focus mineralizing processes.

In summary, the lower magnetic and higher isostatic gravity anomalies (Figs. 6.53a and 6.54a) suggest that, on a regional scale, the sedimentary rock-hosted occurrences are associated with *shallow* crust that is:

- Tectonically over-thickened (see Fig. 6.5d).
- Predominantly sedimentary in character (Fig. 6.56a).
- Relative to surrounding areas, generally lacking in late Cenozoic mafic volcanism and, relative to other regions of Nevada, generally less affected by post–43–34 Ma volcanism (Figs. 6.55, 6.56b, and 6.4).
- Associated with numerous possible deep-seated and upper crustal structural features, including the western craton margin (see Fig. 2.11), the northern Nevada rift zone and its possible extension southeastward, and major thrust faults and thrust root zones (specifically the Roberts Mountain and Golconda thrusts; see Fig. 2.5).

### 6.6.3.2 Volcanic Rock-Hosted Occurrences: Geomagnetic Highs—Isostatic Gravity Lows

The frequency distributions for volcanic rock-hosted occurrences, offset toward positive magnetic values and skewed toward negative isostatic gravity values, indicate that they tend to be found in regions characterized by more magnetic and less dense rocks. The spatial distribution of the magnetic and isostatic gravity anomalies associated with these occurrences is shown in Figures 6.53b and 6.54b. The regional distribution of these geophysical anomalies share broadly similar patterns with the crescent-shaped distribution of the volcanic rock-hosted occurrences, especially in the region of the Walker Lane shear zone (compare to Fig. 6.2).

**Magnetic anomaly highs** in Nevada are primarily associated with basaltic and gabbroic rocks, which contain a relative abundance of magnetic minerals. Three most prominent high-amplitude positive magnetic anomalies (or anomalous regions) are (1) the northern Nevada rift zone, (2) the Walker Lane shear zone, and (3) northwestern Nevada, just northwest of a regional geomagnetic low and isostatic gravity high associated with the Humboldt zone (Figs. 6.45a, features #1, #1a, #2, and #5; 6.53, and 6.54).



The northern Nevada rift zone is most prominently recognized as a long, narrow, and well-defined regional magnetic high, trending north-northwest for 280 km through north-central Nevada, the source of which may extend to a depth of 15 km (Blakely and Jachens, 1991; also see Christiansen and Yeats, 1992). The rift zone is characterized by linear dike swarms and associated lavas (basalt and basaltic andesite) of 17 to 14 Ma age, by a fault-bounded trough, and by a northwest-southeast topographic grain, and has been interpreted to be the surface expression of a deep-seated fracture zone that may have had a complex history of transcurrent movement (see [section 2.7.4](#)). The magnetic signature of the rift suggests that the structure extends only as far south as central Nevada (~N 39° 20' to N 39° 40'), but gravity data suggest that it may extend further southeast into southern Nevada (see [previous section](#)). Blakely and Jachens (1991) suggested that the basaltic and andesitic extrusive and intrusive rocks associated with the northern portion of the rift zone might also be found along its southeastern extension, but if such rocks are present, they remain concealed.

The Walker Lane shear zone is a northwest-trending structural zone 700 km long and from 100 to 300 km wide containing both right-lateral and left-lateral faults. It is currently active, but may have developed primarily during the late Cenozoic, though it may have older origins (see [section 2.6](#)). The Walker Lane is magnetically characterized by a pattern of arcuate anomalies that trend northwestward, generally parallel to the shear zone. Blakely and Jachens (1991) noted that the width of the magnetic anomalies is considerably wider than the structural or topographic expression of the shear zone, extending in some places more than 150 km north-northeast of the Walker Lane and into (under?) basin-range topography characterized by north to northeast structural trends. Further, Blakely and Jachens (1991) suggested that the magnetic anomalies may indicate an underlying tectonic fabric older than modern topography and exposed geology that is perhaps related to the Precambrian breakup of North America. The greater number of higher magnetic anomalies in the Walker Lane belt may also be related to intermediate and mafic rocks, which are more common in western and southwestern Nevada, and more abundant around the margin of the Great Basin in general (see [Fig. 6.55](#)). As with the possible southeastern extension of the northern Nevada rift, mafic and intermediate rocks may intrude the Walker Lane at depth, but are nowhere exposed at the surface.

In northwestern Nevada, a broad belt of patchy geomagnetic highs extends northeast-southwest across the region ([Figs. 6.45a](#), feature #5, and [6.53b](#)). This band is delineated in part by a similarly oriented band of magnetic anomaly lows to the southeast, which is prominently transected by the northern Nevada rift anomaly and west-flanking rift anomalies ([Fig. 6.45a](#), features #1 and #1a). At the regional scale, the juxtaposition of these two magnetic high-low anomaly bands corresponds to the Humboldt zone gravity anomaly high, which stretches northeast-southwest across northern Nevada ([Fig. 6.54a](#)). The magnetic anomaly highs across northwestern Nevada probably reflect the outpourings of Tertiary and younger mafic volcanics in the region and possibly their presence at depth (units such as QTb, Tb, Tba, Tbg, and Tob; see [Appendix A](#)).

**Gravity anomaly lows** in Nevada are related to rocks of lower density, or attributes which effectively lower the density of rocks, such as wide-spread fracturing related to fault and shear zones (Telford et al., 1976; also see Jachens et al., 1989). In Nevada, isostatic gravity lows generally correlate with sediment and volcanic rock-filled inter-range basins, and with the presence of felsic intrusions (Mabey et al., 1983; Saltus, 1988; Blakely and Jachens, 1991). The

dominant feature, visible in both the isostatic and Bouguer anomalies, is a regional-size gravity low that stretches from the Nevada-Utah border across the center of the state into the Walker Lane region (Figs. 6.45b, 6.45c, 6.54b). This low, flanked to the north and south by gravity highs, reflects sources in the pre-Tertiary basement, but its strongest correlation is with the distribution of thick accumulations of Cenozoic volcanic rocks (Blakely and Jachens, 1991; Mabey et al., 1983). The isostatic gravity lows are reasonably well correlated with (1) volcanic rocks erupted during the 34-17 Ma time-slice intervals (see Fig. 6.54b and compare to Fig. 6.4), and (2) a possible east–west-trending structural zone that extends across southern Nevada (the south-central Nevada structural zone; see Kepper et al., 1991, figure 1). The isostatic gravity low is also visible in the Bouguer gravity anomaly, where it is characterized by gross bilateral symmetry that is best developed in east-central Nevada. The axis of symmetry trends northwest and is generally coincident with the northern Nevada rift zone. The Nevada gravity low may actually be part of a larger alternating pattern of northwest-southeast-trending high-low anomalies that stretches from California, across the Great Basin and into Utah (see Jachens et al., 1989, plate 1; Kane and Godson, 1989, plate in back pocket). This larger gravity pattern is probably related to features at the crust-mantle boundary, and is reviewed in greater detail in section 2.7.3.

In summary, the relationship between the volcanic rock-hosted occurrences and regional-scale geologic features, as interpreted through the geophysical anomalies, is not as well-defined as it is for the sedimentary rock-hosted occurrences, however, it appears likely that the volcanic rock-hosted occurrences are associated with *shallow* crust that:

- Has been affected by widespread felsic volcanic activity. The regional distribution of magmatism between 34-6 Ma (particularly between 6-17 Ma) parallels (1) the distribution of volcanic rock-hosted deposits (compare Fig. 6.4 to 6.2 and 6.3) and (2) the Walker Lane shear zone and the Humboldt zone (compare Fig. 6.4 to 1.3, 6.6, and 6.45).
- Is associated with broad and diffuse structural zones that visibly affect basin-range structure, suggestive of regional-scale shear, and may have late Cenozoic movement (Walker Lane shear zone; possibly the Humboldt zone also, as suggested in shaded relief of topography; Figs. 6.6 and 1.2; the Humboldt zone is discussed and illustrated in greater detail in chapter 8).
- Has been intruded by mafic and intermediate magmas, particularly along structural zones (e.g.—figure 4.3 in Smith and Luedke, 1984).

## 6.7 Geochemistry—K/Na and Ba/Na Anomalies

### 6.7.1 Introduction and Summary of Findings

The distribution and spatial association of the gold-silver-bearing occurrences in relation to K/Na (Fig. 6.57b) and Ba/Na (Fig. 6.57c) anomalies are reviewed in this section. The maps were prepared using geochemical data collected as part of the National Uranium Reconnaissance Evaluation (NURE) program in the conterminous western United States between 1976 and 1980, and are depicted as K/Na and Ba/Na ratios, rather than the absolute concentrations of K, Ba, or

Na<sup>5</sup>.

Alteration of aluminosilicate wall-rocks accompanies precious metal mineralization in the sedimentary and volcanic rock-hosted deposits of the Great Basin. In sedimentary rock-hosted deposits, alteration assemblages are characterized by decarbonatization, silicification, argillization and alteration of aluminosilicate minerals to a host of other clay minerals, pyritization, deposition of alunite and barite, oxidation and acid leaching near the surface, as well as the introduction and redistribution of carbon (Bagby and Berger, 1985; Radtke, 1985; Bakken and Einaudi, 1986; Cox and Singer, 1986; Kuehn, 1989; Hofstra, 1994; also see [Table 3.1](#)). Alteration facies do not usually form regional haloes (Christensen, 1995). In general, for sedimentary rock-hosted mineralization, the ratios of K/Na and Ba/Na should increase as (1) Ba is introduced, (2) Na is depleted, and (3) K is either immobile or not as commonly depleted as Na (see Hofstra, 1994). Volcanic rock-hosted deposits may be subdivided into high- and low-sulfidation systems, associated with volcanic-hydrothermal and geothermal environments, respectively (Hedenquist et al., 1996). High-sulfidation systems are characterized by acid-sulfate alteration, whereas low-sulfidation systems are characterized by adularia-sericite alteration (see [Table 3.2](#)). The acid-sulfate (high sulfidation) assemblage shows silicification and advanced argillic alteration near ore bodies and grades outwards to an argillic zone. The adularia-sericite (low sulfidation) assemblage shows K-metasomatism (adularia) and silicification near ore bodies and grades outward to a sericitic-argillic zone. Both alteration assemblages are surrounded by an outermost zone of propylitic alteration, which may form halos hundreds of meters wide around veins (Buchanan, 1981; Hedenquist et al., 1996). In general, for volcanic rock-hosted mineralization, the ratios of K/Na and Ba/Na should increase as (1) Ba (particularly in high-sulfidation systems) and K are introduced, and (2) Na is removed (Sillitoe, 1995; Hedenquist et al., 1996) (Barnes and Rose, 1998, indicate that Na is removed to become a major solute in hydrothermal fluids).

The most significant results of the analyses carried out in this section suggest that occurrences in Nevada, particularly the sedimentary rock-hosted occurrences found along the Battle Mountain–Eureka (Cortez) and Carlin mineral trends, have a strong *spatial association* with high K/Na and Ba/Na anomalies (no genetic link is suggested or implied, although one may exist). As reviewed in chapter 3 ([sections 3.4](#) and [3.6](#)), a number of proposals have been put forth that mineralization along the Battle Mountain–Eureka (Cortez) and Carlin trends is controlled by a regional-scale crustal structure(s) (e.g.—Madrid and Bagby, 1986; Cunningham, 1988; Shawe, 1991; Arehart et al., 1993; Maher et al., 1993; Grauch et al., 1995). The distribution pattern of

---

<sup>5</sup> Samples were selected that contained concentrations for Ba and Na, or K and Na—6,390 samples were chosen for K/Na and 6,460 for Ba/Na, and include mostly (~90%) soil and other sediment samples. The NURE data have a number of well-recognized errors, omissions, and biases, which made regional-scale analysis and comparison of single elements prohibitive. The NURE geochemical data, as published on the USGS DDS-1 CD-ROM (1991), contains a number of inconsistencies which render the data difficult to work with for a regional-scale analysis. Overall, the basic problem with the NURE data is the lack of quality control procedures in both the sampling and laboratory analysis programs. In regional-scale compilations, this led to various “boundary” effects between individual collection-analysis regions. Maps prepared directly from uncorrected Ba, K, or Na concentrations produced maps showing erratic anomaly patterns with no continuity of the patterns across 1° by 2° map sheet blocks. It was determined that by calculating ratios between elements that were analysed using the same techniques, and from samples processed by the same laboratory, the relative magnitude of the geochemical anomaly could be preserved.

the K/Na–Ba/Na anomaly clearly delineates the Battle Mountain–Eureka (Cortez) and Carlin mineral trends, and it is suggested that the geochemical anomalies might *also* be related to presumed crustal structure(s), which control the regional-scale distribution of sedimentary rock-hosted occurrences along the trends.

### 6.7.2 Distribution and Spatial Association of Gold-Silver-Bearing Occurrences

As shown in [Figure 6.57](#), the geochemical evidence layers do not completely cover the study area: they cover only about 50% of the total area of Nevada, however, nearly 70% of the gold-silver-bearing occurrences fall on the K/Na and Ba/Na anomaly maps. Because of the distribution of these data, the results of spatial analysis performed on the sedimentary rock-hosted occurrences is considerably more reliable and stable than for volcanic rock-hosted (compare [Fig. 6.57](#) to [6.2](#)). With respect to weights of evidence modelling, the areas of missing data contribute no weight ( $W^+ = W^- = 0$ ) and the mineral potential (the posterior probability value) is neither up-weighted nor down-weighted (Bonham-Carter, 1994a, p. 327).

Of the total number of primary occurrences (2690), 1840 are located on the K/Na and Ba/Na maps, and of these 1840, the greatest number fall within the lowest geochemical ratio interval (~38% for the K/Na map; ~67% for the Ba/Na map) ([Figs. 6.58](#) and [6.59](#)). Of the total number of sedimentary rock-hosted occurrences (98), 61 are located on the K/Na and Ba/Na maps, and of these 61, over half fall in the top eight K/Na ratio intervals (“6-7” through “≥50”) and in the top five Ba/Na ratio intervals (“0.30-0.35” through “≥0.50”) ([Figs. 6.60](#) and [6.61](#)). Of the total number of volcanic rock-hosted occurrences (415), 270 are located on the K/Na and Ba/Na maps, and of these 270, about 85% fall in the three lowest K/Na ratio intervals (“<1” through “2-3”) and nearly 90% in the lowest Ba/Na ratio interval (“<0.10”) ([Figs. 6.60](#) and [6.61](#)). Keeping in mind that the volcanic rock-hosted occurrences are not well represented with respect to the coverage of the K/Na and Ba/Na geochemical anomaly maps, the most notable difference between the sedimentary and volcanic rock-hosted occurrence frequency distributions is the affinity of sedimentary rock-hosted occurrences for higher geochemical ratio values, especially in the case of Ba/Na.

The spatial association between the K/Na anomaly and both the primary and volcanic rock-hosted occurrences is strongest when the areas of the top five highest ratio intervals are combined (“9-10” through “≥50”) ([Fig. 6.62](#)). The spatial association between the K/Na anomaly and sedimentary rock-hosted occurrences is strongest when the areas of the top three highest ratio intervals are combined (“15-25” through “≥50”) ([Fig. 6.62](#)). In general, the sedimentary rock-hosted and big size primary occurrences show the strongest spatial association with higher K/Na anomalies, while the volcanic rock-hosted occurrences show only a moderate spatial association for mid-range K/Na values. The sedimentary rock-hosted occurrences show the strongest spatial association with the higher Ba/Na anomaly values ([Fig. 6.63](#)). As with the K/Na anomaly, the volcanic rock-hosted occurrences show a weak and even a negative spatial association with Ba/Na anomalies. Again, these relationships reflect the poor distribution of the NURE dataset with respect to the volcanic rock-hosted occurrences.

Three binary-class mineral potential predictor maps were produced from each of the K/Na and Ba/Na geochemical anomaly maps, one for each of the three occurrence samples (primary,

sedimentary and volcanic rock-hosted) (Fig. 6.64). For the K/Na anomaly maps, the six highest ratio intervals (“8-9” through “ $\geq 50$ ”) were combined for the primary occurrences binary predictor map, the three highest intervals (“15-25” through “ $\geq 50$ ”) were combined for the sedimentary rock-hosted occurrence binary predictor map, and the five highest intervals (“9-10” through “ $\geq 50$ ”) were combined to create the volcanic rock-hosted binary predictor map. For the Ba/Na anomaly maps, the eight highest ratio intervals (“0.15-0.20” through “ $\geq 0.50$ ”) were combined for the primary occurrences binary predictor map, the five highest intervals (“0.30-0.35” through “ $\geq 0.50$ ”) were combined to produce the binary predictor maps for both the sedimentary and volcanic rock-hosted occurrence binary predictor maps.

### 6.7.3 Correlations and Interpretive Synthesis

The K/Na and Ba/Na anomalies are mainly associated with the sedimentary rock-hosted occurrences, although geochemical coverage extends only over part of the Walker Lane, which is the principal locale for volcanic rock-hosted occurrences. This restricted coverage reduces the utility of the statistical correlations. The K/Na and Ba/Na anomaly maps display a distinctive “V”-shaped pattern in north-central Nevada that correlate with the Battle Mountain–Eureka (Cortez) and Carlin sedimentary rock-hosted mineral trends (Fig. 6.65). The western northwest-southeast arm of the “V” delineates the Battle Mountain–Eureka (Cortez) trend. The eastern arm of the “V” is north-south from the base of the “V”, then bends northwest along the Carlin trend. The north-south eastern arm extends south of the Carlin trend, near the Emigrant Springs and Rain mines, along a line of mainly small silver-bearing polymetallic occurrences to intersect the western arm of the “V” near a large number of polymetallic replacement and some disseminated deposits around the Eureka district. This north-south section of the eastern arm traces the leading edge of the Roberts Mountain thrust (see Figs. 6.65 and 2.5), but it is not implied here that this forms a connection (structural or otherwise) between the Carlin and Battle Mountain–Eureka (Cortez) mineral trends.

The spatial correlation between Ba/Na and the sedimentary rock-hosted occurrences, which is strongest for the Battle Mountain–Eureka (Cortez) trend, is related to the presence of vein and bedded barite in the stratigraphic sequences of the rock package(s) hosting gold mineralization. Most sedimentary rock-hosted occurrences along the Battle Mountain–Eureka (Cortez) and Carlin trends are associated with structural windows in the upper plate of the Roberts Mountain allochthon (Bagby and Berger, 1985). Paleozoic submarine exhalative bedded barite deposits occur in the upper plate of the Roberts Mountain allochthon, particularly within the units Os and Osv<sup>6</sup> (Papke, 1984), and barium is anomalous in the cherts and argillites of the upper plate (Shawe et al., 1967; Papke, 1984; Byron R. Berger, 1998, personal communication). Structural windows expose the units containing the bedded barite deposits, the barite-enriched cherts and argillites, as well as the units hosting sedimentary rock-hosted gold mineralization. As such, the Ba/Na anomaly *should* be spatially associated with the occurrences. However, it should also be noted that geochemical anomalies of As, U/Th, Al, Sc/V, K, La/K, and Sc/Fe show varying degrees of continuity with, and similarity to, the regional-scale extent of the sedimentary rock-hosted mineral deposit trends and K/Na and Ba/Na anomaly patterns:

---

<sup>6</sup> The units Os and Osv, from the geological map of Nevada (Stewart and Carlson, 1978), have been identified in this study as having a high spatial association with sedimentary rock-hosted occurrences, as illustrated in Figures 6.14 and 6.24.



- The northern Carlin trend (particularly the northern terminus) and the northern Battle Mountain–Eureka (Cortez) trend are well delineated by a linear distribution of anomalous As, in comparison to the region between the trends, which is characterized by less anomalous values.
- The northern Carlin trend (particularly the northern terminus) and the southern Battle Mountain–Eureka (Cortez) trend are relatively well delineated by a linear distribution of anomalous U/Th, in comparison to the region between the trends, which is characterized by less anomalous values.
- The Battle Mountain–Eureka (Cortez) and Carlin trends are delineated by anomalously low Al in comparison to the region between the trends, which is characterized by anomalous values.
- Sc/V and K show moderately-defined anomaly gradient changes along the Battle Mountain–Eureka (Cortez) trend and along the Carlin trend (which is more weakly defined).
- La/K and Sc/Fe show a weak anomaly between the Battle Mountain–Eureka (Cortez) and Carlin trends.

Most of these anomalies are linear and continuous over large distances (at least 240 km for the western arm of the “V”) and trend across and oblique to most mountain ranges and drainages (except along the northernmost portion of Battle Mountain–Eureka (Cortez) trend).

The spatial association of K/Na–Ba/Na anomaly to the Battle Mountain–Eureka (Cortez) and Carlin mineral trends is clear. Any genetic link is, however, inferred. Many samples from bedded barite deposits have been analysed for gold and none found (Byron R. Berger, 1998, personal communication). One possible indirect link is regional-scale structural features associated with the western margin of the Precambrian craton. Cunningham (1988) recognized that a number of important sedimentary rock-hosted deposits are located near the edge of the buried craton (compare Fig. 6.2 to 2.10; see figure 1 in Cunningham). He proposed that deep crustal structures developed along older reactivated zones of weakness at the cratonic boundary, which had a localizing effect on sedimentary rock-hosted mineralization. Papke (1984) interpreted the barite deposits to be exhalative, favoring a magmatic source for the heat and the barium. He suggested that the deposits formed in submarine basins scattered along a 500 km belt, the length and linearity of which suggests a major zone of rifting parallel to the axis of the lower Paleozoic eugeosyncline (see Fig. 2.9; Papke, 1984, figure 1). Structural zones associated with the craton edge may have provided a conduit for the passage of fluids that contained barium, and along different structures and at a later time, gold.

Regardless of the link between the K/Na and Ba/Na anomalies and the Battle Mountain–Eureka (Cortez) and Carlin mineral trends, they are spatially associated with sedimentary rock-hosted mineralization along the trends and do provide reasonably good exploration guides (given the existing dataset). These matters are further discussed in chapter 8.



# Chapter 7. Multi-Map Modelling and Gold-Silver Mineral Potential

## 7.1 Introduction

Chapter 7 is a summary and discussion of the results of mineral potential modelling. In part, the material below represents the second and third of three stages of model building, the *parameter estimation or model fitting* and *model validation* stages, respectively (Chatfield, 1988; see [section 1.4](#)). It constitutes the second of the two procedures that compose the weights of evidence mineral potential modelling method, graphically illustrated in [Figure 4.1](#) as procedure “ii”. The first stage of model building, *model formulation or specification*, was addressed in chapter 6, where, in procedure “i” of weights of evidence modelling, (1) spatial associations between the gold-silver-bearing occurrences and the multi-class mineralization evidence maps were established and measured, (2) the significance of the relationships was determined, and (3) the binary-class mineral predictor maps (“*layers of evidence*”) were created from the mineralization-favorable units composing multi-class evidence maps. The implementation and theoretical aspects of the modelling procedures carried out here are addressed in [Appendix B](#) (summarized in [chapter 4](#)).

The former part of this chapter ([section 7.2](#)) reviews the combination of the binary-class mineral predictor maps (“*layers of evidence*”) generated in [chapter 6](#). The sedimentary and volcanic rock-hosted mineral potential maps are presented in [section 7.3](#). Validation of the mineral potential models, including analysis of conditional independence and error, mineral favorability at known occurrence locations, and blind tests, are discussed in [section 7.4](#). In the latter portion of this chapter ([section 7.5](#)), regional-scale sedimentary and volcanic rock-hosted occurrence exploration targets are delineated, and the important mineral potential evidence within each target region is reviewed. Specific sites for more detailed investigation and further exploration are also suggested. In [chapter 8](#), the mineral potential evidence presented here and the spatial relationships and interpretations presented in [chapter 6](#) are used to identify geologic features that may control the first-order regional-scale distribution of sedimentary and volcanic rock-hosted occurrences in the Great Basin.

The main conclusions of this chapter are that (1) the most significant mineral potential evidence layers examined in this study for predicting sedimentary and volcanic rock-hosted are, in order of importance, geology-related, geochemistry, and geophysics, (2) the sedimentary and volcanic rock-hosted occurrence posterior probability maps have a high degree of statistical certainty and are reliable indicators of mineral potential, despite known conditional dependence problems, and (3) the mineral potential models are valid, as indicated by the prediction of approximately  $\frac{2}{3}$  to  $\frac{3}{4}$  of all occurrences for any given occurrence-type used to train the models, the successful prediction of 15 out of 17 newly discovered occurrences, and by high area cross-correlation with expert-delineated areas of mineral occurrence permissibility. Areas favorable for sedimentary and volcanic rock-hosted mineralization were readily recognized on the mineral potential maps, and promising regional-scale exploration targets were readily identified.

## 7.2 Combination of Mineral Potential Evidence

### 7.2.1 Introduction

The posterior probabilities for predicting mineralization were estimated by combining the layers of evidence for each of the primary, sedimentary and volcanic rock-hosted occurrence-type mineral potential models in two ways: (1) a combination using all of the evidence layers, and (2) a combination using fewer layers, where one or more predictor maps were removed from the model in an attempt to mitigate conditional dependency (CI) violations and posterior probability uncertainty. A total of six posterior probability mineral potential maps were produced.

The weighting factors used to combine the layers of evidence are reviewed in [section 7.2.2](#) below. A review of CI and uncertainty, with respect to mineral potential model validation, is presented later in [section 7.4.2](#). [Appendix C](#) gives detailed examinations of (1) the predictor map combinations, (2) a pair-wise comparison between the two posterior probability maps created for each occurrence-type mineral potential model, and (3) analysis of CI and uncertainty.

### 7.2.2 Combination Weighting Factors

The predictor maps for each of the three mineral occurrence-types were combined using the spatial weights of association ( $W^+$  and  $W^-$ ) listed in [Table 7.1](#). The relative significance, correlation, or “influence”, that a particular layer of evidence has on a posterior probability mineral potential map for a given mineral potential model is taken to be the contrast ( $C=W^+ - W^-$ ), which is the measure of spatial association between the occurrences and a predictor map pattern. The relative influence of the various evidence layers in the mineral potential models is summarized in [Figures 7.1, 7.2, and 7.3](#). In each of these Figures, the evidence is ordered from most influential to least influential layer (i.e.—sorted by “C”).

A collective examination of the Figures reveals that lithology or lithology-related (e.g.—lithotectonic terranes and buffers around plutons) factors rank highly among the top three or four most influential evidence layers, along with geochemical evidence (particularly in the case of sedimentary rock-hosted occurrences). Overall, it appears that geology-related evidence has the highest degree of spatial correlation to the gold-silver-bearing occurrences, followed by geochemical-related evidence and then geophysical-related evidence. These correlations are consistent with those observed by Wright (1996), in a study that compared the merits of four different methods for combining geoscientific spatial data related to volcanic-hosted massive sulfide (VMS) deposits (weights of evidence, weighted logistic regression, fuzzy logic, and Dempster-Shafer belief theory). He found that, in general, stratigraphic evidence (read lithologic here) has the highest degree of correlation to the VMS occurrences, followed by alteration and geochemical evidence, heat-source evidence, and lastly, geophysical evidence (VLF electromagnetics, gravity, and geomagnetics). Another interesting conclusion of Wright (1996) is that the type of evidence used in a model is more critical than the method by which it is combined (see Wright and Bonham-Carter, 1996, for further details).

## 7.3 Sedimentary and Volcanic Rock-Hosted Mineral Potential Maps

### 7.3.1 Introduction

The gold-silver mineral potential maps of Nevada represent areas that are ranked according to their favorability for hosting gold-silver-bearing mineral occurrences (both economic and sub-economic). These areas are the result of unique combinations of overlap among the various binary-class predictor maps. An area is ranked according to its associated posterior probability value, which is based on the degree of spatial association between mineral occurrences and an evidence layer, and on the overlap combinations between the evidence layers (i.e.—the geological attribute binary-class predictor patterns). Areas having posterior probabilities greater than the prior probability, as indicated in the legend for each map, represent a combination of evidence layers that is favorable for the occurrence of gold-silver-bearing mineralization. In these areas, the favorability of finding an occurrence is greater than that which is simply due to chance (the “simply due to chance” condition is represented by the prior probability). Conversely, areas having posterior probabilities equal to or less than the prior probability represent evidence layer combinations that are not favorable for mineralization. In this study, the favorable areas contain greater than 70% of the large and medium size primary, sedimentary and volcanic rock-hosted gold-silver-bearing occurrences (see [section 7.4.3](#) and [Appendix D](#) for details). It is implicit in the weights of modelling technique that this is based upon the distribution of known occurrences and a combination of geological, geophysical or geochemical features spatially associated with these occurrences.

In this and the remaining sections of this study, only two of the six mineral potential maps generated in this study are considered: (1) the 8-layer sedimentary rock-hosted and (2) the 7-layer volcanic rock-hosted (the evidence layers making up these maps are given in [Table 7.1](#); also see [Appendix C](#) for a detailed discussion on these and other mineral potential maps). These maps are presented in [sections 7.3.2](#) and [7.3.3](#), respectively. The mineral potential maps reflect the distribution of known occurrences, but more importantly, they identify areas where yet undiscovered occurrences may exist.

These maps serve as the basis for delineating regional-scale exploration targets, reviewed separately in [section 7.5](#), and for determining the geologic characteristics of high mineral potential areas, which are interpreted with respect to geologic features that may control the regional-scale distribution of the gold-silver-bearing occurrences (the subject of [chapter 8](#)).

### 7.3.2 Favorability for Sedimentary Rock-Hosted Occurrences

The sedimentary rock-hosted occurrence-type posterior probability map is shown in [Figure 7.4](#). This map is based on the 8-layer mineral potential model (see [Table 7.1](#)) and overlain on the shaded relief of topography. Elevated mineral potential areas (light greens, yellow, orange, red) are generally confined to central, north-central, and north-eastern Nevada. The areas of highest mineral potential (yellow-orange-red) form a conspicuous “V”-shape trend of posterior probability values that is largely coincident with the major sedimentary rock-hosted deposit trends (Battle Mountain–Eureka (Cortez), Carlin, Getchell, and Independence group), and which

may parallel possible regional-scale structures, as defined by geophysical (and possibly geochemical) anomalies (see [sections 3.4, 3.6, 6.6, and 6.7](#); further discussed in [chapter 8](#)). These areas represent instances where nearly all of the layers of evidence come into spatial agreement. A typical combination of evidence consists of lithology, the Ba/Na geochemical anomaly, lithotectonic terrane, the geomagnetic anomaly, and distance buffer zones surrounding faults (a more detailed review is presented in [section 8.2.1](#)).

### 7.3.3 Favorability for Volcanic Rock-Hosted Occurrences

The volcanic rock-hosted occurrence-type posterior probability map is shown in [Figure 7.5](#). This map is based on the 7-layer mineral potential model (see [Table 7.1](#)) and overlain on the shaded relief of topography. Elevated mineral potential areas (light greens, yellow, orange, red) are principally distributed along two broad belts: (1) a north-west-trending belt that extends along the southwestern border of Nevada (the Walker Lane belt); and (2) a north-east-trending belt that extends diagonally across northern and northwestern Nevada (correlative to Humboldt zone; see [chapter 8](#)). The two belts intersect in the vicinity of Reno and Carson City, Nevada, between approximately N 39°–40° and W 119°–120°, where the 9-layer posterior probability map shows a relatively strong region of volcanic rock-hosted mineral potential (see [Fig. 7.8a](#) below). The two broad belts of elevated volcanic rock-hosted mineral potential roughly envelop the main region of elevated sedimentary rock-hosted mineral potential (compare [Figs. 7.4 and 7.5](#) to the point distribution of known occurrences in [Fig. 6.2](#)). In comparison to the sedimentary rock-hosted elevated mineral potential areas, the volcanic rock-hosted elevated mineral potential areas are patchy and discontinuous, and generally more evenly distributed across the state. Like the sedimentary rock-hosted mineral potential “highs”, the volcanic rock-hosted “highs” represent instances where nearly all of the layers of evidence come into spatial agreement. A typical combination of evidence consists of lithology, distance buffer zones surrounding plutons, the geomagnetic anomaly, distance buffer zones surrounding faults, lithologic diversity, and the K/Na geochemical anomaly (a more detailed review is presented in [section 8.2.2](#)).

## 7.4 Validation of Mineral Potential Models

### 7.4.1 Introduction

*Model validation* is the third of the three stages of model building (Chatfield, 1988). Validation may be carried out using the same data from which the models were built, where the output of a model is typically analysed for goodness-of-fit and error, and is tested for the ability to predict the distribution of the data from which it was built and specified (training point prediction). Goodness-of-fit and error test are reviewed in [section 7.4.2](#), “*Conditional Independence and Uncertainty of the Mineral Potential Maps*”, and examined in detail in [Appendix C](#). The capacity of the mineral potential models to predict known occurrences is reviewed in [section 7.4.3](#) and detailed in [Appendix D](#). But perhaps more important is the ability of a model to predict the distribution of data which were *not* used to construct the model. Validation of this type is usually referred to as a “blind test”. A blind test of the mineral potential models built here was performed using (1) expert-delineated tracts permissible for sedimentary-rock hosted and epithermal mineralization (in essence an informal blind test; [section 7.4.4](#)), and (2) newly discovered gold occurrences (a true blind test; [section 7.4.5](#)).

The results of the model validation analyses indicate that the posterior probability maps output from the mineral potential models are within acceptable limits. Generally speaking, weights of evidence mineral potential modelling is successful if the resulting mineral potential maps (1) predict the distribution of known mineral occurrences, and/or (2) are useful for delineating or targeting regions of elevated mineral potential for follow-up exploration (Bonham-Carter, 1994b). Both of these criteria were met. The first is discussed in [section 7.4.3](#). The second is discussed in [section 7.4.4](#), and is the subject of [section 7.5](#).

## 7.4.2 Conditional Independence and Uncertainty of the Mineral Potential Maps

The results of CI testing suggest that the mineral potential maps should be considered in terms of relative “*favorability*”, rather than strictly as “*probabilistic*” maps. Both the  $\chi^2$  pairwise and K-S overall tests indicate that the layers of evidence composing these mineral potential models are not conditionally independent with respect to the mineral occurrences, and that this lack of CI is real, in both the statistical and the geological sense. The violation of CI in the mineral potential models is not unexpected, as CI in WOE modelling is always violated to some degree (Bonham-Carter, 1994a; see [chapter 4](#) and [Appendix B](#) for details). The greater the number of evidence maps used in a model, especially if those maps have similar distribution patterns and represent similar types of evidence, the greater the possibility is that conditional *dependency* will exist.

The sedimentary rock-hosted occurrence mineral potential models have a high discrepancy between the number of observed and predicted occurrences. The volcanic rock-hosted occurrences mineral potential models show a lesser amount of CI violation. The lack of CI occurs most notably in the mineral potential models where all of the available binary-class predictor maps were combined. To mitigate some of this CI, the evidence layers that caused the greatest CI violations were rejected from the models. The sedimentary rock-hosted model was reduced from 9 to 8 evidence layers by removing the pluton buffer binary-class predictor map (rejection of 2 or 3 additional combination predictor maps had relatively little additional corrective value). The volcanic rock-hosted model was reduced from 9 to 7 evidence layers by removing the Ba/Na geochemical anomaly and lithotectonic terranes binary-class predictor maps (while not remedying all of the CI problems, removal of these two maps reduced CI violations substantially; see [Appendix C](#) for further explanation). In addition, it was determined that increasingly large numbers of training points result in increasingly larger magnitude and a greater number of CI violations. Therefore, the CI violation exhibited by these mineral potential models may in part be related to the relatively large number of mineral occurrences modelled.

In order to determine whether the violations of CI severely affected the mineral potential maps, comparisons were made between the CI- mitigated and -unmitigated maps, as well as between mineral potential maps generated using the weights of evidence (WOE) and weighted logistic regression (WLR) methods. Maps of absolute difference in posterior probability value between CI- mitigated and -unmitigated mineral potential maps show relatively small discrepancies ([Fig. 7.6](#)). The comparison between the WOE-derived and WLR-derived posterior probability maps for sedimentary and volcanic rock-hosted mineralization shows only minor differences in the distribution of favorable mineral potential areas at the local-scale ([Figs. 7.7](#) and [7.8](#)). At the regional scale, no significant differences are visible in the overall map patterns, although the



WOE mineral potential maps appear to be somewhat “warmer”. The WOE–WLR comparison was chiefly made because the WLR method does not require the assumption of CI. In general, the results of the WLR method appear to be consistent with those of the WOE method, and suggest that, for this study, the results of the WOE method are within acceptable and expected bounds.

Analysis of the “certainty” of the posterior probability estimates also suggests that the mineral potential maps are within acceptable limits. Maps of posterior probability uncertainty for the sedimentary and volcanic rock-hosted mineral potential maps are shown in [Figures 7.9 and 7.10](#), respectively (see [Appendix C](#) for complete analysis). Uncertainty may be due to the variances in weight estimates ( $W^+$  and  $W^-$ ) and/or to one or more of the predictor maps having incomplete coverage (i.e.—missing data) (Bonham-Carter et al., 1989). Uncertainty due to variance in the weights estimates is usually correlated to the posterior probability values, and when mapped, results in an uncertainty map pattern similar to that of the posterior probability map. A measure of relative certainty, consisting of the posterior probability divided by its standard deviation (in effect, a student t-test), indicates the degree of confidence to which the posterior probability mineral potential map patterns are “real”, as opposed to being an artifact of “chance” effects (or due to chance). The t-test is useful for identifying gross violations of the model assumptions. In general, the maps of uncertainty due to variance in weights estimates and due to missing data reflect the large overall variation in the data (i.e.—“noise in the system”). However, the relative certainty maps suggest that, despite this high degree of variability, the mineral potential map favorability patterns are reliable (i.e.—areas of elevated t-value are spatially coincident with areas of high mineral potential).

### 7.4.3 Favorability at Known Gold-Silver-Bearing Occurrence Areas

The mineral potential favorability at known primary, sedimentary and volcanic rock-hosted occurrence locations was determined as follows:

1. Appending the probability calculated with WOE to each occurrence point.
2. Counting the number of occurrences (subdivided by size) having posterior probabilities greater than the prior probability.
3. Comparing the distribution pattern of the point occurrences (as classified by their appended posterior probability) to the distribution pattern of the mineral potential posterior probability map.

Approximately  $\frac{2}{3}$  to  $\frac{3}{4}$  of all occurrences, for any given occurrence-type, have posterior probabilities greater than the prior probability (see [Appendix D](#) for complete listing of data). For the primary occurrences, ~76% of the big (large and medium size) and ~69% of the small size occurrences have posterior probabilities larger than the prior probability, with a total of ~69% of all of the primary occurrences having a higher posterior probability. For the sedimentary rock-hosted occurrences, ~84% of the big and ~82% of the small size occurrences have posterior probabilities larger than the prior probability, with a total of ~83% of all of the sedimentary rock-hosted occurrences having a higher posterior probability ([Fig. 7.11](#)). For the volcanic rock-hosted occurrences, ~72% of the big and ~60% of the small size occurrences have posterior probabilities larger than the prior probability, with a total of ~60% of all of the volcanic rock-hosted occurrences having a higher posterior probability ([Fig. 7.12](#)). The proportion of occurrences with posterior probabilities higher than the prior is roughly the same for the primary



as it is for the volcanic rock-hosted occurrence-type. The sedimentary rock-hosted occurrences, however, show markedly higher proportions, which is mainly due to the greater degree of conditional dependence in the sedimentary rock-hosted occurrence-type mineral potential model.

In addition to a large proportion of the gold-silver-bearing occurrences having elevated posterior probabilities, the spatial distribution of occurrences having elevated posterior probability values is coincident with areas of elevated mineral potential favorability, as predicted by the posterior probability maps. This correlation is particularly noticeable for the sedimentary and volcanic rock-hosted occurrences, as shown in [Figures 7.13](#) and [7.14](#). In both of these Figures, a conspicuous pattern of occurrences is highlighted with a dashed line, and is shown to have a spatially associated and corresponding pattern of areas of elevated posterior probability. The dashed lines on these Figures merely delineate the spatial distribution of the occurrences, and do not necessarily reflect any geologic, structural, or other genetic-related trends.

These observations indicate that (1) a relatively large proportion of occurrences have posterior probability values higher than that of the prior probability, and (2) the distribution of this relatively large proportion of occurrences is correlative to areas of elevated posterior probability. Based upon Bonham-Carter's (1994b) first criterion for successful mineral potential modelling—the *resulting mineral potential maps predict the distribution of known mineral occurrences*—the modelling carried out here, despite known CI problems, was successful.

#### 7.4.4 Comparison to Expert-Delineated Mineral Potential Areas

In 1996 two regional-scale mineral resource assessment studies were published by the U.S. Geological Survey: (1) OFR-96-96, "*Data Base for a National Mineral Resource Assessment of Undiscovered Deposits of Gold, Silver, Copper, Lead, and Zinc in the Conterminous United States*" (Ludington et al., 1996); and (2) OFR-96-2, "*An Analysis of Nevada's Metal-bearing Mineral Resources*" (Singer, 1996). These assessments were conducted over a number of years with the assistance and expert knowledge of a fairly large team of experts from various geological sub-disciplines. The goal of these projects was to provide an analysis of the mineral resources in Nevada and the United States for the purposes of facilitating economic development, land-use and management, and minerals exploration. As part of these surveys, an assessment for undiscovered gold and silver deposits for the Nevada Great Basin was made and deposit "tract maps" delineating regions permissible<sup>1</sup> for various types of sedimentary and volcanic rock-hosted mineralization were produced. For the sediment-hosted gold tract map,

---

<sup>1</sup> In "permissive" areas, the lithologic and/or structural features necessary for ore deposition are present. In "favorable" areas, permissive lithologic and/or structural features are present, as well as other features indicating that potential mineralizing processes have taken place. The term "favorable" used in this study includes mainly *exposed* (not covered by Cenozoic alluvium) "permissive" areas delineated in OFR-96-96 and OFR-96-2, and perhaps indicates a higher degree of mineral potential than "permissive".

only Carlin-style disseminated gold deposits were considered<sup>2</sup>. Tract delineation was based on the distribution of the Roberts Mountain, Golconda, and several other allochthons, and, in the Sevier orogenic belt in eastern Nevada, by patterns of folding and thrust faulting shown on the Stewart and Carlson (1978) geological map of Nevada (Ludington et al., 1996; Singer, 1996). For the epithermal gold-silver tract map, a number of different deposit types were considered<sup>3</sup>. Tract delineation was based on distribution of volcanic rocks, of epithermal mineral deposits, prospects, and occurrences, on the distribution of synvolcanic faults, and on the magnetic anomaly patterns associated with the Walker Lane and northern Nevada rift (Ludington et al., 1996; Singer, 1996). Ludington et al. (1996) and Singer (1996) should be consulted for further details on the mineral assessment methodology, assumptions, and rationale.

Using area cross-correlation analysis, comparisons were made between permissible tracts for sedimentary-hosted gold and epithermal gold-silver mineralization as delineated by the expert mineral assessments and the sedimentary and volcanic rock-hosted mineral potential maps as delineated in this study with weights of evidence (Figs. 7.15 and 7.16). The analysis indicated that:

- Approximately 85% of the favorable and ~95% of the elevated favorable areas for sedimentary rock-hosted gold mineralization lie within the expert-defined permissive tracts for such deposits.
- Approximately 73% of the favorable and ~91% of the elevated favorable areas for volcanic rock-hosted mineralization (epithermal), lie within the expert-defined permissive tracts for such deposits.

Both the sedimentary and volcanic rock-hosted occurrence posterior probability maps display regions of strong mineral potential that are coincident with permissive tracts as delineated by the experts, as well as coinciding with areas hosting important and/or many occurrences. But more important, the mineral potential maps produced in this study highlight regions of strong mineral potential where known occurrences are absent or few in number. Based upon Bonham-Carter's (1994b) second criterion for successful mineral potential modelling—*the resulting mineral potential maps are useful for delineating or targeting regions of elevated mineral potential for follow-up exploration*—the maps created here have successfully outlined areas that might be interesting regional-scale exploration targets. These targets are presented in section 7.5.

### 7.4.5 Blind Test of Mineral Potential Model Predictability

The posterior probability maps produced in this study were built from mineral potential models calibrated (trained) using a 1993 download of *Mineral Resource Data System* (MRDS) database

---

<sup>2</sup> The deposits considered include: (1) an eastern group, exemplified by Bald Mountain, Golden Butte, Alligator Ridge, Illipah, Night Hawk, and Green Springs; (2) a central group, exemplified by deposits in the Jerritt Canyon (Burns Basin) district, the Carlin trend, Marigold, deposits around Cortez, Tonkin Springs, and Northumberland; and (3) a western group, exemplified by deposits in the Getchell trend, Standard, and Fondaway Canyon. Ludington et al. (1996) and Singer (1996) should be consulted for the complete list.

<sup>3</sup> The deposit types considered include: (1) Comstock epithermal vein, exemplified by the Comstock, Tonopah, Jarbidge, National, and Tuscarora districts, (2) quartz-alunite vein, exemplified by the Goldfield district, (3) hot spring gold-silver, exemplified by the Round Mountain, Borealis, Paradise Peak, Hog Ranch, and Lewis deposits, and other epithermal deposits, including hot spring Hg, simple Sb, epithermal Mn, and rhyolite-hosted Sn. Ludington et al. (1996) and Singer (1996) should be consulted for the complete list.

(with some modifications from a 1995 download; see chapter 5). A list of newly discovered occurrences (or at least newly tabulated or reported since the 1993/95 MRDS occurrences used for this study) was compiled from Ludington et al. (1996), the Nevada Mineral Industry reports for 1994, 1995, and 1996 (Nevada Bureau of Mines and Geology staff, 1995-1997), and from Joe V. Tingley of the Nevada Bureau of Mines and Geology (1998, personal communication). These discoveries consist of 12 sediment-hosted occurrences (Gold Canyon, Golden Butte, Pan, Pinon Range–Cord Ranch, Pipeline, Reona, Saddle, South Pipeline, Treasure Hill, Trenton-Valmy, Winters Creek, and Wright Window) and 5 epithermal occurrences (Gemfield, Golden Arrow, Hydra-Hercules, Midway, Mule Canyon).

The blind test was carried out by appending the posterior probability value calculated using the appropriate mineral potential model to the 12 new sedimentary and 5 new volcanic rock-hosted occurrences. Ten of the twelve sedimentary rock-hosted occurrences were estimated to have posterior probabilities higher than the prior probability, where four have notably high posterior probabilities (Fig. 7.17). Five of five epithermal occurrences were estimated to have posterior probabilities higher than the prior probability, where two have notably high posterior probabilities (Fig. 7.18). These results clearly validate the sedimentary and volcanic rock-hosted mineral potential models built in this study and indicate that they have a significant predictive capacity.

## **7.5 Geologic Characterization and Delineation of Regional-Scale Sedimentary and Volcanic Rock-Hosted Occurrence Exploration Targets**

### **7.5.1 Introduction**

A couple of the main purposes of modelling mineral potential are (1) to predict areas where geologic conditions conducive to mineralization exist and where processes resulting in economic ore concentrations are likely to have taken place, and (2) to target regions of high mineral potential for further investigation using the predicted areas as an exploration guide.

The selection of favorable regions for exploration involves identifying areas of elevated posterior probability that have few or no known gold-silver-bearing occurrences. This is most easily accomplished by first superimposing a “mask” of known occurrences over the mineral potential map, and locating those areas within a region of elevated posterior probability that show through the mask. For this study, a mask consisting of a 10 km radius buffer around all known occurrences was used. Ten kilometers is a subjective estimate representing the extent of a mining lease, which may or may not include peripheral “backyard” claims, prospects, or other exploration areas. A radius of 10 km around an ore deposit may also be a fair approximation for the extent of (or at least encompasses) the mineralizing system (i.e.—the extent of district or local-scale hydrothermal circulation; see Nesbitt and Muehlenbachs, 1989; Sillitoe and Bonham, 1990). This estimate may not be appropriate in all instances—10 km may be an overstatement with regard to mineral “showings” or an understatement in cases such as the Comstock or Carlin deposits—but, for all practical purposes, it is considered reasonable for revealing sites of interest.

Using the mineral potential models, promising target sites can be interactively queried “on-

screen” with the GIS in order to investigate which of the evidence layers (or combination of layers) is responsible for the favorability highs in a given region. This provides a “feel” for what geologic factors (according to the data-driven, weights of evidence mineral potential model) might be important for mineralization at a particular site. Such information (supplementing knowledge and experience) can be used to judge whether or not the site is viable. The ability to isolate clearly and understandably which of the evidence layers produce a mineral potential high is one of the important advantages that weights of evidence has over other methods for combining geoscientific spatial data.

This section outlines regional-scale exploration targets for sedimentary and volcanic rock-hosted occurrences. In total, 10 prospective target regions were selected (five for sedimentary rock-hosted occurrences and five for volcanic rock-hosted occurrences). The target regions are presented in as a series of maps:

1. *Regional-Scale Exploration Target Index Maps*—Two Figures that show the sedimentary and volcanic rock-hosted occurrence posterior probability maps overlain with a mask consisting of *all three* occurrence-type samples (primary, sedimentary and volcanic rock-hosted occurrences). The purpose of applying this mask, rather than a mask consisting only of one or another occurrence-type, is to isolate those regions where there is an absence of occurrences of *any* type.
2. *Close-up Maps of Individual Regional-Scale Exploration Targets*—Three or four Figures, where each Figure consists of: (1) a map showing known occurrences relative to predicted favorable areas within the region (some of the more prominent deposits are labelled); (2) the sedimentary or volcanic rock-hosted occurrences posterior probability map shown with respect to regional- and local-scale structures, against shaded relief of topography; and (3) the geological assemblage map for the target region shown with primary occurrences. The occurrences shown on these maps are displayed with a radius of 2 km, rather than 10 km. This was done to reveal more of the area of interest.

The prospective regional-scale exploration targets shown on the two index maps (item #1 above) have a number code that is used to link them to a close-up map (item #2 above) and a detailed description of the lithologic, structural, and tectonomagmatic mineral potential evidence each target region (presented below in [sections 7.5.2](#) and [7.5.3](#) below). For each target region, the following material is reviewed:

- General location.
- Significant deposits hosted by the target region.
- The main mineral potential evidence that qualifies the area as a target region.
- Other significant geologic features conducive to mineralization.
- Potential host lithologies.
- Specific sites (at the mountain-range-scale) for further investigation.

The mineral potential maps presented below are intended to help define *regional-scale* exploration targets for detailed data collection and further investigation—they are *not* intended for delineating drilling targets. The scale of the data compiled here is too small (not “fine” enough) to provide the resolution and information needed to delimit a drilling target. The mineral potential maps are, however, effective for selecting areas that have the proper geologic conditions favorable for gold-silver mineralization. The prospective regional-scale exploration targets presented below are not ranked in any particular order of importance. Geographic references (names of mountain ranges, valleys, creeks, highways, etc.) are from the geological

map of Nevada (Stewart and Carlson, 1978).

## 7.5.2 Sedimentary Rock-Hosted Mineral Potential Regions

The sedimentary rock-hosted occurrence-type regional-scale exploration target index map is shown in [Figure 7.19](#). The individual target regions are shown in [Figures 7.20](#), [7.21](#), and [7.22](#). They consist primarily of elevated mineral potential areas that are not immediately surrounded by sedimentary rock-hosted or other types of occurrences, and areas that are proximal to a few lone scattered occurrences (i.e.—target region #5). The target regions are mainly located along a “V”-shaped trend located in northern Nevada. The individual target regions are described below. A summary of the important geologic mineral potential evidence associated with areas of elevated favorability in the target regions is given in [section 8.2.1](#).

**Region #1**—Located in the northeastern corner of the state, there are no known sedimentary rock-hosted occurrences in this target region (or at least no known occurrences listed in the MRDS database) ([Fig. 7.20a](#)). The Jarbidge district (volcanic rock-hosted deposits) is the most important known gold-silver mineralization in the region. The most significant mineral potential evidence for this region consists of lithology, lithotectonic terrane, and the isostatic gravity anomaly, as well as possible deep-seated structures ([Fig. 7.20b](#)). This region is transected by a number of crustal-scale structural features, which include the  $^{87}\text{Sr}/^{86}\text{Sr}$   $I_{\text{Sr}} = 0.706$  isopleth (presumed to delineate the western edge of the North American Precambrian craton, and may represent a zone of crustal weakness), the Golconda and Roberts Mountain thrust fronts, and several possible deep-seated basement and/or strike-slip features (see Shawe, 1965; Blakely, 1988; Putnam and Henriques, 1991; also see [Figs. 2.5](#), [2.10](#), and [2.11](#)). The northeastern segment of the Nevada paleothermal anomaly, trending roughly northwest–southeast, also extends across this region (see [Fig. 2.10](#)). The areas of highest posterior probability are located proximal to the intersection of many of these features, which could provide fluid pathways for mineralizing fluids at upper crustal levels and facilitate the movement of deep-crustal fluids to higher crustal levels. The crust in this region is also characterized by high present-day heat flow. Lithologies permissive for mineralization include the “Marine and Shelf–Early-Mid PZ” and “Siliceous Rocks–Mid PZ-PC” lithologic assemblages ([Fig. 7.20c](#)). These assemblages were most likely thrust into place, which effectively tectonically over-thickened the crust in this region (as suggested by geophysical anomalies; see [section 6.6.3](#)). These assemblage units have the highest weights of spatial association ( $W^+$ ) with the sedimentary rock-hosted occurrences (see [Fig. 6.12](#)). While the lithology is favorable for ore deposition, the relative fault density over most of the region is not particularly high, although the areas of elevated mineral potential favorability do show moderate lithologic diversity. It is interesting to note that the area of highest relative fault density corresponds the location of the Jarbidge district. Suitable sites for further investigation might include: (1) areas east and southeast of the Arizona mine, along the northeast–southwest-trending length of Knoll Mountain, and the area just north of Jake's Creek, in the westward range across the valley adjacent to (west of) the Arizona mine; (2) in the mountains surrounding the town of Melanoco (Antelope Peak to the west, and Black Mountain to the east), in the vicinity of N 41.28° – W 114.85°; (3) the northernmost Pequop Mountains, just west of the town of Oasis, around N 41.06° – W 114.85° in the vicinity of the Pequop district; (4) the area due-southeast of the Silver Giant Claim Group and Norman mines (Jarbidge district), between Marys River Peak and the source of Anderson Creek; and (5) in the immediate vicinity south of the Coleman and Foss mines (Island Mountain district area), in the mountains just northeast of the town of Wild Horse, and on Cornwall Mountain.

**Region #2**—Located in northern-most central Nevada, just west of target region #1, this target region is host to a number of world-class deposits that include the Independence group and Carlin-trend sedimentary rock-hosted deposits, as well as the Tuscarora district (volcanic rock-hosted deposits), and the Aura and Edgemont polymetallic vein districts ([Fig. 7.20a](#)). This is one of the richest precious metal producing mining regions in the world. The most significant mineral potential evidence for this region consists of lithology, the Ba/Na and K/Na geochemical anomalies, lithotectonic terrane, the isostatic gravity anomaly, as well as many deep-seated and crustal structures ([Fig. 7.20b](#)). Many crustal-scale structural elements come together in this region, all of which may have provided lateral and vertical pathways for fluid movement: the favorable areas are (1) adjacent to the northern Nevada rift zone (see [sections 2.7.4](#), [6.6.3](#), [8.2.1](#), and [8.5.1](#)); (2) flanked to the W-NW by Roberts Mountain thrust and E-SE



by the Golconda thrust fronts (see Fig. 2.5); (3) collateral with the eastern margin of the Nevada paleothermal anomaly (see Fig. 2.10); (4) intersected by a number of possible deep-seated basement structures; and (5) they straddle, at right-angles, the  $^{87}\text{Sr}/^{86}\text{Sr}$   $I_{\text{Sr}} = 0.706$  isopleth, presumed to be the western edge of the North American Precambrian craton (see Figs. 2.10 and 2.11). Other regional characteristics conducive to ore formation include moderate lithologic diversity and a high relative fault density. This region is also characterized by moderately high modern-day heat flow. As with target region #1, the two most permissive lithologic assemblages include “Marine and Shelf–Early-Mid PZ” and “Siliceous Rocks–Mid PZ-PC” (Fig. 7.20c; also see Fig. 6.12). Promising sites for further investigation include: (1) the southern Tuscarora Mountains, on a southerly traverse between the Carlin deposit and the Marys Mountain/Carlin Peaks area (Carlin trend); (2) the hills on the northeastern side of Maggie Creek (the stream), approximately northeast of the Tusc, Gold Quarry, and Maggie Creek deposits (Carlin trend); (3) along a traverse northwest of the Rain and Emigrant Springs deposits to about N 40.70° – W 116.07°; (4) the region along a northeast-southwest traverse through the mountains connecting the northern Carlin trend deposits (i.e.—Post and Meikle area) and the southern Independence group deposits (i.e.—Mill Creek and Burns Basin), especially in the vicinity of Wheeler Mountain; (5) in the southern Independence Mountains, in the vicinity surrounding Swales Mountain, especially areas to the northeast; (6) in the central Independence Mountains, between the Generator Hill and Sammy Creek deposits (Independence group), in the areas west of McAfee and Jacks peaks (possibly under some of the morainal deposits in this area); (7) in the northern (north central?) Independence Mountains, the area immediately southeast of Rocky Bluff and north–northeast of the Sammy Creek deposits (Independence group); and (8) isolated spots in the northern Tuscarora Mountains, in the region surrounded by the Toe Jam Mountain–Dry Creek Mountain–Mount Blitzen–Castile Mountain, and especially the area down-hill to the south of Toe Jam and Castile mountains. It seems that “backyard” prospecting might still be very worthwhile in this region.

**Region #3**—Located in central Nevada, just south of target region #2, this target region is south of the Carlin trend deposits and east of the Battle Mountain–Eureka (Cortez) trend deposits. The Rain, Emigrant Springs, Trout Creek, and South Bullion deposits (Carlin trend) are located in the northern portion of the region, and the Tonkin Springs, Gold Pick, and Gold Bar deposits (Battle Mountain–Eureka trend) are found in the south-southwestern part of the region (Fig. 7.21a). Like region #2, the northern and south-southwestern areas of this target region are very rich in gold. The most significant mineral potential evidence for this region consists of lithology, the Ba/Na or K/Na geochemical anomalies, the isostatic gravity anomaly, as well as numerous crustal-scale structural features (Fig. 7.21b). Of particular interest is a narrow zone of high mineral potential that trends north-south across the target region, and a circular area in the south-central part of the region. The narrow north-south trending favorability zone is collateral with the Roberts Mountain thrust, and is intersected at acute angles by a number of deep-seated basement structures, which are parallel and proximal to the northern Nevada rift zone. The circular zone of favorability is approximately located where the northern Nevada rift zone geomagnetic anomaly intersects the trace of the Roberts Mountain thrust front. These structural arrangements, similar to those found in target region #2, could facilitate fluid passage and mineralizing processes. Both of the favorable zones lie to the east of the eastern margin of the Nevada paleothermal anomaly (see Fig. 2.10). The favorability zones are also characterized by moderate relative fault density, moderate lithologic diversity, and they trend along the eastern-southeastern margin of the present-day Battle Mountain heat high. The two most permissive lithologic assemblage units include “Marine and Shelf–Late PZ” and “Marine and Shelf–Early-Mid PZ” (Fig. 7.21c), slightly different from those found in regions #1 and #2, but also highly rated with respect to their weights of spatial association ( $W^+$ ) with the sedimentary rock-hosted occurrences (see Fig. 6.12). Localities that might warrant further exploration include: (1) areas in the northern Sulphur Spring Range (the Pinon Range), between and west of Buckskin, Spring Canyon, and Pine mountains, proximal and west-northwest of the Rain and Emigrant Springs deposits (Carlin trend); (2) areas in the Pinon Range, east of Pine Mountain, the region between the Rain and Emigrant Springs deposits and the Trout Creek and South Bullion deposits (Carlin trend), in the vicinity of Web Foot (Cu-skarn), Last Chance (polymetallic replacement), and Sylvania mines; (3) the entire length of the narrow north-south-trending zone of mineral potential highs, along the Sulphur Springs Range, roughly extending along Pine Mountain–Coffin Mountain–Union Mountain–Mineral Hill–Bald Mountain–Baily Pass (this target is especially interesting because there is only one deposit of any significance, Mineral Hills, a large polymetallic replacement deposit, located along this range); (4) areas in the Roberts Mountains, immediately surrounding, and to the northeast and southwest of, the Gold Pick, Gold Ridge, and Goldstone deposits (Battle Mountain–Eureka trend), and especially north and east of Roberts Creek Mountain.

**Region #4**—Located in central Nevada, west of region #3, the targets in this region are just southwest of, and



parallel to, the Battle Mountain–Eureka (Cortez) trend deposits. The Cove mine is located in the northwest part of this region, and the Hilltop mine, Gold Acres deposit, Cortez deposit, and Horse Canyon mine (Battle Mountain–Eureka trend) occur in the northeastern portion of the region (Fig. 7.21a). The Tonkin Springs, Gold Pick, Gold Bar, Gold Ridge, and Goldstone deposits (Battle Mountain–Eureka trend) are found in the southeastern part of the region, and were addressed above in the description of region #3. This region, as are regions #2 and #3, is rich in precious metals. The most significant mineral potential evidence in this region consists of lithology, the Ba/Na geochemical anomaly, and lithotectonic terrane, in addition to some crustal-scale structures (Fig. 7.21b). The mineral potential areas of interest are parallel to and bound by the northern Nevada rift zone to the northeast and the Golconda thrust front to the southwest (see Figs. 2.3, 2.5, and 6.45). Further west, the favorable areas are flanked by the  $^{87}\text{Sr}/^{86}\text{Sr}$   $I_{\text{Sr}} = 0.706$  isopleth, presumed to be the western edge of the North American Precambrian craton (see Figs. 2.10 and 2.11), and by a shorter and smaller geomagnetic anomaly related to the northern Nevada rift, presumed to represent a crustal-scale fracture or structural zone (see Fig. 6.45a, feature #1, and sections 2.7.4, 6.6.3, and 8.5.1). In addition, the favorable areas lie largely within and along the eastern margin of the Nevada paleothermal anomaly (see Fig. 2.10). The parallel alignment and proximity of these regional-scale features to one another could have provided through going upper-crust–lower-crust permeability for mineralizing fluids and heat. The areas of high mineral potential are also characterized by moderate relative fault density, moderate to moderately-high lithologic diversity, and anomalously high present-day heat flow (this target region is situated nearly in the center of the Battle Mountain heat high). The most permissive lithologic assemblages are once again the “Marine and Shelf–Early-Mid PZ” and “Siliceous Rocks–Mid PZ-PC”, which have the highest weights of spatial association ( $W^+$ ) with the sedimentary rock-hosted occurrences (Fig. 7.21c; also see Fig. 6.12). Sites that might be considered for further investigation include: (1) areas in the general vicinity of the Shoshone Range, near Mt. Lewis and Goat Peak, especially around and immediately to the southwest of the Elder Creek mine (Battle Mountain–Eureka trend); (2) areas further southwest of the Elder Creek mine in the Shoshone Range, just to the northwest of the central and southern end of Carico Lake Valley, around N 40.05° – W 117.10°; (3) areas in the northern Toiyabe Range, along the eastern margin of Carico Lake Valley, west of Bald Mountain, around N 40.00° – W 116.85°; (4) areas in the northern Toiyabe Range–southern Cortez Mountains, in the vicinity of Bald Mountain along the northwestern margin of the northern end of Grass Valley, around N 40.04° – W 116.67°; (5) areas in the northern Toiyabe Range, immediately southwest of Mt. Callaghan; and (6) areas in the Simpson Park Mountains, just southeast of Twin Peaks and parallel to the Battle Mountain–Eureka trend (northwest–southeast), and along the ridge-line connecting McClusky Peak, Buck Mountain, and Fagin Mountain (trending approximately north–northeast–south–southwest).

**Region #5**—Located in south-central and southwestern Nevada, the principal target areas in this region are located near the Austin Gold Ventures (Quito) mine and the Northumberland mine, in the north-central portion of the region, and near the Candelaria mine in the southwestern part of the region (Fig. 7.22a). Other targets are located just south of the Ratto Canyon mine, in the extreme northeast corner of the region, and north of the Tonopah district (volcanic rock-hosted deposits). With the exception of a few other widely scattered deposits, this target region is generally lacking in sedimentary rock-hosted occurrences, although this region is host to a number of medium- and large-size volcanic rock-hosted deposits and other types of mineralization (see Fig. 7.22a). The most significant mineral potential evidence in this target region consists of the K/Na and Ba/Na geochemical anomalies (where present), lithology, and lithotectonic terrane, as well as the presence of several regional-scale structural features (Fig. 7.22b). The principal mineral potential favorability areas are crossed by the Golconda thrust front and the  $^{87}\text{Sr}/^{86}\text{Sr}$   $I_{\text{Sr}} = 0.706$  isopleth (presumed to represent the western edge of the North American Precambrian craton; see Figs. 2.10 and 2.11), or are proximal to these features. The favorable areas also correspond to locations along the Golconda thrust and  $^{87}\text{Sr}/^{86}\text{Sr}$   $I_{\text{Sr}} = 0.706$  isopleth that are intersected at acute angles or parallel to presumed deep-seated structural features, some of which may be related to transcurrent movement along the Walker Lane belt. In addition, the principal high mineral potential areas lie along the eastern or western margin of the Nevada paleothermal high. The spatial coincidence of these structural zones and the paleothermal heat high may have promoted fluid circulation and facilitated precious metal mineralization. The relative density of faults across the region is variable, but most of the favorable mineral potential targets lie within areas of moderate to slightly higher relative fault densities, and moderate lithologic diversity. Modern-day crustal heat flow in this target region is variable: very high in the western half, which corresponds to the Walker Lane shear zone, and very low in the eastern half, which corresponds to the highlands of central–south-central Nevada. The most permissive lithologic assemblages for hosting occurrences in this region are the “marine and shelf” assemblages, particularly the “Marine and Shelf–Early-Mid PZ” assemblage, which has the second highest weight of spatial association ( $W^+$ ) with sedimentary rock-hosted occurrences (see Fig. 6.12). In general, the areas of interest in this region are fewer and

smaller in extent, as compared to target regions #1–#4, however, the following sites may warrant some consideration: (1) the central Toiyabe Range, along Toiyabe Range Peak–Bunker Hill–Toiyabe Peak–Bob Scotts Summit, especially north and west of Bunker Hill, and in the vicinity of the Austin Gold Ventures (Quito) mine; (2) the central Toiyabe Range, around Petes Summit, Wildcat Peak, and especially south of Wildcat Peak in the vicinity of the Northumberland deposit, but well short of Mount Jefferson; (3) the southernmost Fish Creek Range, well south of Dave Keane Mountain (no known deposits in this area); (4) the northern Hot Creek Range, north of Morey Peak and northwest of Morey district; (5) the Candelaria Hills, in southeastern Mineral County, north and northeast of Miller Mountain, and especially the region west of the Lucky Hill mine and the Candelaria district; and (6) the southwestern Monte Cristo Range, in central northwest Esmeralda county, southwest of the Charley claims along the eastern margin of the Columbus Salt Marsh.

**Other Regions**—In addition to the targets noted above, a number of other promising exploration sites in the Pershing–Lander–Humboldt counties region, which are not reviewed in detail here, include: (1) the northern Tobin Range, north of the Needle Peak and Mount Tobin area, south of the Iron Hat polymetallic vein district and north of the Mount Tobin hot springs deposit; (2) the western (northwestern) half of Battle Mountain, north and northwest of Antler and North peaks; (3) the mountains northwest of the northeastern opening of Pumpnickel Valley, especially in the area surrounding the Golconda Summit; (4) the northwestern Osgood Mountains, to the west and north of the Getchell trend deposits; (5) the Hot Springs Range (west of the Osgood Mountains), the whole of the range but particularly north of Hot Springs Peak in the vicinity of the fault-bound Paleozoic serpentinite units (this lithologic unit, Pzsp, has a high spatial association with distal disseminated occurrences in the Candelaria district in southeastern Mineral County). All of these sites have similar geologic characteristics and attributes to those mentioned in the target regions above.

### 7.5.3 Volcanic Rock-Hosted Mineral Potential Regions

The volcanic rock-hosted occurrence-type regional-scale exploration target index map is shown in [Figure 7.23](#). The individual target regions are shown in [Figures 7.24, 7.25, 7.26, and 7.27](#). They consist primarily of elevated mineral potential areas that are not immediately surrounded by volcanic rock-hosted or other types of occurrences. The target regions are mainly located within the Walker Lane belt and the Humboldt zone, which trends northeast–southwest across northern Nevada. The individual target regions are described below. A summary of the important geologic mineral potential evidence associated with areas of elevated favorability in the target regions is given in [section 8.2.2](#).

**Region #1**—Located in the extreme northwestern corner of Nevada, the main targets in this region are associated with a cluster of Au-Ag hot spring deposits (Virgin Valley district) that occur in the northern portion of this region, and the Western Hog Ranch Au-Ag hot spring mine, which is located in the central part of the region ([Fig. 7.24a](#)). The Crofoot and Lewis mines (Sulphur district) are found in the southeastern part of this target region. The occurrences in this region are principally Au-Ag hot-spring-type. The most significant mineral potential evidence for this region consists of lithology, the geomagnetic anomaly, fault distance buffers, and the isostatic gravity anomaly, as well as numerous possible deep-seated basement structures that trend through the eastern and southern halves of the region ([Fig. 7.24b](#)). In some cases the mineral potential regions of interest are aligned along some of these deep-seated basement structures, while in other instances the favorable areas are proximal to the intersection of the structures. The favorable areas are also characterized by moderate to high relative fault density, and are flanked to the east, southeast, and south by Mesozoic plutons. These structural arrangements could facilitate fluid flow, as well as provide structural traps and the appropriate physio-chemical conditions conducive to ore deposition (see discussion in [sections 3.4, 6.4.3, and 6.5.3](#)). In addition, this region is marginal to the present-day Battle Mountain heat high, and may have a relatively thin crust (~20 km; see Allenby and Schnetzler, 1983; Pakiser, 1989; and [sections 2.7.2 and 2.7.5](#)). If these conditions were present around 27–5 Ma, they most likely contributed heat to the region, promoting magmatic activity and the convection of crustal fluids. The most permissible lithologic assemblage in this region is “Felsic-Intermediate Extrusive & Intrusive–Late CZ”, which is the volcanic assemblage having the highest weight of spatial association (W<sup>+</sup>) with the volcanic rock-hosted occurrences ([Fig. 7.24c](#); also see [Fig. 6.15](#)). The two principal areas of interest are located in the north-central

and west-central portions of the region, with other areas located in the northwest and the east. The following sites may warrant further investigation: (1) north and south of the Western Hog Ranch mine, in the vicinity and north of Fox and Hog Ranch mountains; (2) the hills west and north of Cottonwood Creek (just west of the Western Hog Ranch mine), and especially in the areas northwest and west of High Rock Canyon (no known mines in this area); (3) the Hays Canyon Range, in the vicinity of Hays Canyon Peak (no known mines in this area); (4) the mountains located in northwesternmost Nevada, around  $-118.80^\circ$  longitude– $41.40^\circ$  latitude (no known mines in this area); (5) the general area around the Virgin Valley district, in the vicinity of Catnip, Fish Creek, and Blow Out mountains; (6) northeast of the Virgin Valley district area, in the vicinity of McGee and Big mountains (no known mines in this area); and (7) the Pine Forest Range, along a traverse following Bartlett Peak, Duffer Peak, and extending to the northern part of the range (this area has a large number of small low-sulfide gold-quartz vein deposits).

**Region #2**—Located in northernmost central Nevada, east of target region #1, the principal targets in this region border the southwestern and southeastern margin of relatively broad late Tertiary volcanic plateau, consisting of basalt and associated gravels, known as the Banbury formation (Fig. 7.25a and 7.25c). The most prominent area of mineral potential favorability is located in the northwestern portion of this region, and trends roughly northwest-southeast. It is host to the National district, the Golden Circle (Midas) district, and the Hollister (Ivanhoe) deposits (Fig. 7.25a). Other large volcanic rock-hosted deposits occur in the eastern part of the region, and include the deposits of the Good Hope and Tuscarora districts. This target region also hosts a number of very significant sedimentary rock-hosted deposits, including the Getchell trend, Carlin trend, and Independence group occurrences, making it one of the richest gold-producing areas in the world. The most significant mineral potential evidence for this region consists of lithology, the geomagnetic anomaly, fault distance buffers, and lithologic diversity. In addition, this target region, and in particular the prominent northwest-southeast-trending mineral potential favorability area, is intersected by many crustal-scale lithotectonic features, including: (1) the northern Nevada rift zone, which is roughly coincident with the most significant mineral potential “high” in this region; (2) numerous proposed deep-seated basement structures (Fig. 7.25b); and (3) several strike-slip faults that parallel the Humboldt zone (see Shawe, 1965; Putnam and Henriques, 1991). The main mineral potential favorability area also intersects the  $^{87}\text{Sr}/^{86}\text{Sr}$   $I_{\text{Sr}} = 0.706$  isopleth, presumed to represent the western edge of the North American Precambrian craton (see Figs. 2.10 and 2.11), the Golconda thrust front, and the Nevada paleothermal high. Furthermore, the areas of high mineral potential are characterized by relatively thin crust ( $\sim 20\text{--}28$  km), high present-day heat flow (marginal to the Battle Mountain heat high), and moderate to high relative fault density. Like target region #1, as well as sedimentary rock-hosted target regions #2-4, the configuration of tectonic elements observed in this region could facilitate mineralization processes. The most permissible lithologic assemblages in this region include “Felsic-Intermediate Extrusive & Intrusive–Late CZ” and “Intermediate-Mafic Extrusive & Intrusive–Late CZ”, the former being the volcanic assemblage having the highest weight of spatial association ( $W^+$ ) with the volcanic rock-hosted occurrences, the latter having a moderate weight (Fig. 7.25c; also see Fig. 6.15). Possible exploration sites for further investigation include: (1) the Santa Rosa Range, along a traverse connecting McConnell Peak–Buckskin Mountain–Granite Peak–Santa Rosa Peak–Paradise Peak, but particularly in the vicinity and north of McConnell Peak; (2) the mountains along the southwestern margin of the Banbury formation, along a traverse extending from the McConnell Peak–Capital Peak vicinity to the Gold Circle district, and particularly south of the south fork of the Little Humboldt River and north of the town of Midas; (3) directly east of the town of Red House, the mountains on the far side of the valley, forming the eastern border of the valley; (4) the mountains along the southeastern margin of the Banbury formation, along a traverse extending northeast from the Gold Circle district area to the Cornucopia deposit; (5) the northern Tuscarora Mountains, a small area just southeast of Toe Jam Mountain and southwest of Castile Mountain; and (6) the eastern margin of the Banbury formation, immediately in the vicinity of Hat Peak.

**Region #3**—Located in northeastern corner of Nevada, east of target region #2, this target region is nearly the same in extent as sedimentary rock-hosted target region #1 (Figs. 7.25 and 7.20). The Jarbidge district deposits (mainly Comstock epithermal veins) occur in the northwestern portion of the region, and the principal areas of favorable mineral potential are located in the west and east (Fig. 7.25a). The Independence group sedimentary rock-hosted deposits also occur along the western boundary of the region. The most significant mineral potential evidence for this region consists of lithology, and in varying degrees of frequency and combination, fault distance buffers, pluton distance buffers, the geomagnetic anomaly, lithologic diversity, and the isostatic gravity anomaly, in addition to a number of deep-seated and crustal-scale structures (Fig. 7.25b). This region is transected by several crustal-scale structural features, as is noted for sedimentary rock-hosted exploration target region #1 (see discussion above). The mineral potential favorability area in the western part of the region is located at the intersection of the

$^{87}\text{Sr}/^{86}\text{Sr}$   $I_{\text{Sr}} = 0.706$  isopleth, the Golconda thrust front, a possible deep-seated basement structure, and the Nevada paleothermal high. The two principal favorability areas are associated with crust that has moderate to high relative fault density, and are proximal to Mesozoic plutons. The region is also characterized by high present-day heat flow and a thick crust (30–38 km). The most permissive lithologic assemblage in this region is “Felsic-Intermediate Extrusive & Intrusive–Late CZ”, which is the volcanic assemblage having the highest weight of spatial association ( $W^+$ ) with volcanic rock-hosted occurrences (Fig. 7.25c; also see Fig. 6.15). Potential sites for further exploration include: (1) northeast of the northern Independence Mountains, in “The Mahoganies”, along a traverse extending northeast from the Maggie Summit–Rock Bluff vicinity, through to Haystack and Rough mountains, and up to Hot Springs Butte; (2) the mountains along the eastern side of State Highway 43, between the towns of Wild Horse and North Fork; (3) along the eastern fork of Beaver Creek, within the area of Wild Horse–Mason–Lookout mountains, as well as the area immediately south of the confluence of Beaver Creek and the Humboldt River; (4) the Jarbidge Mountains, in the area between Marys River–Gods Pocket peaks and Twin Buttes (to the northwest), the areas immediately surrounding Marys River–Gods Pocket peaks, and areas further south of Marys River–Gods Pocket peaks; (5) along the northeast–southwest-trending highlands southwest of L&D Mountain; (6) in the immediate vicinity of Tijuana John Peak (in northeastern Nevada); (7) south and southwest of Gollaher Peak (in northeastern Nevada); (8) in the immediate vicinity of White Rock Mountain, and immediately south of Bald Mountain (both in northeastern Nevada); and (8) in the immediate vicinity of China Jim Mountain (in northeastern Nevada).

**Region #4**—Located in central western Nevada, this region is host to some of the largest volcanic rock-hosted deposits in Nevada, including the Buster mines, the Comstock district, and the Como district in the western portion of the region, the Aurora district in the south, and the Wonder district, the Sand Springs district, the Fairview district, the Rawhide deposit, and the Paradise Peak mine in the eastern part of the region (most are Comstock-type epithermal vein deposits) (Fig. 7.26a). The areas of elevated mineral potential are distributed in a semi-uniform manner as a broad belt that trends northwest-southeast across the region. The most significant mineral potential evidence for this region consists of lithology, pluton distance buffers, the geomagnetic anomaly, faults distance buffers, lithologic diversity, and the isostatic gravity anomaly, in addition to numerous possible deep-seated and strike-slip structures (Fig. 7.26b). Clearly, the most important structural feature in this region is the Walker Lane shear zone, along which extends the belt of elevated mineral potential areas. Possibly equally important are a number of linear features, trending northeast-southwest along the Humboldt zone (see Figs. 1.2 and 6.6), which intersect the Walker Lane shear zone in the vicinity of Comstock district (the Humboldt zone and these linear features are discussed in greater detail in sections 8.3.2 and 8.4). The region is in general transected by a number of crustal-scale possible deep-seated basement structures and strike-slip faults (see Shawe, 1965; Blakely, 1988; Putnam and Henriques, 1991). The crust is presumed to be thin (<30 km; see Allenby and Schnetzler, 1983; Allmendinger et al., 1987; Wernicke et al., 1996, and section 2.7.2), and characterized by a variable relative fault density (although the relative density of small linear features interpreted from LANDSAT imagery is moderate to high) and by a density of plutons greater than any other area in Nevada. Present-day heat flow across the region is variable, with a distinct high in the area around Reno, Nevada (Steamboat hot springs), approximately where linear features that parallel the Humboldt zone intersect the Walker Lane shear zone. The structural and crustal conditions in this region appear to have been near-optimal for ore deposition—enhanced fracture and fault permeability, as well as structural traps for mineralization, provided by shearing along the Walker Lane deformational belt, and heat input from widespread volcanism to drive hydrothermal convection. The most permissive lithologic assemblages in this region include “Felsic-Intermediate Extrusive & Intrusive–Late CZ” and “Breccia and Tuffs–Late CZ”, the former being the volcanic assemblage having the highest weight of spatial association ( $W^+$ ) with the volcanic rock-hosted occurrences, the latter having a relatively high weight as well (Fig. 7.26c; also see Fig. 6.15). Sites for further investigation in this region are numerous, and there are far more than can be reviewed here. The following is a list of general areas or groups of sites that have good potential for hosting volcanic rock-hosted precious metal occurrences: (1) the northern Carson Range, the area north of Mount Rose; (2) the Virginia Range, the area north of the Comstock district and south of Interstate Highway 80; (3) the northern Pine Nut Mountains, along a traverse connecting Table Mountain–Rawe Peak–Lyon Peak–Bismark Peak; (4) the southern Pine Nut Mountains, along a traverse connecting Mount Como–Mount Siegel–Eagle Mountain–Wild Oat Mountain; (5) the Wellington Hills, in the vicinity of Desert Creek Peak; (6) the Pine Grove Hills, along a traverse extending north from Bald Mountain through Mount Etna–Mount Wilson–Shamrock Hill to Carson Hill; (7) the Desert Mountains, between Cleaver Peak and Brown Knob; (8) the Gabbs Valley Range, from the northernmost reaches southeast to Table Mountain and south to Pilot Peak; (9) the southernmost Clan Alpine Mountains, south and east of Big Kasock and Slate mountains; (10) the southwestern, central, and northeastern Excelsior Mountains, as well as southeast of the northern end of Huntton Valley; and (11) the central Monte Cristo Range.



**Region #5**—Located in southeastern Nevada, this region is generally lacking in volcanic rock-hosted occurrences as compared to the other target regions, but despite this, it does have a number of elevated mineral potential areas. The notable deposits in the region include the Eagle Valley district deposits (Comstock epithermal veins) in the northeast, the Delamar (Ferguson) district deposits (Comstock epithermal veins) in the east-central part of the region, the Golden Arrow district deposits (Comstock epithermal veins) in the northwest, and in the southwest, the Mother Lode mine, which is just east of the Bullfrog district, host to a number of larger Comstock epithermal vein deposits (Fig. 7.27a). Other deposit types of interest in this region include the Pioche and Highland districts in the northeast (polymetallic replacement deposits), and the Sterling mine in the southwest (sedimentary rock-hosted Au-Ag). The areas of elevated mineral potential are mainly distributed throughout the western half of this region, and concentrated in the east. The most significant mineral potential evidence for this region consists of lithology, pluton distance buffers, the geomagnetic anomaly, faults distance buffers, lithologic diversity, and to some degree, the isostatic gravity anomaly, as well as a number of regional-scale structures (Fig. 7.27b). The area of elevated mineral potential occurring in the eastern part of the region is located along the Sevier thrust front, where it is intersected by several possible deep-seated basement structures and proximal to a number of strike-slip faults (see Shawe, 1965; Blakely, 1988; Putnam and Henriques, 1991). Mineral potential “highs” in the eastern part of the region occur along possible deep-seated basement and/or strike-slip structures and in areas proximal to the intersection of these features. The areas of elevated mineral potential in the east are also marginal to the Nevada paleothermal anomaly. It is also interesting to note that the proposed southeastern extension of the northern Nevada rift zone, as interpreted from the isostatic gravity anomaly (see section 6.6.3), roughly bisects this target region, the two main areas of high mineral potential occurring to either side of the inferred rift structure (also see Figs. 6.45, 6.53, and 6.54). The crust in this region is characterized by moderate to low present-day heat flow, presumed thinning from east to west (~32-34 km to < 30 km; see Allenby and Schnetzler, 1983; Allmendinger et al., 1987; Wernicke et al., 1996, and sections 2.7.2 and 2.7.5), and by variable relative fault density (although the relative density of small linear features interpreted from LANDSAT imagery is moderate to high in favorable areas). Such structural conditions should be conducive to ore formation provided that a heat source(s) was available to drive hydrothermal circulation. The most permissive lithologic assemblage in this region is “Breccia and Tuffs–Late CZ”, which has a relatively high weight of spatial association ( $W^+$ ) with the volcanic rock-hosted occurrences (Fig. 7.27c; also see Fig. 6.15). A number of deposits are also hosted by the “Felsic-Intermediate Extrusive & Intrusive–Late CZ” lithologic assemblage, which has the highest weight of spatial association ( $W^+$ ) with the volcanic rock-hosted occurrences. Possible sites for follow-up exploration include: (1) the whole of the Cactus Range, and east of the southern end of the Cactus Range in the vicinity of Gold Mountain; (2) immediately in the vicinity of Black Mountain on Pahute Mesa; (3) the Kawich Range, south of Kawich Peak to Quartzite Mountain; (4) Shoshone Mountain, immediately northwest-west-southwest of Shoshone Peak; (5) the North Pahroc Range, from Pahroc Summit Pass north to Silver King Mountain; (6) the central Delamar Mountains, just east and southeast of Delamar (Ferguson) district area; (7) northeast of the Cedar Range, along a traverse extending to the Eagle Valley district area; and (8) the eastern Clover Mountains, west and northwest of the Vigo district area.

**Other Regions**—In addition to the targets noted above, a number of other promising exploration sites in the Pershing, northern Nye, and western Nye counties regions, which are not reviewed in detail here, include: (1) the whole of the Seven Troughs Range and Trinity Range (Pershing county); (2) the southern Eugene Mountains (Pershing county); (3) the northern East Range, particularly around Dun Glen Peak (Pershing county); (4) the southern East Range–northern Stillwater Range, between Logan Peak and Granite Mountain (Pershing county); (5) the southern Tobin Range, just south of Mount Tobin (Pershing county); (6) the central Monitor Range, south of Savory Mountain (northern Nye county); (7) the Antelope Range, south of Nine Mile Peak (northern Nye county); (8) Moody Mountain, around Moody Peak, and southeast of Moody Peak to the northern Pancake Range (northern Nye county); (9) the whole of the San Antonio Mountains (western Nye county); and (10) the northern Goldfield Hills, in the vicinity of Blackcap Mountain. The geologic characteristics of these sites vary from area to area, but they are generally consistent with those described in the target regions above.

# Chapter 8. Controls on Sedimentary and Volcanic Rock-Hosted Occurrence Distribution

## 8.1 Introduction

Chapter 8 is a discussion and summary of the geologic and metallogenic interpretation of the mineral potential maps. It brings together the lithologic, structural, and tectonomagmatic mineral potential evidence observed in the target regions reviewed [section 7.5](#) and the spatial relationships and interpretations presented in [chapter 6](#).

The results of mineral potential modelling suggest that there are two distinct and separate sets of crustal structures that control the first-order regional-scale distributions of the sedimentary and volcanic rock-hosted occurrences in the Great Basin:

- *Sedimentary rock-hosted (Carlin-type) mineralization* in northern Nevada appears to be constrained by two, well-defined, sub-parallel, northwest–southeast-trending structural zones, here termed the “Carlin” and “Cortez” structural zones ([Fig. 8.1a](#), red lines).
- *Volcanic rock-hosted (epithermal) mineralization* in northern, western, and southwestern Nevada appears to be constrained by two broad and diffuse structural zones: the Walker Lane shear zone in southwestern Nevada, and a wide belt of possible transcurrent movement that trends northeast–southwest across northern Nevada, here termed the “Humboldt shear(?) zone” ([Fig. 8.2a](#), red transparency).

The presence of these structural zones is in large part suggested by patterns of elevated mineral potential delineated in the sedimentary and volcanic rock-hosted occurrence posterior probability maps ([Figs. 7.4, 7.5, 7.13, and 7.14](#)).

Important mineral potential evidence within the regional-scale exploration target areas is summarized in [section 8.2](#). This evidence helped to recognize and delineate the Humboldt shear(?) zone and the Carlin and Cortez structural zones, which are reviewed [section 8.3](#). The remainder of this chapter discusses geologic evidence for the existence, character, and possible origins of these features ([sections 8.4 and 8.5](#)).

## 8.2 Mineral Potential Evidence Associated with the Gold-Silver-Bearing Occurrences

### 8.2.1 Sedimentary-Rock Hosted Occurrences

In the sedimentary rock-hosted occurrence regional-scale exploration targets ([section 7.5.2](#)) the areas of elevated mineral potential are most commonly associated with the “*Marine and Shelf–Early-Mid PZ*”, “*Siliceous Rocks–Mid PZ-PC*”, and “*Marine and Shelf–Late PZ*” lithologic assemblages (see [Fig. 6.12](#)). Within these assemblages, the lithologic units hosting most of the sedimentary rock-hosted occurrences include Os, St, Dc, and MDs (see [Fig. 6.13](#); note that most of the occurrences apparently “hosted” by the Quaternary cover unit are possibly hosted by units Os, Dc, or MDs, which lie range-ward of the occurrences). The units Os, St, Dc,



and MDs are variably composed of shale (Os, MDs), limestone and dolostone (Os, St, Dc, MDs), silty-limestones–limy-siltstones (St), siltstone (MDs, St), sandstone (Dc, MDs), chert (Os, St), and minor amounts of other detrital and metamorphosed rocks (Os, Dc, MDs) (see [Appendix A](#)). These units in part constitute the “*Siliceous (Western) Assemblage*” (Os), the “*Transitional Assemblage*” (St), the “*Carbonate (Eastern) Assemblage*” (Dc), and the “*Carbonate-Detrital Belt Along Eastern Margin of Antler Orogenic Belt or Western Part of Foreland Basin*” (MDs), as classified by Stewart and Carlson (1978) (see [Appendix A](#)). The targets areas are also proximal to, or related to the intersection of, a number of regional-scale structures, which include the  $^{87}\text{Sr}/^{86}\text{Sr} \text{ } I_{\text{Sr}} = 0.706$  isopleth, presumed to represent the western edge of the Precambrian craton (see [Figs. 2.10](#) and [2.11](#)), the northern Nevada rift zone (see [sections 2.7.4](#) and [6.6.3](#); [Fig. 6.45a](#), feature #1), the Roberts Mountain and Golconda thrust fronts ([Fig. 2.5](#)), and possible deep-seated basement structures interpreted from aeromagnetic data. The nature of the crust in the sedimentary rock-hosted exploration target regions is variable, but in the vicinity of Battle Mountain–Eureka (Cortez) and Carlin mineral trends, the present-day crust is characterized by:

- Thicknesses of greater than 30 km, particularly to the east and northeast of the mineral trends ([Fig. 6.5d](#)).
- Moderate to low relative fault density ([Fig. 6.37c](#)), although LANDSAT linear feature density is high to moderate, and lithologic diversity is moderate to high ([Fig. 6.34](#)).
- General lack of widespread magmatism in relation to surrounding regions ([Figs. 6.4](#) and [6.56](#)).
- Variable heat flow (areas of moderate to high heat flow are proximal to the mineral trends; [Fig. 6.5g](#)). Heat flow may have been higher in the Paleozoic or Mesozoic as evidenced by a paleothermal anomaly ([Fig. 2.10](#)).

The prominent association of elevated sedimentary rock-hosted mineral potential areas with the lithologic and structural features indicated above suggests that, collectively, they probably exercised strong controls on sedimentary rock-hosted precious metal mineralization in the Great Basin. The lithologic associations suggest that certain sedimentary assemblages (1) could have acted as potential source rocks for gold and/or (2) were more suitable host rocks for ore deposition (see [sections 3.5](#), [3.6](#), [6.3.3](#), and [6.4.3](#) for more detailed discussions). The structural associations indicate the importance of local- and regional-scale deformational features to mineralization. Such structures most likely facilitated mineralization by preparing potential host and/or source rocks, concentrating and directing hydrothermal gold-bearing solutions, and increasing permeability, thereby promoting near-surface and deep fluid circulation, vertical and lateral heat transfer, as well as enhancing fluid-wall rock interactions (see discussion in [sections 2.7.6](#), [2.7.7](#), [3.4](#), [3.6](#), [6.4.3](#), and [6.5.3](#)).

## 8.2.2 Volcanic Rock-Hosted Occurrences

In the volcanic rock-hosted occurrence regional-scale exploration targets ([section 7.5.3](#)) the areas of elevated volcanic rock-hosted precious metal mineral potential are most commonly associated with the “*Felsic-Intermediate Extrusive & Intrusive–Late CZ*” and “*Breccia and Tuffs–Late CZ*” lithologic assemblages (see [Fig. 6.15](#)). Within these assemblages, the lithologic units hosting most of the volcanic rock-hosted occurrences include Tt2, Ta3, Tr3, Ta2, and Tba (see [Fig. 6.16](#)). These units are primarily andesite (Ta3, Tba), silicic ash-flow tuffs (Tt2), rhyolite (Tr3, Ta2), and other intermediate rocks, with varying amounts of basalt, and range in age from 34–6 Ma and younger for some basalt units (see [Appendix A](#)). These rocks are generally distributed in semi-circular fashion along the northern–western–southwestern borders of Nevada, and compose in part the 34–17 Ma and 17–6 Ma age units of Stewart and Carlson's (1976) time-slice maps (see

Figs. 6.4, 6.24, and 6.25; section 6.3.3). As observed by Ludington et al. (1993), and shown in Figures 3.1 and 6.2, the volcanic rock-hosted occurrences are distributed in a crescent-shape pattern that coincides with the semi-circular distribution of these units. In particular, they have a high degree of spatial correlation with igneous rocks comprising the 17-6 Ma time-slice (see section 6.3.3; compare Fig. 6.2 to 6.4 and 6.24). Igneous rock composition-slice maps derived from the geological map of Nevada (Stewart and Carlson, 1978) reveal that nearly all units of mafic to intermediate composition are also distributed in a semi-circular manner (see Fig. 6.55), which is coincident in space and time with the 34-17–17-6 Ma igneous rock time-slice ages and with the volcanic rock-hosted occurrence distribution pattern (see Figs. 6.4 and 6.25). The targets areas are also proximal to, aligned along, or located at the intersection of possible deep-seated basement structures, strike-slip faults, thrust fronts, and crustal-scale features, including the  $^{87}\text{Sr}/^{86}\text{Sr} \text{ } I_{\text{Sr}} = 0.706$  isopleth (presumed to represent the western limit of the North American Precambrian craton; see Figs. 2.10 and 2.11) and in some instances, the northern Nevada rift zone or the Nevada paleothermal anomaly (see sections 2.7.4 and 6.6.3; Figs. 2.10 and 6.45a, feature #1). The nature of the crust in the volcanic rock-hosted exploration target regions is variable, but in regions known to host deposits of significant number and size, the present-day crust is characterized by:

- Thicknesses of less than 30 km (Fig. 6.5d).
- Moderate to high relative fault density and/or LANDSAT linear feature density (Fig. 6.37c).
- High relative density of intrusives (primarily Mesozoic in age; Fig. 6.36c).
- Moderate to high present-day heat flow (Fig. 6.5g).

The close spatial association of elevated mineral potential areas with the lithotectonic and crustal features described above indicates that they probably exercised a great deal of control over the distribution and development of volcanic rock-hosted precious metal mineralization in Nevada. The strong spatial and temporal coincidence between the occurrences (formed mostly between 27 and 5 Ma; Ludington et al., 1993) and the volcanic units composing the 34-17–17-6 Ma time-slice age units indicates that mineralization was closely tied to the migration of the inception of magmatism (and extension) across the Nevada Great Basin (see sections 2.5.1.1, 2.5.2.1, and 6.3.3). This coincidence suggests that the 34-17–17-6 Ma time-slice volcanic rocks could have provided heat and contributed gold to volcanic rock-hosted mineral systems (either as source rock to be scavenged or by the input of magmatic ore-bearing fluids into the mineralizing hydrothermal system; see discussions in sections 3.5, 3.6, 6.4.3, and 6.5.3). There is also spatial correlation between the volcanic rock-hosted occurrence distribution pattern and: (1) the intermediate to mafic composition-slice units (see Fig. 6.55); (2) the Walker Lane, which may be intruded by mafic and intermediate rocks at depth, as indicated by a high density of positive geomagnetic anomalies along the Walker Lane (see Fig. 6.45a, feature #2); and (3) the Humboldt shear(?) zone, which may also be intruded by mafic and intermediate rocks at depth, as indicated by a broad belt of high density of positive geomagnetic anomalies north and northwest of the zone (as defined here), as well as at least three prominent cross-cutting anomalies (northern Nevada rift and subordinate rifts to the west) (see Fig. 6.53b and 6.45a, feature #5). These intrusive rocks, which in the Walker Lane are nowhere exposed at the surface, could presumably have contributed gold as well. The structural and crustal features associated with volcanic rock-hosted mineralization could have facilitated the movement of mineralizing fluids and heat, as stated in the preceding section on sedimentary rock-hosted deposits, and as summarized in sections 3.4, 3.6, 6.4.3, and 6.5.3.

## 8.3 Delineation of the Regional-Scale Control Structures

### 8.3.1 Sedimentary Rock-Hosted Mineralization

The regional-scale alignment of sedimentary rock-hosted occurrences along the Carlin and Battle Mountain–Eureka (Cortez) mineral trends strongly suggests the presence of a sub-parallel pair of northwest–southeast-trending crustal-scale structural zones (or segments of zones). Two linear features, here termed the “Carlin” and “Cortez” structural zones ([Fig. 8.1a](#), red lines), have been delineated on the basis of:

- The distribution trend of elevated sedimentary rock-hosted mineral potential ([Figs. 7.4 and 7.13](#)).
- The linear distribution of known occurrences, including volcanic rock-hosted occurrences, along two well-defined mineral trends ([Figs. 1.3, 3.3, 6.2, 6.65, 7.13b, 8.1b](#)).
- The linear arrangement of structural elements visible in the shaded relief of topography ([Figs. 1.2, 6.6, and 8.1](#); also see Thelin and Pike, 1991).
- The distribution pattern of isostatic and Bouguer anomalies and geomagnetic anomalies ([Figs. 6.45, feature #1; 6.53, and 6.54](#)).
- The distinctive “V”-shaped distribution trend of K/Na and Ba/Na geochemical anomalies, although any genetic connection of these anomalies with the Carlin and Cortez structural zones is unclear (see discussion [section 6.7.3; Figs. 6.57 and 6.65](#)).

The Carlin and Cortez structural zones may have acted as fundamental controls over the regional-scale distribution of sedimentary rock-hosted mineralization in northern Nevada. Along these zones, ore-bearing fluids could have been focused and circulated, forming particularly significant deposits at intersections with other structural zones where favorable host-rocks and/or the appropriate physio-chemical conditions were present ([Fig. 8.1](#)). The extents of the Carlin and Cortez structural zones, and the other intersecting linear features depicted in [Figure 8.1](#) (blue lines), are exaggerated in order to highlight structural and mineral trends (i.e.—presented for the purposes of illustration). Assuming that these structural zones and linear features are real, they most likely have a complex history of movement involving more intricate crosscutting relationships than the simple non-offset linear intersections illustrated here.

Sedimentary rock-hosted mineralization is considered to be 42–30 Ma in age (Hofstra, 1997). The Carlin and Cortez structural zones are thought to be mid-Mesozoic or older in age, perhaps dating back to late Proterozoic rifting along the western edge of the North American craton (Grauch, 1995). The most significant recent geologic activity related to these structural zones could be the formation of the northern Nevada rift zone in the mid-Miocene. These topics are further discussed in [section 8.5](#).

### 8.3.2 Volcanic Rock-Hosted Mineralization

The “crescent-shaped” pattern of volcanic rock-hosted occurrences in Nevada suggests that two broad, crustal-scale, structural zones control the regional-scale distribution of epithermal mineralization in northern and southwestern Nevada. The northwest–southeast-trending Walker Lane shear zone in southwestern Nevada, and a belt trending northeast–southwest in northern Nevada, here termed the “*Humboldt shear(?) zone*”, have been delineated on the basis of:

- The distribution trend of elevated volcanic rock-hosted mineral potential ([Figs. 7.5 and 7.14](#)).

- The distribution of known occurrences along two broad and diffuse belts across northern and southwestern Nevada (Figs. 3.1, 6.2, 7.14b, and 8.2b).
- The linear arrangements of structural elements visible in the shaded relief of topography (Figs. 1.2, 6.6, 8.1, and 8.2; also see Thelin and Pike, 1991; used particularly to identify the Humboldt shear(?) zone).
- The broad distributions of 6-17 Ma volcanic rocks (Figs. 6.4 and 6.25).
- The distribution of lithologic units having elevated posterior probabilities for volcanic rock-hosted occurrences (Fig. 6.24b).
- The general distribution of warmer geothermal well and spring waters (Fig. 6.5h; used particularly to identify the Humboldt shear(?) zone).
- The general distribution of areas of higher heat flow (Fig. 6.5g; used particularly to identify the Humboldt shear(?) zone).
- The distribution trend of relative density of plutons (Fig. 6.36c; used particularly to identify the Humboldt shear(?) zone).
- The distribution of higher isostatic and Bouguer gravity anomalies (Figs. 6.45b and 6.45c, feature #5, and 6.54a; used particularly to identify the Humboldt shear(?) zone).
- A moderately defined, bilaterally symmetric, northeast-southwest-trending corridor of geomagnetic lows, juxtaposed along length by highs (Fig. 6.45a, feature #5; 6.53b).

The Walker Lane shear zone and the Humboldt shear(?) zone may have acted as fundamental controls over the regional-scale distribution of the volcanic rock-hosted mineralization in northern, western, and southwestern Nevada (Fig. 8.2; also see Fig. 6.6). The southward sweep of Eocene-Oligocene magmatism across the Nevada Great Basin could have exploited these zones, where heat and mineralizing processes were focused and ore deposits formed. Furthermore, it is suggested that Cenozoic activity along the Humboldt shear(?) zone may have had an *incidental affect* on the post-mineralization distribution sedimentary rock-hosted deposits along the northern termini of the Battle Mountain–Eureka (Cortez) and Carlin trends (as discussed below in section 8.5.4).

The majority of volcanic rock-hosted deposits are considered to have formed between 27 and 5 Ma (Ludington et al., 1993; also see Fig. 3.2). The Walker Lane is thought to be at least Mesozoic in age (Stewart, 1988; Saleeby and Busby-Spera, 1992), or perhaps Precambrian (Blakely and Jachens, 1991), with recent activity documented in the Oligocene or Miocene (Dilles and Gans, 1995) and ongoing today. The Humboldt shear(?) zone is considered to be at least mid-Paleozoic in age (Poole et al., 1992), with possible origins dating back to the mid-Proterozoic assembly of the Laurentian protocraton and/or late Proterozoic rifting (see section 2.4). Latest activity along the Humboldt shear(?) zone is believed to be between mid-Oligocene and mid-Miocene time. The Humboldt shear(?) zone is further discussed in section 8.4.

The Walker Lane shear zone has been the focus of much research (for a review, see sections 2.6 and 6.6.3). Correlations between the Walker Lane and the distribution pattern of epithermal volcanic rock-hosted deposits and the Walker Lane have been proposed by Cox et al. (1991), where they stated “...northwest-trending Walker Lane-style deformation began as early as 27 Ma and provided the tectonic conditions that permitted the formation of volcanic-hosted deposits.” Furthermore, the Walker Lane forms the southwestern portion of Ludington et al. (1993)’s “epithermal crescent” (see Fig. 6.2). It seems well established that the Walker Lane shear zone was an important control over the regional-scale distribution of volcanic rock-hosted occurrences in western and southwestern Nevada. This is further verified by the observations and correlations made in this study in previous sections (6.2, 6.3.3, 6.4.3, 6.5.3, and 6.6.3) and will therefore not be further expanded upon here.

## 8.4 The Humboldt Shear(?) Zone

### 8.4.1 Geologic and Other Evidence

The modelling exercises conducted here suggest that the Humboldt shear(?) zone was potentially as important to volcanic rock-hosted mineralization in the Great Basin as was the Walker Lane shear zone. Control over the regional-scale distribution of volcanic rock-hosted occurrences by the Humboldt shear(?) zone has not been discussed in the literature, other than a few references made to possible northeast–southwest-oriented strike-slip movement across northern Nevada.

The Humboldt shear(?) zone is a controversial feature, and the few comments found in the literature suggest that it may possibly be related to another debatable structure, the northeast-southwest-trending Snake River fault in southern Idaho. The Snake River fault may be part of a broader zone of transcurrent movement, which appears to show latest activity in the mid-Miocene, but could have origins dating back to the mid-Paleozoic or later (see Poole et al., 1977; Poole and Sandberg, 1977; Christiansen and Yeats, 1992, p. 362; Poole et al., 1992, figure 1, text p. 16). Such an interpretation is based on the premise that the northern Nevada rift, the western Snake River graben structure, and the Chief Joseph dike swarm (see Fig. 2.3) are tectonically related (Taubeneck, 1970; also see Zoback and Thompson, 1978), and once formed a continuous 700-plus km long rift zone. A 70 to 100 km right-lateral offset between the northern terminus of the northern Nevada rift and western Snake River graben now exists, and a southward extrapolation along the Humboldt shear(?) zone of the N55°E Snake River Plain trend is an appropriate orientation for a transcurrent structure (Christiansen and Yeats, 1992). In addition, Mabey et al. (1983, p. 314) observed that, in northwest Nevada, the northeast structural grain of the Humboldt gravity zone influenced the trend of the faults, which are generally northeasterly rather than normal to the direction of extension, and thus involve considerable strike-slip movement. Transcurrent movement across northern Nevada would be in accord with a northeastern shift in trend or offset seen in a number of generally north-trending geologic features, including (1) the  $^{87}\text{Sr}/^{86}\text{Sr}$   $I_{\text{Sr}} = 0.706$  isopleth, (2) the Wasatch or hinge line, (3) the eugeoclinal-miogeoclinal transitional facies, (4) the Roberts Mountain, Golconda, and Sevier thrust fronts, and (5) northeast bend in the trend of the Cordilleran Mesozoic batholith belt (see Figs. 2.3, 2.5, 2.9, 2.10, 2.11, and 6.23a). In addition, Smith and Luedke (1984) delineated a northeast-southwest trend of 16–10 Ma volcanic loci that may define a broad structure extending from southern Idaho across northern Nevada (see Smith and Luedke's figure 4.4, and comments on p. 58). Most recently, Wooden et al. (1997) have presented  $^{208}\text{Pb}/^{204}\text{Pb}$  isotopic data that suggest the existence of a major crustal fault or suture north of the Carlin trend (see figure 1 in Wooden et al., 1997). They describe two isopleths ( $^{208}\text{Pb}/^{204}\text{Pb} > 39$  and  $^{208}\text{Pb}/^{204}\text{Pb} < 38.8$ ) that are southwest of, and parallel to, the Battle Mountain–Eureka (Cortez) trend. At the northern termination of the mineral trend, the isopleths swing acutely to the northeast, which may reflect the presence of the Humboldt shear(?) zone.

### 8.4.2 Topographic Expression

The Humboldt shear(?) zone is most readily recognized as a broad and diffuse Bouguer and isostatic gravity high zone that stretches northeast-southwest across northern Nevada (Fig. 6.45b, feature #5, and 6.54a). Of the many datasets compiled and examined for the study, the Humboldt



shear(?) zone is best resolved in shaded relief of topography (based on ~800 meter pixel resolution) (see [Figs. 1.2, 6.6, and 8.2](#); also see Thelin and Pike, 1991). The shaded relief of topography reveals a number of unique structural features and some subtle, but clearly visible, differences in the tectonic grain of the crust between the Humboldt shear(?) zone, the Walker Lane shear zone, and the central–east-central interior of Nevada (these differences are primarily visible northwest of a line that extends from the northeastern corner of the state to Reno, and represents the approximate southeastern limit of the Humboldt shear(?) zone). Some of these features and differences include: (1) the gross orientation of mountain ranges changes between central and northwestern Nevada, from northeast-trending to north-trending in a relatively abrupt manner as the southeastern limit of the Humboldt shear(?) zone is crossed (as delineated in [Fig. 8.2a](#)); (2) on closer inspection, some ranges display domino-style east-west lateral offsets (e.g.—the Independence Mountains, the Osgood Mountains, the Selenite Range, among others); (3) several continuous and segmented linear features traverse northeast-southwest across Nevada, the most prominent of which are seen to cut the topographic expression of the northern Nevada rift zone; and (4) the northern and/or southern ends of a few ranges appear to have a decidedly “sheared” aspect to their morphology (the West Humboldt Range is the most prominent example). All of the features pointed out above either trend roughly northeast-southwest, or are indicative of movement along this direction.

An additional point of interest is the broad and open semi-continuous “S”-shaped curvilinear alignment of ranges visible in the shaded relief ([Figs. 1.2 and 8.2](#)). The northern terminus of this feature, which arcs to the northeast, is presumed to mark the southeastern limit of the Humboldt shear(?) zone (as expressed in basin-range morphology), while the southern terminus, which arcs to the southwest, could indicate the approximate northeastern limit of the Walker Lane shear zone ([Fig. 8.2a](#)). This feature is further discussed in connection with the Carlin and Cortez structural zones in [section 8.5.3](#) below.

### 8.4.3 Origin, Age, and Character of the Humboldt Shear(?) Zone

In addition to the features delineated in shaded relief of topography, a variety of other compelling geological observations and correlations suggest that a broad northeast–southwest-trending zone of transcurrent movement, with possible ancestral heritage, extends across northern Nevada. The following material, presented in point form, further details, characterizes, and demonstrates the existence of the proposed Humboldt shear(?) zone:

*Points that generally contend for the origin, orientation, and age of the Humboldt shear(?) zone include:*

- Northern Nevada is characterized by an isostatic residual gravity anomaly high that stretches northeast-southwest across the region, and by a Bouguer gravity anomaly high located in the northwestern part of the State that appears to be elongated along a northeast–southwest-orientated axis (see [Figs. 6.45b and 6.45c](#), feature #5, and [6.54a](#); [sections 2.7.3 and 6.6.3](#)). Referred to as the Humboldt gravity anomaly or zone (see Mabey et al., 1983), the anomaly is believed to roughly delineate the limits of the Humboldt shear(?) zone.
- At residual Bouguer gravity wavelengths of less than 250 km, the Great Basin is characterized by predominantly northwest trending high-low-alternating anomalies, which extend about the length of the State of Nevada (Kane and Godson, 1989, see plate in back pocket). These anomalies are truncated and severely disrupted by the Humboldt gravity anomaly in northern Nevada, forming a crustal gravity zone boundary with



anomalies of different character to the north. The boundary extends northeast-southwest from the southeastern Idaho–central Wyoming border, across northern Nevada, to the Mendocino triple junction, and may be interpreted as the juxtaposition of major crustal blocks of differing densities, along which a crustal flaw zone or suture zone might exist.

- The Walker Lane is magnetically characterized by a pattern of arcuate anomalies that trend northwestward, generally parallel to the shear zone (Blakely and Jachens, 1991; see [section 6.6.3](#); [Figs. 6.45a](#), feature #2, and [6.53b](#)). This pattern of anomalies is disrupted by a diffuse, northeast–southwest-trending, total residual field geomagnetic low, forming a crustal geomagnetic zone boundary, northwest and north of which geomagnetic highs once again resume (Kane and Godson, 1989, figure 2). The boundary, as delineated by Kane and Godson (1989), parallels the southern limit of a group of magnetic highs that extend southwestward along the southern Snake River Plain, into northern Nevada, and across California to the Mendocino triple junction. This magnetic zone boundary, as well as the gravity zone boundary mentioned above, may be the expression of the primary structural framework of the continental crust (Kane and Godson, 1989), and as such, could represent a crustal flaw-zone or suture zone.
- Neodymium isotopic data that delineate a Precambrian crustal province boundary, which separates the >2.7 Ga Wyoming province from 2.3–2.0 Ga crust, appears to coincide with the Humboldt shear(?) zone (see [Fig. 2.11](#); [section 2.4.2](#)). During the Central Plains and Yavapai-Mazatzal orogenies, between 1.80 and 1.65 Ga, juvenile crust was accreted to the Laurentian protocraton, and if the Humboldt shear(?) zone is related to this suture, then its ultimate age and origin are Middle Proterozoic. Note also that the northeast-southwest trend of the Humboldt shear(?) zone parallels the trend of the  $^{87}\text{Sr}/^{86}\text{Sr}$   $I_{\text{Sr}} = 0.706$  isopleth (presumed to represent the western margin of the North American Precambrian craton) in northern Nevada—either the Humboldt shear(?) zone controls the trace of the  $^{87}\text{Sr}/^{86}\text{Sr}$   $I_{\text{Sr}} = 0.706$  isopleth (has offset it), or the western margin of the Precambrian craton controls the location of the shear zone. Whichever the case, an argument can be made that, if a transcurrent structure is present, it might trend northeast-southwest parallel to the  $^{87}\text{Sr}/^{86}\text{Sr}$   $I_{\text{Sr}} = 0.706$  isopleth in northeastern Nevada.
- The southwestern segment of the Humboldt shear(?) zone may coincide with a region of crustal thinning (~20 km) in northwestern Nevada ([Fig. 6.5d](#); also see Allenby and Schnetzler, 1983, figure 2, Braile et al., 1989, figure 3, and Pakiser, 1989, figure 2). In addition, recent work by Wernicke et al. (1996) suggested that the thin crust of the western Great Basin may extend under the southern Sierra Nevada region. Should this be the case for the northern Sierra Nevada as well, then the zone of thin crust observed in northwestern Nevada would extend farther southwestward along an axis parallel to the Humboldt shear(?) zone. COCORP studies support limited Moho relief in the east-west direction in this area, but do not suggest that the northern Sierra Nevada is much less than 35 km thick (Allmendinger et al., 1987; Knuepfer et al., 1987). There are no data to suggest that the zone of crustal thinning extends northeast under northern Nevada into southern Idaho and western Wyoming, although a ridge in the reflection-surface of the Moho does trend northeast–southwest from northeastern Nevada to east-central Idaho (see Allenby and Schnetzler, 1983, figure 2; Braile et al., 1989, figure 3).
- Northern Nevada is thermally characterized by a northeast–southwest-trending zone of anomalously high present-day heat flow, which extends from the region southwest of the Battle Mountain heat high in northwestern Nevada, across northeastern-Nevada–southeastern-Idaho along the Snake River Plain, to the Yellowstone hot spot (see [Fig. 6.5g](#); also see Blakely, 1988, figure 2; Eaton et al., 1978, figure 3-12; Lachenbruch and Sass, 1978, figure 9-1; Morgan and Gosnold, 1989, figure 12). Present-day anomalous thermal activity along the northeast–southwest extent of the Humboldt shear(?) zone is also expressed by elevated water temperatures in hot springs and geothermal wells ([Fig. 6.5h](#)). It is presumed that thermal activity would be preferentially focused in regions of thinner crust and/or along crustal segments of higher permeability, such as zones of induced permeability that would result from fault or shear activity.
- In addition to the alignment of volcanic rock-hosted occurrences along the Humboldt shear(?) zone ([Figs. 6.2](#), [6.3](#), [7.14b](#), and [8.2b](#)), a map of the relative density of Mesozoic age plutons (see [Fig. 6.36c](#)) shows a broad zone of high pluton density extending northeast-southwest across the northern part of the state. Presumably, both mineralizing fluids and magmas would have taken advantage of the greater permeability

associated with a preexisting structure (i.e.—path of least resistance). Should this be the case, than the Humboldt shear(?) zone could be at least Mesozoic in age.

- Smith and Luedke (1984) delineated a northeast-southwest trend of 16-10 Ma volcanic loci (the Snake River and Humboldt River zones) extending from southern Idaho across northern Nevada (see Smith and Luedke's figure 4.4, and comments on p. 58). The trend of these loci may define a broad zone of crustal weakness, and as stated in the two previous points, it is presumed that heat flow and magmatism would have exploited a preexisting structure such as the Humboldt shear(?) zone.

*Points that generally contend for the transcurrent movement, orientation, and age of the Humboldt shear(?) zone include:*

- The Bouguer gravity anomaly in central–east-central Nevada is characterized by gross bilateral symmetry, the axis of bilateral symmetry trending northwest-southeast and being generally coincident with the northern Nevada rift zone (see Fig. 6.45c, feature #1; sections 2.7.3 and 6.6.3; Eaton et al., 1978, figure 3-8). In northern Nevada, the axis of symmetry disappears, but Eaton et al. (1978) proposed that the axis has been offset eastward and may extend into central Idaho (see Eaton et al., 1978, figure 3-11). The implication is that offset of the axis to the east was achieved along a broad structure characterized by lateral movement. It is also interesting to note that, in Eaton et al.'s (1978) figure 3-11, the dotted line trending northeast–southwest that offsets the axis in central Nevada is coincident to the lower boundary of the Humboldt shear(?) zone, which has been delineated independently in this study from shaded relief of topography (Figs. 8.2a).
- The Humboldt shear(?) zone is parallel to the northeast-southwest-trending inferred Snake River fault in southern Idaho, which is suspected to be a strike-slip fault (Poole et al., 1977; Poole and Sandberg, 1977; Poole et al., 1992, figure 1). Poole et al. (1992, p. 16) noted that evidence for the Snake River fault can be demonstrated by offset of the Sevier thrust system across the Snake River Plain (see Figs. 2.4 and 2.5, and Poole et al., 1992, figure 1), and evidence for both left- and right-lateral movements can be demonstrated by significantly different amounts of offset of thickness trends of Devonian and Mississippian rocks (Poole et al., 1977, have proposed 200 km of Paleozoic left-lateral offset on a fault along the trend of the Snake River plain). The Snake River fault is more than likely to be related to, or is an element of, the Humboldt shear(?) zone, and assuming this to be true, the evidence provided by Poole et al. (1992) indicates that the Humboldt shear(?) zone could be at least mid-Paleozoic in age.
- The presence of a transcurrent feature extending along the trend of the Humboldt shear(?) zone can be inferred based upon the premise that the northern Nevada rift, the western Snake River graben structure, and the Chief Joseph dike swarm (see Fig. 2.3) are tectonically related, and once formed a continuous 700-plus km long rift zone (Taubeneck, 1970; also see Zoback and Thompson, 1978). A 70 to 100 km right-lateral offset between the northern terminus of the northern Nevada rift and western Snake River graben now exists, and a southward extrapolation along the Humboldt shear(?) zone of the N55°E Snake River Plain trend is an appropriate orientation for a transcurrent structure (see Christiansen and Yeats, 1992, p. 362-363). Assuming this premise is correct, and that the lateral displacement between these features is the result of transcurrent movement along the Humboldt shear(?) zone, then the time of latest movement along the shear zone would be at least mid-Miocene.
- Several generally north-trending crustal-scale structures and features of varying ages and types show an eastward deflection, right-lateral offset, or discontinuity across the Humboldt shear(?) zone, which would be consistent with transcurrent movement along a northeast-southwest trend, and include: (1) the  $^{87}\text{Sr}/^{86}\text{Sr}$   $I_{\text{Sr}} = 0.706$  isopleth, presumed to represent the western margin of the North American Precambrian craton (see Figs. 2.3, 2.10, 2.11); (2) the Wasatch or “hinge” line (see Fig. 2.3); (3) the Cordilleran Mesozoic batholith belt (see Fig. 2.3); (4) the Roberts Mountain, Golconda, Luning-Fencemaker(?), and Sevier thrust fronts (see Figs. 2.4 and 2.5; also see Poole et al., 1992, p. 16); (5) the Nevada paleothermal anomaly (see Fig. 2.10); and (6) the northern Nevada rift zone and its postulated northern extension (either the Brothers fault zone or the Snake River graben structure; see Fig. 2.3, and section 2.6; also see Christiansen and Yeats, 1992, p. 362-363, 367).

The material presented above argues strongly in favor of the existence of Humboldt shear(?) zone, and that it may have exercised a fundamental control over the distribution and formation of volcanic rock-hosted occurrences. The Humboldt shear(?) zone may also have had an incidental affect on the distribution of the sedimentary rock-hosted occurrences. Right-lateral, post-mineralization transcurrent movement along the Humboldt shear(?) zone may have displaced the Getchell trend and Independence group deposits northeastward of the northern termini of the Battle Mountain-Eureka (Cortez) and Carlin mineral trends (respectively). This is suggested by a bend to the northeast of As and U/Th geochemical anomalies, believed to have some spatial association with the mineral trends, and by eastward lateral offsets in Basin-Range structure, that are visible in shaded relief of topography. This proposal is investigated in greater detail below in [section 8.5.4](#), where it is suggested that the Getchell trend represents the northeastward-sheared extension of the Battle Mountain–Eureka (Cortez) trend and that the Independence group deposits (trend) represent the northeastward-sheared extension of the Carlin trend.

## 8.5 The Carlin and Cortez Structural Zones

### 8.5.1 Geophysical and Geochemical Evidence

The isostatic gravity and geomagnetic anomalies examined in [section 6.6](#) provide some support for the existence of the Carlin and Cortez structural zones. The K/Na and Ba/Na geochemical anomalies show strong spatial association with the sedimentary rock-hosted occurrences and clearly delineate the Battle Mountain–Eureka (Cortez) and Carlin mineral trends, but it is unclear whether or not the anomalies have any genetic association with mineralization (see [section 6.7.3](#)). The geochemical anomalies, however, may provide some additional insight by augmenting the interpretations made from the geophysical data.

In [section 6.6](#) (“Geophysics–Geomagnetic and Gravity Anomalies”), it was shown that the frequency distribution of gold-silver-bearing occurrences with respect to the geophysical anomalies is approximately normal, with the distribution modes located in the ranges that are transitional between the high-end and low-end of the magnetic and gravity anomaly intensity spectrums (mode lies slightly negative of the zero value, see [Figs. 6.46, 6.47, 6.49, and 6.50](#)). The near-zero-centered distribution modes for the occurrences indicate that the majority are located in regions that are transitional between rocks that are more highly and less highly magnetized, and transitional between rocks of higher and lower density. In general, anomaly gradient contrasts are thought to be indicative of crustal structures, such as terrane boundaries, structural trends, and fault and shear zones. Such structures could facilitate the convection of hydrothermal fluids at shallow crustal levels and the vertical movement of heat and deep-seated fluids from lower crustal levels (see [sections 3.4, 3.6, 6.4.3, and 6.5.3](#) for additional details). Kutina and Hildenbrand (1987) reported that some of the principal endogenic ore deposits of the western United States cluster in or adjacent to regions of gravity lows (e.g.—the majority of deposits of the Colorado mineral belt). Gold-silver-bearing occurrences in Nevada possess similar characteristics not only in relation to gravity anomalies but also in relation to magnetic anomalies. Grauch et al. (1995, p. 206) found an overall statistical tendency for gold occurrences to be spatially related to major density boundaries, which they explained as either (1) a major change in lithology of the crust associated with a terrane boundary or strike-slip fault, or (2) as a regional-scale structure that juxtaposes high-density basement material against low-density.

Examples of large and medium size sedimentary rock-hosted occurrences within transition regions between (1) low and high magnetic anomalies include the Goldstrike mine and the northern Carlin trend deposits, (2) low and high gravity anomalies include the Atlanta, Cortez Gold, Gold Acres, Florida Canyon, Gold Bar deposits/mines, and the deposits of the northern Carlin trend, and (3) low and high magnetic *and* gravity anomalies include the Gold Bar mine and northern Carlin trend deposits.

Shallow-source magnetic and pre-Tertiary basement gravity anomalies in north-central Nevada, particularly along the Battle Mountain–Eureka (Cortez) mineral trend, and the distribution of the K/Na–Ba/Na geochemical anomaly, may reflect the Cortez and Carlin structural zones. [Figure 8.3](#) illustrates the spatial relationship between the sedimentary rock-hosted occurrences and these geophysical and geochemical anomalies.

[Figures 8.3e](#) and [8.3f](#) show the trend of the K/Na anomaly (and the occurrences) relative to the isostatic and Bouguer gravity anomaly (respectively), which in Nevada, reflects sources in the pre-Tertiary basement as well as representing the density distribution of late Cenozoic masses in the upper (5–10 km) crust (Mabey et al., 1983; Blakely and Jachens, 1991; Shawe, 1991, figure 3; also see [section 6.6.3](#)). The gravity anomalies show close alignment with the mineral and geochemical trends (the “V”), expressed by a relatively sharp and well-defined changes in gradient between regions of gravity lows and adjacent areas of moderate to high intensities (particularly for the isostatic gravity anomaly). The gravity gradient paralleling the Eureka–Battle Mountain (Cortez) arm of the “V” is believed to be the northern extension of the gravity-low bilateral axis of symmetry in Nevada, and represents the northern segment of a linear isostatic gravitational gradient ridge that may delineate the southern extension of the northern Nevada rift zone (Blakely, 1988; also see [sections 2.7.4](#) and [6.6.3](#); [Figs. 6.45b](#), feature #1, and [6.54](#)).

[Figures 8.3b](#) and [8.3c](#) show the trend of the K/Na anomaly relative to the total residual magnetic anomaly, and [Figure 8.3d](#) shows the K/Na anomaly highs against a shaded relief rendition of the magnetic data. The magnetic anomaly highs depicted in the [Figure 8.3](#) (lighter, brighter colors) are believed to represent shallow magnetic sources (~1 km, Blakely and Jachens, 1991; also see [section 6.6.3](#)). The northern Nevada rift is the main magnetic anomaly feature in [Figure 8.3](#) (a long, narrow, arcuate, magnetic high trending roughly NW–SE; see [sections 2.7.4](#) and [6.6.3](#)), and has been interpreted as a mid-Miocene (~17–14 Ma) rift zone (Zoback et al., 1994; also see Mabey et al., 1983). Two smaller rift systems can also be seen flanking the northern Nevada rift to the west. The northern Nevada rift zone magnetic anomaly is not as closely aligned with the mineral and geochemical trends as the gravity anomalies, and can clearly be seen to extend sub-parallel along the Eureka–Battle Mountain (Cortez) arm of the trends *between* the K/Na anomalies ([Fig. 8.3d](#); also see [8.1](#), green line), forming an alternating geochemical-anomaly–magnetic-anomaly pattern. There appears to be a *conspicuous lack* of Ba/Na or K/Na geochemical anomalies or mineral occurrences (either sedimentary *or* volcanic rock-hosted) along much of the length of the northern Nevada rift—neither the Battle Mountain–Eureka (Cortez) trend nor the Carlin trend deposits, or their associated K/Na–Ba/Na geochemical anomaly, show close spatial coincidence with the *axis* of the rift zone. Rather, they envelop the rift to the west and the east. However, this may be due to sampling bias, although, given the large amount of mineral exploration activity in northern Nevada, this seems unlikely. Alternatively, the absence of K/Na or Ba/Na anomalies may reflect the distribution of Cenozoic

volcanic cover in the area, where the geochemical anomalies are concentrated along the eroded or flow-edges of the units (see [section 6.7.3](#))

The deeper basement features imaged by the gravity anomalies show much better spatial correlation with the Battle Mountain–Eureka (Cortez) and Carlin mineral trends and the K/Na anomaly pattern than does the shallow feature revealed by the geomagnetic anomaly. This correlation, as well as the relative “sharpness” and linearity of the gravity and geochemical anomalies (and of the geomagnetic anomaly too), suggest the presence of a crustal-scale structural feature, such as a suture zone, terrane boundary, or dip- and/or strike-slip fault zone. This is supported by recent work by Tosdal and Wooden (1997) and Wooden et al. (1997), who have been able to subdivide the northern Great Basin into four crustal provinces based on Pb 206/204 and 208/204 isotopic ratios: western, central, and eastern provinces, flanked to the east by Archean crust. The boundary between the central and eastern provinces ( $^{208}\text{Pb}/^{204}\text{Pb} > 39.5$  isopleth) is coincident with the Carlin trend. The sharpness of this boundary suggest to Tosdal and Wooden (1997) and Wooden et al. (1997) that it represents a major crustal fault. In addition, the results of a magnetotelluric survey across the Battle Mountain–Eureka (Cortez) and Carlin mineral trends (Rodriguez, 1997) have revealed deep-penetrating regional structures which appear to be major structural breaks in the crust. The presence of regional-scale structural zones along the Battle Mountain–Eureka (Cortez) and Carlin mineral trends is also consistent with proposals made by Arehart et al. (1993), Grauch et al. (1995), Madrid and Bagby (1986), Maher et al. (1993), and Shawe (1965, 1991) (further discussed below, and previously in [sections 3.4](#) and [3.6](#)).

### 8.5.2 Age and Origin of the Carlin and Cortez Structural Zones

Assuming that the Carlin and Cortez structural zones do exist, and that they did exercise strong control over the distribution of sedimentary rock-hosted deposits in north-central Nevada, then the inferred crustal structures would had to have been in place prior to ore-deposition, or formed as a result of (and during) the processes that led to mineralization. Sedimentary rock-hosted mineralization along the Battle Mountain–Eureka (Cortez) and Carlin trends is generally considered to be Upper Eocene–Early Oligocene (42–30 Ma) in age (Bagby and Berger, 1985; Maher et al., 1993; Hofstra, 1994, 1997; Ilchik, 1995; Thorman et al., 1995; Emsbo et al., 1996; Hofstra, 1994, 1997; Ilchik and Barton, 1997), but ages as old as Lower–Upper Cretaceous have been suggested (see Kuehn, 1989; Arehart et al., 1993, 1995). The northern Nevada rift trends sub-parallel to the Battle Mountain–Eureka (Cortez) trend ([Fig. 8.3c](#)). The age of the northern Nevada rifting event has been determined by Zoback et al. (1994) to be ~17–14 Ma, which is based on new radiometric dating of north-northwest-trending dikes and flows occurring within the rift. The authors also pointed out that, the northern Nevada rift is equivalent in age, trend, and composition to feeder dikes that fed the main eruptive pulse of the Columbia River flood basalts in northern Oregon ~15.5–16.5 Ma (Zoback et al., 1994) (see [Fig. 2.3](#)). Assuming the age estimates of mineralization and rifting are correct, the sedimentary rock-hosted deposits are some 20–100 m.y. or so *older* than the rift structure, suggesting that the rift, in its present manifestation, did not play a key role in mineralization.

Alternatively, the dikes and flows associated with the northern Nevada rift, which are the source of the magnetic anomaly delineating the rift zone, may be the product of magmas that were focused along and ascended through a zone of preexisting weakness in the crust, in effect using



the crustal flaw zone as a conduit (see, for example, Cameron and Hattori, 1995). This, contended Zoback et al. (1994), was not the case. Zoback et al. (1994) observed that the orientations of the magnetic anomaly, exposed basaltic feeder dike swarms, and structural troughs associated with the rift zone, all trend uniformly N20°–25°W, and this consistency, they argued, indicates that the northern Nevada rift zone developed in response to the prevailing least principal stress at the time of formation (horizontal and oriented N65°–70°W), rather than by exploiting a pre-existing zone of crustal weakness. While *latest activity* may in fact have taken place in this environment (i.e.—rifting), the observations and spatial relationships among the geophysical and geochemical anomalies and the mineral trends presented in [section 8.5.1](#) suggest that a pre-existing crustal weakness may indeed exist. This proposal is in accord with Grauch et al. (1995). They suggested that a pre-existing basement structure played a major role in the formation and/or location of other nearby geologic features of similar trend (i.e.—the northern Nevada rift), as well as having focused magmatism (heat) and the flow of deep-seated and/or high-level convecting ore-related fluids, which resulted in the formation of Battle Mountain–Eureka (Cortez) and Carlin mineral trends. Furthermore, Grauch et al. (1995) suggested that the basement feature must have developed during or prior to Jurassic time, as determined by the oldest alignment of geologic features along its trend (Jurassic intrusive rocks and probable mid-Jurassic folds). The northerly orientation of the basement gravity gradient, and its location proximal to tectonic activity directed at the continental margin, led Grauch et al. (1995) to conclude that this feature may be associated with the rifted Precambrian continental margin. This interpretation places the inferred structural feature in an acceptable geologic environment and chronological order with respect to Upper Eocene–Early Oligocene mineralization and mid-Miocene rifting:

1. Development of a Jurassic or *older* crustal-scale structural feature, which may represent (1) a normal fault related to the Precambrian rifting event that acted as a buttress against later tectonic compression, producing ramped thrust plates and parallel fold belts, or (2) just one manifestation of a general structural grain in the Precambrian continent (Grauch et al., 1995).
2. Focusing of heat and mineralizing fluids along the crustal-scale structural feature to produce the alignment of Upper Eocene–Early Oligocene age sedimentary rock-hosted occurrences along the Battle Mountain–Eureka (Cortez) mineral trend and possibly the Carlin trend.
3. Formation of the northern Nevada rift zone proximal to the crustal-scale structural feature during the mid-Miocene in an extensional tectonic regime, where the preexisting Jurassic or older structural feature influenced the location of rifting and associated magmatism.

These findings are also consistent with Maher et al. (1993), where it was suggested that the northern Nevada rift is the most recent manifestation of activity related to an “older” Paleozoic or pre-Late Cretaceous fundamental structure in the crust.

The observations made in this study, in addition to those mentioned above, further support the possibility that mineralization along the Battle-Mountain–Eureka (Cortez) and Carlin trends could be the result of heat and mineralizing fluids distributed laterally along regional-scale crustal structural zones of mid-Jurassic or older origin.

### 8.5.3 Transcurrent Movement

The presence of sedimentary rock-hosted occurrences in east-central Nevada suggests that the Carlin and Cortez structural zones may be extrapolated along trend to the southeast of the



northerly-trending Roberts Mountain thrust front (see [Figs. 8.1a](#), dashed red lines). This notion is based on a number of structural elements visible in shaded relief of topography (derived from ~800 meter pixel resolution), as well as by isostatic gravity data, which shows a linear gradient ridge running sub-parallel to, and south of, the northern Nevada rift zone, and may represent the northern extension of the Bouguer gravity-low bilateral axis of symmetry in Nevada (Blakely, 1988; also see [sections 6.6.3](#) and [2.7.3](#); [Figs. 6.45b](#) and [6.45c](#), feature #1, and [6.54](#)). The Bald Mountain district, Alligator area deposits, and Illipah deposit occur approximately along strike of the southeastern extension of the Carlin mineral trend, and roughly on the eastern side of the bilateral axis of symmetry. The Eureka district and the Ratto Canyon deposit occur along strike of the southeastern extension of the Battle Mountain–Eureka (Cortez) mineral trend, and to the west of the bilateral axis of symmetry. In between the Carlin and Battle Mountain–Eureka (Cortez) mineral trends, and roughly within the bilateral axis zone, the Easy Junior–Night Hawk and Green Springs deposits are found.

Shaded relief of topography may give some indications of transcurrent movement along (or between) the Carlin and Cortez structural zones. The southeastern extensions of the Carlin and Cortez structural zones, as delineated in [Figures 8.1a](#) (dashed red lines), roughly bisect a broad and open semi-continuous “S”-shaped topographic curvature. This feature, which is clearly visible in shaded relief (located just east of center in [Fig. 8.1](#)), is formed by the curvilinear alignment of (from north to south) the Ruby Mountains and the White Pine–Horse–Grant–Quinn Canyon ranges. Left- or right-lateral movement, widely distributed between the southeastern extensions of the Carlin and Cortez structural zones, could have produced this topographic feature:

- Assuming that this topographic feature was originally continuous, left-lateral movement could have displaced the northeast–southwest-trending northern and southern segments, and during the process, realigned the ranges in the zone of transcurrent movement along a more northerly orientation (central segment of the “S”, area between dashed red lines in [Fig. 8.1a](#)).
- Assuming that this topographic feature was not originally continuous, right-lateral movement could have realigned the ranges in the central portion of the “S” from roughly northeast–southwest-trending to north–northwest–south–southeast-trending, effectively “joining” the northern and southern segments of the “S”.

Evidence for both left- and right-lateral motion sense are found along the Carlin structural zone. The Alligator group deposits occur near the southern extension of the Carlin structural zone, and as a group, parallel the ranges in the central part of the “S”-shaped topographic structure (compare [Fig. 8.1](#) and [3.3](#)). Recent mapping in the Alligator Ridge area has documented Eocene, left-lateral, transpressive deformation structures (Nutt, 1997; Nutt and Good, 1998). In sedimentary rock-hosted deposits along the northern Carlin trend, right-lateral strike-slip faulting has been recognized by a number of Newmont Exploration Ltd. geologists (1990, personal communication), Putnam and Enriquez (1991), Teal and Jackson (1997), and Byron R. Berger (1998, personal communication; e.g.—Genesis and Post-Betze pits). Right-lateral movement on a regional scale has been suggested by Carey (1955, 1958, 1976, 1988), Shawe (1965), Atwater (1970), Livaccari (1979), and Ward (1988, 1991). In order to reconcile the conflicting sense of kinematic motion, Tosdal and Nutt (1998) suggested that the Carlin mineral trend (which includes the “southern extension” deposits of the Alligator group) delineates a transfer or accommodation zone, linking geographic offset or steps in extending domains and thereby allowing for opposing movement (see [Faulds and Varga, 1998](#)).

Transcurrent movement between the Carlin and Cortez structures may also be supported by the trend of Pb isotope values of Jurassic, Cretaceous, and Tertiary granitic rocks. Wooden et al. (1997) have identified a number of Pb isotopic boundaries in northern Nevada, an eastern boundary ( $^{208}\text{Pb}/^{204}\text{Pb} > 39.5$ ) that coincides with the Carlin trend and a western boundary ( $^{208}\text{Pb}/^{204}\text{Pb} > 39$ ) that lies parallel but to the southwest of the Battle Mountain–Eureka (Cortez) trend (see figure 1 in Wooden et al., 1997). They indicate that the westernmost Pb boundary appears to swing northeast, possibly encountering the Humboldt shear(?) zone as suggested in [section 8.4.1](#), *except* at the Battle Mountain–Eureka (Cortez) trend, where there is a prominent southeast deflection (Tosdal and Wooden, 1997). The boundary then bends back to the northeast toward the Carlin trend where it appears to turn further northward (Wooden et al., 1997, figure 1; Richard M. Tosdal, 1998, personal communication). The “jog” in the northeast-trending  $^{208}\text{Pb}/^{204}\text{Pb} > 39$  isopleth across the Carlin and Battle Mountain–Eureka (Cortez) mineral trends could have been the result of transcurrent movement along and/or between the Carlin and Cortez structural zones.

Finally, the northern Nevada rift zone may provide some support for transcurrent activity along the Carlin and Cortez structural zones. The rift zone trends between and sub-parallel to the structural zones ([Figs. 8.1a](#), green line; also see [8.3c](#)), suggesting that it could be related to these features (although they may differ in age; see discussion in [sections 8.5.1](#) and [8.5.2](#)). The northern Nevada rift zone has been postulated to be the southern extension of the Brothers fault zone (see [sections 2.7.4](#) and [6.6.3](#); [Fig. 2.3](#)). Together, they form the Oregon–Nevada lineament (Stewart et al., 1975), which has been interpreted to be the surface expression of a deep-seated fracture zone (up 15 km deep) that may have had a complex history of strike-slip and transcurrent movement (Stewart et al., 1975; Blakely and Jachens, 1991; also see Christiansen and Yeats, 1992).

#### **8.5.4 Truncation of the Battle Mountain–Eureka (Cortez) and Carlin Mineral Trends by the Humboldt Shear(?) Zone**

As discussed in [section 8.4](#), broad northeast–southwest-trending zone of transcurrent movement, with possible ancestral heritage, is believed to extend across northern Nevada and to be responsible for controlling the regional-scale distribution of volcanic rock-hosted occurrences in this area. Termed the Humboldt shear(?) zone, it has, to a large degree, been delineated in this study on the basis of topographic expression. Within this zone, a number of northeast–southwest-trending linear features have been identified (see [Fig. 8.1a](#), features “A”, “B”, and “C”). The intersection of these linear features with the proposed Carlin and Cortez structural zones and the northern Nevada rift zone correlate with (1) some degree of deposit clustering (see text in caption of [Fig. 8.1](#)), (2) discontinuities along the geomagnetic signature of the northern Nevada rift zone (particularly in the flanking rift signatures to the west; see [Figs. 6.45a](#) and [6.53b](#)), and (3) lateral offsets and discontinuities in the K/Na–Ba/Na geochemical anomaly pattern (see [Fig. 6.65](#)). Associated with these linear features is the abrupt termination of the Carlin and Mountain–Eureka (Cortez) mineral trends in the vicinity of the Dee, Bootstrap, and Capstone deposits, and the Lone Tree and Stone House deposits<sup>1</sup>, respectively. In both instances, a group

---

<sup>1</sup> Or perhaps in the vicinity of the Preble deposit, if only the alignment of deposits with the Battle Mountain–Eureka (Cortez) mineral trend is considered.

of sedimentary rock-hosted deposits are encountered to the northeast of the northern termini of the mineral trends: the Independence group deposits to the northeast of the Carlin trend, and the Getchell trend deposits to the northeast of the Battle Mountain–Eureka (Cortez) trend.

It is not unreasonable to assume that the Battle Mountain–Eureka (Cortez) and Carlin mineral trends continue northwestward along the same approximate strike. As previously discussed ([section 6.7.3](#)), the K/Na–Ba/Na geochemical anomaly is spatially, if not genetically, associated with the sedimentary rock-hosted occurrences and clearly delineates the mineral trends. As such, the K/Na–Ba/Na geochemical anomaly might also extend further northwestward. Unfortunately, the NURE K/Na and Ba/Na geochemical datasets examined for this study do not significantly extend north of the northern termini of the Battle Mountain–Eureka (Cortez) or Carlin trends. However, the NURE U/Th and As datasets do extend further north, and they show anomaly distribution patterns that are very similar to the K/Na–Ba/Na anomaly pattern and to the distribution of deposits along the northern reaches of the mineral trends (see [section 6.7.3](#)). It appears that the U/Th and As anomaly patterns do not extend northwestward, rather they appear to bend to the northeast:

- In the vicinity of the Kramer Hill and Preble deposits, the As anomaly bends to the northeast and extends along the Getchell trend deposits.
- North of the Dee, Bootstrap, and Capstone deposits, the As and U/Th anomalies bend to the northeast, then northward to parallel the Independence group deposits.

It is uncertain whether the northeast bend observed in these anomaly patterns is real, or if they reflect the extent of Cenozoic volcanic cover of the Banbury formation, or perhaps a sampling bias. In support of the northeast bend are the points presented in [section 8.4.3](#), and in particular, eastward lateral offsets in basin-range structure visible (1) north of the northern terminus of the Battle Mountain–Eureka (Cortez) trend along the Getchell trend deposits (in the Osgood Mountains), and (2) north of the northern terminus of the Carlin trend, between the Dee deposit (north Carlin trend) and the Burns Basin and Mill Creek deposits (southern end of the Independence group deposits; southwestern spur of the Independence Mountains). The implication is that the Getchell trend represents the northeastward-displaced (sheared?) extension of the Battle Mountain–Eureka (Cortez) trend, and the Independence group deposits (trend) represent the northeastward-displaced (sheared?) extension of the Carlin trend. Lateral displacement of the Getchell and Independence trend deposits away from the Battle Mountain–Eureka (Cortez) and Carlin trend deposits (respectively) could have been achieved by right-lateral transcurrent movement within the Humboldt shear(?) zone, parallel to the northeast–southwest-trending linear features depicted in [Figures 8.1a](#).

Such a scenario requires that certain age and kinematic relationships along the structural zones be satisfied: (1) the age of mineralization at the “sheared-off” ends of the deposit trends should be roughly the same—the deposits of the Carlin trend roughly equal in age to those in the Independence group; the Battle Mountain–Eureka (Cortez) trend deposits roughly equal to those of the Getchell trend, and (2) mid-Miocene, right-lateral movement along the Humboldt shear(?) zone should be reconciled with right-lateral movement along the Cortez and Carlin structural zones and the Walker Lane shear zone.

Hofstra (1997) commented that “evidence continues to mount that Carlin-type deposits formed in the mid-Tertiary (42 to 30 Ma)” (see references in Hofstra). For the Carlin trend deposits,

Christensen (1995) reported two radiometric age date groupings of 95-117 Ma and 36-40 Ma, with dates as young as 8-35 Ma, and as old as ~120 Ma (Kuehn, 1989; also see Arehart et al., 1993, 1995). Thorman et al. (1995) proposed that the many of the Carlin trend deposits are Eocene-Oligocene. Ilchik (1995), based on a reanalysis of data published by Arehart et al. (1993), suggested that the most reasonable age for the formation of the Post-Betze deposit is slightly younger than 39 Ma. Most recently, Emsbo et al. (1996) were able to constrain mineralization at the Meikle and Post-Betze deposit to <38.8 Ma based upon relationships among igneous dikes on the Goldstrike property. At the southern end of the Independence group deposits, recent work in the Jeritt Canyon district has produced mineralization age dates of ~40 Ma (Hofstra, 1994; also see Folger et al., 1997; Hofstra, 1997; Wise and Gorman, 1997). Along the length of the Battle Mountain–Eureka (Cortez) trend, Maher et al. (1993) bracketed the age of the most economically significant Carlin-style gold producing mines to late-Eocene–early-Oligocene time (radiometric age dates compiled for his study for this time period range from ~40 to ~34 Ma). These ages are comparable with recent Getchell trend mineralization age dates for the Twin Creeks deposit (Rabbit and Chimney Creek deposits; ~42 Ma; Groff, 1996, Groff et al., 1997; Hall et al., 1997) and Pinson (42.7±5 Ma; Byron R. Berger, 1998, personal communication). These age data bridge the timing of mineralization across the Carlin trend and Independence group deposits and across the Battle Mountain–Eureka (Cortez) and Getchell trend deposits. This is consistent with the proposal made here that the Getchell trend and Independence group of deposits represent the sheared-off northern extensions of the Battle Mountain–Eureka (Cortez) and Carlin mineral trends. Furthermore, if this postulate is correct, then it may be possible to constrain the most recent movement along the Humboldt shear(?) zone to between the formation of the Carlin-type deposits (42 to 30 Ma; Hofstra, 1997) and the most recent igneous activity along the northern Nevada rift zone (~17-14 Ma; Zoback et al., 1994), which transects the Humboldt shear(?) zone but shows no distinct lateral offsets in its geomagnetic signature (i.e.—latest appreciable movement occurred between 42-30 to 17-14 Ma).

Questions remain as to the tectonic origin of the Humboldt shear(?) zone, its activity throughout geologic history, and its relationship to other regional-scale features, such as the Carlin and Cortez structural zones and the Walker Lane shear zone. As indicated above, there is evidence as well as a plausible explanation for left-lateral movement along the Carlin structural zone. Left-lateral motion-sense is kinematically consistent with right-lateral movement along the Humboldt shear(?) zone. However, given the proposal here that right-lateral movement within the Humboldt shear(?) zone may have taken place ten's of millions of years after mineralization along the Cortez and Carlin structural zones, and presuming that movement along the Humboldt shear(?) and Carlin structural zones therefore was *not* concurrent, it is unclear whether or not motion-sense relationships between these features must or can be resolved. It is perhaps more important to reconcile motion-sense between the Humboldt shear(?) zone and the Walker Lane, which has documented activity in the middle and late Tertiary (see Dilles and Gans, 1995; [section 2.6](#)). Research conducted by Hardyman and Oldow (1991) may provide a possible resolution. Based on field work in the central Walker Lane (Carson sink area, south to Tonopah, Nevada), Hardyman and Oldow (1991) have outlined a three-stage tectonic history that involves a 70° to 90° rotation in the extension direction since 19-15 Ma: an early 28-17 Ma stage of extension that was oriented north-northeast–south-southwest, followed by east-west extension between 17-11 Ma, and, after about 10 Ma, southeast-northwest oriented extension. The result of this last extensional stage (post-10 Ma through present day) has been dominant right-lateral movement on northwest-striking faults in the Walker Lane shear zone. To be kinematically

correct, this sense of motion would require *left-lateral* movement along the Humboldt shear(?) zone, contrary to what is proposed here. However, during the period of early extension (28-17 Ma), Hardyman and Oldow (1991) indicate that extension was oriented north-northeasterly, resulting in a *left-lateral* strike-slip regime. This time period of left-lateral strike-slip along the Walker Lane is in large part concurrent with latest movement within the Humboldt shear(?) zone proposed here (42-30 to 17-14 Ma), and is kinematically consistent with the right-lateral movement needed to displace the Getchell and Independence trend deposits northeastward away from the northern termini of the Battle Mountain–Eureka (Cortez) and Carlin trend deposits (respectively). Left-lateral motion within the Walker Lane shear zone between 28-17 Ma may also be related to left-lateral motion along the Carlin structural zone.

## 8.6 A Mantle Plume

There has recently been a noticeable increase in the number of regional-scale studies suggesting that a mantle plume or upwelling asthenosphere could be responsible for the tectonomagmatic evolution, metallogenesis, and present-day character of the Basin and Range Province and surrounding environs (see for example, Smith, 1978; Fitton and James, 1987; Mutschler et al., 1987; Fitton et al., 1988; Leeman and Fitton, 1989; Westaway, 1989; Draper, 1991; Fitton et al., 1991; Mutschler et al., 1992; Parsons et al., 1994; Saltus and Thompson, 1995; Oppliger et al., 1997; Murphy et al., 1998; Murphy et al., 1999). Many of the researchers cited above believe that a mantle plume fits the geographic, geologic, geophysical, and geochemical data observed in the Great Basin, and that in fact the Great Basin is an example of a plume-related orogenic process that has been overlooked (Murphy et al., 1998; Murphy et al., 1999). A mantle plume or diapiric activated/controlled mechanism for magma generation accommodates (1) the chemistry and isotopic characteristics of mid- and late Cenozoic basalt (Fitton and James, 1987; Fitton et al., 1988; Glazner and Ussler, 1989; Leeman and Fitton, 1989; Fitton et al., 1991; Leeman and Harry, 1993), (2) the space-time magmatic and extensional migration patterns across the region (Armstrong et al., 1969; Stewart 1980; Silberman 1985; White 1985; Seedorff, 1991), and (3) correlates well with the work on the physics and chemistry of mantle plumes conducted by Courtney and White (1986), Richards et al. (1989), and DePaolo et al. (1991).

A number of datasets compiled for this study, some of which were not directly applied to the mineral potential modelling performed here (see [section 5.3.3](#)), support the presence of a plume or upwelling asthenosphere. These datasets include (1) igneous rock radiometric age dates (RAD-B), (2) metallic mineral deposits rock radiometric age dates, (3) Cenozoic igneous rock time-slices maps, (4) Cenozoic igneous rock composition-slices, (5)  $^{87}\text{Sr}/^{86}\text{Sr}$  initial values of Mesozoic and Cenozoic igneous rocks, (6) dip attitude of Tertiary rocks, and (7) mountain peak elevation. In the Great Basin, magmatism and extension migrated southwestward, spreading concentrically outward from the northeastern Nevada during the middle Tertiary early rapid extension through subsequent late Tertiary slow extension stages (see [Fig. 6.4](#) and [section 2.5](#)). (Magmatism in the Great Basin completes only a portion of this ring, forming an arcuate band in Nevada as shown in [Figure 6.4](#), but the remainder could be concealed under younger strata to the north or northeast). This outward radiating ring of event inception times follows the time-transgressive effects that a mantle plume could have on magmatism as suggested by a theoretical model proposed by Courtney and White (1986), where an outward-younging radial and concentric trend of magmatic inception times is produced above a plume. Maps generated from the seven aforementioned datasets are all consistent with the time-transgressive effects that a



mantle plume could have on regional-scale tectonomagmatism. The space-time migration of inception times of magmatism is particularly well developed in the igneous rock radiometric age dates (RAD-B) dataset (Fig. 8.4), while the dip attitude of Tertiary rocks is suggestive of an overall “doming” or “arching” to the region, as might be expected over a mantle plume or upwelling asthenosphere.

A mantle plume, in conjunction with preexisting crustal-scale structures such as the Carlin and Cortez structural zones and the Walker Lane and Humboldt shear(?) zones, could have had profound effects on the development of the Great Basin as a metallogenic province. The southwesterly absolute motion of the North American plate suggests that the Basin and Range province lies in the “wake” of the plume (Fitton et al., 1991). A mantle plume is believed to have emerged (made contact with the lower crust?) in northernmost central Nevada, near the borders of Oregon and Idaho, at the triple-junction intersection of Brothers fault zone, the Snake River Plain, and the northern Nevada rift zone (see Fig. 2.3) (Parsons et al., 1994; see also Mutschler et al., 1992). Murphy et al. (1998, 1999) track the plume a little farther south, through Battle Mountain, Nevada, and along a path which parallels the Humboldt shear(?) zone, as delineated in this study. However, if the RADB data (Fig. 8.4) and the Stewart and Carlson (1978) volcanic rock time-slice maps (Fig. 6.4) are any indication of where initial Cenozoic magmatism was centered in the Great Basin, then slightly north of east-central Nevada is where the plume may have made contact with the crust. The current location of the plume is thought to be either under the southern Rocky Mountains, in the region of the Colorado Plateau (Fitton et al., 1991; Parsons and McCarthy, 1993), or under the region of Yellowstone Park (the “Yellowstone hot spot”) (Smith, 1978; Westaway, 1989; Draper, 1991; Parsons et al., 1994; Oppliger et al., 1997; Murphy et al., 1998; Murphy et al., 1999). Oppliger et al. (1997) have suggested that the ancestral Yellowstone hotspot may have been responsible for sedimentary rock-hosted mineralization in north-central Nevada, having provided (1) a source for gold (a la Rock and Groves, 1988), (2) a mechanism for metamorphic devolatilization in the lower crust (see Sedorff, 1991, for metamorphic devolatilization sedimentary rock-hosted model), and (3) a regional-scale heat source that drove fluid convection in the upper crust.

The formation and distribution of the volcanic rock-hosted occurrences could also be related to plume activity. In context of the arcuate time-transgressive migration pattern of magmatism across Nevada (Fig. 6.4), the generalized distribution pattern of the sedimentary rock-hosted occurrences is spatially coincident with the older “core” of the sequence, whereas the volcanic rock-hosted “epithermal crescent”, which encompasses the sedimentary rock-hosted occurrences, is coincident with a younger “ring” (see Fig. 6.2 and sections 6.2.2 and 6.2.3). As indicated in section 8.1 and subsequent sections, the Walker Lane shear zone and the Humboldt shear(?) zone are believed to have acted as first-order controls over the regional-scale distribution of the volcanic rock-hosted occurrences. Plume-driven magmatism may have acted as a second-order control. As Eocene-Oligocene magmatism expanded in a arcuate time-transgressive manner across the region, it encountered and exploited the Walker Lane shear zone and the Humboldt shear(?) zone, where together magmatism and preexisting tectonic conditions provided a favorable environment for ore deposit formation (see, for example, sections 8.2.2, 8.2.1, 3.4, 3.6, 6.4.3, and 6.5.3).



## References

- Agterberg, F. P., 1974, Automatic contouring of geological maps to detect target areas for mineral exploration: *Journal of Mathematic Geology*, v. 6, p. 373-395.
- Agterberg, F. P., 1989a, Computer programs for mineral exploration: *Science*, v. 245, p. 76-81.
- Agterberg, F. P., 1989b, Systematic approach to dealing with uncertainty of geoscience information in mineral exploration, *in*, Weiss, A., editor, *Proceedings of the 21<sup>st</sup> Symposium on "Application of Computers and Operations Research in the Mineral Industry"*, Society of Mining engineers, Inc., Littleton, Colorado, 1989, p. 165-178.
- Agterberg, F. P., 1992a, Combining indicator patterns in weights of evidence modelling for resource evaluation: *Nonrenewable Resources*, v. 1, p. 39-50.
- Agterberg, F. P., 1992b, Computer applications in geology: *Encyclopaedia of Earth System Science*, v. 1, p. 565-579.
- Agterberg, F. P., 1992c, Estimating the probability of occurrence of mineral deposits from multiple map patterns, *in*, Merriam, D. F., and Kürzl, H., editors, *Use of Microcomputers in Geology*, Plenum Press, New York, p. 73-92.
- Agterberg, F. P., Bonham-Carter, G. F., Cheng, Q., and Wright, D. F., 1993, Weights of evidence modelling and weighted logistic regression for mineral potential mapping, *in*, Davis, J. C., and Herzfeld, U. C., editors, *Computers in Geology—25 Years of Progress*: Oxford University Press, New York, p. 13-32.
- Agterberg, F. P., Bonham-Carter, G. F., Wright, D. F., 1990, Statistical pattern integration for mineral exploration, *in*, Gaál, G., and Merriam, D. F., editors, *Computer Applications in Resource Estimation Prediction and Assessment of Metals and Petroleum*: Pergamon Press, Oxford-New York, p. 1. 12.
- Albers, J. P., 1981, A lithologic-tectonic framework for the metallogenic provinces of California: *Economic Geology*, v. 76, p. 765-790.
- Albers, J. P., 1983, Distribution of mineral deposits in accreted terranes and cratonal rocks of western United States: *Canadian Journal Earth Sciences*, v. 20, p. 1019-1029.
- Allenby, R. J., and Schnetzler, C. C., 1983, United States crustal thickness: *Tectonophysics*, v. 93, p. 13-31.
- Allmendinger, R. W., 1992, Fold and thrust tectonics of the western United States exclusive of the accreted terranes, *in*, Burchfiel, B. C., Lipman, P. W., and Zoback, M. L., editors, *The Cordilleran Orogen: The conterminous U. S., the geology of North America*, volume G-3: Geological Society of America, p. 583-607.

- Allmendinger, R. W., Hauge, T. A., Hauser, E. C., Potter, C. J., Klemperer, S. L., Nelson, K. D., Knuepfer, P., and Oliver, J., 1987, Overview of the COCORP 40°N Transect, western United States: The fabric of an orogenic belt: *Geological Society of America Bulletin*, v. 98, p. 308-319.
- Allmendinger, R. W., Sharp, J. W., Von Tish, D., Serpa, L., Kaufman, S., Oliver, J., and Smith, R. B., 1983, Cenozoic and Mesozoic structure of the eastern Basin and Range province, Utah, from COCORP seismic-reflection data: *Geology*, v. 11, p. 532-319.
- An, P., Moon, W. M., and Rencz, A., 1991, Application of fuzzy set theory to integrated mineral exploration: *Canadian Journal of Exploration Geophysics*, v. 27, p. 1-11.
- Anders, M. H., Geissman, J. W., and Sleep, N. H., 1990, Comment and Reply on “Northeastern Basin and Range province active tectonics: An alternative view”: *Geology*, v. 18 p. 914-917.
- Anderson, J. L., 1983, Proterozoic anorogenic granite plutonism of North America, *in*, Medaris, L. H., Jr., Byers, C. W., Mickelson, D. M., and Shanks, W. C., editors, *Proterozoic geology: Geological Society of America Memoir 161*, p 133-154.
- Anderson, J. L., 1988, Core complexes of the Mojave-Sonoran desert: Conditions of plutonism, mylonitization, and decompression, *in*, Ernst, W. G., editor, *Metamorphism and crustal evolution of the western United States: Rubey Volume VII*, Prentice Hall, Englewood Cliffs, New Jersey, p. 502-525.
- Anderson, R. E., 1989, Tectonic evolution of the Intermontane System; Basin and Range, Colorado Plateau, and High Lava Plains, *in*, Pakiser, L. C., and Mooney, W. D., editors, *Geophysical Framework of the Continental United States: Geological Society of America Memoir 172*, p. 163-176.
- Anhaeusser, C. R., 1981, The relation of mineral deposits to early crustal evolution, *in*, Skinner, B. J., editor, *Economic Geology Seventy-Fifth Anniversary Volume: El Paso, Texas, Economic Geology Publishing Company*, p. 42-62.
- Anonymous, 1997, Production and jobs—The world's largest gold producing countries (1995): The Gold Institute, Washington, D. C., United States, <http://www.goldinstitute.com/worldprod.html>.
- Antenucci, J. C., Brown, K., Croswell, P. L., Kevany, M. J., and Archer, H., 1991, *Geographic Information Systems, A guide to the technology*: Van Nostrand Reinhold, New York, 301 p.
- Archbold, N. L., 1972, Modified geological map of Nevada: Nevada Bureau of Mines and Geology Map 44.
- Arehart, G. B., 1995, Origin of sediments-hosted disseminated gold deposits: A review [abs.], *in*, *Geology and Ore Deposits of the American Cordillera*, symposium, program with abstracts: Geological Society of Nevada, Reno/Sparks, Nevada, p. A10.

- Arehart, G. B., Foland, K. A., Naeser, C. W., and Kesler, S. E., 1995,  $^{40}\text{Ar}/^{39}\text{Ar}$ , K/Ar, and fission track geochronology of sediments-hosted disseminated gold deposits at Post-Betze, Carlin trend, northeastern Nevada—A Reply: *Economic Geology*, v. 90, p. 208-212.
- Arehart, G. B., Foland, K. A., Naeser, C. W., and Kesler, S. E., 1993,  $^{40}\text{Ar}/^{39}\text{Ar}$ , K/Ar, and fission-track geochronology of sediment-hosted disseminated gold deposits at Post-Betze, Carlin Trend, northeastern Nevada: *Economic Geology*, v. 88, p. 622-646.
- Armstrong, R. L., 1968, Sevier orogenic belt in Nevada and Utah: *Geological Society of America Bulletin*, v. 79, p. 429-458.
- Armstrong, R. L., Ekren, E. B., McKee, E. H., and Noble, D. C., 1969, Space-time relations of Cenozoic silicic volcanism in the Great Basin of the western United States: *American Journal of Science*, v. 267, p. 478-490.
- Armstrong, R. L., and Suppe, S., 1973, Potassium-argon geochronometry of Mesozoic igneous rocks in Nevada, Utah, and southern California: *Geological Society of America Bulletin*, v. 84, p. 1375-1392.
- Armstrong, R. L., and Ward, P., 1991, Evolving geographic patterns of Cenozoic magmatism in the North American Cordillera: The temporal and spatial association of magmatism and metamorphic core complexes: *Journal of Geophysical Research*, v. 96, N° B8, p. 13201-13224.
- Armstrong, R. L., Ekren, E. B., McKee, E. H., and Noble, D. C., 1969, Space-time relations of Cenozoic silicic volcanism in the Great Basin of the western United States: *American Journal of Science*, v. 267, p. 478-490.
- Aronoff, S., 1989, *Geographic Information Systems: A management perspective*: WDL Publications, Ottawa, Canada, 294 p.
- Atwater, T., 1989, Plate tectonic history of the northeast Pacific and western North America, *in*, Winterer, E. L., Hussong, D. M., Decker, R. W., editors, *The Eastern Pacific Ocean and Hawaii*: Bolder, Colorado, Geological Society of America, *The Geology of North America*, v. N, p. 21-72.
- Atwater, T., 1970, Implications of plate tectonics for the Cenozoic tectonic evolution of western North America: *Geological Society of America Bulletin*, v. 81, p. 3513-3536.
- Ausburn, K. E., 1991, Ore-petrogenesis of Tertiary volcanic hosted epithermal gold mineralization at the Hart mining district, Castle Mountains, NE San Bernardino County, California, *in*, Raines, G. L., Lisle, R. E., Schafer, R. W., and Wilkinson, W. H., editors, *Geology and Ore Deposits of the Great Basin, Symposium Proceedings Volume 2: Geological Society of Nevada, Reno/Sparks, Nevada*, p. 1147-1188.
- Axen, G. J., Taylor, W. J., and Bartley, J. M., 1993, Space-time patterns and tectonic controls of Tertiary extension and magmatism in the Great Basin of the western United States: *Geological Society of America Bulletin*, v. 105, p. 56-76.

- Babcock, J. W., 1984, Introduction to geologic ore deposit modelling: Mining Engineering, v. 36, p. 1631-1636.
- Bacon, C. R., 1983, Possible relations between magmatism, rates of extension, and the states of stress in the crust [abs.]: Geological Society of America Abstracts with Programs, v. 15, p. 288.
- Bacon, C. R., Kurasawa, H., Delevaux, M. H., Kistler, R. W., and Doe, B. R., 1984, Lead and strontium isotopic evidence for crustal interaction and compositional zonation in the source regions of Pleistocene basaltic and rhyolitic magmas of Coso volcanic field, California: Contributions to Mineralogy and Petrology, v. 85, p. 366-375.
- Bagby, W. C., and Berger, B. R., 1985, Geologic characteristics of sediment-hosted, disseminated precious-metal deposits in the western United States, *in*, Berger, B. R., and Bethke, P. M., editors, Geology and Geochemistry of Epithermal Systems: Reviews in Economic Geology, v. 2, p. 169-202.
- Baker, P. E., 1982, Evolution and classification of orogenic volcanic rocks, *in*, Thorpe, R. S., editor, Andesites—Orogenic Andesites and Related Rocks: Wiley and Sons, New York, p. 11-23.
- Bakken, B. M., 1990, Gold mineralization, wall rock alteration, and the geochemical evolution of the hydrothermal system in the main ore body, Carlin mine, Nevada: Unpublished Ph. D. thesis, Stanford University, 236 p.
- Bakken, B. M., and Einaudi, M. T., 1986, Spatial and temporal relations between wall rock alteration and gold mineralization, main pit, Carlin mine, Nevada, U. S. A., *in*, Macdonald, A. J., editor, Gold '86—an International Symposium on the Geology of Gold Deposits, Proceedings Volume: Toronto, Ontario, Gold '86, p. 388-403.
- Bakken, B. M., Hochella, M. F., Einaudi, M. T., and Marshall, A. F., 1987, The quest for gold: High resolution microscopy of ore from the Carlin mine, Nevada: Geological Society of America Abstracts with Programs, v. 19, p. 578.
- Bally, A. W., and Palmer, A. R., editors, 1989, The Geology of North America: An Overview: Boulder, Colorado, Geological Society of America, The Geology of North America, v. A, 619 p.
- Barbarin, B., 1990, Granitoids: Main petrogenetic classifications in relation to origin and tectonic setting: Geological Journal, v. 25, p. 227-238.
- Barnes, H. L., 1979. Solubilities of ore minerals, *in*, H. L. Barnes, ed., Geochemistry of Hydrothermal Ore Deposits, 2nd. ed., John-Wiley & Sons, New York, p. 404-460.
- Barnes, H. L., and Rose, A. W., 1998, Origins of hydrothermal ores: Science, v. 279, March 1998, p. 2064-2065.
- Barton, M. D., 1990, Cretaceous magmatism, metamorphism, and metallogeny in the east-central

- Great Basin, *in*, Anderson, J. L., editor, The Nature and Origin of Cordilleran Magmatism: Geological Society of America Memoir 174, p. 283-302.
- Barton, M. D., Battles, D. A., Bebout, G. E., Capo, R. C., Christensen, J. N., Davis, S. R., Hansen, R. B., Michelsen, C. J., Trim, H. E., 1988, Mesozoic contact metamorphism in the western United States, *in*, Ernst, W. G., editor, Metamorphism and Crustal Evolution of the Western United States: Rubey Volume VII, Prentice Hall, Englewood Cliffs, New Jersey, p. 110-178.
- Barton, P. B., Jr., 1986, User-friendly mineral deposit models, *in*, Cargill, S. M. and Green, S. B., editors, Prospects for Mineral Resource Assessments of Public Lands: Proceedings of the Leesburg Workshop: U. S. Geological Survey Circular 980, p. 94-110.
- Bean, R. E. and Titley, S. R., 1981, Porphyry copper Deposits, part II, hydrothermal alteration and mineralization, *in*, Skinner, B. J., editor, Economic Geology Seventy-Fifth Anniversary Volume: El Paso, Texas, Economic Geology Publishing Company, p. 235-269.
- Beghoul, N., and Barazangi, M., 1989, Mapping high P-velocity beneath the Colorado Plateau constrains uplift models: Journal of Geophysical Research, v. 94, p. 7083-7104.
- Bennett, V. C., and DePaolo, D. J., 1987, Proterozoic crustal history of the western United States as determined by neodymium isotopic mapping: Geological Society of America Bulletin, v. 99, p. 674-685.
- Benz, H. M., Smith, R. B., and Mooney, W. D., 1990, Crustal structure of the northwestern Basin and Range province from the 1986 Program for Array Seismic Studies of the Continental Lithosphere seismic experiment: Journal of Geophysical Research, v. 95, p. 21,823-21,842.
- Berg, A. W., and Carrillo, F. V., 1980, MILS: The mineral industry location system of the Federal Bureau of Mines: U. S. Bureau of Mines Information Circular 8815, 24 p.
- Berger, B. R., 1985, Geologic-geochemical features of hot- springs precious-metal deposits, *in*, Tooker, E. W., editor, Geologic Characteristics of Sediment- and Volcanic- Hosted Disseminated Gold Deposits—search for an Occurrence Model: U. S. Geological Survey Bulletin 1646, p. 47-53.
- Berger, B. R., 1996, Constraining structural environments during fault motion inversion; requisite for bonanza orebody formation, Comstock Lode, Virginia City, Nevada, *in*, Geological Society of America, 28<sup>th</sup> annual meeting, Abstracts with Programs, v. 28, p. 94.
- Berger, B. R., and Bethke, P. M., editors, 1985, Geology and Geochemistry of Epithermal Systems: Reviews in Economic Geology, v. 2, 298 p.
- Berger, B. R., and Bonham, H. F., 1990, Epithermal gold-silver deposits in western United States: Time-space products of evolving plutonic, volcanic and tectonic environments: Journal of Geochemical Exploration, v. 36, p. 103-142.

- Berger, B. R., and Eimon, P. I., 1982, Comparative models of epithermal silver-gold deposits: Society of Mining Engineers of American Institute of Mining, Metallurgical, and Petroleum Engineers, Inc., Preprint N° 82-13, 25 p.
- Berger, B. R., and Henley, R. W., 1989, Advances in the understanding of epithermal gold-silver deposits, with special reference to the western United States, *in*, Keays, R. R., Ramsay, R. H., and Groves, D. I., editors, *The Geology of Gold Deposits: The Perspective in 1988: Economic Geology Monograph 6*, p. 405-423.
- Berger, B. R., and Jefferson, C. W., 1986, Deposit type models: A quantitative base for resource assessment, *in*, Cargill, S. M., and Green, S. B., editors, *Prospects for mineral resource assessments on public lands: Proceedings of the Leesburg Workshop: U.S. Geological Survey Circular 980*, p. 271-274.
- Berry, G. W., Grim, P. J., and Ikelman, J. A., 1980, Thermal springs list for the United States: National Oceanic and Atmospheric Administration Key to Geophysical Records Documentation N° 12, National Geophysical and Solar-Terrestrial Data Center, Datamapping Group, Code D64, Boulder, 59 p.
- Best, M. G., and Christiansen, E. H., 1991, Limited extension during peak Tertiary volcanism, Great Basin of Nevada and Utah: *Journal of Geophysical Research*, v. 96, N° B8, p. 13509-13528.
- Best, M. G., Christiansen, E. H., Deino, A. L., Grommé, C. S., McKee, E. H., and Noble, D. C., 1989, Excursion 3A: Eocene through Miocene volcanism in the Great Basin of the western United States, *in*, Chapin, C. E., and Zidek, J., editors, *Field Excursions to Volcanic Terranes in the Western United States, V. II: Cascades and Intermountain West: New Mexico Bureau of Mines and Mineral Resources Memoir 47*, p. 91-133.
- Billings, M. P., 1972, *Structural Geology*, Prentice-Hall, Inc., Englewood Cliffs, New Jersey, Third edition, 606 p.
- Birak, D. J., 1986, Exploration and geologic development of the Jerritt Canyon gold deposit, Elko County, Nevada, U. S. A., *in*, Macdonald, A. J., editor, *Gold '86—an International Symposium on the Geology of Gold Deposits, Proceedings Volume: Toronto, Ontario, Gold '86*, p. 488-496.
- Birak, D. J., Mancuso, T. K., and Dahl, A. R., 1987, Sediment-hosted disseminated gold mineralization at Jerritt Canyon, Nevada. I—Jasperoids as the key to the time-space framework: *Geological Society of America Abstracts with Programs*, v. 19, p. 589.
- Bird, P., 1988, Formation of the Rocky Mountains, western United States: A continuum computer model: *Science*, v. 239, p. 1501-1507.
- Blackwell, D. D., 1978, Heat flow and energy loss in the western United States, *in*, Smith R. B., and Eaton, G. P., editors, *Cenozoic Tectonics and Regional Geophysics of the Western Cordillera: Geological Society of America Memoir 152*, p. 175-208.



- Blake, M. C. Jr., Jayko, A. S., McLaughlin, R. J., and Underwood, M. B., 1988, Metamorphic and tectonic evolution of the Franciscan Complex, Northern California, *in*, Ernst, W. G., editor, *Metamorphism and Crustal Evolution of the Western United States: Rubey Volume VII*, Prentice Hall, Englewood Cliffs, New Jersey, p. 1035-1060.
- Blakely, R. J., 1988, Curie temperature isotherm analysis and tectonic implications of aeromagnetic data from Nevada: *Journal of Geophysical Research*, v. 93, p. 11,817-11,832.
- Blakely, R. J., and Connard, G. G., 1989, Crustal studies using magnetic data, *in*, Pakiser, L. C., and Mooney, W. D., editors, *Geophysical Framework of the Continental United States: Geological Society of America Memoir 172*, p. 45-60.
- Blakely, R. J., and Jachens, R. C., 1991, Concealed mineral deposits in Nevada—Insights from three-dimensional analysis of gravity and magnetic anomalies, *in*, Raines, G. L., Lisle, R. E., Schafer, R. W., and Wilkinson, W. H., editors, *Geology and Ore Deposits of the Great Basin, Symposium Proceedings Volume 1: Geological Society of Nevada, Reno/Sparks, Nevada*, p. 185-192.
- Blenkinsop, T., 1994, The fractal distribution of gold deposits: Two examples from the Zimbabwe Archaean Craton, *in*, Kruhl, J. H., editor, *Fractals and Dynamic Systems in Geoscience*, Springer-Verlag, New York, p. 247-258.
- Bliss, J. D., 1992, Developments in mineral deposit modelling: *U. S. Geological Survey Bulletin* 2004, 168 p.
- Bliss, J. D., and Menzie, D. W., 1990, Mineral deposit spatial models [abs.]: 8<sup>th</sup> International Association on the Genesis of Ore Deposits (IAGOD), Program with Abstracts, p. A228.
- Bliss J. D., editor, 1992, *Development in Mineral Deposit Modeling*. U.S. Geological Survey Bulletin 2004, p. 168.
- Bogen, N. L., and Schweickert, R. A., 1985, Magnitude of crustal extension across the northern Basin and Range province: Constraints from paleomagnetism: *Earth and Planetary Science Letters*, v. 75, p. 93-100.
- Bohannon, R. G., and Parsons, T., 1995, Tectonic implications of post-30 Ma Pacific and North American relative plate motions: *Geological Society of America Bulletin*, v. 107, p. 937-959.
- Bonham, H. F., 1982, Reserves, host rocks, and ages of bulk-minable precious metal deposits in Nevada: Nevada Bureau of Mines and Geology Open-File Report 81-1 and Preliminary Report 82-9, 4 p.
- Bonham, H. F., Jr., 1985, Characteristics of bulk-minable gold-silver deposits in cordilleran and island-arc settings, *in*, Tooker, E. W., editor, *Geologic Characteristics of Sediment- and Volcanic-hosted Disseminated Gold Deposits—Search for an Occurrence Model*: U. S. Geological Survey Bulletin 1646, p. 71-77.

- Bonham, H. F., Jr., 1988, Models for volcanic-hosted epithermal precious metal deposits, *in*, Schafer, R. W., Cooper, J. J., Vikre, P. G., editors, Bulk Mineable Precious Metal Deposits of the Western United States, The Geological Society of Nevada, Reno, p. 259-271.
- Bonham-Carter, G., Agterberg, F., Fowler, T., Brodaric, B., instructors, 1994, GIS: A short course for geoscientists, course notes, University of Ottawa.
- Bonham-Carter, G. F., 1989, Comparison of image analysis and geographic information systems for integrating geoscientific maps, *in*, Agterberg, F. P., and Bonham-Carter, G. F., editors, Statistical Analysis in the Earth Sciences, Geological Survey of Canada, Paper 89-9, p. 141-155.
- Bonham-Carter, G. F., 1991, Integration of geoscientific data using GIS, *in*, Maguire, D. J., Goodchild, M. F., and Rhind, D. W., editors, Geographical Information Systems, Volume 2: Applications: Longman Scientific and Technical, John Wiley and Sons, Inc., New York, p. 171-184.
- Bonham-Carter, G. F., 1994a, Geographic Information Systems for Geoscientists: Modelling with GIS (Computer Methods in the Geosciences Volume 13): Pergamon Press/Elsevier Science Publications, Tarrytown, New York, 398 p.
- Bonham-Carter, G. F., 1994b, When to use the Weights of Evidence method for map data: Proceedings of the Spatial Data Modelling Workshop: Macaulay Institute for Soil Science, Aberdeen, Scotland, September 1-3, 1994, 14 p.
- Bonham-Carter, G. F., Agterberg, F. P., and Wright, D. F., 1989, Weights of evidence modelling: A new approach to mapping mineral potential, *in*, Agterberg, F. P., and Bonham-Carter, G. F., editors, Statistical Applications in the Earth Science: Geological Survey of Canada, Paper 89-9, p. 171-183.
- Bonham-Carter, G. F., Agterberg, F. P., and Wright, D. F., 1988, Integration of geological datasets for gold exploration in Nova Scotia: Photogrammetric Engineering and Remote Sensing (PE&RS), v. 54, p. 1585-1592.
- Bookstrom, A. A., 1995, Plate motions, magmatism, and metallogenesis on the cordilleran margin of the U. S. A. : II. Evidence from deep seismic tomography [abs.], *in*, Geology and Ore Deposits of the American Cordillera, symposium, program with abstracts: Geological Society of Nevada, Reno/Sparks, Nevada, p. A13.
- Borisenko, A. D., Miller, A. D., and Fisher, E. I., 1972, The abundance of gold in ultrabasic rocks: *Geokhimiya*, №. 2, p. 188-196.
- Bowers, T. S., 1991, The deposition of gold and other metals: Pressure-induced fluid immiscibility and associated stable isotope signatures: *Geochimica et Cosmochimica Acta*, v. 55, p. 2417-2434.
- Boyle, R. W., 1979, The geochemistry of gold and its deposits: Geological Survey of Canada

Bulletin 280, 584 p.

Brace, W. F., 1984, Permeability of crystalline rocks: New in situ measurements: *Journal of Geophysical Research*, v. 84, p. 4327-4330.

Braile, L. W., Hinze, W. J., von Frese, R. R. B., and Keller, G. R., 1989, Seismic properties of the crust and uppermost mantle of the conterminous United States and adjacent Canada, *in*, Pakiser, L. C., and Mooney, W. D., editors, *Geophysical Framework of the Continental United States: Geological Society of America Memoir 172*, p. 655-680.

Braux, C., Delpont, G., Bonnefoy, D., Cassard, D., Bonnemaïson, M., 1990, Interpretation of remotely sensed data over the South Armorican shear zone, Brittany, France: contribution to exploration for gold mineralization, *in*, Symposium IMM Londres, October 1990, *Remote Sensing: An operational technology for mining and petroleum industries special issue*, p. 191-203.

Brookfield, M. E., 1993, Neoproterozoic Laurentia-Australia fit: *Geology*, v. 21, p. 683-686.

Bryant, B., and Nichols, D. J., 1988, Late Mesozoic and early Tertiary reactivation of an ancient crustal boundary along the Uinta Trend and its interaction with the Sevier Orogenic belts, *in*, Perry, W. J., and Schmidt, C. J., editors, *Interactions of the Rocky Mountain Foreland and Cordilleran Thrust Belt: Geological Society of America Memoir 171*, p. 411-430.

Buchanan, L. J., 1981, Precious metal deposits associated with volcanic environments in the southwest, *in*, Dickinson, W. R., and Payne, W. D., editors, *Relations of Tectonics to Ore Deposits in the Southern Cordillera: Arizona Geological Society Digest*, v. 14, p. 237-262.

Buck, W. R., 1991, Modes of continental lithospheric extension: *Journal of Geophysical Research*, v. 96, p. 20,161-20,178.

Burchfiel, B. C., Cowan, D. S., and Davis, G. A., 1992, Tectonic overview of the Cordilleran orogen in the western United States, *in*, Burchfiel, B. C., Lipman, P. W., and Zoback, M. L., editors, *The Cordilleran Orogen: The Conterminous U. S., the Geology of North America, Volume G-3: Geological Society of America*, p. 407-480.

Cameron, E. M., 1987, Archaean gold mineralization and oxidized hydrothermal fluids: *Economic Geology*, v. 82, p. 1177-1191.

Cameron, E. M., 1988, Archaean gold: Relation to granulite formation and redox zoning in the crust: *Geology*, v. 16, p. 109-112.

Cameron, E. M., 1993, Precambrian gold: Perspectives from the top and bottom of shear zones: *Canadian Mineralogist*, v. 31, p. 917-944.

Cameron, E. M., and Hattori, K., 1995, Highly oxidized deep metamorphic zones: occurrence and origin, [ext. abs.]: Goldschmidt Conference, Edinburg, *Mineralogical Magazine*, v. 58A, p. 142-143.

- Campa, M. F., and Coney, P. J., 1983, Tectono-stratigraphic terranes and mineral resources distributions in Mexico: *Canadian Journal of Earth Science*, v. 20, p. 1040-1051.
- Campbell, I. H., and Griffiths, R. W., 1992, The changing nature of mantle hotspots through time: Implication for the chemical evolution of the mantle: *The journal of Geology*, v. 92, p. 497-523.
- Canfield, K. S., 1983, Gold in the United States, *in*, Reese, D. A., editor, *Precious metals 1983—Proceedings of the Seventh International Precious Metals Institute Conference*, San Francisco, California, June, 1983: New York, New York, Pergamon Press, p. 153-166.
- Carbonell, R., and Smithson, S. B., 1991, Large-scale anisotropy within the crust in the Basin and Range province: *Geology*, v. 19, p. 698-701.
- Carey, S. W., 1955, The orocline concept in geotectonics, *Proceedings of the Royal Society of Tasmania*, v. 89, p. 255-288.
- Carey, S. W., 1958, The tectonic approach to continental drift, *in* S. W. Carey, editor, *Continental Drift: A Symposium*, p. 177-363, Hobart: University of Tasmania.
- Carey, S. W., 1976, *The Expanding Earth*: Elsevier, Amsterdam, 487 p.
- Carey, S. W., 1989, *Theories of the Earth and Universe—A History of Dogma in the Earth Sciences*: Stanford University Press, Stanford, California, 413 p.
- Carlson, C. A., 1991, Spatial distribution of ore deposits: *Geology*, v. 19, p. 111-114.
- Carlson, D. H., Fleck, R. J., Moyer, F. J., and Fox, K. F., 1991, Geology, geochemistry and isotopic character of the Colville igneous complex, northeastern Washington: *Journal of Geophysical Research*, v. 96, p. 13,313-13,333.
- Carlson, R. W., 1984, Tectonic influence on magma composition of Cenozoic basalts from the Columbia Plateau and northwestern Great Basin, U. S. A., *in*, *Explosive volcanism: Inception, evolution, and hazards*: Washington, D. C., National Academy Press, p. 23-33.
- Catchings, R. D., 1992, A relation among geology, tectonics, and velocity structure, western to central Nevada Basin and Range: *Geological Society of America Bulletin*, v. 104, p. 1178-1192. 13 figs.
- Catchings, R. D., and Mooney, W. D., 1991, Basin and Range crustal and upper mantle structure, northwest to central Nevada: *Journal of Geophysical Research*, v. 96, 6247-6268.
- Champigny, N., and Sinclair, A. J., 1985, Progress report on the geology of the Specogna (Babe) gold deposit, *in*, Tooker, E. W., editor, *Geologic Characteristics of Sediment- and Volcanic-hosted Disseminated Gold Deposits—Search for an Occurrence Model*: U. S. Geological Survey Bulletin 1646, p. 139-145.

- Chatfield, C., 1988, Problem solving—A Statistician's Guide: Chapman and Hall, London, United Kingdom, 261 p.
- Cheng, Q., Agterberg, F. P., and Ballantyne, S. B., 1994, The Separation of Geochemical anomalies from background by fractal methods: *Journal of Geochemical Exploration*, v. 51, p. 109-130.
- Chrisman, N. R., 1991, The error component in spatial data, *in*, Maguire, D. J., Goodchild, M. F., and Rhind, D. W., editors, *Geographical Information Systems: Principles and Applications*, Volume 1: Principles: Longman Scientific and Technical, John Wiley and Sons, New York, p. 165- 174.
- Christensen, N. I., and Wepfer, W., W., 1989, Laboratory techniques for determining seismic velocities and attenuations, with applications to the continental lithosphere, *in*, Pakiser, L. C., and Mooney, W. D., editors, *Geophysical Framework of the Continental United States: Geological Society of America Memoir 172*, p. 91-102.
- Christensen, O. D., 1985, Sedimentary-rock-hosted gold deposits of the Carlin trend, Nevada: [abs.], Thayer Lindsley Visiting Lecturer, Carlton University, 1 p.
- Christensen, O. D., 1995, The Carlin trend giant gold camp: is it the strata, the structure or the stock? [ext. abs.], *in*, Clark, A. H., editor, *Giant Ore Deposits-ii: Controls on the Scale of Orogenic Magmatic-Hydrothermal Mineralization*, *Proceedings of the Second Giant Ore Deposits Workshop*, QminEx Associates and Queen's University, Kingston, p. 340-357.
- Christiansen, R. L., and Lipman, P. W., 1972, Cenozoic volcanism and plate-tectonic evolution of the western United States. II. Late Cenozoic: *Philosophical Transactions of the Royal Society of London, Series A*, v. 249, p. 249-284.
- Christiansen, R. L., and McKee, E. H., 1978, Late Cenozoic volcanic and tectonic evolution of the Great Basin and Columbia Intermontane regions, *in*, Smith, R. B., and Eaton, G. P., editors, *Cenozoic Tectonics and Regional Geophysics of the Western Cordillera: Geological Society of America Memoir 152*, p. 283-311.
- Christiansen, R. L., and Yeats, R. S., 1992, Post-Laramide geology of the U. S. Cordilleran region, *in*, Burchfiel, B. C., Lipman, P. W., and Zoback, M. L., editors, *The Cordilleran Orogen: The Conterminous U. S., the Geology of North America, Volume G-3: Geological Society of America*, p. 261-406.
- Christie-Blick, N., and Biddle, K. T., 1985, Deformation and Basin formation along strike-slip faults, *in*, Biddle, K. T., and Christie-Blick, N., editors, *Strike-Slip Deformation, Basin Formation, and Sedimentation: The Society of Economic Paleontologists and Mineralogists*, special publication no 37, Tulsa, Oklahoma, p. 1-34.
- Chung, C. J. F., 1995, Workshop on the concepts and techniques in modelling for GIS, a collection of published and unpublished papers related to modelling in GIS: The 7<sup>th</sup> International Conference on Geomatics, June 12<sup>th</sup>, Ottawa, Ontario, Canada, unpaginated.

- Chung, C. J. F., and Agterberg, F. P., 1980, Regression models for estimating mineral resources from geological map data: *Mathematical Geology*, v. 12, p. 473-488.
- Chung, C. J. F., and Moon, W. M., 1990, Combination rules of spatial geoscience data from mineral exploration, *in*, Shoji, T., editor, *The Proceedings of the International Symposium on Mineral Exploration: The Use of Artificial Intelligence*, 1990, October 29 – November 2, Tokyo, Japan, p. 1-37.
- Clark, T. M., Ehman, K. D., and Axelrod, D. I., 1985, Late Eocene extensional faulting in the northern Basin and Range province, Elko County, Nevada [abs.]: *Geological Society of America Abstracts with Program*, v. 17, p. 348.
- Cline, J. S., Hofstra, A., Landis, G., and Rye, R., 1997, Ore fluids at the Getchell, Carlin-Type gold deposit, North-Central Nevada, *in*, Vikre, P., Thompson, T. B., Bettles, K., Christensen, O., and Parratt, R., editors, *Carlin-Type Gold Deposits Field Conference*, Society of Economic Geologists, Guidebook Series, v. 28, p. 155-166.
- Coney, P. J., 1978, Mesozoic-Cenozoic Cordilleran plate tectonics, *in*, Smith, R. B., and Eaton, G. P., editors, *Cenozoic Tectonics and Regional Geophysics of the Western Cordillera*: Geological Society of America Memoir 152, p. 33-50.
- Coney, P. J., 1980, Cordilleran metamorphic core complexes: An overview: *in*, Crittenden, M. D., Jr., Coney, P. J., and Davis, G. H., editors, *Cordilleran Metamorphic Complexes*: Geological Society of America Memoir 153, p. 7-31.
- Coney, P. J., 1987, The regional tectonic setting and possible causes of Cenozoic extension in the North American Cordillera, *in*, Coward, M. P., Dewey, J. F., and Hancock, P. L., editors, *Continental Extensional Tectonics*: Geological Society Special Publication number 28, p. 177-186.
- Coney, P. J., and Harms, T. A., 1984, Cordilleran metamorphic core complexes: Cenozoic extensional relics of Mesozoic compressions: *Geology*, v. 12, p. 550-554.
- Coney, P. J., and Reynolds, S. J., 1977, Cordilleran Benioff zones: *Natures*, v. 270, p. 403-406.
- Cook, D. R., 1986, Analysis of significant mineral discoveries in the last 40 years and future trends: *Mining Engineering*, v. 38, p. 87-94.
- Coope, J. A., 1991, The Carlin trend exploration history: Discovery of the Carlin deposit: Nevada Bureau of Mines and Geology Special Publication 13, Mackay School of Mines, University of Reno, Nevada, 16 p.
- Couch, R. W., and Riddihough, R. P., 1989, The crustal structure of the western continental margin of North America, *in*, Pakiser, L. C., and Mooney, W. D., editors, *Geophysical Framework of the Continental United States*: Geological Society of America Memoir 172, p. 103-128.



- Courtney, R. C., and White, R. S., 1986, Anomalous heat flow and geoid across the Cape Verde Rise; Evidence for dynamic support from a thermal plume in the mantle: *Geophysical Journal of the Royal Astronomical Society*, v. 87, p. 815-867.
- Cowan, D. S., and Bruhn, R. L., 1992, Late Jurassic to early Late Cretaceous geology of the U. S. Cordillera, *in*, Burchfiel, B. C., Lipman, P. W., and Zoback, M. L., editors, *The Cordilleran Orogen: The conterminous U. S., the Geology of North America, Volume G-3: Geological Society of America*, p. 169-203.
- Coward, M. P., Dewey, J. F., and Hancock, P. L., editors, 1987, *Continental Extensional Tectonics*, Geological Society of London Special Publication 28, 637 p.
- Cox, D. P., 1992, Descriptive Model of Distal Disseminated Ag-Au, *in*, Bliss J. D., editor, *Development in Mineral Deposit Modeling*. U.S. Geological Survey Bulletin 2004, p. 168.
- Cox, D. P., and Singer, D. A., 1992, Grade and Tonnage of Distal Disseminated Ag-Au, *in*, Bliss J. D., editor, *Development in Mineral Deposit Modeling*. U.S. Geological Survey Bulletin 2004, p. 168.
- Cox, D. P., and Singer, D. A., 1986, Mineral deposit models: U. S. Geological Survey Bulletin 1693, 379 p.
- Cox, D. P., Ludington, S., Sherlock, M. G., Singer, D. A., Berger, B. R., and Tingley, J. V., 1991, Mineralization pattern in time and space in the Great Basin of Nevada, *in*, Raines, G. L., Lisle, R. E., Schafer, R. W., and Wilkinson, W. H., editors, *Geology and Ore Deposits of the Great Basin, Symposium Proceedings Volume 1: Geological Society of Nevada, Reno/Sparks, Nevada*, p. 193-198.
- Crittenden, M. D., Jr., Coney, P. J., and Davis, G. H., editors, 1980, *Cordilleran Metamorphic Complexes: Geological Society of America Memoir 153*, 490 p.
- Crowell, J. C., 1987, The tectonically active margin of the western U. S. A. : *Episodes*, v. 10., p. 278-282.
- Cunningham, C. G., 1986, Genetic model for disseminated gold deposits related to a regional paleothermal anomaly in Nevada: *Geological Society of America Abstracts with Programs*, v. 18, p. 578.
- Cunningham, C. G., 1988, The relationship between some disseminated gold deposits, the western edge of the Precambrian Craton, and paleothermal anomalies in Nevada, *in*, Schafer, R. W., Cooper, J. J., and Vikre, P. G., editors, *Bulk Mineable Precious Metal Deposits of the Western United States: The Geological Society of Nevada, Reno*, p. 35-48.
- Daly, W. E., Doe, T. C., and Loranger, R. J., 1991, Geology of the northern Independence Mountains, Elko County, Nevada, *in*, Raines, G. L., Lisle, R. E., Schafer, R. W., and Wilkinson, W. H., editors, *Geology and Ore Deposits of the Great Basin, Symposium Proceedings Volume 1: Geological Society of Nevada, Reno/Sparks, Nevada*, p. 583-602.

- Damon, P. E., and Mauger, R. L., 1966, Epeirogeny-orogeny viewed from the Basin and Range province: Society of Mining Engineers, Transactions, v. 235, N° 1, p. 99-112.
- Davis, J. C., 1973, Statistics and data analysis in geology: John Wiley and Sons, New York, 550 p.
- Davis, J. C., 1986, Statistics and data analysis in geology, 2<sup>nd</sup> Ed.: John Wiley and Sons, New York, 646 p.
- DePaolo, D. J., Stolper, E. M., and Thomas, D. M., 1991, Physics and chemistry of mantle plumes: EOS, Transactions, American Geophysical Union, v. 72, p. 236-237.
- Dewelley, P. C., 1984, Geology, mineralization, and fluid inclusion analysis of the Ajax vein system, Cripple Creek mining district, Colorado: Fort Collins, Colorado, Colorado State University M. S. thesis, 167 p.
- Dewey, J. F., 1988, Extensional collapse of orogens: Tectonic, v. 7, p. 1123-1139.
- Dewey, J. W., Hill, D. P., Ellsworth, W. L., and Engdahl, E. R., 1989, Earthquakes, faults, and the seismotectonic framework of the contiguous United States, *in*, Pakiser, L. C., and Mooney, W. D., editors, Geophysical Framework of the Continental United States: Geological Society of America Memoir 172, p. 541-575.
- Dickinson, W. R., 1981, Plate tectonic evolution of the southern Cordillera, *in*, Dickinson, W. R., and Payne, W. D., editors, Relations of Tectonics to Ore Deposits in the Southern Cordillera: Arizona Geological Society Digest Volume XIV, p. 113-135.
- Dickinson, W. R., 1992, Cordilleran sedimentary assemblages, *in*, Burchfiel, B. C., Lipman, P. W., and Zoback, M. L., editors, The Cordilleran Orogen: The conterminous U. S., The Geology of North America, Volume G-3: Geological Society of America, p. 539-551.
- Dickinson, W. R., and Snyder, W. S., 1978, Plate tectonics of the Laramide orogeny, *in*, Matthews, V., III, editor, Laramide Folding Associated with Basement Block Faulting in the Western United States: Geological Society of America Memoir 151, p. 355-366.
- Dickson, F. W., Rye, R. D., and Radtke, D. S., 1979, The Carlin gold deposit as a product of rock-water interactions: Nevada Bureau of Mines Report 33, p. 101-108.
- Dilles, J. H., and Gans, P. B., 1995, The chronology of Cenozoic volcanism and deformation in the Yerington area, western Basin and Range and Walker Lane: Geological Society of America Bulletin, v. 107, p. 474-486.
- Douglas, M. S., Jr., Albinson, T., and Sawkins, F. J., 1982, Geologic and fluid inclusion studies of the Tayoltita silver-gold vein deposit, Durango, Mexico: Economic Geology, v. 77, p. 1120-1145.
- Downes, H., 1990, Shear zones in the upper mantle - relation between geochemical enrichment

- and deformation in mantle peridotites: *Geology*, v. 18, p. 374-377.
- Draper, D. S., 1988, Geochemical trends in basalts of the northern Basin and Range Province [abs.]: *EOS, Transactions, American Geophysical Union*, v. 69, p. 1479.
- Draper, D. S., 1991, Late Cenozoic bimodal magmatism in the northern Basin and Range Province of southeastern Oregon: *Journal of Volcanology and Geothermal Research*, v. 47, p. 299-328.
- Dreier, J., 1984, Regional tectonic control of epithermal veins in the western United States and Mexico, *in*, Wilkins, J. Jr., editor, *Gold and Silver Deposits of the Basin and Range Province Western U. S. A. : Arizona Geological Society Digest*, v. 15, p. 28-50.
- Drewes, H., 1991, Description and development of the Cordilleran orogenic belt in the southwestern United States and northern Mexico: *U. S. Geological Survey Professional Paper* 1512, p. 1-5.
- Dunbar, J. A., and Sawyer, D. S., 1989, How preexisting weaknesses control the style of continental breakup: *Journal of Geophysical Research*, v. 94, N° B6, p. 7278-7292.
- Durning, W. P., and Buchanan, L. J., 1984, The geology and ore deposits of Oatman, Arizona: *Arizona Geological Society Digest*, v. 15, p. 141-158.
- Duval, J. S., 1991, Potassium, uranium and thorium geochemical maps of the conterminous U. S. A. : *Transactions of the Institute of Mining and Metallurgy, (Sect. B: Applied Earth Science)*, 100, p. B66-B73.
- Eardley, A. J., 1951, *Structural geology of North America*: New York, Harper and Row, 624 p.
- Eaton, G. P., 1980, Geophysical and geological characteristics of the crust of the Basin and Range province, *in*, *Continental Tectonics, Studies in Geophysics*, National Academy of Sciences Panel on Continental Tectonics, Burchfiel, B. C., Oliver, J. E., and Silver, L. T., Chairmen, p. 96-113.
- Eaton, G. P., 1982, The Basin and Range Province: Origin and tectonic significance: *Annual Reviews of Earth and Planetary Science*, v. 10, p. 409-440.
- Eaton, G. P., 1983, Cenozoic magmatism, crustal deformation and mineralization in the western U. S. [abs.]: *Geological Society of America Abstracts with Programs*, v. 15, p. 288.
- Eaton, G. P., 1984, Mineral abundance in the North American Cordillera: *American Scientist*, v. 72, p. 368-377.
- Eaton, G. P., 1986, A tectonic redefinition of the southern Rocky Mountains: *Tectonophysics*, v. 132, 163-193.
- Eaton, G. P., 1987, Topography and origin of the southern Rocky Mountains and Alvarado

- Ridge, *in*, Coward, M. P., Dewey J. F., and Hancock, P. L., editors, Continental Extensional Tectonics, Geological Society Special Publication, London, v. 28, p. 355-369.
- Eaton, G. P., Wahl, R. R., Prostka, H. J., Mabey, D. R., and Kleinkopf, M. D., 1978, Regional gravity and tectonic patterns: Their relation to late Cenozoic epeirogeny and lateral spreading in the western Cordillera, *in*, Smith, R. B., and Eaton, G. P., editors, Cenozoic Tectonics and Regional Geophysics of the Western Cordillera: Geological Society of America Memoir 152, p. 51-91.
- Eckstrand, O. R., editor, 1984, Canadian Mineral Deposit Types: a Geological Synopsis: Geological Survey of Canada Economic Geology Report 36, 86 p.
- Edward, G., and McLaughlin, W. A., 1972, Shell list N° 1-K-Ar and Rb-Sr age determinations of California, Nevada and Utah rocks and minerals: Isochron/West, N°3, January
- Eggler, D. H., 1987, Solubility of major and trace elements in mantle metasomatic fluids: Experimental constraints, *in*, Menzies, M. A., and Hawkesworth, C. J., editors, Mantle Metasomatism: Academic Press, London, p. 21-41.
- Eggler, D. H., Meen, J. K., Welt, Fred, Dudas, F. O., Furlong, K. P., McCallum, M. E., and Carlson, R. W., 1988, Tectonomagmatism of the Wyoming province: Colorado School of Mines Quarterly, v. 83, N° 2, p. 25-40.
- Einaudi, M. T., and Burt, D. M., 1982, Introduction—Terminology, classification and composition of skarn deposits: Economic Geology, v. 77, p. 745-754.
- Einaudi, M. T., Meinert, L. D., and Newberry, R. J., 1981, Skarn deposits, *in*, Skinner, B. J., editor, Economic Geology Seventy-Fifth Anniversary Volume: El Paso, Texas, Economic Geology Publishing Company, p. 317-391.
- Elevatorski, E. A., 1981, Gold mines of the world: Dana Point, California, Minobras, 107 p.
- Elison, M. W., Speed, R. C., and Kistler, R. W., 1990, Geologic and isotopic constraints on crustal structure of the northern Great Basin: Geological Society of America Bulletin, v. 102, p. 1077-1092.
- Elston, W. E., 1982, The Basin and Range province: Origin and tectonic significance: Annual Reviews of Earth and Planetary Science, v. 10, p. 409-440.
- Elston, W. E., 1983, Mid-Tertiary volcanism of southwestern United States: arc or backarc? [abs.]: The Geological Society of America Abstracts with Programs, v. 15, p. 288.
- Elston, W. E., 1984, Subduction of young oceanic lithosphere and extensional orogeny in southwestern North America during mid-Tertiary time: Tectonics, v. 3, p. 229-250.
- Elston, W. E., 1986, Evolution of Rio Grande Rift and Basin and Range Province: A 60-Ma continuum [abs.]: Geological Society of America Abstracts with Programs, v. 18, p. 594.

- Elston, W. E., 1987, Areal and temporal patterns in post-40 Ma extension and volcanism, North American Basin and Range Province [abs.]: EOS, Transactions, American Geophysical Union, v. 68, p. 1529.
- Emsbo, P., Hofstra, A., Zimmerman, J. M., Snee, L., 1996, September 6, 1998A mid-Tertiary age constraint on alteration and mineralization in igneous dikes on the Goldstrike property, Carlin Trend, Nevada, Geological Society of Nevada, abstract with program.
- Eng, T., 1991, Geology and mineralization of the Freedom Flats gold deposit, Borealis mine, Mineral County, Nevada, *in*, Raines, G. L., Lisle, R. E., Schafer, R. W., and Wilkinson, W. H., editors, Geology and Ore Deposits of the Great Basin, Symposium Proceedings Volume 2: Geological Society of Nevada, Reno/Sparks, Nevada, p. 995-1019.
- Ernst, W. G., 1992, Metamorphism of the western Cordillera and its relationship to tectonics, *in*, Burchfiel, B. C., Lipman, P. W., and Zoback, M. L., editors, the Cordilleran Orogen: the Conterminous U. S., the Geology of North America, Volume G-3: Geological Society of America, p. 515-538.
- Ernst, W. G., editor, 1988, Metamorphism and Crustal Evolution of the Western United States: Rubey Volume VII, Prentice Hall, Englewood Cliffs, New Jersey, 1153 p.
- Farmer, G. L., 1988, Isotope geochemistry of Mesozoic and Tertiary igneous rocks in the western United States and implications for the structure and composition of the deep continental lithosphere, *in*, Ernst, W. G., editor, Metamorphism and Crustal Evolution of the Western United States: Rubey Volume VII, Prentice Hall, Englewood Cliffs, New Jersey, p. 87-109.
- Farmer, G. L., and DePaolo, D. J., 1984, Origin of Mesozoic and Tertiary granite in the western United States and implications for pre-Mesozoic crustal structure - 2. Nd and Sr isotopic studies of unmineralized and Cu- and Mo-mineralized granite in the Precambrian craton: Journal of Geophysical Research, v. 89, N° B12, p. 10141-10160.
- Farmer, G. L., and DePaolo, D. J., 1983, Origin of Mesozoic and Tertiary granite in the western United States and implications for pre-Mesozoic crustal structure - 1. Nd and Sr isotopic studies in the geocline of the northern Great Basin: Journal of Geophysical Research, v. 88, N° B4, p. 3379-3401.
- Farmer, G. L., Perry, F. V., Semken, S., Crowe, B., Curtis, D., and DePaolo, D. J., 1989, Isotopic evidence on the structure and origin of subcontinental lithospheric mantle in southern Nevada: Journal of Geophysical Research, v. 94, N° B6, p. 7885-7898.
- Faulds, J. E., and Varga, R. J., 1998, The role of accommodation zones and transfer zones in the regional segmentation of extended terranes: Geological Society of America Special Paper 323, p. 1-46.
- Fenneman, N. M., and Johnson, D. W., 1946, Physical divisions of the United States: U. S. Geological Survey, 1: 7,000,000 scale map sheet.

- Fisher, P. F., 1991, Spatial data sources and data problems, *in*, Maguire, D. J., Goodchild, M. F., and Rhind, D. W., editors, *Geographical Information Systems, Volume 1: Principles and Applications*: John Wiley & Sons, New York, 649 p.
- Fitton, J. G., and James, D., 1987, The relationship between late Cenozoic extension and magmatism in the western U. S. A. [abs.]: EOS, Transactions, American Geophysical Union, v. 68, p. 1530.
- Fitton, J. G., James, D., Kempton, P. D., Ormerod, D. S., and Leeman, W. P., 1988, The role of lithospheric mantle in the generation of late Cenozoic basic magmas in the western United States: *Journal of Petrology, Special Lithosphere Issue*, p. 331-349.
- Fitton, J. G., James, D., and Leeman, W. P., 1991, Basic magmatism associated with late Cenozoic extension in the Western United States: compositional variations in space and time: *Journal of Geophysical Research*, v. 96, N° B8, pages 13,693-13,711.
- Fleck, R. J., and Criss, R. E., 1985, Strontium and oxygen isotopic variations in Mesozoic and Tertiary plutons of central Idaho: *Contribution to mineralogy and Petrology*, v. 90, p. 291-308.
- Flowerdew, R., 1991, Spatial data integration, *in*, Maguire, D. J., Goodchild, M. F., and Rhind, D. W., editors, *Geographical Information Systems: Principles and Applications, Volume 1: Principles*: Longman Scientific and Technical, New York, John Wiley and Sons, p. 375-387.
- Folger, H., 1995, Unravelling the history of a rock: U. S. Geological Survey Mineral Resources Newsletter, v. 6, N° 1, p. 1.
- Folger, H. A., Eberl, D. D., Hofstra, A. H., and Snee, L. W., 1997, Illite crystallinity- A key to understanding  $^{40}\text{Ar}/^{39}\text{Ar}$  dates from gold deposits in the Jerritt Canyon district, Nevada, [abs.]: Geological Society of America, Abstract with Program, v. 29, Abstract No 51470, <http://www.geosociety.org/cgi-bin/gsa97hl.pl?hofstra^annual/s/abs/51470.htm~>
- Fountain, D. M., and Christensen, N. I., 1989, Composition of the continental crust and upper mantle; A review, *in*, Pakiser, L. C., and Mooney, W. D., editors, *Geophysical Framework of the Continental United States: Geological Society of America Memoir 172*, p. 711-742.
- Franklin, J. M., Lydon, J. W., and Sangster, D. F., 1981, Volcanogenic-associated massive sulfide deposits, *in*, Skinner, B. J., editor, *Economic Geology Seventy-Fifth Anniversary Volume*: El Paso, Texas, Economic Geology Publishing Company, p. 485-627.
- Gammons, C. H., 1997, Thermochemical sulfate reduction: A key step in the origin of sediment-hosted disseminated gold deposits, *in*, Vikre, P., Thompson, T. B., Bettles, K., Christensen, O., and Parratt, R., editors, *Carlin-Type Gold Deposits Field Conference, Society of Economic Geologists, Guidebook Series*, v. 28, p. 141-146.
- Gans, P. B., 1987, An open-system, two-layer crustal stretching model for the eastern Great Basin: *Tectonics*, v. 6, p. 1-12.



- Gans, P. B., 1990, Space-time patterns of Cenozoic N-S extension, N-S shorting, E-W extension, and magmatism in the Basin and Range Province: Evidence for active Rifting [abs.]: Geological Society of America Abstracts with Programs, v. 22, p. 24.
- Gans, P. B., and Mahood, G., 1987, Synextensional magmatism in the Basin and Range Province: A case study from the eastern Great Basin [abs.]: Geological Society of America Abstracts with Programs, v. 19, p. 671.
- Gans, P. B., and Miller, E. L., 1983, Style of mid-Tertiary extension in east-central Nevada, *in*, Geological Society of America Field Trip Guidebook, Utah Geological and Mineral Survey Special Studies 59, p. 107-160.
- Gans, P. B., Mahood, G. A., and Schermer, E., 1989, Synextensional magmatism in the Basin and Range Province: A case study from the eastern Great Basin: Geological Society of America Special Paper 233, 53 p.
- Gastil, R. G., 1979, A conceptual hypothesis for the relation of differing tectonic terranes to plutonic emplacement: *Geology*, v. 7, p. 542-544.
- George, H., and Bonham-Carter, G. F., 1989, Spatial modelling of geological data for gold exploration, Star Lake area, Saskatchewan, *in*, Agterberg, F. P. and Bonham-Carter, G. F., editors, Statistical Applications in the Earth Sciences: Geological Survey of Canada, Paper 89-9, p. 157-169.
- Giggenbach, W. F., 1992a, The composition of gases in geothermal and volcanic systems as a function of tectonic setting, *in*, Kharaka, Y. K., and Maest, A. S., editors, Water-Rock Interaction, Volume 2 Moderate and High Temperature Environment, Proceeding of the 7<sup>th</sup> International Symposium on Water-Rock Interaction, Balkema, Rotterdam, p. 873-878.
- Giggenbach, W. F., 1992b, Isotopic shifts in waters from geothermal and volcanic systems along convergent plate boundaries and their origin: *Earth and Planetary Science Letters*, v. 113, p. 495-510.
- Giggenbach, W. F., 1992c, Magma degassing and mineral deposition in hydrothermal systems along convergent plate boundaries: *Economic Geology*, v. 87, p. 1927-1944.
- Glazner, A. F., and Bartley, J. M., 1985, Evolution of lithospheric strength after thrusting: *Geology*, v. 13, p. 42-45.
- Glazner, A. F., and Bartley, J. M., 1990, Contrasting Cenozoic tectonomagmatic histories of the northern and southern Basin and Range [abs.]: Geological Society of America Abstracts with Programs, v. 22, p. 25.
- Glazner, A. F., and Ussler III, W., 1989, Crustal extension, crustal density, and the evolution of Cenozoic magmatism in the Basin and Range of the western United States: *Journal of Geophysical Research*, v. 94, N° B6, p. 7952-7960.

- Glazner, A. F., and Ussler III, W., 1987, Lithospheric extension and the change of intermediate to basaltic volcanism in the western United States [abs.]: EOS, Transactions, American Geophysical Union, v. 68, p. 1529.
- Goodchild, M. F., 1995, Error estimates: Workshop for Geomatics 95, Ottawa, Congress Centre, Geomatics Workshop, 42 p.
- Gott, G. B., McCarthy, J. H., Jr., VanSickle, G. H., and McHugh, J. G., 1969, Distribution of gold and other metals in the Cripple Creek district, Colorado: U. S. Geological Survey Professional Paper 625-A, p. A1-A17.
- Gottfried, D., Rowe, J. J., and Tilling, R. I., 1972, Distribution of gold in igneous rocks: Geological Survey Professional Paper 727, 42 p.
- Govett, G. J. S., 1983, Rock Geochemistry in Mineral Exploration, Handbook of Exploration Geochemistry: Elsevier Science Publishing Company Inc., New York, v. 3, 473 p.
- Grauch, V. J. S., Jachens, R. C., and Blakely, R. J., 1995, Evidence for a basement feature related to the Cortez disseminated gold trend and implications for regional exploration in Nevada: Economic Geology, v. 90, p. 203-207.
- Griffiths, J. C., and Smith Jr., C. M., 1992, Mineral resources versus geologic diversity in small areas: Computers & Geosciences, v. 18, p. 477-486.
- Groff, J. A., 1996,  $^{40}\text{Ar}/^{39}\text{Ar}$  geochronology of gold mineralization and origin of auriferous fluids for the Getchell and Twin Creeks mines, Humboldt County, Nevada: New Mexico Institute of Mining and Technology PhD. dissertation, 291 p.
- Groff, J. A., Heizler, M. T., McIntosh, W. C., and Norman, D. I., 1997,  $^{40}\text{Ar}/^{39}\text{Ar}$  dating and mineral paragenesis for Carlin-type gold deposits along the Getchell trend, Nevada: Evidence for Cretaceous and Tertiary gold mineralization: Economic Geology, v. 92, p. 601-622.
- Guilbert, J. M., and Park, C. F., Jr., 1986, The geology of ore deposits: New York, New York, W. H. Freeman and Company, 985 p.
- Guild, P. W., 1968, Metallogenic Map of North America: Comm. Geol. Map World (International Geological Congress—International Union of Geological Scientists) Bulletin 8, p. 77-90.
- Guild, P. W., 1985, The Basin-and-Range metallogenic province: Product of Horizontal or vertical stresses?: Global Tectonics and Metallogeny, v. 3, N° 1, p. 18-19.
- Hall, C. M., Simon, G., Kesler, S. E., 1997, Age of mineralization at the Twin Creeks SHMG deposit, Nevada, *in*, Vikre, P., Thompson, T. B., Bettles, K., Christensen, O., and Parratt, R., editors, Carlin-Type Gold Deposits Field Conference, Society of Economic Geologists, Guidebook Series, v. 28, p. 151-154.

- Hamilton, W., 1987, Crustal extension in the Basin and Range province, southwestern United States, *in*, Coward, M. P., Dewey, J. F., and Hancock, P. L., editors, Continental Extensional Tectonics, Geological Society of London Special Publication 28, p. 155-176.
- Hamilton, W., and Myers, W. B., 1966, Cenozoic tectonics of the Western United States: Reviews in Geophysics, v. 4, p. 509-549.
- Hamilton, W. B., 1987, Plate-tectonic evolution of the western U. S. A. : Episodes, v. 10, p. 271-276.
- Hamilton, W. B., 1988, Tectonic setting and variations with depth of some Cretaceous and Cenozoic structural and magmatic systems of the western United States, *in*, Ernst, W. G., editor, Metamorphism and Crustal Evolution of the Western United States: Rubey Volume VII, Prentice Hall, Englewood Cliffs, New Jersey, p. 1-40.
- Hamilton, W. B., 1989, Crustal geologic processes of the United States, *in*, Pakiser, L. C., and Mooney, W. D., editors, Geophysical Framework of the Continental United States: Geological Society of America Memoir 172, p. 743-781.
- Hardyman, R. F., and Oldow, J. S., 1991, Tertiary tectonic framework and Cenozoic History of the Central Walker Lane, Nevada, *in*, Raines, G. L., Lisle, R. E., Schafer, R. W., and Wilkinson, W. H., editors, Geology and Ore Deposits of the Great Basin, Symposium Proceedings Volume 1: Geological Society of Nevada, Reno/Sparks, Nevada, p. 279-301.
- Harland, W. B., Armstrong, R. L., Cox, A. V., Smith, A. G., and Smith, D. G., 1990, A geologic time scale 1989: Cambridge University Press, Cambridge, 263 p.
- Harris, A. G., Wardlaw, B. R., Rust, C. C., and Merrill, G. K., 1980, Maps for assessing thermal maturity (conodont color alteration index maps) in Ordovician through Triassic rocks in Nevada and Utah: U. S. Geological Survey Miscellaneous Investigations Series Map I-1249.
- Harry, D. L., Oldow, J. S., and Sawyer, D. S., 1995, The growth of orogenic belts and the role of crustal heterogeneities in decollement tectonics: Geological Society of America Bulletin, v. 107, p. 1411-1426.
- Harry, D. L., Sawyer, D. S., and Leeman, W. P., 1993, The mechanics of continental extension in western North America: Implications for the magmatic and structural evolution of the Great Basin: Earth and Planetary Science Letters, v. 117, p. 59-71.
- Hauge, T. A., Allmendinger, R. W., Caruso, C., Hauser, E., Klemperer, S., Opdyke, S., Potter, C., Sanford, W., Brown, L., Kaufman, S., and Oliver, J., 1987, Crustal structure of western Nevada from COCORP deep seismic reflection data: Geological Society of America Bulletin, v. 98, p. 320-329.
- Hausen, D. M., Akright, R., Kerr, P. F., 1967, Colloidal gold mineralization in Palaeozoic sediments of the Lynn mining district, Nevada: Transactions of the Institute of Mining and Metallurgy, (Sect. B: Applied Earth Science), 732, p. B225.

- Hauser, E. C., and Lundy, J., 1989, COCORP deep reflection: Moho at 50 km beneath Colorado Plateau: *Journal of Geophysical Research*, v. 94, p. 7071-7089.
- Hauser, E., Potter, C., Hauge, T., Burgess, S., Burtch, S., Mutschler, J., Allmendinger, R., Brown, L., Kaufman, S., Oliver, J., 1987, Crustal structure of eastern Nevada from COCORP deep seismic refraction data: *Geological Society of America Bulletin*, v. 99, p. 833-844.
- Hayashi, K. I., and Ohmoto, H., 1991, Solubility of gold in NaCl- and H<sub>2</sub>S-bearing aqueous solutions at 250° C-350° C: *Geochimica et Cosmochimica Acta*, v. 55, p. 2111-2126.
- Hayba, D. O., Bethke, P. M., Heald, P., and Foley, N. K., 1985, Geologic, mineralogic, and geochemical characteristics of volcanic-hosted epithermal precious-metal deposits, *in*, Berger, B. R., and Bethke, P. M., editors, *Geology and Geochemistry of Epithermal Systems: Reviews in Economic Geology*, v. 2, p. 129-167.
- Heald, P., Foley, N. K., and Hayba, D. O., 1987, Comparative anatomy of volcanic-hosted epithermal deposits: Acid-sulfate, and adularia-sericite types: *Economic Geology*, v. 82, p. 1-26.
- Hearn, T., Beghoul, N., and Barazangi, M., 1991, Tomography of the western United States from regional arrival times: *Journal of Geophysical Research*, v. 96, p. 16,369-16,381.
- Hedenquist, J. W., 1997, The porphyry to epithermal continuum: Evidence from volcanoes and ore deposits: Thayer Lindsley Lecture of the Society of Economic Geologists, October 9 1997, Ottawa-Carleton Geoscience Centre, Ottawa, ON.
- Hedenquist, J. W., and Lowenstern, J. B., 1994, The role of magmas in the formation of hydrothermal ore deposits: *Nature*, v. 370, N° 18, p. 519-527.
- Hedenquist, J. W., Izawa, E., Arribas, A., and White, N. C., 1996, Epithermal gold deposits: Styles, characteristics, and exploration: Society of Resource Geology, *Resource Geology Special Publication Number 1*, Tokyo.
- Hendricks, J. D., and Plescia, J. B., 1991, A review of the regional geophysics of the transition zone: *Journal of Geophysical Research*, v. 96, p. 12,351-12,374.
- Henley, R. W., 1983, The geothermal framework of epithermal deposits, *in*, Berger, B. R., and Bethke, P. M., editors, *Geology and Geochemistry of Epithermal Systems: Reviews in Economic Geology*, v. 2, p. 1-24.
- Henley, R. W., and Ellis, A. J., 1983, Geothermal systems ancient and modern: A geochemical review: *Earth- Science Reviews*, v. 19, p. 1-50.
- Henry, C. D., and Boden, D. R., 1997, Eocene magmatism of the Tuscarora volcanic field, Elko County, Nevada, and implications for Carlin-Type mineralization, *in*, Vikre, P., Thompson, T. B., Bettles, K., Christensen, O., and Parratt, R., editors, *Carlin-Type Gold Deposits Field Conference*, Society of Economic Geologists, *Guidebook Series*, v. 28, p. 193-202.

- Henry, C. D., Elson, H. B., McIntosh, W. C., Heizler, M. T., and Castor, S. B., 1997, Brief duration of hydrothermal activity at Round Mountain, Nevada, determined from  $^{40}\text{Ar}/^{39}\text{Ar}$  geochronology: *Economic Geology*, v. 92, p. 807-826.
- Hildenbrand, T. G., and Kucks, R. P., 1988, Filtered magnetic anomaly maps of Nevada: Nevada Bureau of Mines and Geology Map 93B, 5 sheets.
- Hildenbrand, T. G., Simpson, R. W., Godson, R. H., and Kane, M. F., 1982, Digital colored residual and regional bouguer gravity maps of the conterminous United States with cut-off wavelengths of 250 km and 1000 km: U. S. Geological Survey, Map GP-953-A.
- Hill, R. I., Campbell, I. H., Davies, G. F., and Griffiths, R. W., 1992, Mantle plumes and continental tectonics: *Science*, v. 256, p. 186-193.
- Hitchborn, A. D., Arbonies, D. G., Peters, S. G., Conners, K. A., Noble, D. C., Larson, L. T., Beebe, J. S., and McKee, E. H., 1996, Geology and gold deposits of the Bald Mountain mining district, White Pine County, Nevada, *in*, Coyner, A. R., and Fahey, P. L., editors, *Geology and Ore Deposits of the American Cordillera: Geological Society of Nevada Symposium Proceedings*, Reno/Sparks, Nevada, April 1995, p. 505-546.
- Hittelman, A. M., Habermann, R. E., Dater, D. T., and Di, L., compilers, 1992, Gravity earth system data CD-ROM (alpha release): National Oceanic and Atmospheric Administration, National Geophysical Data Center, Boulder, CO.
- Hittelman, A. M., Kinsfather, J. O., and Meyers, H., compilers, 1990, Geophysics of North America CD-ROM (release 1. 1, July): National Oceanic and Atmospheric Administration, National Geophysical Data Center, Boulder, CO.
- Hodges, K. V., and Walker, J. D., 1992, Extension in the Cretaceous Sevier orogen, North American Cordillera: *Geological Society of America Bulletin*, v. 104, p. 560-569.
- Hodgson, C. J., 1995, The case for upper crustal control on metal assemblages and the scale of mineralization of some hydrothermal ore deposits: A speculative genetic model, *in*, Clark, A. H., editor, *Giant Ore Deposits-II, Controls on the Scale of Orogenic Magmatic-hydrothermal Mineralization: QminEx Associates and Queen's University, Kingston*, p. 414-449.
- Hoffman, J. D., Gunnells, G. B., and McNeal, J. M., 1991, National geochemical data base: National Uranium resource evaluation data for the conterminous western United State CD-ROM: U. S. Geological Survey Digital Data Series DDS-1.
- Hoffman, P. F., 1989, Precambrian geology and tectonic history of North America, *in*, Bally, A. W., and Palmer, A. R., editors, *The Geology of North America: An Overview: Boulder, Colorado, Geological Society of America, The Geology of North America*, v. A, p. 447-512.
- Hofstra, A. H., 1994, Geology and genesis of the Carlin-type gold deposits in the Jerritt Canyon district, Nevada: Ph.D. Dissertation, University of Colorado, Boulder, 719 p.

- Hofstra, A. H., 1997, Isotopic composition of Sulfur in Carlin-type gold deposits: Implication for genetic models, *in*, Vikre, P., Thompson, T. B., Bettles, K., Christensen, O., and Parratt, R., editors, Carlin-Type Gold Deposits Field Conference, Society of Economic Geologists, Guidebook Series, v. 28, p. 119-129.
- Hofstra, A. H., and Rowe, W. A., 1987, Sediment-hosted disseminated gold mineralization at Jerritt Canyon, Nevada. II—Jasperoid paragenesis and occurrence of gold: Geological Society of America Abstracts with Programs, v. 19, p. 704.
- Hofstra, A. H., Landis, G. P., Rye, R. O., Birak, D. J., Dahl, A. R., Daly, W. E., and Jones, M. B., 1989, Geology and origin of the Jerritt Canyon sediment-hosted disseminated gold deposits, Nevada [abs.]: USGS Research on Mineral Resource—1989, Program and Abstracts, Fifth Annual V. E. McKelvey Forum on Mineral and Energy Resources, U. S. Geological Survey Circular 1035, p. 30-32.
- Hofstra, A. H., Landis, G. P., and Rowe, W. A., 1987, Sediment-hosted disseminated gold mineralization at Jerritt Canyon, Nevada. IV—Fluid geochemistry: Geological Society of America Abstracts with Programs, v. 19, p. 704.
- Hofstra, A. H., Landis, G. P., Leventhal, J. S., Northrop, H. R., Rye, R. O., Doe, T. C., and Dahl, A. R., 1991, Genesis of sediment-hosted, disseminated gold deposits by fluid mixing and sulfidation of iron in the host rocks—Chemical reaction path modeling of ore depositional processes at Jerritt Canyon, Nevada, *in*, Raines, G. L., Lisle, R. E., Schafer, R. W., and Wilkinson, W. H., editors, Geology and Ore Deposits of the Great Basin, Symposium Proceedings: Geological Society of Nevada, p.235-237.
- Hofstra, A. H., Northrop, H. R., Rye, R. O., Landis, G. P., and Birak, D. J., 1988, Origin of sediment-hosted disseminated gold deposits by fluid mixing: Evidence from jasperoids in the Jerritt Canyon gold district, Nevada, USA, *in*, Goode, A. D. T., and Bosma, L. I., compilers, Bicentennial Gold 88, Melbourne Symposium 1988: Geological Society of Australia, v. 22, p. 284-289.
- Holland, P. T., Beaty, D. W., and Snow, G. G., 1988, Comparative elemental and oxygen isotope geochemistry of jasperoid in the northern Great Basin; evidence for distinctive fluid evolution in gold-producing hydrothermal systems: Economic Geology, v. 83, p. 1401-1423.
- Horton, R. C., 1964, Hotsprings, sinter deposits, and volcanic cinder cones in Nevada: Nevada Bureau of Mines Map 25, University of Nevada, Reno, NV.
- Humphreys, E. D., 1995, Post-Laramide removal of the Farallon slab, western United States: Geology, v. 23, p. 987-990.
- Hutchinson, R. W., and Albers, J. P., 1992, Metallogenic evolution of the Cordilleran region of the western United States, *in*, Burchfiel, B. C., Lipman, P. W., and Zoback, M. L., editors, The Cordilleran Orogen: The Conterminous U. S., the Geology of North America, Volume G-3: Geological Society of America, p. 629-652.



- Idnurm, M., and Giddings, J. W., 1995, Paleoproterozoic-Neoproterozoic North America-Australia link: New evidence from paleomagnetism: *Geology*, v. 23, p. 149-152.
- Ilchik, R. P., 1995,  $^{40}\text{Ar}/^{39}\text{Ar}$ , and fission track geochronology of sediment-hosted disseminated gold deposits at Post-Betze, Carlin trend, northeastern Nevada—A discussion: *Economic Geology*, v. 90, p. 208-212.
- Ilchik, R. P., and Barton, M. D., 1996, Physical and chemical constraints for an amagmatic origin of Carlin-type gold deposits, a source-sink approach: Geological Society of Nevada Symposium, Reno/Sparks, Nevada, April 1995, p. 687-708.
- Ilchik, R. P., and Barton, M. D., 1997, An amagmatic origin for carlin-type gold deposits: *Economic Geology*, v. 92, p. 269-288.
- Iyer, H. M., and Hitchcock, T., 1989, Upper-mantle velocity structure in the continental U. S. and Canada, *in*, Pakiser, L. C., and Mooney, W. D., editors, *Geophysical Framework of the Continental United States: Geological Society of America Memoir 172*, p. 681-710.
- Jachens, R. C., Simpson, R. W., Blakely, R. J., and Saltus, R. W., 1989, Isostatic residual gravity and crustal geology of the United States, *in*, Pakiser, L. C., and Mooney, W. D., editors, *Geophysical Framework of the Continental United States: Geological Society of America Memoir 172*, p. 405-424.
- Jachens, R. C., Simpson, R. W., and Blakely, R. J., 1989, Isostatic and crustal geology of the United States, *in*, Pakiser, L. C., and Mooney, W. D., editors, *Geophysical Framework of the Continental United States: Geological Society of America Memoir 172*, p. 405-424.
- Jensen, M. L., and Bateman, A. M., 1981, *Economic Mineral Deposits*, 3<sup>rd</sup> edition: New York, New York, John Wiley and Sons, 593 p.
- John, D. A., Nash, J. T., Clark, C. W., and Wulftange, W. H., 1991, Geology, hydrothermal alteration, and mineralization at the Paradise Peak gold-silver-mercury deposits, Nye County, Nevada, *in*, Raines, G. L., Lisle, R. E., Schafer, R. W., and Wilkinson, W. H., editors, *Geology and Ore Deposits of the Great Basin, Symposium Proceedings Volume 2: Geological Society of Nevada, Reno/Sparks, Nevada*, p. 1020-1050.
- Johnson, C. M., 1991, Large-scale crust formation and lithosphere modification beneath middle to late Cenozoic calderas and volcanic fields, western North America: *Journal of Geophysical Research*, v. 96, N<sup>o</sup>. B8, p. 13485-13507.
- Jones, D. L., Cox, Allan, Coney, Peter, and Beck, 1982, The growth of western North America: *Scientific American*, v. 247, p. 70-84.
- Jones, R. B., 1989, Carlin trend gold belt: The geology: *Mining Magazine*, v. 161, p. 256-261.
- Jones, R. S., 1969, Gold in igneous, sedimentary and metamorphic rocks: U. S., Geological Survey Circular, v. 610, 28 p.

- Kane, M. F., and Godson, R. H., 1989, A crust/mantle structural framework of the conterminous United States based on gravity and magnetic trends, *in*, Pakiser, L. C., and Mooney, W. D., editors, *Geophysical Framework of the Continental United States: Geological Society of America Memoir 172*, p. 383-403.
- Keays, R. R., and Scott, R. B., 1976, Precious metals in ocean-ridge basalts: Implications for basalts as source rocks for gold mineralization: *Economic Geology*, v. 71, Nº. 4, p. 705-720.
- Keith, S. B., 1978, Paleosubduction geometries inferred from Cretaceous and Tertiary magmatic patterns in southwestern North America: *Geology*, v. 6, p. 516-521.
- Keller, G. V., 1989, Electrical structure of the crust and upper mantle beneath the United States; Part 2, Survey of data and interpretation, *in*, Pakiser, L. C., and Mooney, W. D., editors, *Geophysical Framework of the Continental United States: Geological Society of America Memoir 172*, p. 425-446.
- Kempton, P. D., Fitton, J. G., Hawkesworth, C. J., and Ormerod, D. S., 1991, Isotopic and trace element constraints on the composition and evolution of the lithosphere beneath the southwestern United States: *Journal of Geophysical Research*, v. 96, Nº. B8, p. 13713-13735.
- Kepper, J. C., Lugaski, T. P., and Aymard, W., 1991, Precious metal deposits, structural blacks and volcanism in the central structural zone, *in*, Raines, G. L., Lisle, R. E., Schafer, R. W., and Wilkinson, W. H., editors, *Geology and Ore Deposits of the Great Basin, Symposium Proceedings Volume 1: Geological Society of Nevada, Reno/Sparks, Nevada*, p. 213-234.
- Kerr, R. A., 1988, Geophysics: Ancient air, ozone, and fault: Making faults weak enough to slip: *Science*, v. 239, p. 144.
- Kerr, R. A., 1996, Putting stiffness in Earth's mantle: *Science*, v. 271, p. 1053-1054.
- Kerr, R. A., 1997, Why the west stands tall: *Science*, v. 275, p. 1564-1565.
- Kerrick, R., 1986, Fluid infiltration into fault zones: Chemical, isotopic, and mechanical effects: *Pageoph*, v. 124, p. 225-268.
- Kerrick, R., and Fyfe, W. S., 1981, The gold-carbonate association: Source of CO<sub>2</sub>, and CO<sub>2</sub> fixation reactions in Archaean lode deposits: *Chemical Geology*, v. 33, p. 265-294.
- Kesler, S. E., Russell, N., Seaward, M., Rivera, J., McCurdy, K., Cumming, G. L., and Sutter, J. F., 1981, Geology and geochemistry of sulfide mineralization underlying the Pueblo Viejo gold-silver oxide deposit, Dominican Republic: *Economic geology*, v.76, p. 1096-1117.
- Ketner, K. B., 1983, Strata-bound, silver-bearing, iron, lead and zinc sulphide deposits in Silurian and Ordovician rocks of allochthonous terrains, Nevada and Northern Mexico. U. S. Geological Survey Open File Report, 83-792.
- King, P. B., 1969, The tectonics of North America —A discussion to accompany the tectonic

- map of North America, scale 1: 5,000,000: U. S. Geological Survey Prof. Paper 628, 94 p.
- Kirkham, R. V., Sinclair, W. D., Thorpe, R. I., and Duke, J. M. (editors), 1993, Mineral Deposit Modeling: Geological Association of Canada Special Paper 40, 770 p.
- Kistler, R. W., 1990, Two different lithosphere types in the Sierra Nevada, California, *in*, Anderson, J. L., editor, The Nature of Cordilleran Magmatism: Geological Society of America Memoir 174, p. 271-281.
- Kistler, R. W., and Lee, D. E., 1989, Rubidium, Strontium and Strontium isotopic data for a suite of granitoid rocks from the Basin and Range Province, Arizona, California, Nevada, and Utah: U. S. Geological Survey Open-File Report 89-199, 13 p.
- Kistler, R. W., and Peterman, Z. E., 1978, Reconstruction of crustal blocks of California on the basis of initial strontium isotopic compositions of Mesozoic granitic rocks: U.S. Geological Survey Professional paper 1071, 17p.
- Kistler, R. W., and Peterman, Z. E., 1973, Variations in Sr, Rb, K, Na, and initial  $^{87}\text{Sr}/^{86}\text{Sr}$  in Mesozoic granitic rocks and intruded wall rocks in central California: Geological Society of America Bulletin, v. 84, p. 3489-3512.
- Kistler, R. W., and Ross, D. C., 1990, A strontium isotopic study of plutons and associated rocks of the southern Sierra Nevada and vicinity, California: U. S. Geological Survey Bulletin 1920, 20 p.
- Kligfield, R., Crespi, J., Naruk, S., and Davis, G. H., 1984, Displacement and strain patterns of extensional orogens: Tectonics, v. 3, p. 577-609.
- Knuepfer, P. L. K., Lemiszki, P. J., Hauge, T. A., Brown, L. D., Kaufman, S., and Oliver, J. E., 1987, Crustal structure of the Basin and Range—Sierra Nevada transition from COCORP deep seismic reflection profiling: Geological Society of America Bulletin, v. 98, p. 488-496.
- Korobeynikov, A. F., 1985, Gold distribution in black shale associations: Geokhimiya, № 12, p. 1747-1757.
- Korobeynikov, A. F., 1986, The distribution in differentiation products of basic and acid magmas of various ages: Geokhimiya, № 3, p. 328-338.
- Korobeynikov, A. F., 1988, Gold from endogenic processes of crust and mantle: Doklady Akademii Nauk SSSR, v. 299, № 5, p. 1233-1237.
- Korobeynikov, A. F., 1991, Background gold-bearing capacity of rocks of ancient greenstone belts of the earth's crust: Geokhimiya, № 2, p. 195-204.
- Korobeynikov, A. F., and Goncharenko, A. I., 1986, Gold in ophiolite complexes in the Altai-Sayan folded region: Geochemistry International. Scripta publishing, American Geological Institute Washington, v. 23, No 6, p. 43-55.

- Koschmann, A. H., and Bergendahl, M. H., 1968, Principal gold-producing districts of the United States: U. S. Geological Survey Professional Paper 610, 283 p.
- Kozlovsky, Ye. A., 1987, The superdeep well of the Kola Peninsula: Berlin, Springer-Verlag, 558 p.
- Krauskopf, K. B., 1979, Introduction to geochemistry, 2<sup>nd</sup> Ed. : New York, McGraw-Hill, 616 p.
- Kretschmer, E. L., 1991, Geology of the Kramer Hill gold deposit, Humboldt County, Nevada: , *in*, Raines, G. L., Lisle, R. E., Schafer, R. W., and Wilkinson, W. H., editors, Geology and Ore Deposits of the Great Basin, Symposium Proceedings Volume 2: Geological Society of Nevada, Reno/Sparks, Nevada, p. 857-863.
- Krupp, R. E., and Seward, T. M., 1987, The Rotokawa geothermal system, New Zealand: An active epithermal gold-depositing environment: *Economic Geology*, v. 82, p. 1109-1129.
- Kuehn, C. A., 1989, Studies of disseminated gold deposits near Carlin, Nevada: Evidence for a deep geologic setting of ore formation: Ph.D. dissertation, Pennsylvania State University, University Park, PA, 396 p.
- Kuehn, C. A., and Rose, A. W., 1987, Chemical and mineralogical zonation associated with low pH hydrothermal alteration at Carlin gold deposit, NV: *Geological Society of America Abstracts with Programs*, v. 19, p. 734.
- Kusznir, N. J., and Matthews, D. H., 1988, Deep seismic reflections and deformational mechanics of the continental lithosphere: *Journal of Petrology*, Special Lithosphere Issue, p. 63-87.
- Kusznir, N. J., and Park, R. G., 1987, The extensional strength of the continental lithosphere: its dependence on geothermal gradient, and crustal composition and thickness: *in* Coward, M. P., and Hancock, P. L., (eds. ), *Continental Extensional Tectonics*, Geological Society Special Publication N° 28, p. 35-52.
- Kutina, J., and Hildenbrand, T. G., 1987, Ore deposits of the western United States in relation to mass distribution in the crust and mantle: *Geological Society of America Bulletin*, v. 99, p. 30-41.
- Lachenbruch, A. H., and Sass, 1978, Models of an extending lithosphere and heat flow in the Basin and Range Province, *in*, Smith, R. B., and Eaton, G. P., editors, *Cenozoic Tectonics and Regional Geophysics of the Western Cordillera*: Geological Society of America Memoir 152, p. 209-250.
- Lamb, J. B., and Cline J., 1997, Depths of formation of the Meikle and Betze/Post deposits, *in*, Vikre, P., Thompson, T. B., Bettles, K., Christensen, O., and Parratt, R., editors, *Carlin-Type Gold Deposits Field Conference*, Society of Economic Geologists, Guidebook Series, v. 28, p. 101-107.

- Latin, D., and White, N., 1990, Generating melt during lithospheric extension: Pure shear vs. simple shear: *Geology*, v. 18, p. 327-331.
- Lee, D. E., Kistler, R. W., and Robinson, A. C., 1986, The strontium isotope composition of granitoid rocks of the southern Snake Range, Nevada: *U. S. Geological Survey Bulletin* 1622, p. 171-179.
- Lee, T., Richards, J. A., and Swain, P. H., 1987, Probabilistic and evidential approaches for multi-source data analysis: *IEEE Transactions on geoscience and Remote Sensing*, v. 25, p. 283-292.
- Leeman, W. P., 1970, The isotopic composition of strontium in late-Cenozoic basalts from the Basin—Range Province, western United States: *Geochimica et Cosmochimica Acta*, v. 34, p. 857-872.
- Leeman, W. P., 1982, Tectonic and magmatic significance of strontium isotopic variations in Cenozoic volcanic rocks from the western United States: *Geological Society of America Bulletin*, v. 93, p. 487-503.
- Leeman, W. P., 1987, Geochemical provinciality of late Cenozoic basaltic magmatism in the western U. S. : Evidence for lithospheric mantle heterogeneities [abs.]: *EOS, Transaction, American Geophysical Union*, v. 68, p. 1529.
- Leeman, W. P., and Fitton, J. G., 1989, Magmatism associated with lithospheric extension: Introduction: *Journal of Geophysical Research*, v. 94, p. 7682-7684.
- Leeman, W. P., and Harry, D. L., 1993, A binary source model for extension-related magmatism in the Great Basin, western North America: *Science*, v. 262, p. 1550-1554.
- Leroux, H., Warne, J. E., and Doukhan, J., 1995, Shocked quartz in the Alamo breccia, southern Nevada: Evidence for a Devonian impact event: *Geology*, v. 23, p. 1003-1006.
- Leventhal, J. A., Hofstra, A. H., and Mancuso, T. B., 1987, Sediment-hosted disseminated gold mineralization at Jerritt Canyon, Nevada. III—Role of organic carbon: *Geological Society of America Abstracts with Programs*, v. 19, p. 745.
- Leventhal, J. A., Reid, M. R., Montana, A., and Holden, P., 1995, Mesozoic invasion of crust by MORB-source asthenospheric magmas, U. S. Cordilleran interior: *Geology*, v. 23, p. 399-402.
- Leverington, D. W., and Duguay, C. R., 1994, Prediction of depth to frozen ground using satellite imagery and digital topographic data: Mayo, Y. T., *Proceedings: 1994 International Association for mathematical Geology Annual Conference, Mont Tremblant*, p. 218-222.
- Levy, M., and Christie-Blick, N., 1989, Pre-Mesozoic palinspastic reconstruction of the eastern Great Basin (western United States): *Science*, v. 245, p. 1454-1461.

- Lindgren, W., and Ransome, F. L., 1906, Geology and gold deposits of the Cripple Creek district, Colorado: U. S. Geological Survey Professional Paper 54, 516 p.
- Lipman, P. W., 1983, Cenozoic magmatism associated with extensional tectonics in the Rocky Mountains [abs.]: Geological Society of America Abstracts with Programs, v. 15, p. 288.
- Lipman, P. W., 1992, Magmatism in the Cordilleran United States; Progress and problems, *in*, Burchfiel, B. C., Lipman, P. W., and Zoback, M. L., editors, The Cordilleran Orogen: The Conterminous U. S., the Geology of North America, Volume G-3: Geological Society of America, p. 481-514.
- Lipman, P. W., Prostka, H. J., and Christiansen, R. L., 1972, Cenozoic volcanism and plate-tectonic evolution of the western United States. I. Early and middle Cenozoic: Philosophical Transactions of the Royal Society of London, Series A, v. 271, p. 217-248.
- Lister, G. S., and Baldwin, S. L., 1993, Plutonism and the origin of metamorphic core complexes: *Geology*, v. 21, p. 607-610.
- Lister, G. S., and Davies, G. A., 1989, The origin of metamorphic core complexes and detachment faults formed during Tertiary continental extension in the northern Colorado River region, U. S. A. : *Journal of Structural Geology*, v. 11, p. 65-94.
- Lister, G. S., Etheridge, M. A., and Symonds, P. A., 1986, Detachment faulting and the evolution of passive continental margins: *Geology*, v. 14, p. 246-250.
- Livaccari, R. F., 1979, Late Cenozoic tectonic evolution of the western United States: *Geology*, v. 7, p. 72-75.
- Livaccari, R. F., and Perry, F. V., 1993, Isotopic evidence for preservation of Cordilleran lithospheric mantle during the Sevier-Laramide orogeny, western United States: *Geology*, v. 21, p. 719-722.
- Lowe, N. T., Ramey, G. R., and Norberg, J. R., 1985, Principal deposits of strategic and critical minerals in Nevada: Bureau of Mines Information Circular 9035, 202 p.
- Lowry, A. R., and Smith, R. B., 1995, Strength and rheology of the western U. S. Cordillera [abs.]: *Journal of Geophysical Research*, v. 100, N° B9, p. 25.
- Ludington, S., Cox, D. P., Singer, D. A., Sherlock, M. G., Berger, B. R., and Tingley, J. V., 1993, Spatial and temporal analysis of precious-metal deposits for a mineral resource assessment of Nevada, *in*, Kirkham, R. V., Sinclair, W. D., Thorpe, R. I., Duke, J. M., editors, Mineral Deposit Modelling: Geological Association of Canada, Special Paper 40, p. 31-40.
- Ludington, S., Cox, D. (editors), and McCammon (project chief), 1996, Data Base for a National Mineral-resource Assessment of Undiscovered Deposits of Gold, Silver, Copper, Lead, and Zinc in the Conterminous United States by U.S. Geological Survey Minerals Team: U.S. Geological Survey Open File Report 96-96, CD-ROM.



- Lynch, H. D., and Morgan, P., 1987, The tensile strength of the lithosphere and the localization of extension, *in*, Coward, M. P., Dewey, J. F., and Hancock, P. L., editors, *Continental Extensional Tectonics: Geological Society Special Publication N° 28*, p. 53-65.
- Mabey, D. R., Oliver, H. W., and Hildenbrand, T. G., 1983, Regional gravity and magnetic anomalies in the northern Basin and Range province: Geothermal Resources Council, Special Report no13, p. 307-315.
- Madrid, R. J., and Bagby, W. C., 1986, Structural alignment of sediment-hosted gold deposits in north-central Nevada: An example of inherited fabrics [abs.]: Geological Society of America Abstract with Programs, v. 18, p.393.
- Maguire, D. J., Goodchild, M. F., and Rhind, D. W., editors, 1991, *Geographical Information Systems—Volume1: Principles, Volume2: Applications*: Longman Scientific and Technical, John Wiley and Sons, Inc., New York, 649 p. v. 1, 447 p. v. 2.
- Maher, B. J., Browne, Q. J., and McKee, E. H., 1993, Constraints on the age of gold mineralization and metallogenesis in the Battle Mountain-Eureka mineral belt, Nevada: *Economic Geology*, p. 469-478.
- Malavieille, J., and Taboada, A., 1991, Kinematic model for postorogenic Basin and Range extension: *Geology*, v. 19, p. 555-558.
- Mann, G. M., and Meyer, C. E., 1993, Late Cenozoic structure and correlations to seismicity along the Olympic-Wallowa lineament, northwest United States: *Geological Society of America Bulletin*, v. 105, p. 853-871.
- Marshak, S., and Paulsen, T., 1996, Midcontinent U. S. fault and fold zones: A legacy of Proterozoic intracratonic extensional tectonism?: *Geology*, v. 24, p. 151-154.
- Mathews, V., III, and Anderson, C. E., 1973, Yellowstone convection plume and break-up of the western United States: *Nature*, v. 243, p. 158-159.
- Maxson, J., and Tikoff, B., 1996, Hit-and-run collision model for the Laramide orogeny, western United States: *Geology*, v. 24, p. 968-972.
- Mayer, L., 1986, Topographic constraints on models of lithospheric stretching of the Basin and Range Province, western United States, *in*, Mayer, L., editor, *Extensional Tectonics of the Southwestern United States: A Perspective on Processes and Kinematics*: Geological Society of America Special Paper 206, p. 1-14.
- McCaig, A. M., 1988, Deep fluid circulation in fault zones: *Geology*, v. 16, p. 867-870.
- McCarthy, J., and Parsons, T., 1994, Insights into the kinematic Cenozoic evolution of the Basin and Range-Colorado Plateau transition from coincident seismic refraction and reflection data: *Geological Society of America Bulletin*, v. 106, p. 747-759.

- McCulloch, M. T., and Gamble, J. A., 1991, Geochemical and geodynamical constraints on subduction zone magmatism: *Earth and Planetary Science Letters*, v. 102, p. 358-274.
- McKee, E. H., 1971, Tertiary igneous chronology of the Great Basin of the western United States; implication for tectonic models: *Geological Society of America Bulletin*, v. 82, p. 3497-3502.
- McKee, E. H., 1977, Cenozoic volcanism of the northern Great Basin [abs.]: *EOS, Transactions, American Geophysical Union*, v. 58, p. 1237.
- McKee, E. H., 1995, Cenozoic magmatism and mineralization in Nevada [abs.], *in*, *Geology and Ore Deposits of the American Cordillera*, symposium program with abstracts: Geological Society of Nevada, Reno/Sparks, Nevada, p. A54.
- McKenzie, D., and Bickle, M. J., 1988, The volume and composition of melt generated by extension of the lithosphere: *Journal of Petrology*, v. 29, p. 625-679.
- Meeuwig, D., 1995, Nevada's mineral production in 1994: Quarterly Newsletter of the Nevada Bureau of Mines and Geology, Summer 1995, <http://www.nbmng.unr.edu/nl/nl.htm>.
- Meeuwig, D., 1996, Nevada's mineral production in 1995: Quarterly Newsletter of the Nevada Bureau of Mines and Geology, August 1996, <http://www.nbmng.unr.edu/nl/nl.htm>.
- Meeuwig, D., 1997, Nevada's mineral production in 1996: Quarterly Newsletter of the Nevada Bureau of Mines and Geology, June 1997, <http://www.nbmng.unr.edu/nl/nl.htm>.
- Mellott, M. G., and Hart, W. K., 1987, Petrogenesis and tectonic significance of andesites from the northern Basin and Range, Nevada [abs.]: *Geological Society of America Abstracts with Programs*, v. 19, p. 770.
- Mendenhall, W., and Reinmuth, J. E., 1974, *Statistics for management and economics*, 2<sup>nd</sup> Ed.: Duxbury Press, North Scituate, Massachusetts, 596 p.
- Mihalasky, M. J., 1988, *GOLDY—A database and mineral deposit models for the giant lode gold camps of North America*: MSc. thesis, Eastern Washington University, Cheney, Washington, 290 p.
- Miller, C. F., and Barton, M. D., 1990, Phanerozoic plutonism in the Cordilleran interior, U. S. A., *in*, Kay, S. M., and Rapela, C. W., editors, *Plutonism from America to Alaska*: Boulder, Colorado, Geological Society of America Special Paper 241, p. 213-231.
- Miller, D. M., Nilsen, T. H., and Bilodeau, W. L., 1992, Late Cretaceous to early Eocene geologic evolution of the U. S. Cordillera, *in*, Burchfiel, B. C., Lipman, P. W., and Zoback, M. L., editors, *The Cordilleran Orogen: The Conterminous U. S., the Geology of North America*, Volume G-3: Geological Society of America, p. 205-260.
- Miller, E. L., Gams, P. B., Wright, J. E., and Sutter, J. F., 1988, Metamorphic history of the east-

- central Basin and Range Province: Tectonic setting and relationship to magmatism, *in*, Ernst, W. G., editor, *Metamorphism and Crustal Evolution of the Western United States: Rubey Volume VII*, Prentice Hall, Englewood Cliffs, New Jersey, p. 649-682.
- Miller, E. L., Gans, P. B., Wright, J. E., and Sutter, J. F., 1986, Metamorphic history of the east-central Basin and Range Province: Tectonic setting and relationship to magmatism [abs.]: *Geological Society of America Abstracts with Programs*, v. 18, p. 158.
- Miller, E. L., Miller, M. M., Stevens, C. H., Wright, J. E., and Madrid, R., 1992, Late Paleozoic paleogeographic and tectonic evolution of the western U. S. Cordillera, *in*, Burchfiel, B. C., Lipman, P. W., and Zoback, M. L., editors, *The Cordilleran Orogen: the Conterminous U. S., the Geology of North America, Volume G-3*: Geological Society of America, p. 57-106.
- Mills, B. A., 1984, Geology of the Round Mountain gold deposit, Nye County, Nevada: *Arizona Geological Society Digest*, v. 15, p. 89-99.
- Mitchell, A. W., 1977, Geology of bedded barite deposits, north-central Nevada [M.Sc.]: University of Nevada, Reno, 58 p.
- Mohide, T. P., 1981, Gold: Mineral policy background paper N° 12, Ministry of Natural Resources, Mineral Resources Branch, Toronto, Ontario, Canada, 275 p.
- Moon, W. M., 1990, Integration of geophysical and geological data using evidential belief function: *IEEE Transactions on Geoscience and Remote Sensing*, v. 28, N° 4, p. 711-720.
- Mooney, T. C., Mutschler, F. E., 1990, Lineaments, mantle melts, and gold deposits; new prospecting paradigms or old fables?: *Abstracts with Programs- Geological Society of America*, v. 22, N° 3, Pages 70.
- Mooney, W. D., and Pakiser, L. C., 1989, Geophysical framework of the continental United States; Progress, problems, and opportunities for research, *in*, Pakiser, L. C., and Mooney, W. D., editors, *Geophysical Framework of the Continental United States*: Geological Society of America Memoir 172, p. 799-811.
- Mooney, W. D., and Weaver, C. S., 1989, Regional crustal structure and tectonics of the Pacific Coastal States; California, Oregon, and Washington, *in*, Pakiser, L. C., and Mooney, W. D., editors, *Geophysical Framework of the Continental United States*: Geological Society of America Memoir 172, p. 129-161.
- Morgan, P., and Gosnold, W. D., 1989, Heat flow and thermal regimes in the continental United States, *in*, Pakiser, L. C., and Mooney, W. D., editors, *Geophysical Framework of the Continental United States*: Geological Society of America Memoir 172, p. 493-522.
- Morgan, P., and Sass, J. H., 1984, Thermal regime of the continental lithosphere: *Journal of Geodynamic*, v. 1. p143-166.
- Mosier, D. L., Menzie, W. D., and Kleinhampl, F. J., 1986, Geologic and grade-tonnage

- information on Tertiary epithermal precious- and base-metal vein districts associated with volcanic rocks: U. S. Geological Survey Bulletin 1666, 39 p.
- Mosier, D. L., Singer, D. A., Bagby, W. C., and Menzie, W. D., 1992, Grade and Tonnage Model of Sediment-Hosted Au, *in*, Bliss J. D., editor, Development in Mineral Deposit Modeling. U.S. Geological Survey Bulletin 2004, p. 168.
- Muffler, P. L. J., Hedenquist, J. W., Kesler, S. E., and Izawa, E (editors), 1992, Magmatic Contributions to Hydrothermal Systems: Report of a Seminar Held Nov. 10-16, 1991 in Japan, Geological Survey of Japan report number 279, 353 p.
- Murphy, J. B., Oppliger, G. L., Brimhall, G. H., 1998, Plume-modified orogeny: An example from the southwestern United States: *Geology*, v. 26, p. 731-734.
- Murphy, J. B., Oppliger, G. L., Brimhall, G. H., and Hynes, A. Jr., 1999, Mantle plumes and mountain building: *American Scientist*, v. 87, N° 2, p. 146-153.
- Mutschler, F. E., Larson, E. E., and Gaskill, D. L., 1992, The fate of the Colorado Plateau- A view from the mantle: unpublished manuscript, Department of Geology, Eastern Washington University, Cheney, Washington, 14p.
- Mutschler, F. E., Larson, E. E., and Bruce, R. M., 1987, Laramide and younger magmatism in Colorado—New petrologic and tectonic variations on old themes: *Colorado School of Mines Quarterly*, v. 82, N° 4, p. 1-47.
- Mutschler, F. E., Mooney, T. C., and Johnson, D. C., 1991, Precious metal deposits related to alkaline igneous rocks—a space-time trip through the cordillera: *Mining Engineering*, v. 43, N° 3, p. 304-309.
- Mutschler, F. E., Rougon, D. J., Lavin, O. P., and Hughes, R. D., (compilers), 1981, PETROS—A data bank of major element chemical analyses of igneous rocks for research and teaching (version 6. 1): Eastern Washington University, Department of Geology, Washington (Distributed by: National Oceanic and Atmospheric Administration, Marine Geology & Geophysics Division, National Geophysical Data Center, Boulder, Colorado, USA, NGDC Data Set # 0030).
- Naruk, S. J., 1984, A model for detachment fault gold mineralization: *Geological Society of America Abstracts with Programs*, v. 16, p. 607.
- Nash, J. T., Utterback, W. C., and Saunders, J. A., 1991, Geology and geochemistry of the Sleeper gold deposits, Humboldt County, Nevada; an interim report, *in*, Raines, G. L., Lisle, R. E., Schafer, R. W., and Wilkinson, W. H., editors, *Geology and Ore Deposits of the Great Basin, Symposium Proceedings Volume 2: Geological Society of Nevada, Reno/Sparks, Nevada*, p. 1063-1084.
- Nelson, C. E., 1991, Metalliferous marine black shales and fossil petroleum reservoirs —Source rock and host environment for Carlin-type gold deposits, *in*, Raines, G. L., Lisle, R. E.,

- Schafer, R. W., and Wilkinson, W. H., editors, *Geology and Ore Deposits of the Great Basin, Symposium Proceedings Volume 1: Geological Society of Nevada, Reno/Sparks, Nevada*, p. 249-254.
- Nesbitt, B. E., and Muehlenbachs, K., 1989, Origins of movement of fluids during deformation and metamorphism in the Canadian Cordillera: *Science*, v. 245, p. 733-736.
- Nevada Bureau of Mines and Geology staff, 1995-1997, *The Nevada mineral industry - 1994, 1995, 1996: Nevada Bureau of Mines and Geology Special Publications MI-1994, MI-1995, MI-1996*, <http://www.nbmng.unr.edu/mi/>
- Newton, R. C., Smith, J. V., and Windley, B. F., 1980, Carbonic metamorphism, granulites, and crustal growth: *Nature*, v. 288, p. 45-49.
- Nichols, S. L., and Lutsey, I. A., 1972, *Topographic map of Nevada: Nevada Bureau of Mines and Geology Map 43*.
- Noble, D. C., 1972, Some observations on the Cenozoic volcano-tectonic evolution of the Great Basin, western United States: *Earth and Planetary Science Letters*, v. 17, p. 142-150.
- Noble, D. C., McCormack, J. K., McKee, E. H., Silverman, M. L., and Wallace, A. B., 1988, Time of mineralization in the evolution of the McDermitt caldera complex, Nevada-Oregon, and the relation of middle Miocene mineralization in the northern Great Basin to coeval regional basaltic magmatic activity: *Economic Geology*, v. 83, p. 859-863.
- Norman, D. I., Groff, J., Kamali, C., Musgrave, J., and Moore, J. N., 1996, Gaseous species in fluid inclusions: Indicators of magmatic input into ore-forming geothermal systems [abs.]: Geological Society of America, Abstract with program, p. A-401.
- Northrop, H. R., Rye, R. O., Landis, G. P., Lustwerk, R., Jones, M. B., and Daly, W. E., 1987, Sediment-hosted disseminated gold mineralization at Jerrett Canyon, Nevada. V—Stable isotope geochemistry and a model of ore deposition: *Geological Society of America Abstracts with Programs*, v. 19, p. 791.
- Nutt, C. J., 1997, Sequence of deformational events and the recognition of Eocene(?) deformation in the Alligator Ridge Area, East-central Nevada, *in*, Vikre, P., Thompson, T. B., Bettles, K., Christensen, O., and Parratt, R., editors, *Carlin-Type Gold Deposits Field Conference, Society of Economic Geologists, Guidebook Series*, v. 28, p. 203-211.
- Nutt, C. J., and Good, S. C., 1998, Recognition and significance of Eocene deformation in the Alligator Ridge area, central Nevada, *in*, Tosdal, R. M., editor, *Contributions to the gold metallogeny of northern Nevada: U.S. Geological Survey Open-File Report 98-338*, p. 141-150.
- O'Neil, J. R., and Silberman, M. L., 1974, Stable Isotope Relations in Epithermal Au-Ag Deposits: *Economic Geology*, v. 69, p. 902-909.

- O'Neil, J. R., Silberman, M. L., Fabbi, B. P., and Chesterman, C. W., 1973, Stable isotope and chemical relations during mineralization in the Bodie mining district, Mono County, California: *Economic Geology*, v. 68, p. 765-784.
- Oldow, J. S., Bally, A. W., Ave Lallement, H. G., and Leeman, W. P., 1989, Phanerozoic evolution of the North American Cordillera: United States and Canada, *in*, Bally, A. W., and Palmer, A. P., editors, *The Geology of North America: An Overview*: Boulder, Colorado, Geological Society of America, *The Geology of North America*, v. A, p. 139-232.
- Oliver, J., 1986, Fluids expelled tectonically from orogenic belts: Their role in hydrocarbon migration and other geologic phenomena: *Geology*, v. 14, p. 99-102.
- Oppliger, G. L., Murphy, J. B., and Brimhall Jr., G. H., 1997, Is the ancestral Yellowstone hotspot responsible for the Tertiary "Carlin" mineralization in the Great Basin?: *Geology*, v. 25, p. 627-630.
- Ormerod, D. S., Hawkesworth, C. J., Rogers, N. W., Leeman, W. P., and Menzies, M. A., 1988, Tectonic and magmatic transition in the western Great Basin, USA: *Nature*, v. 333, N° 26, p. 349-353.
- Ott, L. E., Groody, D., Follis, E. L., and Siems, P. L., 1986, Stratigraphy, structural geology, ore mineralogy and hydrothermal alteration at the Cannon mine, Chelan County, Washington, U. S. A., *in*, Macdonald, A. J., editor, *Gold '86—An International Symposium on the Geology of Gold Deposits, Proceedings Volume*: Toronto, Ontario, Gold '86, p. 425-435.
- Overstreet, W. C., and Marsh, S. P., 1981, Some concepts and technics in geochemical exploration, *in*, Skinner, B. J., editor, *Economic Geology Seventy-Fifth Anniversary Volume*: El Paso, Texas, Economic Geology Publishing Company, . 775-805.
- O'Neill, J. M., and Lopez, D. A., 1985, Character and significance of Great Falls tectonic zone, east-central Idaho and west-central Montana: *American Association of Petroleum Geologist Bulletin*, v. 69, p. 437-447.
- Pakiser, L. C., 1989, Geophysics of the Intermontane system, *in*, Pakiser, L. C., and Mooney, W. D., editors, *Geophysical Framework of the Continental United States*: Geological Society of America Memoir 172, p. 235-247.
- Pakiser, L. C., and Mooney, W. D., editors, 1989, *Geophysical Framework of the Continental United States*: Geological Society of America Memoir 172, 826 p.
- Palmer, A. R., 1990, History of data compilation, decade of North American geology overview, *in*, Hittelman, A. M., Kinsfather, J. O., and Meyers, H., compilers, 1990, *Geophysics of North America CD-ROM, user's manual (release 1. 1, July)*: National Oceanic and Atmospheric Administration, National Geophysical Data Center, Boulder, CO., p. 5-1.
- Panteleyev, A., 1986, Ore Deposits #10. A Canadian Cordilleran model for epithermal gold-silver deposits: *Geoscience Canada*, v. 13, N° 2, p. 101-111.



- Papke, K. G., 1984, Barite in Nevada: Nevada Bureau of Mines and Geology, Bulletin 98, University of Nevada, 125 p.
- Parsons, T., and McCarthy, J., 1993, The active Southwest margin of the Colorado Plateau: Uplift of mantle origin, [abs.]: Geological society of America Abstract with programs, p. A-143.
- Parsons, T., Thompson, G. A., and Sleep, N. H., 1994, Mantle plume influence on the Neogene uplift and extension of the U. S. western Cordillera?: *Geology*, v. 22, p. 83-86.
- Paterson, S. R., and Fowler, T. K. Jr., 1993, Extensional pluton-emplacement models: Do they work for large plutonic complexes?: *Geology*, v. 21, p. 781-784.
- Patino-Douce, A., and Humphreys, E., 1987, Magmatic evolution in the Great Basin [abs.]: EOS, Transactions, American Geophysical Union, v. 68, p. 1474.
- Peacock, S. M., 1988, Inverted metamorphic gradients in the westernmost cordillera, *in*, Ernst, W. G., editor, *Metamorphism and Crustal Evolution of the Western United States: Rubey Volume VII*, Prentice Hall, Englewood Cliffs, New Jersey, p. 953-975.
- Percival, T. J., Bagby, W. C., and Radtke, A. S., 1988, Physical and chemical features of precious metals deposits hosted by sedimentary rocks in the Western United States, *in*, Schafer, R. W., Cooper, J. J., and Vikre, P. G., editors, *Bulk Mineable Precious Metal Deposits of the Western United States*, The Geological Society of Nevada, Reno, p. 11-34.
- Perry, F. V., DePaolo, D. J., and Baldrige, W. S., 1993, Neodymium isotopic evidence for decreasing crustal contributions to Cenozoic ignimbrites of the western United States: Implications for the thermal evolution of the Cordilleran crust: *Geological Society of America Bulletin*, v. 105, p. 872-882.
- Peters, S. G., Nash, J. T., John, D. A., Spanski, G. T., King, H. D., Connors, K. A., Moring, B. C., Doebrich, J. L., McGuire, D. J., Albino, G. V., Dunn, V. C., Theodore, T. G., and Ludington, S., 1996, Metallic mineral resources in the U.S. Bureau of Land Management's Winnemucca District and Surprise Resource Area, northwest Nevada and northeast California: U.S. Geological Survey Open File Report 96-712, 147 p.
- Picha, F., and Gibson, R. I., 1985, Cordilleran hingeline: Late Precambrian rifted margin of the North American craton and its impact on the depositional and structural history, Utah and Nevada: *Geology*, v. 13, p. 465-468.
- Plouff, D., 1986, Role of magma in localization of Basin-Range valleys [abs.]: EOS, Transactions, American Geophysical Union, v. 67, p. 1226.
- Plummer, R. W., 1992, Using a geographic information system as a tool in mineral exploration: *The Canadian Mining and Metallurgical Bulletin (CIM Bulletin)*, v. 85, p. 67-71.
- Poole F. G., and Sandberg, C. A., 1977, Mississippian paleogeography and tectonics of the

- western United States, *in*, Stewart, J. H., Stevens, C. H., and Fritsche, A. E., editors, Paleozoic Paleogeography of the Western United States, Pacific Coast Paleogeography Symposium 1: Society of Economic Paleontologists and Mineralogists, p. 67-85.
- Poole F. G., Sandberg, C. A., and Boucot, A. J., 1977, Silurian and Devonian paleogeography of the western United States, *in*, Stewart, J. H., Stevens, C. H., and Fritsche, A. E., editors, Paleozoic Paleogeography of the Western United States, Pacific Coast Paleogeography Symposium 1: Society of Economic Paleontologists and Mineralogists, p. 39-55.
- Poole, F. G., Stewart, J. H., Palmer, A. R., Sandberg, C. A., Madrid, R. J., Ross, R. J., Jr., Hintze, L. F., Miller, M. M., and Wrucke, C. T., 1992, Latest Precambrian to latest Devonian time; Development of a continental margin, *in*, Burchfiel, B. C., Lipman, P. W., and Zoback, M. L., editors, The Cordilleran Orogen: The conterminous U. S., the Geology of North America, Volume G-3: Geological Society of America, p. 9-56.
- Porter, E. W., Ripley, E., 1985, Petrologic and stable isotope study of the gold-bearing breccia pipe at the Golden Sunlight deposit, Montana: Economic Geology, v. 80, p. 1689-1706.
- Potter, C. J., Liu, C.-S., Huang, J., Zheng, L., Hauge, T. A., Hauser, E. C., Allmendinger, R. W., Oliver, J. E., Kaufman, S., and Brown, L., 1987, Crustal structure of north-central Nevada: Results from COCORP deep seismic profiling: Geological Society of America Bulletin, v. 98, p. 330-337.
- Proffett, J. M., Jr., 1977, Cenozoic geology of the Yerington district, Nevada, and implications for the nature and origin of Basin and Range faulting: Geological Society of America Bulletin, v. 88, p. 247-266.
- Proffett, J. M., Jr., 1989, Cenozoic extension and tilting recorded in the Upper Cretaceous and Tertiary rocks at the Hall molybdenum deposit, northern San Antonio Mountains, Nevada: Discussion: Geological Society of America Bulletin, v. 101, p. 440.
- Putnam III, B. R., and Henriques, E. Q. B., 1991, Geology and mineralization at the South Bullion Deposit, Pinon Range, Elko County, Nevada: Implications for western United States Cenozoic tectonics, *in*, Raines, G. L., Lisle, R. E., Schafer, R. W., and Wilkinson, W. H., editors, Geology and Ore Deposits of the Great Basin, Symposium Proceedings Volume 2: Geological Society of Nevada, Reno/Sparks, Nevada, p. 713-728.
- Radtke, A. S., 1980, Genesis of gold-bearing quartz veins of the Alleghany district, California, *in*, Silberman, M. L., Field, C. W., and Berry, A. L., editors, Proceedings of the Symposium on Mineral Deposits of the Pacific Northwest, Geological Society of America, Cordilleran Section Meeting: U. S. Geological Survey Open-File Report 81-355, p. 279.
- Radtke, A. S., 1981, Geology of the Carlin gold deposit, Nevada: U. S. Geological Survey Open-File Report 81-97, 154 p.
- Radtke, A. S., 1985, Geology of the Carlin gold deposit, Nevada: U. S. Geological Survey Professional Paper 1267, 124 p.

- Radtke, A. S., Rye, R. O., and Dickson, F. W., 1980, Geology and stable isotope studies of the Carlin gold deposit, Nevada: *Economic Geology*, v. 75, p. 641-672.
- Raines, G. L., 1978, Porphyry copper exploration model for northern Sonora, Mexico: *Journal of Research of the U. S. Geological Survey*, v. 6, Nº 1, p. 51-58.
- Raines, G. L., Lisle, R. E., Schafer, R. W., and Wilkinson, W. H., editors, 1991, *Geology and Ore Deposits of the Great Basin*, Symposium Proceedings Volume 1: Geological Society of Nevada, Reno/Sparks, Nevada, p. 618.
- Randall, J. A., 1972, Metallization sequence in the Tayoltita region, San Dimas, Durango, Mexico: *International Geological Congress*, 24<sup>th</sup>, Montreal, Canada, Section 4, p. 309-317.
- Reddy, R. K. T., Agterberg, F. P., and Bonham-Carter, G. F., 1991, Application of GIS-based logistic models to base-metal potential mapping in Snow Lake area, Manitoba, *in*, *Proceedings of the Canadian Conference on GIS*, Ottawa, Canada, March 18-22, 1991, p. 607-618.
- Reddy, R. K. T., and Bonham-Carter, G. F., 1991, A decision-tree approach to mineral potential mapping in Snow Lake area, Manitoba: *Canadian Journal of Remote Sensing*, v. 17, p. 191-200.
- Rehrig, W. A., 1986, Processes of regional Tertiary extension in the western Cordillera: Insights from the metamorphic core complexes, *in*, Mayer, L., editor, *Extensional Tectonics of the Southwestern United States: a Perspective on Processes and Kinematics*: Geological Society of America Special Paper 206, p. 97-122.
- Reidel, S. P., and Tolan, T. L., 1994, Late Cenozoic structure and correlation to seismicity along the Olympic-Wallowa Lineament, northwestern United States: *Discussion: Geological Society of America Bulletin*, v. 106, p. 1634-1638.
- Richards, J. P., 1995, Alkaline-type epithermal gold deposits- A review, *in*, Thompson, J. F. H., editor, *Magma, Fluids, and Ore Deposits: Mineralogical Association of Canada, Short Course Series*, v. 23, p. 367-400.
- Richards, M. A., Duncan, R. A., Courtillot, V. E., 1989, Flood basalts and hot-spot tracks: Plume heads and tails: *Science*, v. 246, p. 103-107.
- Riter, J. C. A., and Smith, D., 1996, Xenolith constraints on the thermal history of the mantle below the Colorado Plateau: *Geology*, v. 24, p. 267-270.
- Roberts, R. G., and Sheahan, P. A., editors, 1988, *Ore Deposit Models*: Geoscience Canada Reprint Series 3, Geological Association of Canada, Memorial University of Newfoundland, St. John's, Newfoundland, Canada, 194 p.
- Roberts, R. J., 1960, Alinement of mining districts in north-central Nevada: *U.S. Geological Survey Professional paper* 400-B, p. B17-B19

- Roberts, R. J., 1964, Exploration targets in north-central Nevada: U.S. Geological Survey Open-File Report, 21 p.
- Roberts, R. J., 1966, Metallogenic provinces and mineral belts in Nevada: Nevada Bureau of Mines, Report 13, p. 47-72.
- Roberts, R. J., and Crittenden, M. D., Jr., 1973, Orogenic mechanisms, Sevier orogenic belt, Nevada and Utah, *in*, De Jong, K. A., and Scholten, R., editors, Gravity and Tectonics: New York, John Wiley and Sons, Inc., p. 409-428.
- Robinson, A. C., 1995, Regionally coherent lower-crustal sources for continental subduction-generated magmas and metallogenesis: A Sr and Nd isotopic comparison of Mesozoic granitoids in Nevada and eastern California with Mesozoic to Holocene granitoid and volcanic rocks in Chile [abs]: Geology and ore deposits of the American Cordillera, symposium program with abstracts: Geological Society of Nevada, Reno/Sparks, Nevada, p. 67-68.
- Rock, N. M. S., and Groves, D. I., 1988, Can lamprophyres resolve the genetic controversy over mesothermal gold deposits?: *Geology*, v. 16, p. 538-541.
- Rock, N. M. S., Groves, D. I., Perring, C. S., and Golding, S. D., 1989, Gold, Lamprophyres, and Porphyries: What does their association mean?, *in*, Keays, R. R., Ramsay, R. H., and Groves, D. I., editors, The Geology of Gold Deposits: The Perspective in 1988: Economic Geology Monograph 6, p. 609-625.
- Rock, N. M. S., Groves, D. I., Perring, C. S., and Golding, S. D., 1989, Gold, lamprophyres, and porphyries: What does their association mean?, *in*, Keays, R. R., Ramsay, R. H., and Groves, D. I., editors, The Geology of Gold Deposits: The Perspective in 1988: Economic Geology Monograph 6, p. 609-625.
- Rodriguez, B. D., 1997, Deep regional resistivity structure across the Carlin Trend, *in*, Vikre, P., Thompson, T. B., Bettles, K., Christensen, O., and Parratt, R., editors, Carlin-Type Gold Deposits Field Conference, Society of Economic Geologists, Guidebook Series, v. 28, p. 39-46.
- Rodriguez, B. D., 1997, Deep regional resistivity structure across the Carlin Trend, *in*, Vikre, P., Thompson, T. B., Bettles, K., Christensen, O., and Parratt, R., editors, Carlin-Type Gold Deposits Field Conference, Society of Economic Geologists, Guidebook Series, v. 28, p. 38-45.
- Romberger, S. B., 1986, Ore deposits #9. Disseminated gold deposits: *Geoscience Canada*, v. 13, p. 23-31.
- Rose, A. W., and Kuehn, C. A., 1987, Ore deposition from highly acidic CO<sub>2</sub>-enriched solutions at the Carlin gold deposit, Eureka County, Nevada [abs.]: Geological Society of America, Abstract with Programs, v. 19, p. 824.
- Rose, A. W. and Kuehn, C. A., 1987, Ore deposition from acidic CO<sub>2</sub>-rich solutions at the Carlin

- gold deposit, Eureka county, Nevada [abs.]: Geological Society of America Abstracts with Programs, v. 19, p. 824.
- Rose, A. W., Hawkes, H. E., and Webb, J. S., 1979, *Geochemistry in mineral exploration*, 2<sup>nd</sup> Ed. : New York, Academic Press, 657 p.
- Rowan, L. C., and Wetlaufer, P. H., 1979, Geologic evaluation of major LANDSAT lineaments in Nevada and their relationship to ore districts: U. S. Geological Survey Open File Report 79-544.
- Rowley, P. D., 1996, The syntectonic caldera—A new caldera type boundary by synchronous linear faults [abs.]: Geological Society of America, Abstract with Programs, Denver 1996, p. A-449.
- Russell, N., Polanco, J., and Kesler, S. E., 1986, Geology of the Monte Negro gold-silver deposit, Pueblo Viejo district, Dominican Republic, *in*, Macdonald, A. J., editor, *Gold '86—an International Symposium on the Geology of Gold Deposits, Proceedings Volume: Toronto, Ontario, Gold '86*, p. 497-503.
- Rye, R. O., 1985, A model for the formation of carbonate-hosted disseminated gold deposits based on geologic, fluid-inclusion, geochemical, and stable isotope studies of the Carlin and Cortez deposits, Nevada, *in*, Tooker, E. W., editor, *Geologic Characteristics of Sediments- and Volcanic-hosted Disseminated Gold Deposits: Search for an Occurrence Model*: U. S. Geological Survey Bulletin 1646, p. 35-42.
- Saleeby, J. B., and Busby-Spera, C., 1992, Early Mesozoic tectonic evolution of the western U. S. Cordillera, *in*, Burchfiel, B. C., Lipman, P. W., and Zoback, M. L., editors, *The Cordilleran Orogen: The Conterminous U. S., the Geology of North America, Volume G-3: Geological Society of America*, p. 107-168.
- Saleeby, J. B., Sams, D. B., and Kistler, R. W., 1987, U/Pb Zircon, Strontium and Oxygen isotopic and geochronological study of the southernmost Sierra Nevada Batholith, California: *Journal of Geophysical Research*, v. 92, Nº B10, p. 10443-10466.
- Saleeby, J. B., Hannah, J. L., and Varga, R. J., 1987, Isotopic age constraints on middle Paleozoic deformation in the northern Sierra Nevada, California: *Geology*, v. 15, p. 757-766.
- Saltus, R. W., 1988, Regional, residual, and derivative gravity maps of Nevada: Prepared by the U. S. Geological Survey in cooperation with the Nevada Bureau of Mines and Geology, Mackay School of Mines, University of Nevada, Reno, Nevada, four 1: 1,000,000 gravity anomaly maps, two 1:1,250,000 topography and isostatic regional gravity maps.
- Saltus, R. W., and Thompson, G. A., 1995, Why is it downhill from Tonopah to Las Vegas?: A case for mantle plume support of the High Northern Basin and Range [abs.]: *Tectonics*, v. 14, Nº. 6, p. 1235-1244.
- Sanderson, D. J., and Marchini, W. R. D., 1984, Transpression: *Journal of Structural Geology*,

v. 6, p.449-458.

Sawatzky, D. L., and Raines, G. L., 1981, Geologic uses of linear-feature maps derived from small-scale images, *in*, O'Leary, D. W., and Earle, J. L., editors, Proceedings of the Third International Conference on Basement Tectonics, Durango, Colorado, 1978: Basement Tectonics Committee, Denver, Colorado, p. 91-100.

Sawkins, F. J., 1976, Widespread continental rifting: Some considerations of timing and mechanism: *Geology*, v. 4, p. 427-430.

Schafer, R. W., Cooper, J. J., and Vikre, P. G., editors, 1988, Bulk Mineable Precious Metal Deposits of the Western United States, The Geological Society of Nevada, Reno, 755 p.

Schermer, E. R., 1985, Isotope and trace element geochemistry of syn-extensional rocks, east-central Nevada [abs.]: EOS, Transactions, American Geophysical Union, v. 66, p. 1138.

Schmeling, H., and Marquart, G., 1990, A mechanism for crustal thinning without lateral extension: *Geophysical Research Letters*, v. 17, p. 2417-2420.

Seedorff, E., 1991, Magmatism, extension, and ore deposits of Eocene to Holocene age in the Great Basin—Mutual effects and preliminary proposed genetic relationships, *in*, Raines, G. L., Lisle, R. E., Schafer, R. W., and Wilkinson, W. H., editors, *Geology and Ore Deposits of the Great Basin, Symposium Proceedings Volume 1: Geological Society of Nevada, Reno/Sparks, Nevada*, p. 133-177.

Sengor, A. M. C., and Burke, K., 1978, Relative timing of rifting and volcanism on earth and its tectonic implications: *Geophysical Research Letters*, v. 5, p. 419-421.

Seward, T. M., 1984, The transport and deposition of gold in hydrothermal systems, *in*, Foster, R. P., editor, *Gold '82—The Geology, Geochemistry and Genesis of Gold Deposits: Geological Society of Zimbabwe Special Publication N° 1: Rotterdam, A. A. Balkema*, p. 165-181.

Seward, T. M., 1989, The hydrothermal chemistry of gold and its implication for ore formation: Boiling and conductive cooling as examples, *in*, Keays, R. R., Ramsay, R. H., and Groves, D. I., editors, *The Geology of Gold Deposits: The Perspective in 1988: Economic Geology Monograph 6*, p. 398-404.

Sha, P., 1993, Geochemistry and genesis of carbonate-hosted disseminated gold mineralization at the Gold Quarry mine, Nevada: Ph.D. Dissertation, University of Alabama, 218 p.

Shawe, D. R., 1965, Strike-slip control of Basin-Range structure indicated by historical faults in western Nevada: *Geological Society of America Bulletin*, v. 76, p. 1361-1378.

Shawe, D. R., 1977, Continent-margin tectonics and ore deposits, western United States: *Transactions of the American Institute of Mining, Metallurgical, and Petroleum Engineers*, v. 262, p. 185-190.

- Shawe, D. R., 1991, Structurally controlled gold trends imply large gold resources in Nevada, *in*, Raines, G. L., Lisle, R. E., Schafer, W. R., and Wilkinson, W. H., editors, *Geology and Ore Deposits of the Great Basin*, v. 1, Geological Survey of Nevada, Reno, p. 199-212.
- Shawe, D. R., 1995, Geologic map of the Round Mountain quadrangle, Nye county, Nevada: U. S. Department of the Interior, U. S. Geological Survey, Geologic quadrangle map.
- Shawe, D. R., and Stewart, J. H., 1976, Ore deposits as related to tectonics and magmatism, Nevada and Utah: Society of Mining Engineers, AIME, Transactions-v. 260, p. 225-231.
- Shenberger, D. M., and Barnes, H. L., 1989, Solubility of gold in aqueous sulfide solutions from 150 to 350°C: *Geochimica Cosmochimica Acta*, v. 53, p. 269-278.
- Sherrod D. R., and Tosdal, R. M., 1991, Geological setting and southeastern California: *Journal of Geophysical Research*, v. 96, p. 12,407-12,423.
- Sibson, R. H., 1987 Earthquake rupturing as a mineralizing agent in hydrothermal systems: *Geology*, v. 15, p. 701-704.
- Silberling, N. J., 1991, Allochthonous terranes of western Nevada—Current status, *in*, Raines, G. L., Lisle, R. E., Schafer, R. W., and Wilkinson, W. H., editors, *Geology and Ore Deposits of the Great Basin*, Symposium Proceedings Volume 1: Geological Society of Nevada, Reno/Sparks, Nevada, p. 101-102
- Silberling, N. J., Jones, D. L., Blake, M. C., Jr., and Howell, D. G., 1987, Lithotectonic terrane map of the western conterminous United States: U.S. Geological Survey Miscellaneous Field Studies Map MF-1874-C, 20 p., scale 1:2,500,000.
- Silberman, M. L., 1983, Geochronology of hydrothermal alteration and mineralization: Tertiary epithermal precious metal deposits in the Great Basin: Geothermal Resources Council Special Report 13, p. 287-303.
- Silberman, M. L., 1985, Geochronology of hydrothermal alteration and mineralization: Tertiary epithermal precious-metal deposits in the Great Basin, *in*, Tooker, E. W., editor, *Geologic Characteristics of Sediment- and Volcanic-hosted Disseminated Gold Deposits—search for an Occurrence Model*: U. S. Geological Survey Bulletin 1646, p. 55-70.
- Silberman, M. L., and McKee, E. H., 1974, Ages of Tertiary volcanic rocks and hydrothermal precious metal deposits in central and western Nevada: Nevada Bureau of Mines and Geology Report 19, p. 67-72.
- Silberman, M. L., Stewart, J. H., and McKee, H., 1976, Igneous activity, tectonics, and hydrothermal precious-metal mineralization in the Great Basin during Cenozoic time: *American Institute of Mining, Metallurgy, and Petroleum Engineers Transactions*, v. 260, p. 253-263.
- Sillitoe, R. H., 1995, The influence of magmatic-hydrothermal model on exploration strategies



- for volcano-plutonic arcs, *in*, Thompson, J. F. H., editor, *Magmas, Fluids, and Ore Deposits: Mineralogical Association of Canada, Short Course Series*, v. 23, p. 511-525.
- Sillitoe, R. H., 1995, The influence of magmatic-hydrothermal models on exploration strategies for volcano-plutonic arcs, *in*, Thompson, J. F. H., editor, *Magmas, Fluids, and Ore Deposits: Mineralogical Association of Canada, Short Course Series*, v. 23, p. 367-400.
- Sillitoe, R. H., and Bonham, H. F., Jr., 1990, Sediments-hosted gold deposits: Distal products of magmatic-hydrothermal systems: *Geology*, v. 18, p. 157-161.
- Sillitoe, R. H., Graubeger, G. L., and Elliott, J. E., 1985, A diatreme-hosted gold deposit at Montana Tunnels, Montana: *Economic Geology*, v. 80, p. 1707-1721.
- Silver, L. T., and Anderson, T. H., 1974, Possible left-lateral early to middle Mesozoic disruption of the southwestern North American craton margin: *Geological Society of America Abstracts with Programs*, v. 6, p. 955.
- Singer, D. A., editor, 1996, An analysis of Nevada's Metal-bearing Mineral Resources: Nevada Bureau of Mines and Geology Open-file Report 96-2, <http://www.nbmj.unr.edu/ofr962/> and [ftp://ftp.nbmj.unr.edu/NBMG/nbmj\\_ofr96\\_2/](ftp://ftp.nbmj.unr.edu/NBMG/nbmj_ofr96_2/).
- Singer, D. A., 1993, Basic concepts in three-part quantitative assessments of undiscovered mineral resources; *Nonrenewable Resources*, v. 2, N° 2, p. 69-81.
- Singer, D. A., and Cox, D. P., 1988, Applications of mineral deposit models to resource assessments: *U.S. Geological Survey Yearbook Fiscal Year 1987*, p. 55-57.
- Skinner, B. J., 1979, The many origins of hydrothermal mineral deposits: Chapter 1, *in*, Barnes, H. L., *Geochemistry of hydrothermal ore deposits*, John Wiley & Sons, p. 1-21.
- Smith, D. L., Gans, P. B., and Miller, E. L., 1991, Palinspastic restoration of Cenozoic extension in the central and eastern Basin and Range province at Latitude 39-40° N, *in*, Raines, G. L., Lisle, R. E., Schafer, R. W., and Wilkinson, W. H., editors, *Geology and Ore Deposits of the Great Basin, Symposium Proceedings Volume 1: Geological Society of Nevada, Reno/Sparks, Nevada*, p. 75-86.
- Smith, D. M., Jr., Albinson, T., Sawkins, F. J., 1982, Geologic and fluid inclusions studies of the Tayoltita silver-gold vein deposit, Durango, Mexico: *Economic Geology*, v. 77, p. 1120-1145.
- Smith, R. B., 1978, Seismicity, crustal structure, and intraplate tectonics of the interior of the western Cordillera, *in*, Smith, R. B., and Eaton, G. P., editors, *Cenozoic Tectonics and Regional Geophysics of the Western Cordillera: Geological Society of America Memoir 152*, p. 111-141.
- Smith R. B., and Eaton, G. P., editors, 1978, *Cenozoic Tectonics and Regional Geophysics of the Western Cordillera: Geological Society of America Memoir 152*, 388 p.

- Smith, R. B., Nagy, W. C., Julander, K. A., Viveiros, J. J., Barker, C. A., and Gants, D. G., 1989, Geophysical and tectonic framework of the eastern Basin and Range-Colorado Plateau-Rocky Mountain transition, *in*, Pakiser, L. C., and Mooney, W. D., editors, Geophysical Framework of the Continental United States: Geological Society of America Memoir 172, p. 205-233.
- Smith, R. L., and Luedke, R. G., 1984, Potentially active volcanic lineaments and loci in western conterminous United States, *in*, Explosive volcanism: Inception, evolution, and hazards: Washington, D. C., National Academy Press, p. 47-65.
- Smithson, S. B., and Johnson, R. A., 1989, Crustal structure of the western U. S. based on reflection seismology, *in*, Pakiser, L. C., and Mooney, W. D., editors, Geophysical Framework of the Continental United States: Geological Society of America Memoir 172, p. 577-612.
- Snoke, A. W., Miller, D. M., 1988, Metamorphic and tectonic history of the Northeastern Great Basin, *in*, Ernst, W. G., editor, Metamorphism and Crustal Evolution of the Western United States: Rubey Volume VII, Prentice Hall, Englewood Cliffs, New Jersey, p. 606-648.
- Snow, J. K., 1992, Large-magnitude Permian shortening and continental-margin tectonics in the southern Cordillera: Geological Society of America Bulletin, v. 104, p. 80-105.
- Snyder, D. B., England, R. W., and McBride, J. H., 1997, Linkage between mantle and crustal structures and its bearing on inherited structures in northwestern Scotland: Journal of the Geological Society, London, v. 154, p. 79-83.
- Snyder, W. S., Dickinson, W. R., and Silberman, M. L., 1976, Tectonic implications of space time patterns of Cenozoic magmatism in the Western United States: Earth and Planetary Sciences Letters, v. 32, p. 91-106.
- Sonder, L. J., and England, P., 1986, Vertical averages of rheology of the continental lithosphere: relation to thin sheet parameters: Earth and Planetary Science Letter, v. 77, p81-90.
- Sonder, L. J., England, P. C., Wernicke, B. P., and Christiansen, R. L., 1987, A physical model for Cenozoic extension of western North America, *in*, Coward, M. P., Dewey, J. F., and Hancock, P. L., editors, Continental Extensional Tectonics: Geological Society Special Publication Number 28, p. 187-201.
- Speed, R. C., 1983, Pre-Cenozoic tectonic evolution of northeastern Nevada: Geothermal Resources Council, Special Report N° 13, p. 11-24.
- Speed, R. C., Elison, M. W., and Heck, F. R., 1988, Phanerozoic tectonic evolution of the Great Basin, *in*, Ernst, W. G., editor, Metamorphism and Crustal Evolution of the Western United States: Rubey Volume VII, Prentice Hall, Englewood Cliffs, New Jersey, p. 572-605.
- Spencer, J. E., and Chase, C. G., 1989, Role of crustal flexure in initiation of low-angle normal faults and implications for structural evolution of the Basin and Range province: Journal of Geophysical Research, v. 94, 1765-1775.

- Spiegelhalter, D. J., and Knill-Jones, R. P., 1984, Statistical and knowledge-based approaches to clinical decision-support systems, with an application in gastroenterology: *Journal of the Royal Statistical Society, A*, Part 1, p. 35-77.
- Spiers, C. J., and Peach, C. J., 1989, Development of dilation and permeability in rocks during creep: Experiments on salt as a rock analog [abs.]: *Abstracts of the International Geological Congress*, V. 3, p. 162-163.
- Stager, H. K., and Tingley, J. V., 1988, Tungsten deposits in Nevada: *Nevada Bureau of Mines and Geology Bulletin* 105, 256 p.
- Star, J., and Estes, J., 1990, *Geographic information systems, an introduction*: Prentice Hall, Englewood Cliffs, NJ, 303 p.
- Stevens, C. H., 1992, A speculative reconstruction of the middle Paleozoic continental margin of southwestern North America: *Tectonics*, v. 11, N<sup>o</sup>. 2, p. 405-419.
- Steward, J. H., 1980, *Geology of Nevada; A discussion to Accompany the Geologic Map of Nevada*: Nevada Bureau of Mines and Geology, Special publication 4, 136p.
- Stewart, J. H., 1976, Late Precambrian evolution of North America: Plate tectonics implication: *Geology*, v. 4, p. 11-15.
- Stewart, J. H., 1978, Basin and Range structure in western North America—A review, *in*, Smith, R. B., and Eaton, G. P., editors, *Cenozoic Tectonics and Regional Geophysics of the Western Cordillera*: Geological Society of America Memoir 152, p. 1-31.
- Stewart, J. H., 1980, *Geology of Nevada: A discussion to accompany the geological map of Nevada*: Nevada Bureau of Mines and Geology Special Report 4, 136 p.
- Stewart, J. H., 1983, Cenozoic structure and tectonics of the northern Basin and Range Province, California, Nevada, and Utah: *Geothermal Resources Council, Special Report* N<sup>o</sup> 13, p. 25-40.
- Stewart, J. H., 1988, Tectonics of the Walker Lane Belt, Western Great Basin: Mesozoic and Cenozoic deformation in a zone of shear, *in*, Ernst, W. G., editor, *Metamorphism and Crustal Evolution of the Western United States: Rubey Volume VII*, Prentice Hall, Englewood Cliffs, New Jersey, p. 683-713.
- Stewart, J. H., and Carlson, J. E., 1978, *Geologic map of Nevada*: Prepared by U. S. Geological Survey in cooperation with the Nevada Bureau of Mines and Geology, scale 1: 500,000, 2 sheets.
- Stewart, J. H., and Carlson, J. E., 1976, Cenozoic rocks of Nevada—Four maps and a brief description of distribution, lithology, age, and centers of volcanism: *Nevada Bureau of Mines and Geology Map* 52, scale 1:1,000,000.
- Stewart, J. H., and Crowell, J. C., 1992, Strike-slip tectonics in the Cordilleran region, western

- United States, *in*, Burchfiel, B. C., Lipman, P. W., and Zoback, M. L., editors, The Cordilleran Orogen: The Conterminous U. S., The Geology of North America, Volume G-3: Geological Society of America, p. 609-628.
- Stewart, J. H., and Poole, F. G., 1974, Lower Paleozoic and uppermost Precambrian of the Cordilleran miogeocline, Great Basin, western United States, *in*, Dickinson, W. R., editors, Tectonics and Sedimentation: Society of Economic Mineralogists and Paleontologists Special Publication, v. 22, p.28-57.
- Stewart, J. H., and Suczek, C. A., 1977, Cambrian and latest Precambrian paleogeography and tectonic in the western United States, *in*, Stewart, J. H., Stevens, C. H., and Fritsche, A. E., editors, Paleozoic Paleogeography of the Western United States: Society of Economic Palaeontologists and Mineralogists, Pacific Section, Pacific Coast Paleogeography Symposium I, p. 1-17.
- Stewart, J. H., Walker, G. W., and Kleinhampl, F. J., 1975, Oregon-Nevada lineament: Geology, v. 3, p. 265-268.
- Stoffregen, R., 1987, Genesis of acid-sulfate alteration and Au-Cu-Ag mineralization at Summitville, Colorado: Economic Geology, v. 82, p. 1575-1591.
- Stokes, W. L., 1976, What is the Wasatch Line?, *in*, Hill, J., editor, Geology of the Cordilleran Hingeline: Rocky mountain Association of Geologists, p. 11-26
- Suppe, J., 1985, Principles of structural geology: Prentice Hall, Englewood Cliffs, New Jersey, 537 p.
- Sweeney, T. M., 1990, Active or significant Nevada gold properties: U.S. Bureau of Mines, Western field operations center, Spokane, Washington, map with properties list, 1 sheet.
- Swinden, H. S., 1984, The Chetwynd prospect, southwestern Newfoundland: Department of Mines and Energy, Mineral Development Division, Government of Newfoundland and Labrador, Open File 110/09/148, 10 p.
- Talapatra, A. K., and Mukhopadhyay, M. K., 1993, Mineral belt modelling: A statistical approach applied to some selected Indian base-metal deposits, *in*, Kirkham, R. V., Sinclair, W. D., Thorpe, R. I., and Duke, J. M., editors, Mineral Deposit Modelling: Geological association of Canada, Special Paper 40, p. 761-770.
- Taubeneck, W. H., 1970, Dikes of the Columbia River Basalt in northeastern Oregon, Western Idaho, and southeastern Oregon, *in*, Gilmour, E. H., and Stradling, D., editors, Proceedings, Second Columbia River Basalt Symposium: Cheney, Eastern Washington State College, p. 73-76.
- Taylor, B. E., 1996, Epithermal gold deposits, *in*, Eckstrand, O. R., Sinclair, W. D., and Thorpe, R. I., editors, Geology of Canadian Mineral Deposits Types: Geological Survey of Canada, Geology of Canada, N° 8, p. 327-350.

- Teal, L., and Jackson, M., 1997, Geologic overview of the Carlin Trend gold deposits and description of recent deep discoveries, *in*, Vikre, P., Thompson, T. B., Bettles, K., Christensen, O., and Parratt, R., editors, Carlin-Type Gold Deposits Field Conference, Society of Economic Geologists, Guidebook Series, v. 28, p. 3-37.
- Telford, W. M., Geldart, L. P., Sheriff, R. E., and Keys, D. A., 1976, Applied geophysics: Cambridge, Cambridge University Press, 860 p.
- Teyssier, C., Tikoff, B., and Markley, M., 1995, Oblique plate motion and continental tectonics: *Geology*, v. 23, p. 447-450.
- Thelin, G. P., and Pike, R. J., 1991, Landforms of the conterminous United States - A digital shaded-relief portrayal: U. S. Geological Survey, Miscellaneous Investigation Series, Map 1-2206, scale 1: 350 000, Accompanying Booklet, 16 p.
- Thompson, G. A., and Zoback, M. L., 1979, Regional geophysics of the Colorado Plateau: *Tectonophysics*, v. 61, p. 149-181.
- Thompson, G. A., Catchings, R., Goodwin, E., Holbrook, S., Jarchow, C., Mann, C., McCarthy, J., and Okaya, D., 1989, Geophysics of the western Basin and Range province, *in*, Pakiser, L. C., and Mooney, W. D., editors, Geophysical Framework of the Continental United States: Geological Society of America Memoir 172, p. 177-203.
- Thompson, G., and McCarthy, J., 1986, Geophysical evidence for igneous inflation of the crust in highly extended terranes [abs.]: EOS, Transactions, American Geophysical Union, v. 67, p. 1184.
- Thompson, J. F. K., 1993, Application of deposit models to exploration, *in*, Kirkham, R. V., Sinclair, W. D., Thorpe, R. I., Duke, J. M., editors, Mineral Deposit Modelling: Geological Association of Canada, Special Paper 40, p. 51-67.
- Thompson, T. B., 1986, Precious metals in the Leadville district, Colorado: Geological Society of America Abstracts with Programs, v. 18, p. 773.
- Thompson, T. B., Trippel, A. D., and Dewelley, P. C., 1985, Mineralized veins and breccias of the Cripple Creek district, Colorado: *Economic Geology*, v. 80, p. 1669-1688.
- Thorman, C. H., and Christensen, O. D., 1991, Geologic settings of gold deposits in the Great Basin, western United States, *in*, Ladeira, E. A., editor, Brazil gold '91, Balkema, Rotterdam, p. 65-75.
- Thorman, C. H., Brooks, W. E., Snee, L. W., Hofstra, A. H., Christensen, O. D., and Wilton, D. T., 1995, Eocene-Oligocene model for Carlin-type deposits in northern Nevada [abs.]: *Geology and ore deposits of the American Cordillera, symposium program with abstracts*: Geological Society of Nevada, Reno/Sparks, Nevada, p. 75.
- Thorman, C. H., Ketner, K. B., Brooks, W. E., Snee, L. W., and Zimmermann, R. A., 1991, Late

- Mesozoic-Cenozoic tectonics in northeastern Nevada, *in*, Raines, G. L., Lisle, R. E., Schafer, R. W., and Wilkinson, W. H., editors, *Geology and Ore Deposits of the Great Basin, Symposium Proceedings Volume 1: Geological Society of Nevada, Reno/Sparks, Nevada*, p. 25-45.
- Tilling, R. I., Gottfried, D., Rowe, J. J., 1973, Gold abundance in igneous rocks: Bearing on gold mineralization: *Economic Geology*, v. 68, p. 168-186.
- Tingley, J. V., and Berger, B. R., 1985, Lode gold deposits of Round Mountain, Nevada: Nevada Bureau of Mines and Geology Bulletin 100, 62 p.
- Titley, S. R., 1978, Copper, molybdenum, and gold content of some porphyry copper systems of the southwestern and western Pacific: *Economic Geology*, v. 73, p. 977-981.
- Titley, S. R., 1987, The crustal heritage of silver and gold ratios in Arizona ores: *Geological Society of America Bulletin*, v. 99, p. 814-826.
- Titley, S. R., 1989, Regional variation of silver and gold ratios in vein ores of Arizona, *in*, Keays, R. R., Ramsay, R. H., and Groves, D. I., editors, *The Geology of Gold Deposits: The Perspective in 1988: Economic Geology Monograph 6*, p. 626-636.
- Titley, S. R., 1991, Correspondence of ores of silver and gold with basement terranes in the American southwest: *Mineralium Deposita*, v. 26, p. 66-71.
- Titley, S. R., and Beane, R. E., 1981, Porphyry copper deposits—Part I. Geologic settings, petrology, and tectogenesis—Part II. Hydrothermal alteration and mineralization, *in*, Skinner, B. J., editor, *Economic Geology Seventy-Fifth Anniversary Volume: El Paso, Texas, Economic Geology Publishing Company*, p. 214-269.
- Tooker, E. W., 1983, Correlation of metal occurrence and terrane attributes in the northwestern conterminous United States: *Canadian Journal of Earth Science*, v. 20, p. 1030-1039.
- Tooker, E. W., 1985, Discussion of the disseminated gold ore occurrence model, *in*, Tooker, E. W., editor, *Geologic Characteristics of Sediment- and Volcanic-hosted Disseminated Gold Deposits—search for an Occurrence Model: U. S. Geological Survey Bulletin 1646*, p. 107-150.
- Tosdal, R. M., and Nutt, C. J., 1998, Localization of sedimentary rock-hosted Au deposits of the Carlin trend Nevada, along an Eocene accommodation zone: *Geological Society of America Abstracts with Programs*, v. 30, № 7, p. A-372.
- Tosdal, R. M., and Wooden, J. L., 1997, Granites, Pb isotopes, and the Carlin and Battle Mountain-Eureka trends, Nevada, [abs.]: *Geological Society of America, Abstract with Program*, v. 29, Abstract No 50295, <http://www.geosociety.org/cgi-bin/gsa97hl.pl?carlin^annual/s/abs/50295.htm~>
- Trexler, D. T., Flynn, T., Koenig, B. A., and Ghush, G. Jr., 1983, Geothermal resources of

- Nevada: Division of Earth Sciences, Environmental Research Center, University of Nevada, Las Vegas, NV.
- Turcotte, D. L., and Emerman, S. H., 1983, Mechanism of active and passive rifting, *in*, Morgan, P. and Baker, B. H., editors, *Processes of Continental Rifting*: Elsevier, Amsterdam, p. 39-50.
- Turner, D. D., 1997, Predictive GIS for sediment-hosted gold deposits, North-central Nevada, USA, *in*, Gubins, A. G., editor, *Proceedings of Exploration 97: Fourth Decennial International Conference on Mineral Exploration*, p. 115-126.
- Turner, M. R., and Bawiec, W. J., 1991, *Geology of Nevada: A digital representation of the 1978 geologic map of Nevada*: U. S. Geological Survey Digital Data Series DDS-2, CD-ROM.
- Tweto, O., 1979, The Rio Grande rift system in Colorado, *in*, Riecker, R. E., editor, *Rio Grande Rift: Tectonics and Magmatism*: American Geophysical Union, Washington, D. C., p. 33-56.
- TYDAC Technologies Inc., 1991, *Spatial Analysis System Reference Guides, Version 5. 2*, Ottawa, Ontario, Canada.
- U. S. Bureau of Mines, 1992, *Minerals Availability System (MAS)*, Spokane, Washington.
- U. S. Geological Survey, 1984, *The State of Nevada (shaded-relief topographic map)*, edition of 1967.
- U. S. Geological Survey, 1990a, *Side-looking airborne radar (SLAR)—Western Mosaics CD-ROM*: Earth Science Information Center, EROS Data Center, Sioux Falls, SD.
- U. S. Geological Survey, 1990b, *Conterminous U. S. AVHRR—1990 bi-weekly composites CD-ROM*: Earth Science Information Center, EROS Data Center, Sioux Falls, SD.
- U. S. Geological Survey, 1990c, *Digital line graphs from 1: 2,000,000-scale maps CD-ROM*: Earth Science Information Center, Reston, VA.
- U. S. Geological Survey, 1993, 1995, *Mineral Resource Data System (MRDS)*, USGS Field Station, Reno, Nevada.
- U. S. Geological Survey, 1996, *North American 30 arc-second DEM: EROS Data Center Distributed Active Archive Center (EDC DAAC)*, EROS Data Center in Sioux Falls, South Dakota, [http://edcftp.cr.usgs.gov:80/pub/data/30ASDCWDEM/NORTH\\_AMERICA/](http://edcftp.cr.usgs.gov:80/pub/data/30ASDCWDEM/NORTH_AMERICA/) and <ftp://edcftp.cr.usgs.gov/pub/data/gtopo30/global/>.
- Van Eysinga, F. W. B. (compiler), 1975, *Geological time table*, 3<sup>rd</sup> edition: Elsevier, Amsterdam, 1 wall-poster sheet.
- Veregin, H., 1989, *A taxonomy of error in spatial databases*: Technical Paper 89-12, National Center for Geographic Information and Analysis University of California, Santa Barbara, California.



- Vielzeuf, D., and Kornprobst, J., 1984, Crustal splitting and the emplacement of Pyrenean Iherzolites and granulites: *Earth Planetary Science Letters*, v. 67, p. 87-96.
- Vikre, P. G., McKee, E. H., and Silverman, M. L., 1988, Chronology of Miocene hydrothermal and igneous events in the western Virginia Range, Washoe, Storey, and Lyon counties, Nevada: *Economic Geology*, v. 83, p. 864-874.
- Vikre, P., Thompson, T. B., Bettles, K., Christensen, O., and Parratt, R., editors, 1997, Carlin-Type Gold Deposits Field Conference, Society of Economic Geologists, Guidebook Series, v. 28, 287 p.
- Wallace, A. R., 1991, Effect of Late Miocene extension on the exposure of gold deposits in north-central Nevada, *in*, Raines, G. L., Lisle, R. E., Schafer, R. W., and Wilkinson, W. H., editors, *Geology and Ore Deposits of the Great Basin, Symposium Proceedings Volume 1: Geological Society of Nevada, Reno/Sparks, Nevada*, p. 179-183.
- Ward, P. L., 1986, Volcanism and plate tectonics of the western United States [abs.]: *EOS, Transactions, American Geophysical Union*, v. 67, p. 1226.
- Ward, P. L., 1988, North America-Pacific plate boundary, an elastic-plastic megashear; Evidence from very long baseline interferometry: *Journal of Geophysical Research*, v. 93, p. 7716-7728.
- Ward, P. L., 1991, On plate tectonics and the geologic evolution of southwestern North America: *Journal of Geophysical Research*, v. 96, N<sup>o</sup>. B7, p. 12479-12496.
- Warne, J. E., and Sandberg, C. A., 1996, Alamo megabreccia: Record of a late Devonian impact in southern Nevada: *GSA Today*, v. 6, p. 1-7.
- Warner, L. A., 1978, The Colorado lineament: A middle Precambrian wrench fault system: *Geological Society of America Bulletin*, v. 89, p. 161-171.
- Watson, G. P., and Rencz, A. N., 1989, Data integration studies in northern New Brunswick, *in*, Agterberg, F. P., and Bonham-Carter, G. F., editors, *Statistical Analysis in the Earth Sciences*, Geological Survey of Canada, Paper 89-9, p. 185-191.
- Wernicke, B., 1981, Low angle normal faults in the Basin and Range province—Nappe tectonics in an extension orogen: *Nature*, v. 291, p. 645-648.
- Wernicke, B. P., 1985, Uniform-sense normal simple shear of the continental lithosphere: *Canadian Journal of Earth Science*, v. 22, p. 108-125.
- Wernicke, B. P., 1990, The fluid crustal layer and its implications for continental dynamics, *in*, Salisbury, M. H., and Fountain, D. M., editors, *Exposed Cross-sections of the Continental Crust: Kluwer Academic Publishers, Netherlands*, p. 509-544.
- Wernicke, B. P., 1992, Cenozoic extensional tectonics of the U. S. Cordillera, *in*, Burchfiel, B. C., Lipman, P. W., and Zoback, M. L., editors, *The Cordilleran Orogen: The Conterminous U.*

- S., the Geology of North America, Volume G-3: Geological Society of America, p. 553-581.
- Wernicke, B. P., Axen, G. J., and Snow, J. K., 1988, Basin and Range extensional tectonics at the latitude of Las Vegas, Nevada: Geological Society of America bulletin, v. 100, p. 1738-1757.
- Wernicke, B. P., Christiansen, R. L., England, P. C., and Sonder, L. J., 1987, The tectonomagmatic evolution of Cenozoic extension in the North American Cordillera, *in*, Coward, M. P., Dewey, J. F., and Hancock, P. L., editors, Continental Extensional Tectonics: Geological Society Special Publication number 28, p. 203-221.
- Wernicke, B. P., Clayton, R., Ducea, M., Jones, C. H., Park, S., Ruppert, S., Saleeby, J., Snow, J. K., Squires, L., Fliedner, M., Jiracek, G., Keller, R., Klemperer, S., Luetgert, J., Malin, P., Miller, K., Mooney, W., Oliver, H., and Phinney, R., 1996, Origin of high mountains in the continents: The southern Sierra Nevada: Science, v. 271, p. 190-193.
- Wernicke, B., Spencer, J. E., Burchfiel, B. C., and Guth, P. L., 1982, Magnitude of crustal extension in the southern Great Basin: Geology v. 10, p. 499-502.
- Westaway, R., 1989, Deformation of the NE Basin and Range Province: the response of the lithosphere to the Yellowstone plume?: Geophysics Journal Int., 99, 33-62.
- White, D. E., 1974, Diverse origins of hydrothermal ore fluids: Economic Geology, v. 69, p. 954-973.
- White, D. E., 1981, Active geothermal systems and hydrothermal ore deposits, *in*, Skinner, B. J., editor, Economic Geology Seventy-Fifth Anniversary Volume: El Paso, Texas, Economic Geology Publishing Company, p. 392-423.
- White, D. E., 1985, Vein and disseminated gold-silver deposits of the Great Basin through space and time, *in*, Tooker, E. W., editor, Geologic Characteristics of Sediment- and Volcanic-hosted Disseminated Gold Deposits—search for an Occurrence Model: U. S. Geological Survey Bulletin 1646, p. 5-14.
- White, D. E., and Heropoulos, C., 1983, Active and fossil hydrothermal-convection systems of the Great Basin: Geothermal Resources Council, Special Report N<sup>o</sup>. 13, p. 41-53.
- Wilkins, J. Jr., 1984, The distribution of gold- and silver-bearing deposits in the Basin and Range Province, western United States *in*, Wilkins, J. Jr., editor, Gold and Silver Deposits of the Basin and Range Province Western USA : Arizona Geological Society Digest, v. 15, p. 1-27.
- Wise, J. M., and Gorman, J. A., 1997, Modern and historic fluid interaction with the new deep fault, Jerritt Canyon district, Nevada, [abs.]: Geological Society of America, Abstract with Program, v. 29, Abstract N<sup>o</sup> 51205, <http://www.geosociety.org/cgi-bin/gsa97hl.pl?carlin^annual/s/abs/51205.htm~>
- Wood, S. A., Crerar, D. A., and Borcsik, M. P., 1987, Solubility of the assemblage pyrite-

- pyrrhotite-magnetite-sphalerite-galena-gold-stibnite-bismuthinite-argentite-molybdenite in H<sub>2</sub>O-NaCl-CO<sub>2</sub> solutions from 200° C to 350° C: *Economic Geology*, v. 82, p. 1864-1887.
- Woodall, R., 1984, Success in mineral exploration: Confidence in science and ore deposit models: *Geoscience Canada*, v. 11, № 3, p. 127-132.
- Wooden, J. L., Stacey, J. S., Howard, K. A., Doe, B. R., and Miller, D. M., 1988, Pb isotopic evidence for the formation of Proterozoic crust in the southwestern United States, *in*, Ernst, W. G., editor, *Metamorphism and Crustal Evolution of the Western United States: Rubey Volume VII*, Prentice Hall, Englewood Cliffs, New Jersey, p. 69-86.
- Wooden, J. L., Tosdal, R. M., and Kistler, R. W., 1997, Pb and Sr mapping of crustal structure in the Northern Great Basin, *in*, Vikre, P., Thompson, T. B., Bettles, K., Christensen, O., and Parratt, R., editors, *Carlin-Type Gold Deposits Field Conference*, Society of Economic Geologists, Guidebook Series, v. 28, p. 47-51.
- Woodward, L. A., 1984, Basement control of Tertiary intrusions and Associated mineral deposits along Tijeras-Canoncito fault system, New Mexico: *Geology*, v. 12, p. 531-533.
- Wright, D. F., 1990, Gold potential for eastern Meguma Terrane, Nova Scotia, using weights of evidence modelling [abs.]: 8<sup>th</sup> International Association on the Genesis of Ore Deposits (IAGOD), Program with Abstracts, p. A46.
- Wright, D. F., 1996, Evaluating volcanic hosted massive sulphide favourability using GIS-based spatial data integration models, Snow Lake area, Manitoba: Ph.D. dissertation, University of Ottawa, Ottawa, Canada, 344 p.
- Wright, D. F., and Bonham-Carter, G. F., 1996, VHMS favourability mapping with GIS- based integration models, Chisel Lake-Anderson Lake area: Exploration '97 Workshop, Bonham-Carter, G., and Wright, D., workshop coordinators, Ottawa, September 9-1, 1997,
- Wright, D. F., Bonham-Carter, G. F., 1996, VHMS favourability mapping with GIS-based integration models, Chisel Lake-Anderson Lake area, *in*, Bonham-Carter, G. F., Galley, A. G., and Hall, G. E. M., editors, *EXTECH I: A Multidisciplinary Approach to Massive Sulphide Research in the Rusty Lake-Snow Lake Greenstone Belts*, Manitoba: Geological Survey of Canada, Bulletin 426, p. 339-376, 387-401.
- Zartman, R. E., 1974, Lead isotopic provinces of the western United States and their geologic significance: *Economic Geology*, v. 69, p. 792-805.
- Zoback, M. L., 1989, State of stress and modern deformation of the northern Basin and Range Province: *Journal of Geophysical Research*, v. 94, p. 7105-7128.
- Zoback, M. L., and Thompson, G. A., 1978, Basin and Range rifting in northern Nevada: Clues from a mid-Miocene rift and its subsequent offsets: *Geology*, v. 6, p. 111-116.
- Zoback, M. L., and Zoback, M. D., 1989, Tectonic stress field of the continental United States,

*in*, Pakiser, L. C., and Mooney, W. D., editors, Geophysical Framework of the Continental United States: Geological Society of America Memoir 172, p. 523-539.

Zoback, M. L., Anderson, R. E., and Thompson, G. A., 1981, Cainozoic evolution of the state of stress and style of tectonism of the Basin and Range Province of the western United States: Royal Society of London, Philosophical Transactions, v. A-300, p. 407-434.

Zoback, M. L., McKee, E. H., Blakely, R. J., and Thompson, G. A., 1994, The northern Nevada rift: Regional tectono-magmatic relations and middle Miocene stress direction: Geological Society of America Bulletin, v. 106, p. 371-382.

Class	Type of Relationship	Examples	
		Field	Model
<i>Theoretical</i>	Physical/Chemical Principles	Groundwater Flow	Equations of Motion
<i>Hybrid</i>	Semi-Empirical	Sediment Transport	Transport Equations
<i>Empirical</i>	Heuristic or Statistical	Mineral Prediction	Statistical Regression

*Table 1.1.* Types of models used in the geosciences (Bonham-Carter, 1994a).

Type	Model Parameters	Examples
<i>Data-driven</i>	Calculated From Training Dataset	<i>Weights of Evidence</i> Logistic Regression Neural network
<i>Knowledge-driven</i>	Estimated by an Expert	Fuzzy Logic Dempster-Shafer Belief Theory

**Table 1.2.** Types of mineral potential models (Bonham-Carter, 1994a).

<i>Population</i>	<i>Metallic and Non-Metallic Mineral Occurrences</i>											
	<i>Primary-Product Gold-Silver-Bearing Occurrences (all types) (2690)</i>				<i>Sedimentary Rock- Hosted Gold-Silver- Bearing Occurrences (98)</i>				<i>Volcanic Rock-Hosted Gold-Silver-Bearing Occurrences (415)</i>			
	<i>Lrg. (59)</i>	<i>Med. (118)</i>	<i>Sml. (2269)</i>	<i>Unkn. (244)</i>	<i>Lrg. (8)</i>	<i>Med. (30)</i>	<i>Sml. (57)</i>	<i>Unkn. (3)</i>	<i>Lrg. (33)</i>	<i>Med. (43)</i>	<i>Sml. (317)</i>	<i>Unkn. (22)</i>

**Table 1.3.** The gold-silver-bearing occurrences examined in this study.



## SEDIMENTARY ROCK-HOSTED DEPOSIT-TYPE SYNOPTIC MODEL

### *SYNONYMS AND DESCRIPTIONS:*

Carlin-type; carbonate rock-hosted Au; disseminated replacement-type Au; disseminated Au; invisible Au; sediment-hosted micron Au (SHMG); erroneously referred to as "epithermal" disseminated as well. Stratiform deposits of sub-microscopic to microscopic Au coating disseminated sulfide minerals in carbonaceous calcareous sedimentary rocks.

### *COMMODITIES (principal recovered products; by-products in parentheses):*

Au Ag (Hg)

### *EXAMPLES: (within the Great Basin)*

In Nevada: Carlin trend deposits (Bootstrap, Dee, Carlin Gold mine, Genesis, Gold Strike, Pete, Post, Gold Quarry, Maggie Creek, Rain, etc.), Cortez trend deposits (Gold Acres, Cortez, Horse Canyon, Pipeline, etc.), Tonkin Springs, Gold Bar, Northumberland, Getchell trend deposits (Twin Creeks (Chimney Creek and Rabbit Creek), Getchell, Pinson, Preble), Independence group deposits (Big Springs-Sammy Creek, Burns Basin, Jerritt Canyon, Winters Creek, Wright Window, etc.), Alligator group deposits (Alligator Ridge, Bald Mountain, Golden Butte, Illipah, White Pine, Yankee, etc.), Standard, Fondaway Canyon, Night Hawk, and Green Springs. In Utah: Mercur, Barney's Canyon, Tecoma, and Melco.

### *TYPICAL GRADE AND TONNAGE (Troy ounces; U.S. short tons):*

Gold: 0.015-0.3; up to 0.7-0.8 oz/t

Silver: data sparse; generally much lower than Au (0.02 oz/t Alligator; 0.7 oz/t Dee)

Tonnage: 2-8 to 50 to >500 million tons

### *ASSOCIATED DEPOSIT TYPES (other genetically related deposit types):*

Veins containing stibnite, barite, realgar, and orpiment.

### *GEOLOGIC SETTING:*

Deformed basin and/or platform sediments in mobile belt or stable craton settings. Carbonaceous, calcareous rocks cut by high-angle normal faults. Many deposits in Nevada aligned along inferred regional-scale structures, en echelon fault belts, belts of thrust faulting (including fensters in allochthonous plate), and/or zones of crustal weakness?

### *MINERALIZED AND HOST ROCKS:*

Calcareous sedimentary rocks high in carbon (3-15% C). Rock types usually range from calcareous shale to silty limestone or dolostone. Commonly thinly bedded. Coarse to fine clastic sedimentary rocks with high carbon content occur as hosts in some deposits (e.g.—Getchell). Units of high permeability most favorable host rocks.

### *ASSOCIATED ROCKS (spatially associated non-mineralized igneous rocks):*

Calc-alkaline and/or alkaline plutons and dikes occur at or near most deposits. Intrusives pre-ore or post-ore at most deposits, although appear to be syn-ore at some. Hydrothermal breccias may be present in ore zones. Genetic association unclear (may have acted as heat engine in some cases?).

**Table 3.1.** Synoptic mineral deposit model for sedimentary rock-hosted disseminated precious metal deposits. This model is derived from the attributes of North American "giant" deposits ( $\geq 1,000,000$  Troy ounces Au production and/or reserves) in the Great Basin.

**FORM OF DEPOSIT** (*ore body and gold mineralization*):

Stratabound. Irregular to tabular ore bodies extending out from faults intersecting favorable host rocks. Some deposits may show vertical continuity of mineralization with no change in mineralogy over vertical intervals in excess of 700-1000 meters. Mineralization is disseminated, fine grained and decreases away from fault zone or heat source. Most Au is "invisible" (0.03-10 microns). Au content varies widely within ore zone. Ore may be partially oxidized. Small veins and stockworks may occur within orebodies. Jasperoid replacement bodies common and may be ore grade. Au-quartz veins rare.

**ORE CONTROLS:**

Permeable carbonaceous calcareous sedimentary rocks. Geochemically favorable horizons. Proximity to high angle faults, thrust faults, and/or low-angle normal or reverse faults. At some deposits breccia zones/pipes and impermeable "capping" stratigraphy or structures important (some units or structures may have acted as local aquitards, blocking upward movement of fluids and redirecting them laterally along permeable units). Regional antiformal doming and localized (minor) anticlinal folding ("structural domes") important at some deposits (fracturing and brecciation along crest). Folding is Mesozoic in Nevada.

**MINERALOGY** (*mode of gold occurrence in ore; other metallic, accessory and gangue minerals*):

Native Au: exceedingly fine grained; sub-microscopic to microscopic, usually less than one micron; rarely visible. Occurs as thin films and fracture fillings on pyrite which may be disseminated, encapsulated in quartz, or in veins. Free Au also occurs as disseminations in quartz or barite, between quartz and clay grains, on grains of amorphous carbon or hematite, and as inclusions in other sulfides. Veins contain barite, calcite, pyrite, realgar, orpiment, other sulfides, sulfosalts, and carbonaceous material. Carbonaceous material may include hydrocarbons, amorphous carbon, microcrystalline graphite, and humic acids. Minerals in the unoxidized ore zone include arsenopyrite, pyrrhotite, marcasite, cinnabar, realgar, orpiment, stibnite, lorandite, tennantite, getchellite, jordanite, galkhaite, gratonite, christite, ellisite, weissbergite, boulangerite, tetrahedrite, carlinite, galena, sphalerite, chalcocopyrite, covellite, chalcocite and molybdenite. Other hydrothermal minerals include quartz (often jasperoid), calcite, dolomite, barite, fluorite, jarosite, alunite, frankdicksonite, and clay minerals. Oxidized ore zone may contain hematite, goethite, schuetteite, arsenolite, carminite, scorodite, arseniosiderite, mimetite, stibiconite, valentinite, cervantite, avicennite, litharge, massicot, anglesite, cerussite, smithsonite, malachite, azurite, chrysocolla and turquoise.

**ALTERATION:**

Decarbonatization, silicification, argillization, pyritization, and oxidation and acid leaching near surface. Introduction and redistribution of carbon. At the Carlin deposit (Nevada), Au is generally associated with intermediate alteration zones of carbonate removal. Volume loss related to decarbonatization produces apparent enrichment in Al, Fe, and K, but there is little change except for major Ca, Mg, CO<sub>2</sub> and minor K loss, and SiO<sub>2</sub> gain.

**AGE RANGE:**

Host: Cambrian to Tertiary (generally Cambrian through Pennsylvanian for deposits in north-central Nevada)

Ore: Tertiary (42-30 Ma in Nevada)

**GENETIC MODEL:**

Unresolved. For the Great Basin, three basic models have been proposed: (1) Related to regional-scale crustal extension, where the southward sweep of Tertiary magmatism and the onset of extensional (and strike-slip?) tectonism facilitated deep fluid circulation by increasing the geothermal temperature gradient (thinning of the crust) and crustal permeability via brittle faulting and fracturing in the upper crust. (2) Related to regional metamorphism, where deep-seated, possibly mantle-derived magmatic activity, preceded crustal extension and provided fluids (by metamorphic devolatilization reactions at deeper levels) and created sufficient heat (a regional "geothermal environment") to circulate fluids. Deeply convecting unevolved meteoric fluids mix at deep crustal levels with ascending gas-rich metal-bearing fluids that were released at the onset of extension.

**Table 3.1**, continued.

(3) Igneous-related (distal disseminated), where deposits form in the distal portions of magmatic hydrothermal systems. Magmas provided energy to drive hydrothermal circulation were the source for some fluid components and metals. Deposits formed within approximately <3 to >5 km of the surface (as compared to ~1km for epithermal mineralization). Main-stage ore depositing fluids were evolved meteoric (mixed) waters, with elevated CO<sub>2</sub> and H<sub>2</sub>S, low in salinity (<0.2-10 equivalent wt% NaCl; generally <5 wt%, but up to 18% or higher at boiling), temperature (150-250°C; most deposits 190 to 225°C), and SO<sub>4</sub>. Several generations of hydrothermal brecciation at some deposits suggest multiple mineralizing events. Late-stage ore and/or post-ore fluids may redistribute Au to some degree. Metals derived at depth from underlying sedimentary pile (Late Proterozoic miogeoclinal pelitic rocks) or from magmatic sources. Bisulfide, thiosulfide, arsenic, and/or other poorly documented complexes may transport Au.

*COMPILED FROM:*

Arehart et al. (1993), Bakken et al. (1987), Bakken and Einaudi (1986), Bakken (1990), Birak et al. (1987), Birak (1986), Bonham (1985), Cline et al. (1997), Cox and Singer (1986), Cunningham (1988), Dickson et al. (1979), Hall et al. (1997), Hausen et al. (1967), Henry and Boden (1997), Hitchborn et al. (1996), Hofstra et al. (1988), Hofstra and Rowe (1987), Hofstra et al. (1987), Hofstra (1997), Hofstra (1994), Holland et al. (1988), Ilchik and Barton (1997), Ilchik and Barton (1996), Kuehn and Rose (1987), Kuehn (1989), Lamb and Cline (1997), Leventhal et al. (1987), Lowe et al. (1985), Ludington et al. (1993), Ludington et al. (1996), Maher et al. (1993), Norman et al. (1996), Northrop et al. (1987), Percival et al. (1988), Radtke (1981), Radtke (1985), Radtke et al. (1980), Rodriguez (1997), Romberger (1986), Rose and Kuehn (1987), Rye (1985), Seedorff (1991), Singer (1996), Teal and Jackson (1997), Tooker (1985), White (1985), and Wooden et al. (1997).

## VOLCANIC ROCK-HOSTED DEPOSIT-TYPE SYNOPTIC MODEL

### *SYNONYMS AND DESCRIPTIONS:*

Epithermal veins; volcanic disseminated Au. Epithermal vein and/or disseminated deposits (often co-occurring) of Au and Au-bearing minerals in or associated with a variety of fault zones, breccia zones, fracture zones, shear zones, and diatremes in volcanic and spatially associated rock types. Formed at relatively shallow depths (< 1 km) below paleosurface in geothermal system. May be divided into low-sulfidation systems (LS) characterized by adularia-sericite alteration or (high-sulfidation systems (HS) characterized by acid-sulfate alteration. Systems may be Au-dominated (LS or HS) or Ag-dominated (LS).

### *COMMODITIES (principal recovered products; by-products in parentheses):*

LS: Au, Ag, Zn, Pb, (Cu, Sb, As, Hg, Se)

HS: Cu, Au, Ag, As, (Pb, Hg, Sb, Te, Sn, Mo, Bi)

### *EXAMPLES (including notable deposits outside of the Great Basin):*

*Vein mineralization generally more common than disseminated:*

Aurora (Nevada), Bullfrog (Nevada; Ag-dominated), Comstock (Nevada; Ag-dominated), Goldfield (Nevada), Rawhide (Nevada), Rochester (Nevada; Ag-dominated), Sleeper (Nevada), Tonopah (Nevada; Ag-dominated), Oatman (Arizona), Bodie (California), Zaca (California; Ag-dominated), Cripple Creek (Colorado), Silverton-Telluride (Colorado), Summitville (Colorado), Silver City-Delamar (Idaho; Ag-dominated), Republic (Washington), Guadalupe y Calvo (Chihuahua), Guanacevi (Durango; Ag-dominated), Tayoltita (Durango; Ag-dominated), Guanajuato (Guanajuato; Ag-dominated), Pachuca (Hidalgo; Ag-dominated), El Oro (Michoacan), Abangares (Costa Rica), San Sebastian (El Salvador), El Rosario (Honduras; Ag-dominated), Coco mine (Nicaragua), and Pis Pis (Nicaragua).

*Disseminated mineralization generally more common than vein:*

Hollister-Ivanhoe (Nevada), Paradise Peak (Nevada), Round Mountain (Nevada), Golden Sunlight (Montana), Los Cacaos (Dominican Republic), Montana Tunnels (Montana), and Pueblo Viejo (Dominican Republic).

### *TYPICAL GRADE AND TONNAGE (Troy ounces; U.S. short tons):*

*LS generally higher than HS*

*Vein deposits:*

Gold: 0.06-0.79 to 1.7; up to 2.24 oz/t

Silver: 0.047-0.3 to 3-30; up to 73 oz/t

Tonnage: 0.07-8.8 to 20-90; up to 118 million tons

*Disseminated deposits:*

Gold: 0.034-0.14 to 0.55; up to 1.1 oz/t

Silver: 0.08-3.5 to 5 oz/t

Tonnage: 0.12 to 12.3-86; up to 195 million tons

### *ASSOCIATED DEPOSIT TYPES (other genetically related deposit types):*

Volcanic rock-hosted vein and disseminated mineralization commonly co-occur. Mantos and vein deposits in sedimentary rocks may occur with vein deposits. Granite molybdenite systems may occur with vein and/or disseminated deposits hosted by high-silica rhyolite. Sedimentary rock-hosted disseminated Au may be spatially associated with volcanic rock-hosted disseminated Au mineralization.

**Table 3.2.** Synoptic mineral deposit model for volcanic rock-hosted gold-silver deposits. This model is derived from the attributes of North American "giant" deposits ( $\geq 1,000,000$  Troy ounces Au production and/or reserves), and is primarily based on, but not limited to, deposits in the Great Basin.

**GEOLOGIC SETTING:**

**LS:** Geothermal environment.

**HS:** Volcanic-hydrothermal environment, closer to volcanic centers.

Volcanic centers in tectonic mobile belts or in anorogenic or extensional tectonic regimes. Commonly, but not necessarily, associated with volcanic collapse structures.

**MINERALIZED AND HOST ROCKS:**

Felsic to intermediate calc-alkaline volcanics most common; in some cases alkaline volcanics (e.g.—Cripple Creek, Colorado). Accompanying mafic volcanics, subvolcanic and epizonal plutons, volcaniclastic, and sedimentary rocks sometimes mineralized. Includes rhyolite, rhyodacite, latite, dacite, andesite, trachyandesite, trachyte, phonolite, basalt, granite, shale, sandstone, conglomerate. Acid-altered rock, a silica residue termed vuggy quartz, is commonly the ore host in HS deposits. High-silica rhyolite source rocks typically produce Ag-dominated deposits.

**ASSOCIATED ROCKS (*spatially associated non-mineralized igneous rocks*):**

Intermediate to felsic calc-alkaline or alkaline pre-ore volcanic, subvolcanic, and plutonic rocks; mafic rocks may be present. Includes rhyolite, rhyodacite, latite, dacite, andesite, trachyte, phonolite, monchiquite, vogesite, basalt, olivine basalt, tonalite, granodiorite, diorite, monzonite, and syenite. Post-ore igneous rocks rare.

**FORM OF DEPOSIT (*ore body and gold mineralization*):**

**LS:** Open-space vein fillings dominant, stockwork ore common. Disseminated and replacement ore minor.

**HS:** Disseminated ore dominant, replacement ore common. Stockwork ore minor, veins commonly subordinate.

***Vein deposits:***

Au-bearing quartz-carbonate-sulfide veins in, or spatially associated with various faults (high-angle normal, listric normal, detachment structures, and strike-slip), shear zones, breccia zones, fracture zones, and diatremes. Formed at relatively shallow depths (< 1 km) below paleosurface by open-space filling. Includes stringers, stockworks, sheeted veinlet systems, and single or multiple anastomosing, sigmoidal, and bifurcating veins; rhythmic banding, crustification, and comb textures typical. Larger veins contain high-grade ore shoots, and involve replacement mineralization. Disseminated mineralization surrounding veins common. Except in alkaline rock-related systems (e.g.—Cripple Creek, Colorado), vein systems show distinct vertical zoning; a "barren gap" occurs below bonanza Au and other Au-Ag mineralization, and above deeper Ag-rich and base-metal mineralization. The productive horizon within a district is typically domal and delimited by changes in grade and type of mineralization. Some systems Au-dominated near surface, passing downward into Ag-dominated, grading into base-metal dominated at depth. Zonation may be telescoped, or more generally expressed as a precious-metal zone overlying a base-metal zone. Zonation may not be consistent within an individual orebody, within a deposit, or between deposits within a district. Volcanic rock-hosted disseminated deposits gradational with vein deposits.

***Disseminated deposits:***

Disseminations of medium- to fine-grained ore minerals in diatremes, breccia zones, surrounding vein and shear zones, and proximal to changes in attitude of major vein systems; usually within zones of pervasive silicification. Disseminations may also occur as uniformly dispersed or wispy masses within large vein systems. Quartz-carbonate veins commonly present. Most disseminated deposits show precious and base-metal zonation as a function of depth; Au-dominated near paleosurface, passing downward into Ag-dominated, grading into base-metal dominated at depth. Zoning may be telescoped, or more generally expressed as a precious-metal zone overlying a base-metal zone. Zonation may not be consistent between deposits in same district. Volcanic rock-hosted vein deposits gradational with disseminated deposits.

**Table 3.2,** continued.

**ORE CONTROLS:***Vein deposits:*

Structure; fracture, fault, breccia, and shear zones. Changes in pressure-temperature-composition conditions.

*Disseminated deposits:*

Usually structure, but may be concealed. Permeable zones; breccia pipes, shear and fracture zones. Areas surrounding major bends or strike change of vein systems. Changes in pressure-temperature-composition conditions.

**MINERALOGY (mode of gold occurrence in ore; other metallic, accessory and gangue minerals):***Vein deposits:*

Native Au: as microscopic to visible grains, plates, wires, clots, fracture fillings, and crystalline masses interstitial to and replacing gangue; as inclusions in, and as fine grained coating on, pyrite and other sulfides. Au-bearing tellurides (calaverite, krennerite, petzite, sylvanite, and nagyagite) major ore minerals in alkaline rock-related systems. Other important ore minerals may include native Ag, argentite, and Ag-bearing As-Sb sulfosalts and selenides. Cinnabar, realgar, stibnite, and tetrahedrite may be locally important. Principal base-metal sulfides and ferroalloy minerals include pyrite, arsenopyrite, chalcopyrite, galena, sphalerite, and bornite. Main gangue minerals are quartz and calcite. Fluorite, barite, alunite, and adularia locally may be main gangue minerals. Cryptocrystalline quartz, various carbonates, and sheet silicates also present in gangue. Ag-dominated deposits are distinguished from Au-dominated deposits by relative abundance of sulfosalts (especially ruby silvers) and base-metal sulfides, and by the general absence of As-, Sb-, and Hg-bearing phases. Au-dominated deposits are relatively enriched in As- and Sb-bearing minerals and may be depleted in base-metal sulfides. Ag-dominated deposits may be relatively enriched in Se-bearing phases whereas Au-dominated deposits may show Te-bearing phases.

*Disseminated deposits:*

Native Au: as submicroscopic to microscopic grains of Au dispersed in gangue (sometimes encapsulated in quartz), as inclusions in disseminated pyrite, and less commonly as fine-grained coatings on sulfide grains. Au-bearing tellurides (calaverite, krennerite, petzite, sylvanite, and nagyagite) locally major ore minerals. Other important ore minerals include native Ag, argentite, and Ag-bearing As-Sb sulfosalts and selenides. Cinnabar, realgar, stibnite, and tetrahedrite may be locally important. Principal base-metal sulfides and ferroalloy minerals include pyrite, arsenopyrite, chalcopyrite, galena, sphalerite, and bornite. Main gangue minerals are quartz and calcite. Fluorite, barite, alunite and adularia locally may be main gangue minerals. Cryptocrystalline quartz, various carbonates, and sheet silicates also present in gangue. Ag-dominated deposits are distinguished from Au-dominated deposits by relative abundance of sulfosalts (especially ruby silvers) and base-metal sulfides, and by the general absence of As-, Sb-, and Hg-bearing phases. Au-dominated deposits are relatively enriched in As- and Sb-bearing minerals and depleted in base-metal sulfides. Ag-dominated deposits may be relatively enriched in Se-bearing phases whereas Au-dominated deposits may show Te-bearing phases.

**LS:** Low-sulfidation state minerals. Distinguished from HS by common occurrence of Zn-Pb minerals (sphalerite and galena), and electrum. Ore mineralogy generally less diverse than HS, as reflected by higher Ag/Au ratio.

**HS:** High-sulfidation state sulfide minerals. Distinguished from LS by common occurrence of Cu-As minerals (enargite-group minerals, chalcopyrite, tennantite, covellite) and Au-Ag tellurides (usually present but seldom in major amounts).

**ALTERATION:**

**LS:** Quartz-adularia-sericite±carbonate assemblage shows silicification and K-metasomatism in or immediately adjacent to veins or near disseminated ore bodies, and grades outward to kaolinite and illite or sericite marginal to ore bodies, to outermost propylitic zone (possibly extensive). Adularia is the characteristic alteration mineral, which does not occur in HS systems and indicates near neutral pH and reducing conditions.

**Table 3.2,** continued.

**HS:** Advanced argillic assemblages (quartz-alunite±sericite±kaolinite±S±barite±pyrophyllite±zunyite±diaspore) in and adjacent to veins or near disseminated ore bodies, and grades outward to sericitic-argillic zone, to outermost propylitic zone. Outermost propylitic zone commonly of regional extent. Alunite is the characteristic alteration mineral, which is not common to LS systems and indicates relatively acidic and oxidizing conditions.

**AGE RANGE:**

**Host:** Tertiary; few Paleozoic and Mesozoic (Tertiary in Nevada)

**Ore:** Same as host rock; most formed between 27 to 5 Ma in Nevada

**GENETIC MODEL:**

Au mineralization at shallow depths (within ~1 km) below paleosurface in geothermal or hot springs system (LS) or volcanic hydrothermal system (HS). Mineralizing system forms during waning stages of magmatic events, contemporaneous to extension, and during waning extensional activity. Formed in relatively short order (0.05-0.5 to 3 m.y.) under conditions of unrestricted flow (high-permeability). Deeply circulating fluids leach metals at depth from volcano-sedimentary pile (underlying rocks) and exit along structural channel ways. Mineralization is episodic, taking place when system ruptures, rapidly releasing confining pressure and decreasing temperature. After physiochemical equilibrium is achieved, the system seals for another cycle of mineralization. Ore minerals precipitate as fluids boil (effervesce) and/or mix (dilution) with cooler oxygenated ground waters. Bisulfide, thiosulfide, or other complexes that are not well understood (e.g.—cyanide or arsenide complexes) may transport Au in upper levels of system; chloride complexes in lower levels. Vertical metal zoning common; base-metal zone often underlies precious metal zone.

**LS:** Form from near neutral-pH, reduced waters close to equilibrium with host rocks. Fluids are low-salinity (<1 wt% NaCl equiv.), relatively gas-rich (1-2 wt% CO<sub>2</sub>, subordinate H<sub>2</sub>S), at 140 to 325°C (240°C average during precious metal deposition), and are meteoric-water dominant; however, there is evidence for an early magmatic component that may also introduce ore metals to the system. Boiling is the critical process to deposit high concentrations of Au.

**HS:** Processes responsible for Au deposition are not understood since the ore fluid has not been characterized fully, though ore minerals, and hence ore fluid, evolve with time to less acidic and more reduced conditions. Have a significant magmatic component throughout their history, particularly in the early, leaching stage when the fluid is most acidic and oxidized. Meteoric-water involvement may increase as magmatic plume collapses. A continuum may exist between hydrothermal processes related to mineralization in a porphyry to an epithermal environment (suggesting critical link to late magmatic fluid input).

**COMPILED FROM:**

Berger and Eimon (1982), Berger and Henley (1989), Berger and Bonham (1990), Bonham (1988), Buchanan (1981), Cox and Singer (1986), Cox et al. (1991), Dewelley (1984), Douglas et al. (1982), Durning and Buchanan (1984), Gott et al. (1969), Hayba et al. (1985), Heald et al. (1987), Hedenquist (1997), Hedenquist and Lowenstern (1994), Hedenquist et al. (1996), Henry et al. (1997), Henley (1983), John et al. (1991), Henry et al. (1997), Kesler et al. (1981), Krupp and Seward (1987), Lindgren and Ransome (1906), Ludington et al. (1993), Mills (1984), Mosier et al. (1986), Nash et al. (1991), O'Neil et al. (1973), Panteleyev (1986), Porter and Ripley (1985), Randall (1972), Russell et al. (1986), Seedorff (1991), Seward (1989), Silberman (1983), Sillitoe et al. (1985), Sillitoe (1995), Smith et al. (1982), Stoffregen (1987), Swinden (1984), Taylor (1996), Thompson et al. (1985), Thorman and Christensen (1991), Tingley and Berger (1985), White (1981), and White and Heropoulos (1983).



DATA SET	DATA TYPE	OBJECT-TYPE	SOURCE DATA	NUMBER OF ENTITIES	SIZE (bytes)	COVERAGE	DATASET SOURCE(S)
----------	-----------	-------------	-------------	--------------------	--------------	----------	-------------------

REGIONAL GEOLOGY							
<b>Bedrock and Surficial Geology</b>	Nominal	Line, Area	ARC INFO, Vectors	84,955	36,778,743	Nevada	Turner and Bawiec (1991)
<b>Metamorphic Rocks</b>	Nominal	Line, Area	SPANS, Digitized Lines	158	108,228	Nevada	Ernst (1992)
<b>Metamorphic Core Complex Locations</b>	Binary	Point	SPANS, Digitized Points	25	2,145	Great Basin	Axen et al. (1993)
<b>Corridor of Metamorphic Core Complex Distribution</b>	Binary	Line, Area	SPANS, Digitized Lines	1	490	Great Basin	Axen et al. (1993)
<b>Volcanic Centers</b>	Nominal	Line, Area	SPANS, Digitized Lines	77	46,629	Nevada	Stewart (1980)
<b>Cinder Cones</b>	Binary	Point	SPANS, Digitized Points	19	757	Nevada	Horton (1964)
<b>Mesozoic Plutons Distribution Percentage</b>	Ordinal	Line, Area	SPANS, Digitized Lines	3	3,456	Nevada	Barton (1990)

**Table 5.1.** The geoscience datasets composing the Nevada and Great Basin GIS database. The data are grouped by discipline and characterized by: *DATASET*–the data composing a dataset; *DATA TYPE*–the scale of measurement in which the data are expressed; *OBJECT-TYPE*–the spatial object-type of the dataset as it exists after processing with SPANS GIS; *SOURCE DATA*–the file format, and/or spatial data model (raster or vector), and/or spatial object-type of the dataset as it was obtained, before pre-processing and integration into the database; *NUMBER OF ENTITIES*–the number of sample points or arcs making up the dataset; *SIZE*–the approximate size in bytes of the source data file; *COVERAGE*–the areal extent of the dataset and distribution of points where appropriate; *DATASET SOURCE(S)*–the origin of the source dataset and/or source of the data composing the dataset.

DATA SET	DATA TYPE	OBJECT-TYPE	SOURCE DATA	NUMBER OF ENTITIES	SIZE (bytes)	COVERAGE	DATASET SOURCE(S)
<b>Cordilleran Geosyncline Facies Boundaries</b>	Nominal	Line	SPANS, Digitized Lines	3	18,052	Nevada	Thorman and Christensen (1991)
<b>Regions of Strong Upper Crustal Extension</b>	Binary	Line, Area	SPANS, Digitized Lines	24	33,300	Nevada	Wernicke (1992)
<b>Fault Coverage—Nevada</b>	Binary	Line	ARC INFO, Vectors	13,471	~ 3,116,375	Nevada	Sawatzky (1992, personal communication), from Stewart and Carlson (1978)
<b>Fault Coverage—Historical</b>	Binary	Line	Generic ASCII Plotter Output File	116	39	Nevada	Dohrenwend (1995, personal communication), from unpublished maps
<b>Fault Coverage—Holocene</b>	Binary	Line	Generic ASCII Plotter Output File	489	118,242	Nevada	Dohrenwend (1995, personal communication), from unpublished maps
<b>Fault Coverage—Holocene - Late Pleistocene</b>	Binary	Line	Generic ASCII Plotter Output File	860	209,004	Nevada	Dohrenwend (1995, personal communication), from unpublished maps
<b>Fault Coverage—Late Pleistocene</b>	Binary	Line	Generic ASCII Plotter Output File	1,169	319,494	Nevada	Dohrenwend (1995, personal communication), from unpublished maps
<b>Fault Coverage—Offsetting Volcanics</b>	Binary	Line	Generic ASCII Plotter Output File	2,374	604,221	Nevada	Dohrenwend (1995, personal communication), from unpublished maps
<b>Fault Coverage—Undifferentiated</b>	Binary	Line	Generic ASCII Plotter Output File	1,979	509,379	Nevada	Dohrenwend (1995, personal communication), from unpublished maps

Table 5.1, continued.

DATA SET	DATA TYPE	OBJECT-TYPE	SOURCE DATA	NUMBER OF ENTITIES	SIZE (bytes)	COVERAGE	DATASET SOURCE(S)
<b>Fault Coverage—Undated</b>	Binary	Line	Generic ASCII Plotter Output File	2,778	773,232	Nevada	Dohrenwend (1995, personal communication), from unpublished maps
<b>Fault Coverage—Regional</b>	Binary	Line	ARC INFO, Vectors	18,549	4,291,117	Great Basin	Sawatzky (1992, personal communication)
<b>Strike-Slip Faults</b>	Binary	Line	SPANS, Digitized Lines	96	9,376	Nevada	Putnam III and Henriques (1991); Modified from Shawe (1965)
<b>Golconda Thrust Front</b>	Binary	Line	SPANS, Digitized Lines	1	1,568	Great Basin	Stewart (1980)
<b>Roberts Mountain Thrust Front</b>	Binary	Line	SPANS, Digitized Lines	1	1,247	Great Basin	Stewart (1980)
<b>Deep-Seated Basement Fracture Systems</b> (Interpreted from aeromagnetic data)	Binary	Line	SPANS, Digitized Lines	126	12,834	Nevada	Blakely (1988)
<b>Furnace Creek Fault</b>	Binary	Line	SPANS, Digitized Lines	1	6,051	Great Basin	Poole et al. (1992)
<b>Garlock Fault</b>	Binary	Line	SPANS, Digitized Lines	1	4,917	—	Poole et al. (1992)
<b>Las Vegas Fault</b>	Binary	Line	SPANS, Digitized Lines	1	2,867	Nevada	Poole et al. (1992)
<b>San Andreas Fault</b>	Binary	Line	SPANS, Digitized Lines	1	19,629	—	Poole et al. (1992)

Table 5.1, continued.

DATA SET	DATA TYPE	OBJECT-TYPE	SOURCE DATA	NUMBER OF ENTITIES	SIZE (bytes)	COVERAGE	DATASET SOURCE(S)
Stewart Valley Fault	Binary	Line	SPANS, Digitized Lines	1	3,056	Great Basin	Poole et al. (1992)
Snake River Fault	Binary	Line	SPANS, Digitized Lines	1	4,674	—	Poole et al. (1992)
Antler Orogenic Belt	Binary	Line	SPANS, Digitized Lines	1	20,388	Great Basin	Poole et al. (1992)
Sevier Orogenic Belt	Binary	Line	SPANS, Digitized Lines	8	37,023	Great Basin	Poole et al. (1992)
Sonoma Orogenic Belt	Binary	Line	SPANS, Digitized Lines	1	21,630	Great Basin	Poole et al. (1992)
Northeastern Snake River Plain Outline	Binary	Line	SPANS, Digitized Lines	1	17,439	Great Basin	Oppenheimer (1995, personal communication), source unknown
Lithotectonic Terranes	Nominal	Line, Area	ARC INFO, Vectors	145	222,475	Great Basin	Raines (1995, personal communication), from Silberling et al. (1987); Silberling (1991)
Attitude of Tertiary Rocks	Interval	Point, Surface	SPANS, Digitized Points	392	13,695	Nevada, Irregular Distribution	Stewart (1978)
<b>PHYSICAL GEOGRAPHY</b>							
Elevation / Topography (30 Arc-Second Grid)	Interval	Surface	Raster	—	77,000,000	Western US, Great Basin ~ 801 m Grid	U.S. Geological Survey (1996)
Elevation / Topography (5 Arc-Minute Grid)	Interval	Point, Surface	ASCII Flat File, Points	11,664	315,221	Great Basin ~ 8 km Grid	Hittelman et al. (1990)

Table 5.1, continued.

DATA SET	DATA TYPE	OBJECT-TYPE	SOURCE DATA	NUMBER OF ENTITIES	SIZE (bytes)	COVERAGE	DATASET SOURCE(S)
<b>Mountain Peak Heights</b>	Interval	Point, Surface	SPANS, Digitized Points	417	26,697	Nevada	U.S. Geological Survey (1984)
<b>Great Basin Physiographic Province</b> (Generalized)	Binary	Line, Area	SPANS, Digitized Lines	1	4,427	Great Basin	Wilkins (1984)
<b>Great Basin Physiographic Province</b> (Detailed)	Binary	Line, Area	SPANS, Digitized Lines	1	12,077	Great Basin	Thelin and Pike (1991)
<b>GEOPHYSICS</b>							
<b>Gravity Anomaly - Observed, Free Air, Bouguer, Isostatic</b>	Interval	Point, Surface	ASCII Flat File, Points	79,704	8,156,456	Nevada, Irregular Distribution	Hittelman et al. (1992)
<b>Geomagnetism - Total Residual Field Anomaly</b>	Interval	Point, Surface	ASCII Flat File, Points	288,983	8,669,771	Nevada, 1 km Grid	Buhmann (1992, personal communication)
<b>Geothermal Heat Flow</b>	Interval	Point, Surface	ASCII Flat File, Points	1,080	85,933	Great Basin, Irregular Distribution	Blackwell (1994, personal communication); Hittelman et al. (1990)
<b>Geothermal Conductivity</b> (Gradient)	Interval	Point, Surface	ASCII Flat File, Points	1,059	86,124	Great Basin, Irregular Distribution	Blackwell (1994, personal communication)
<b>Geothermal Heat Production</b>	Interval	Point, Surface	ASCII Flat File, Points	1,059	86,124	Great Basin, Irregular Distribution	Blackwell (1994, personal communication)
<b>Geothermal Wells/Springs Temperature</b>	Interval	Point, Surface	SPANS, Digitized Points	795	77,609	Nevada	Trexler et al. (1983); Berry et al. (1980)

Table 5.1, continued.

DATA SET	DATA TYPE	OBJECT-TYPE	SOURCE DATA	NUMBER OF ENTITIES	SIZE (bytes)	COVERAGE	DATASET SOURCE(S)
<b>Paleothermal Anomaly</b>	Binary	Line, Surface	SPANS, Digitized Lines	1	3,846	Nevada	Cunningham (1988); Harris et al. (1980)
<b>SEISMOLOGY</b>							
<b>Crustal Thickness</b> (Depth to Reflection Moho)	Interval	Point, Surface	SPANS, Digitized Points	103	3,663	Great Basin, Irregular Distribution	Allenby and Schnetzler (1983); Smith et al. (1989)
<b>Seismicity</b> (Earthquake density, depth to focus, and magnitude)	Interval	Point, Surface	ASCII Flat File, Points	15,045	681,140	Great Basin	Hittelman et al. (1990)
<b>Orientation of Minimum Principal Crustal Stress</b> ( 0-5 Ma, 5-38 Ma, 38-65 Ma)	Interval	Line	SPANS, Digitized Lines	118	11,991	Nevada, Irregular Distribution	Eaton (1982); Zoback et al. (1981)
<b>GEOCHEMISTRY</b>							
<b>Radiometric Ages— Igneous Rocks (RAD-B)</b>	Ratio	Point, Surface	ASCII Flat File, Points	4,819	1,041,127	Great Basin, Irregular Distribution	Ward (1991, personal communication)
<b>Radiometric Ages— Metallic Mineralization</b>	Ratio	Point, Surface	ASCII Flat File, Points	157	59,644	Nevada, Irregular Distribution	Bonham (1982); Buchanan (1981); Dreier (1984); Jones (1989); Kuehn (1989); Nobel et al. (1988); Mosier et al. (1986); Seedorff (1991); Silberman et al. (1976); Stager and Tingley (1988); Thorman and Christensen (1991); Tooker (1985); Vikre et al. (1988); White (1985); White and Heropoulos (1983); Wilkins (1984)

Table 5.1, continued.

DATA SET	DATA TYPE	OBJECT-TYPE	SOURCE DATA	NUMBER OF ENTITIES	SIZE (bytes)	COVERAGE	DATASET SOURCE(S)
<b>Strontium Isotope—<sup>87</sup>Sr/<sup>86</sup>Sr Initial Values</b>	Ratio	Point, Surface	ASCII Flat File, Points	511	52,847	Great Basin, Irregular Distribution	Bacon et al (1984); Edwards and McLaughlin (1972); Elison et al (1990); Farmer (1989); Gans et al (1989); Kistler (1993, personal communication); Kistler and Ross (1990); Kistler and Lee (1989); Lee et al (1986); Leeman (1970); Ormerod (1988); Saleeby et al (1987)
<b><sup>87</sup>Sr/<sup>86</sup>Sr I<sub>Sr</sub> = 0.706 Isoleth</b>	Nominal	Line	SPANS, Digitized Lines	3	7,969	Great Basin	Farmer and DePaolo (1983); Kistler and Ross (1990)
<b><sup>87</sup>Sr/<sup>86</sup>Sr I<sub>Sr</sub> = 0.706 Isoleth, Restored</b>	Nominal	Line	SPANS, Digitized Lines	1	1,486	Great Basin	Levy and Christie-Blick (1989)
<b><sup>87</sup>Sr/<sup>86</sup>Sr I<sub>Sr</sub> = 0.708 Isoleth</b>	Nominal	Line	SPANS, Digitized Lines	1	783	Great Basin	Farmer and DePaolo (1983); Kistler and Ross (1990)
<b>NURE</b> (Major and Minor Element Geochemistry)	Ratio	Point, Surface	ASCII Flat File, Points	Varies by Element	> 10,000	Nevada	Hoffman et al. (1991)
<b>PETROS</b> (Igneous Rock Major Element Geochemistry)	Ratio	Point, Surface	ASCII Flat File, Points	37,300	8,196,802	Global	Mutschler et al. (1981)
<b>REMOTE SENSING</b>							
<b>Linear Features From LANDSAT Imagery</b>	Binary	Line	ARC INFO, Vectors	6,398	1,410,596	Great Basin	Sawatzky (1992, personal communication)
<b>Radar Imagery</b>	—	—	(on microfiche)	—	—	Portions of Nevada	U.S. Geological Survey (1990a)

Table 5.1, continued.



DATA SET	DATA TYPE	OBJECT-TYPE	SOURCE DATA	NUMBER OF ENTITIES	SIZE (bytes)	COVERAGE	DATASET SOURCE(S)
<b>AVHRR Satellite Imagery</b>	Nominal	Surface	Raster	—	Variable	Conterminous US	U.S. Geological Survey (1990b)
<b>ECONOMIC GEOLOGY</b>							
<b>MRDS Metallic Mineral Occurrences</b>	Binary, Nominal, Ordinal	Point, Surface	ASCII Flat File, Points	6,197	7,295,344	Nevada	U. S. Geological Survey (1993; 1995)
<b>Mineralization Belts and Trends</b>	Binary	Line	SPANS, Digitized Lines	22	4,816	Nevada	Roberts (1966); Shawe and Stewart (1976)
<b>MAS Minerals Availability System</b>	Binary, Nominal, Ordinal	(Attributes)	ASCII Flat File	7,571	6,269,300	Nevada	U. S. Bureau of Mines (1992)
<b>Million Ounce Gold Camps</b> (current through 1984)	Binary, Ratio	Point	ASCII Flat File, Points	15	9,000	Nevada	Mihalasky (1988)
<b>HYDROLOGY</b>							
<b>Drainage Divides</b>	Nominal	Line, Area	SPANS, Digitized Lines	46	108,489	Nevada	Archbold (1972)
<b>Streams</b>	Binary	Line	DLG, Vectors	2,363	2,780,800	Nevada	U.S. Geological Survey (1990c)
<b>Water Bodies</b>	Binary	Line, Area	DLG, Vectors	1,164	1,246,560	Nevada	U.S. Geological Survey (1990c)
<b>HUMAN FEATURES</b>							
<b>Major Cities</b>	Binary	Point	SPANS, Digitized Points	153	10,445	Nevada	Nichols and Lutsey (1972)

Table 5.1, continued.

DATA SET	DATA TYPE	OBJECT-TYPE	SOURCE DATA	NUMBER OF ENTITIES	SIZE (bytes)	COVERAGE	DATASET SOURCE(S)
<b>County Borders</b>	Nominal	Line	DLG, Vectors	327	386,880	Nevada	U.S. Geological Survey (1990c)
<b>Nevada State Border—High Resolution</b>	Binary	Line, Area	ARC INFO, Vectors	1	342,000	Nevada	Turner and Bawiec (1991)
<b>Nevada State Border—Low Resolution</b>	Binary	Line	DLG, Vectors	1	54,170	Nevada	U.S. Geological Survey (1990c)
<b>Borders of Neighbouring States</b>	Nominal	Line	DLG, Vectors	176	57,738	—	U.S. Geological Survey (1990c)
<b>Roads and Highways</b>	Binary	Line	DLG, Vectors	1,008	1,054,880	Nevada	U.S. Geological Survey (1990c)
<b>Railways</b>	Binary	Line	DLG, Vectors	397	449,920	Nevada	U.S. Geological Survey (1990c)

*Table 5.1*, continued.

<i>Sample</i>		<i>Primary Gold-Silver</i>	<i>Sedimentary Rock-Host.</i>	<i>Volcanic Rock-Host.</i>
<i>Sub-Sample</i>	<i>Large</i>	59	8	33
	<i>Medium</i>	118	30	43
	<i>Small</i>	2269	57	317
	<i>Unknown</i>	244	3	22
<i>Grand Totals:</i>		2690	98	415

**Table 5.2.** Total number of observations in all gold-silver-bearing occurrence-type samples.

Binary Map	Area of Pattern Present (km <sup>2</sup> )	Occurrences	W <sup>+</sup>	Stdev (W <sup>+</sup> )	W <sup>-</sup>	Stdev (W <sup>-</sup> )	C	Stdev (C)	Stud C C/Stdev(C)	Description of Binary-Class Predictor Map
------------	--	-------------	----------------	-------------------------	----------------	-------------------------	---	-----------	----------------------	---

<i>Primary (Occurrences of all Sizes and Types) Mineral Potential Model Evidence Layers and Associated Weights</i>										
BANABIPR	21740	445	<b>0.7790</b>	0.0479	<b>-0.1019</b>	0.0212	0.8809	0.0524	16.8176	Ba/Na geochemical anomaly (mainly soil and sediment samples)
BFFTBIPIR	77225	1361	<b>0.6264</b>	0.0273	<b>-0.3898</b>	0.0275	1.0162	0.0388	26.1929	Buffer zones surrounding faults(all types and ages; 0.0, 0.5, 1.0, 1.5, 2.5, 5.0, 10.0 km)
BFPLBIPR	21185	810	<b>1.4221</b>	0.0358	<b>-0.2829</b>	0.0231	1.7050	0.0427	39.9717	Buffer zones surrounding plutons (mainly Mesozoic; 0.0, 0.5, 1.0, 1.5, 2.5, 5.0, 10.0 km)
GEDVBIPR	43805	1070	<b>0.9598</b>	0.0310	<b>-0.3418</b>	0.0249	1.3016	0.0397	32.7513	Diversity of lithology (units per 2.5 X 2.5 km neighbourhood cell; geologic map of Nevada)
GEOBIHI	2925	342	<b>2.6252</b>	0.0575	<b>-0.1267</b>	0.0207	2.7520	0.0612	44.9958	Lithology—higher W <sup>+</sup> (geologic map of Nevada)
GEOBILOW	11473	349	<b>1.1853</b>	0.0544	<b>-0.0985</b>	0.0208	1.2838	0.0582	22.0630	Lithology—lower W <sup>+</sup> (geologic map of Nevada)
GEOBIMED	12761	709	<b>1.8140</b>	0.0386	<b>-0.2620</b>	0.0226	2.0760	0.0447	46.3991	Lithology—medium W <sup>+</sup> (geologic map of Nevada)
GISOBIPR	152680	1792	<b>0.2139</b>	0.0238	<b>-0.3252</b>	0.0335	0.5391	0.0411	13.1306	Isostatic gravity anomaly
KNABIPR	4398	153	<b>1.3241</b>	0.0823	<b>-0.0433</b>	0.0199	1.3674	0.0847	16.1493	K/Na geochemical anomaly (mainly soil and sediment samples)
MAGBIPR	81957	1145	<b>0.3904</b>	0.0298	<b>-0.2147</b>	0.0255	0.6052	0.0392	15.4309	Total residual field geomagnetic anomaly
TRRNBIPIR	76290	1166	<b>0.4816</b>	0.0295	<b>-0.2565</b>	0.0257	0.7381	0.0391	18.8573	Lithotectonic (allochthonous) terranes

<i>Sedimentary Rock-Hosted Mineral Potential Model Evidence Layers and Associated Weights</i>										
BANABISD	10604	34	<b>2.2292</b>	0.1718	<b>-0.3880</b>	0.1250	2.6173	0.2125	12.3195	Ba/Na geochemical anomaly (mainly soil and sediment samples)
BFFTBIISD	77225	56	<b>0.7403</b>	0.1337	<b>-0.5291</b>	0.1543	1.2693	0.2042	6.2171	Buffer zones surrounding faults(all types and ages; 0.0, 0.5, 1.0, 1.5, 2.5, 5.0, 10.0 km)
BFPLBIISD	21185	15	<b>0.7164</b>	0.2583	<b>-0.0884</b>	0.1098	0.8048	0.2807	2.8675	Buffer zones surrounding plutons (mainly Mesozoic; 0.0, 0.5, 1.0, 1.5, 2.5, 5.0, 10.0 km)
GEDVBIISD	43805	43	<b>1.0433</b>	0.1526	<b>-0.4097</b>	0.1349	1.4531	0.2036	7.1359	Diversity of lithology (units per 2.5 X 2.5 km neighbourhood cell; geologic map of Nevada)
GEOBIISD	14367	64	<b>2.5593</b>	0.1253	<b>-1.0068</b>	0.1715	3.5661	0.2124	16.7901	Lithology (geologic map of Nevada)
GISOBISD	21401	40	<b>1.6882</b>	0.1583	<b>-0.4461</b>	0.1313	2.1343	0.2057	10.3783	Isostatic gravity anomaly
KNABISD	923	12	<b>3.6390</b>	0.2906	<b>-0.1274</b>	0.1078	3.7664	0.3099	12.1521	K/Na geochemical anomaly (mainly soil and sediment samples)
MAGBIISD	119721	71	<b>0.5390</b>	0.1187	<b>-0.7399</b>	0.1925	1.2789	0.2261	5.6556	Total residual field geomagnetic anomaly
TRRNBIISD	50690	71	<b>1.3993</b>	0.1188	<b>-1.0922</b>	0.1925	2.4914	0.2262	11.0165	Lithotectonic (allochthonous) terranes

**Table 7.1.** Evidence layers for the primary and sedimentary rock-hosted occurrence-type mineral potential models. Light grey rows represent predictor maps removed from the models in an attempt to mitigate severe conditional dependence (see [section 7.4.2](#) and [Appendix C](#) for details). White rows represent predictor maps included in the primary 7-layer (top) and sedimentary rock-hosted 8-layer (bottom) mineral potential models. White and light grey rows represent predictor maps included in the primary 11-layer (top) and sedimentary rock-hosted 9-layer (bottom) mineral potential models (i.e.—conditional dependence was not mitigated). The weighting factors used to combine binary-class predictor maps are highlighted in bold.

Binary Map	Area of Pattern Present (km <sup>2</sup> )	Occurrences	W <sup>+</sup>	Stdev (W <sup>+</sup> )	W <sup>-</sup>	Stdev (W <sup>-</sup> )	C	Stdev (C)	Stud C C/Stdev(C)	Description of Binary-Class Predictor Map
------------	--	-------------	----------------	-------------------------	----------------	-------------------------	---	-----------	----------------------	---

<i>Volcanic Rock-Hosted Mineral Potential Model Evidence Layers and Associated Weights</i>										
BANABIVL	10604	17	<b>0.0901</b>	0.2427	<b>-0.0037</b>	0.0502	0.0937	0.2479	0.3782	Ba/Na geochemical anomaly (mainly soil and sediment samples)
BFFTBIVL	77225	205	<b>0.5954</b>	0.0699	<b>-0.3632</b>	0.0690	0.9587	0.0983	9.7550	Buffer zones surrounding faults(all types and ages; 0.0, 0.5, 1.0, 1.5, 2.5, 5.0, 10.0 km)
BFPLBIVL	21185	81	<b>0.9615</b>	0.1113	<b>-0.1396</b>	0.0548	1.1010	0.1241	8.8751	Buffer zones surrounding plutons (mainly Mesozoic; 0.0, 0.5, 1.0, 1.5, 2.5, 5.0, 10.0 km)
GEDVBIVL	43805	110	<b>0.5397</b>	0.0955	<b>-0.1401</b>	0.0573	0.6799	0.1113	6.1061	Diversity of lithology (units per 2.5 X 2.5 km neighbourhood cell; geologic map of Nevada)
GEOBIVL	21955	194	<b>1.8042</b>	0.0721	<b>-0.5500</b>	0.0673	2.3543	0.0986	23.8679	Lithology (geologic map of Nevada)
GISOBIVL	154093	260	<b>0.1413</b>	0.0621	<b>-0.1997</b>	0.0804	0.3410	0.1015	3.3578	Isostatic gravity anomaly
KNABIVL	3274	9	<b>0.6304</b>	0.3338	<b>-0.0103</b>	0.0497	0.6408	0.3375	1.8987	K/Na geochemical anomaly (mainly soil and sediment samples)
MAGBIVL	50725	136	<b>0.6054</b>	0.0859	<b>-0.2000</b>	0.0599	0.8054	0.1047	7.6925	Total residual field geomagnetic anomaly
TRRNBIVL	41229	191	<b>1.1543</b>	0.0725	<b>-0.4598</b>	0.0668	1.6141	0.0986	16.3648	Lithotectonic (allochthonous) terranes

**Table 7.1, continued.** Evidence layers for the volcanic rock-hosted occurrence-type mineral potential model. Light grey rows represent predictor maps removed from the model in an attempt to mitigate severe conditional dependence (see [section 7.4.2](#) and [Appendix C](#) for details). White rows represent predictor maps included in the volcanic rock-hosted 7-layer mineral potential model. White and light grey rows represent predictor maps included in the volcanic rock-hosted 9-layer mineral potential model (i.e.—conditional dependence was not mitigated). The weighting factors used to combine binary-class predictor maps are highlighted in bold.

# Great Basin Physiographic Province, Southwestern United States

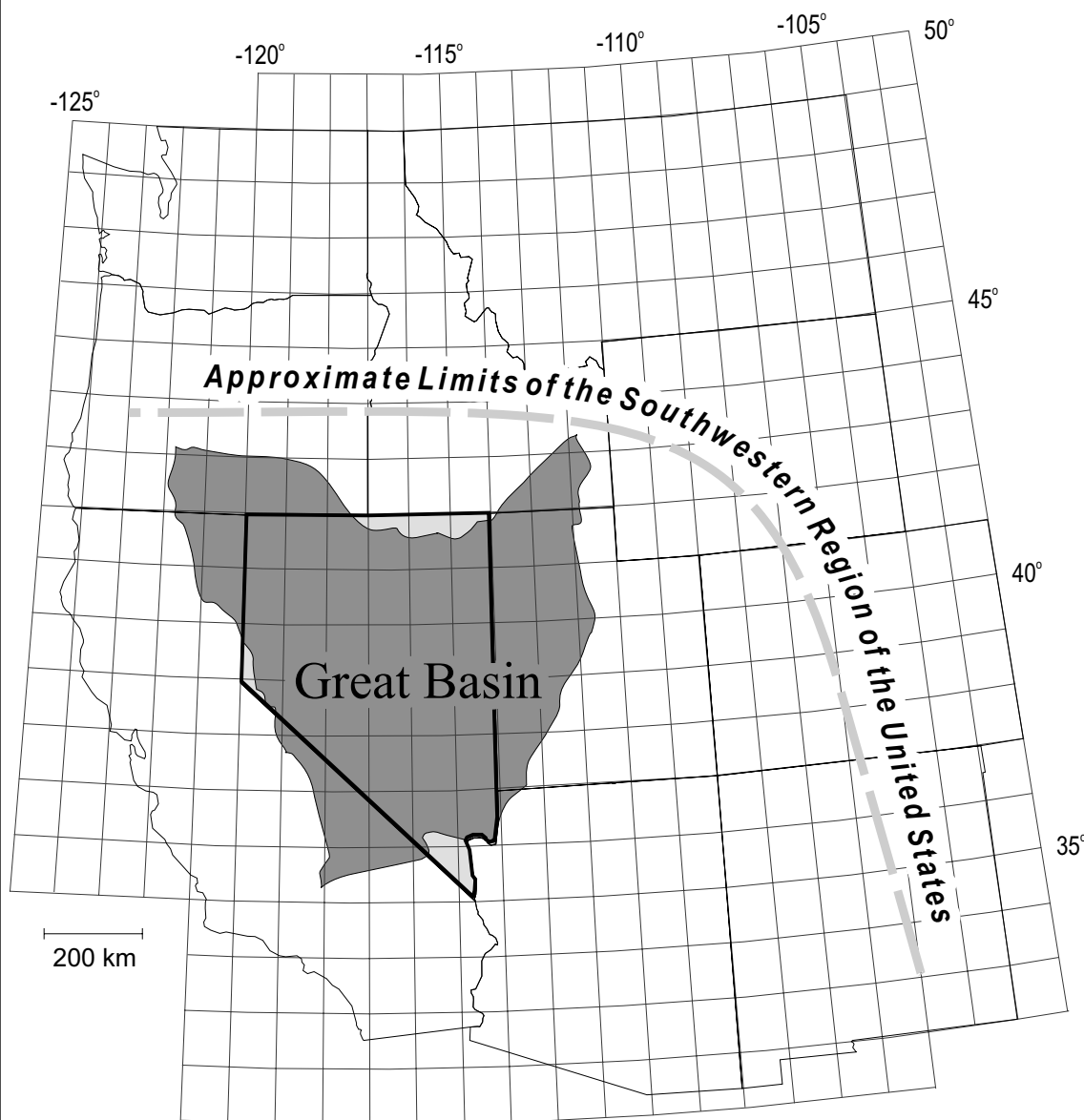


**Figure 1.1.** Location map of the Great Basin (highlighted in darker grey). The State of Nevada is lighter grey and outlined in black. For the purpose of this study, the "southwestern" United States encompasses the region south and west of the grey dashed line, particularly the Great Basin, Colorado Plateau, and southern Basin and Range provinces, as well as part of the Pacific Mountain System, and small portions of the Columbia and Snake River Plateaus and the Rocky Mountain System. The "western" United States is herein defined as those states composing this base; Washington, Idaho, Montana, Oregon, Wyoming, California, Nevada, Utah, Colorado, Arizona, and New Mexico. The Great Basin covers  $\sim 452,340 \text{ km}^2$  (as circumscribed by Thelin and Pike, 1991). Nevada covers  $\sim 283,219 \text{ km}^2$ . The Great Basin occupies about 95% of Nevada. Great Basin boundary from Thelin and Pike (1991).

## *"Basin and Range" Topography*

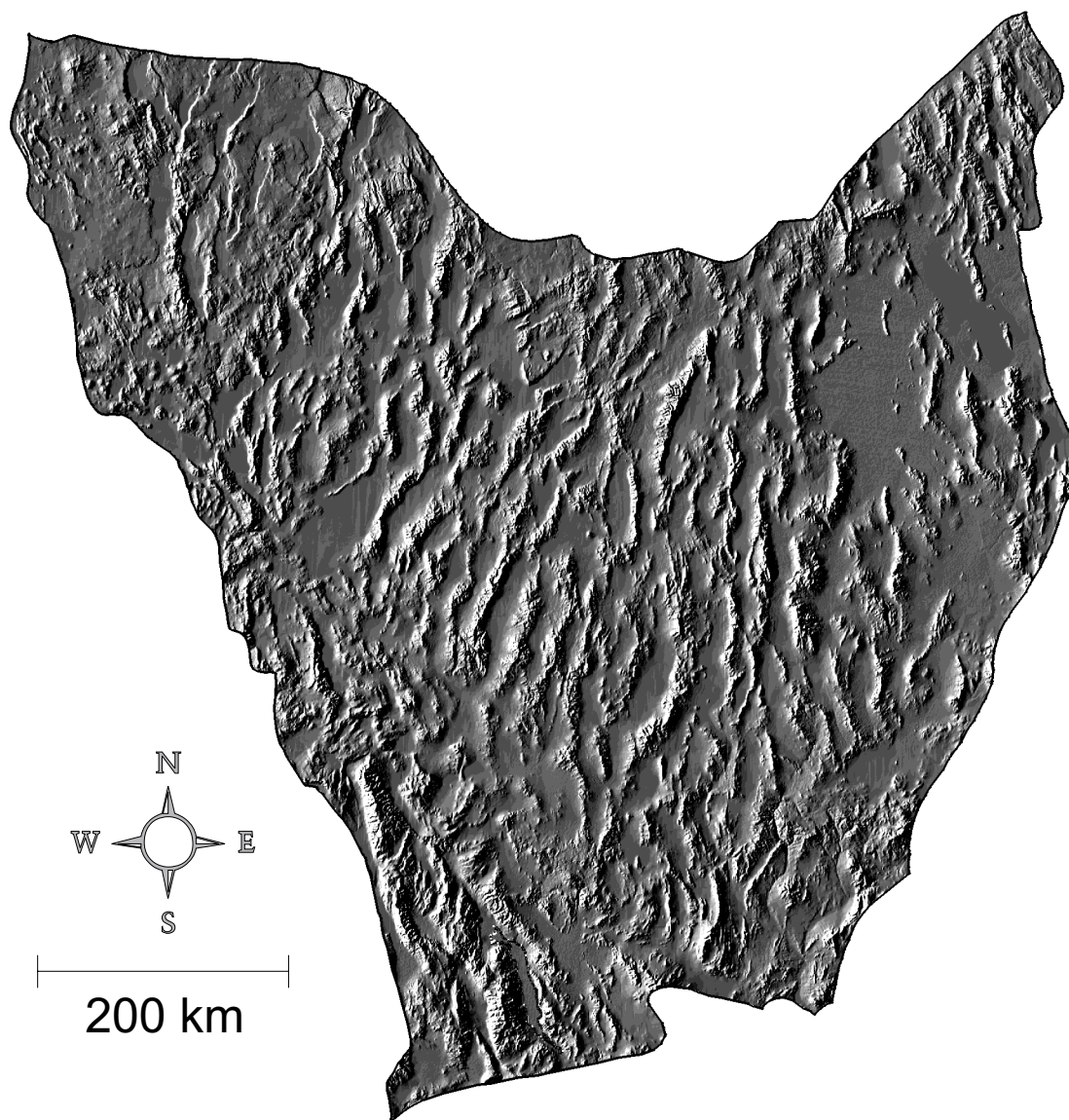


**Figure 1.2.** Shaded relief of the topography of the Great Basin, illuminated by an artificial light source located at 290° azimuth and 45° zenith. *"Basin and Range"* topography consists of alternating, unusually even-spaced, parallel mountain ranges and intervening broad, flat, alluviated desert basins. The ranges and valleys trend roughly north-south ( $\pm 10^\circ$ ) and are typically 15-20 to 50 km across, giving the Great Basin a pronounced north-northeast–south-southwest structural grain. The ranges are large coherent tilted fault blocks, bound on one or more sides by high-angle normal or reverse faults, and the basins are adjacent grabens and half-grabens. The tilts of the fault blocks range from a few degrees to about 30 degrees from horizontal. Basin-range topography was not attained before ~10 Ma (at the earliest), and formed as a result of block-faulting during late (~17-0 Ma) brittle extension of the upper crust. Text modified from Stewart (1978), Wilkins (1984), and Zoback et al., (1981). Great Basin outline from Thelin and Pike (1991). Digital elevation data from U.S. Geological Survey (1996).



## Principal Metallogenic Features of the Great Basin

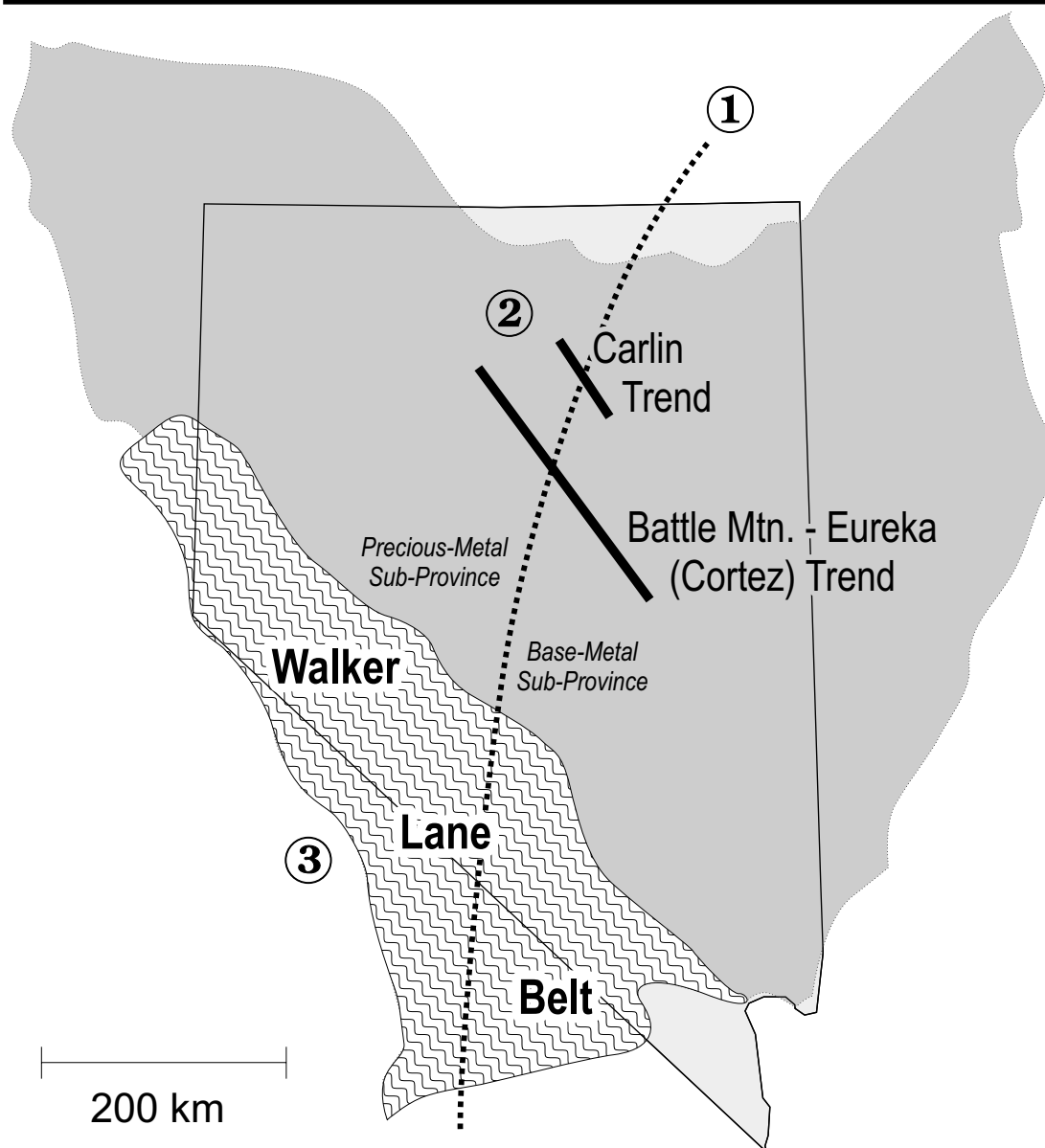


**Figure 1.3.** Principal precious-metal deposit trends, locations, and metallogenic subdivisions in the Great Basin. **1**—The Great Basin metallogenic province can be divided into an eastern base-metal and a western precious-metal metallogenic sub-province (dotted black line). The east-west sub-province division is mainly defined by the preferential distribution of gold-bearing deposits for the western half of the basin. **2**—The main sedimentary rock hosted deposits are aligned along the Carlin and Battle Mountain-Eureka (Cortez) mineral trends. **3**—The main volcanic rock-hosted deposits occur within (or proximal to) the Walker Lane belt, a broad zone of shear deformation (wavy fill pattern). Nevada in light gray shading. Great Basin in dark gray shading. Metallogenic sub-provincial boundary adopted from Roberts (1966). Walker Lane belt from Stewart (1988). Great Basin boundary from Thelin and Pike (1991).

# Cordilleran Orogenic Belt North America

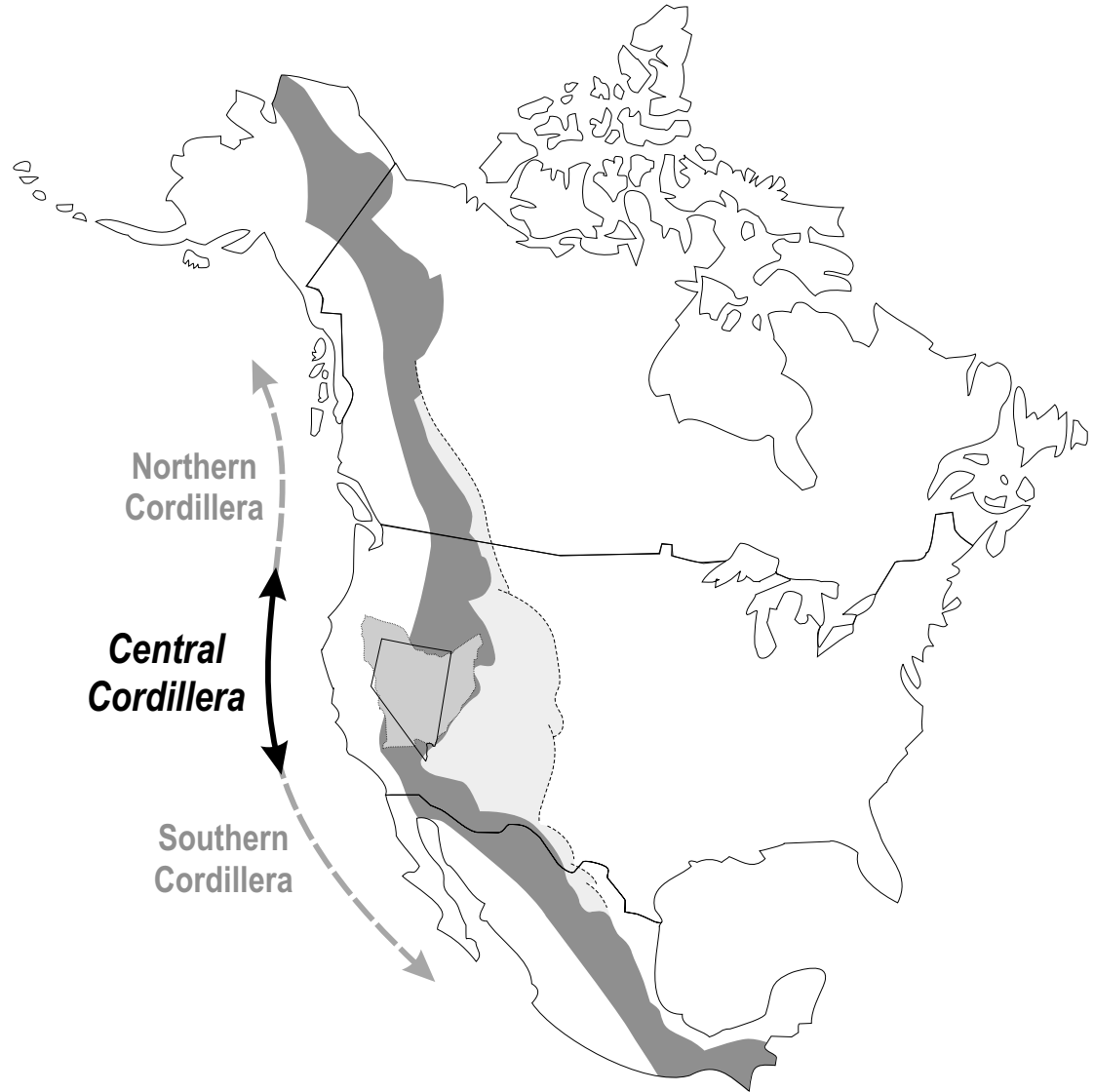


**Figure 2.1.** Generalized extent of the Cordilleran orogen in North America (darkest and lightest gray). The Great Basin physiographic province (medium gray) lies in the "*central*" Cordillera, as opposed to regions north and south. The Cordilleran orogenic belt proper (western hinterland and eastern foreland fold-thrust belt) in darkest gray. The Cordilleran foreland (lightest gray, typically related to the Laramide phase of the Cordilleran orogeny) lies northeast of and beneath the eastern foreland fold-thrust belt, and is assumed to be external to the hinterland and the foreland fold-thrust belt because brittle deformation structures in the foreland are probably not continuous with those of the orogenic belt proper. Dashed line indicates eastern limit of foreland (thrust front may or may not be present). The Cordilleran orogenic belt is one of the two largest orogenic belts in the world, and extends several thousands of kilometers from northern Alaska (possibly even from Siberia), down through Canada, the United States, and Mexico, across the Bartlett transform in Central America, southward along the western margin of South America into Chile, and ends(?) on the Palmer Peninsula of Antarctica. Text and figure modified from Drewes (1991). Great Basin boundary from Thelin and Pike (1991).

## The Great Basin and Environs



**Figure 2.2.** Major physiographic divisions (heavy weight lines), provinces (medium weight lines), subprovinces (dotted lines), and State boundaries (light weight lines) of the western United States. Great Basin physiographic province in dark gray shading. State of Nevada in light gray shading. Province boundaries from Thelin and Pike (1991). Province names from Fenneman and Johnson (1946).

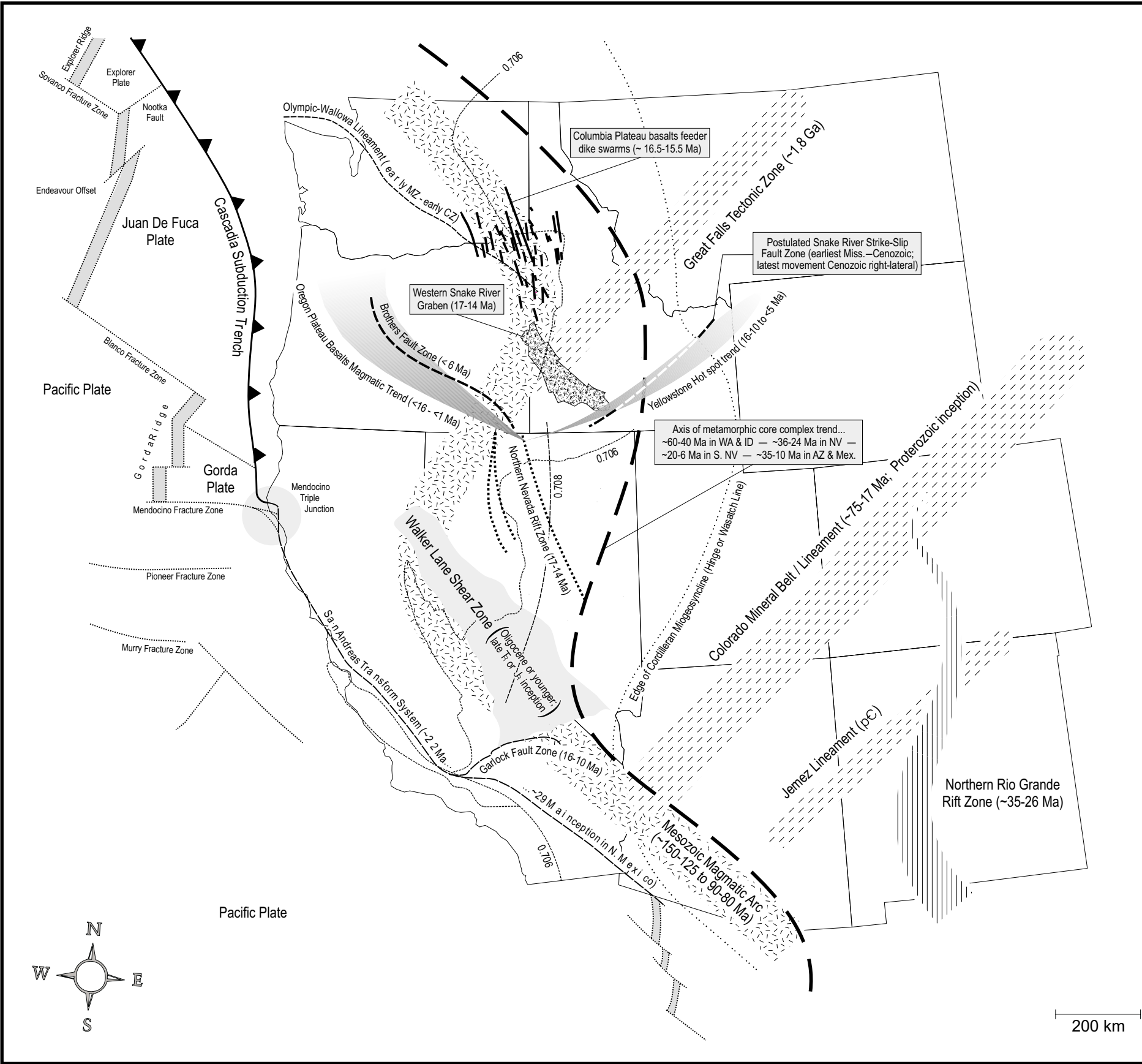


# Plate Tectonic Setting and Selected Tectonomagmatic Elements of the Western United States

**Figure 2.3.** Present-day tectonic setting of the western United States showing the approximate locations and extents of major Precambrian and Phanerozoic tectonic and magmatic elements. The age of a tectonic feature, in parentheses, represents the approximate time of initial activity. In the case of trends (i.e. –Yellowstone hot spot trend), the ages span the period of earliest to latest activity. The dashed line labelled "0.706" is the initial  $^{87}\text{Sr}/^{86}\text{Sr}$  isopleth = 0.706 for Mesozoic plutons, and approximates the edge of the Precambrian crust (from Mutschler et al., 1992; modified from Carlson et al., 1991; Fleck and Criss, 1985; Kistler, 1990; Kistler and Peterman, 1973; Farmer and DePaolo, 1983). The dash-double-dot line labelled "0.708" is the  $\epsilon\text{Nd} = -7$  and initial  $^{87}\text{Sr}/^{86}\text{Sr} = 0.708$  contour, which is interpreted as the edge of the Precambrian crust by Farmer and DePaolo (1983). Compiled from Armstrong and Ward (1991); Atwater (1970); Axen et al. (1993); Burchfiel et al. (1992); Christiansen and Yeats (1992); Cowan and Bruhn (1992); Dilles and Gans (1995); Eaton (1982); Hoffman (1989); Lipman (1992); Mann and Meyer, (1993); Miller et al. (1992); Mutschler et al. (1987); Reidel and Tolan, (1994); Stewart (1988); Stewart et al. (1975); Stewart and Crowell (1992); Suppe (1985); Thelin and Pike (1991); Thorman and Christensen (1991); Warner (1978); Zoback et al. (1981); and Zoback et al. (1994). Older age for inception of Garlock fault from Craig Jones (1994, personal communication). Trace of Snake River fault from Poole et al. (1992).

# Primary Tectonic Subdivisions of the Central Cordilleran Orogen

**Figure 2.4.** First-order tectonic subdivisions of the Cordilleran orogen in the western United States. The descriptions below are keyed by number to the tectonic subdivisions illustrated on the next page.

**#1**—Paleozoic and Mesozoic accretionary belt (shaded light grey, slightly darker where subdivisions #1 and #2 overlap; heavy line delimits approximate western edge of the Precambrian craton, dashed where inferred). Composed of native and exotic terranes of deep-oceanic, shelf-slope, island-arc, and continental origin that were accreted and obducted onto the margin of the Precambrian cratonal shelf in a passive-margin setting (sub-island arc subduction) during the Paleozoic Antler orogeny and the Paleozoic-Mesozoic Sonoma orogeny. Oceanic and displaced terranes of arc affiliation were again accreted during the Mesozoic Nevadan orogeny in an active-margin setting (sub-continental subduction). The accretionary belt makes up from 20 to 50 percent of the width of the Cordillera at different latitudes (Burchfiel et al., 1992).

**#2**—Late Jurassic to Tertiary Sevier hinterland, also known as the *central Cordilleran interior*, and as the *western region* of the Cordilleran orogen (shaded dark grey, slightly lighter where subdivisions #1 and #2 overlap). Defined as the region east of the Mesozoic Andean-type arc (stipple pattern, greatly generalized) and west of the Sevier foreland fold-thrust belt (#3), and includes the Roberts Mountain, Golconda, and Luning-Fencemaker thrust sheets (see Leventhal et al., 1995; Miller et al., 1992). Affected by: (1) middle Paleozoic to earliest Mesozoic thin-skinned deformation of latest Proterozoic to Middle Paleozoic continental shelf clastics and carbonates (miogeoclinal) strata during the Antler and Sonoma passive-margin orogenies; and (2) Mesozoic thin-skinned thrusting and folding of earlier deformed terrain during the Cordilleran active-margin orogeny (includes the Nevadan-Elko and Sevier phases, and possibly the westernmost earliest Laramide phase deformation). This region was most active and initially established during Mesozoic (Sevier) deformation and is in part underlain by subdivision #1. It is within this region that the Great Basin would develop in the Cenozoic.

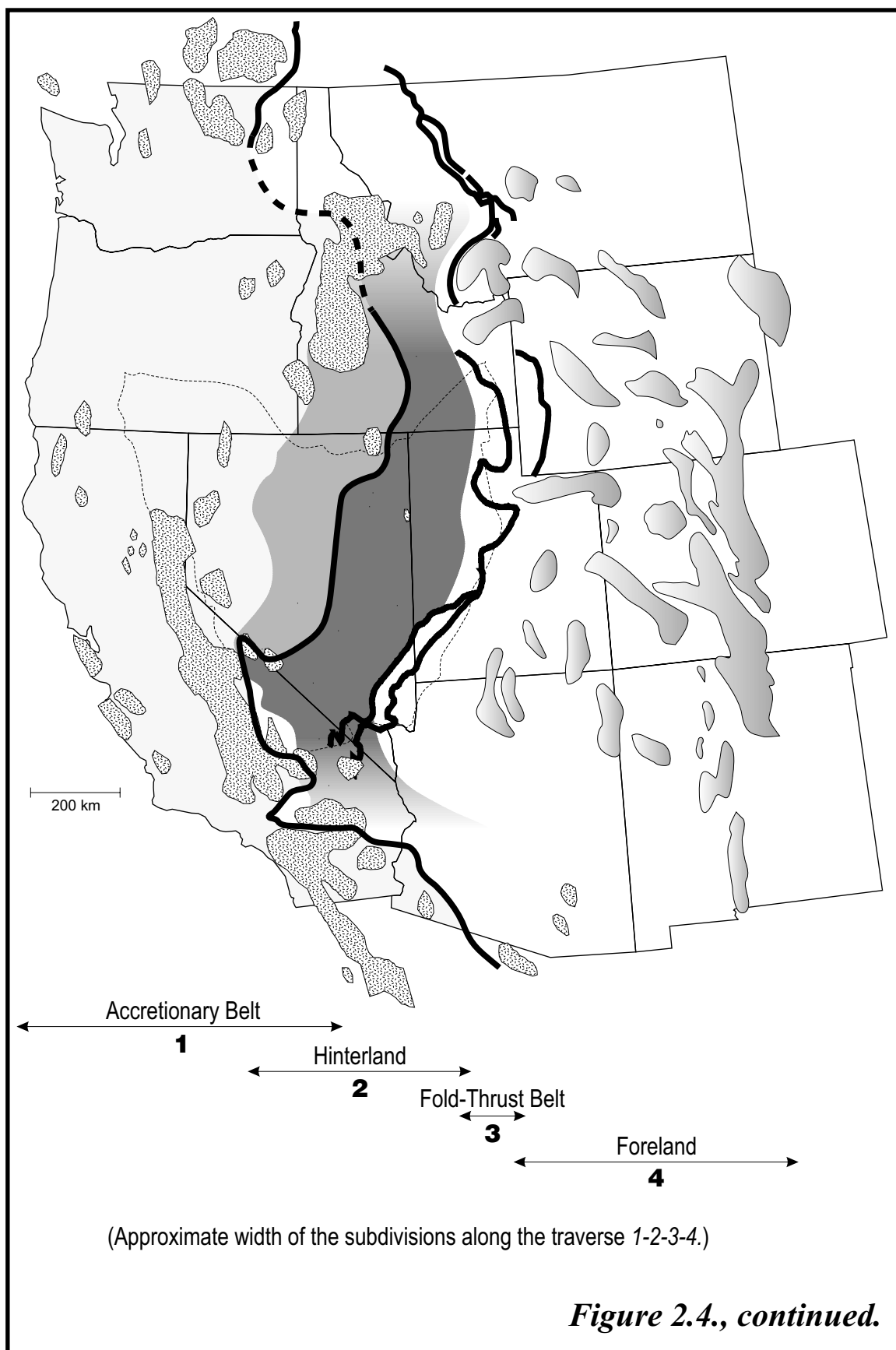
**#3**—Latest Cretaceous to Tertiary Sevier foreland fold and thrust belt, includes the regions immediately west and adjacent to the frontal Sevier foreland thrust (series of heavy and subparallel broken lines). Delineates the eastern limit of the Sevier hinterland and the western limit of Laramide deformation in the Rocky Mountain foreland region. Coeval and to the west of Sevier deformation, the Pacific margin magmatic arc batholiths were emplaced into accreted Paleozoic and Mesozoic continental crust (northern California), Cordilleran miogeoclinal-eugeoclinal sequences (south-central California), and Paleozoic craton (southern California and Arizona) (Suppe, 1985).

**#4**—Latest Cretaceous through middle-late Eocene Rocky Mountain foreland (Laramide deformational belt), also referred to as the *eastern region* of the Cordilleran orogen. "Classic" Laramide deformational features are fault-bounded, basement-cored, asymmetric anticlinal uplifts in the central Rocky Mountains (gradient-filled polygons; approximate locations). The uplifts are adjacent to deep basins filled with marine and continental clastic sediments, largely derived from the Sevier orogenic belt (Hamilton, 1987; Mutschler, 1987). The uplifts developed during the latest Cretaceous to Eocene, and are believed to be related to basement contraction in response to a decrease in the dip of the subducted slab at depth beneath the southern Cordillera (Dickinson, 1981).

**#2 & #3**—The Cordilleran orogenic belt proper, composed of a western hinterland region (#2) and an eastern foreland fold and thrust belt (#3). In the southwestern United States, the Cordilleran orogenic belt is locally referred to the *Sevier orogenic belt* (Cowan and Bruhn, 1992).

**#2, #3, & #4**—The "central" Cordilleran orogen of the western United States, relative to the "northern" segment in Montana and British Columbia, and the "southern" segment in southeastern California, southern Arizona, and southwestern New Mexico (Burchfiel et al., 1992; Cowan and Bruhn, 1992).

Figure based on Burchfiel et al. (1992). Accretionary belt from Burchfiel et al. (1992). Sevier thrust front from Pool et al. (1992). Sevier hinterland (central Cordilleran interior) from Leventhal et al. (1995). Mesozoic magmatic arc from Suppe (1985). Laramide deformation uplifts from Mutschler et al. (1987). Boundary of Great Basin from Thelin and Pike (1991).



# Major Orogenic Belts and Thrusts of the Central Cordilleran Interior

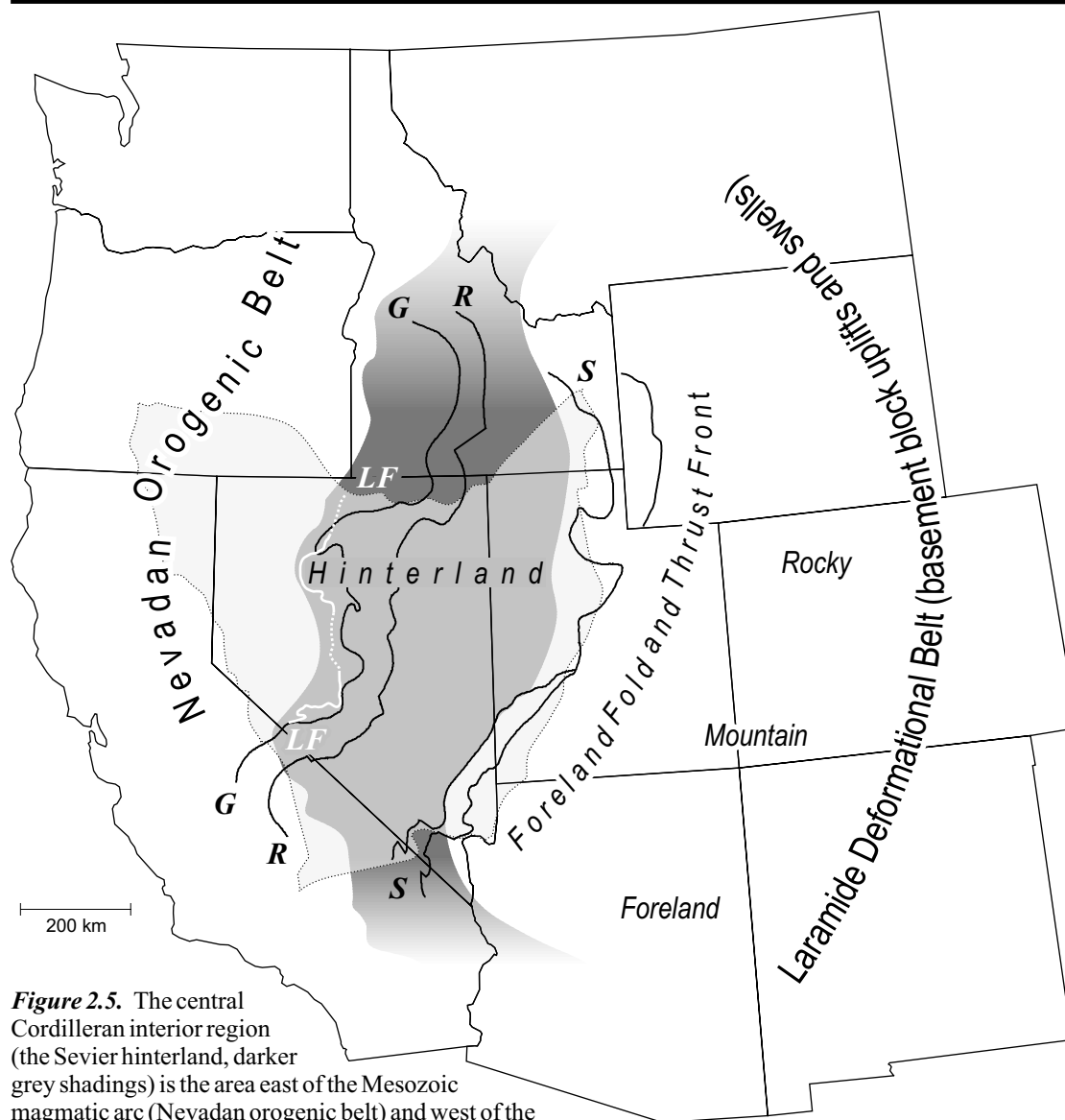


**Figure 2.5.** The central Cordilleran interior region (the Sevier hinterland, darker grey shadings) is the area east of the Mesozoic magmatic arc (Nevadan orogenic belt) and west of the Sevier foreland fold-thrust belt (Miller et al., 1992), and was most active during the Mesozoic (Sevier activity). Great Basin in lighter gray shadings. Phanerozoic thrust fronts: **R**—Roberts Mountain (Antler orogeny, Upper Devonian to Upper Mississippian); **G**—Golconda (Sonoma orogeny, mid- to Upper-Permian); **LF**—Luning-Fencemaker (Nevadan-Elko activity, Middle-Late Jurassic to Early Cretaceous; western counterpart to coeval "*Elko orogeny*" in northeastern Nevada and northwestern Utah, both probably related to emplacement of the Sierra Nevada magmatic arc); and **S**—Sevier (Sevier activity, eastern limit of the Sevier foreland fold-thrust belt, western limit of Laramide deformation; thrusts are Sevier and earliest Laramide in age, Late Jurassic to early Tertiary). The Nevadan orogenic belt is delineated by great batholithic complexes (i.e.—Sierra Nevada and Idaho batholiths), emplaced during the Late Jurassic to Upper Cretaceous. Laramide deformation (latest Cretaceous through mid- to Late-Eocene) delineates the Rocky Mountain foreland region. Thrust fronts from Poole et al. (1992) and Hardyman and Oldow (1991). Central Cordilleran interior (Sevier hinterland) from Leventhal et al. (1995). Boundary of Great Basin from Thelin and Pike (1991).



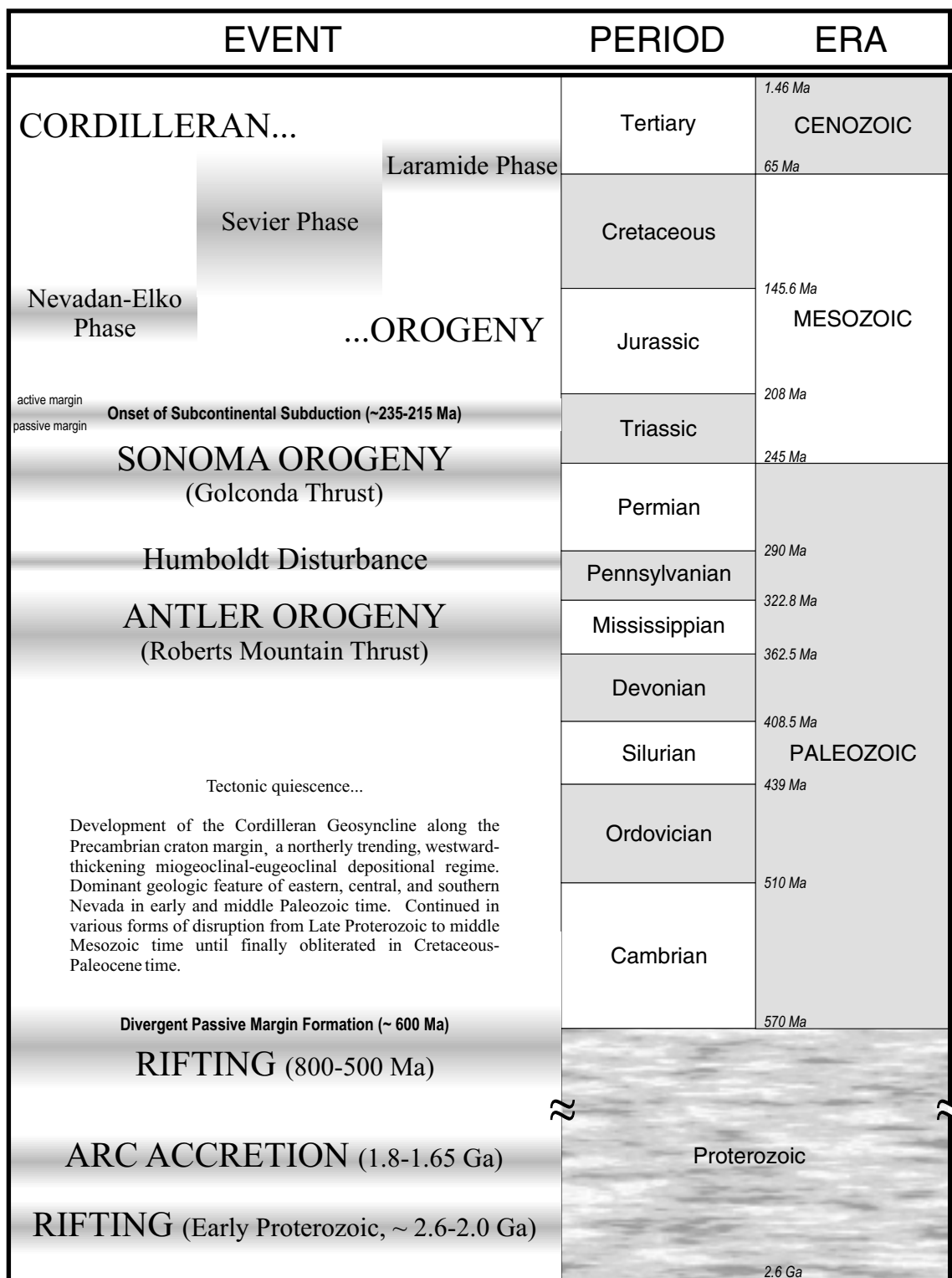


**Figure 2.6.** Time chart of orogenic events affecting the Great Basin. Compiled from Burchfiel et al. (1992), Cowan and Bruhn, (1992), Eaton (1982), Hoffman (1989), Miller et al. (1992), Poole et al. (1992), Speed (1983), Speed et al. (1988), Stewart (1980), Suppe (1985), Thorman and Christensen (1991), and Thorman et al. (1991). Inset text modified from Thorman and Christensen (1991). Period bounding dates from Harland et al. (1990). Lower Proterozoic boundary from Van Eysinga (1975).

# Phases of the Cordilleran Orogeny— Space-Time Relationships

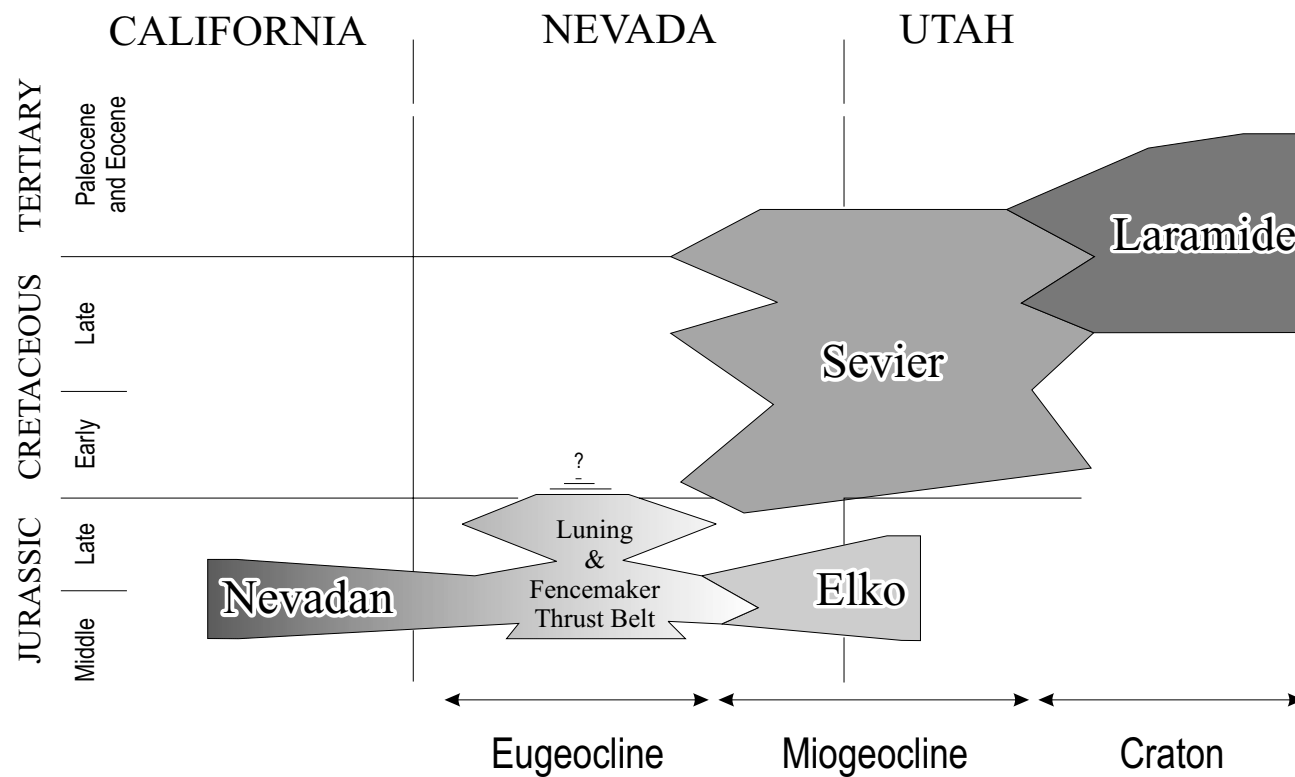


**Figure 2.7.** Diagrammatic time and space relationships between Mesozoic and early Cenozoic orogenies in the Great Basin and adjoining areas. Figure from Thorman and Christensen (1991), with modifications incorporated from Cowan and Bruhn (1992), Eaton (1982), Miller et al. (1992), and Speed et al. (1988).

# Geologic Events Affecting the Great Basin and Environs During the Cenozoic

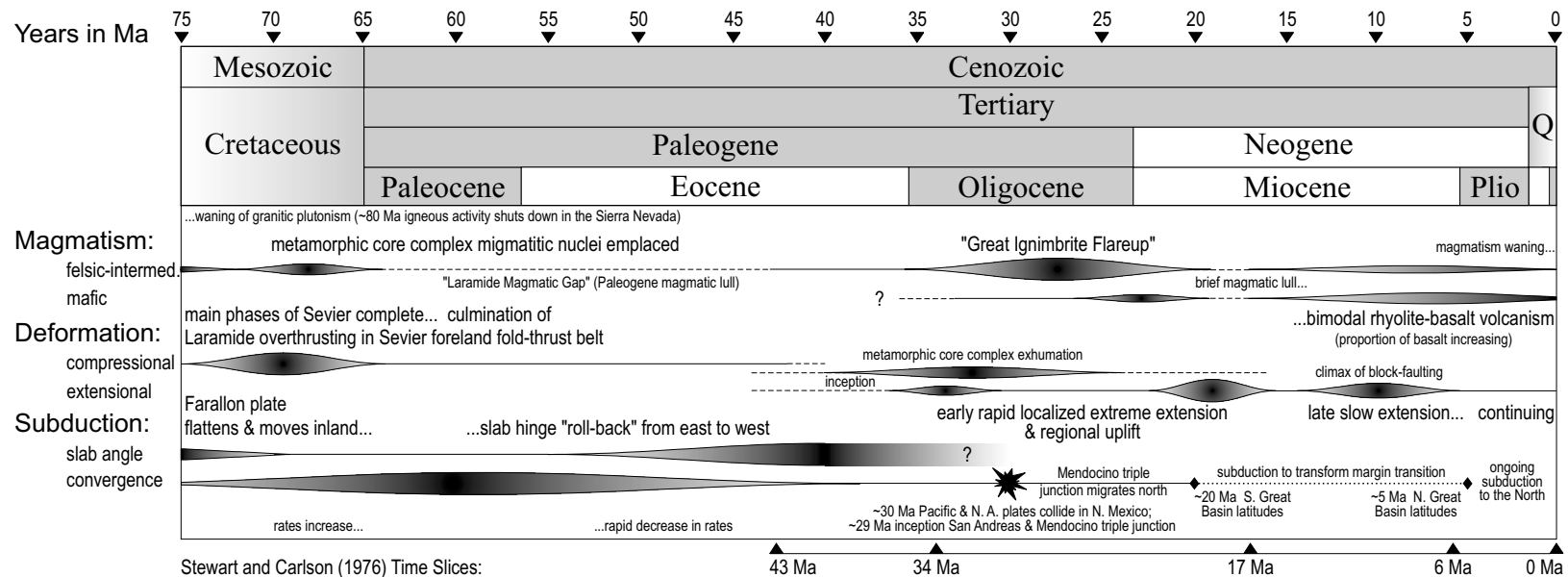


**Figure 2.8.** Time-line summary of the major tectonomagmatic events affecting the Great Basin in Cenozoic time. The thickness of a time-line indicates the relative intensity of an event. Compiled from Allmendinger (1992), Armstrong et al. (1969), Armstrong and Ward (1991), Atwater (1970, 1989), Axen et al. (1993), Best and Christiansen (1991), Berger and Bonham (1990), Christensen and Yeats (1992), Coney (1980), Dickinson (1992), Dickinson and Snyder (1978), Eaton (1982), Elston (1986), Gans and Mahood (1987), Hamilton (1987), Harry et al. (1993), Humphreys (1995), Hutchinson and Albers (1992), Livaccari and Perry (1993), Miller et al. (1992), Mutschler et al. (1987), Patino-Douce and Humphreys (1987), Rehrig (1986), Sedorff (1991), Speed et al. (1988), Stewart (1978), Stewart (1980), Stewart and Carlson (1976), Suppe (1985), Thorman and Christensen (1991), Ward (1991), Wernicke et al. (1987), and Zoback et al. (1981).

# Depositional Framework of the Cordilleran Geosyncline

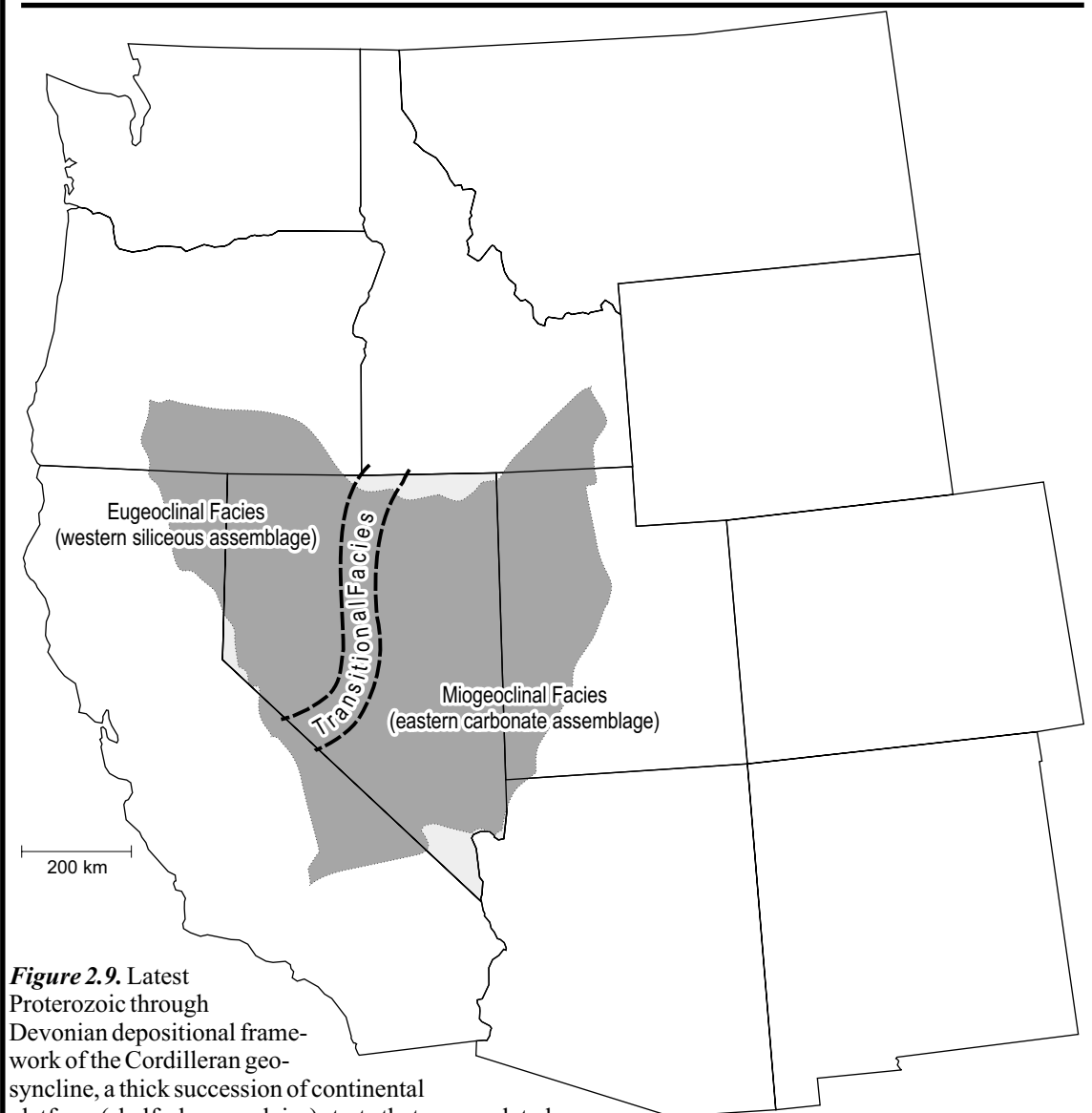


**Figure 2.9.** Latest Proterozoic through Devonian depositional framework of the Cordilleran geosyncline, a thick succession of continental platform (shelf, slope, and rise) strata that accumulated along the western margin of the craton in a broad northerly-trending two-fold miogeoclinal-eugeoclinal belt. The miogeoclinal facies (*eastern carbonate assemblage*) was deposited on the continental shelf in a shallow-water subtidal to supratidal environment, forming an apron of thin terrigenous siliciclastic detrital material, a few hundred meters thick in cratonic areas in central Utah, that extended west across the craton margin, thickening into a prism of siliciclastic carbonate sequences over 15 km thick in central Nevada. The eugeoclinal facies (*western siliceous assemblage*) was deposited on the continental slope and rise in a deep-water environment, coeval with miogeoclinal strata, and consisted of siliciclastic-chert-volcanic sequences, shale, radiolarian chert, quartzite, and mafic pillow lavas. A transitional facies is recognized where the miogeoclinal shelf facies interfingers with the eugeoclinal slope-rise facies. Facies boundary from Roberts (1966), Stewart (1980), and Thorman and Christensen (1991). Great Basin boundary from Thelin and Pike (1991). Great Basin in dark grey. Text from Dickinson (1981), Hamilton (1987), Hutchinson and Albers (1992), Thorman et al. (1991), and Thorman and Christensen (1991).

## The Western Edge of Precambrian North America

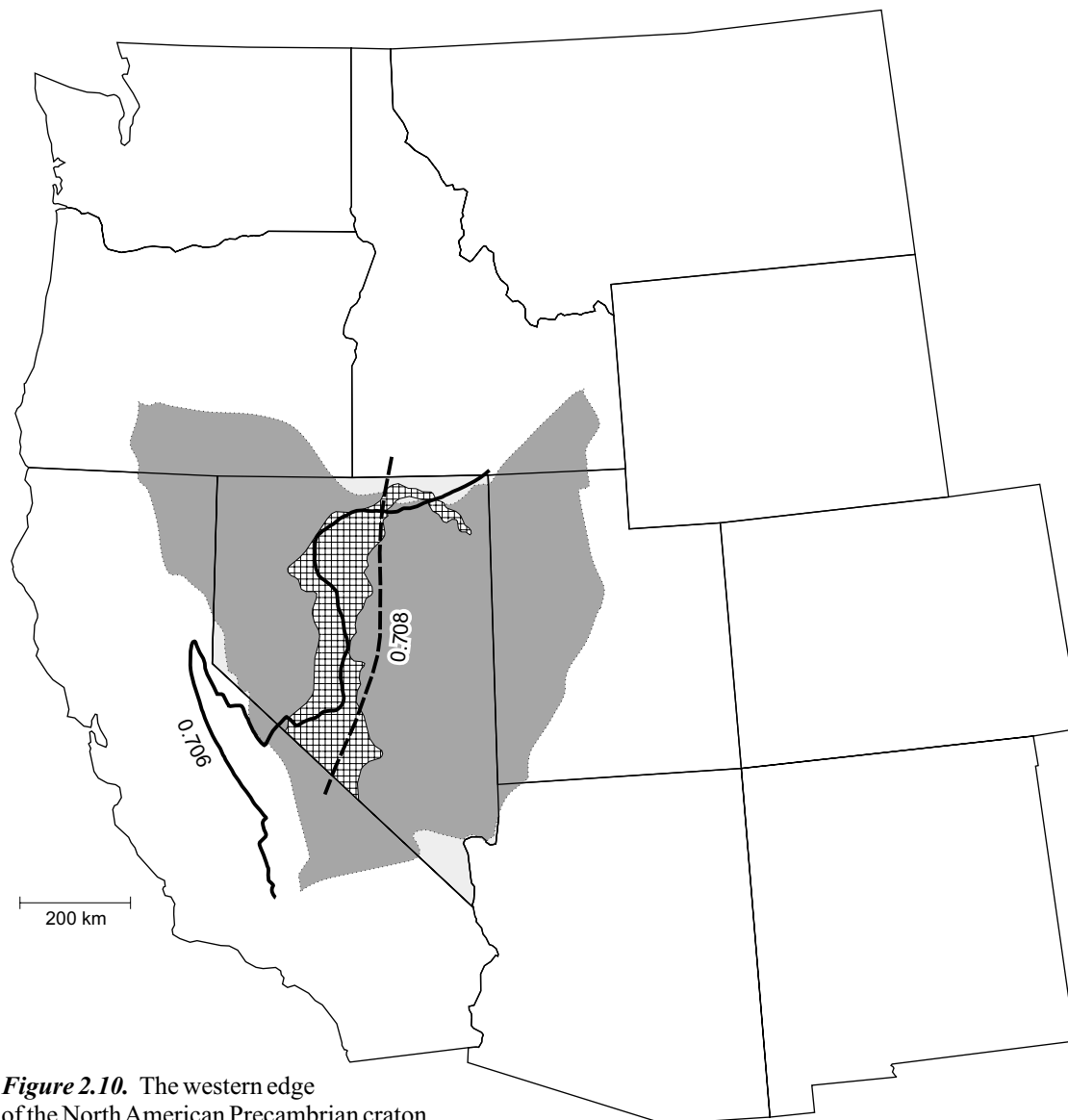


**Figure 2.10.** The western edge of the North American Precambrian craton, as delineated by isotopic and paleothermal data. The heavy black line labelled "0.706" is the initial  $^{87}\text{Sr}/^{86}\text{Sr}$  isopleth = 0.706 for Mesozoic plutons, and is thought to approximate the edge of the Precambrian crust (Kistler and Peterman, 1973). The dashed line labelled "0.708" represents the initial  $^{87}\text{Sr}/^{86}\text{Sr} = 0.708$  and the  $\epsilon\text{Nd} = -7$  contours, and is interpreted as the edge of the Precambrian crust by Farmer and DePaolo (1983). The gridded area outlines a regional paleothermal anomaly, as defined by the distribution of Devonian rocks containing conodonts with a conodont color alteration index over 4.5. The age of the anomaly is uncertain, but a major episode of regional heating took place in the late Paleozoic and in the early Mesozoic. The eastern edge of the paleothermal anomaly may be a sensitive indicator of the position of the edge of the buried craton. Nevada in light gray shading. Boundary of Great Basin in dark gray shading. Paleothermal anomaly from Cunningham (1988). Boundary of Great Basin from Thelin and Pike (1991). Text modified from Cunningham (1988).

# Crustal Formation Provinces of the Western United States

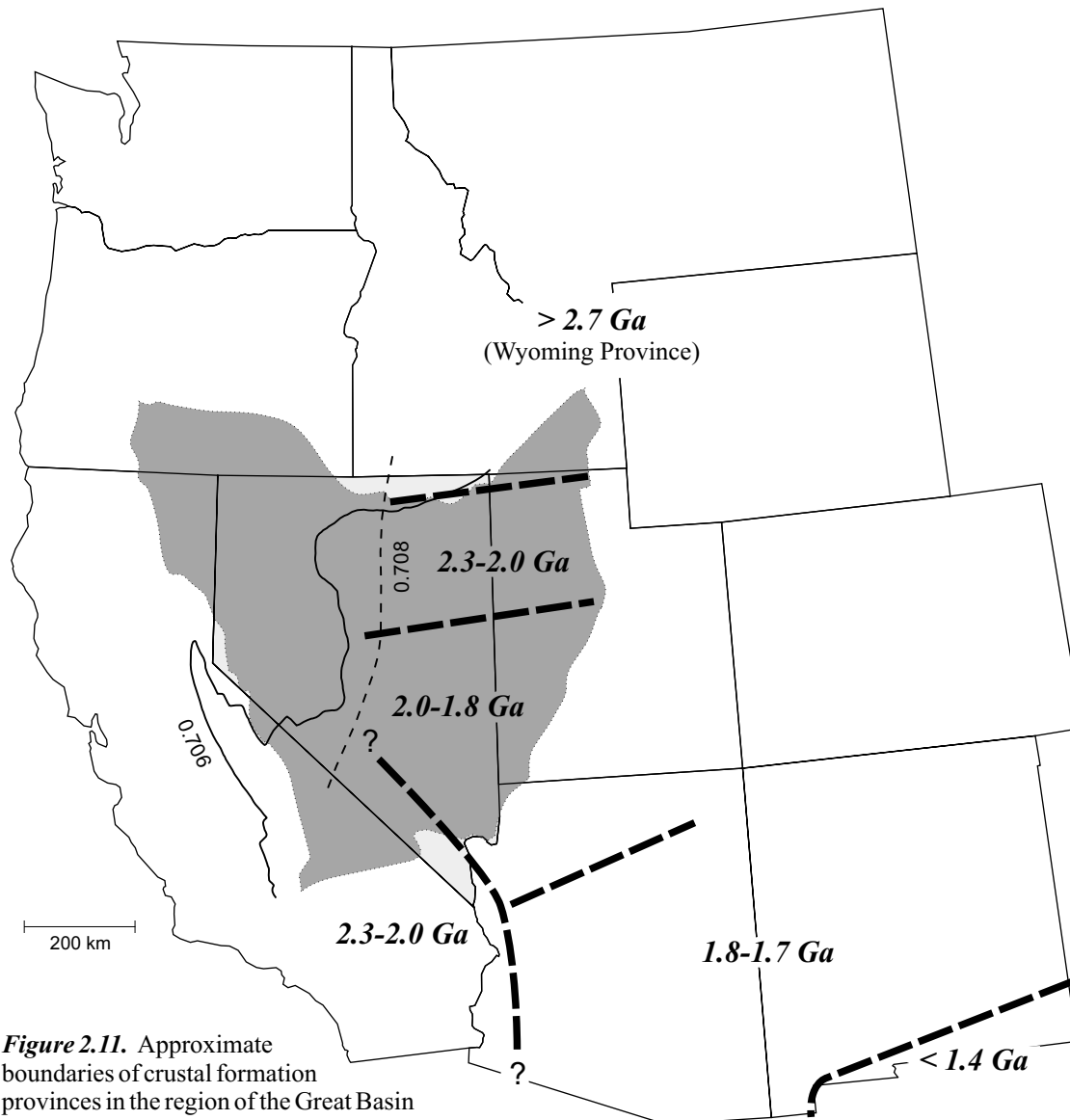


**Figure 2.11.** Approximate boundaries of crustal formation provinces in the region of the Great Basin (heavy dashed lines; ages as indicated). Provinces are distinguished on the basis of regional differences in Nd isotopic evolution paths as determined by measurements of crustally derived granitoids of various ages. The western edge of the Precambrian craton is commonly thought to be approximated by the initial  $^{87}\text{Sr}/^{86}\text{Sr}$   $I_{\text{Sr}} = 0.706$  isopleth for Mesozoic plutons (line labelled "0.706"). The dashed line labelled "0.708" represents the initial  $^{87}\text{Sr}/^{86}\text{Sr}$   $I_{\text{Sr}} = 0.708$  ( $\epsilon_{\text{Nd}} = -7$ ) isopleth, which is interpreted as the edge of the Precambrian crust by Farmer and DePaolo (1983). Nevada in light gray shading. Boundary of Great Basin in dark gray shading. Province boundaries based on Farmer et al. (1988), with modifications from Bennett and DePaolo (1987) and Livaccari and Perry (1993).  $^{87}\text{Sr}/^{86}\text{Sr}$   $I_{\text{Sr}}$  isopleth based on Kistler and Peterman (1973) and Farmer and DePaolo (1983); this trace from Mutschler et al. (1992), who had incorporated modifications from Carlson et al. (1991), Fleck and Criss (1985), and Kistler (1990). Boundary of Great Basin from Thelin and Pike (1991). Text modified from Bennett and DePaolo (1987).

## Variability of Selected Geologic Attributes Across the Southern Great Basin

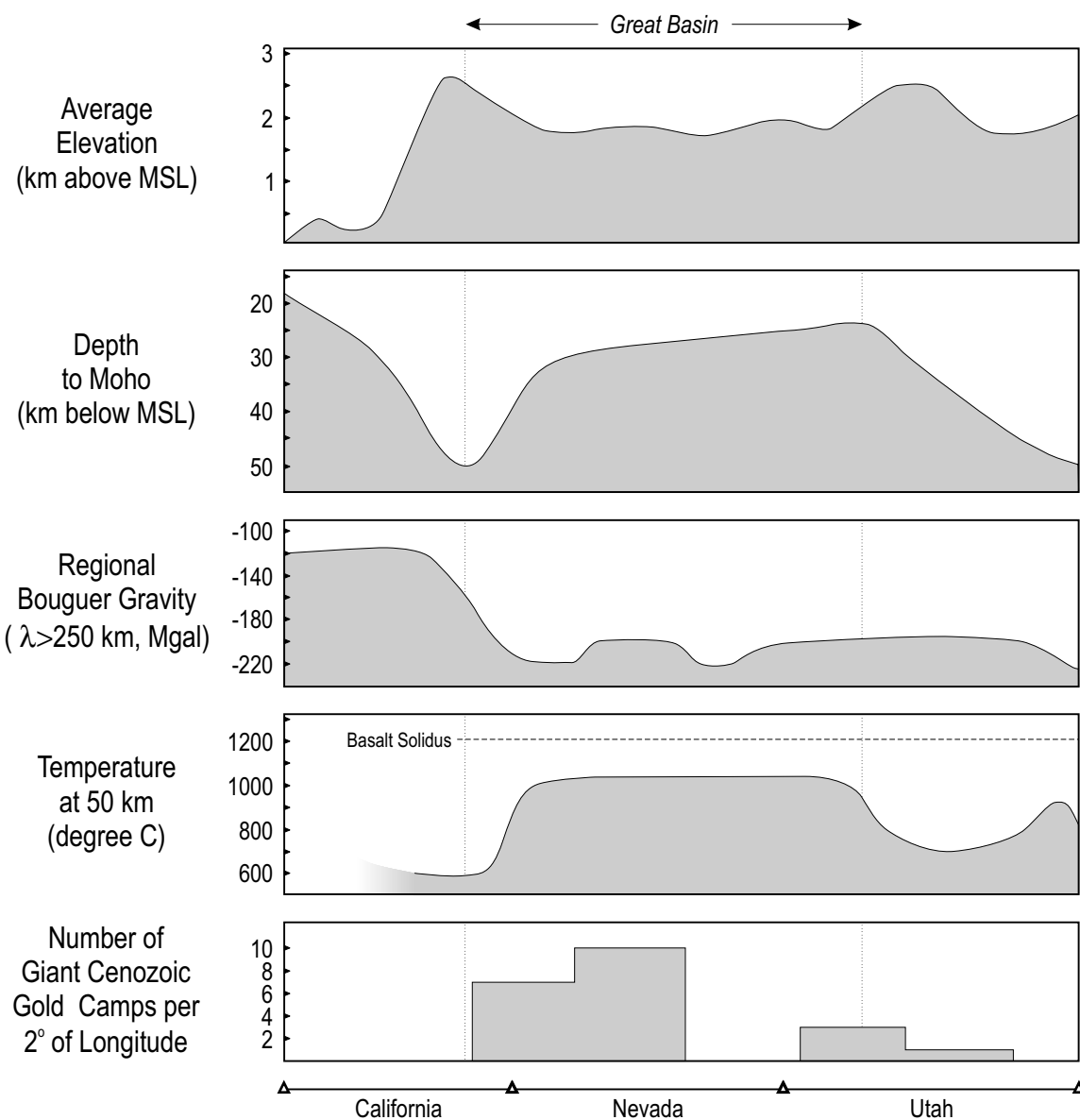


**Figure 2.12.** Simplified profiles at 38° latitude showing the relationships between average elevation, crustal thickness (Allenby and Schnetzler, 1983), long wavelength regional Bouguer gravity (Hildenbrand et al., 1982), temperature at depth (Eaton et al., 1978; Eggler et al., 1988), and giant Cenozoic gold camps (production and/or reserves of 1,000,000 Troy ounces or more Au). Redrawn from Mooney and Mutschler (1990).



# Phanerozoic Tectonostratigraphy of The Great Basin

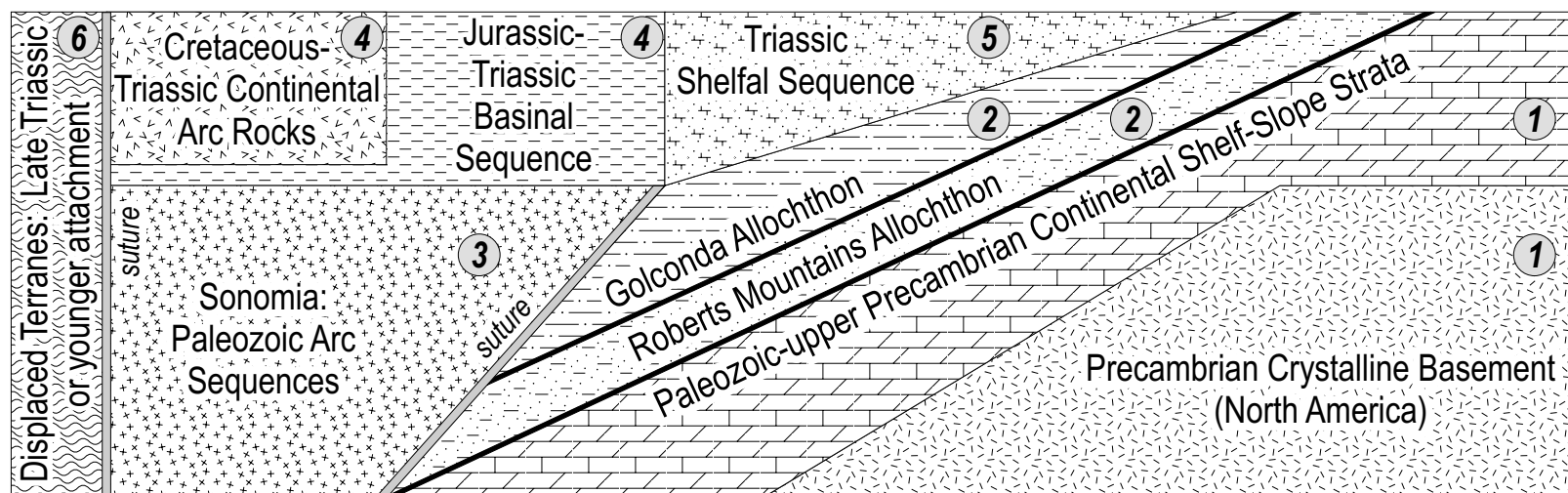
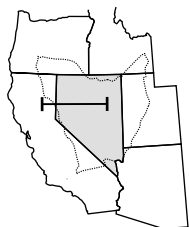


**Figure 2.13.** Stacking diagram of regional tectonostratigraphic units at the surface in the western Great Basin and surrounding environs. The stacking section trends east-west approximately along 40° N between the Sierra Nevada and Elko, Nevada (see inset lower left). Heavy lines and sutures are tectonic boundaries, light lines are depositional. Unit 1 constitutes Precambrian sialic North America plus parautochthonous cover, and probably remained relatively coherent over Phanerozoic time. Unit 2 represents the eastward thrusting of eugeoclinal rocks (siliceous and volcanic assemblages) over coeval miogeoclinal rocks (carbonate shelf-slope strata), during Antler (Roberts Mountains thrust) and Sonoma (Golconda thrust) orogenies, respectively. Unit 3 is presumed to be a microplate, or collection of microplates, whose subsurface extent is unknown. Unit 4 formed as parautochthonous Mesozoic cover strata, mainly basinal, but locally shelfal, to unit 3 after it was accreted to North America. Unit 5 is presumed to be the source region for the Jurassic-Triassic basinal sequences of unit 4. Unit 6 consists of displaced and suture-related terranes of Mesozoic melange or of arc affiliation. The contact of unit 6 with units 3 and 4 is the Sierra Nevada Foothills suture, a major accretionary surface that separates terranes that attached to the passive margin of North America before Middle Triassic time from those that arrived during the later active margin phase of orogenesis (see figure 2.2, #1). The suture separating unit 3 from units 1 and 2 is presumed to exist, and is probably blind. Quaternary and upper Cretaceous cover (Unit 7) not shown (see text). Figure redrawn from Speed et al. (1988). Text modified from Speed et al. (1988) and Speed (1983).



# Distribution of Sedimentary Rock-Hosted and Volcanic Rock-Hosted Gold-Silver Deposits

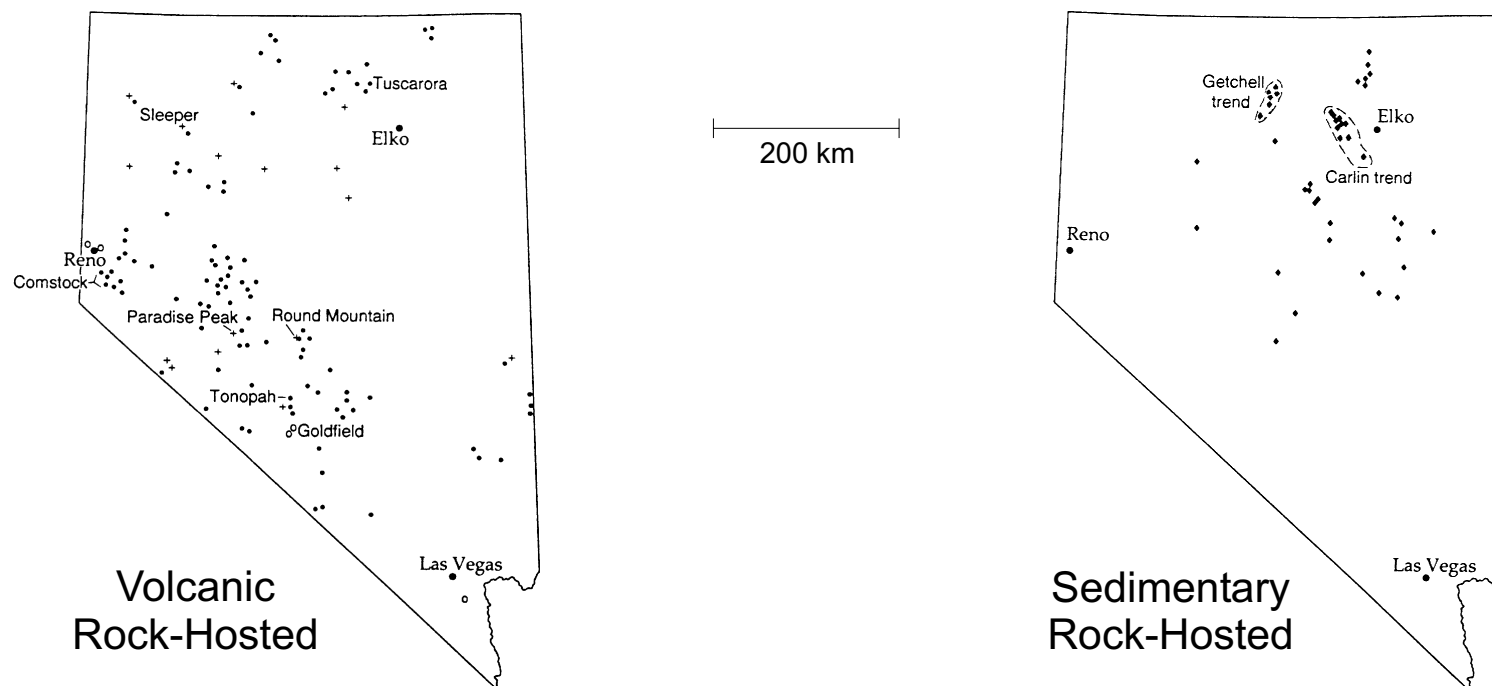


**Figure 3.1.** Spatial distribution of sedimentary rock-hosted and volcanic rock-hosted gold-silver deposits. Volcanic rock-hosted deposits include disseminated, vein, and other fracture-related (i.e.—breccia zones) epithermal mineralization which is hosted primarily by volcanic rocks, and less commonly by associated volcanoclastic and sedimentary rocks closely associated with proximal subvolcanic intrusions. Solid circles represent quartz-adularia veins; open circles, quartz-alunite veins; crosses, hot spring gold deposits. Note the crescent-shape distribution (the "*epithermal crescent*"), and conspicuous lack of volcanic rock-hosted deposits in the central and eastern regions of Nevada. Sedimentary rock-hosted deposits include disseminated mineralization hosted by clastic as well as carbonate sedimentary rocks, and by and large have no obvious association with volcanic centers. The sedimentary rock-hosted deposits lie mainly inward of the epithermal crescent, forming a "*core*" to the epithermal crescent in central and eastern Nevada, and are older and formed deeper than the volcanic rock-hosted deposits. Figure from Ludington et al. (1993). Text modified from Ludington et al. (1993).

# Sedimentary and Volcanic Rock-Hosted Deposit Age Boundary

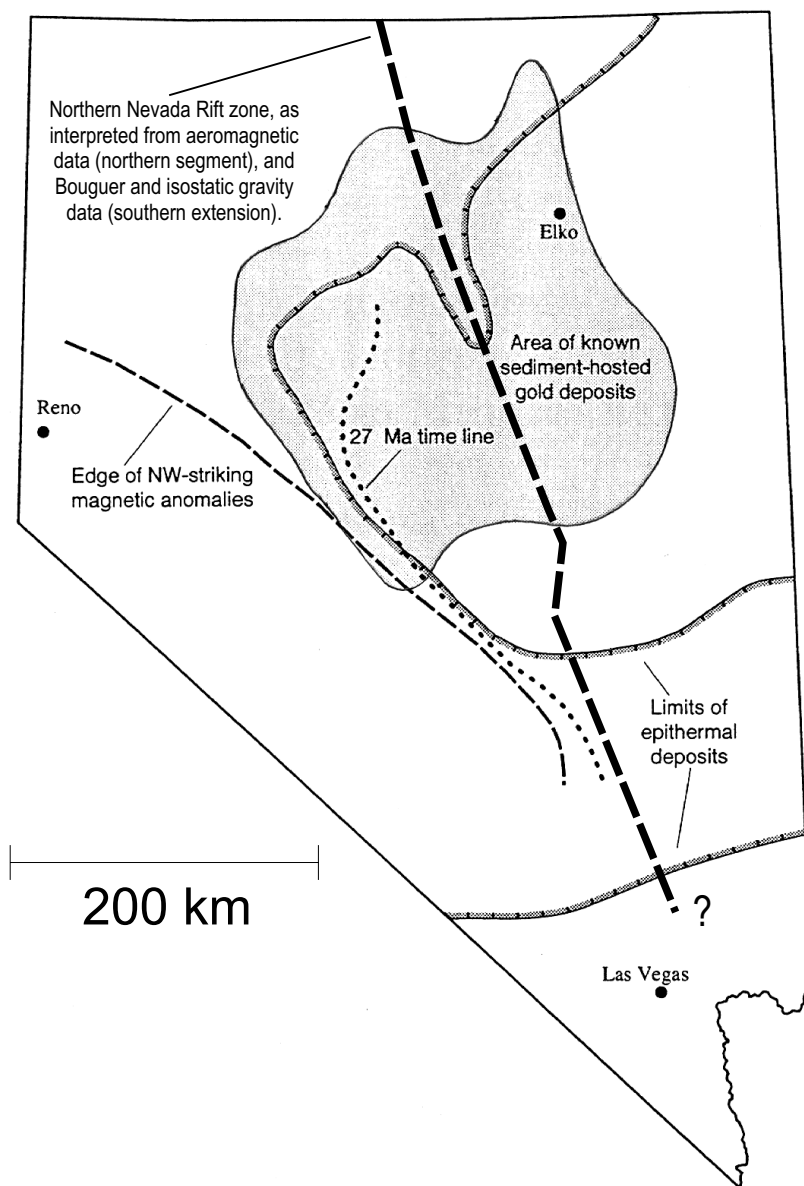


**Figure 3.2.** The 27 Ma age boundary between sedimentary and volcanic rock-hosted deposits. The sedimentary rock-hosted deposits are believed to be generally pre-27 Ma in age, whereas the volcanic rock-hosted deposits are primarily post-27 Ma in age. The 27 Ma age boundary is based on the spatial coincidence of: (1) the western extent of sedimentary rock-hosted deposits and the eastern extent of volcanic rock-hosted deposits (line delimiting eastern extent of volcanic rock-hosted deposits in central Nevada, and shaded area marking region of known sedimentary rock-hosted deposits); (2) the position of a volcanic time-line that separates calderas and other volcanic source regions with ages that are pre- or post-27 Ma (dotted line); and (3) the northeastern limit of Walker Lane shear zone deformation, as delineated by northwest-trending geomagnetic anomalies (dashed line). Figure and text modified from Ludington et al. (1993) and Cox et al. (1991).

# Mineral Trends and Belts of Nevada

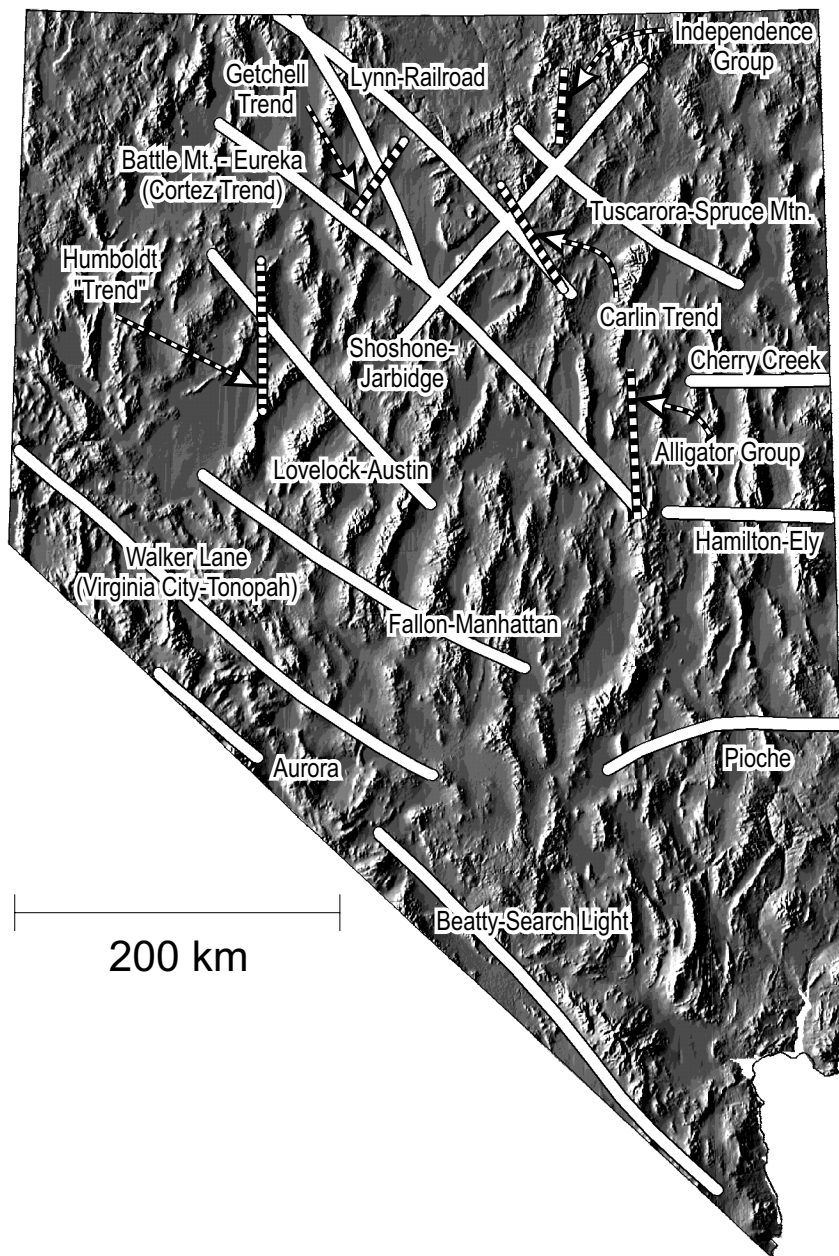


**Figure 3.3.** Principal mineral trends and belts of Nevada. Trends and belts are labelled and illustrated as dashed white lines (trends) and heavy white lines (belts) superimposed on a shaded relief map of topography. Mineral belts commonly refer to regional-scale alignments of deposits, which may or may not be of the same age or type, while mineral trends refer to district-scale deposit alignments (Seedorff, 1991). The topography effectively shows the north-northeast trending structural grain of Nevada in contrast to most trends and belts, which are oriented northwest-southeast. Mineral belts from Roberts (1966) and Shawe and Stewart (1976). Trends from Sweeney (1990), with additions from Thorman and Christensen (1991) and Percival et al. (1988).

# Weights of Evidence Mineral Potential Modelling Method

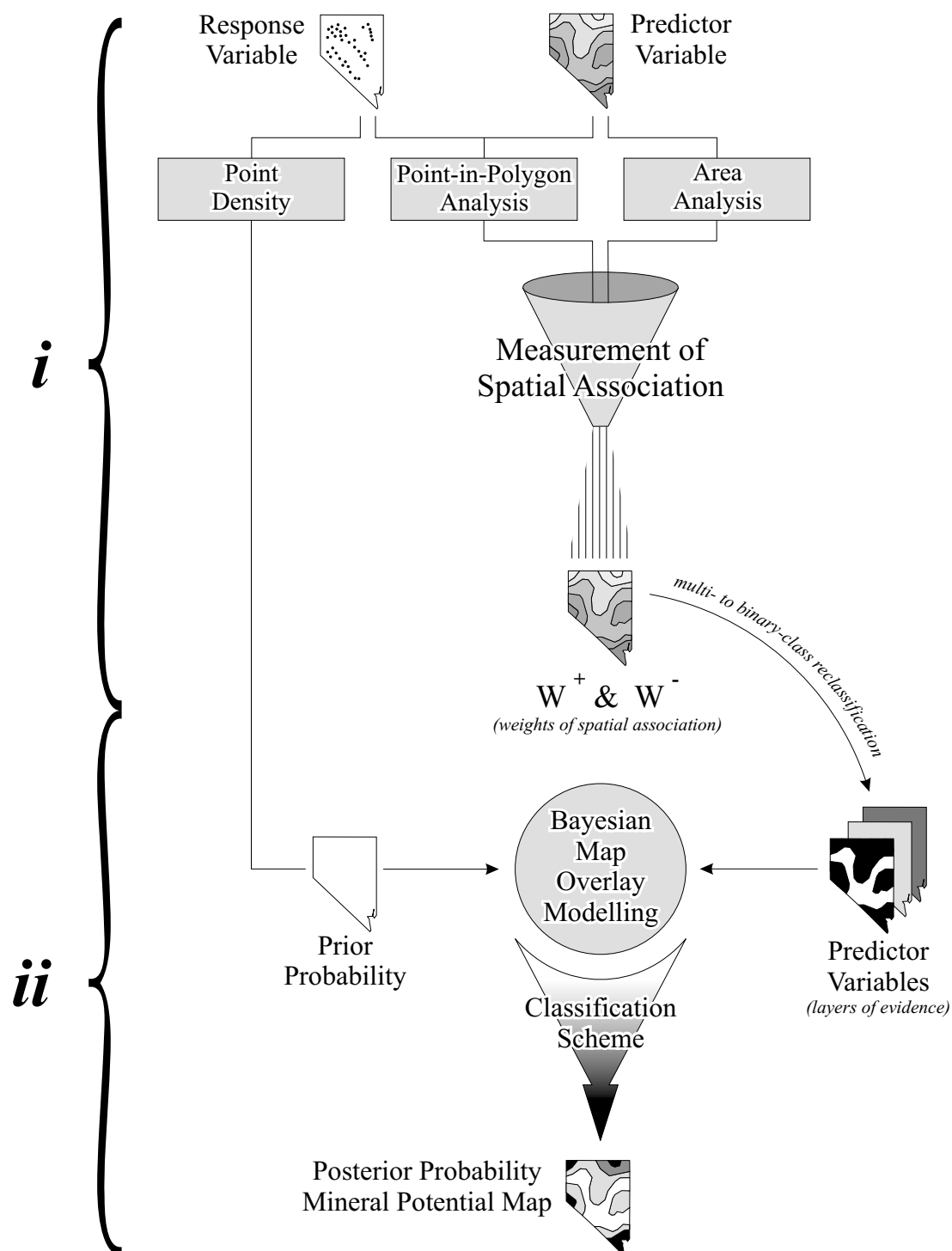
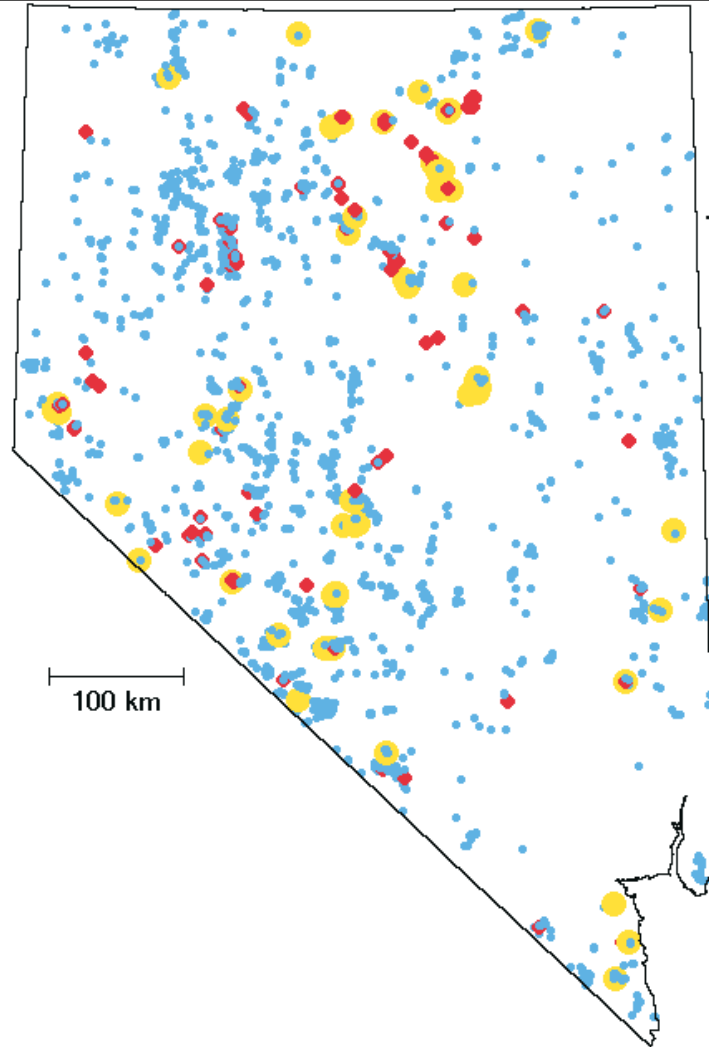


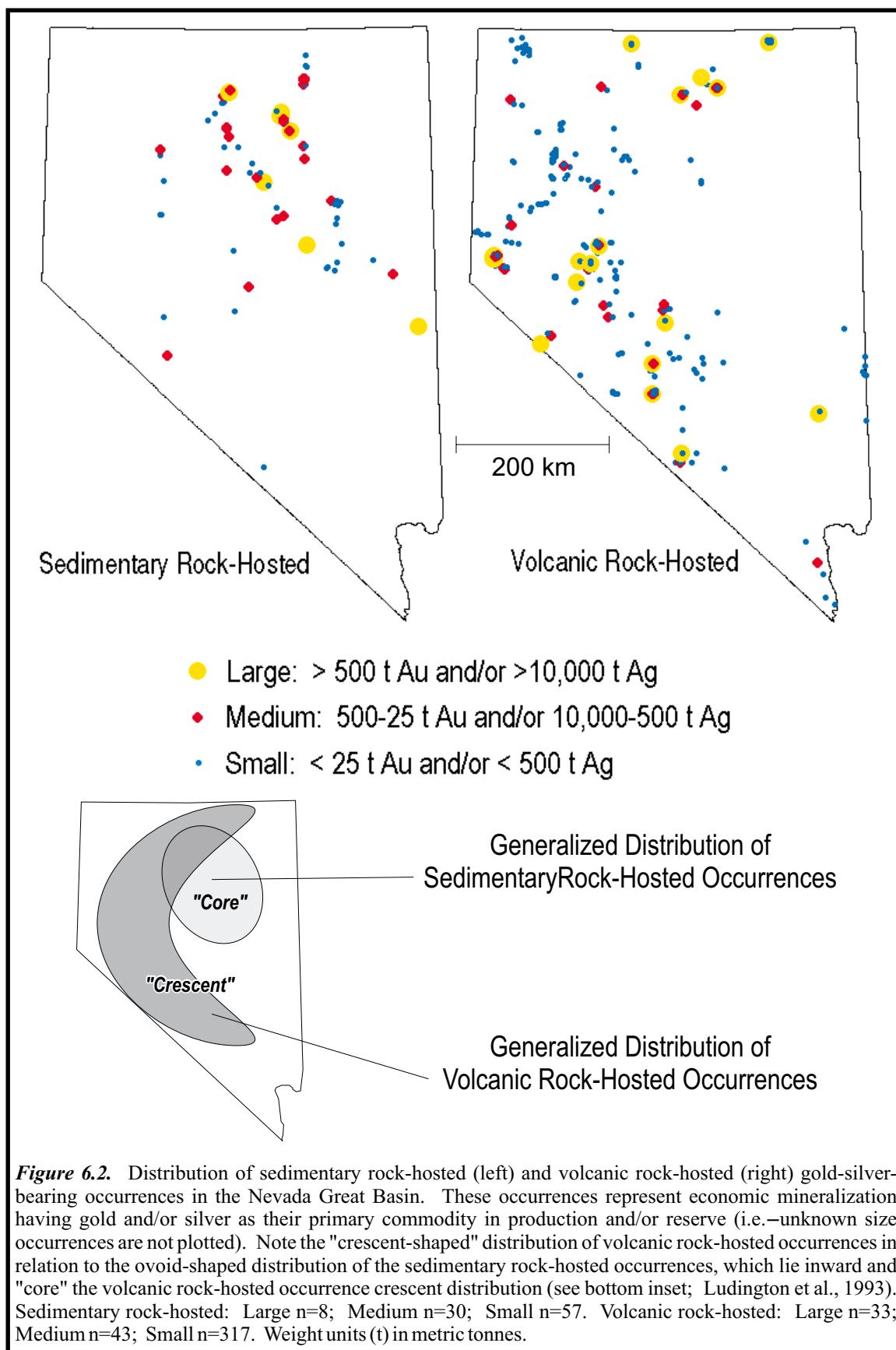
**Figure 4.1.** Flow chart illustrating the weights of evidence mineral potential modelling method.

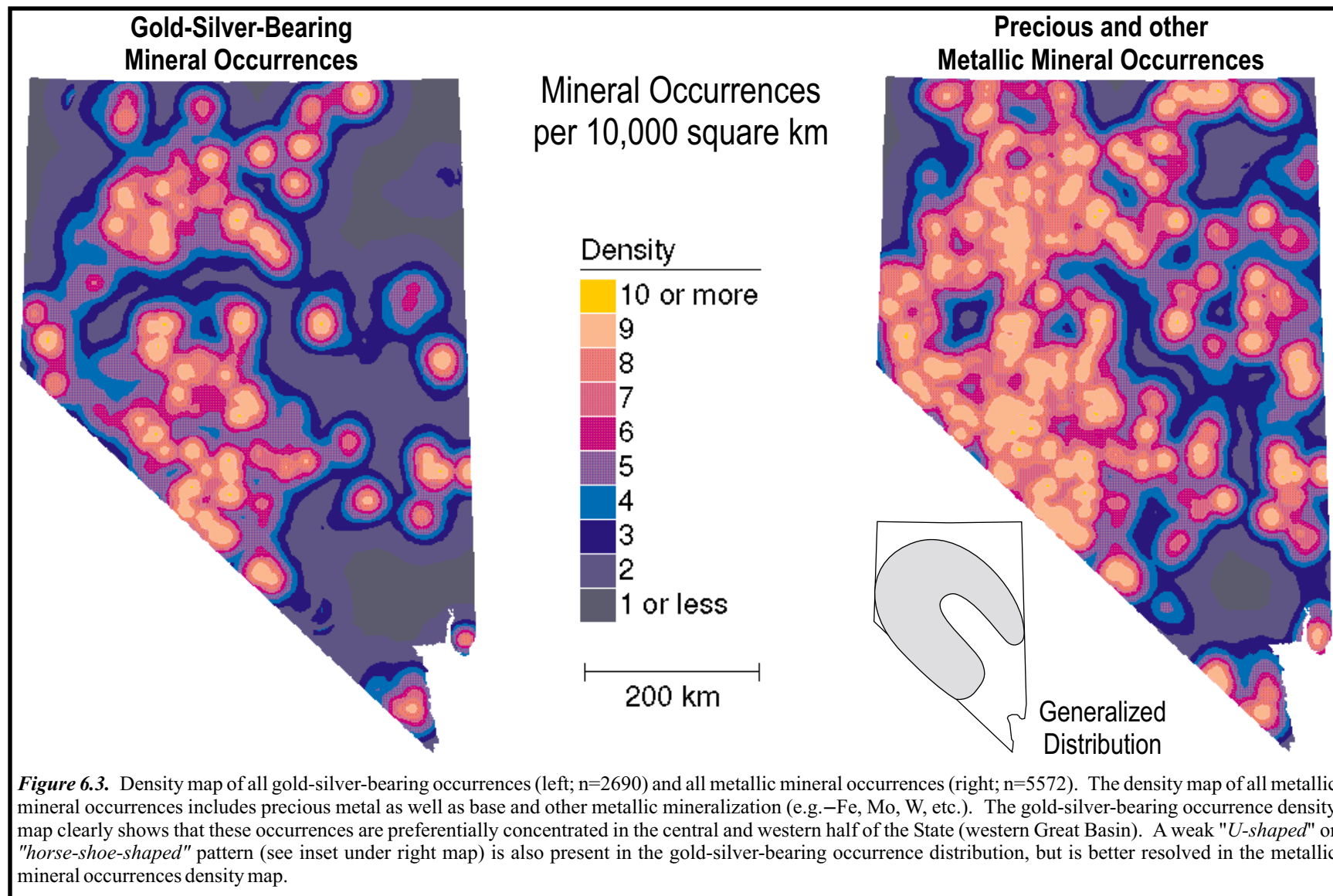
# Gold-Silver Occurrences Nevada, USA



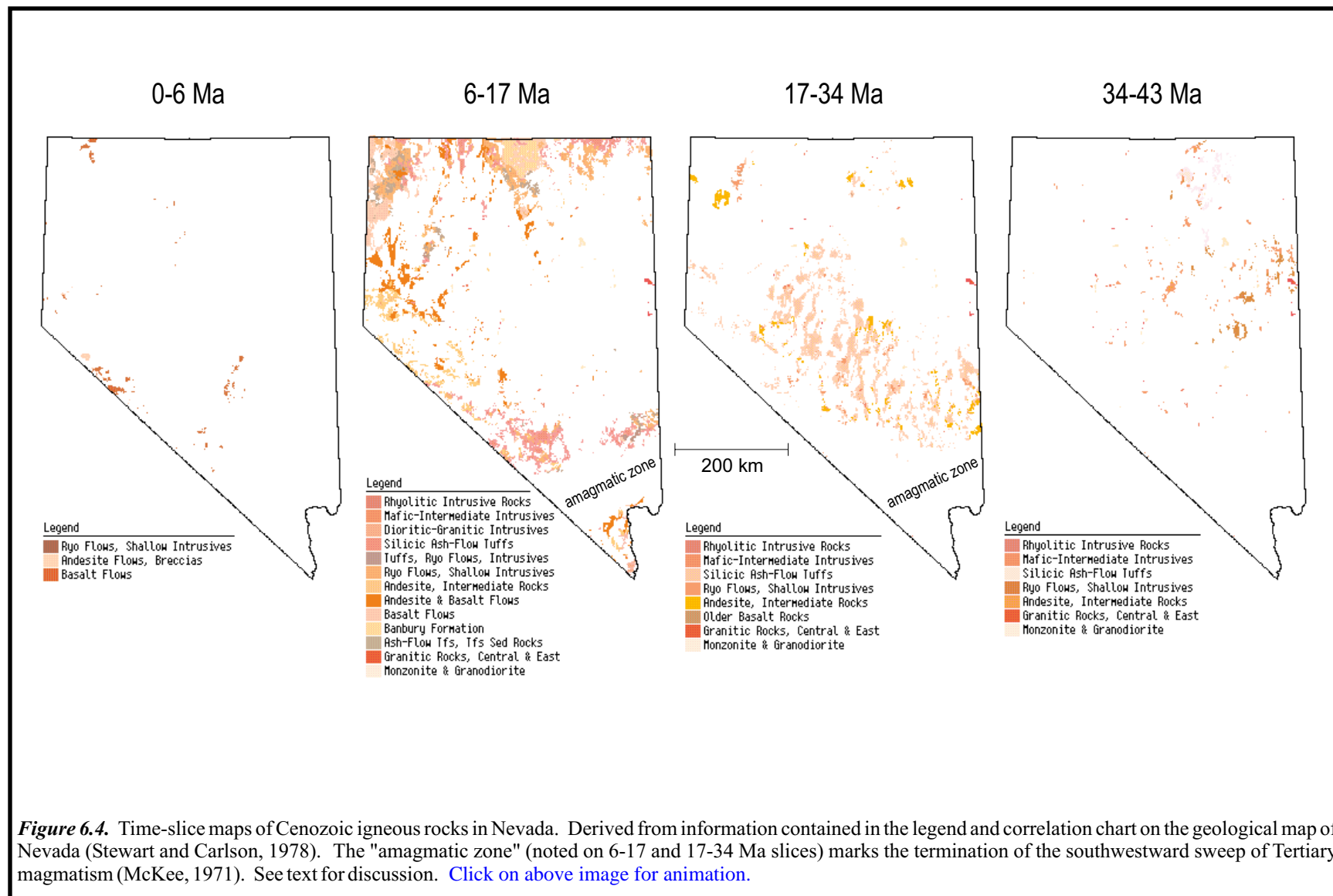
- Large: > 500 t Au and/or >10,000 t Ag
- Medium: 500-25 t Au and/or 10,000-500 t Ag
- Small: < 25 t Au and/or < 500 t Ag

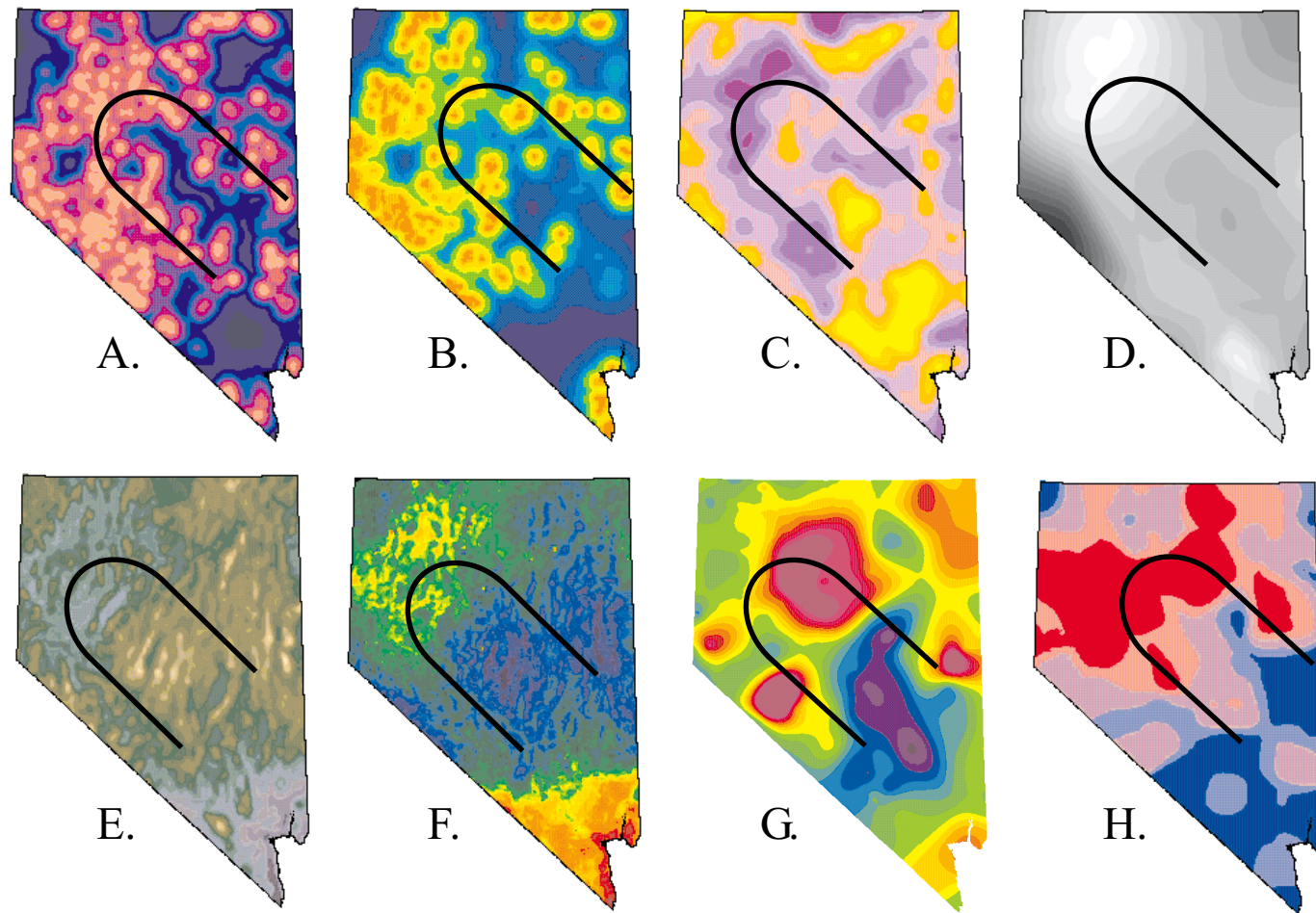
**Figure 6.1.** Distribution of gold-silver-bearing occurrences in the Nevada Great Basin. These occurrences represent economic mineralization having gold and/or silver as its primary commodity in production and/or reserve (i.e.—unknown size occurrences are not plotted). Large: n=59; Medium n=118; Small n=2269. Weight unit (t) in metric tonnes. See text for discussion.



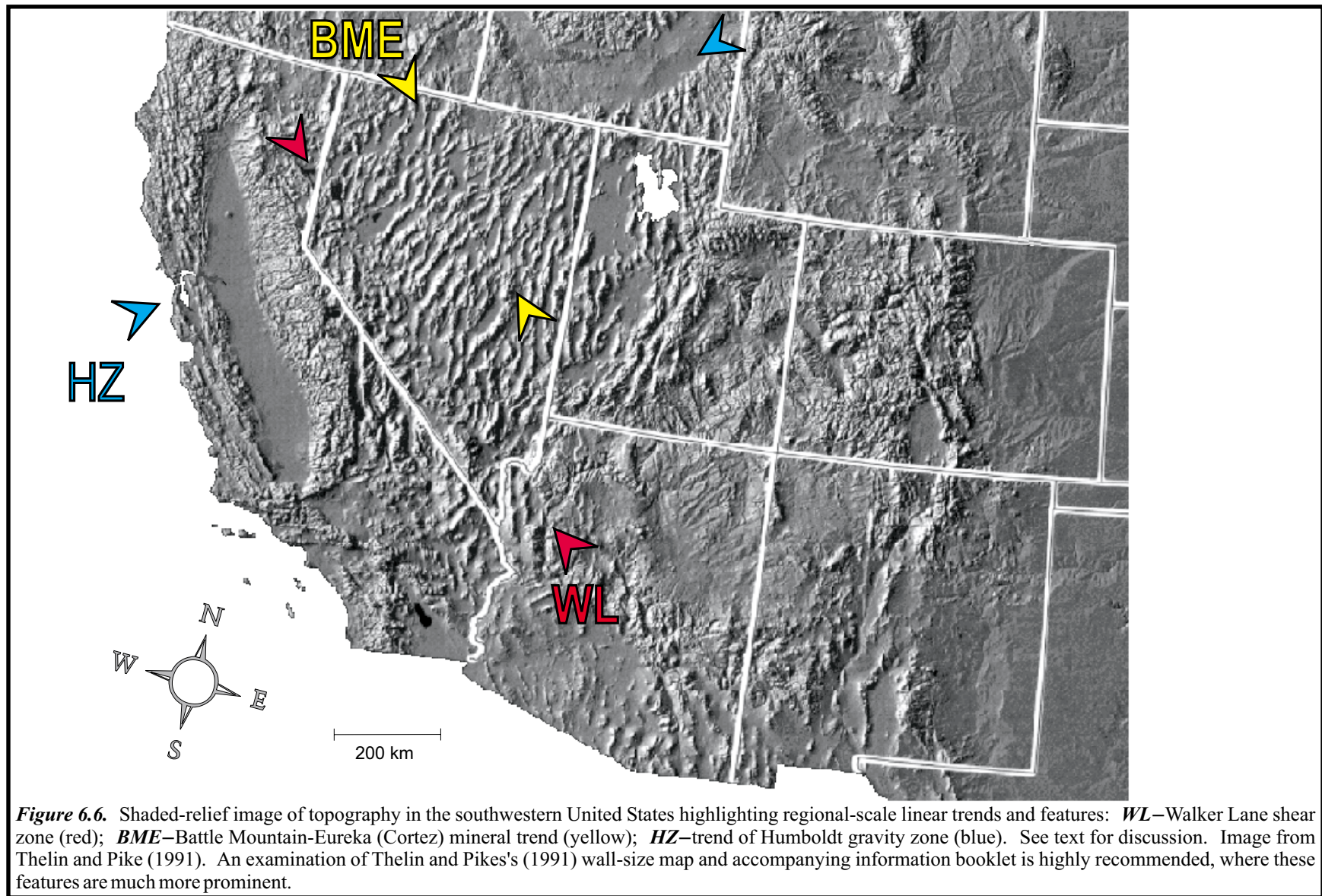








**Figure 6.5.** Map patterns of various geoscientific datasets reflecting the "U-shaped" or "horse-shoe-shaped" distribution pattern of the precious- and non-precious-metal occurrences in Nevada (note line on each map highlighting "U-shaped" trend). Brighter "warmer" colors denote higher magnitudes of the phenomenon mapped (i.e.—denser, higher, warmer, etc.), whereas darker "cooler" colors represent lower magnitudes (i.e.—less dense, lower, cooler, etc.), with the exception of map "D" (crustal thickness), where darker greys indicate thicker crust. *A*—precious and non-precious metal occurrence density; *B*—density of Mesozoic plutonic rocks; *C*—density of mapped faults; *D*—depth to reflection Moho; *E*—topography; *F*—Bouguer gravity; *G*—heat flow; *H*—temperature of geothermal wells and springs.





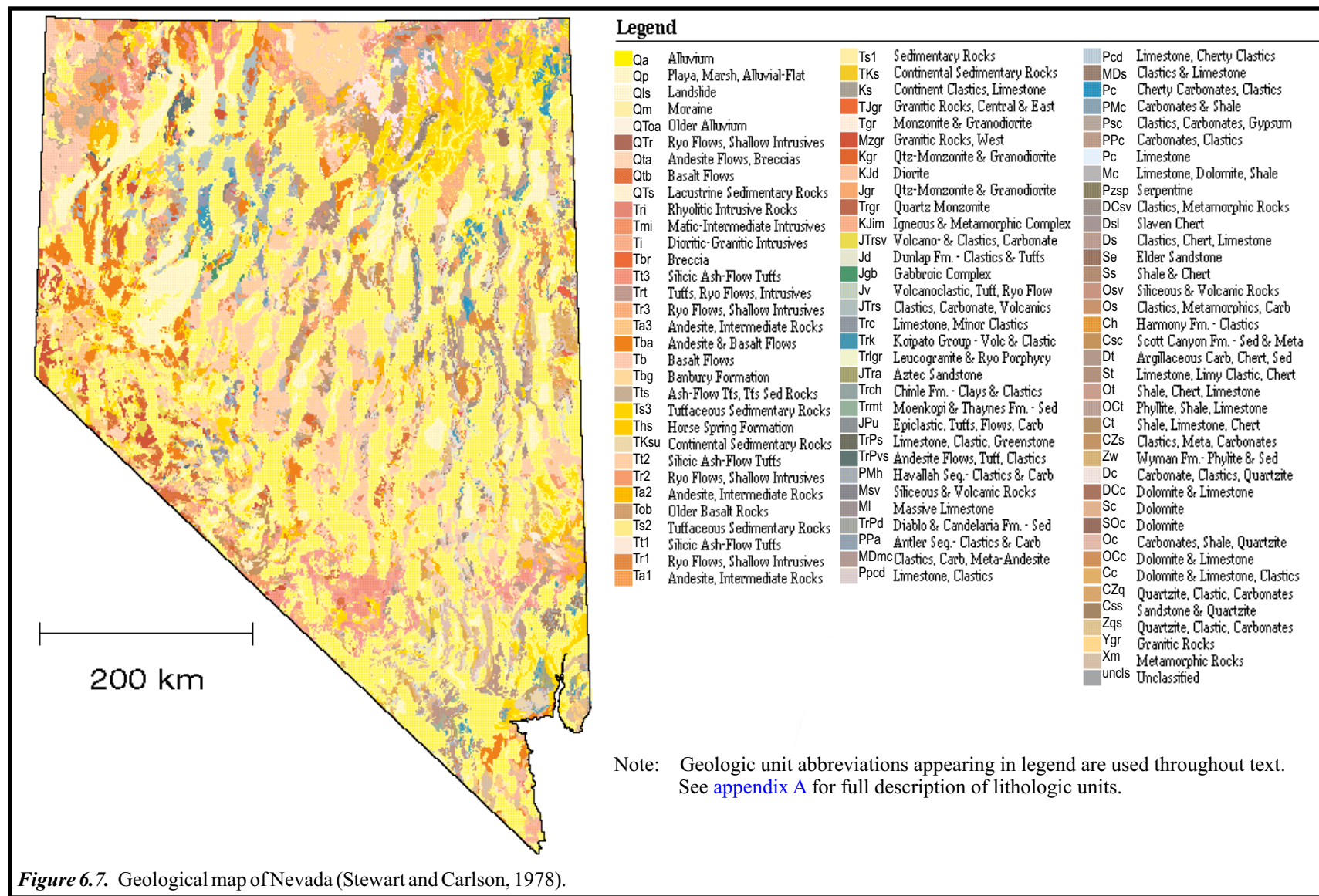
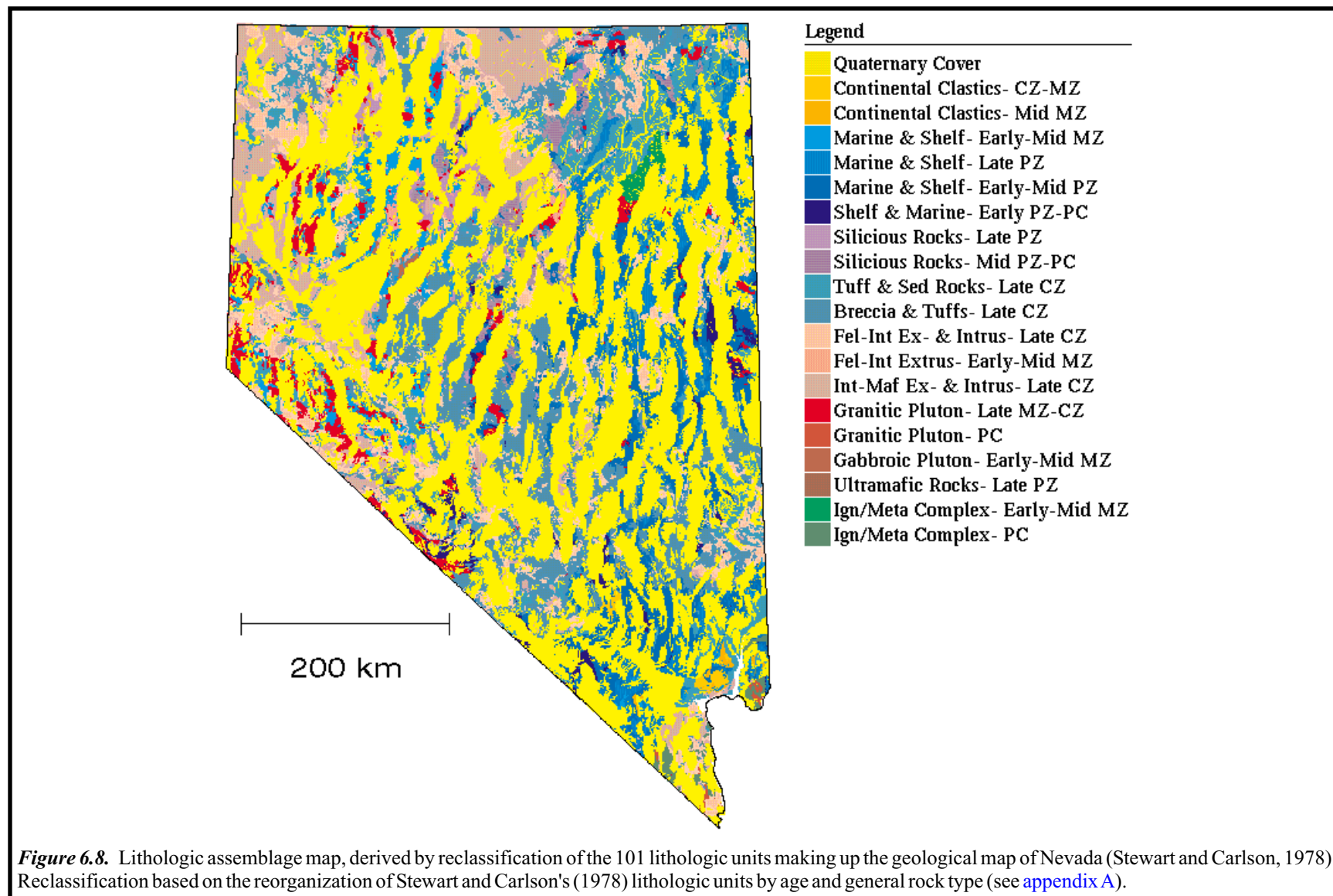
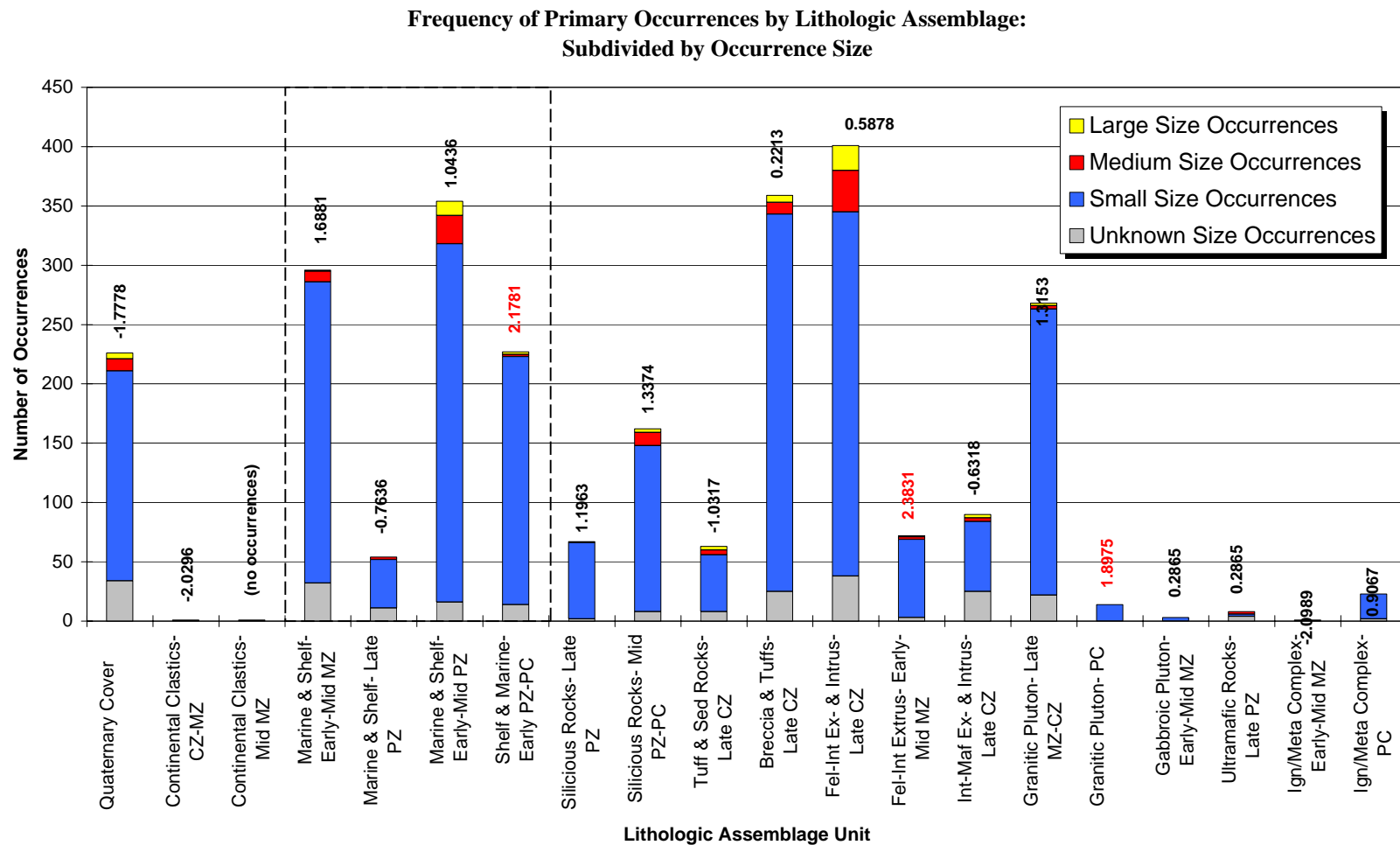
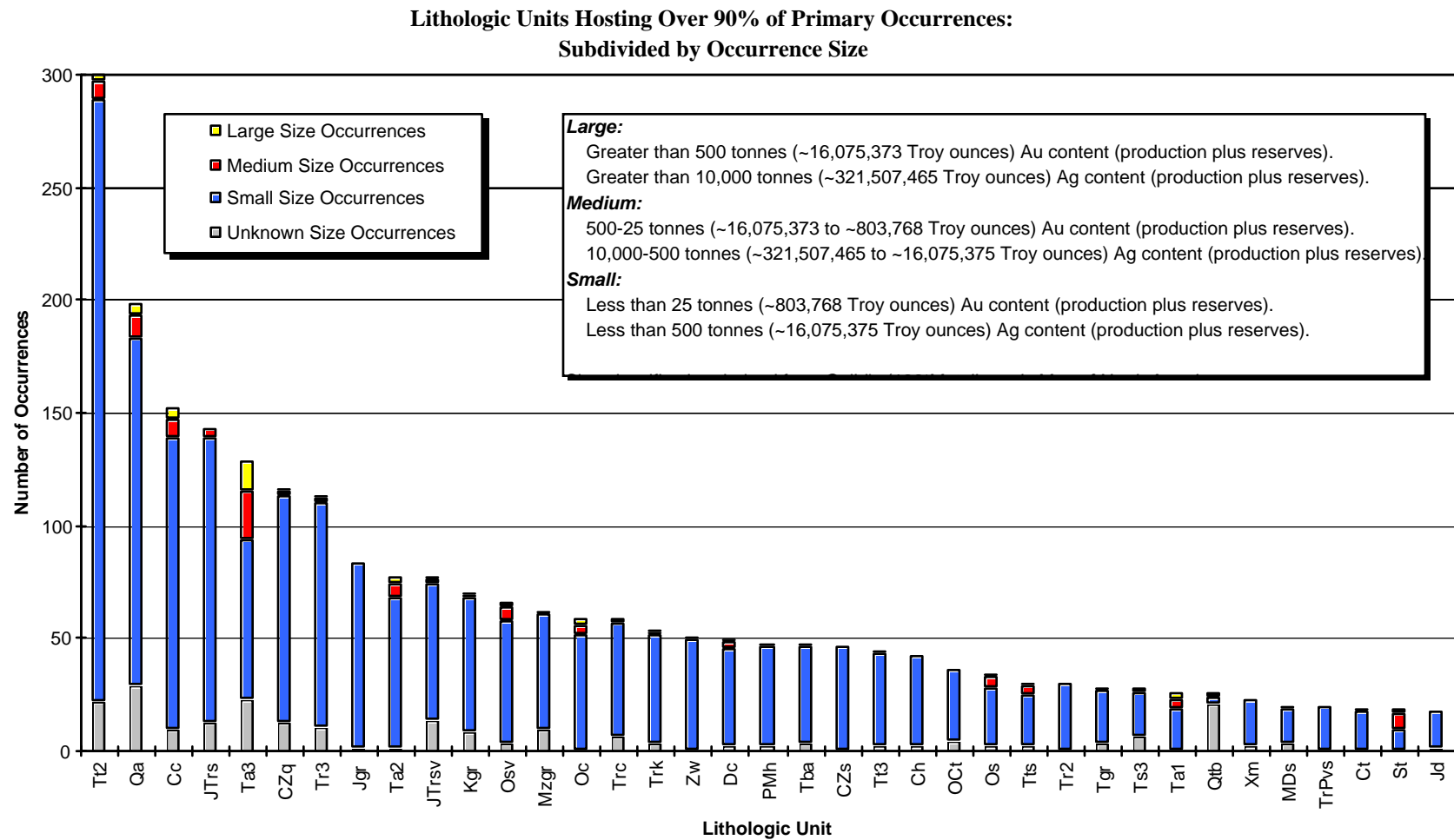


Figure 6.7. Geological map of Nevada (Stewart and Carlson, 1978).





**Figure 6.9.** Number of primary occurrences (subdivided by size) per lithologic assemblage unit. W+ shown for units (highest in red).



**Figure 6.10.** These 37 lithologic units (of 101) host over 90% of the primary occurrences (subdivided by size). See [Appendix A](#) for unit abbreviations.

### Lithologic Units Having a Strong Spatial Association with Primary Occurrences

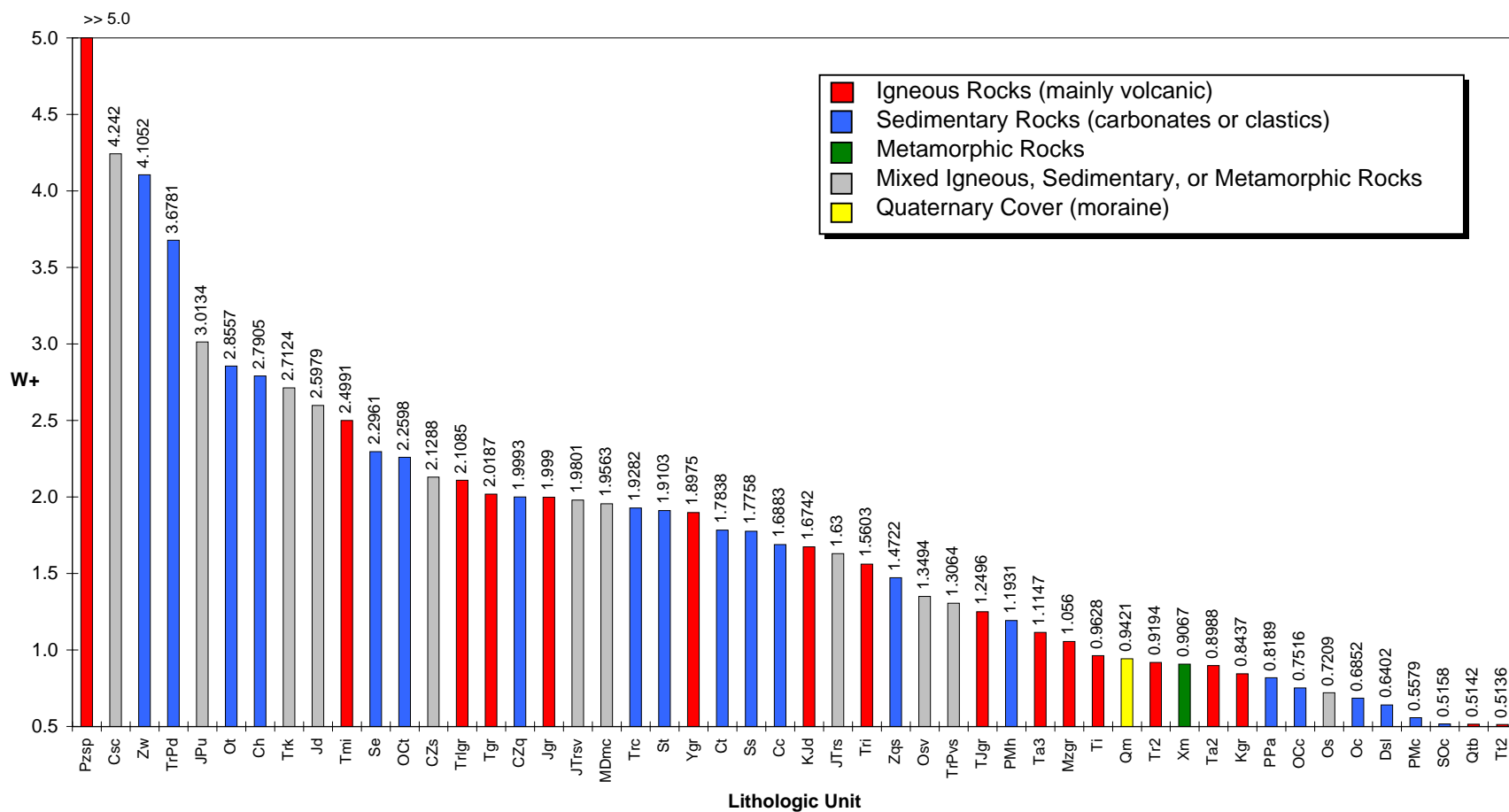


**Figure 6.11.** Lithologic units having a strong spatial association with primary occurrences. These units represent those in the 10th and higher percentile range of W+.



Frequency of Sedimentary Rock-Hosted Occurrences by Lithologic Assemblage:  
Subdivided by Occurrence Size

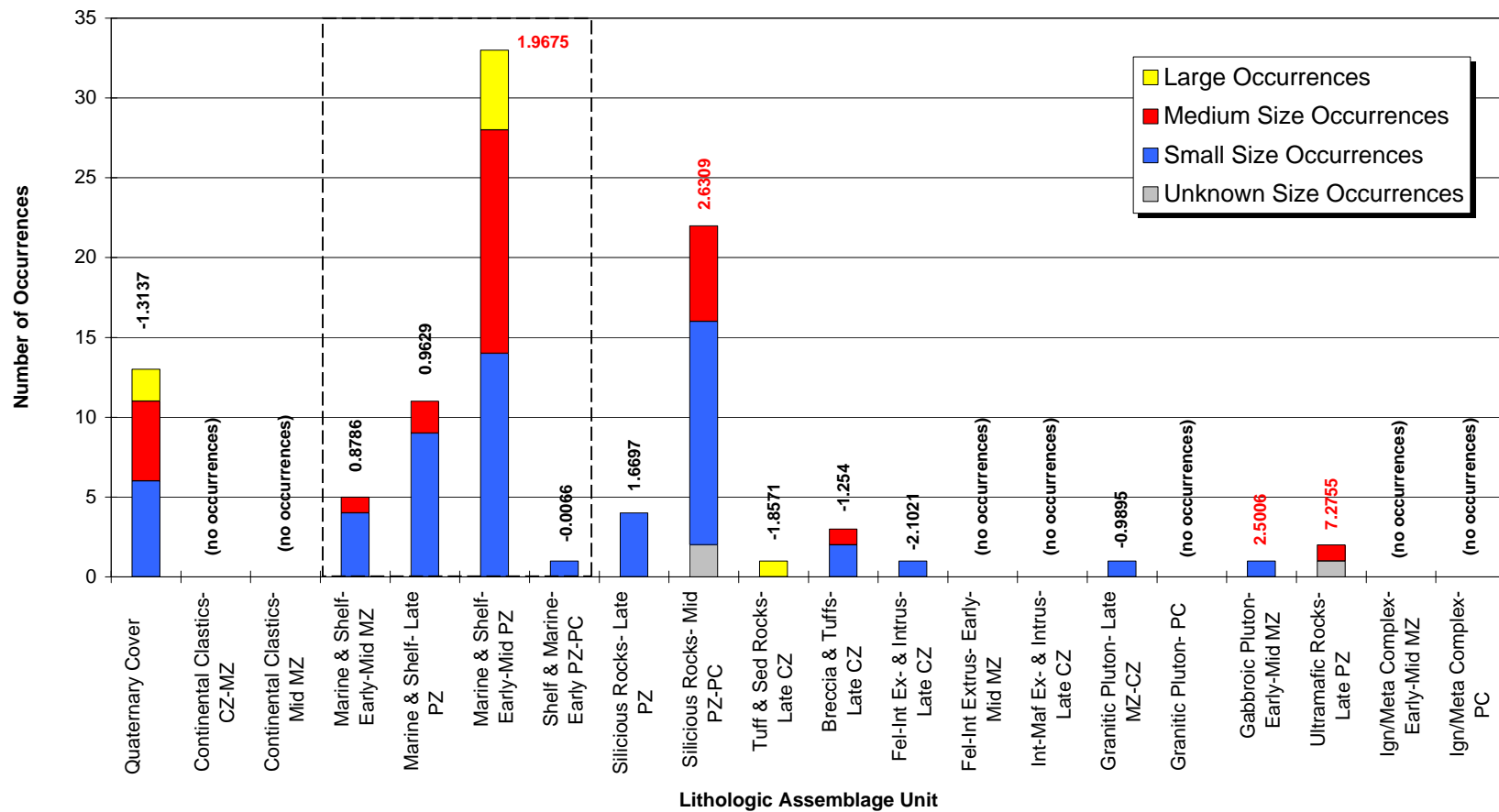
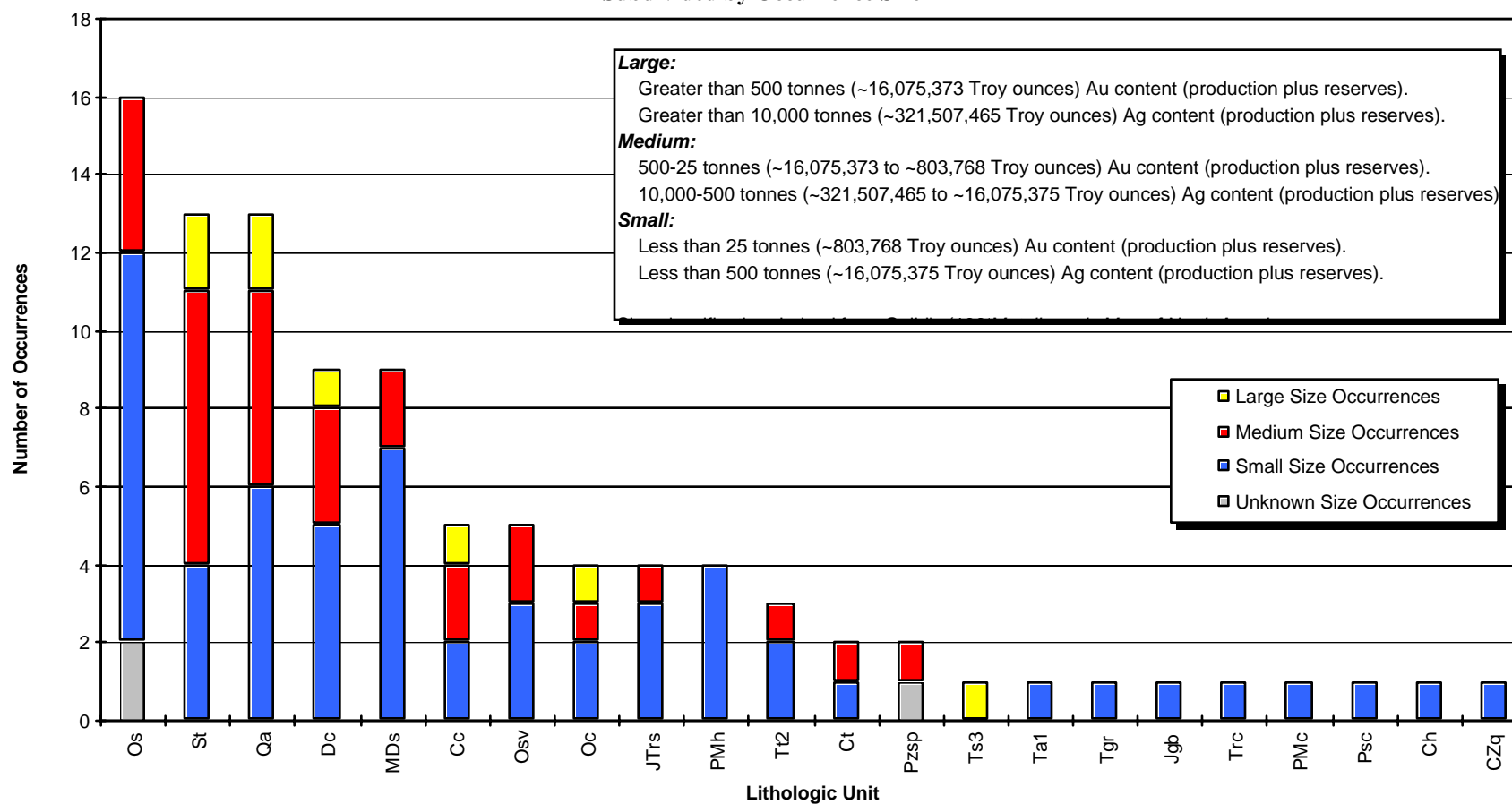


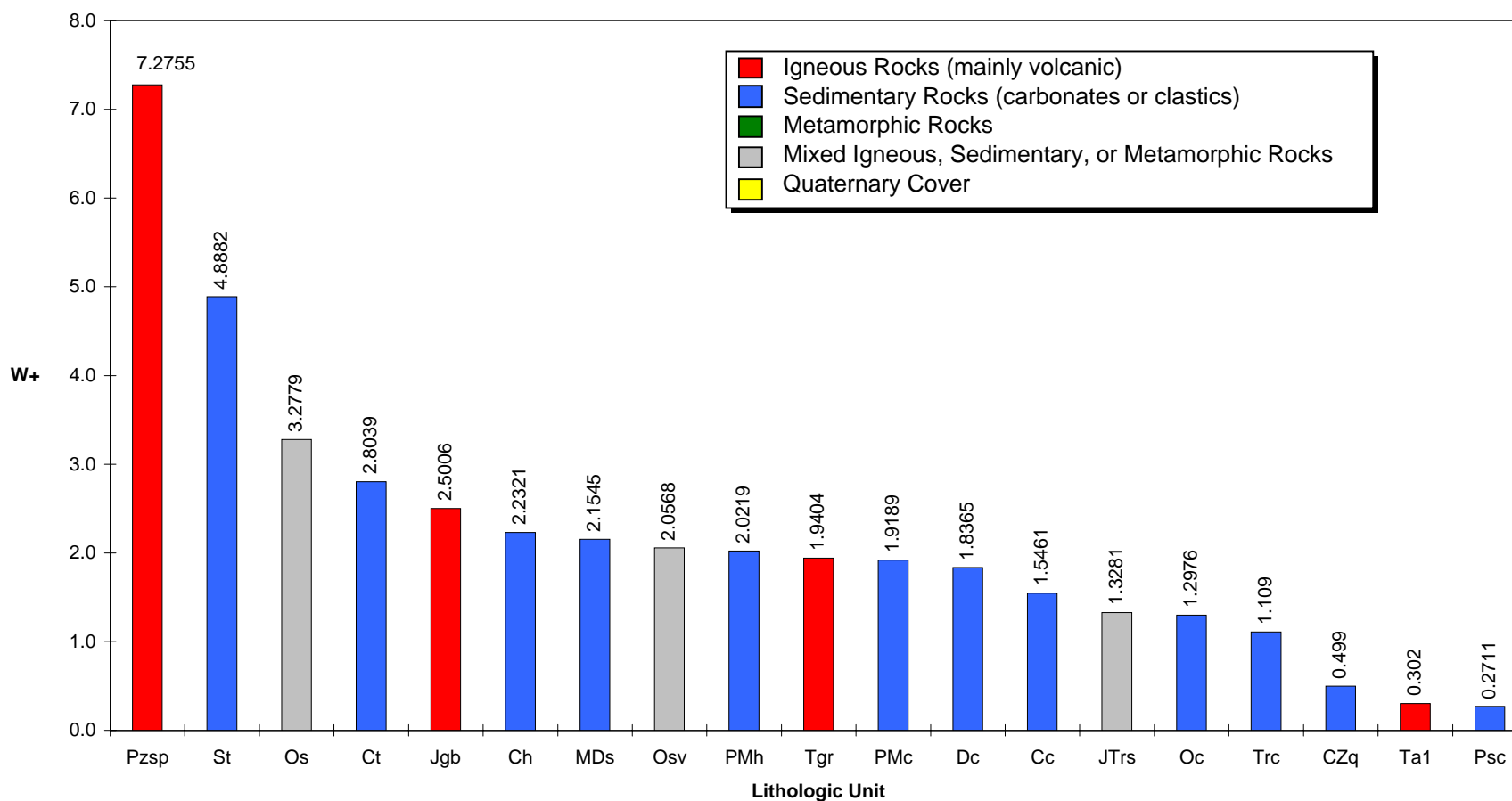
Figure 6.12. Number of sedimentary rock-hosted occurrences (subdivided by size) per lithologic assemblage unit. W+ shown for units (highest in red).

**Lithologic Units Hosting 100% of Sedimentary Rock-Hosted Occurrences:  
Subdivided by Occurrence Size**

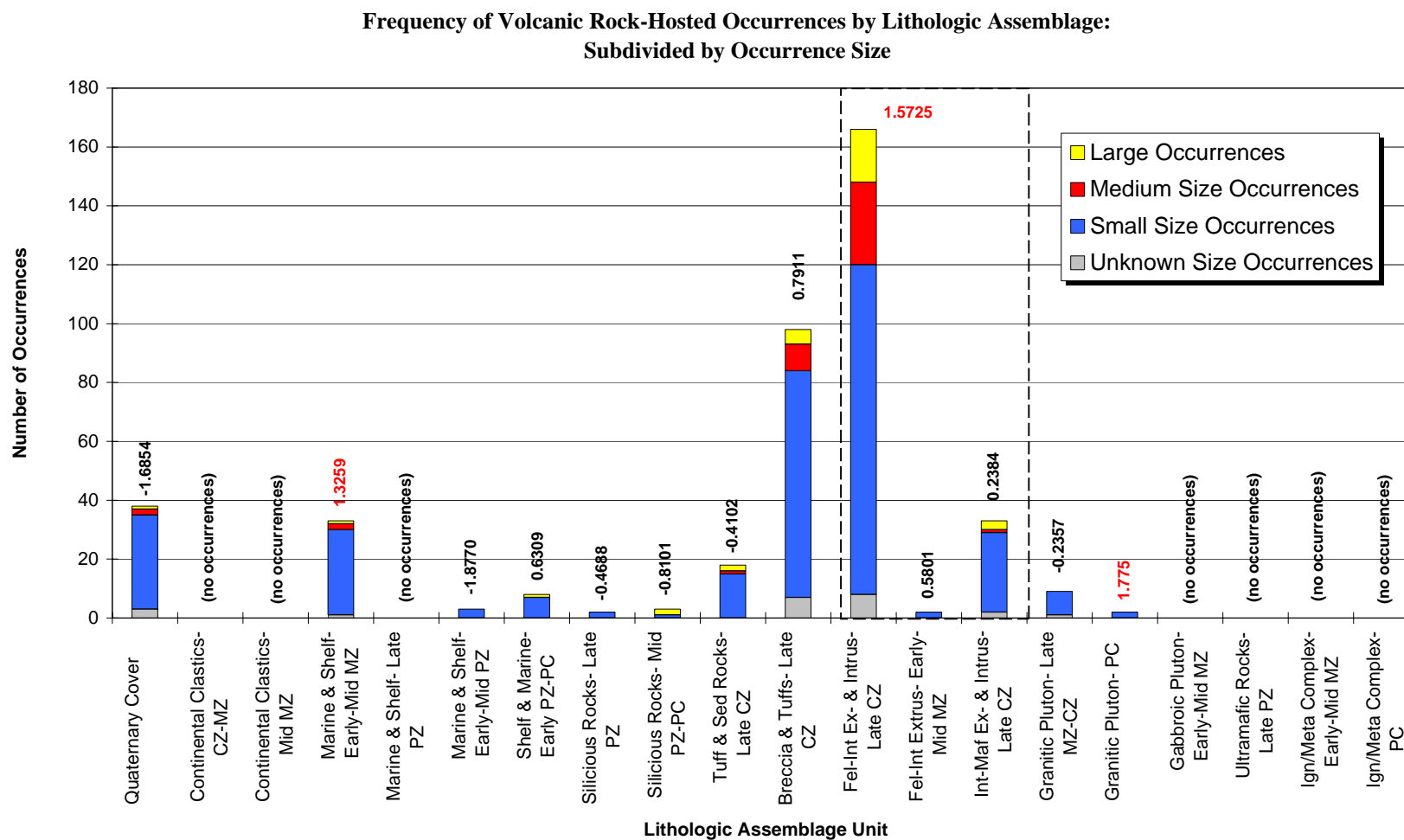


**Figure 6.13.** These 22 lithologic units (of 101) host 100% of the sedimentary rock-hosted occurrences (subdivided by size). See [Appendix A](#) for unit abbreviations.

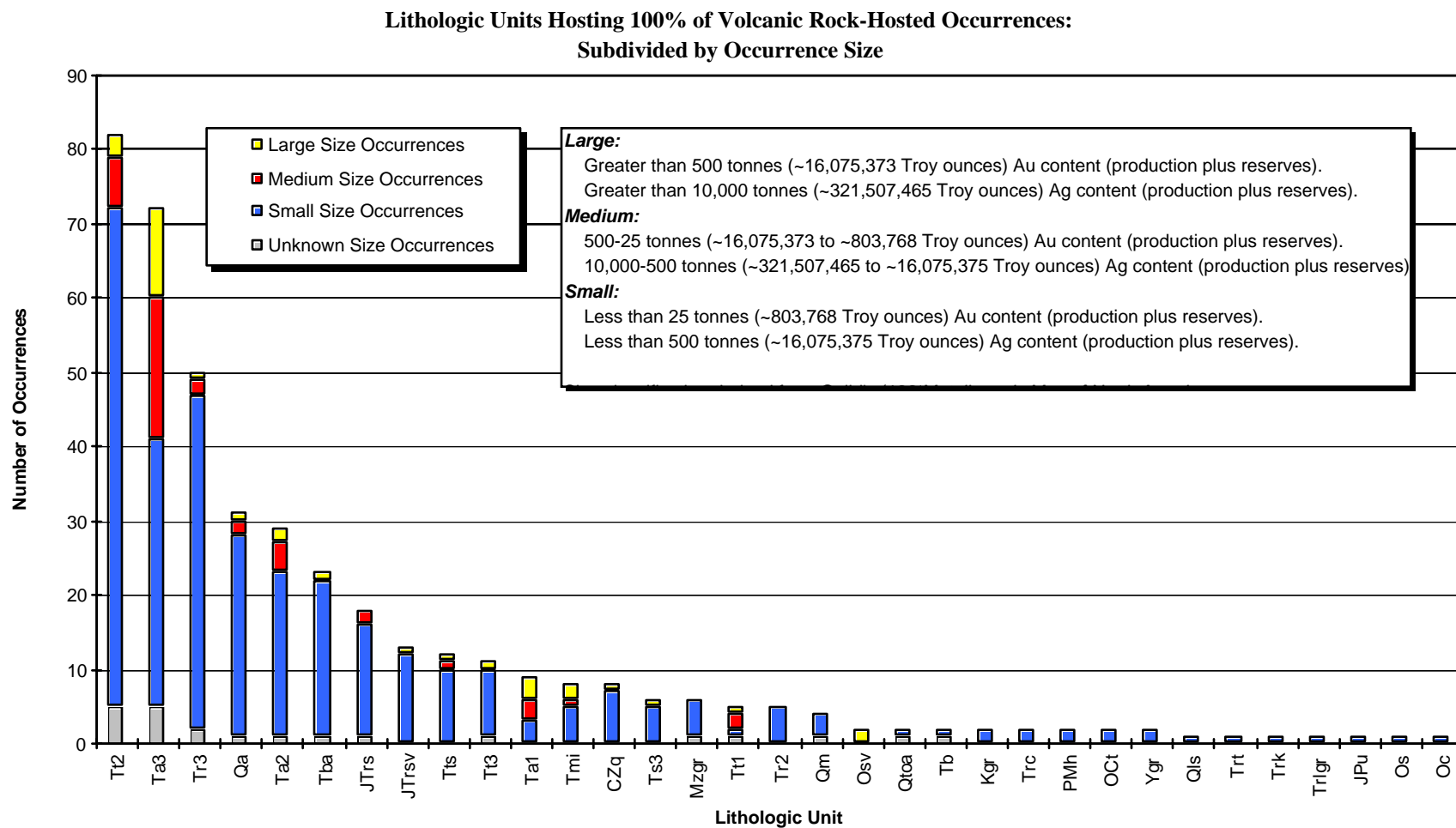
### Lithologic Units Having a Strong Spatial Association with Sedimentary Rock-Hosted Occurrences



**Figure 6.14.** Lithologic units having a strong spatial association with sedimentary rock-hosted occurrences. These units represent all of those having a positive value for  $W_+$ .

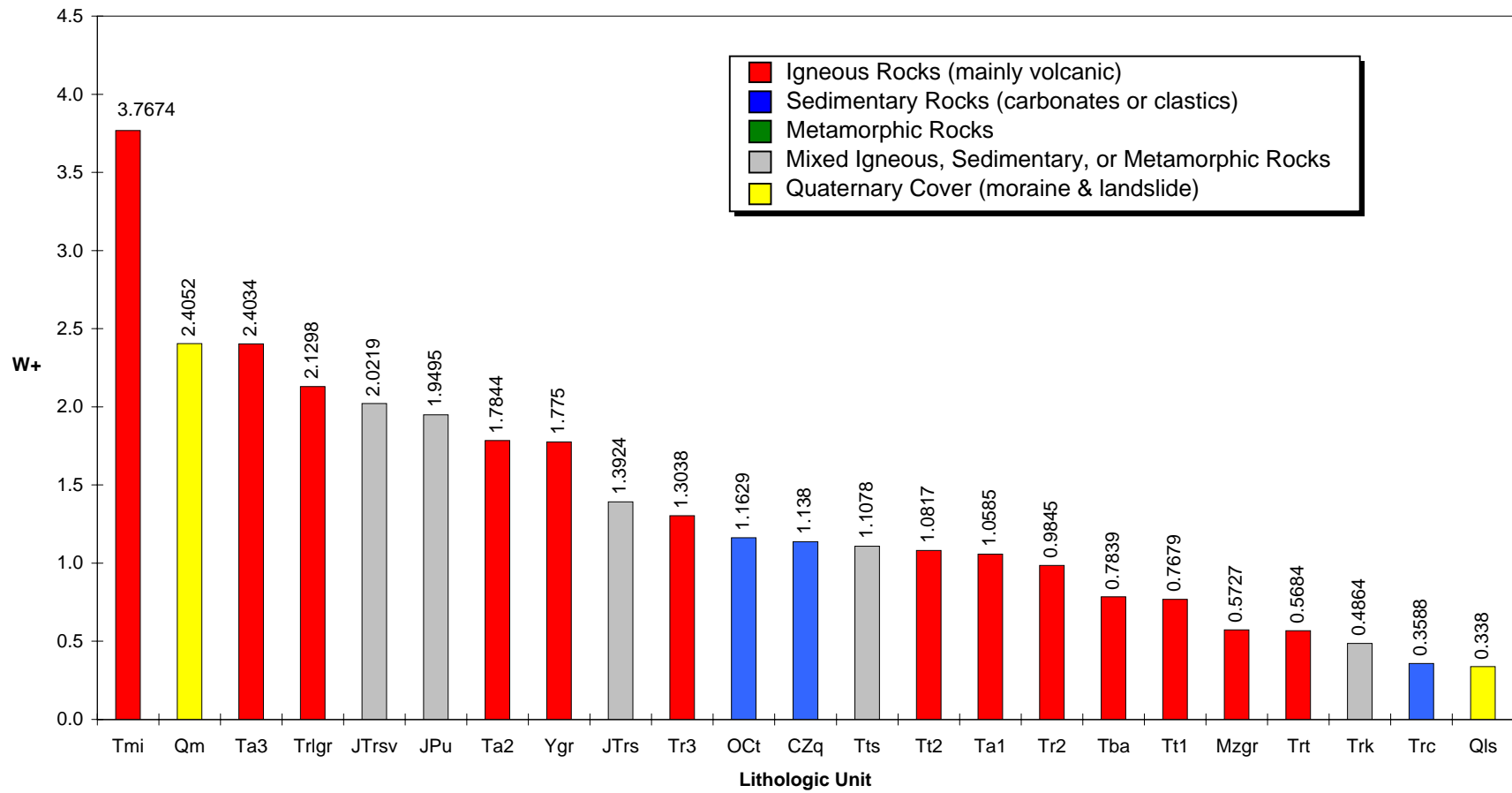


**Figure 6.15.** Number of volcanic rock-hosted occurrences (subdivided by size) per lithologic assemblage unit. W+ shown for units (highest in red).

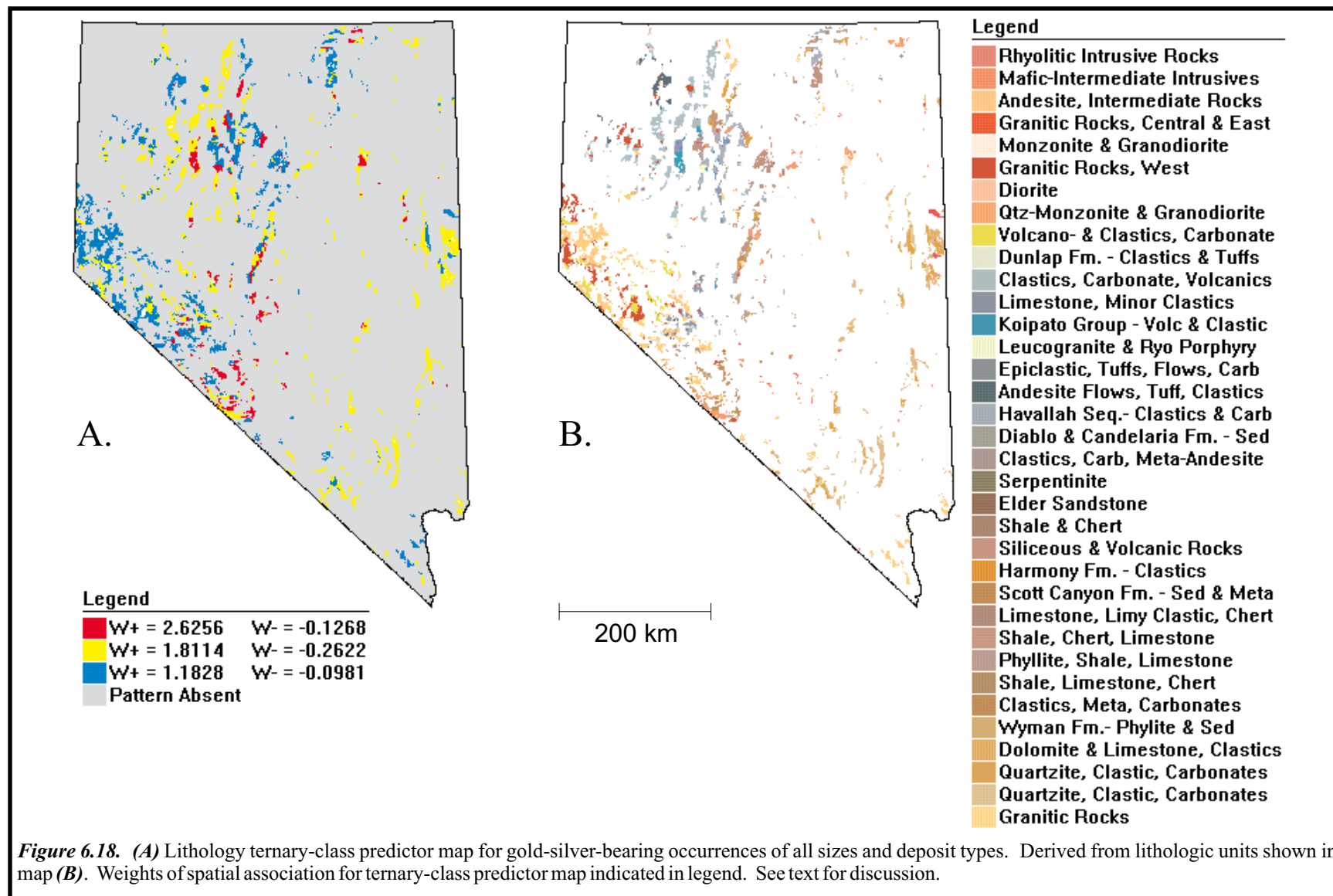


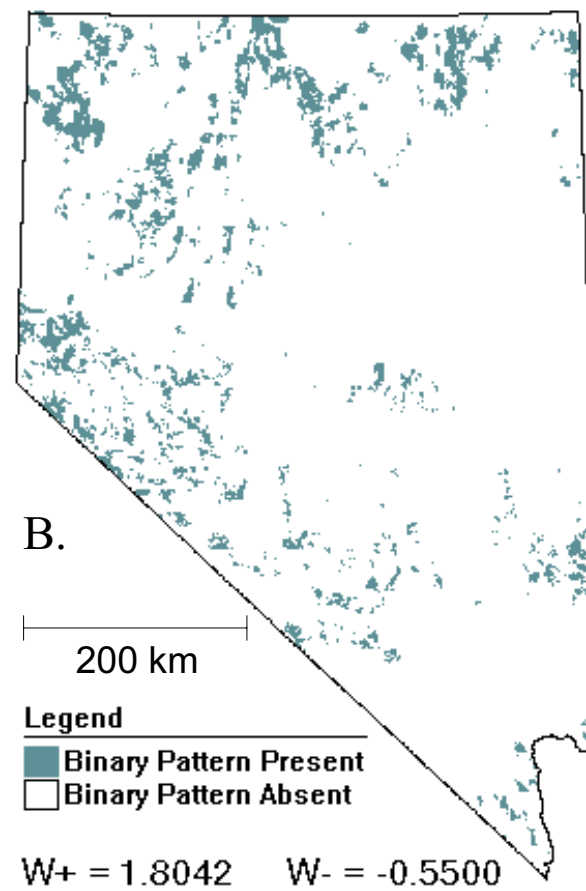
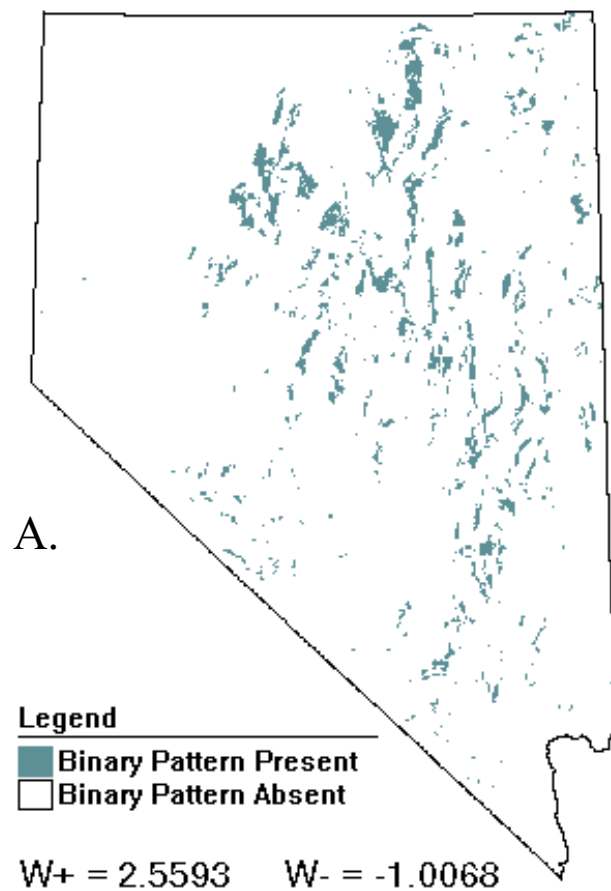
**Figure 6.16.** These 33 lithologic units (of 101) host 100% of the volcanic rock-hosted occurrences (subdivided by size). See [Appendix A](#) for unit abbreviations.

### Lithologic Units Having a Strong Spatial Association with Volcanic Rock-Hosted Occurrences



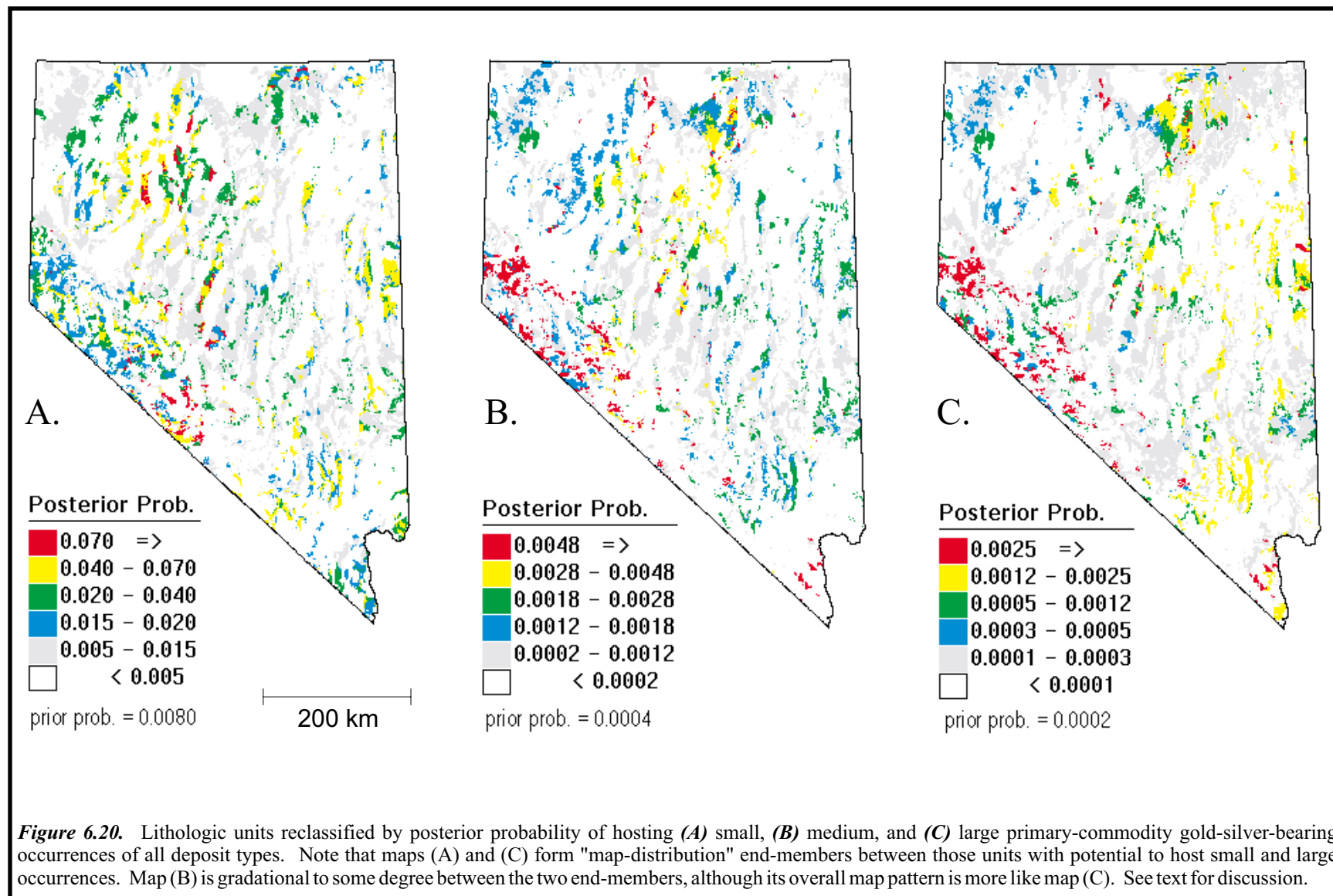
**Figure 6.17.** Lithologic units having a strong spatial association with volcanic rock-hosted occurrences. These units represent all of those having a positive value for  $W_+$ .

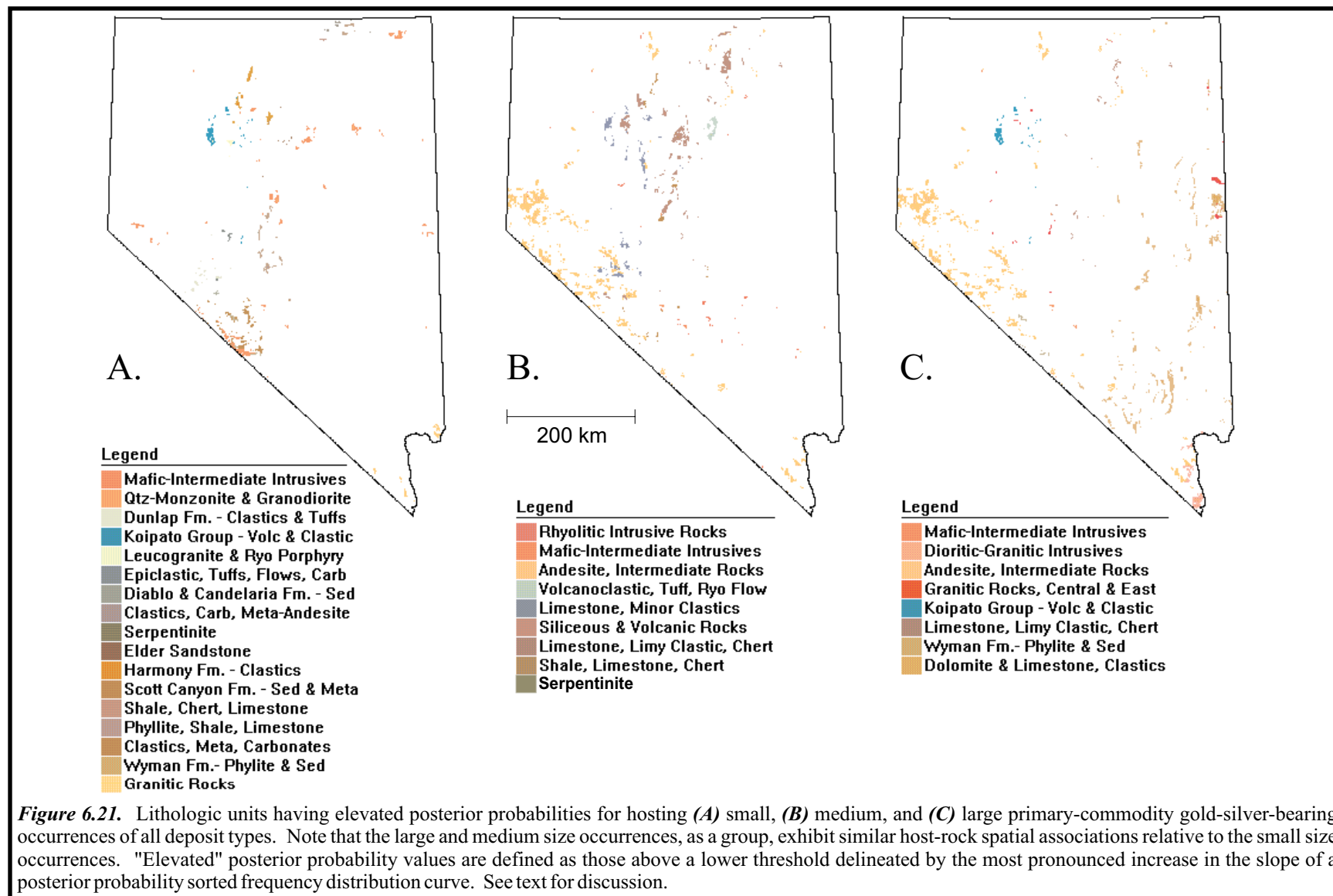


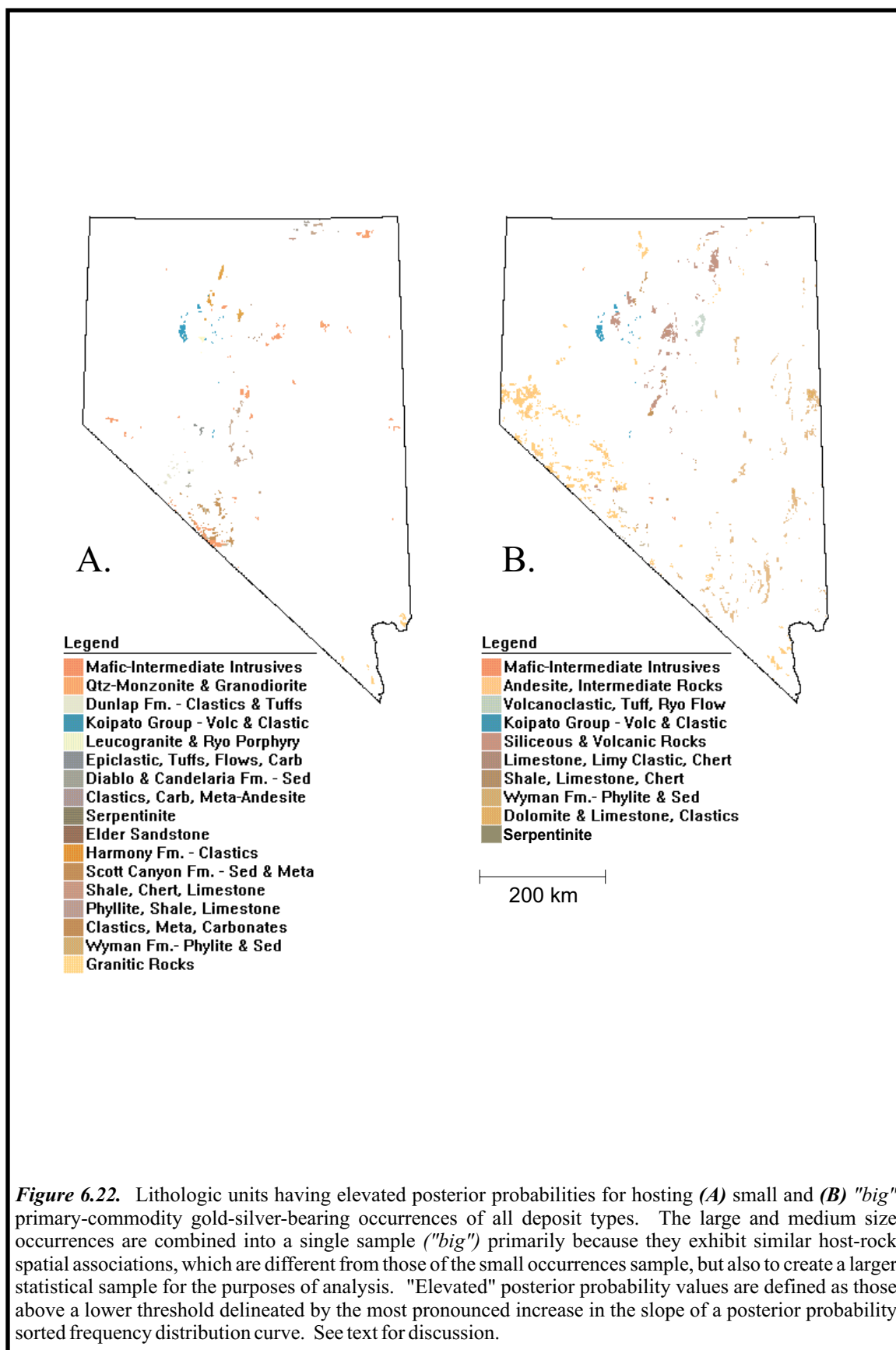


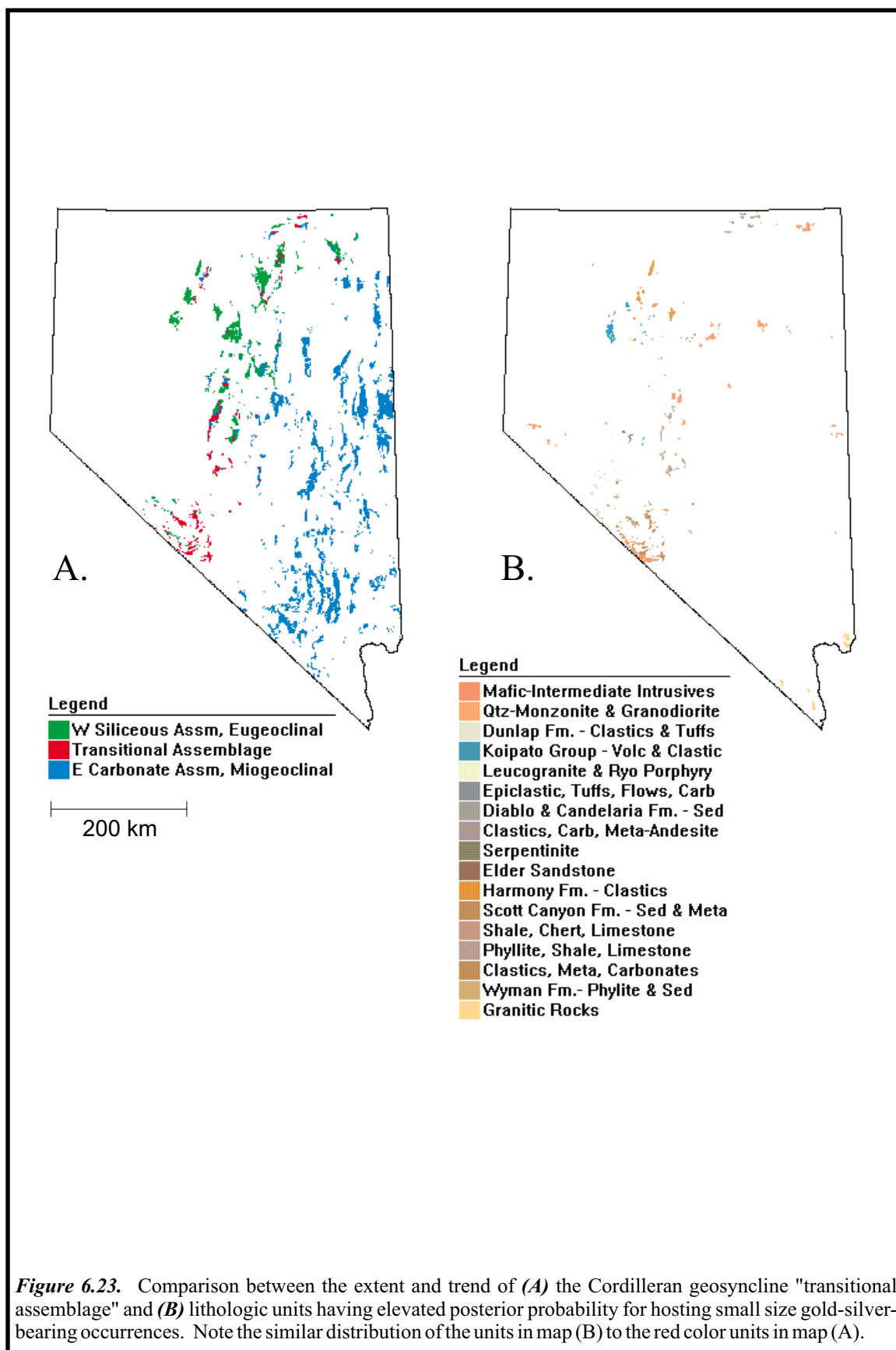
**Figure 6.19.** Lithology binary-class predictor maps for (A) sedimentary and (B) volcanic rock-hosted gold-silver-bearing occurrences of all sizes. Weights of spatial association for binary-class predictor maps indicated in legend. See text for discussion.

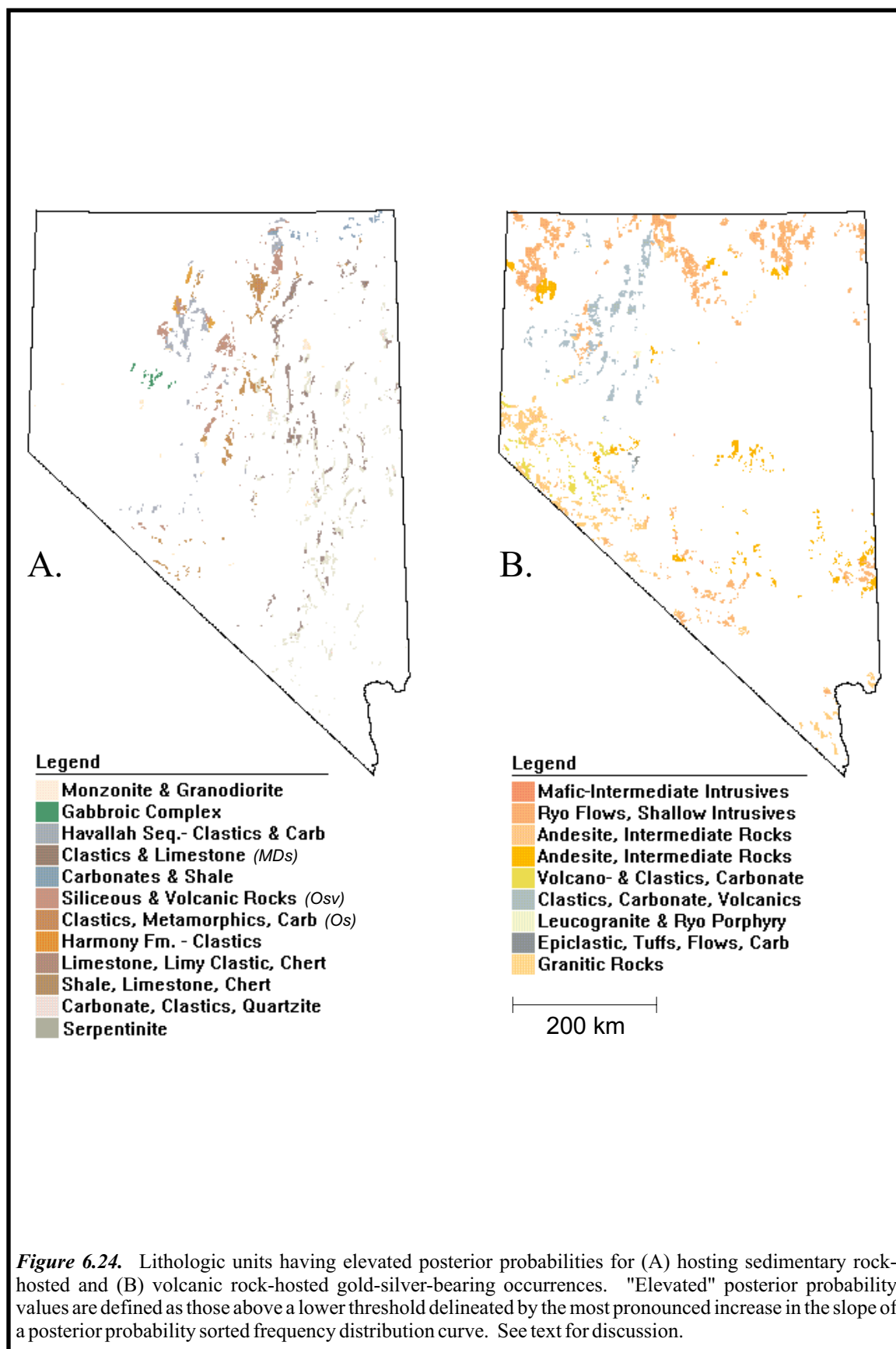


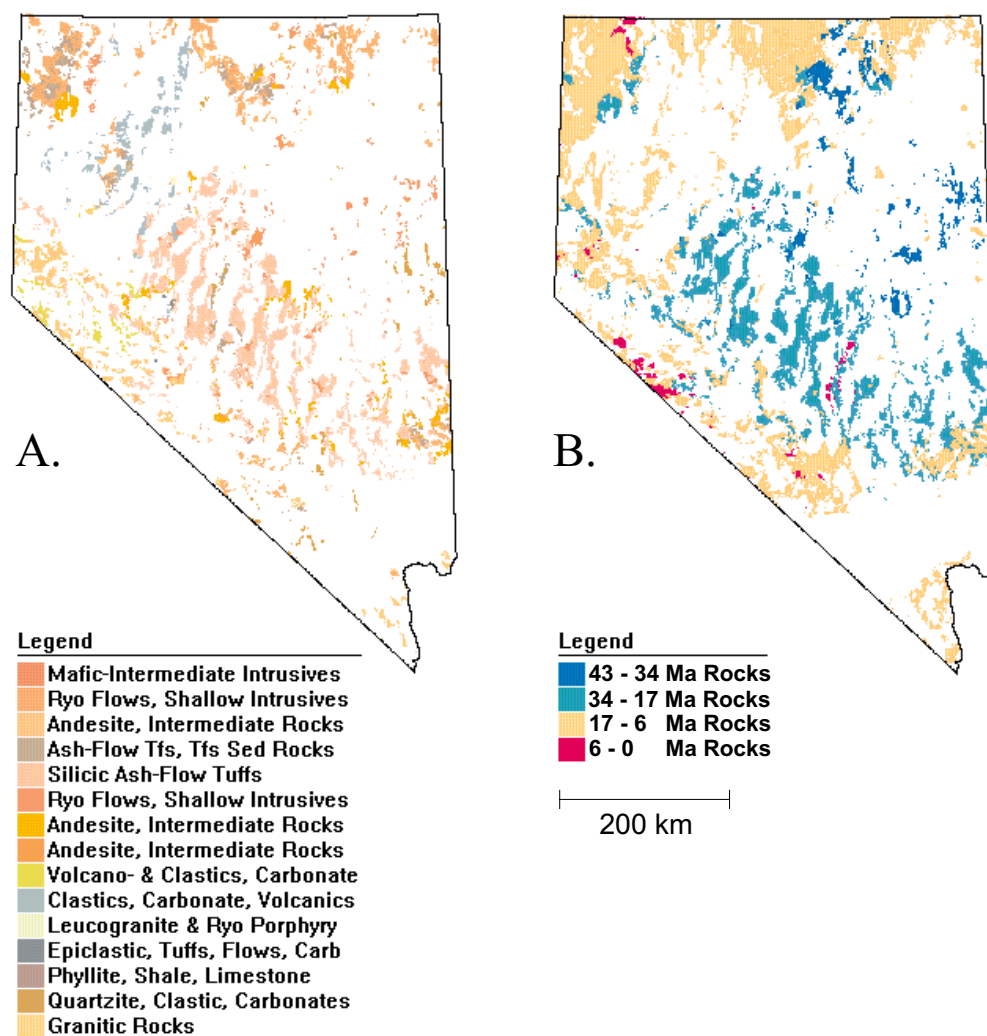




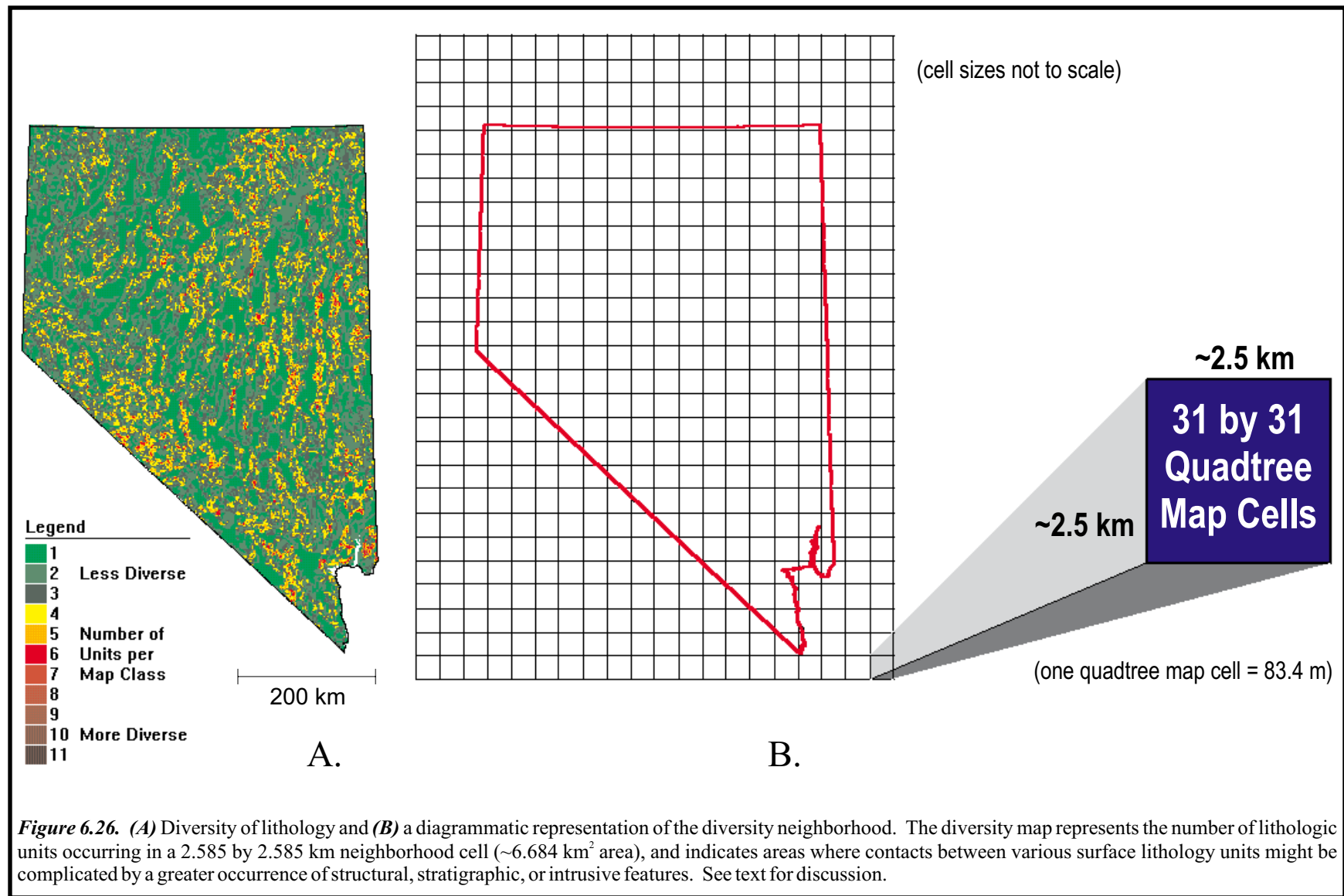








**Figure 6.25.** Lithologic units having "substantial" posterior probabilities for (A) hosting volcanic rock-hosted gold-silver-bearing occurrences, compared to a map illustrating (B) the space-time distribution of volcanic rocks in Nevada. Note the spatial coincidence between the units in map (A) to those of the 34-17—17-6 Ma units in map (B). "Substantial" posterior probability values are defined as those equal to and greater than the 25th percentile. See text for discussion.





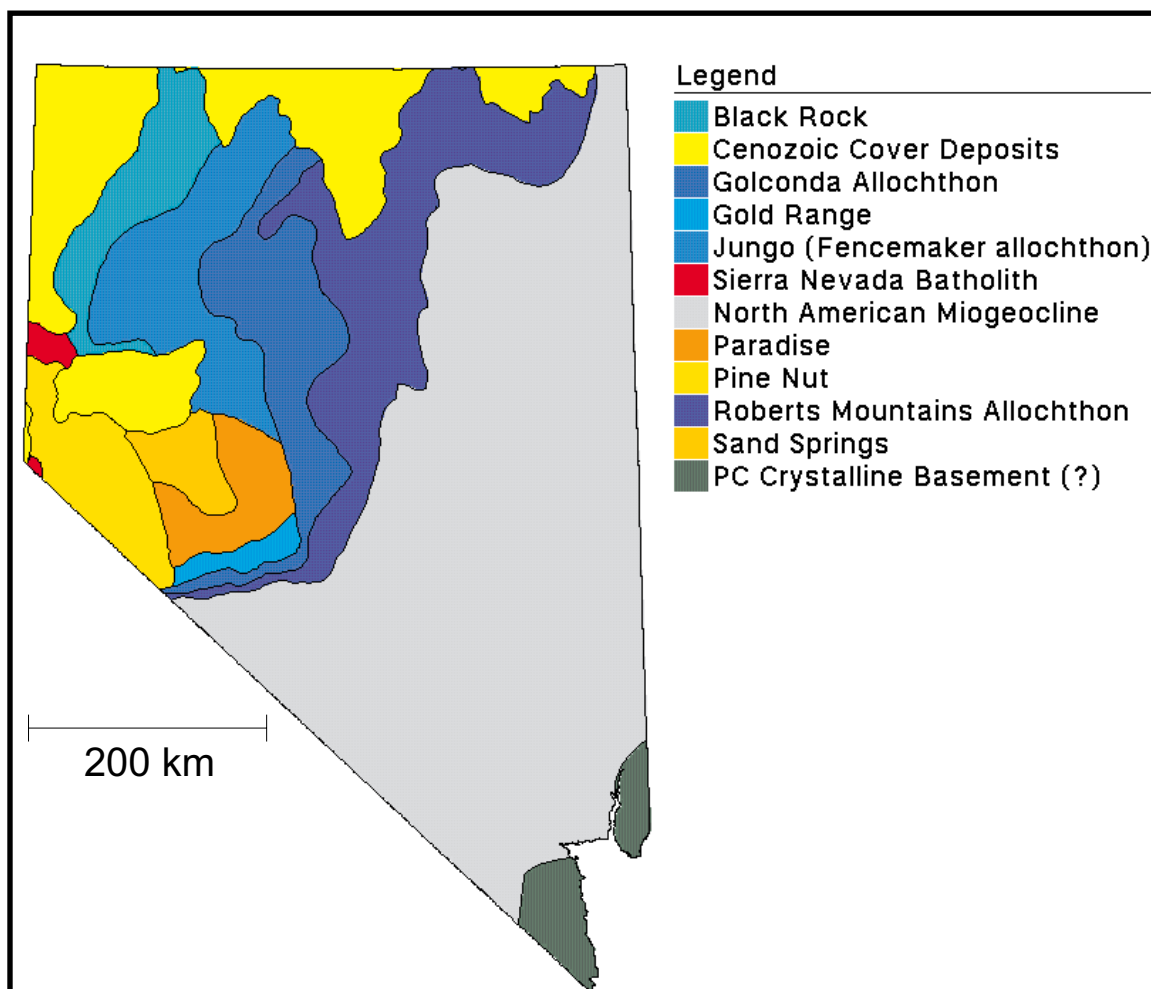


**Figure 6.27.** Lithotectonic terranes of Nevada. The terrane map coverage is a generalized representation of allochthonous terranes, with particular focus on the area of the Great Basin. Most of this coverage is based on the maps of N. J. Silberling (Silberling et al., 1987; Silberling, 1991), which should be consulted for a better understanding of the lithotectonic units. In order to provide full map coverage for Nevada, an additional map unit labelled "PC Crystalline Basement (?)" was added. It is approximate in extent and is derived from the position of Precambrian rock outcrops on the geological map of Nevada (Stewart and Carlson, 1978). The following information about this coverage was provided by G. L. Raines (1995, personal communication), the source of which is N. J. Silberling. The area between the Sand Springs and Jungo terranes is an area of controversial terrane assignment, belonging to either terrane. The lines bounding Cenozoic cover have a convoluted nature that gives them an aspect of false precision, and should be treated as approximate contacts only. An understanding of the distribution of the terranes in the third dimension is important to interpreting the map pattern. For example, lines bounding the eastern sides of the Roberts Mountain and Golconda allochthonous, unlike other terranes, simply indicate the easternmost exposures of these terranes—thus within the area of the Roberts Mountain allochthon, there are "windows" of the North American miogeocline, and within the area of the Golconda allochthon, there are windows of both the Roberts Mountain terrane and the North American miogeocline. The configuration of the eastern-bounding lines for these terranes reflect the present position of rocks whose exposures are controlled by a variety of compressional and extensional structures ranging from Paleozoic to Cenozoic in age. Only a minor part (at most) of the upper crustal thickness is actually composed of rocks characteristic of the named terranes. To some degree this is also true of the younger, more westerly terranes, particularly when their bounding faults were originally thin-skinned thrusts. In general, the boundaries of the terranes are discrete faults and, while even in two dimensions their regional map pattern is not well constrained, the terrane pattern can be regarded as a surface boundary. The crustal thickness of various terranes is variable and a matter of interpretation.

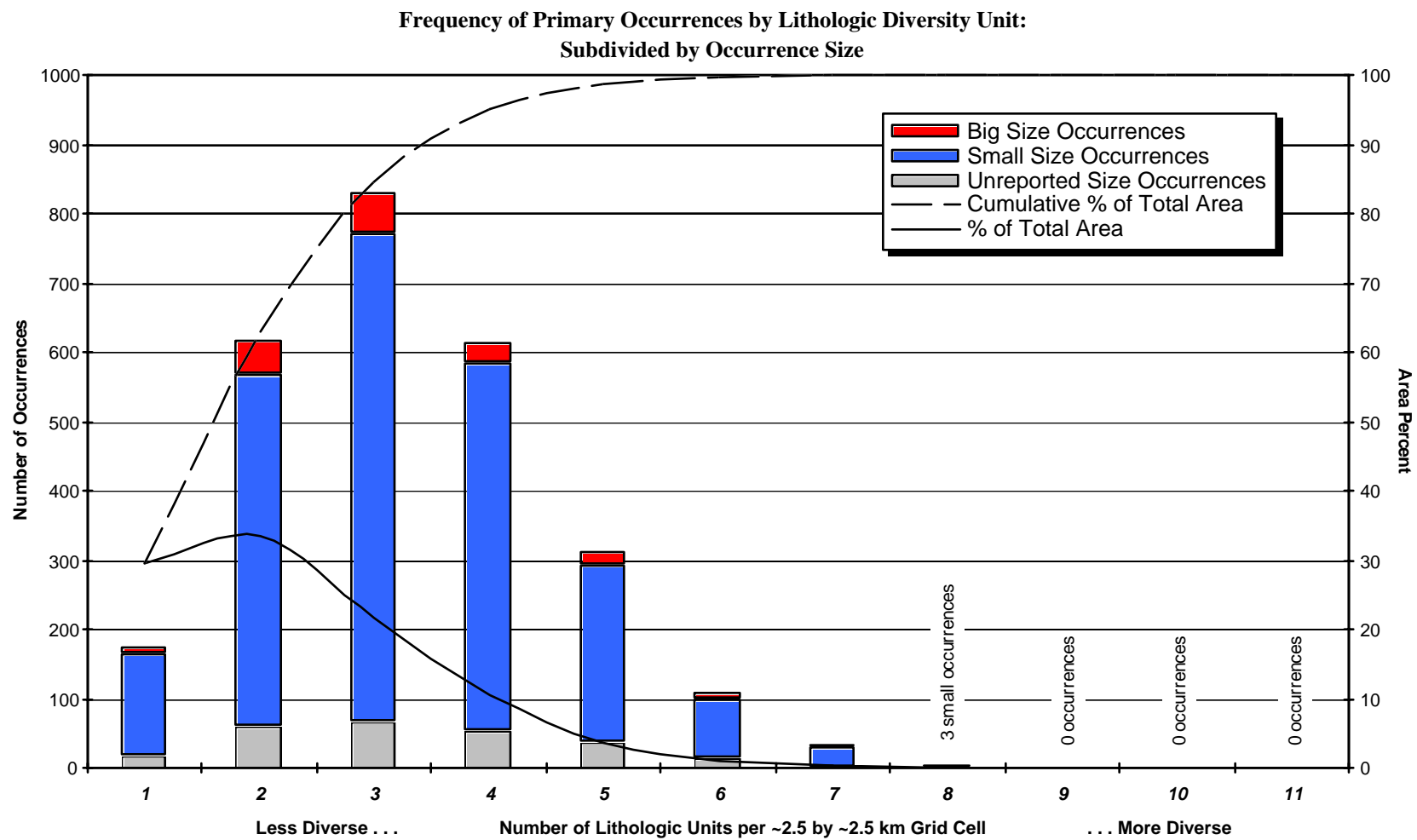


**Figure 6.28** Number of primary occurrences per lithologic diversity unit (subdivided by size).

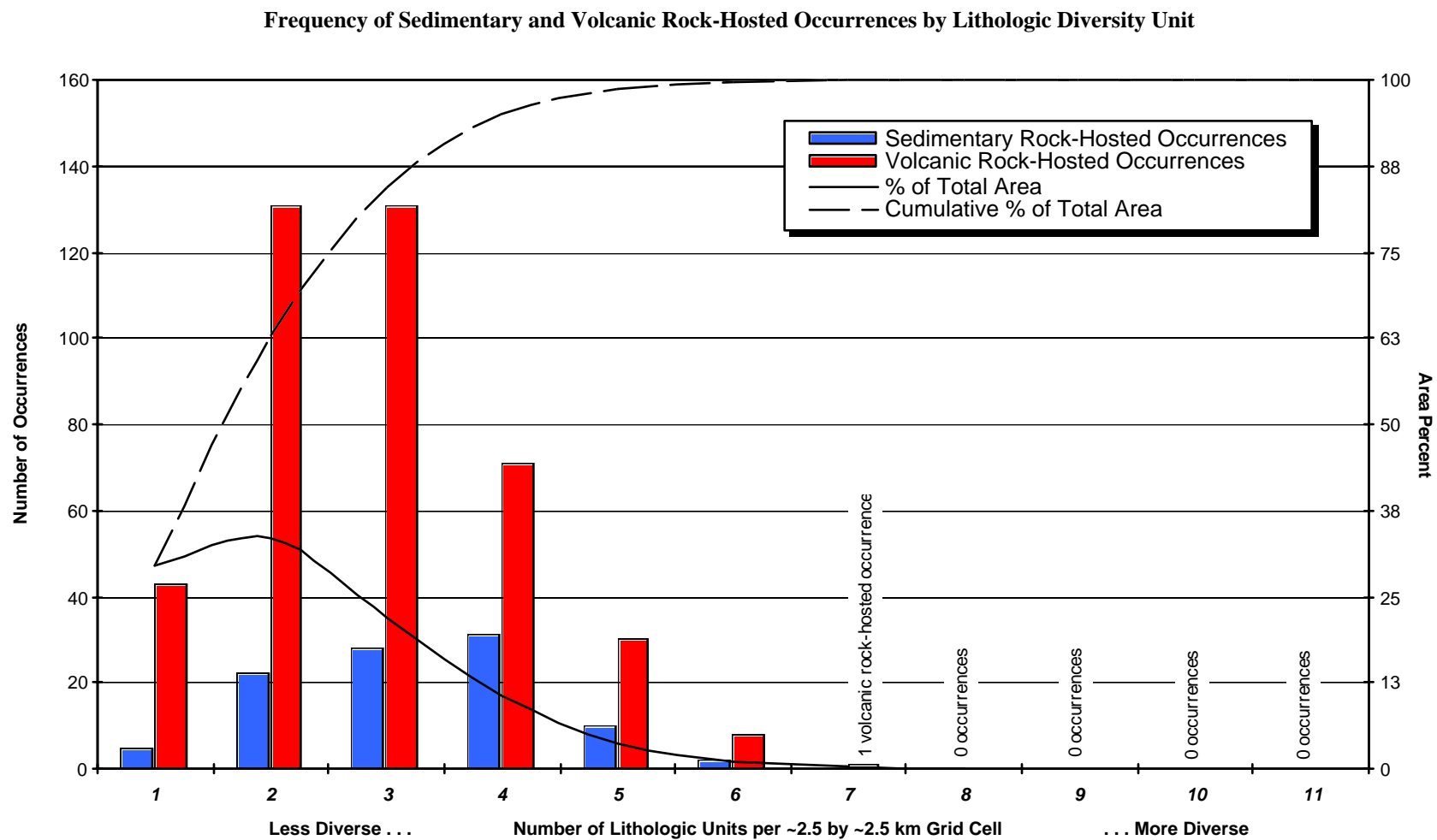


**Figure 6.29** Number of sedimentary and volcanic rock-hosted occurrences per lithologic diversity unit.

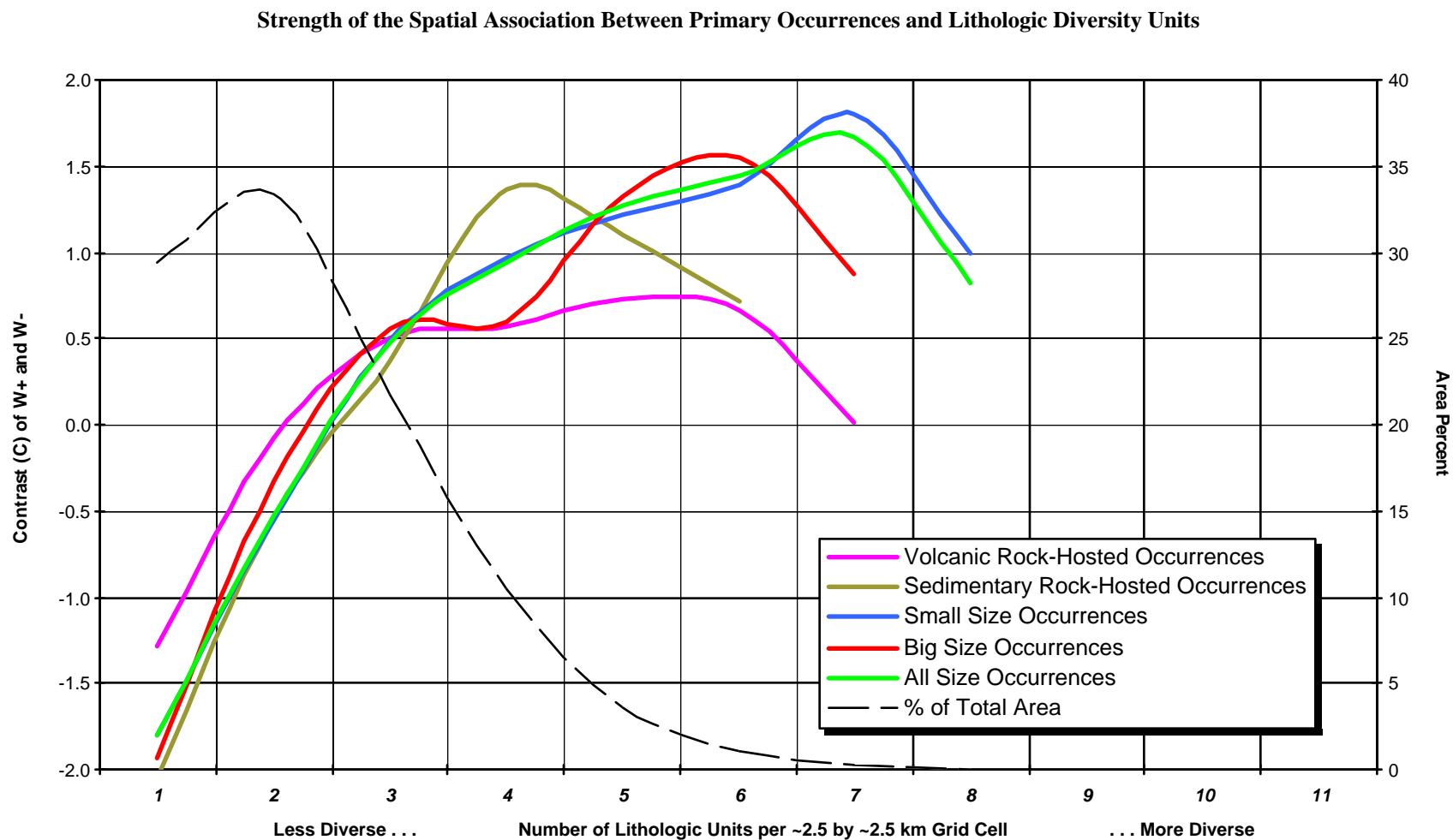


**Figure 6.30** Strength of spatial association (C) between lithologic diversity units and primary occurrences (subdivided by type and size). Note that (C) is non-area-cumulative

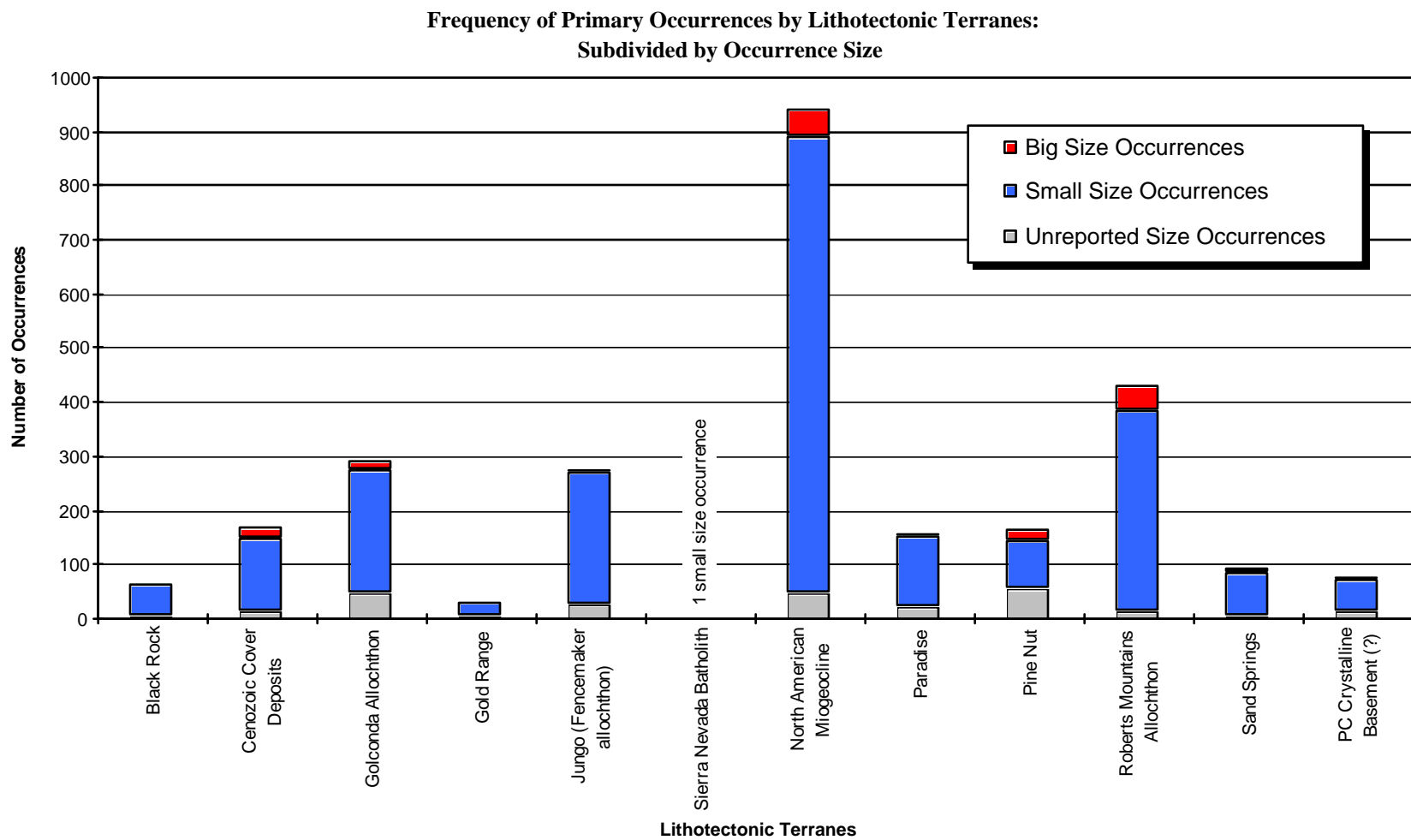


**Figure 6.31** Number of primary occurrences per lithotectonic terrane unit (subdivided by size).

**Frequency of Sedimentary and Volcanic Rock-Hosted by Lithotectonic Terrane**

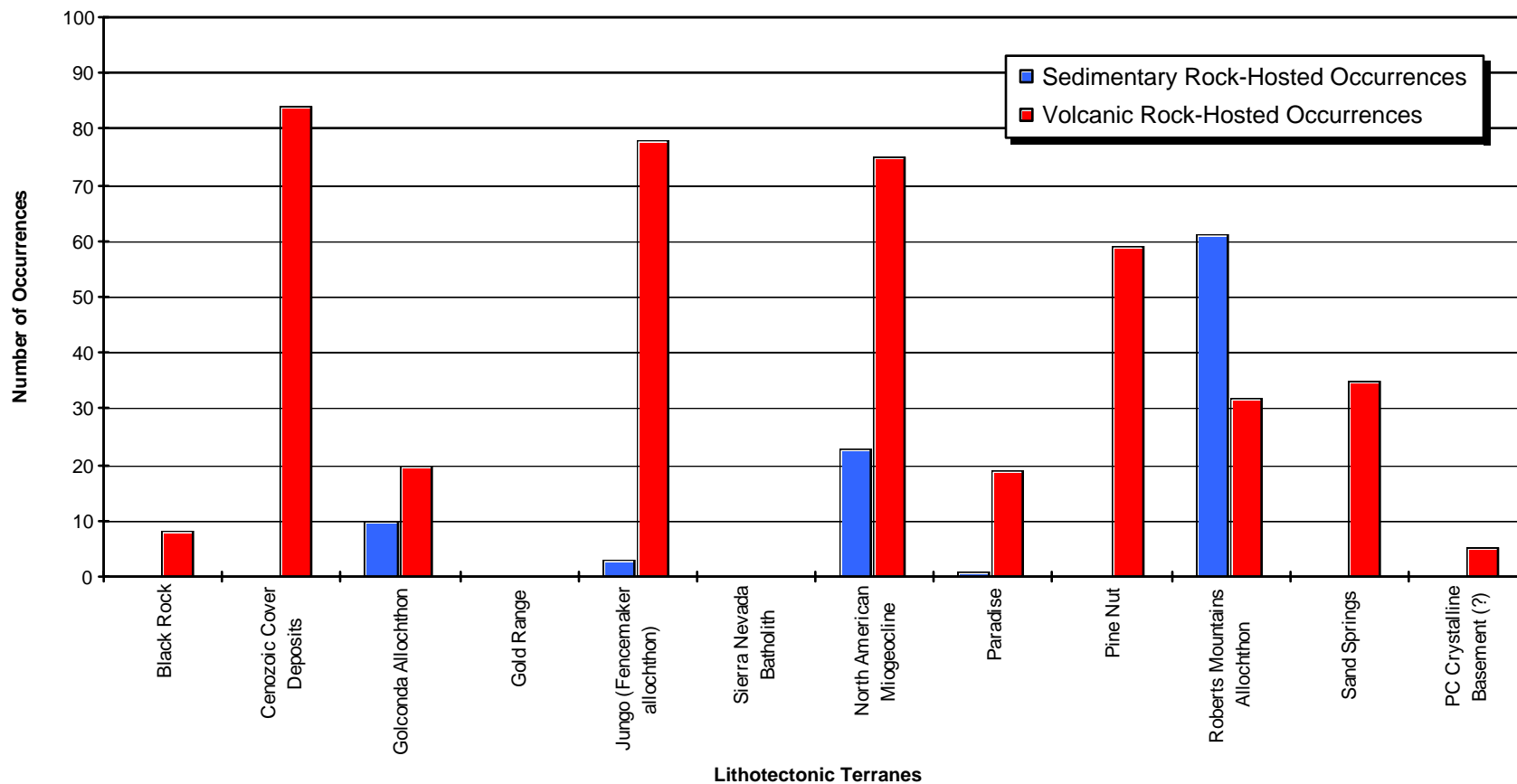


**Figure 6.32** Number of sedimentary and volcanic rock-hosted occurrences per lithotectonic terrane unit.

### Strength of the Spatial Association Between Primary Occurrences and Lithotectonic Terranes

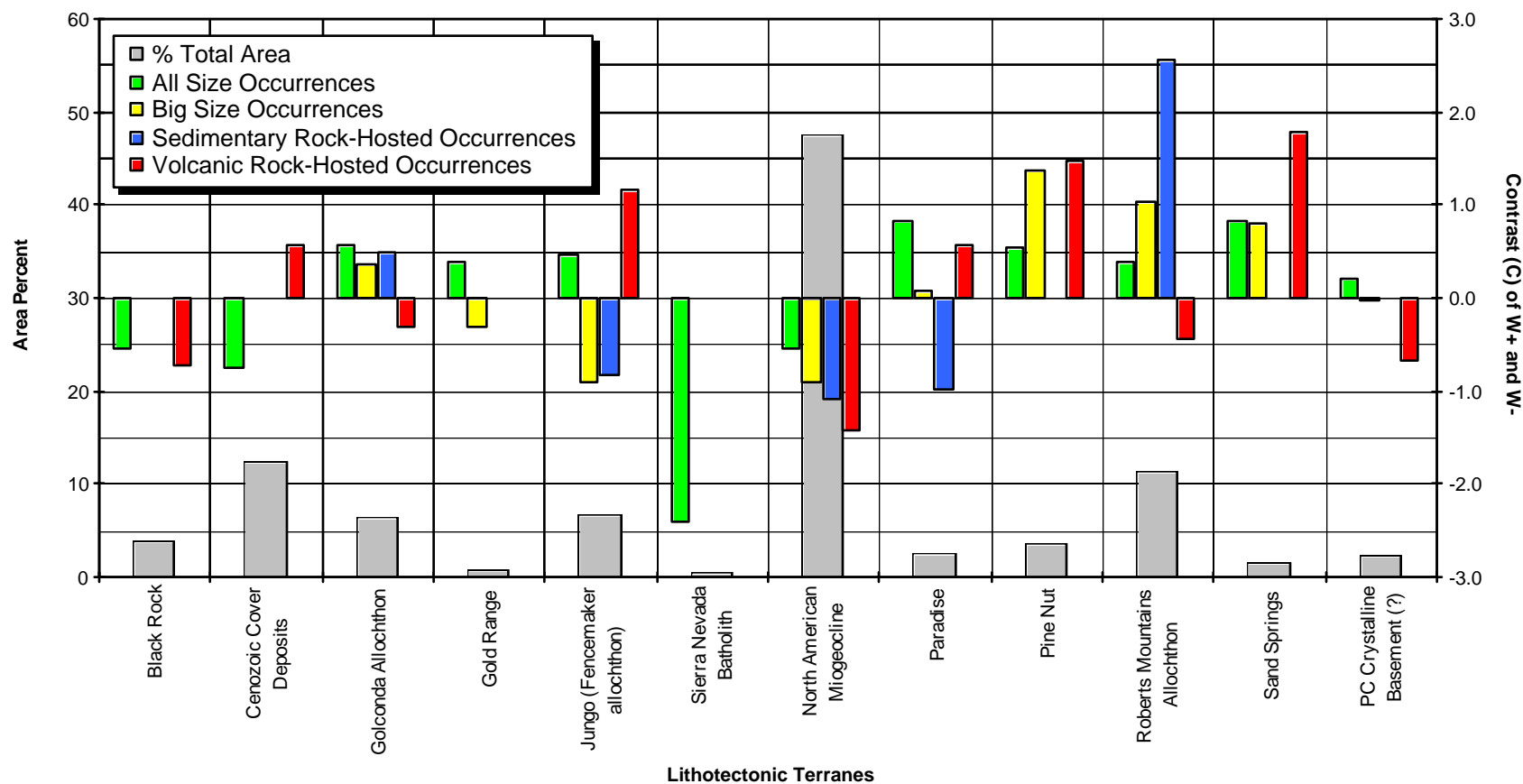


**Figure 6.33** Strength of spatial association (C) between lithotectonic terrane units and primary occurrences (subdivided by occurrence type and size).

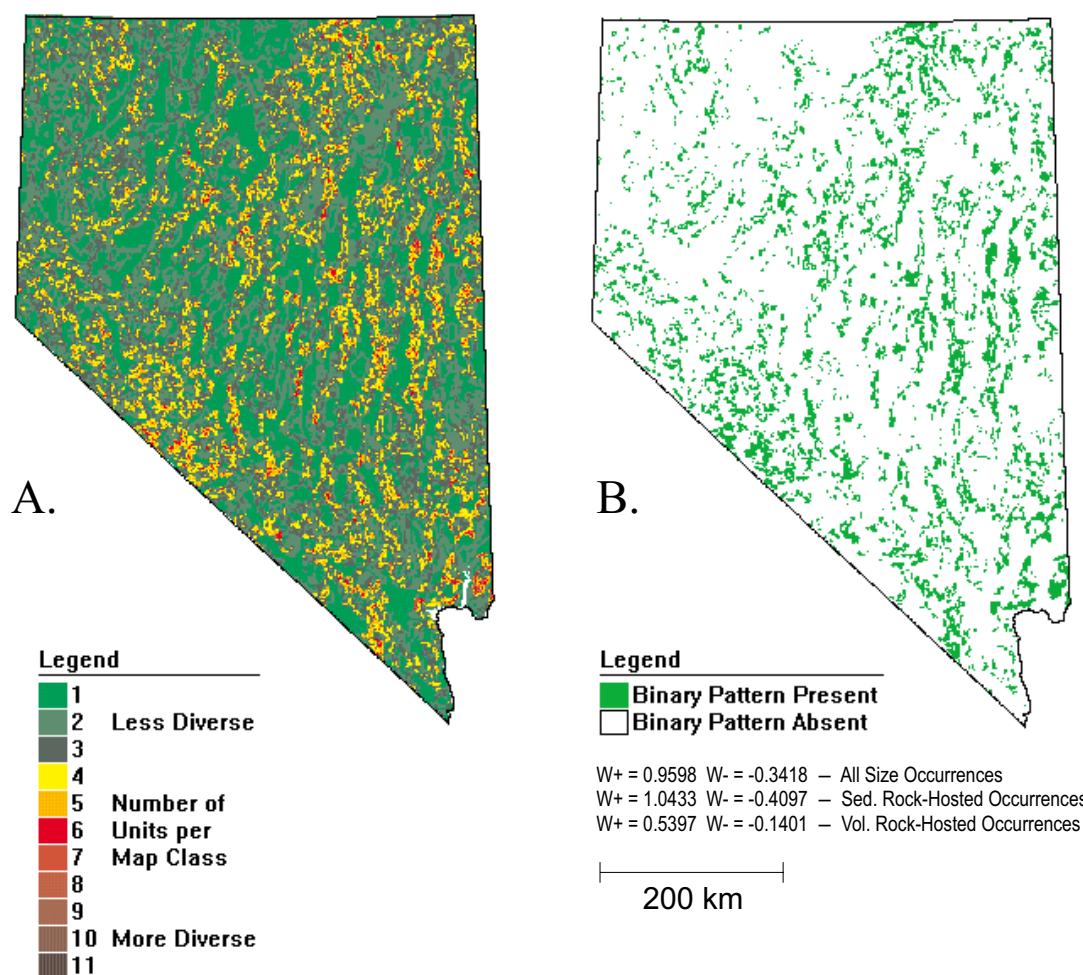
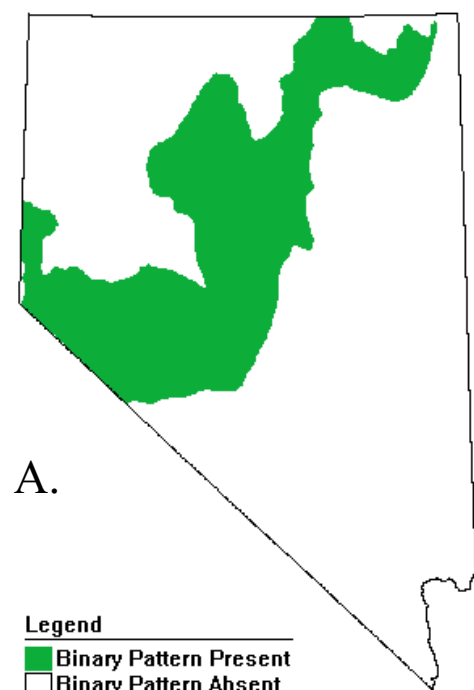
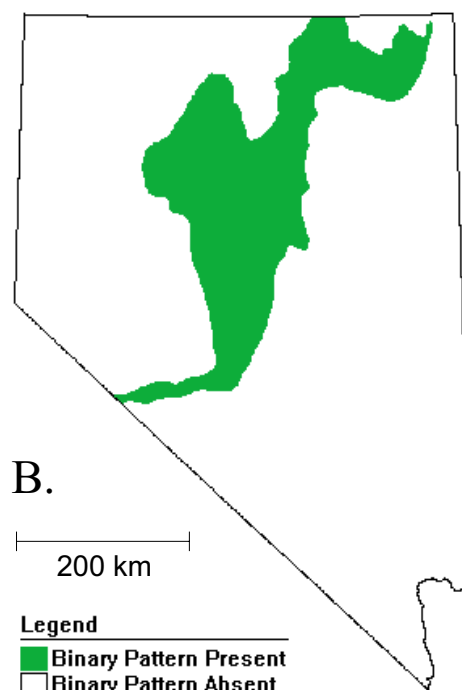


**Figure 6.34.** (A) Diversity of lithology map and (B) diversity binary-class predictor map for gold-silver-bearing occurrences of all sizes and types, sedimentary rock-hosted occurrences, and volcanic rock-hosted occurrences. The diversity map represents the number of lithologic units occurring in a ~2.5 by ~2.5 km neighborhood cell (~6.684 km<sup>2</sup> area), and indicates areas where contacts between various surface lithology units might be complicated by a greater occurrence of structural, stratigraphic, or intrusive features. Weights of spatial association for binary-class predictor map indicated in legend. See text for discussion.

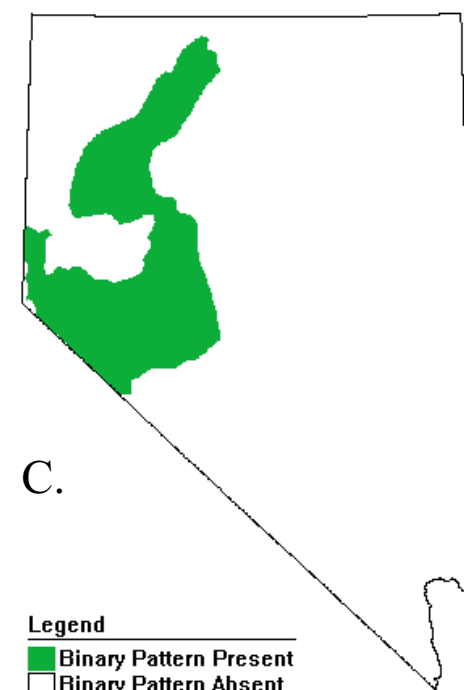




W+ = 0.4816 W- = -0.2565 — All Size and Type Occurrences



W+ = 1.3993 W- = -1.0922 — Sed. Rock-Hosted Occurrences



W+ = 1.1543 W- = -0.4598 — Vol. Rock-Hosted Occurrences

**Figure 6.35.** Lithologic terrane binary-class predictor maps for gold-silver-bearing occurrences of (A) all sizes and types, (B) sedimentary rock-hosted occurrences, and (C) volcanic rock-hosted occurrences. Weights of spatial association for binary-class predictor maps indicated in legend. In descending order of contrast, the terranes composing the binary predictor maps are as follows: map (A)—Paradise, Sand Springs, Golconda Allochthon, Pine Nut, Jungo (Fencemaker allochthon), Roberts Mountain allochthon, and the Gold Range; map (B)—Roberts Mountain allochthon and Golconda allochthon; map (C)—Sand Springs, Pine Nut, Jungo (Fencemaker allochthon), and Paradise. See text for discussion.

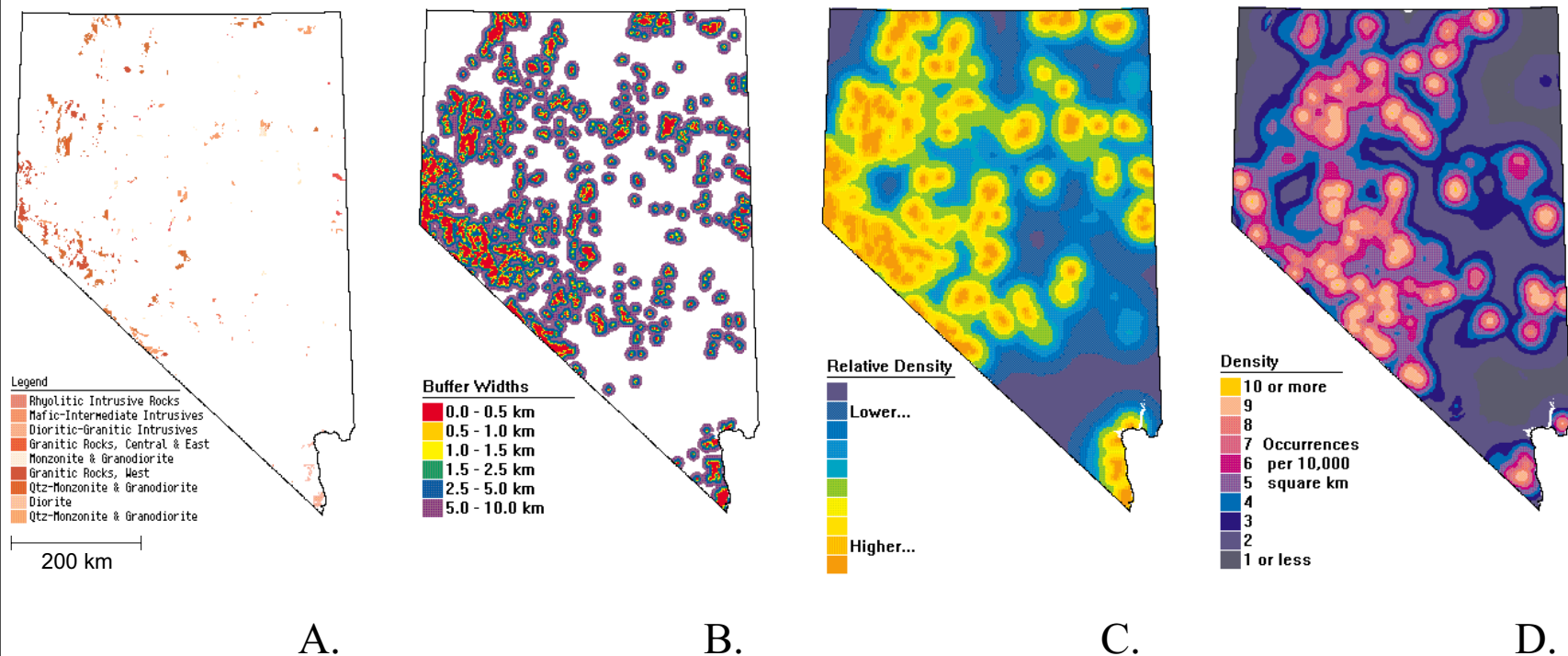
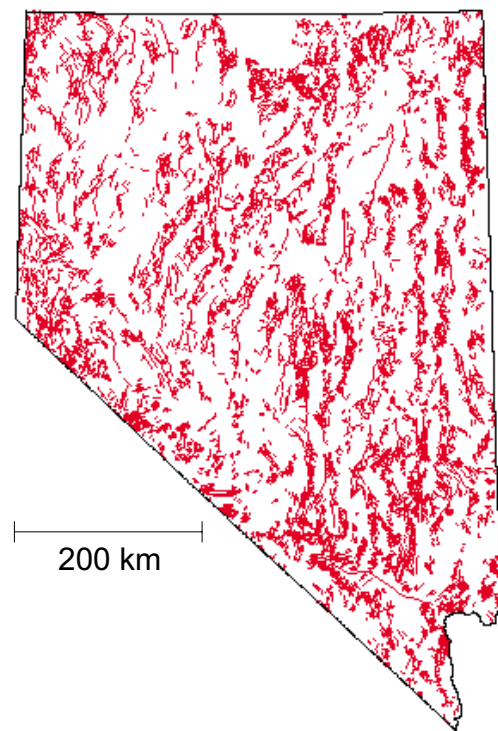
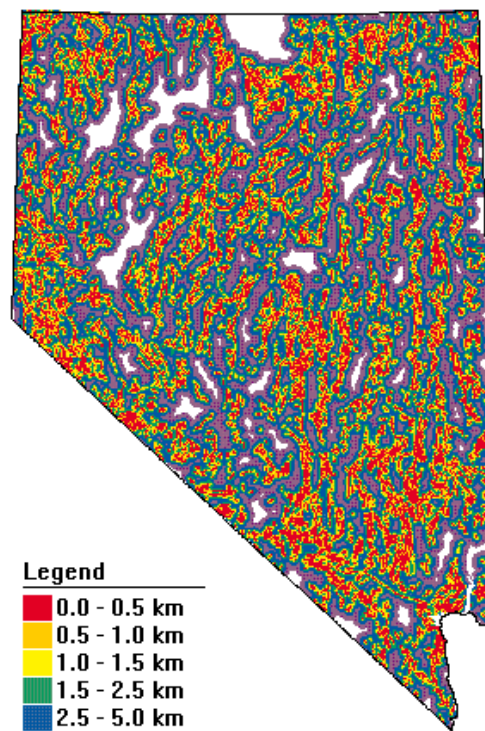


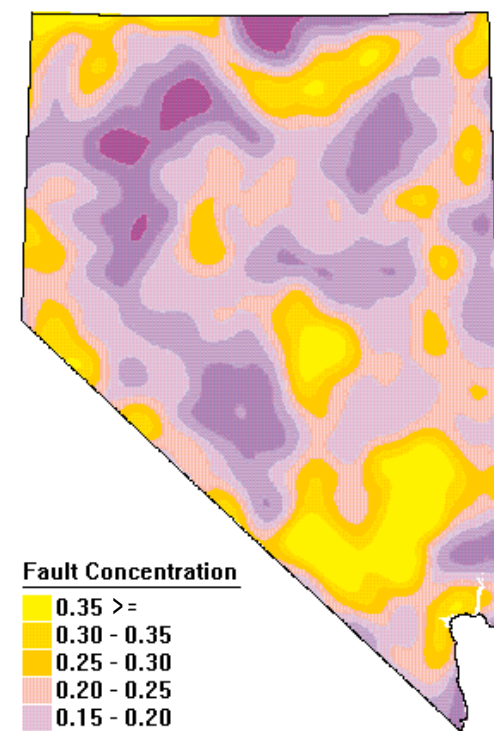
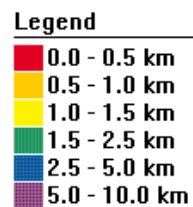
**Figure 6.36.** (A) Plutonic rocks of Nevada, (B) buffered plutons, (C) pluton density, and (D) the density of all gold-silver-bearing occurrences. The plutonic rocks are dominantly Mesozoic in age, the remainder are Cenozoic intrusive rocks. Pluton buffers do not extend into the plutonic bodies—the 0.0-0.5 km buffer represents areas within and surrounding the plutonic body to a distance of 0.5 km. The pluton density map illustrates a relative measure of density. Note the broad similarity between (C) the pluton density distribution pattern and (D) the gold-silver-bearing occurrences density distribution pattern. See text for discussion.



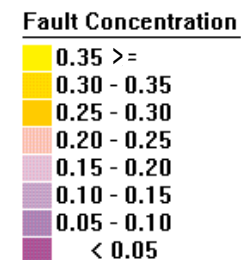
A.



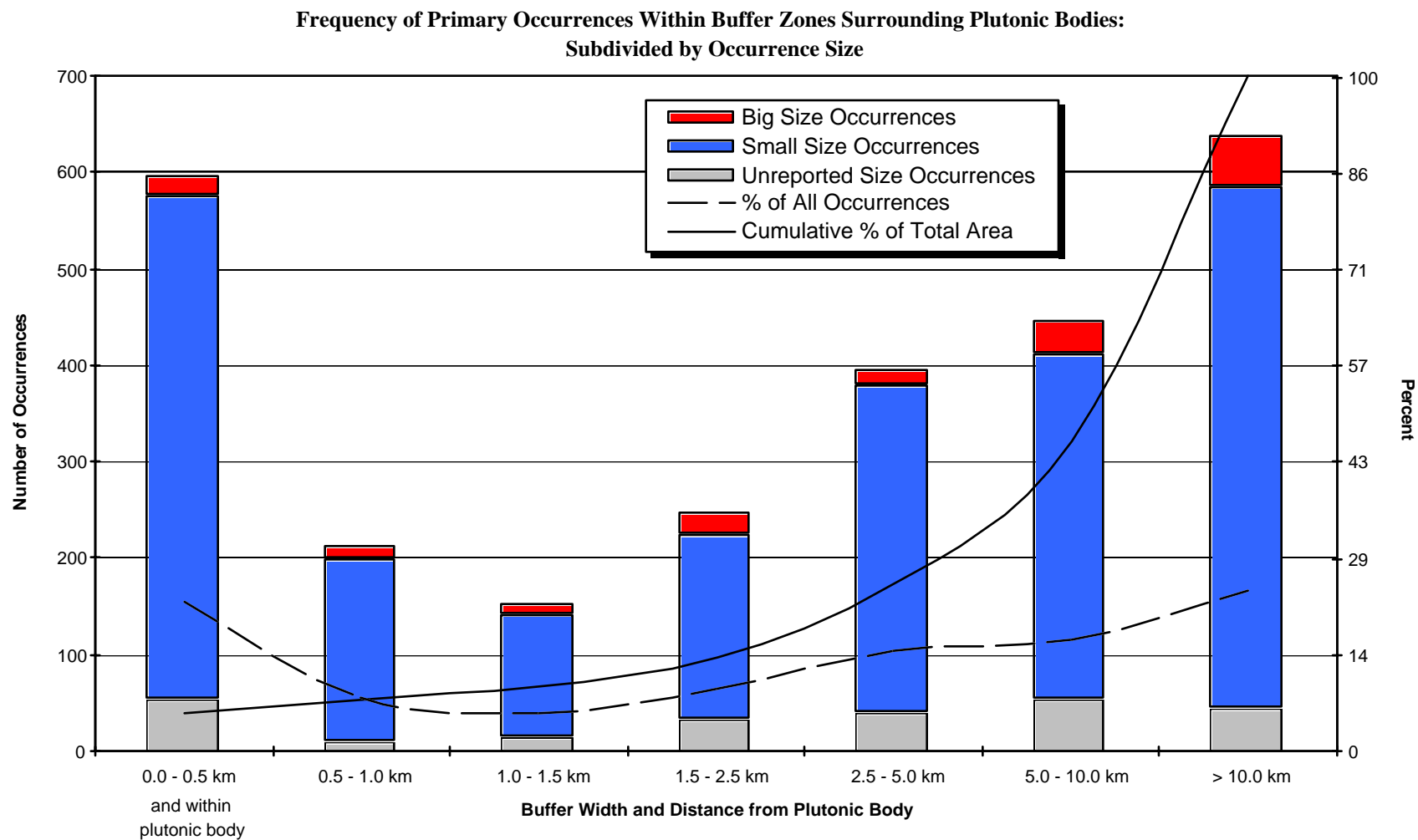
B.



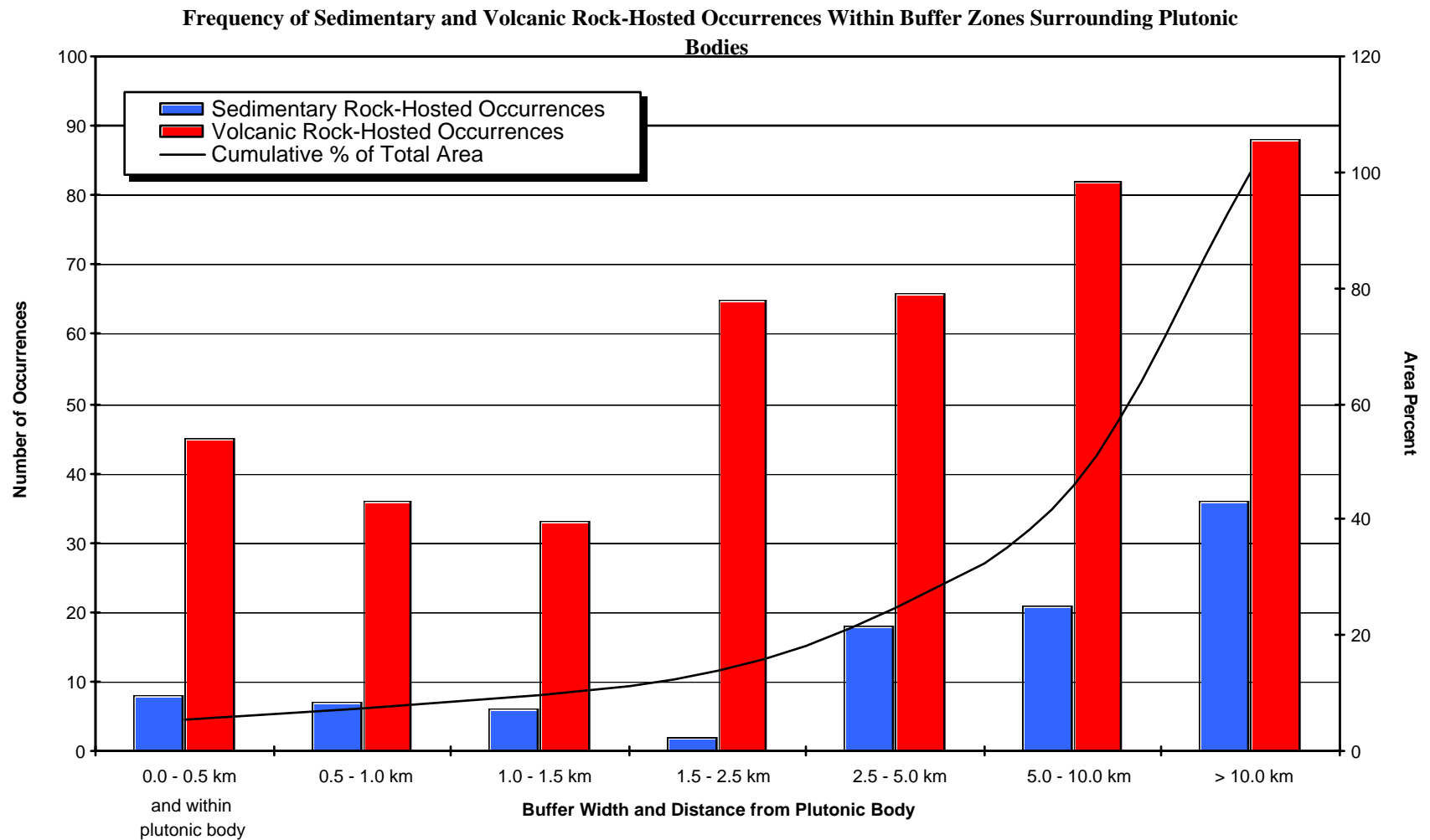
C.



**Figure 6.37.** (A) Faults from the geological map of Nevada, (B) fault distance buffers, and (C) density of faults. The faults are of all types (dip-slip, strike-slip, etc.) and ages. The measure of concentration for the fault density map is the total length of faults within a grid cell (~ 8.6 by 8.6 km) in geographic data units (latitude and longitude), normalized to the relative frequency per unit area of the grid (for further explanation, see Raines, 1978). A 10-times smoothing factor was applied to the data to highlight regional-scale trends. For all practical purposes, the fault density map illustrates where there is a high concentration of faults per unit area, and is shown here only for the purpose of visual comparison. See Sawatsky and Raines (1981) for additional details on the fault density mapping techniques. See text for discussion

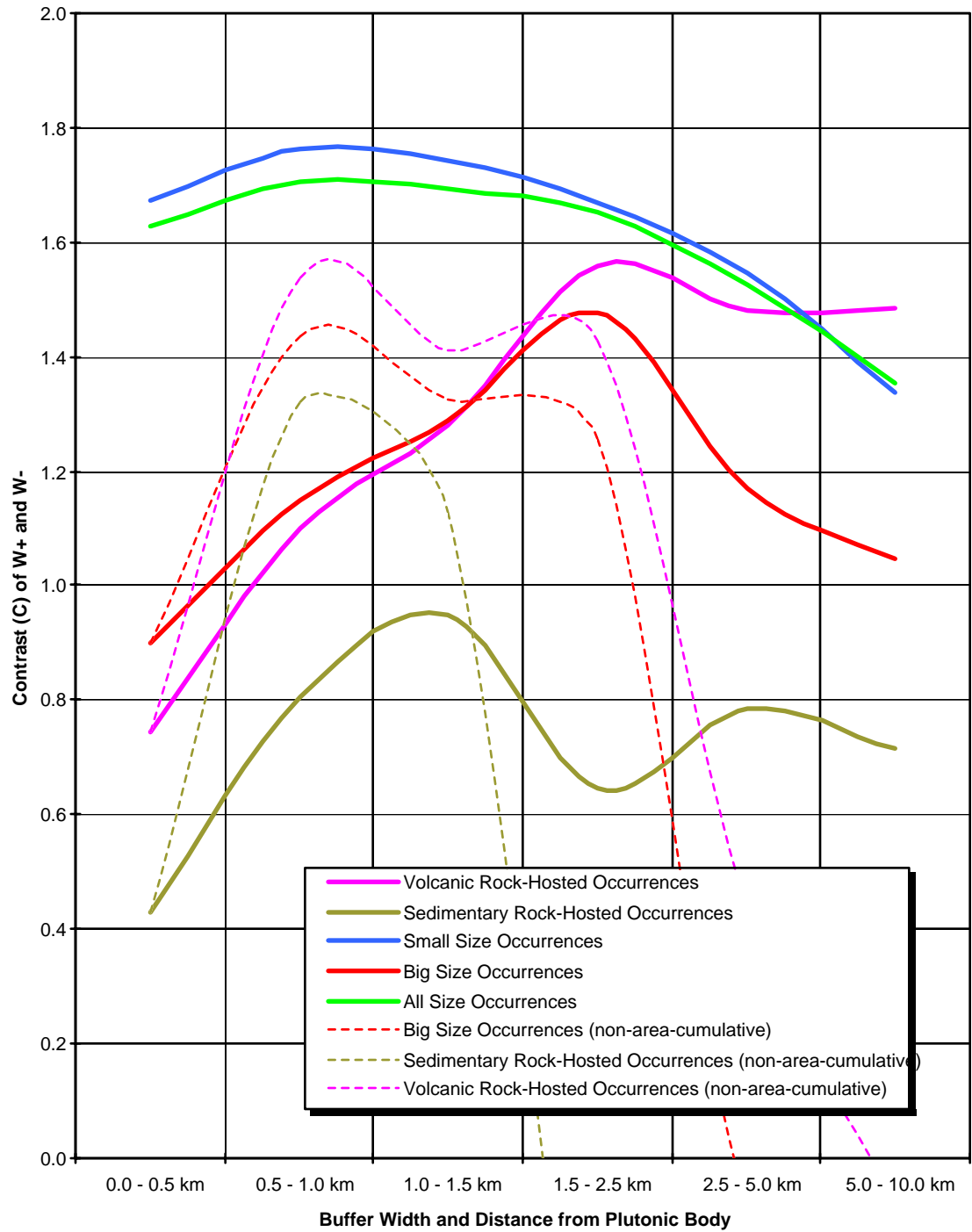


**Figure 6.38** Number of primary occurrences (subdivided by size) within buffer zones surrounding plutonic and intrusive bodies (predominantly Mesozoic).



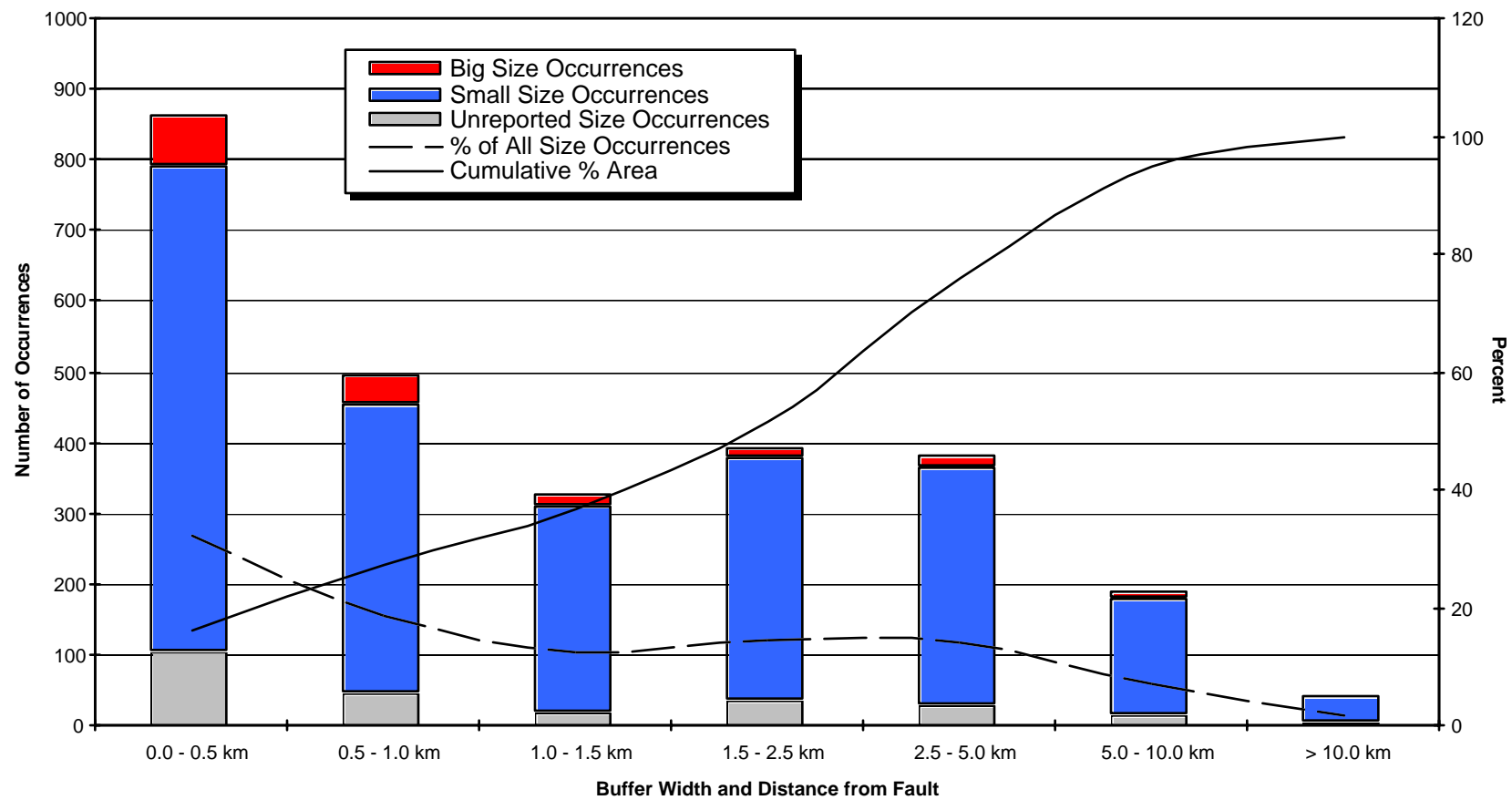
**Figure 6.39** Number of sedimentary and volcanic rock-hosted occurrences within buffer zones surrounding plutonic and intrusive bodies (predominantly Mesozoic).

**Variation of Contrast (C) with Successive Area-Cumulative Distance Intervals from Plutonic Bodies for Primary Occurrences**



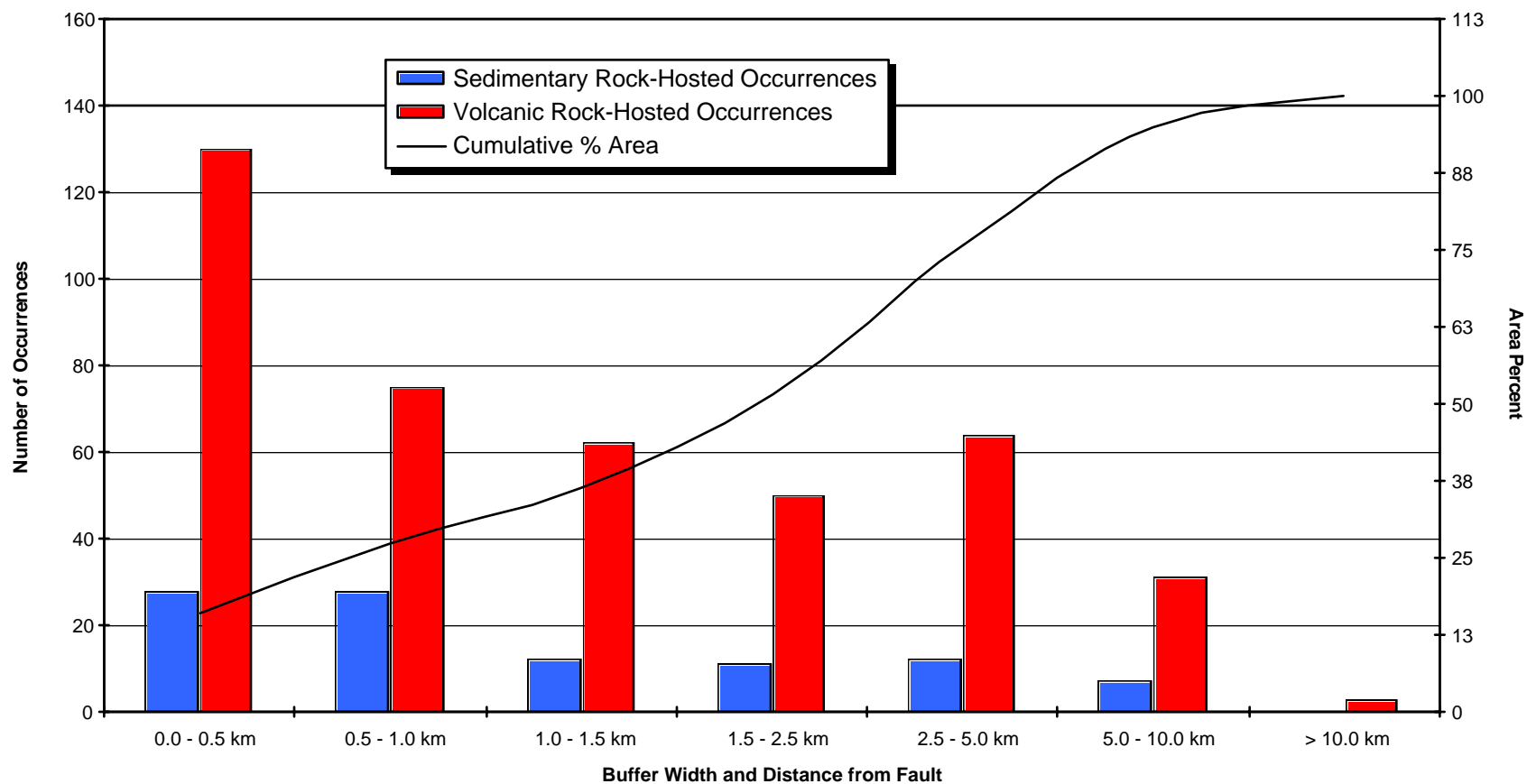
**Figure 6.40.** Variation in contrast (C) across distance intervals surrounding plutonic and intrusive rocks for primary occurrences (subdivided by type and size).

**Frequency of Primary Occurrences Within Buffer Zones Surrounding Faults:  
Subdivided by Occurrence Size**



**Figure 6.41** Number of primary occurrences (subdivided by size) within buffer zones surrounding faults (predominantly Cenozoic).

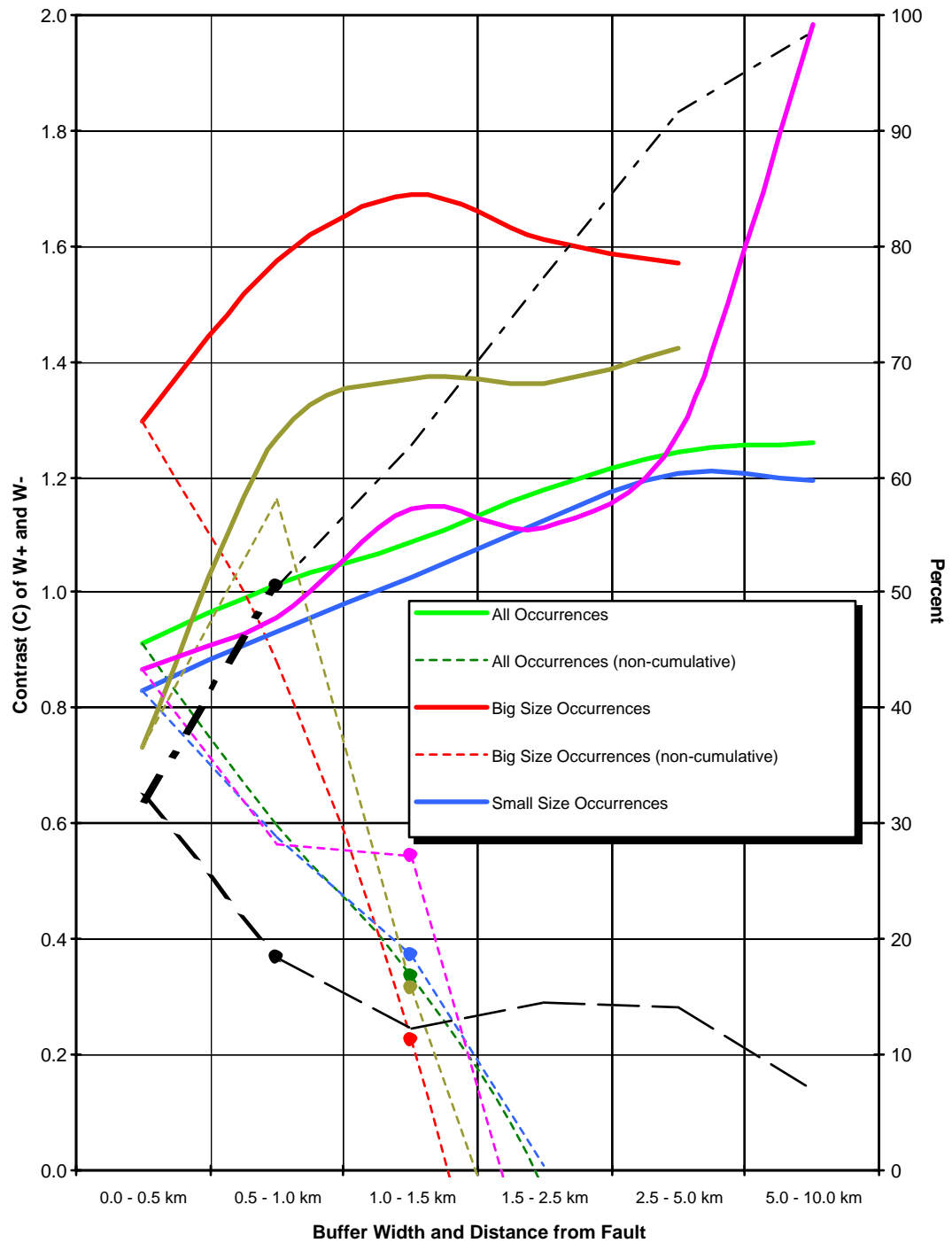
**Frequency of Sedimentary and Volcanic Rock-Hosted Occurrences Within Buffer Zones Surrounding Faults**



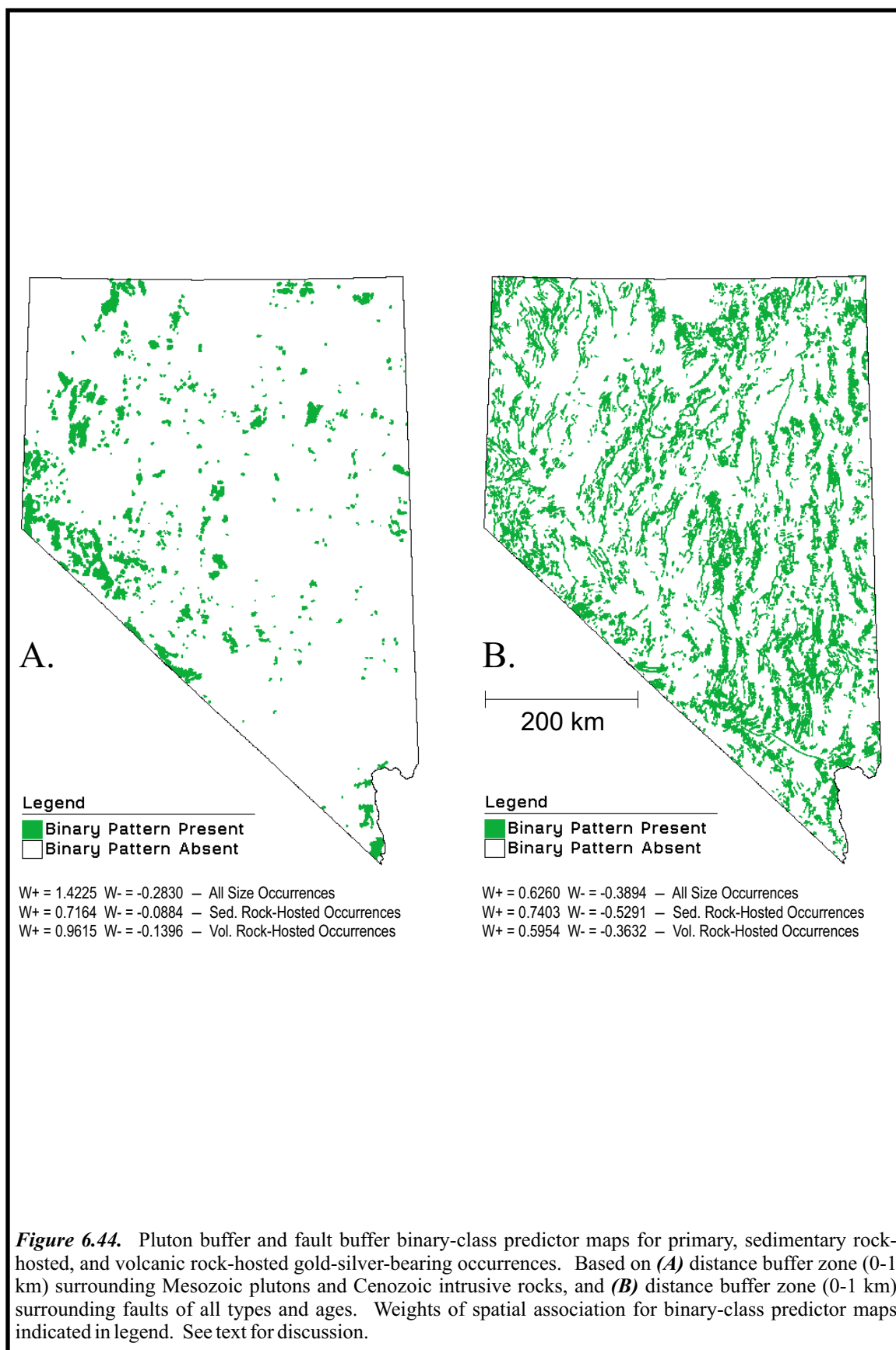
**Figure 6.42** Number of sedimentary and volcanic rock-hosted occurrences within buffer zones surrounding faults (predominantly Cenozoic).

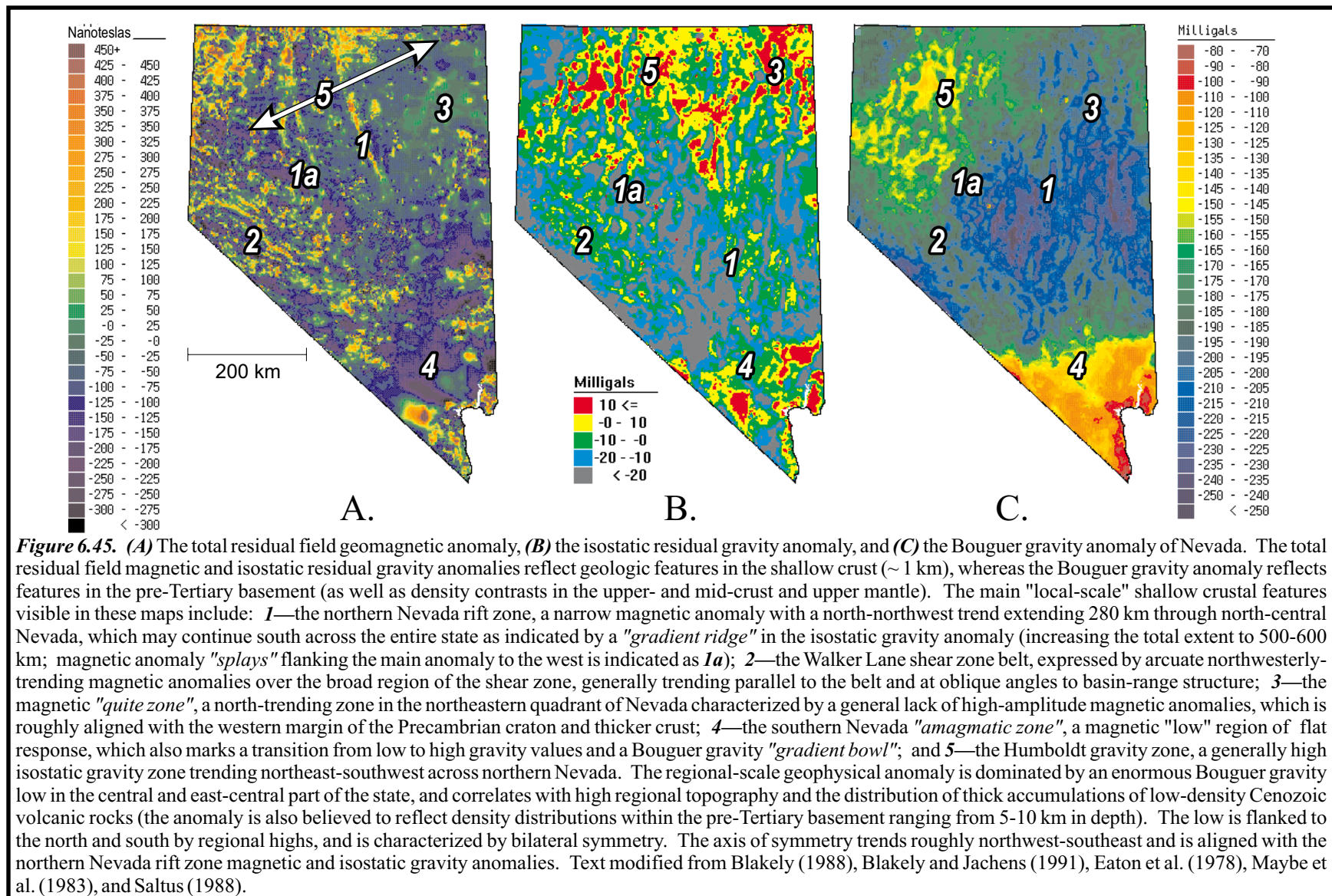


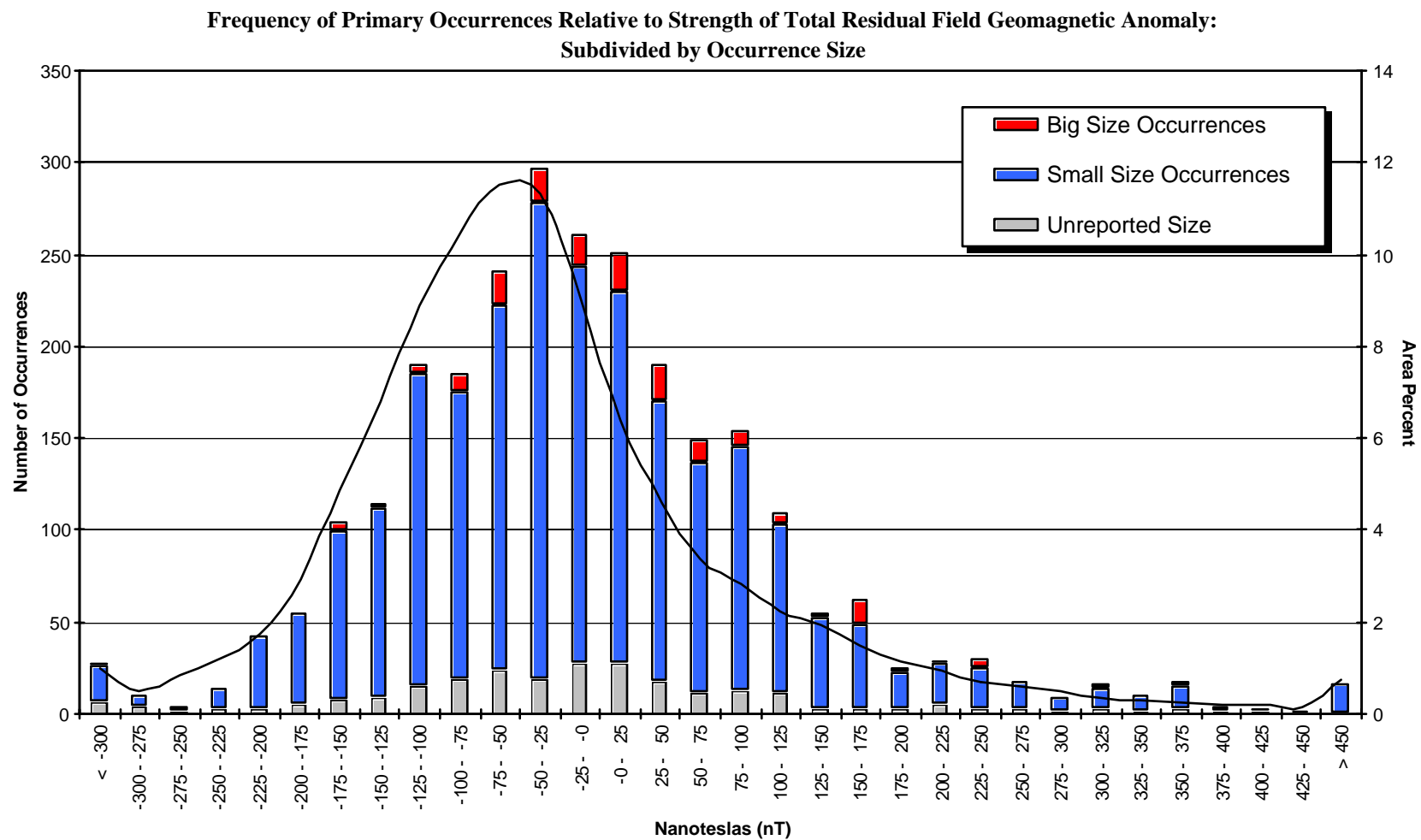
**Variation of Contrast (C) with Successive Area-Cumulative Distance Intervals from Faults for Primary Occurrences**



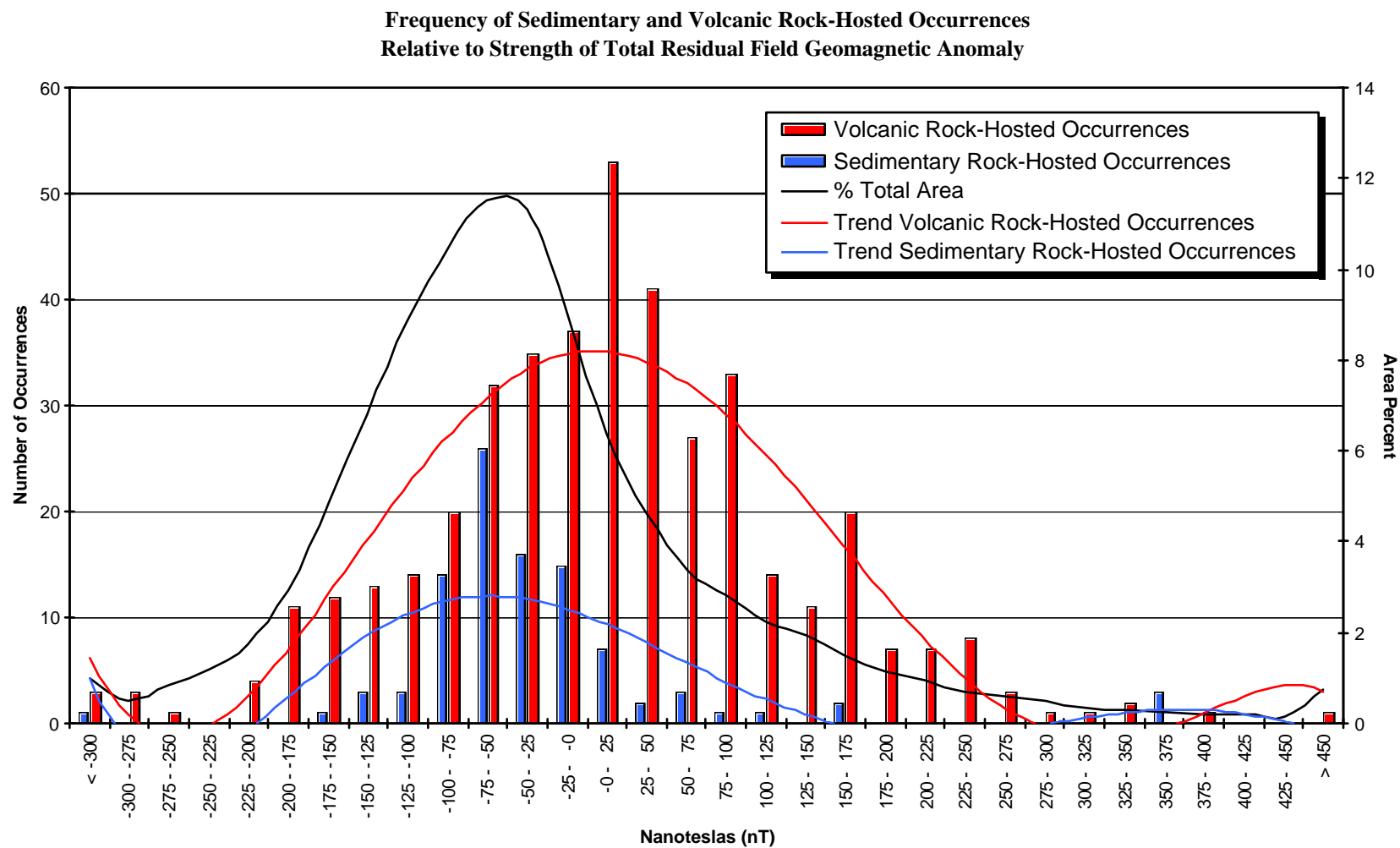
**Figure 6.43.** Variation in contrast (C) across distance intervals surrounding faults for primary occurrences (subdivided by type and size).



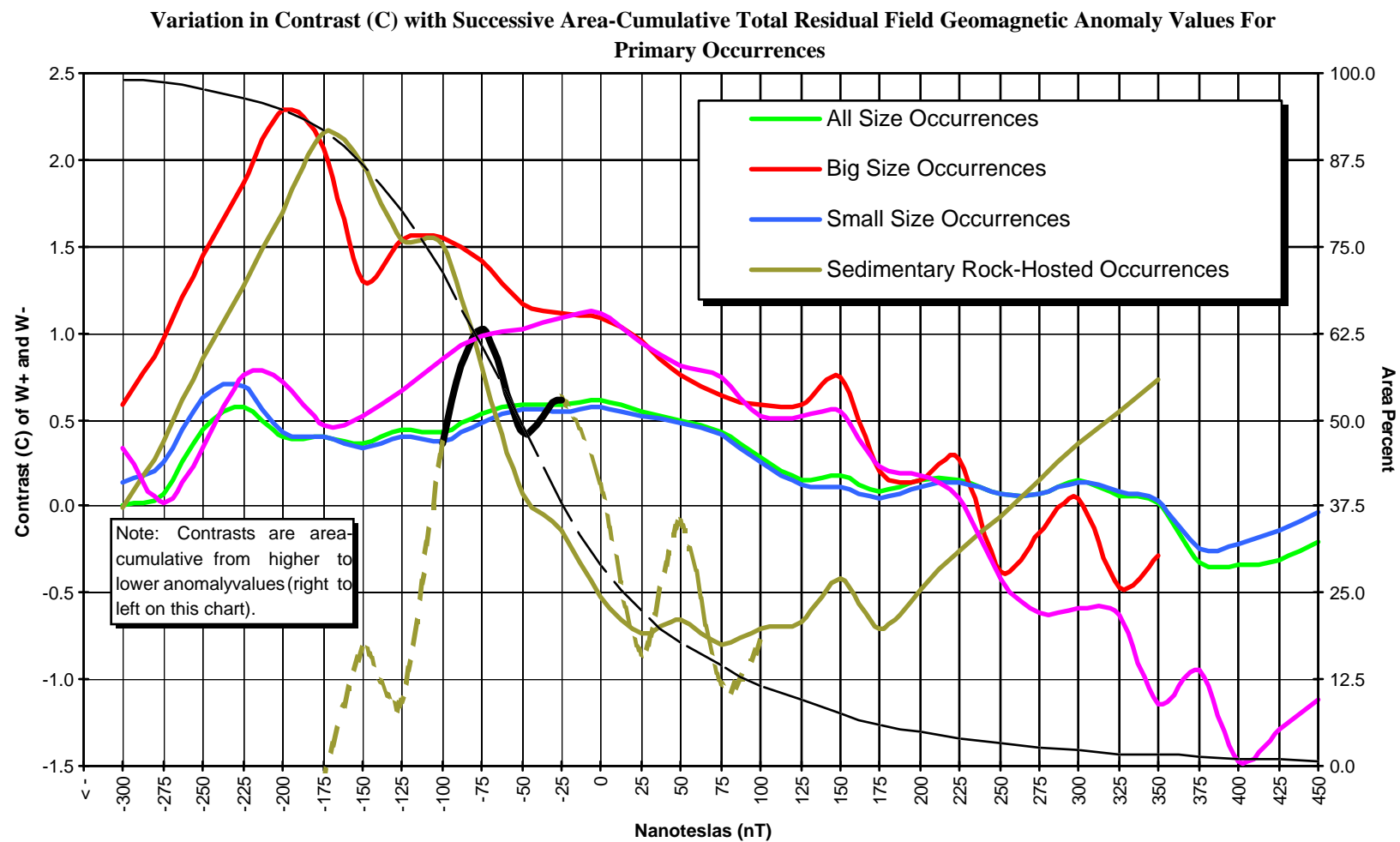




**Figure 6.46.** Number of primary occurrences relative to total residual field geomagnetic anomaly strength (subdivided by size).

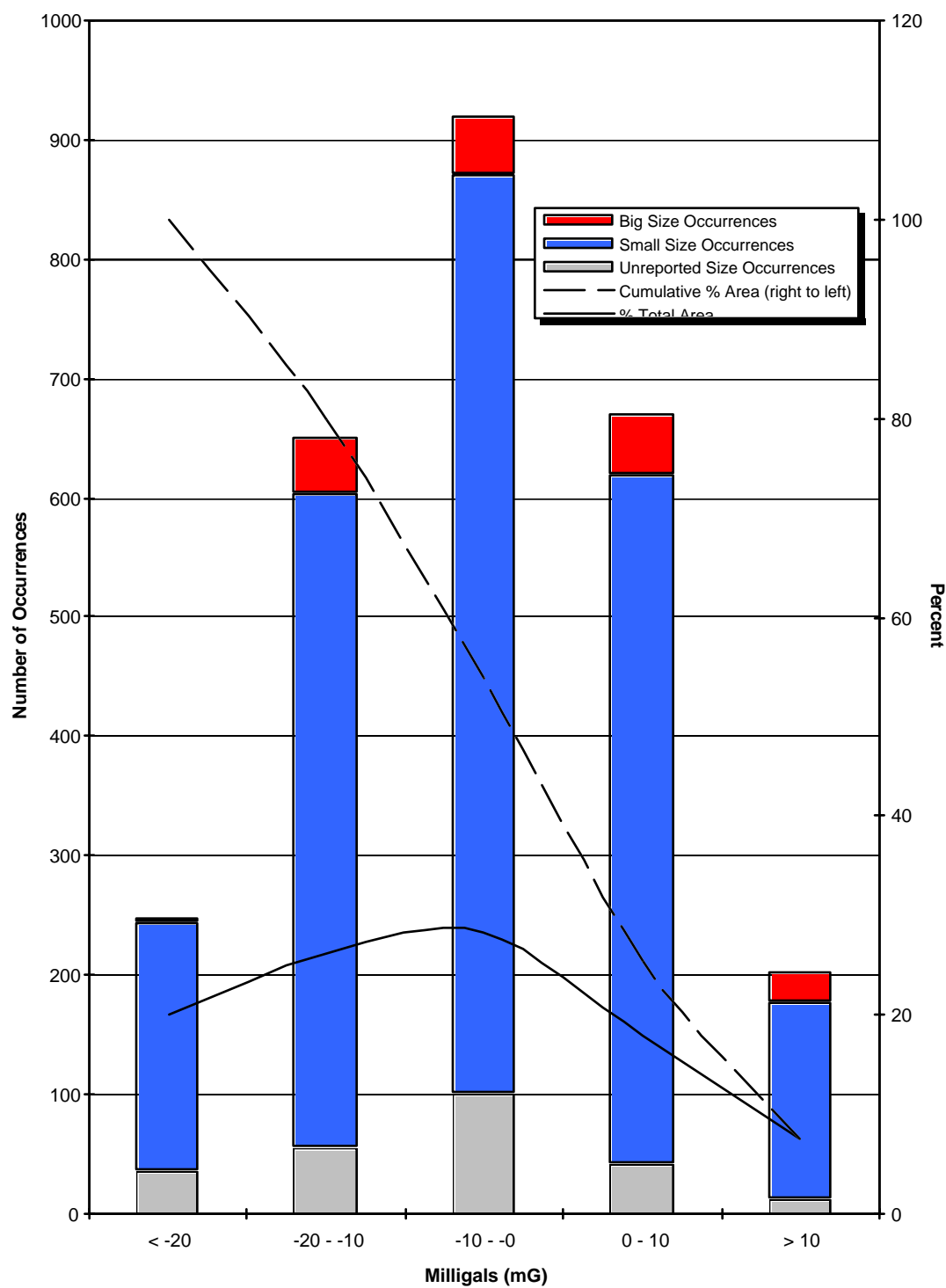


**Figure 6.47.** Number of sedimentary and volcanic rock-hosted occurrences relative to total residual field geomagnetic anomaly strength.



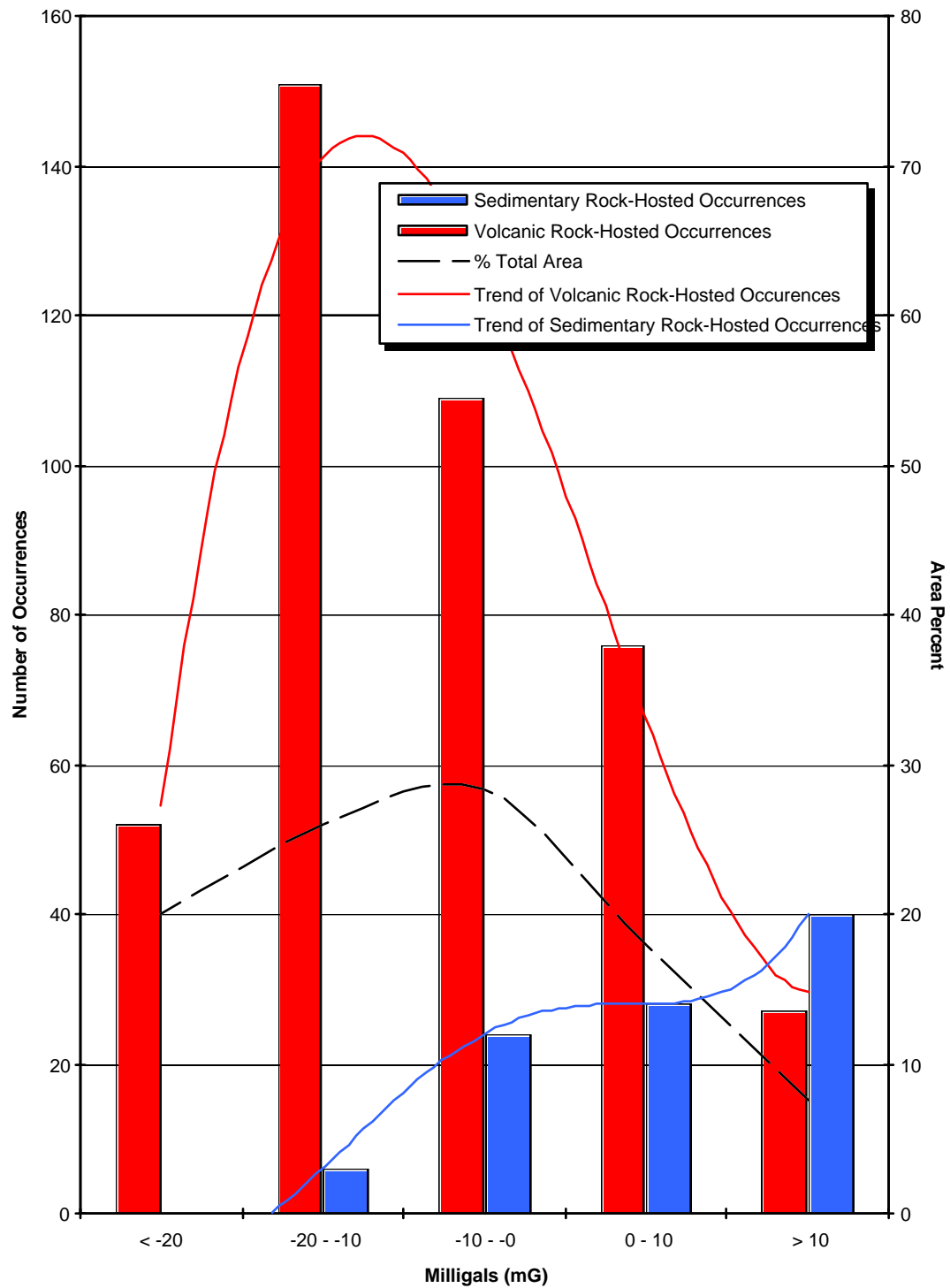
**Figure 6.48** . Variation in contrast (C) across total residual field geomagnetic anomaly intervals for primary occurrences (subdivided by type and size).

**Frequency of Primary Occurrences Relative to  
Strength of Isostatic Residual Gravity Anomaly:  
Subdivided by Occurrence Size**



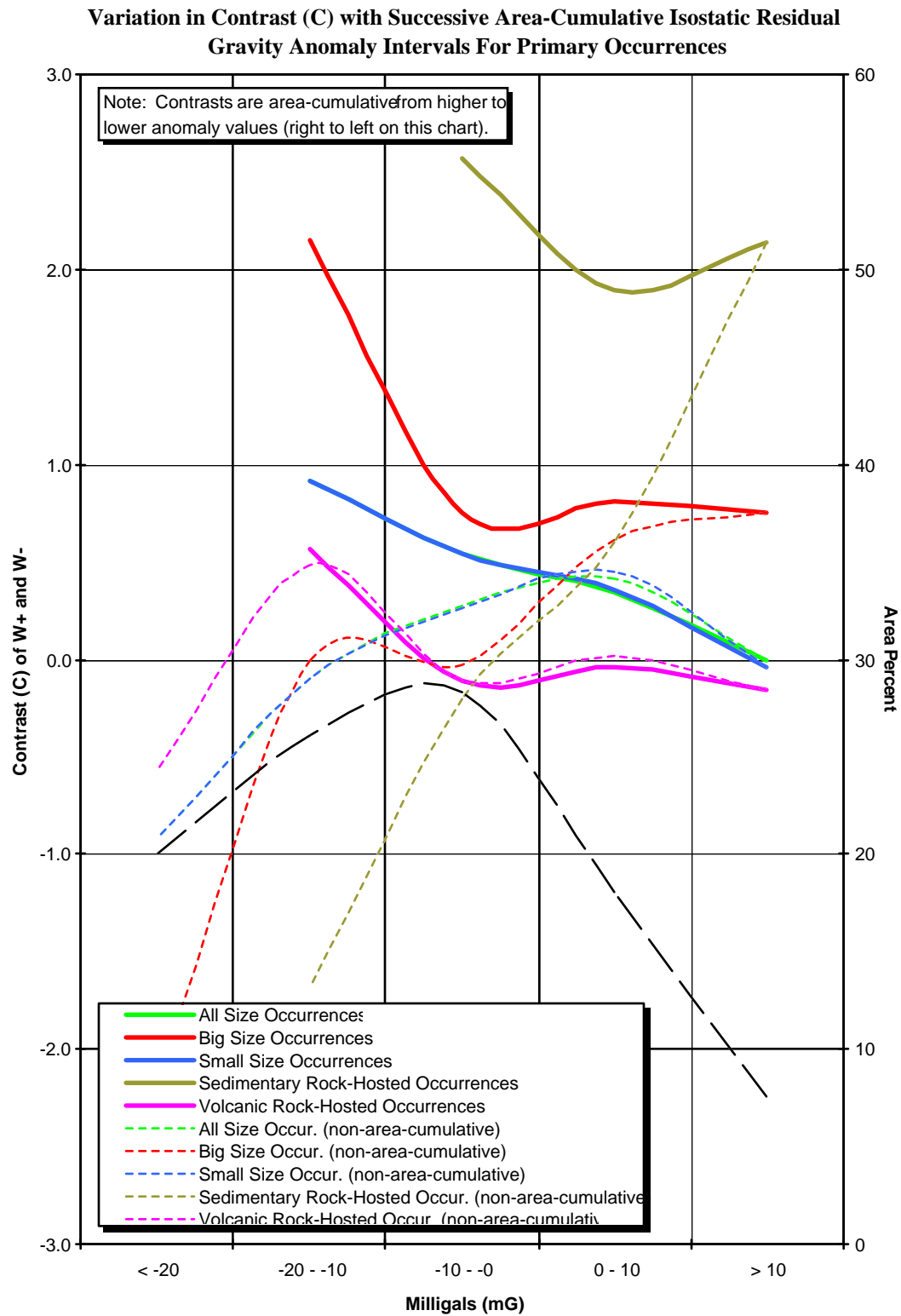
**Figure 6.49.** Number of primary occurrences relative to isostatic residual gravity anomaly strength (subdivided by size).

**Frequency of Sedimentary and Volcanic Rock-Hosted Occurrences  
Relative to Strength of Isostatic Residual Gravity Anomaly**

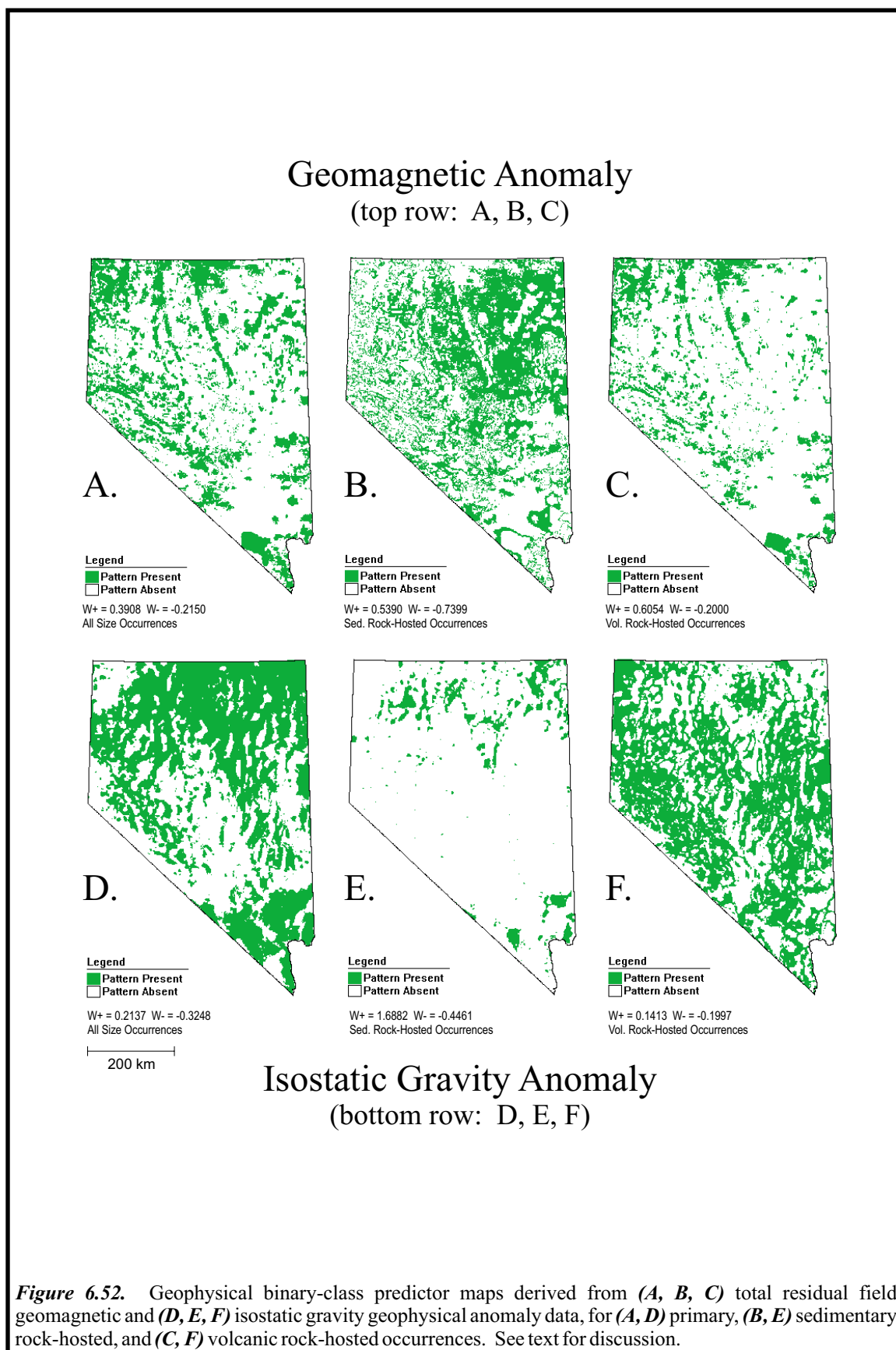


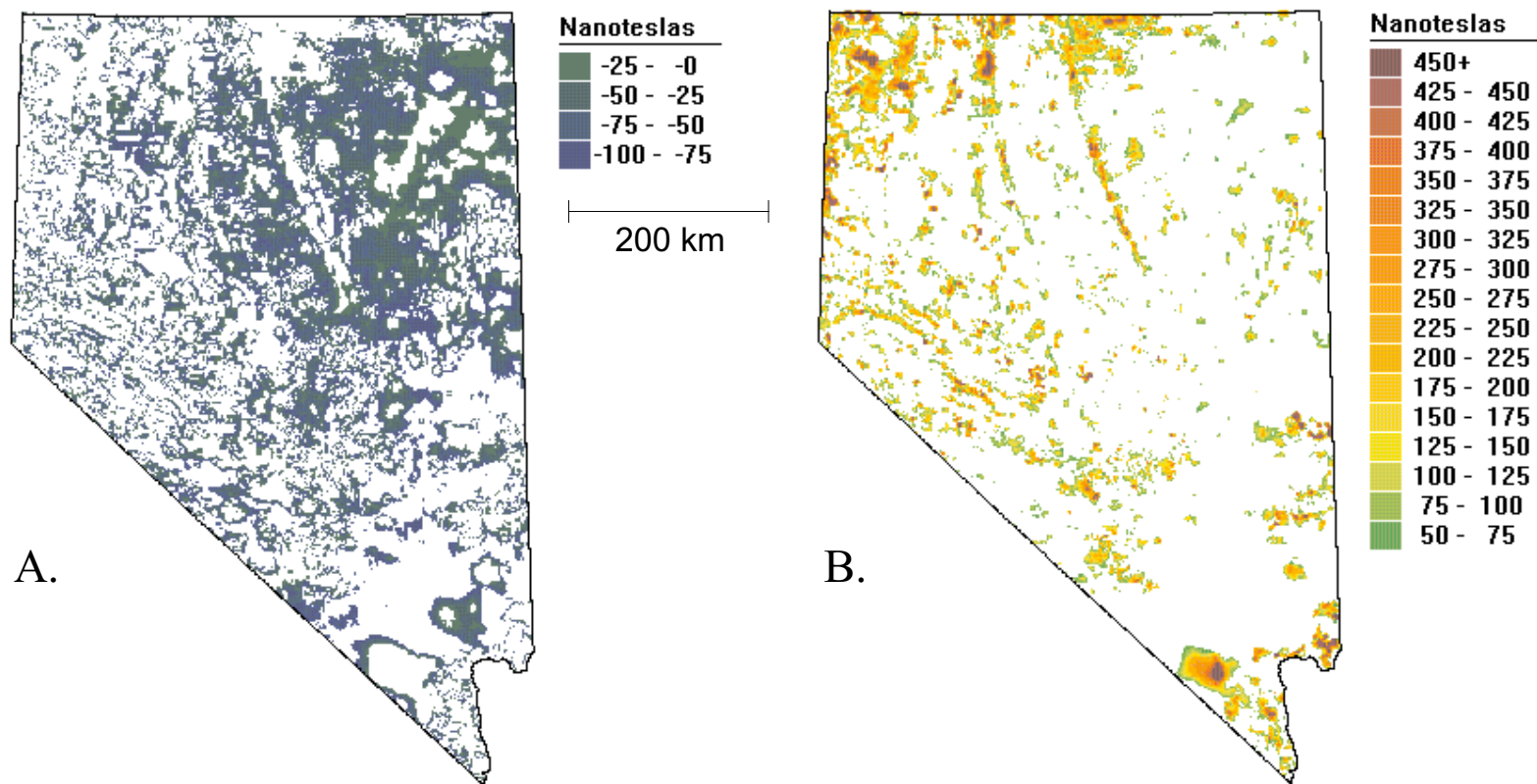
**Figure 6.50.** Number of sedimentary and volcanic rock-hosted occurrences relative to isostatic residual gravity anomaly strength.



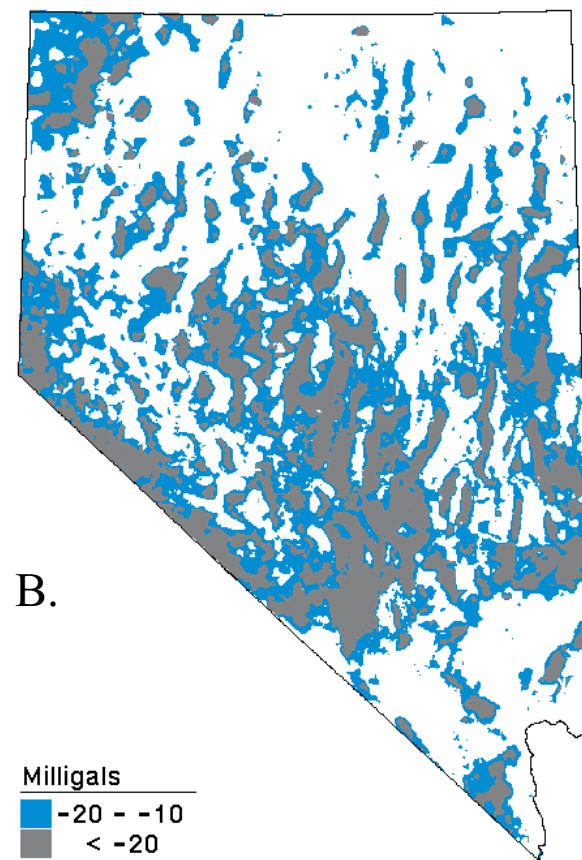
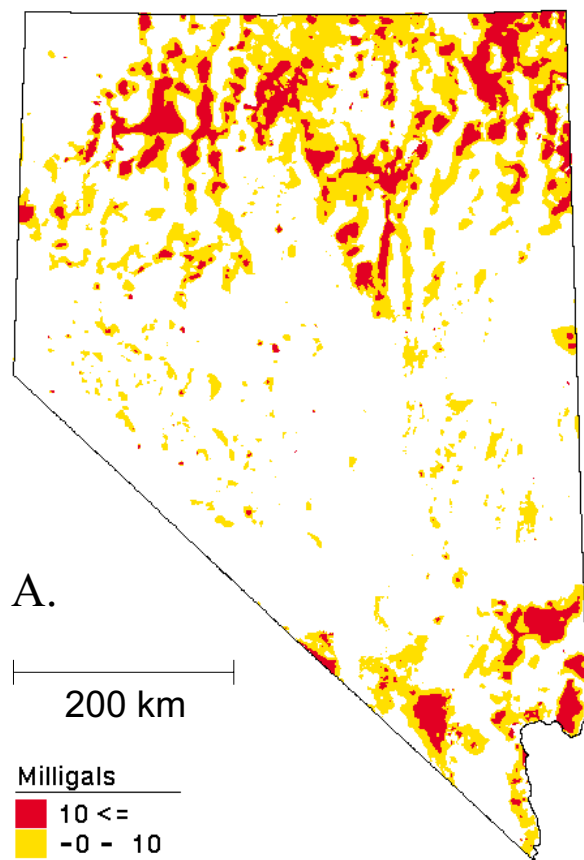


**Figure 6.51** . Variation in contrast (C) across isostatic residual gravity anomaly intervals for primary occurrences (subdivided by type and size)..

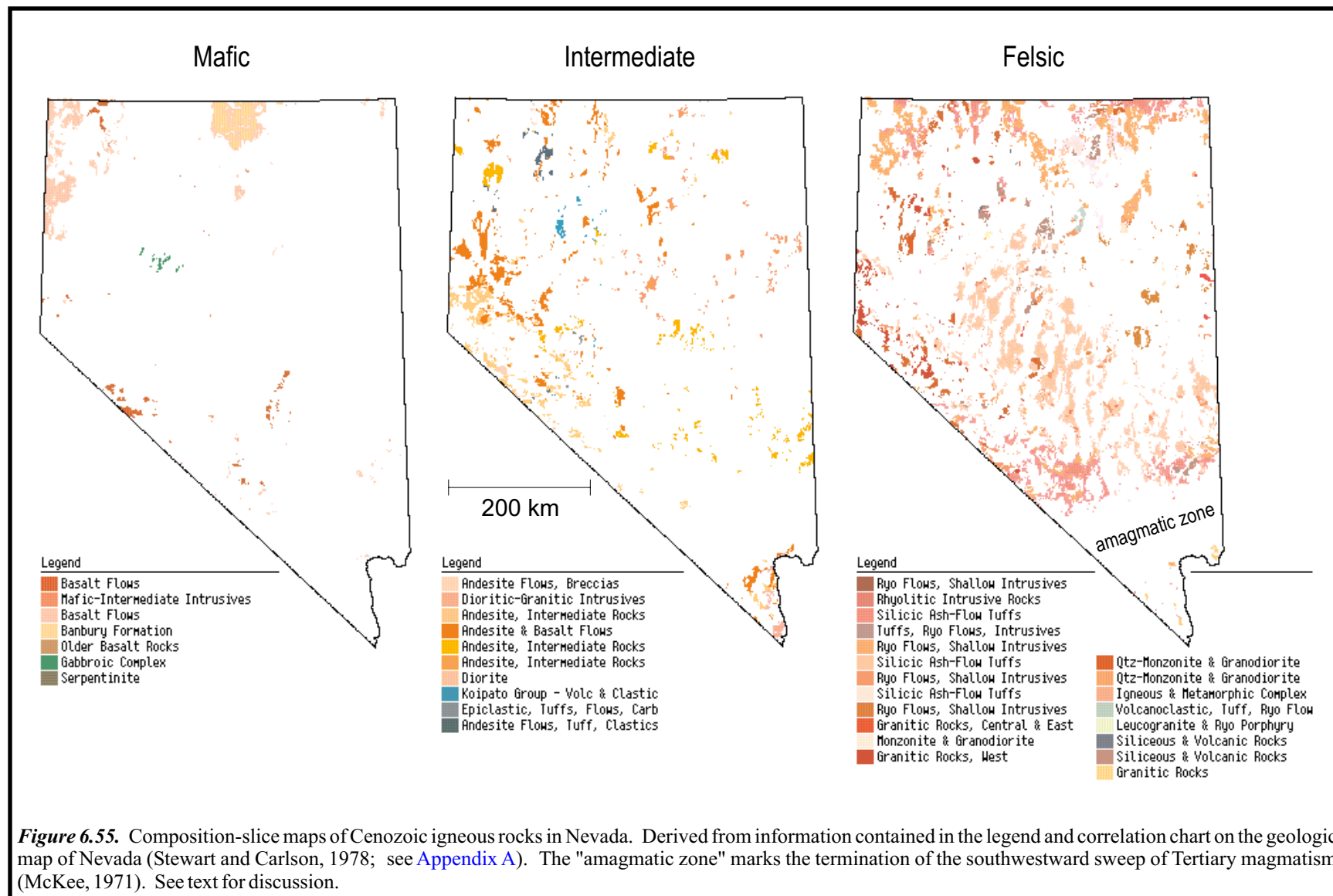




**Figure 6.53.** The total residual field geomagnetic anomaly intervals determined to have a strong spatial association with **(A)** sedimentary rock-hosted occurrences and **(B)** volcanic rock-hosted occurrences. On a regional level, the generally round shape of the broad low-amplitude anomaly in the northeastern quadrant of Nevada (map A) is coincident in extent with the distribution of sedimentary rock-hosted occurrences. This area is part of the "*magnetic quiet zone*", a region of low-amplitude anomalies that stretches along the eastern part of the state and into the "*amagmatic zone*" of the Laramide magmatic gap. In contrast, the high-amplitude anomalies (map B) are most widespread in the Walker Lane shear zone (with the exception of the northern Nevada rift anomalies), and along an arcuate distribution trend that mirrors the crescent-shape distribution of the volcanic rock-hosted occurrences. See text for discussion.



**Figure 6.54.** The isostatic residual gravity anomaly intervals that are spatially associated with **(A)** sedimentary rock-hosted occurrences, and **(B)** volcanic rock-hosted occurrences. The overall distribution of the isostatic gravity highs in the northeastern quadrant of Nevada (map A) is broadly coincident in extent with the distribution of sedimentary rock-hosted gold-silver-bearing occurrences. This region of gravity high is referred to as the "*Humboldt zone*", and corresponds to the "*magnetic quiet zone*". The gravity lows (map B) reflect the presence of thick accumulations of low-density Cenozoic volcanic rocks (as well as sediments) within basins and volcanotectonic depressions, and on a regional level, are broadly correlative to the crescent-shape distribution of volcanic rock-hosted occurrences. See text for discussion.







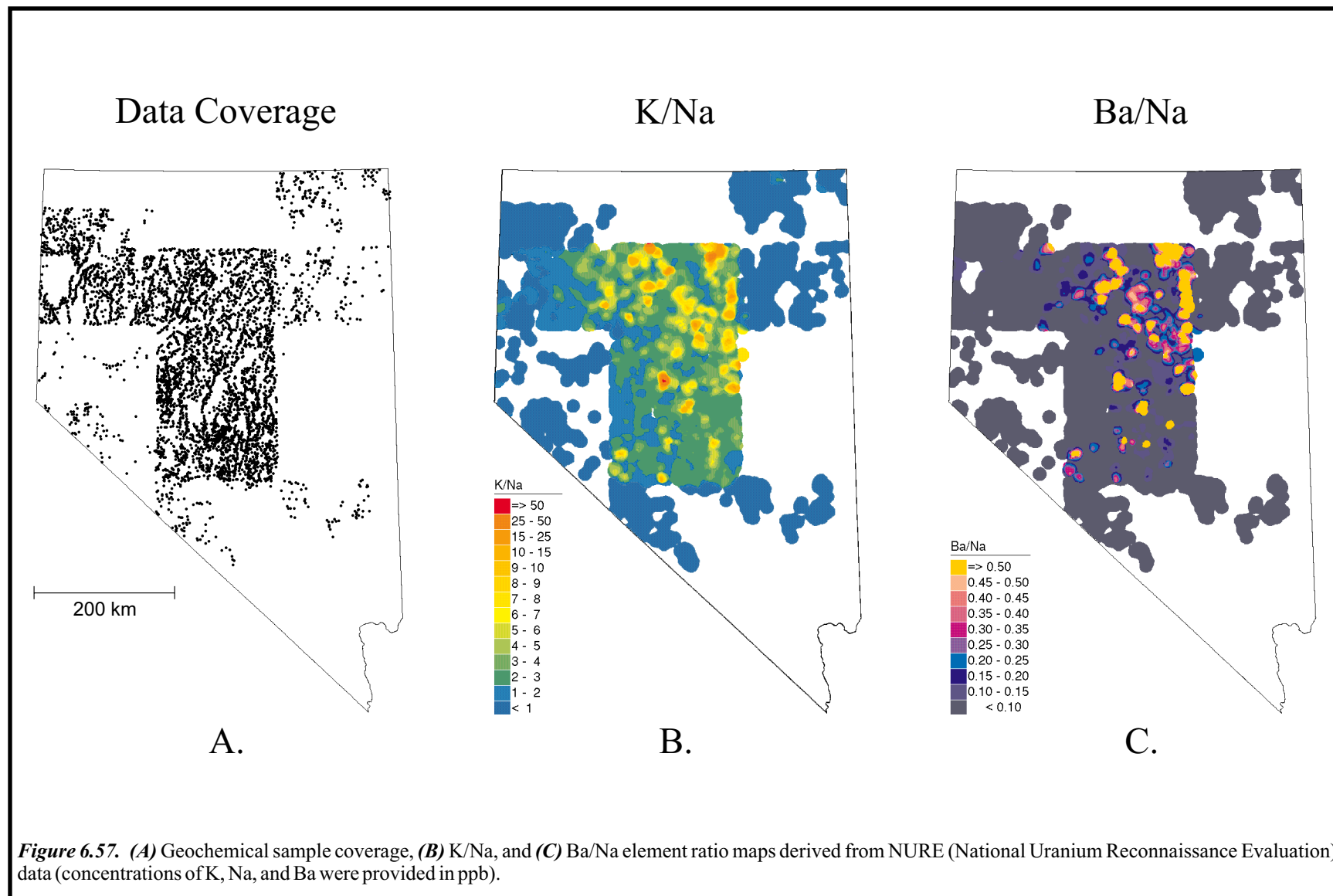


**Figure 6.57.** (A) Geochemical sample coverage, (B) K/Na, and (C) Ba/Na element ratio maps derived from NURE (National Uranium Reconnaissance Evaluation) data (concentrations of K, Na, and Ba were provided in ppb).

Frequency of Primary Occurrences Relative to K/Na Anomaly:  
Subdivided by Occurrence Size

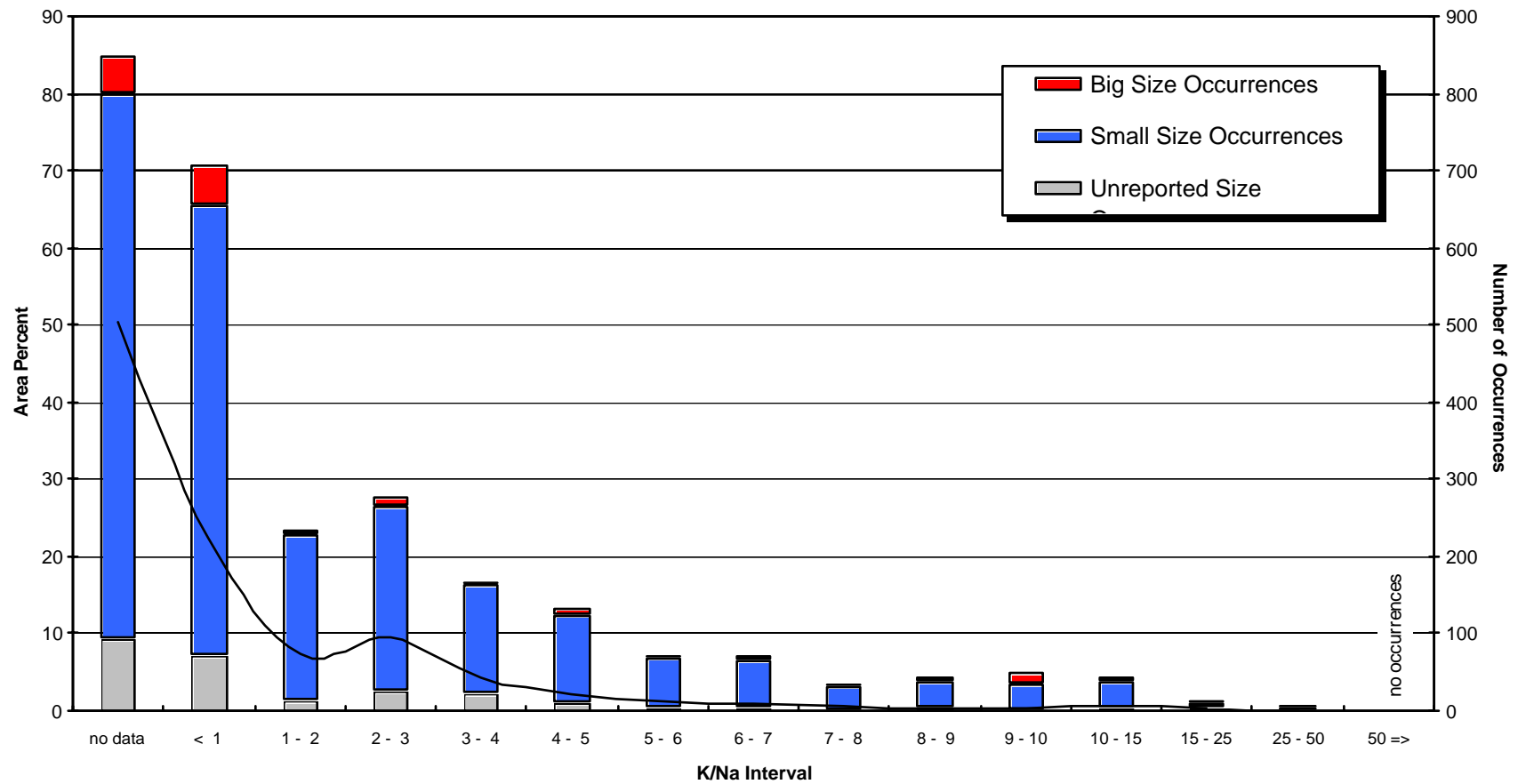
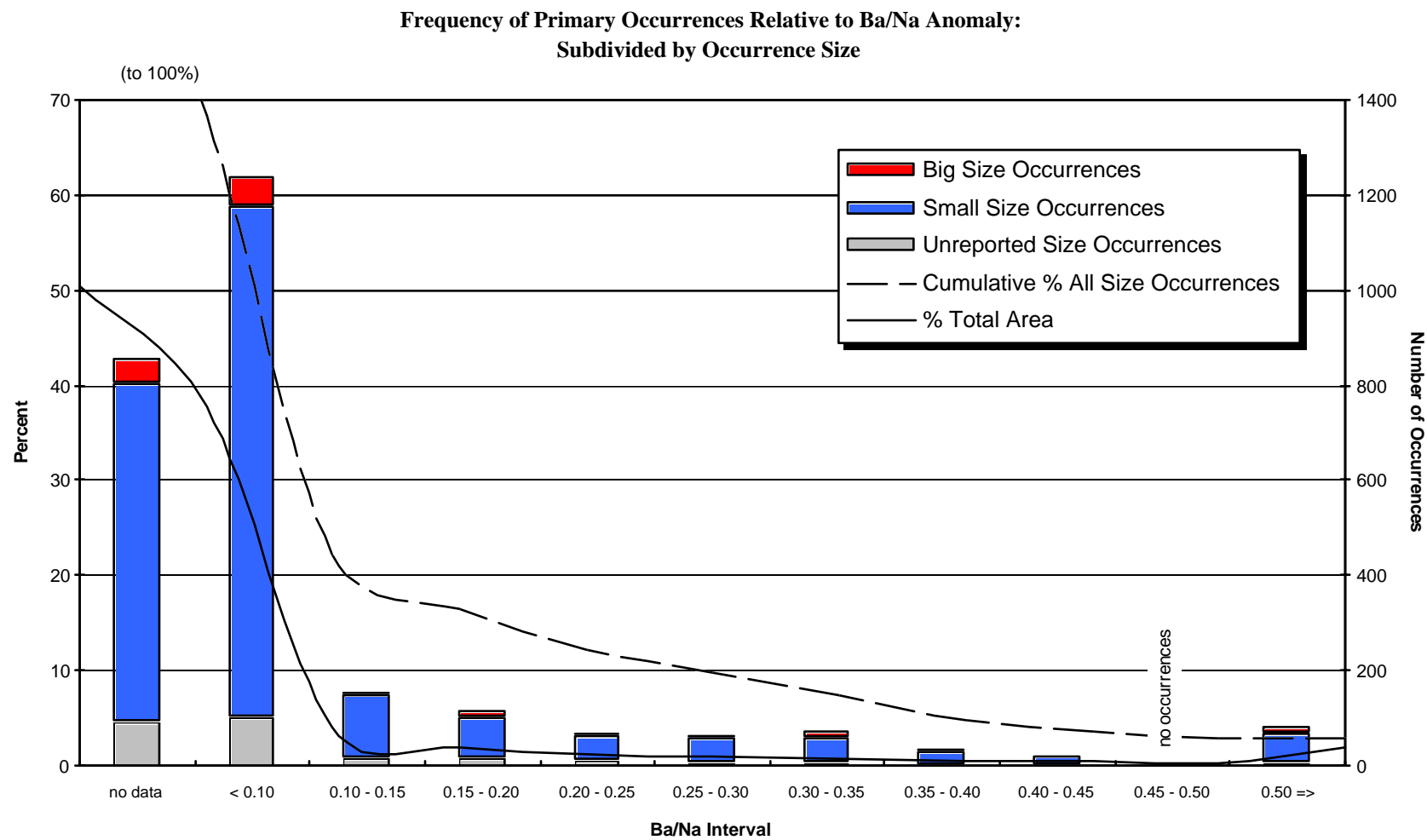


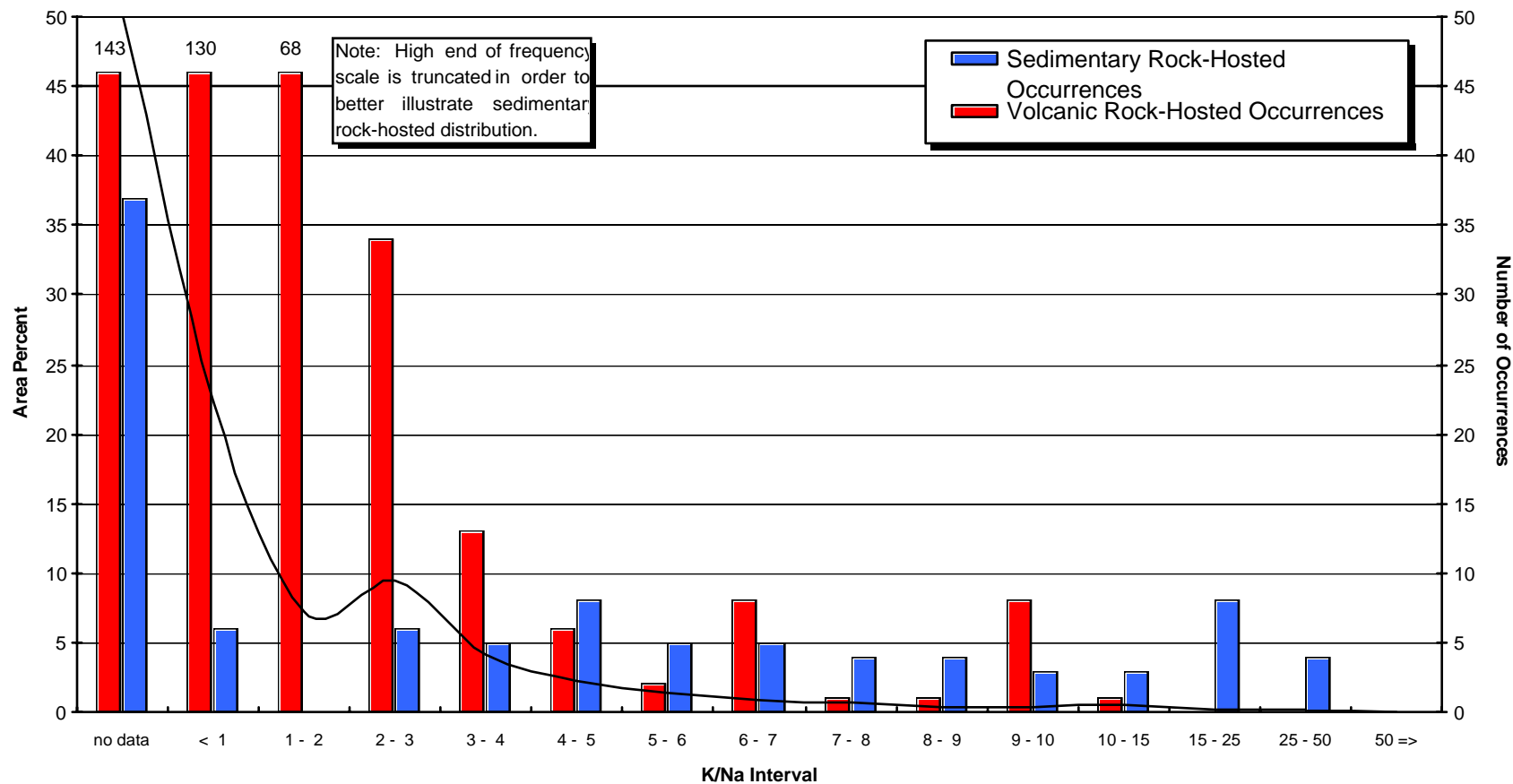
Figure 6.58. Number of primary occurrences per K/Na anomaly interval (subdivided by size).





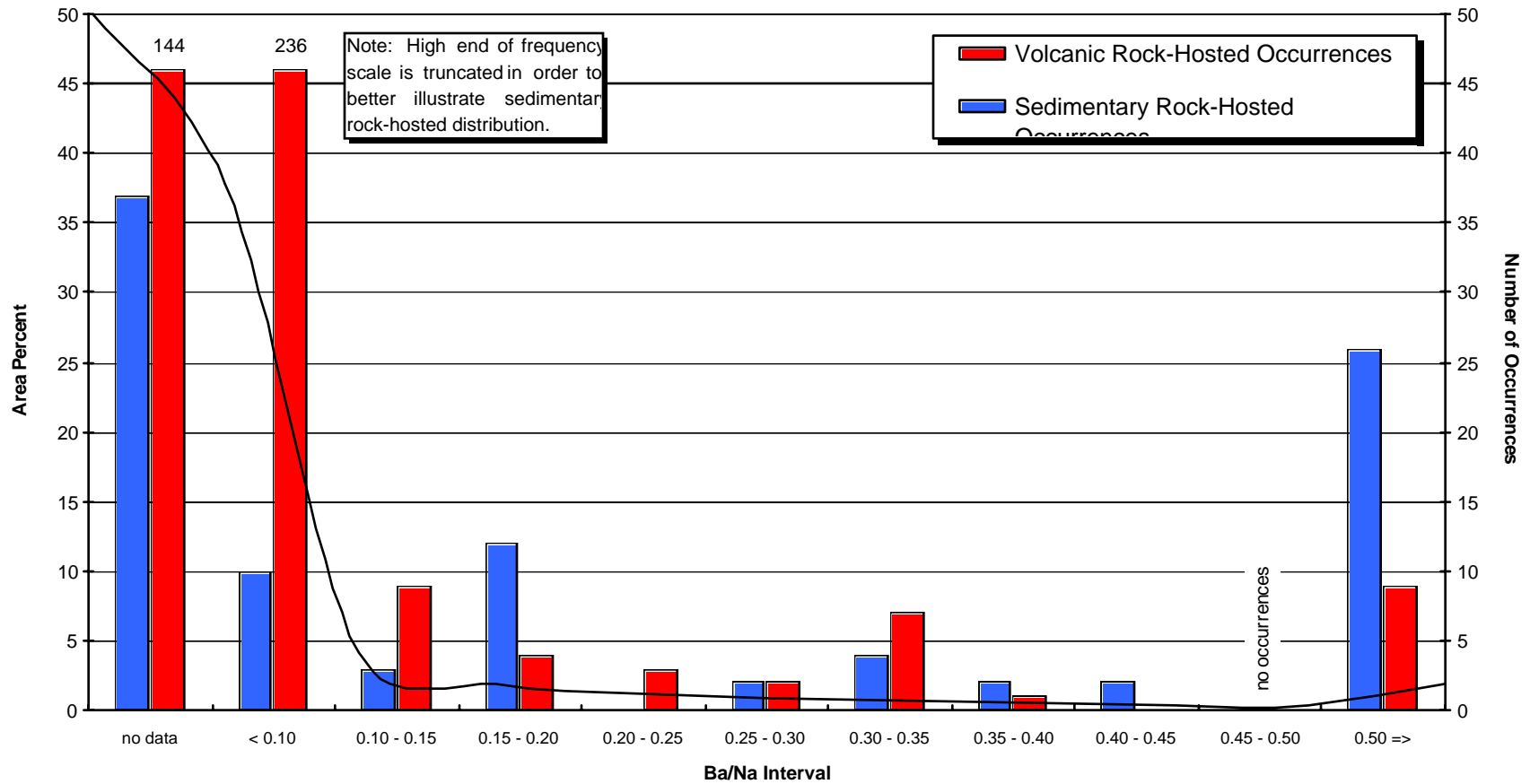
**Figure 6.59.** Number of primary occurrences per Ba/Na anomaly interval (subdivided by size).

### Frequency of Sedimentary and Volcanic Rock-Hosted Occurrences Relative to K/Na Anomaly

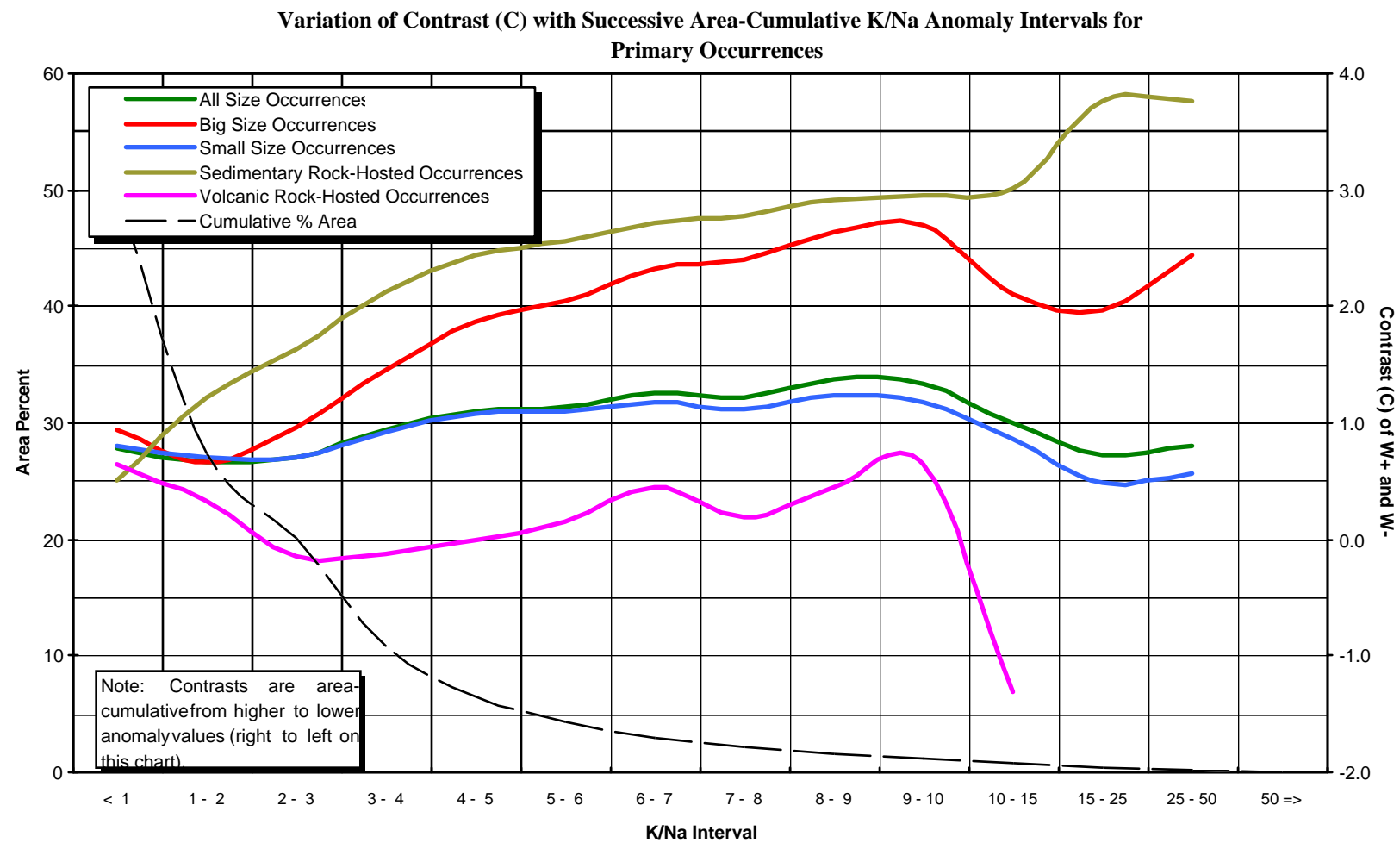


**Figure 6.60.** Number of sedimentary and volcanic rock-hosted occurrences per K/Na anomaly interval.

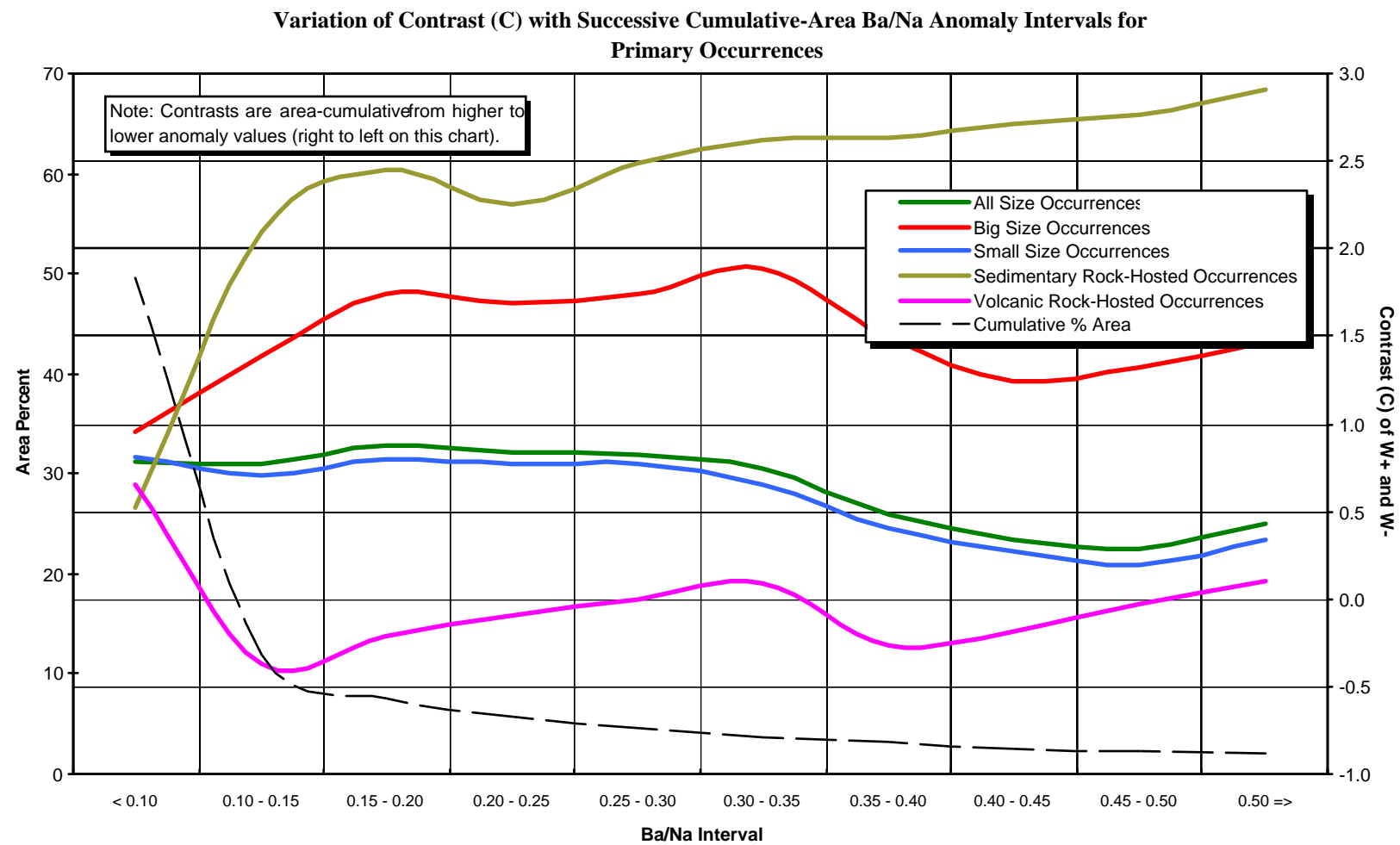
### Frequency of Sedimentary and Volcanic Rock-Hosted Occurrences Relative to Ba/Na Anomaly



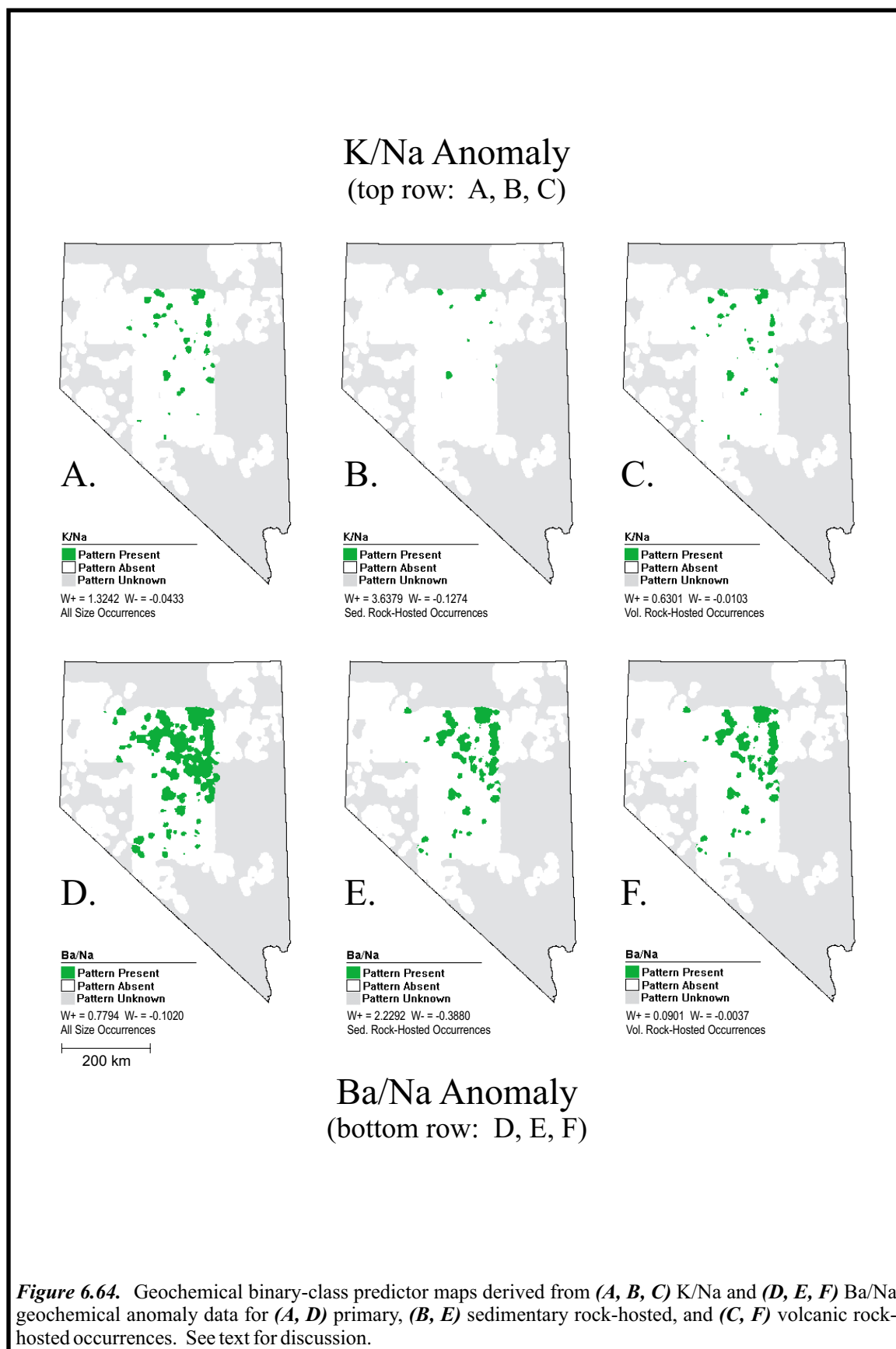
**Figure 6.61.** Number of sedimentary and volcanic rock-hosted occurrences per Ba/Na anomaly interval.

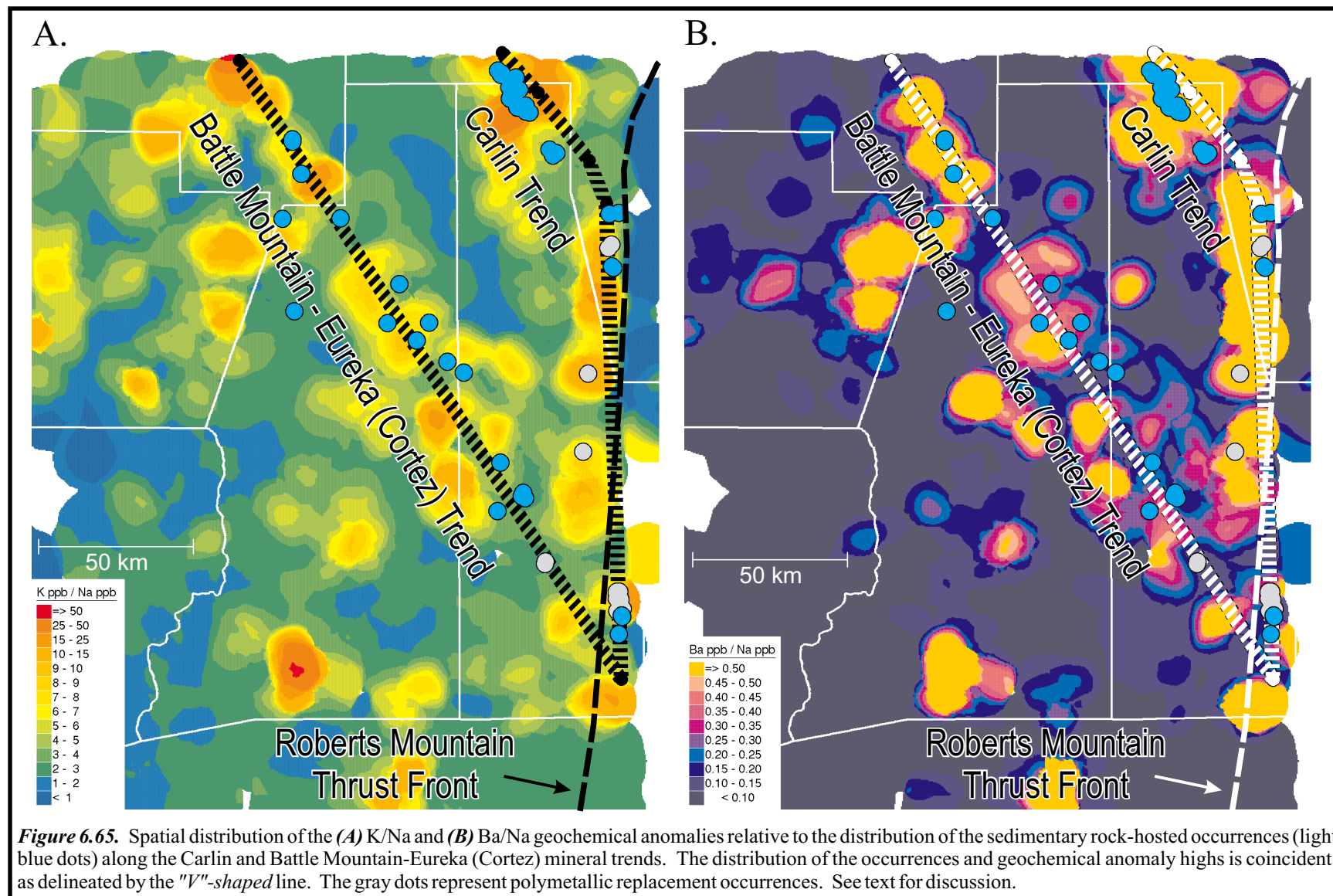


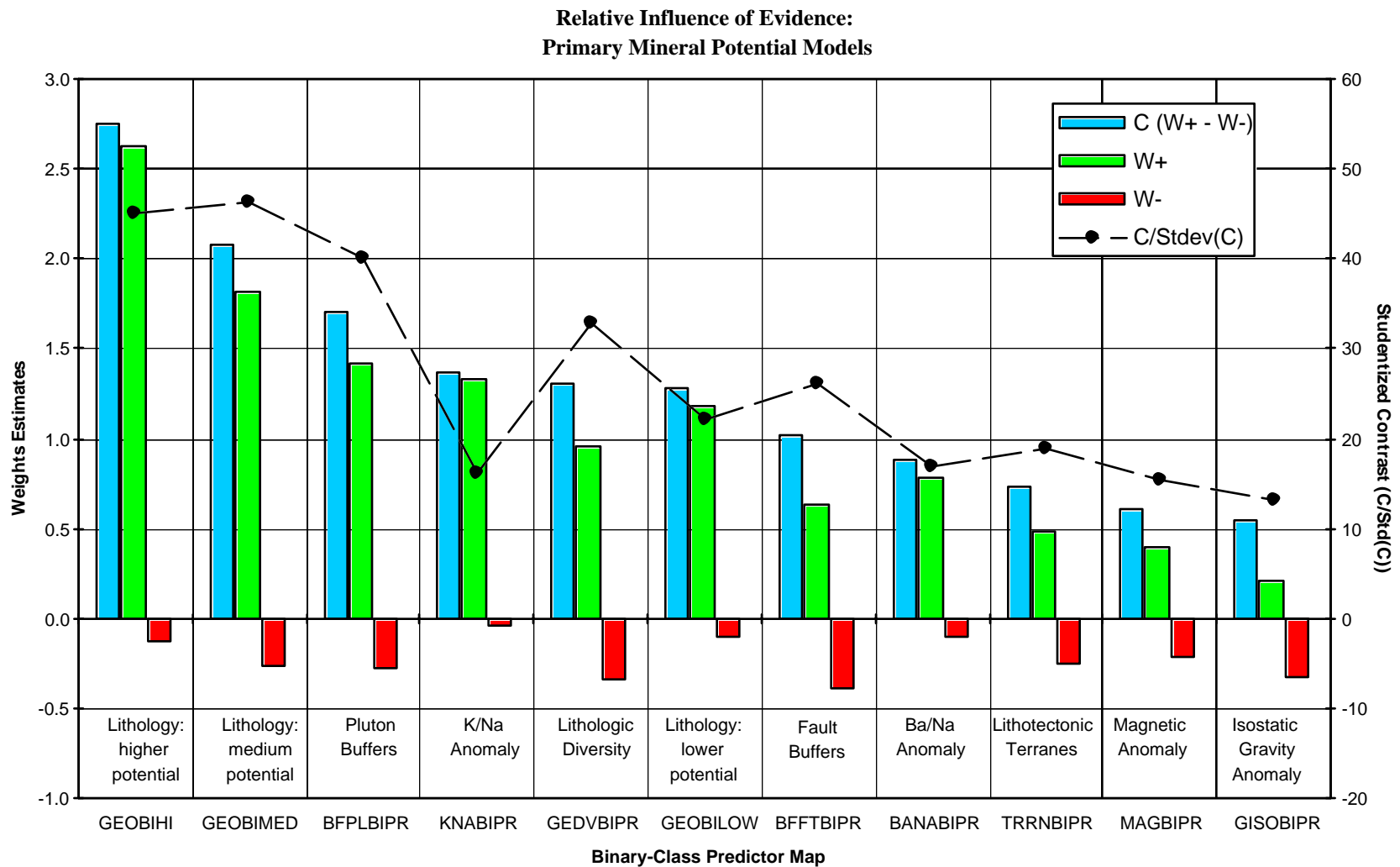
**Figure 6.62** Variation in contrast (C) across K/Na anomaly intervals (subdivided by type and size).



**Figure 6.63** . Variation in contrast (C) across Ba/Na anomaly intervals (subdivided by type and size).

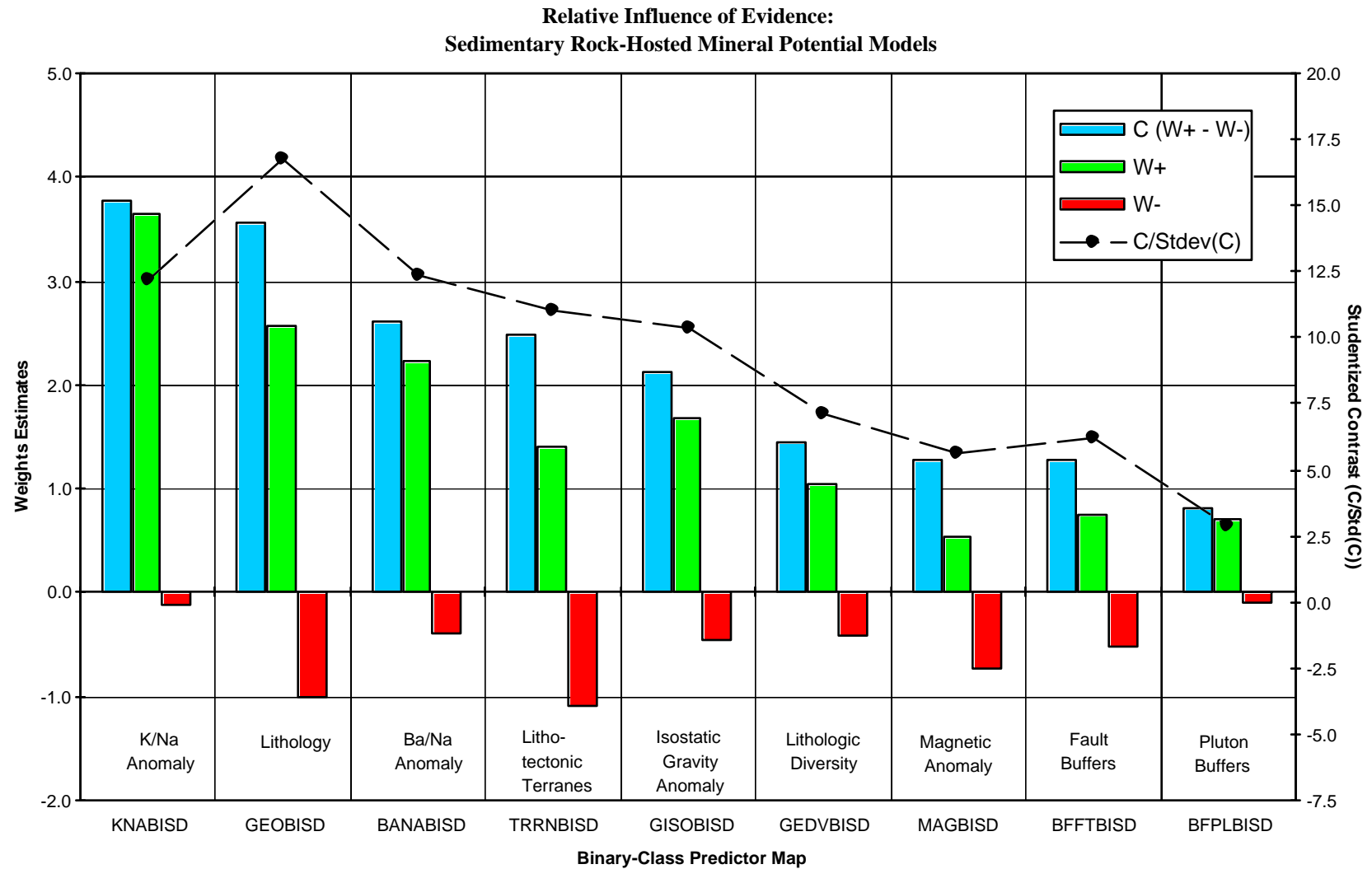




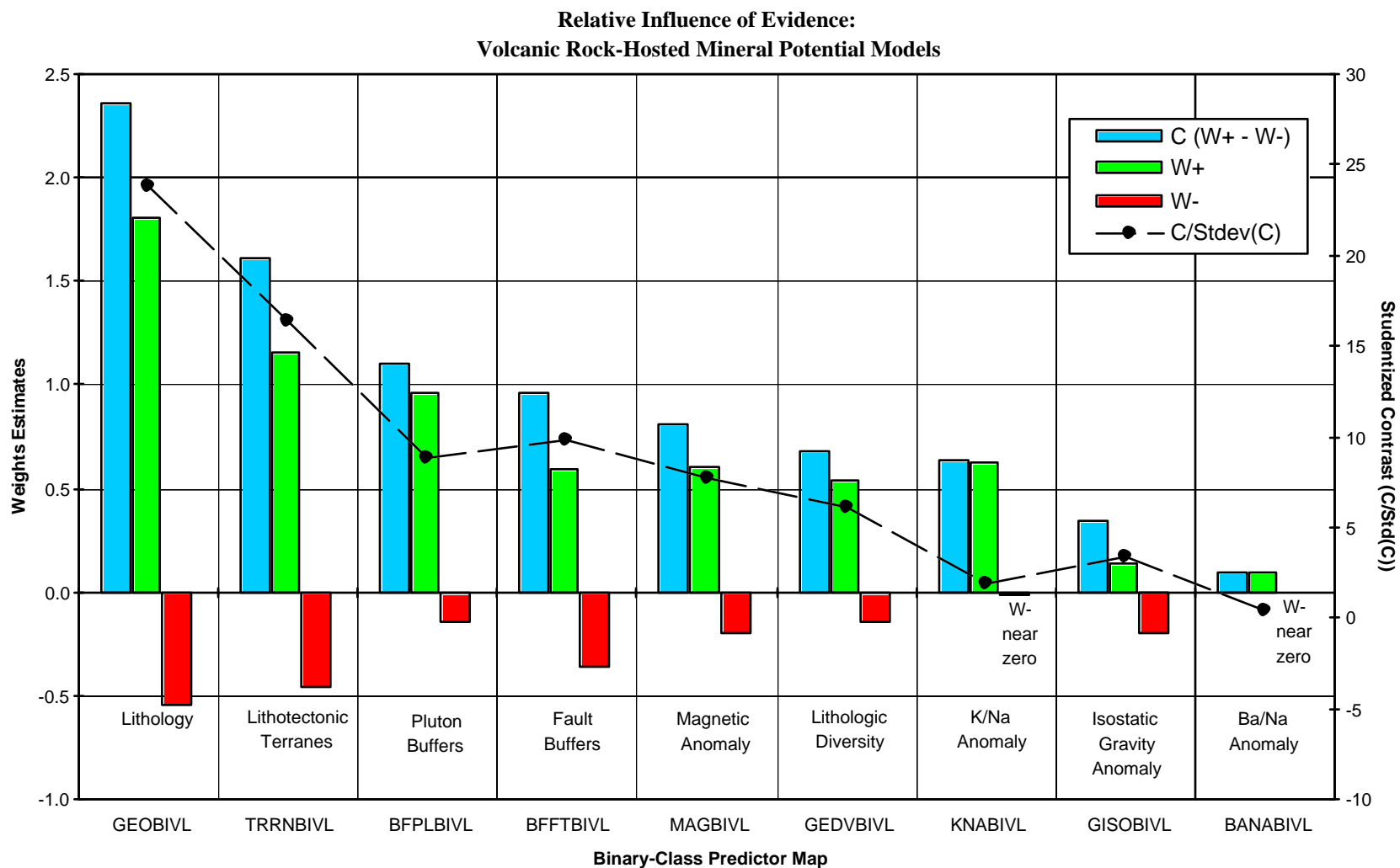


**Figure 7.1.** The influence of predictor maps used in the primary occurrence-type mineral potential models, and the strength of spatial association between the evidence and the occurrences

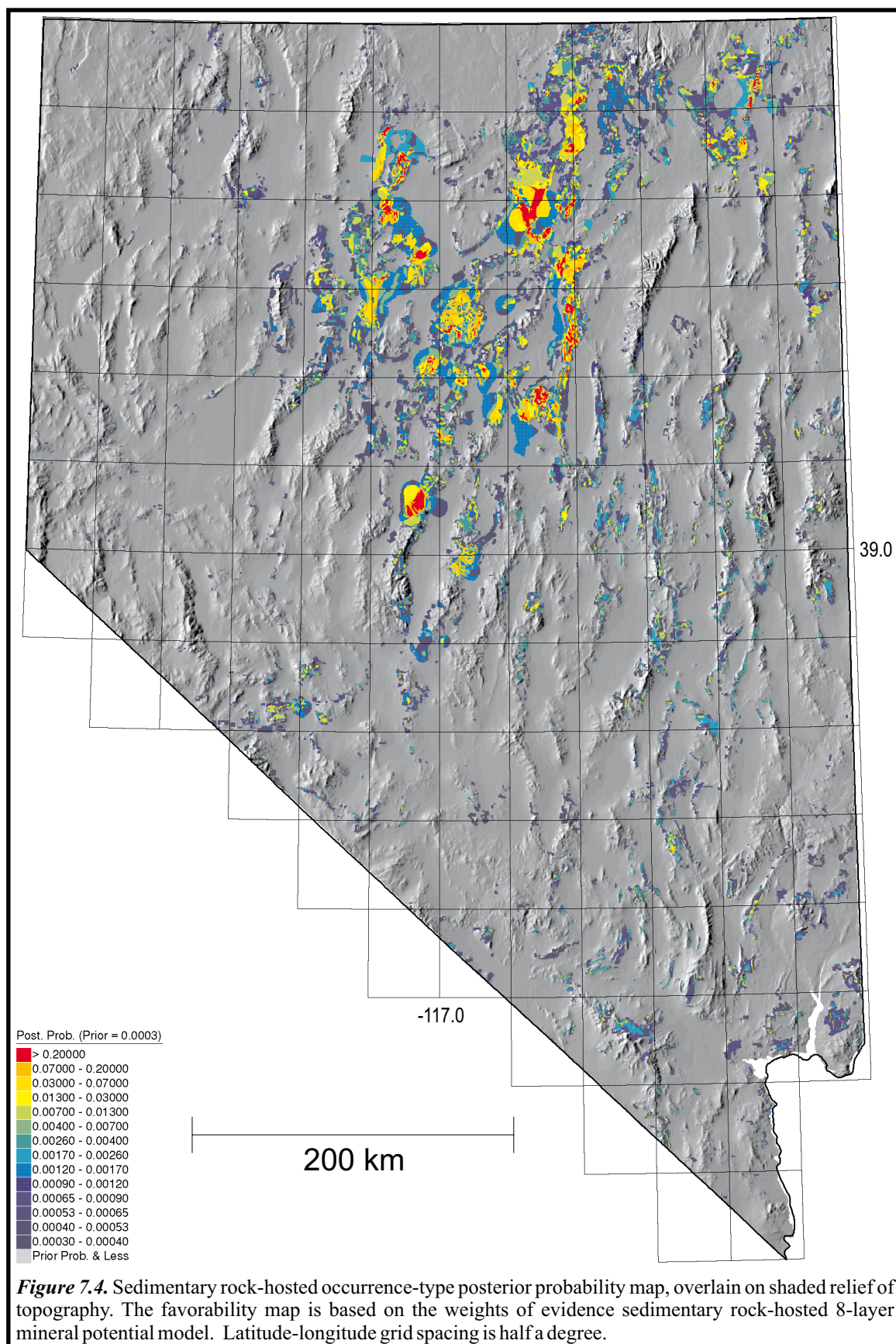




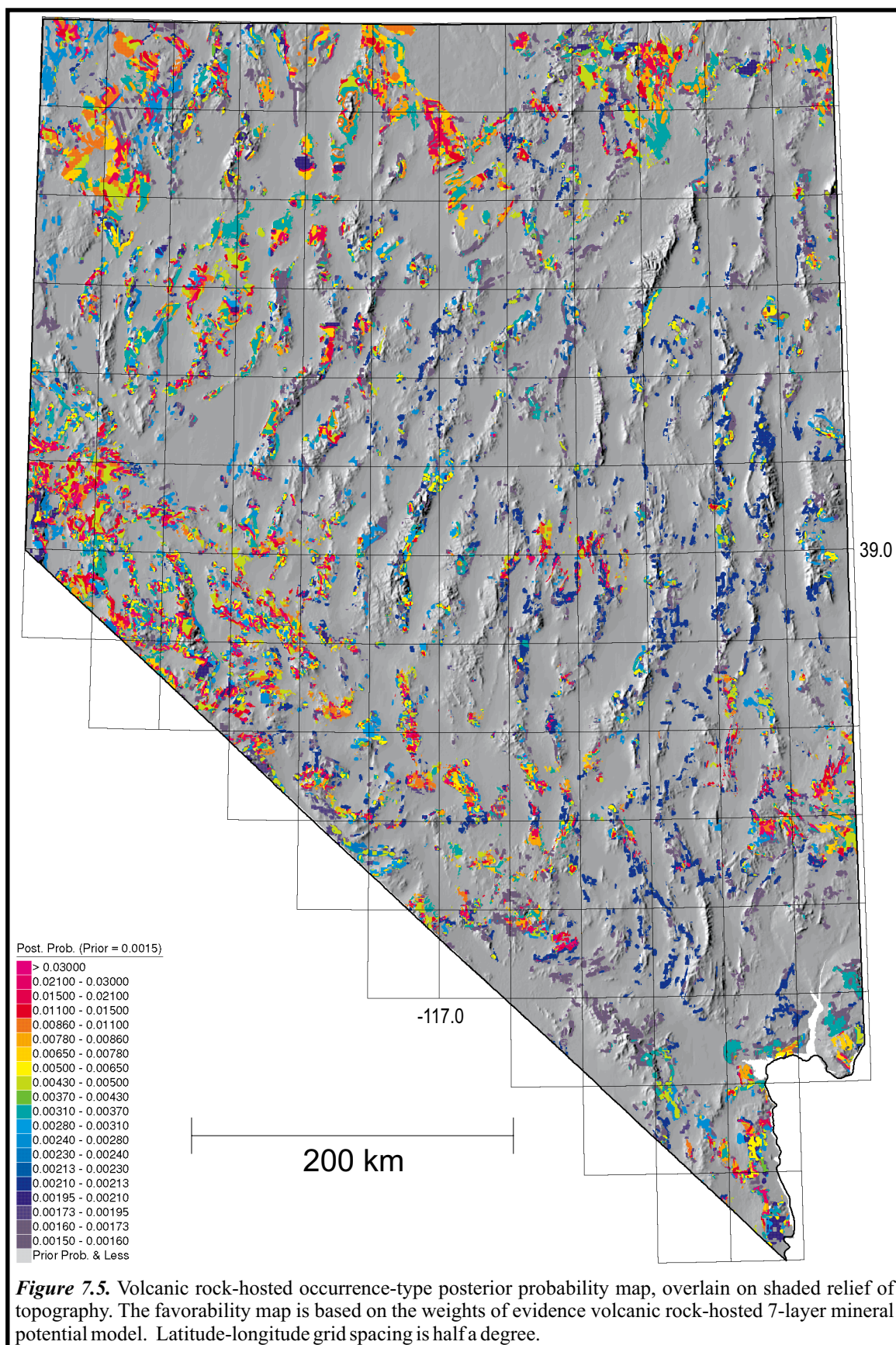
**Figure 7.2.** The influence of predictor maps used in the sed. rock-host. occurrences mineral potential models, and the strength of spatial association between the evidence and the occurrences

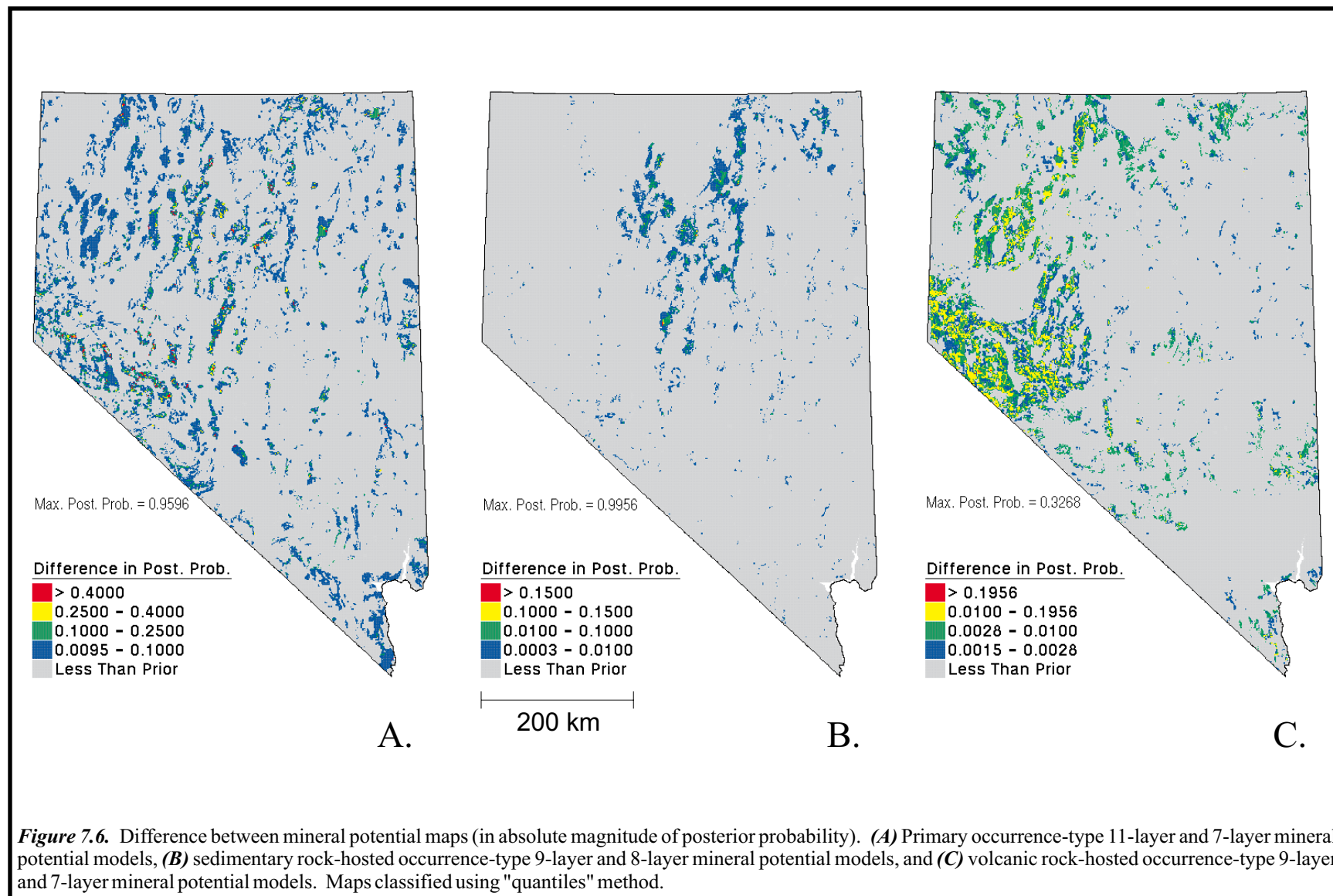


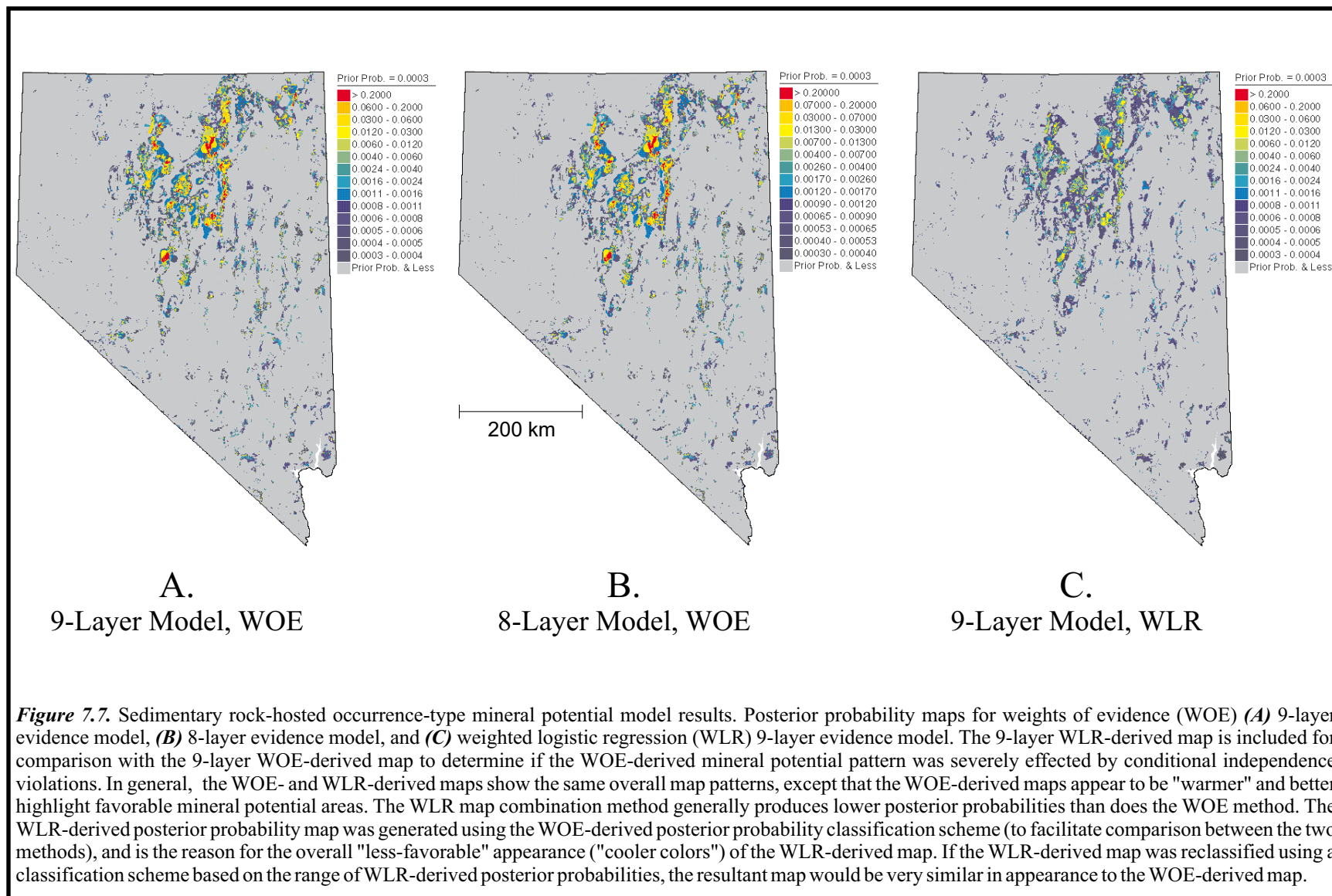
**Figure 7.3.** The influence of predictor maps used in the vol. rock-host. occurrences mineral potential models, and the strength of spatial association between the evidence and the occurrences



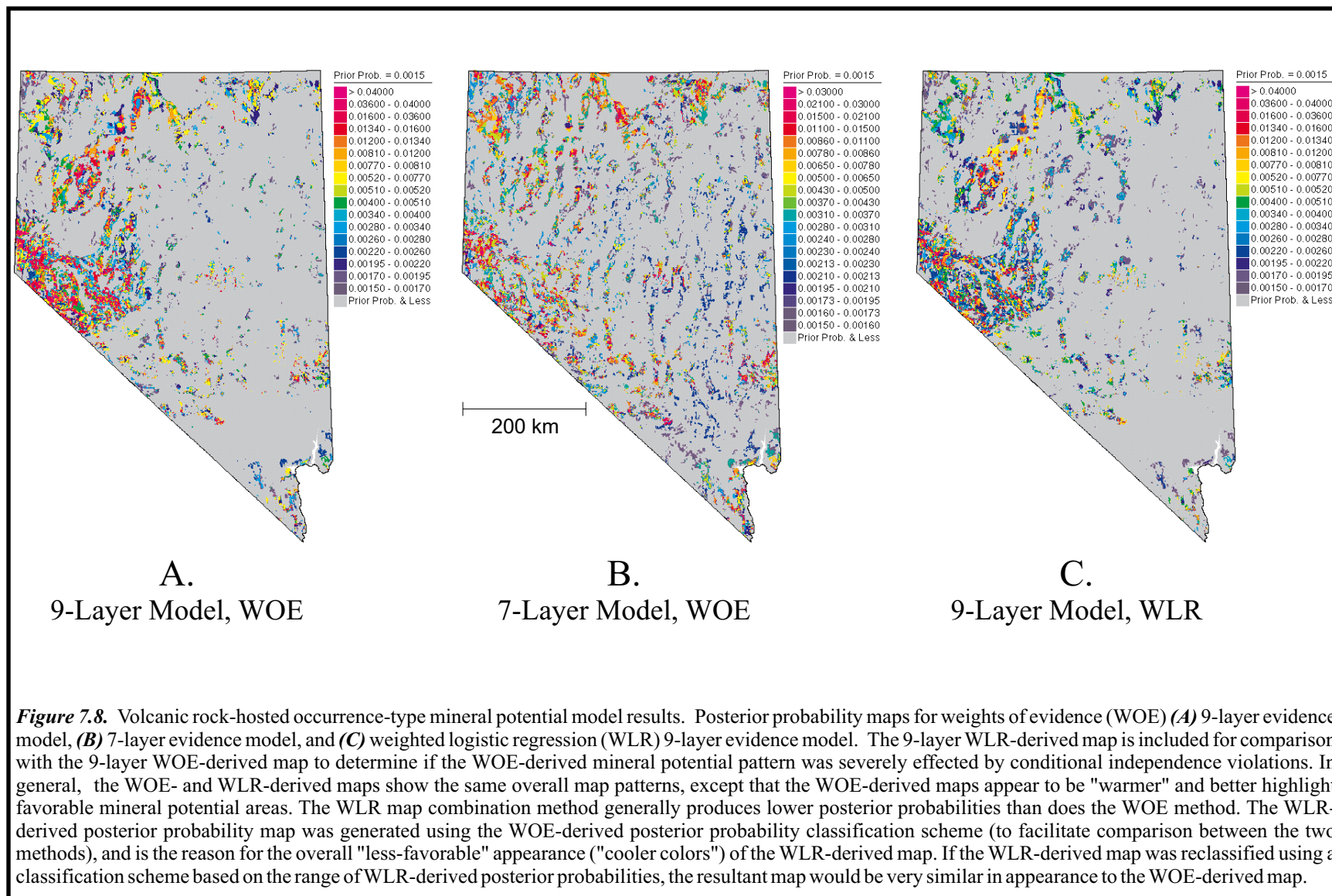




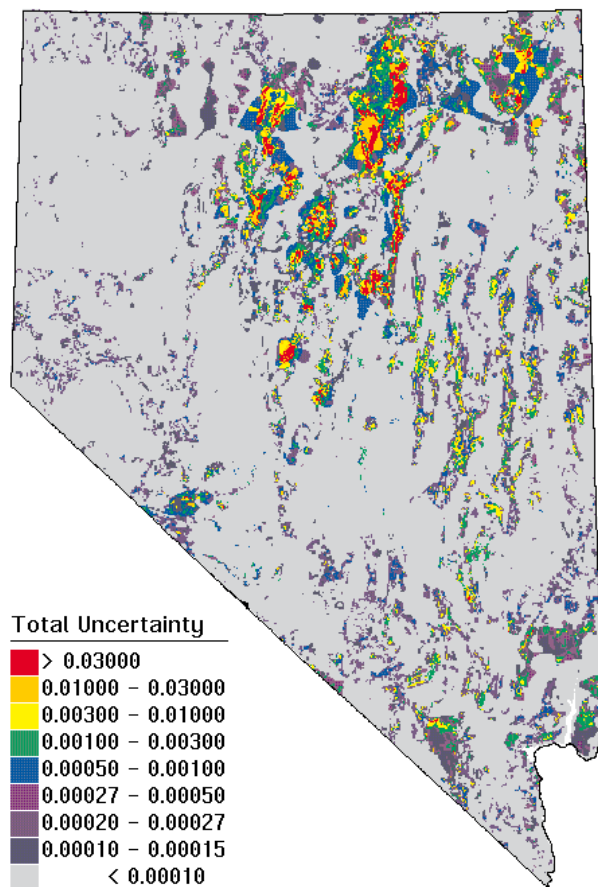








A.



B.

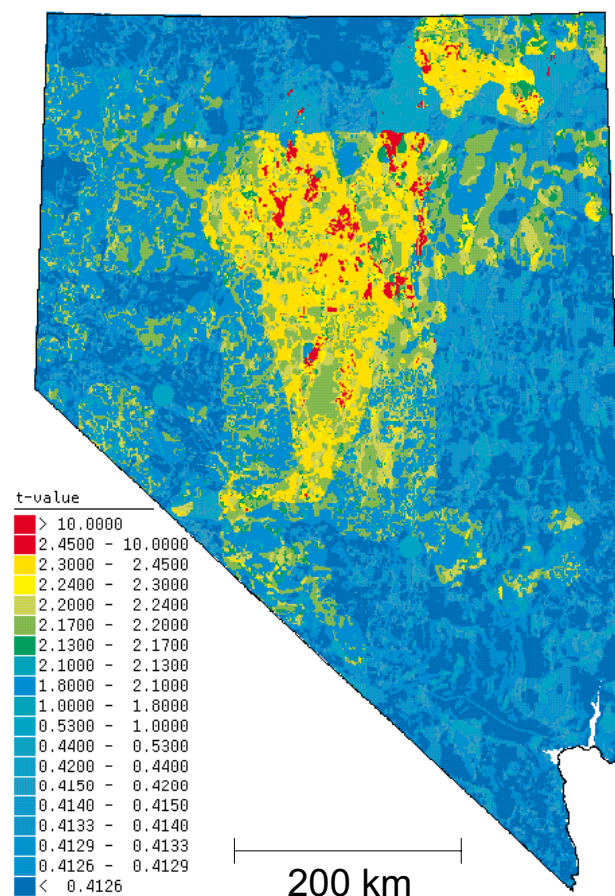
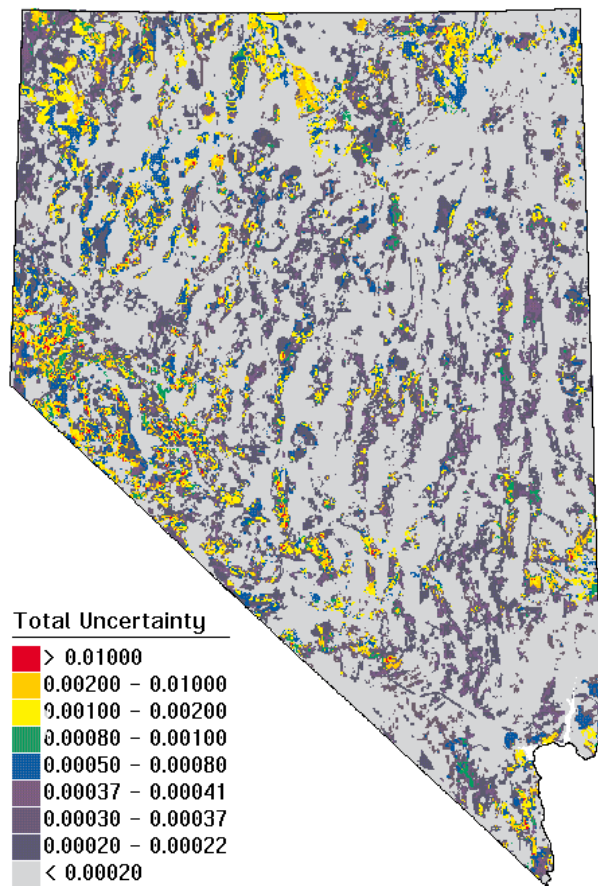


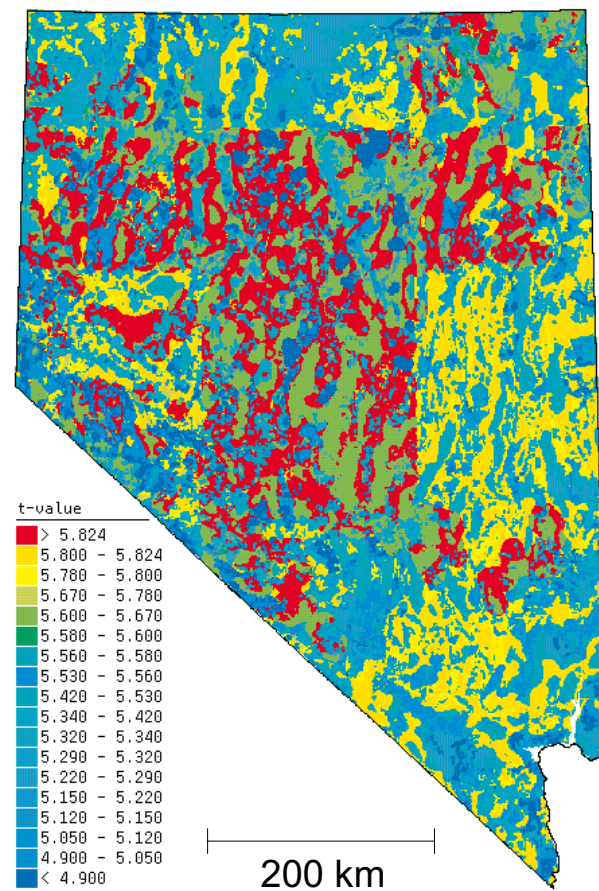
**Figure 7.9.** Uncertainty of posterior probabilities used to generate sedimentary rock-hosted occurrence-type 8-layer mineral potential map. (A) Total uncertainty (uncertainty due to variances of weights, plus, sum of uncertainty due to missing data) and (B) relative certainty of the posterior probability (posterior probability divided by its standard deviation, in effect, the application of an approximate t-test).



A.

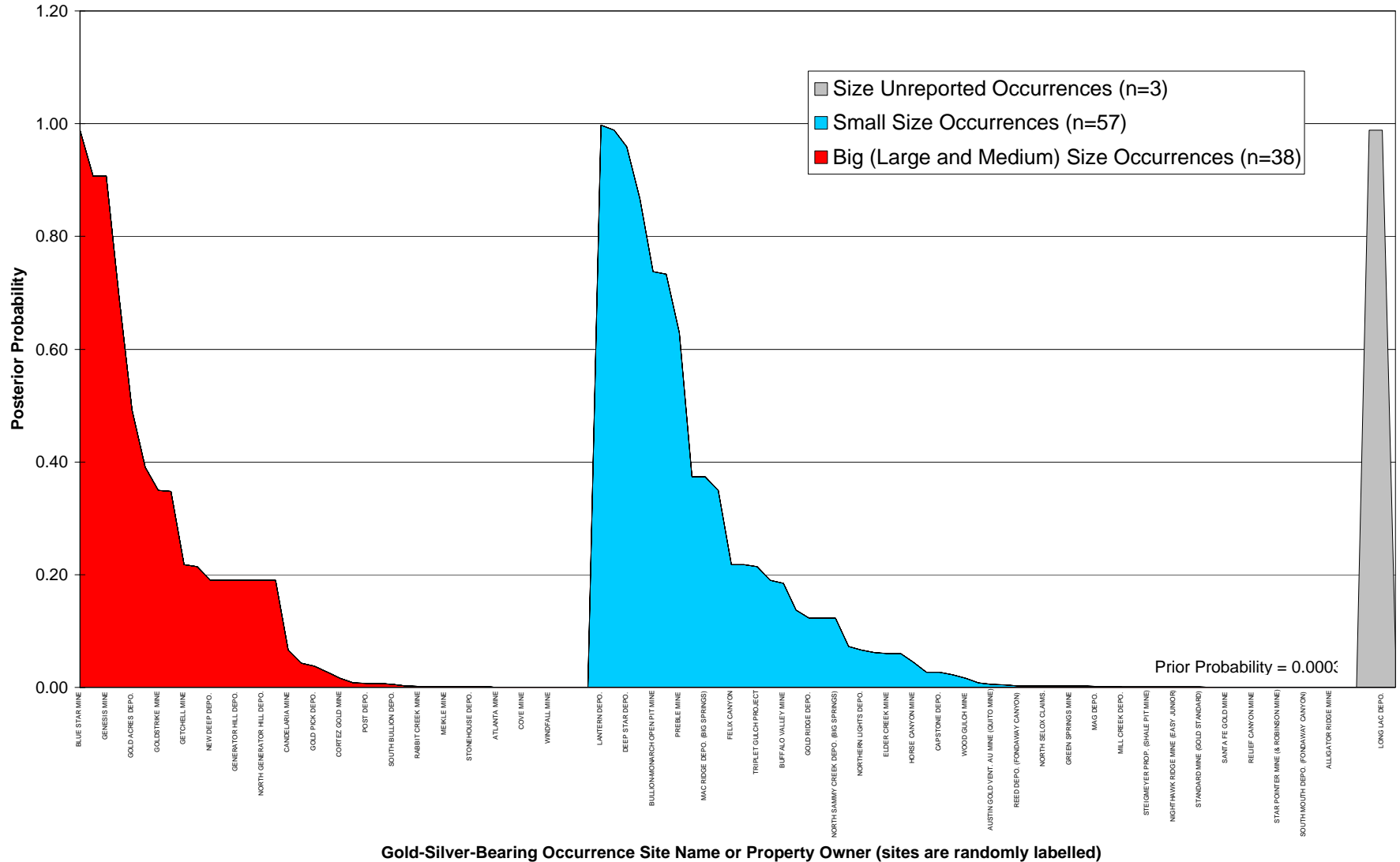


B.



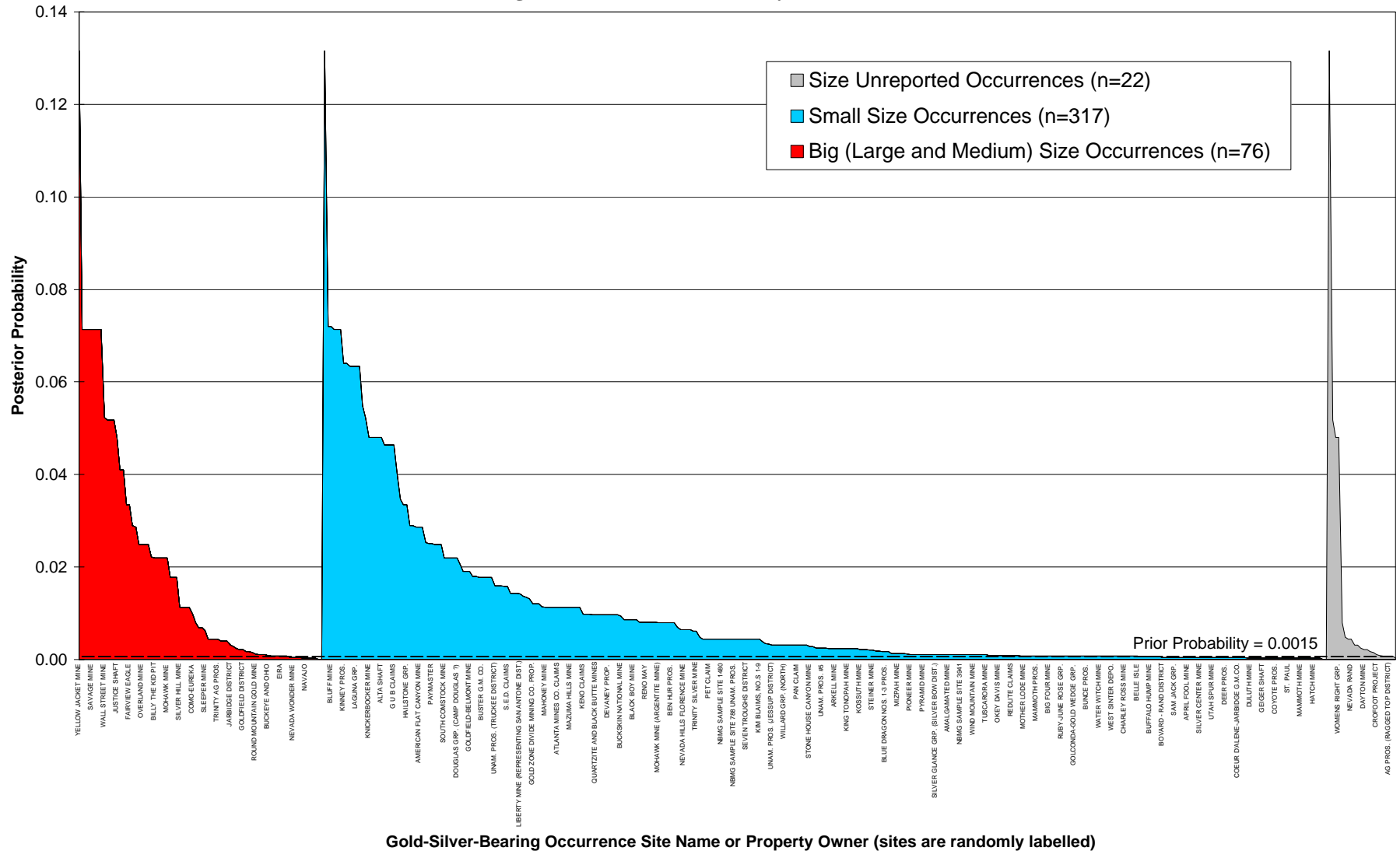
**Figure 7.10.** Uncertainty of posterior probabilities used to generate volcanic rock-hosted occurrence-type 7-layer mineral potential map. (A) Total uncertainty (uncertainty due to variances of weights, plus, sum of uncertainty due to missing data) and (B) relative certainty of the posterior probability (posterior probability divided by its standard deviation, in effect, the application of an approximate t-test).

**Posterior Probabilities Appended to Sedimentary Rock-Hosted Gold-Silver-Bearing Occurrences:  
Calculated Using Sedimentary Rock-Hosted 8-Layer Mineral Potential Model**

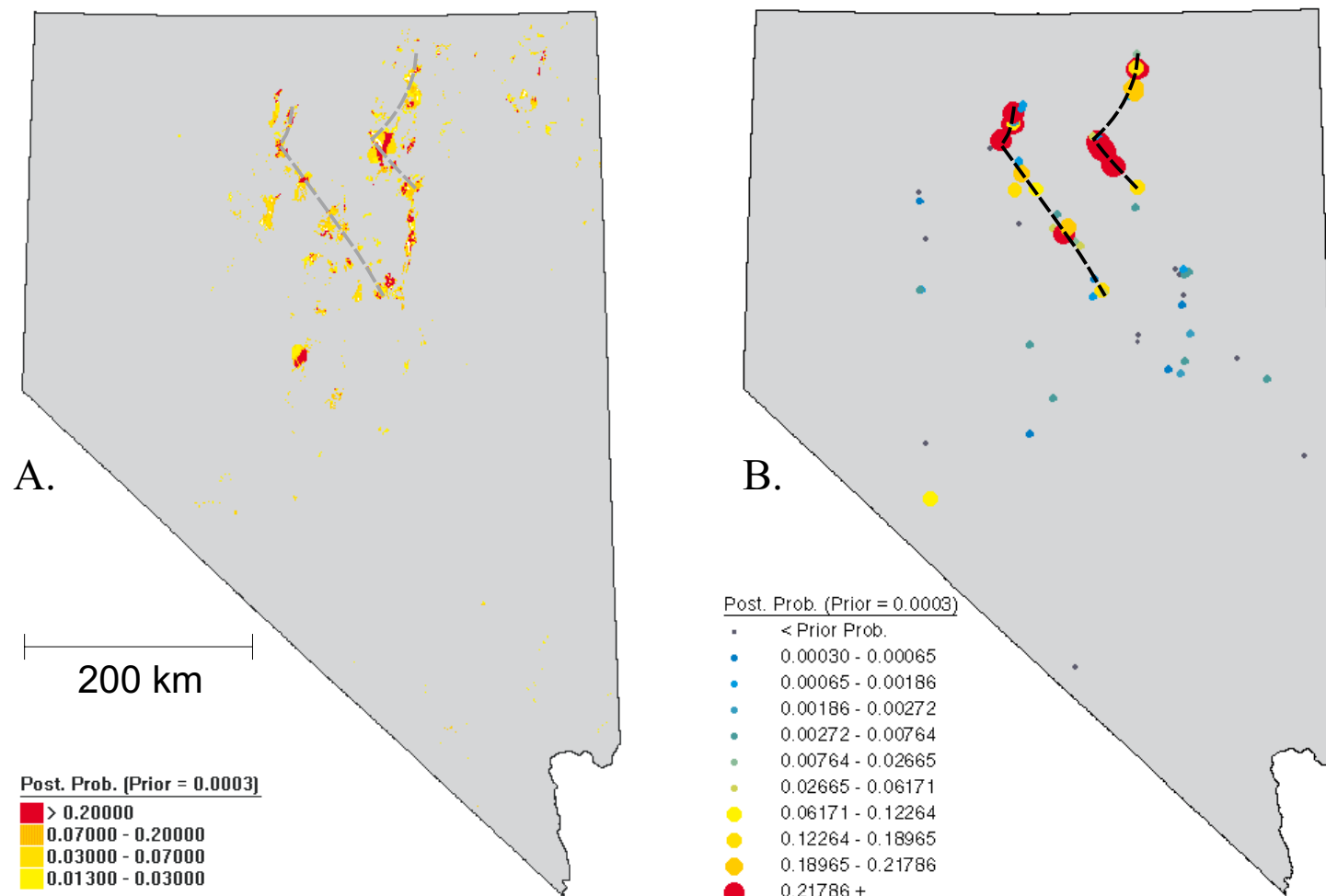


**Figure 7.11.** Distribution of posterior probabilities associated with big (large and medium), small, and unknown size sedimentary rock-hosted occurrences. 298

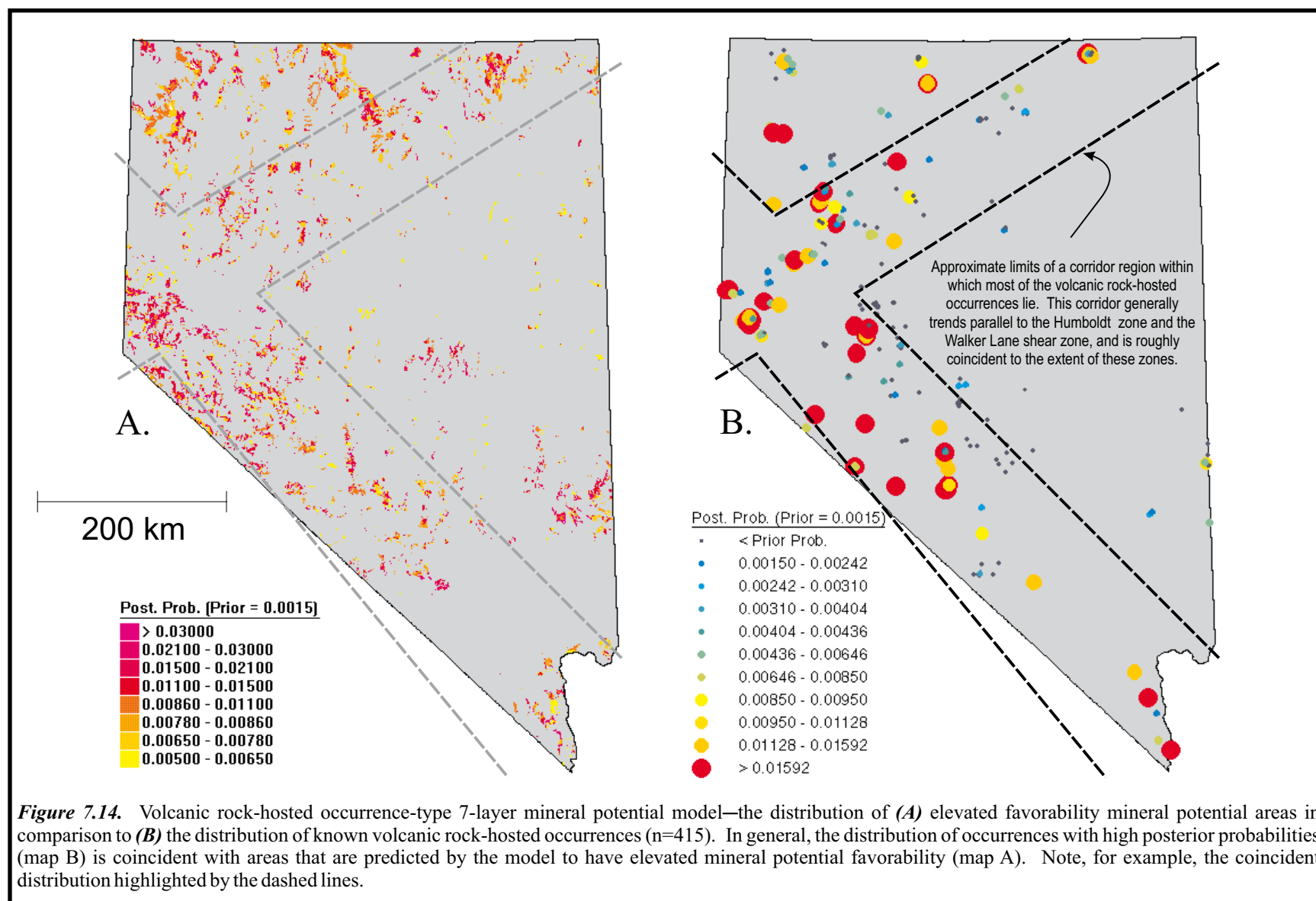
**Posterior Probabilities Appended to Volcanic Rock-Hosted Gold-Silver-Bearing Occurrences:  
Calculated Using Volcanic Rock-Hosted 7-Layer Mineral Potential Model**

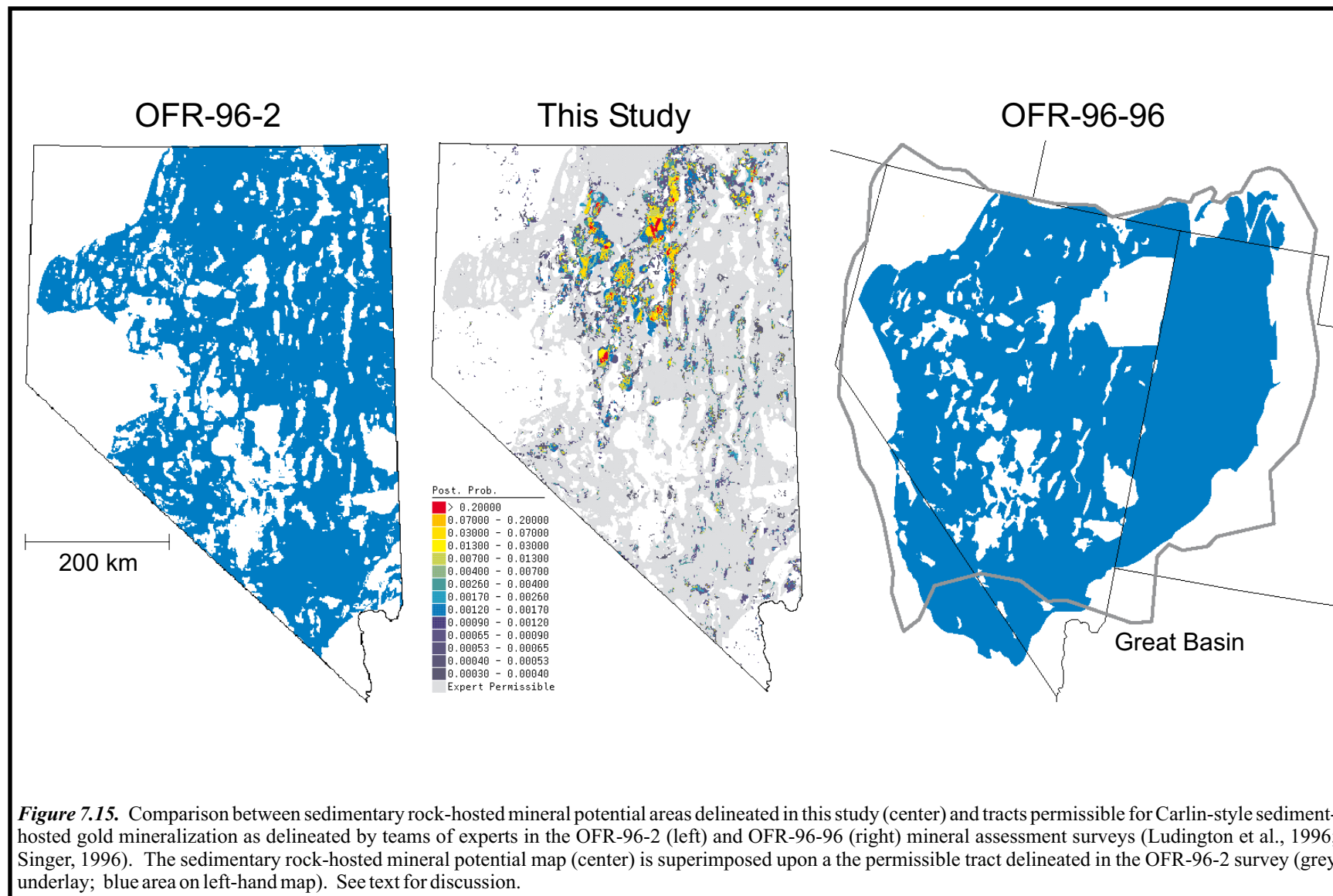


**Figure 7.12.** Distribution of posterior probabilities associated with big (large and medium), small, and unknown size volcanic rock-hosted occurrences. 299

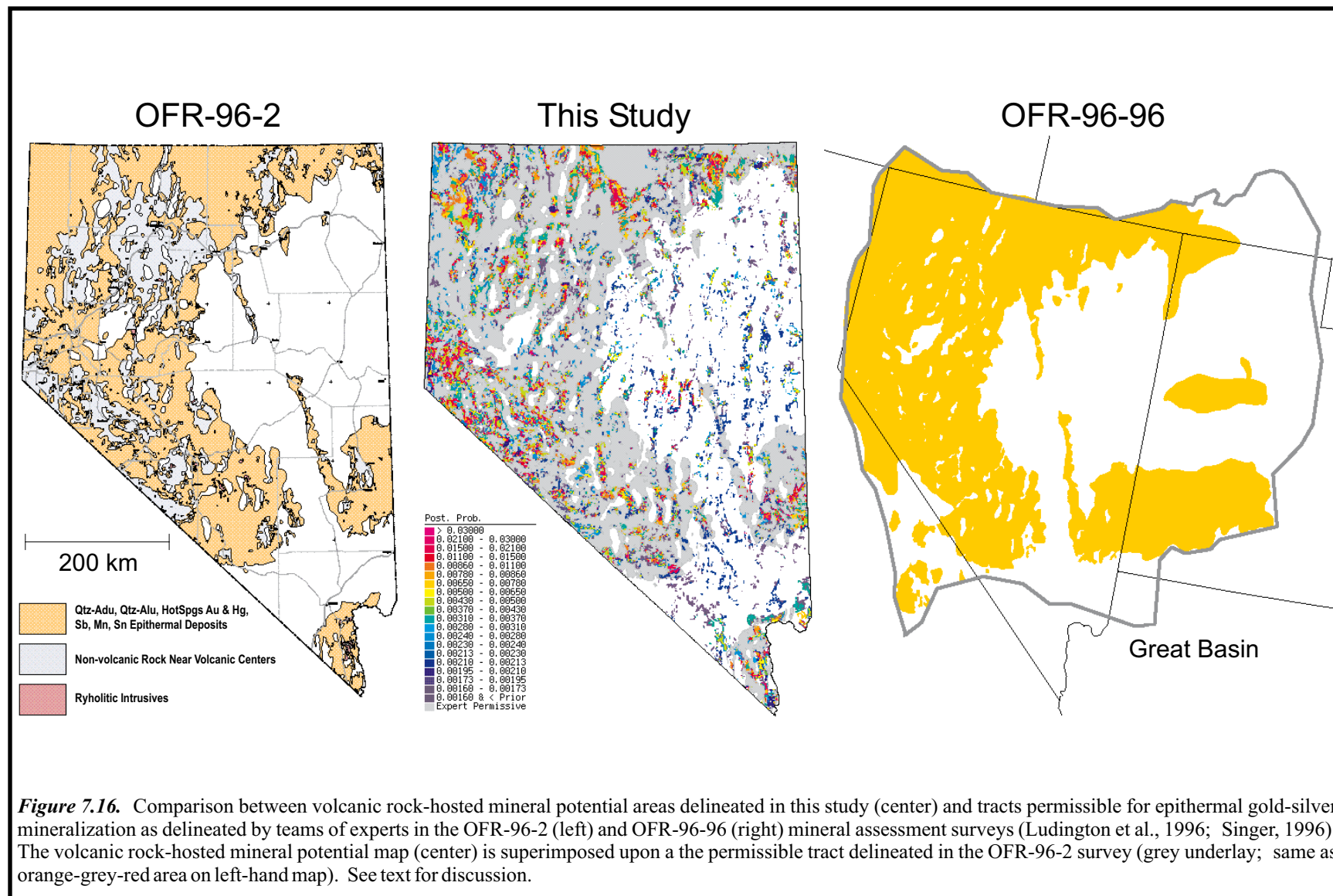


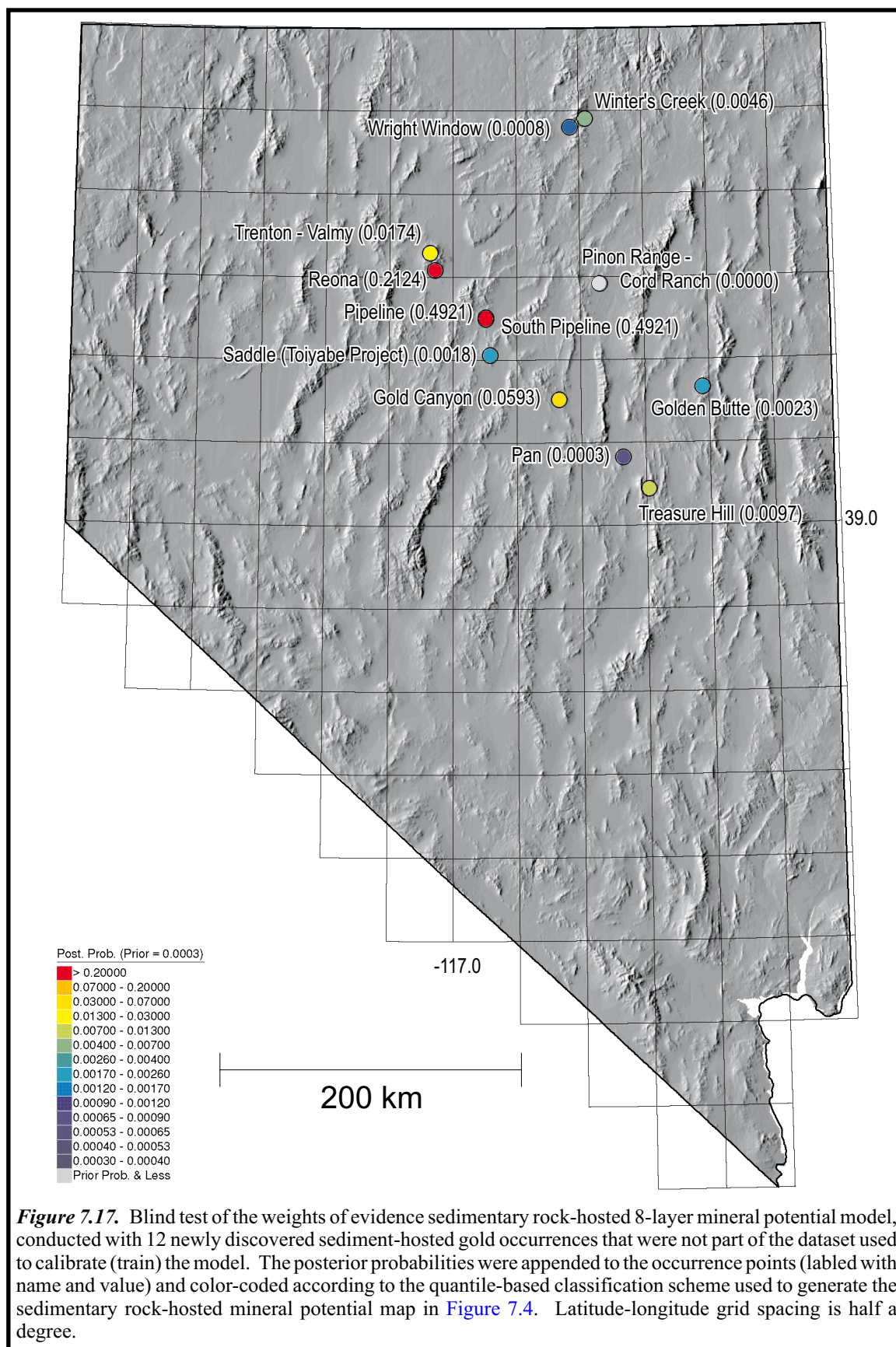
**Figure 7.13.** Sedimentary rock-hosted occurrence-type 8-layer mineral potential model—the distribution of (A) elevated favorability mineral potential areas in comparison to the distribution of (B) known sedimentary rock-hosted occurrences (n=98). In general, the distribution of occurrences with high posterior probabilities (map B) is coincident with areas that are predicted by the model to have elevated mineral potential favorability (map A). Note, for example, the coincident distribution highlighted by the dashed lines.





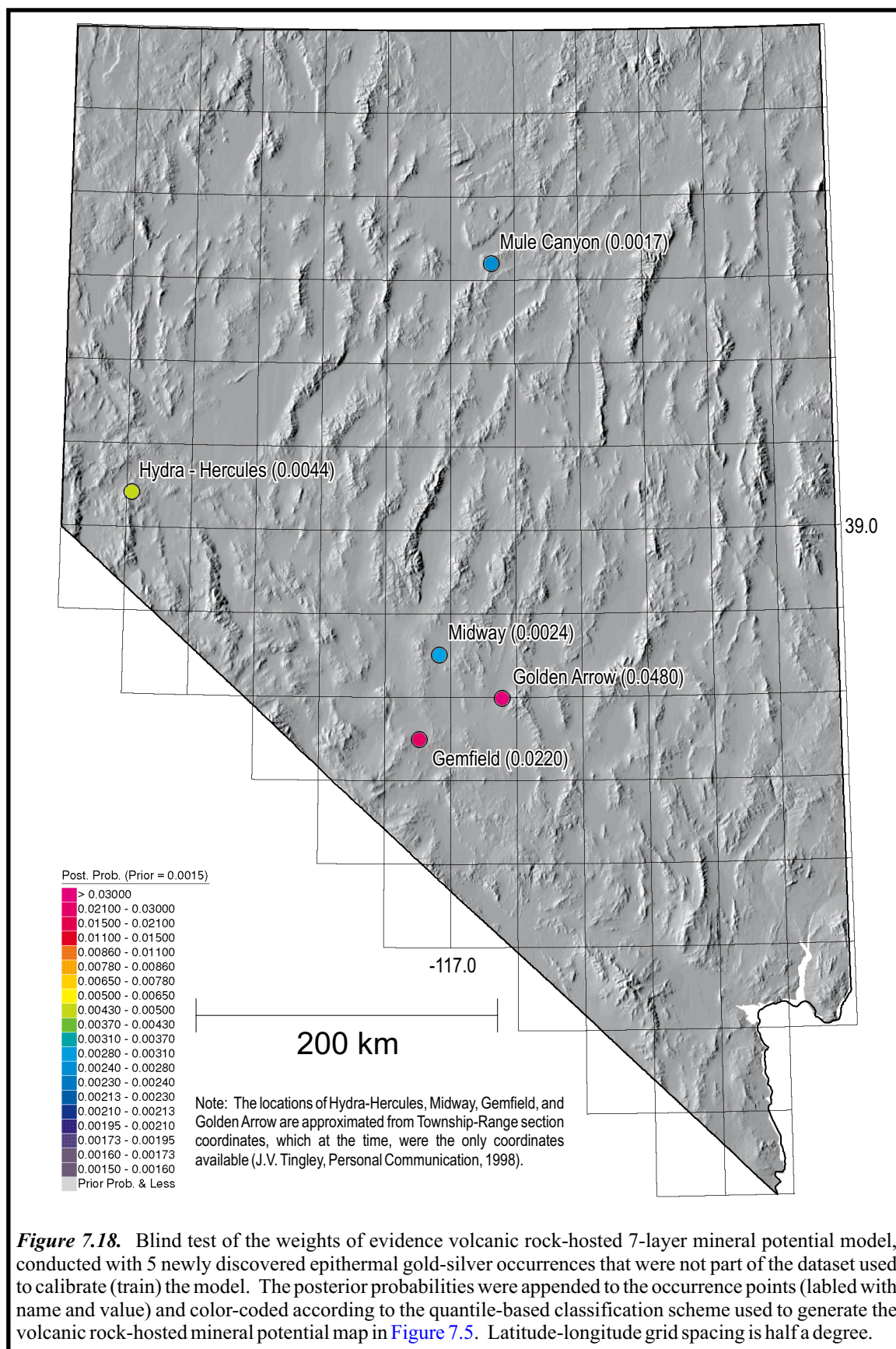


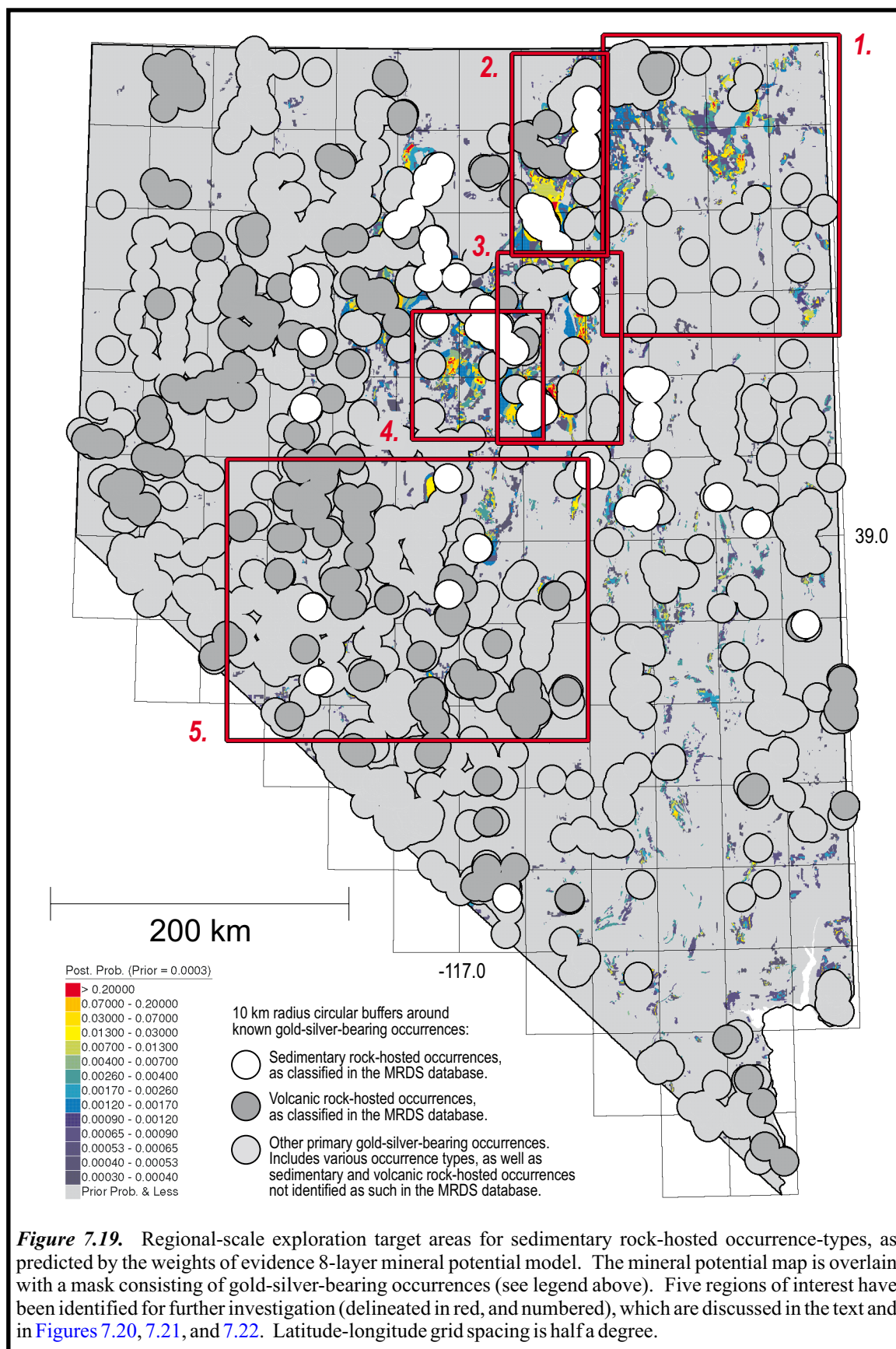


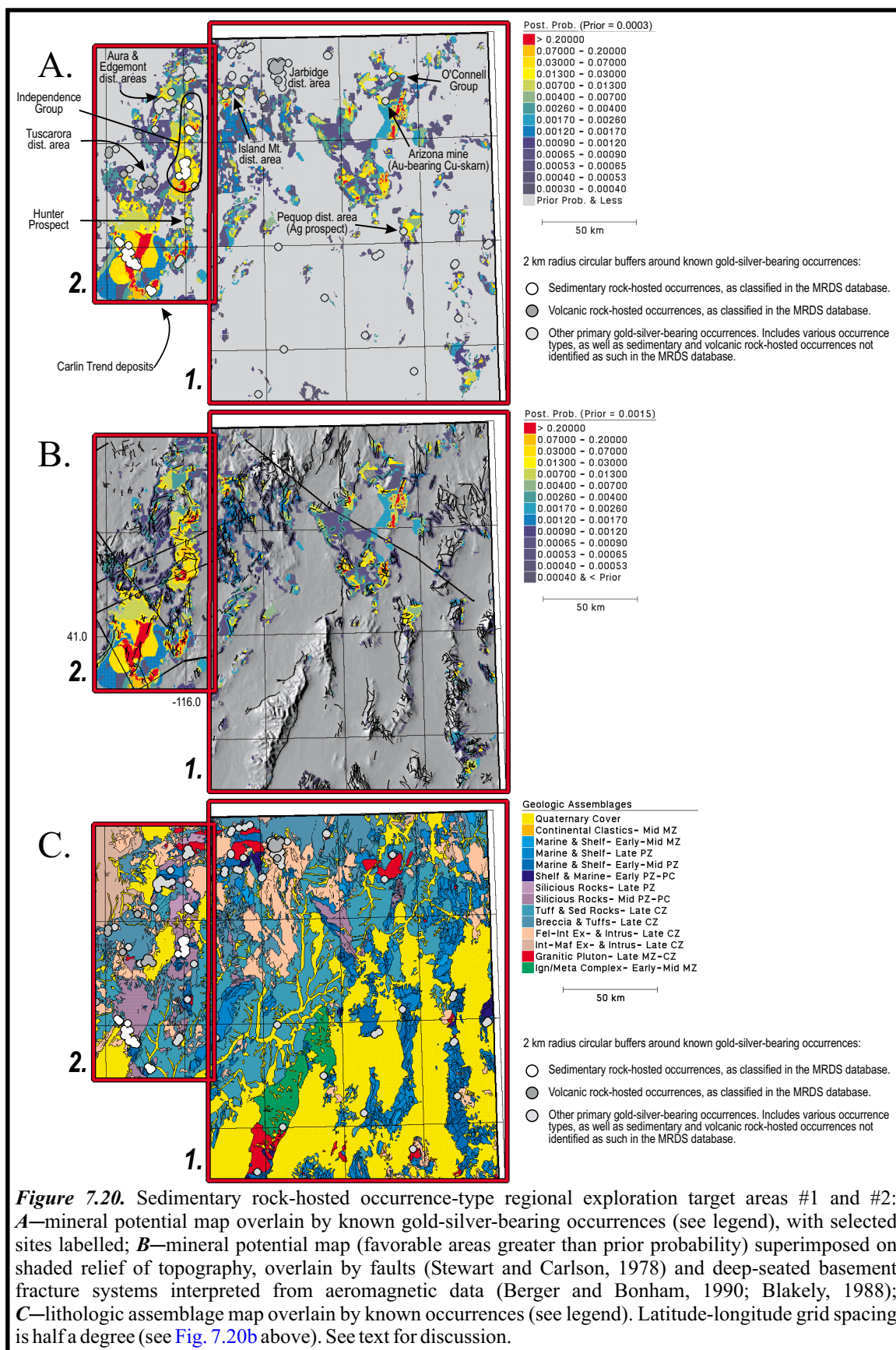


**Figure 7.17.** Blind test of the weights of evidence sedimentary rock-hosted 8-layer mineral potential model, conducted with 12 newly discovered sediment-hosted gold occurrences that were not part of the dataset used to calibrate (train) the model. The posterior probabilities were appended to the occurrence points (labeled with name and value) and color-coded according to the quantile-based classification scheme used to generate the sedimentary rock-hosted mineral potential map in [Figure 7.4](#). Latitude-longitude grid spacing is half a degree.

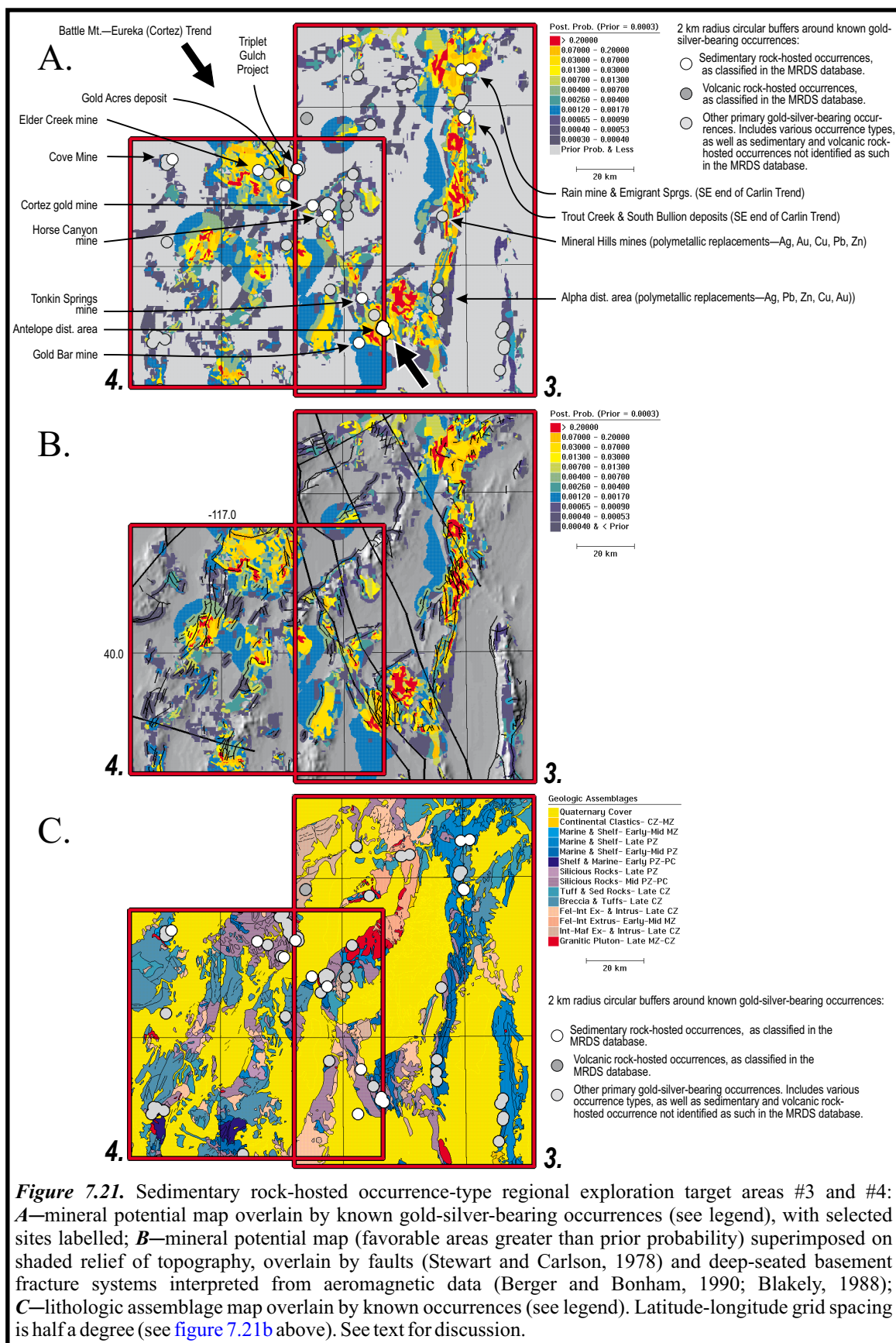


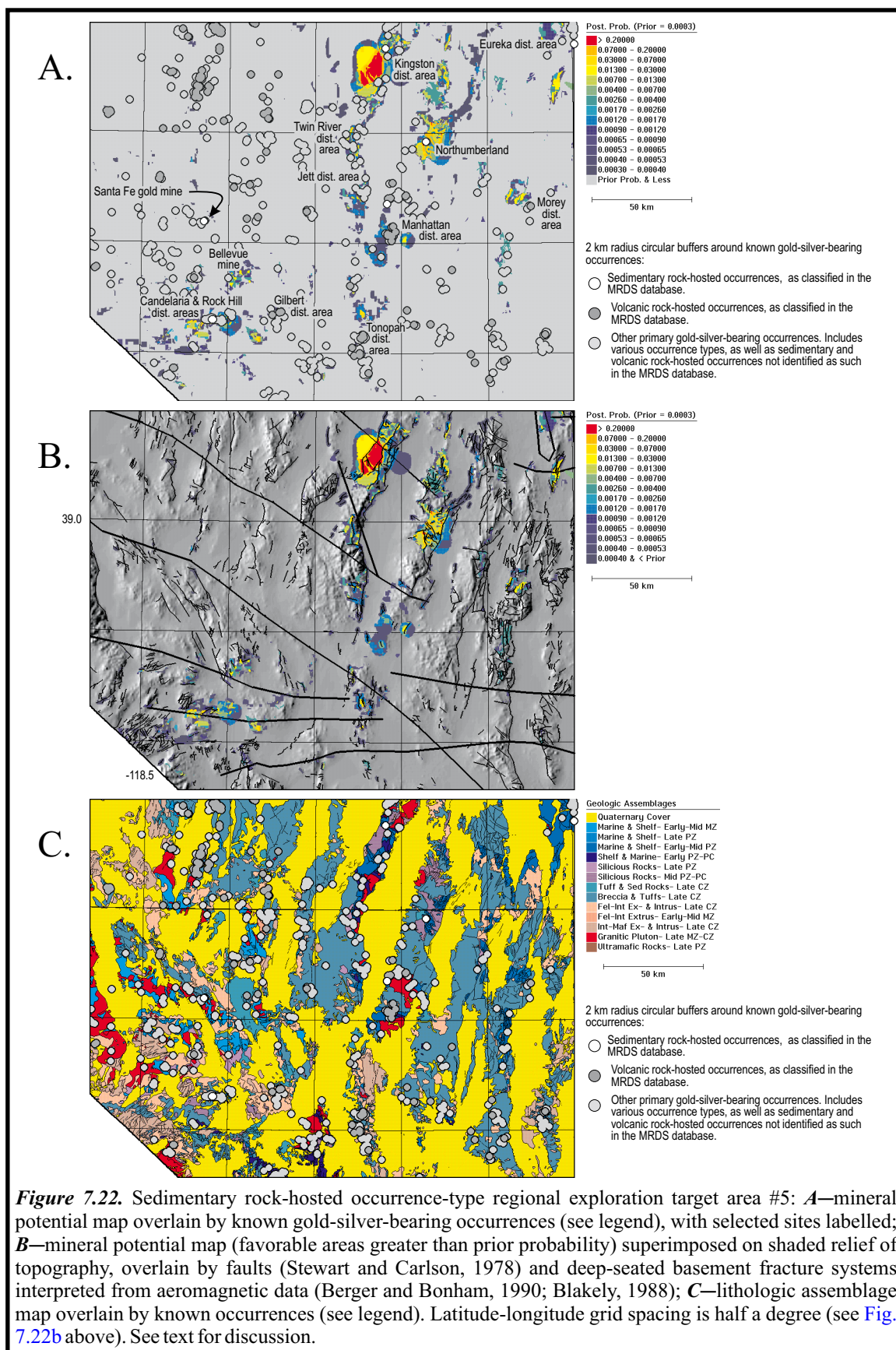


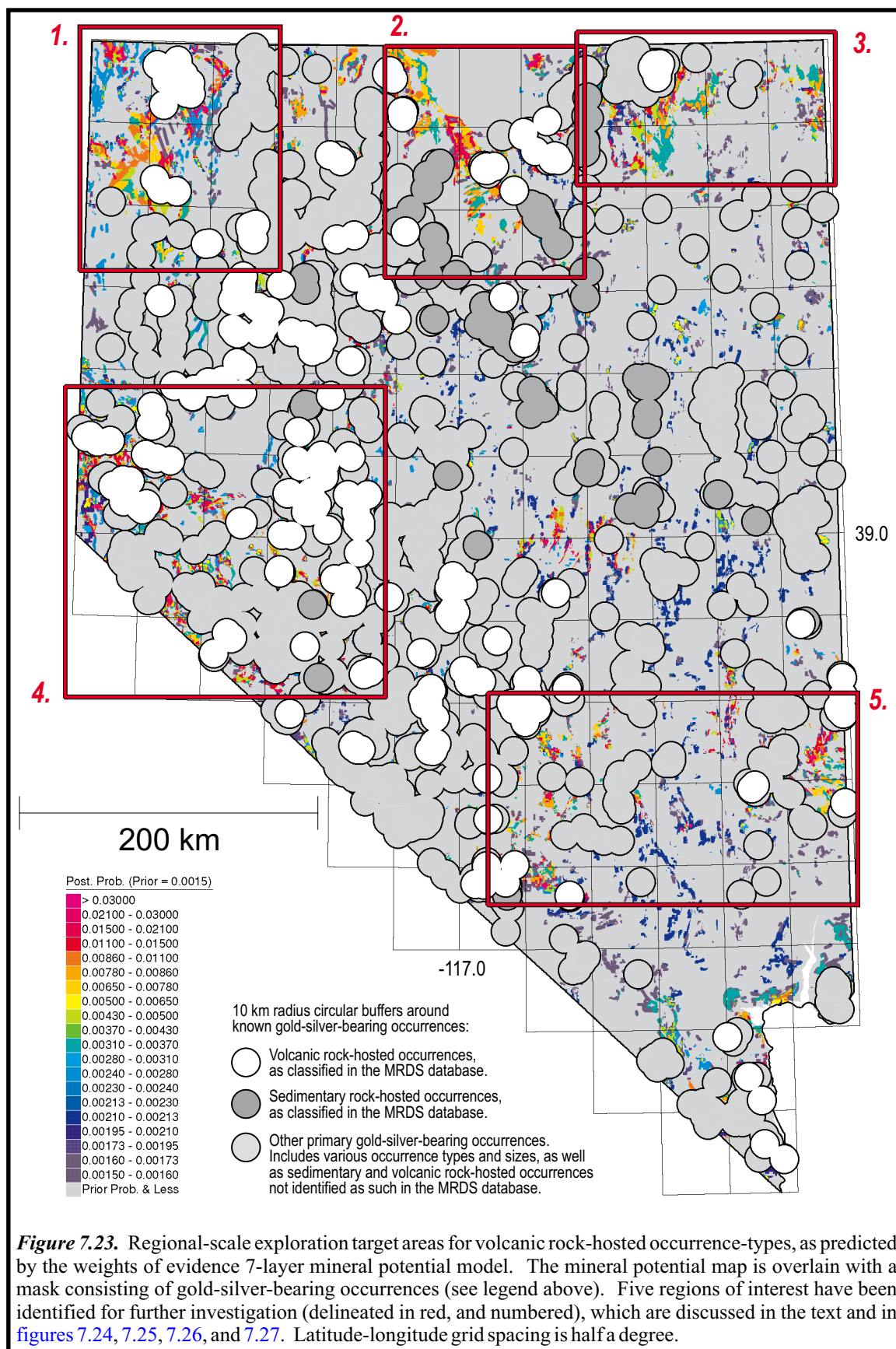




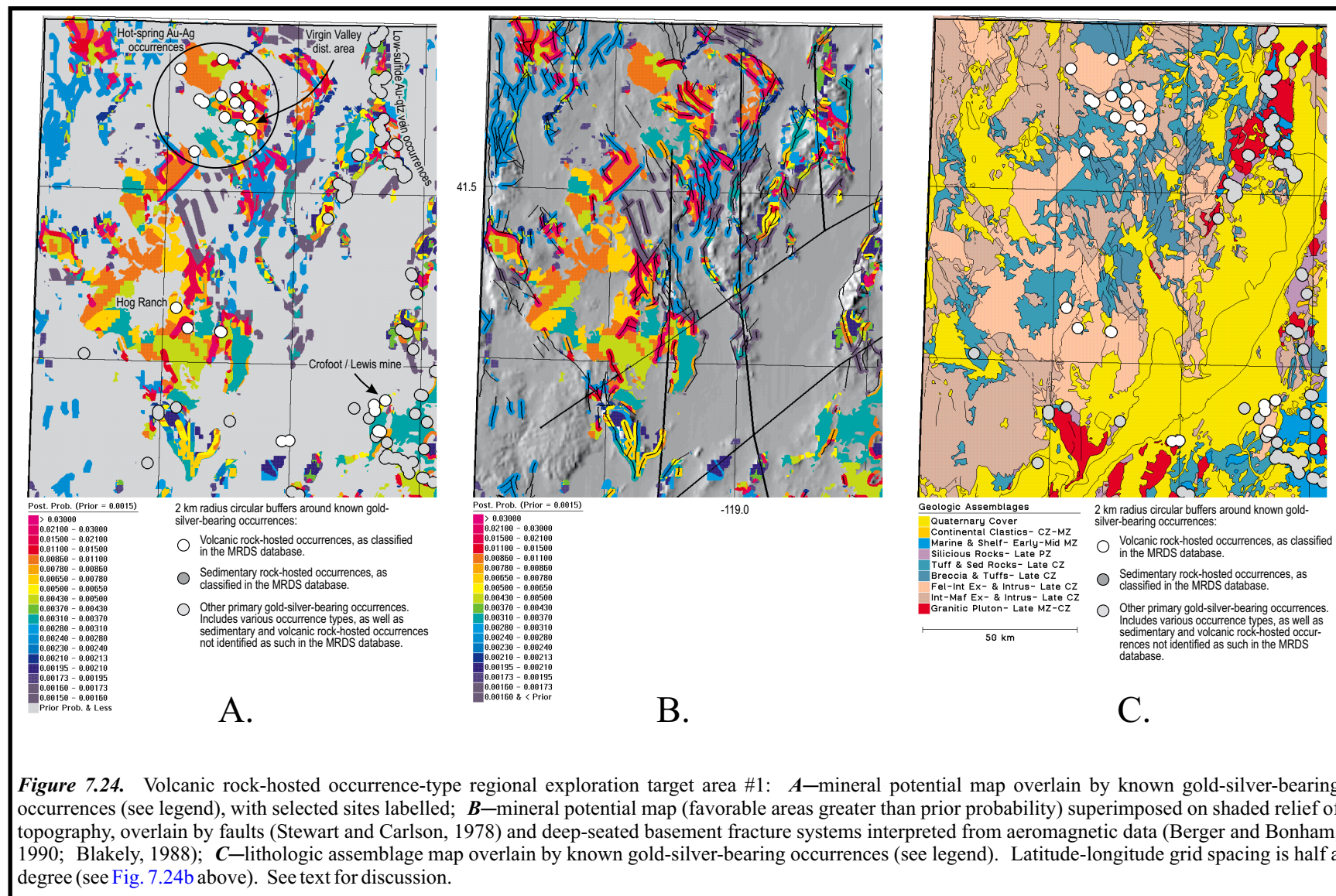




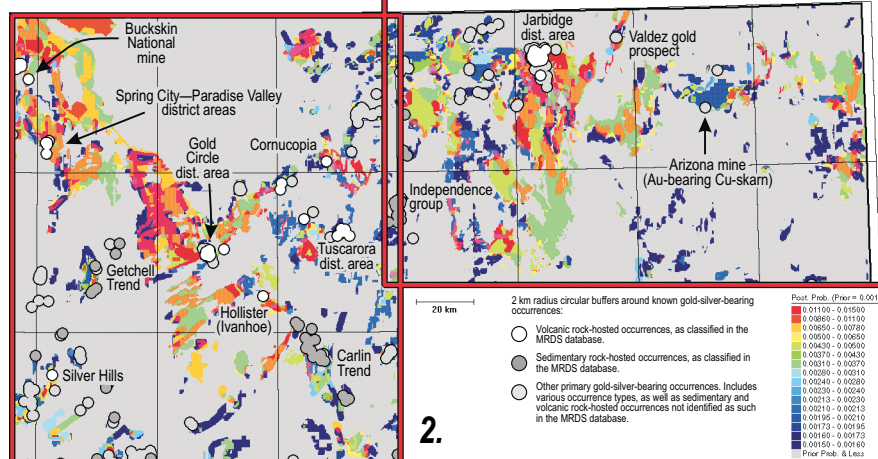






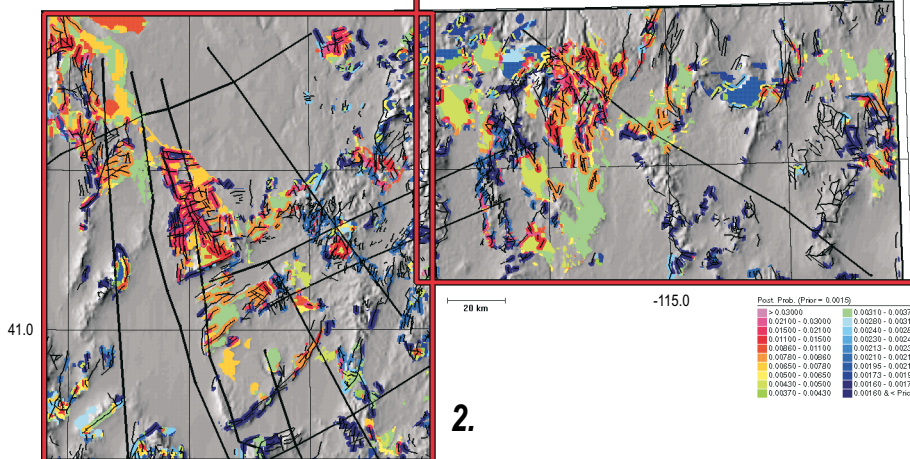


A.



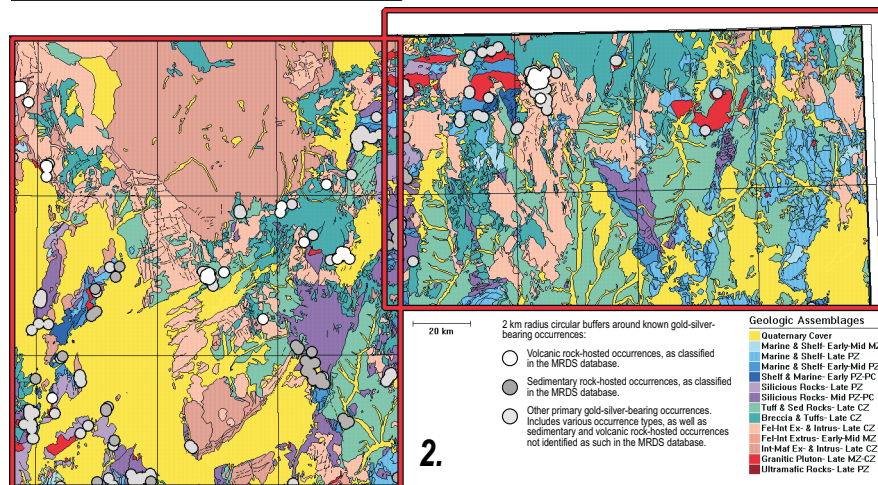
3.

B.



3.

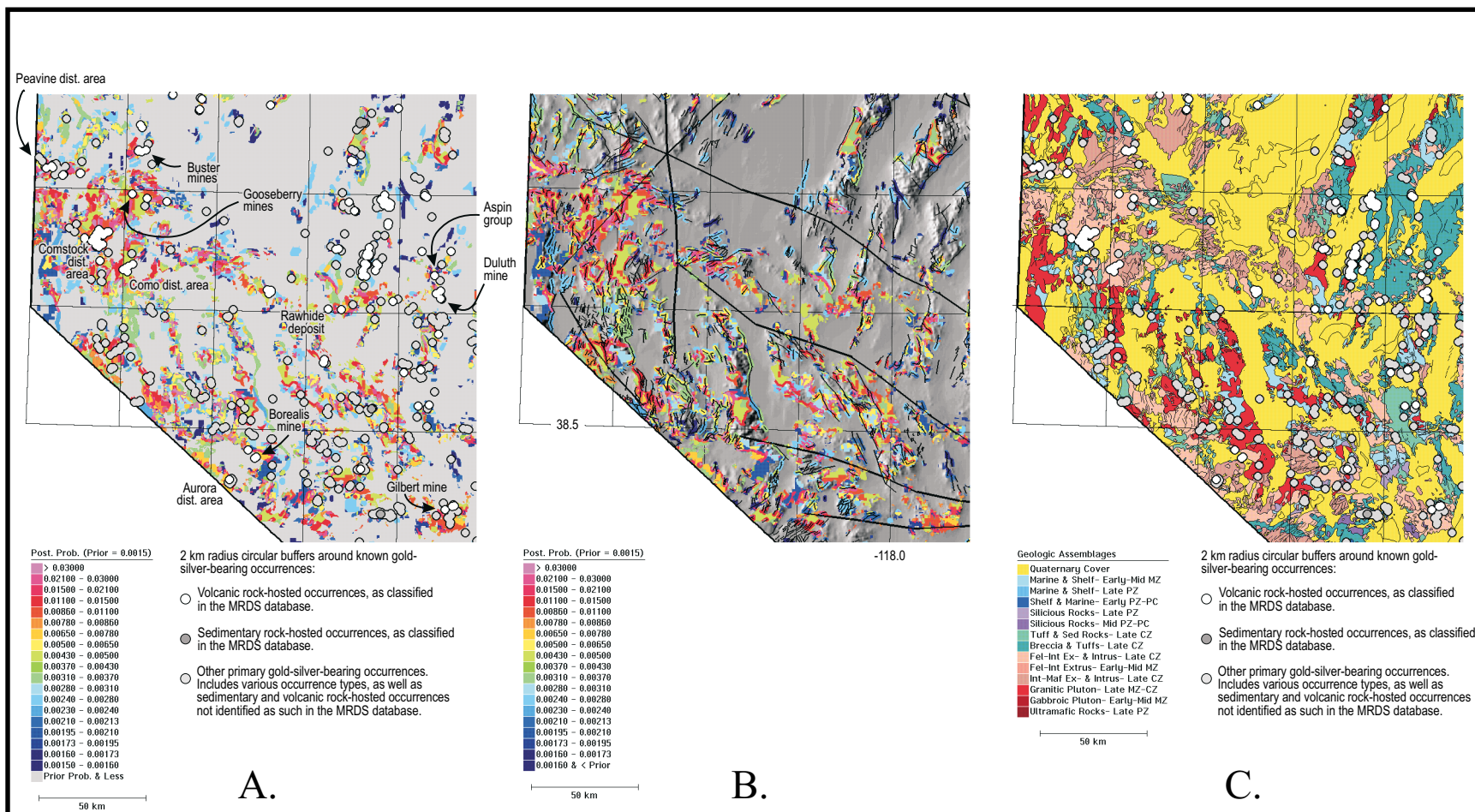
C.



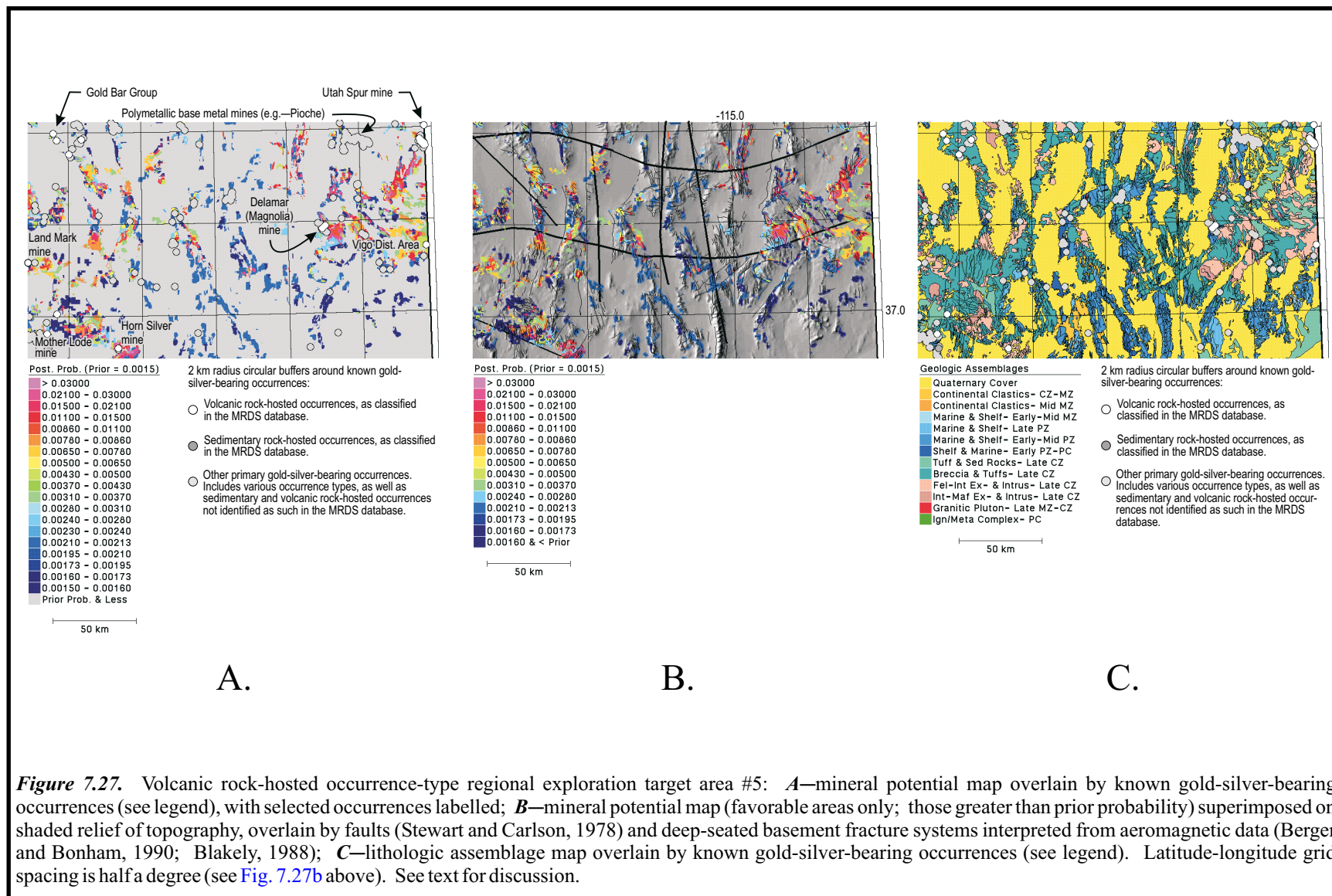
3.

**Figure 7.25.** Volcanic rock-hosted occurrence-type regional exploration target areas #2 and #3: **A**—mineral potential map overlay by known gold-silver-bearing occurrences (see legend), with selected sites labelled; **B**—mineral potential map (favorable areas greater than prior probability) superimposed on shaded relief of topography, overlay by faults (Stewart and Carlson, 1978) and deep-seated basement fracture systems interpreted from aeromagnetic data (Berger and Bonham, 1990; Blakely, 1988); **C**—lithologic assemblage map overlay by known gold-silver-bearing occurrences (see legend). Latitude-longitude grid spacing is half a degree (see Fig. 7.25b above). See text for discussion.





**Figure 7.26.** Volcanic rock-hosted occurrence-type regional exploration target area #4: **A**—mineral potential map overlain by known gold-silver-bearing occurrences (see legend), with selected occurrences and districts labelled; **B**—mineral potential map (favorable areas only; those greater than prior probability) superimposed on shaded relief of topography, overlain by faults (Stewart and Carlson, 1978) and deep-seated basement fracture systems interpreted from aeromagnetic data (Berger and Bonham, 1990; Blakely, 1988); **C**—lithologic assemblage map overlain by known gold-silver-bearing occurrences (see legend). Latitude-longitude grid spacing is half a degree (see Fig. 7.26b above). See text for discussion.





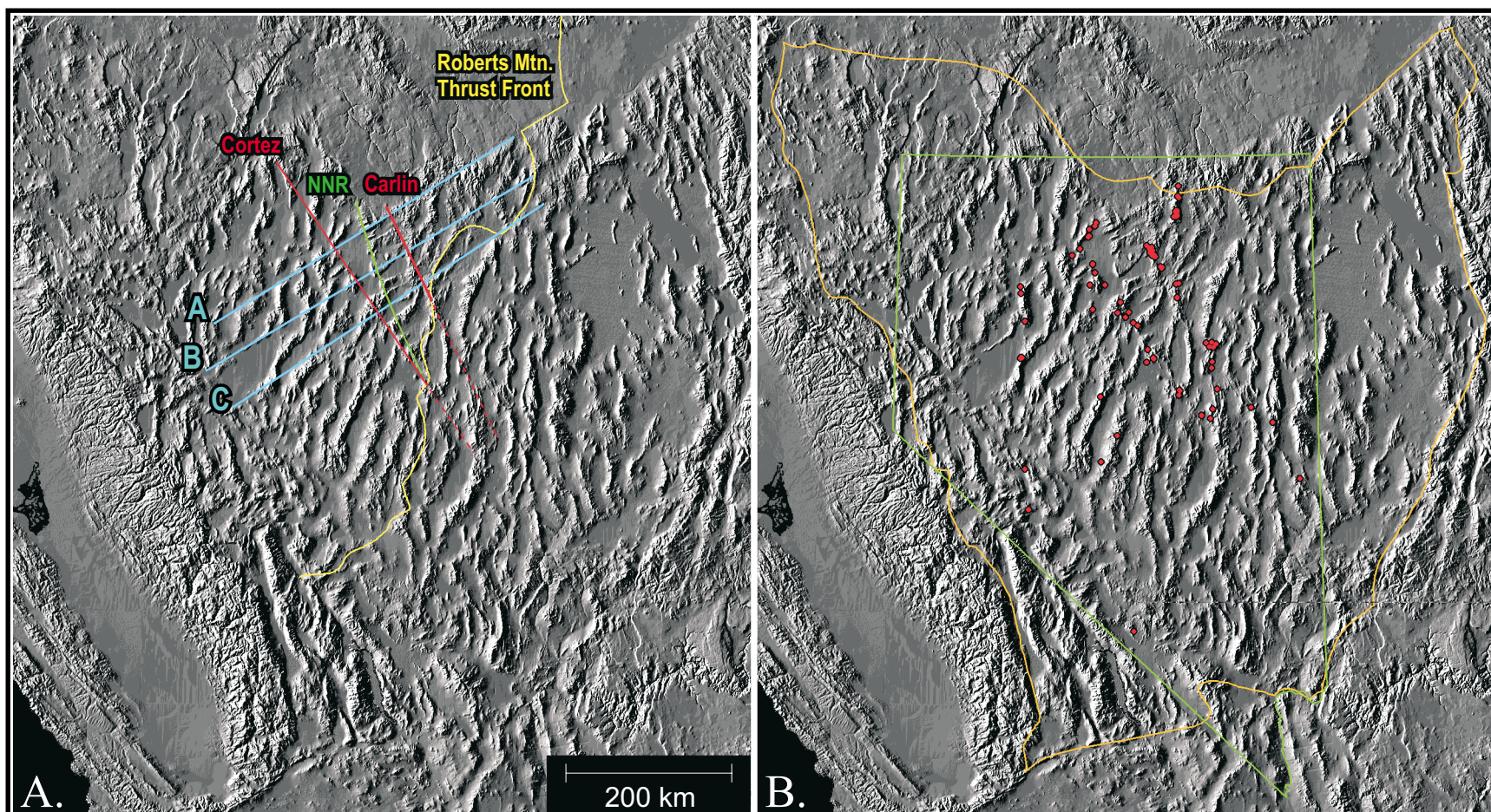


**Figure 8.1.** (A) Linear trends highlighting possible regional-scale crustal features that may have been important to the localization of sedimentary rock-hosted occurrences. (B) Distribution of sedimentary rock-hosted occurrences. The trace of all linear trends were fit to fault and fracture patterns visible in shaded relief as offsets in mountain ranges and in smaller linear features, and to the distribution pattern of occurrences (red dots; Fig. 8.1b). The positioning and extent of the linear trends is approximate. NNR is the northern Nevada rift zone, as interpreted from geomagnetics. The *Cortez* and *Carlin* structural zones are parallel to the Battle Mountain—Eureka (*Cortez*) and Carlin mineral trends, and sub-parallel to the NNR. The linear features labelled "A", "B", and "C" are parallel to, and occur within, the proposed Humboldt shear(?) zone. Important deposits and districts occur at the intersection of most of these linear features: the Preble and Kramer Hill mines (southern Getchell trend) at *Cortez* and "A"; the Battle Mountain district (Marigold mine) at *Cortez* and "B"; the Bullion district (Gold Acres deposit) at *Cortez* and "C"; the *Cortez* and Antelope districts in the vicinity where NNR, *Roberts Mountains thrust front*, and *Cortez* intersect; the Windfall and Ratto Canyon deposits just south of where *Cortez* intersects the *Roberts Mountain thrust front*; the northern Carlin trend deposits at *Carlin* and "B"; the southern Carlin trend deposits (Rain and Emigrant Springs) at *Carlin*, "C", and the *Roberts Mountain thrust front*. Nevada border in green. Great Basin boundary in orange (from Thelin and Pike, 1991). *Roberts Mountain thrust front* in yellow (from Poole et al., 1992). The crosscutting relationships between these linear features is not intended to denote relative age.



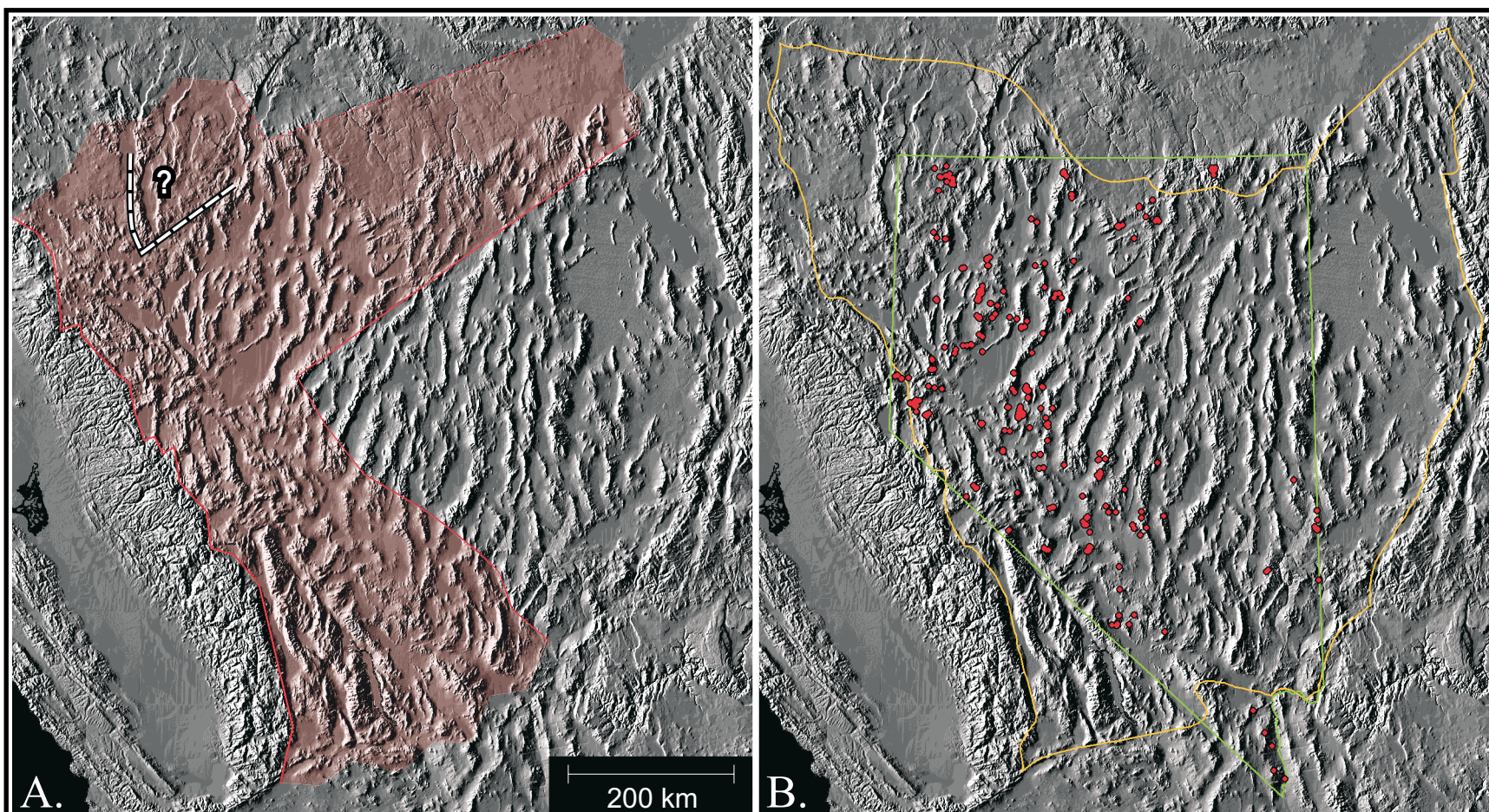


**Figure 8.2.** The "epithermal cross-roads". **(A)** Broad regional-scale crustal structures that may have been important to the localization of volcanic rock-hosted occurrences. **(B)** Distribution of volcanic rock-hosted occurrences. The red transparency in (A) envelopes the NW–SE-trending Walker Lane shear zone in southwestern Nevada and the proposed NE–SW-trending Humboldt shear(?) zone in northern Nevada. The extents of these two features were fit to fault and fracture patterns visible in shaded relief as offsets in mountain ranges, significant changes in the orientation (trend) of mountain ranges, and to the distribution pattern of mineral deposits (red dots; Fig. 8.2b). The positioning and extent of these boundaries is approximate. The northern boundary of the Humboldt shear(?) zone and the northeastern boundary of the northern Walker Lane shear zone is convoluted in the shaded relief, and is probably greatly complicated by the intersection of these features and concealed beneath late Cenozoic volcanic cover. This boundary, provisionally denoted with a dashed red line, may be represented in the shaded relief by any of a myriad of faults or fracture zones, or may be a broad zone that is gradational with adjacent tectonic elements. A rough boundary might consist of the postulated Snake River fault zone, which underlies the Snake River volcanic plateau, and the Brothers fault zone in Oregon, which has been proposed as a northern extension of northern Nevada rift zone (see Pool et al., 1992; Christiansen and Yeats, 1992). Irrespective, nearly all of the volcanic rock-hosted occurrences lie within the Walker Lane and Humboldt(?) shear zones. Nevada border in green. Great Basin boundary in orange (from Thelin and Pike, 1991).



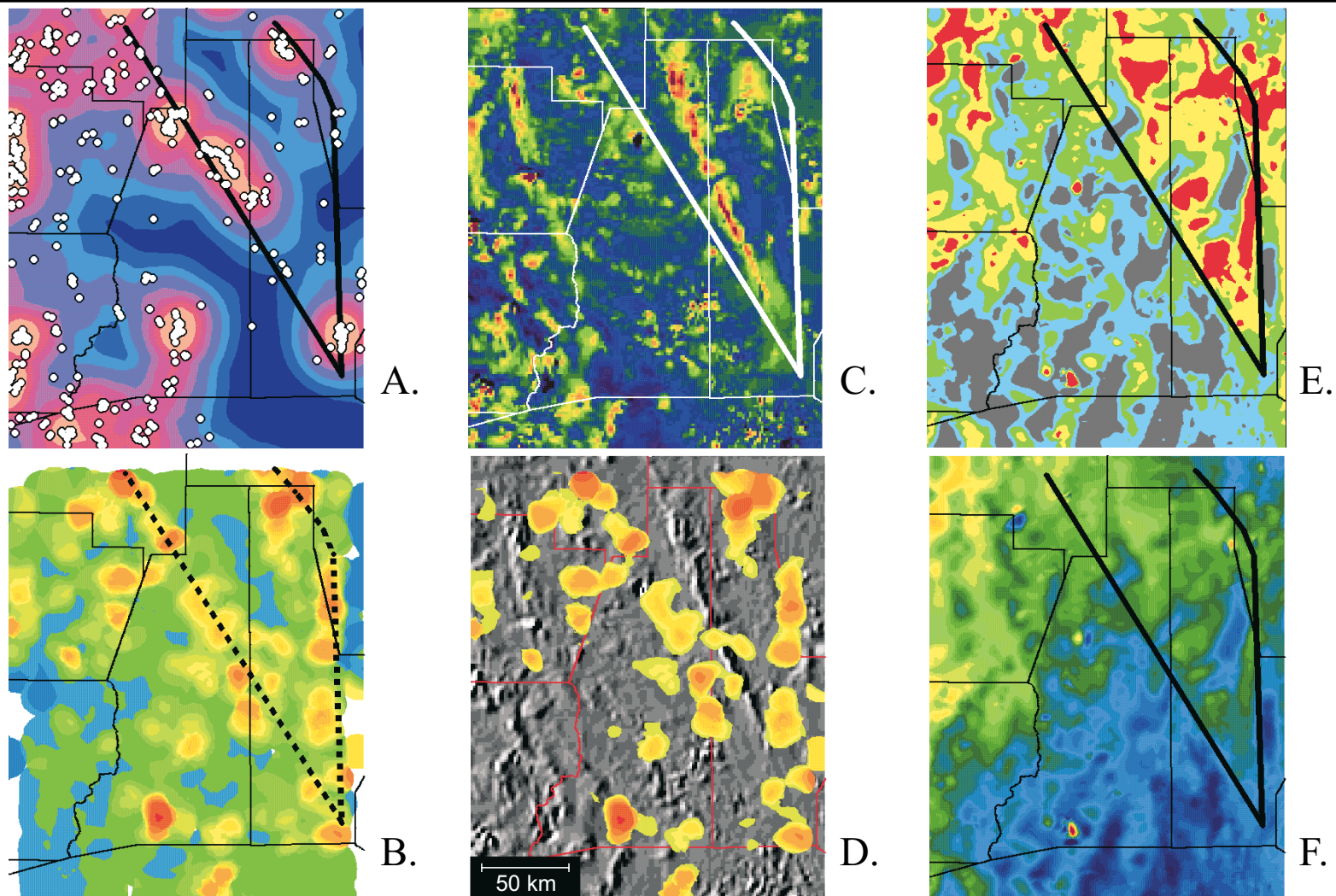
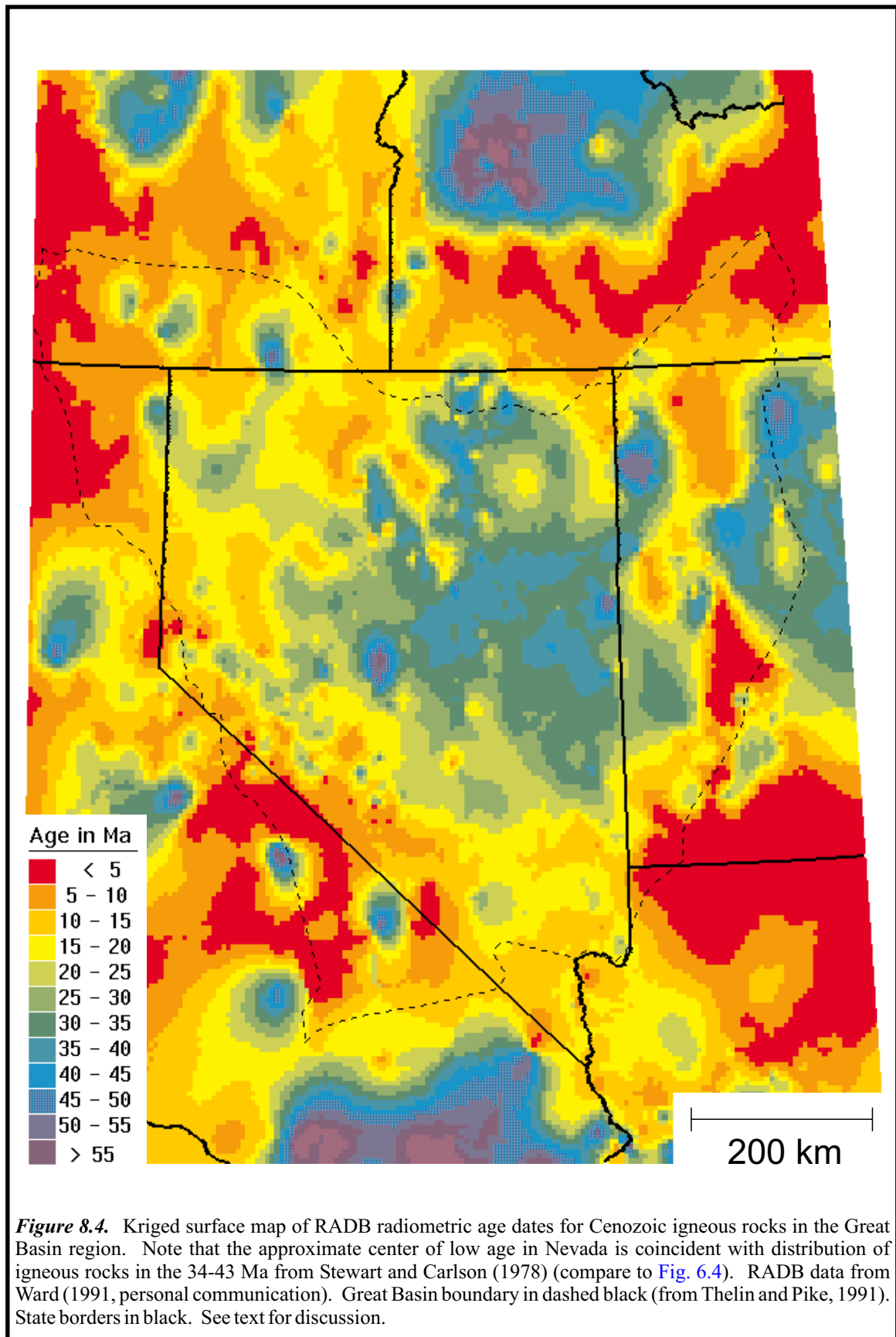


**Figure 8.3.** Spatial distribution relationships among (A) all gold-silver-bearing occurrences, overlain on occurrence density, (B) K/Na geochemical anomaly, (C) geomagnetic anomaly, (D) K/Na anomaly highs overlain on shaded relief of geomagnetic anomaly, (E) isostatic gravity anomaly, and (F) Bouguer gravity anomaly. The distribution of the occurrences and K/Na anomaly highs is coincident, as delineated by the "V"-shaped line. Also see [Fig. 6.65](#).



# **APPENDIX A**

## **Stratigraphy And Description Of Lithologic Units— Geologic Map of Nevada**

### **Section Contents:**

- A.1** [Correlation Chart of Geologic Map Units with Accompanying Table of Unit Descriptions](#)
- A.2** [Key to GIS Geological Map Legend and Lithologic Unit Abbreviations Appearing of Digital Maps](#)
- A.3** [Key to Lithologic Units Composing Assemblage Map Units](#)



## A.1 Correlation of Geologic Units in Nevada

*Figure A.1* Correlation of geologic map units. This figure is derived from the “correlation of map units” shown on Stewart and Carlson’s (1978) geologic map of Nevada, and includes additional description of the units and assemblages from various sources (see Fig. A.1 caption).

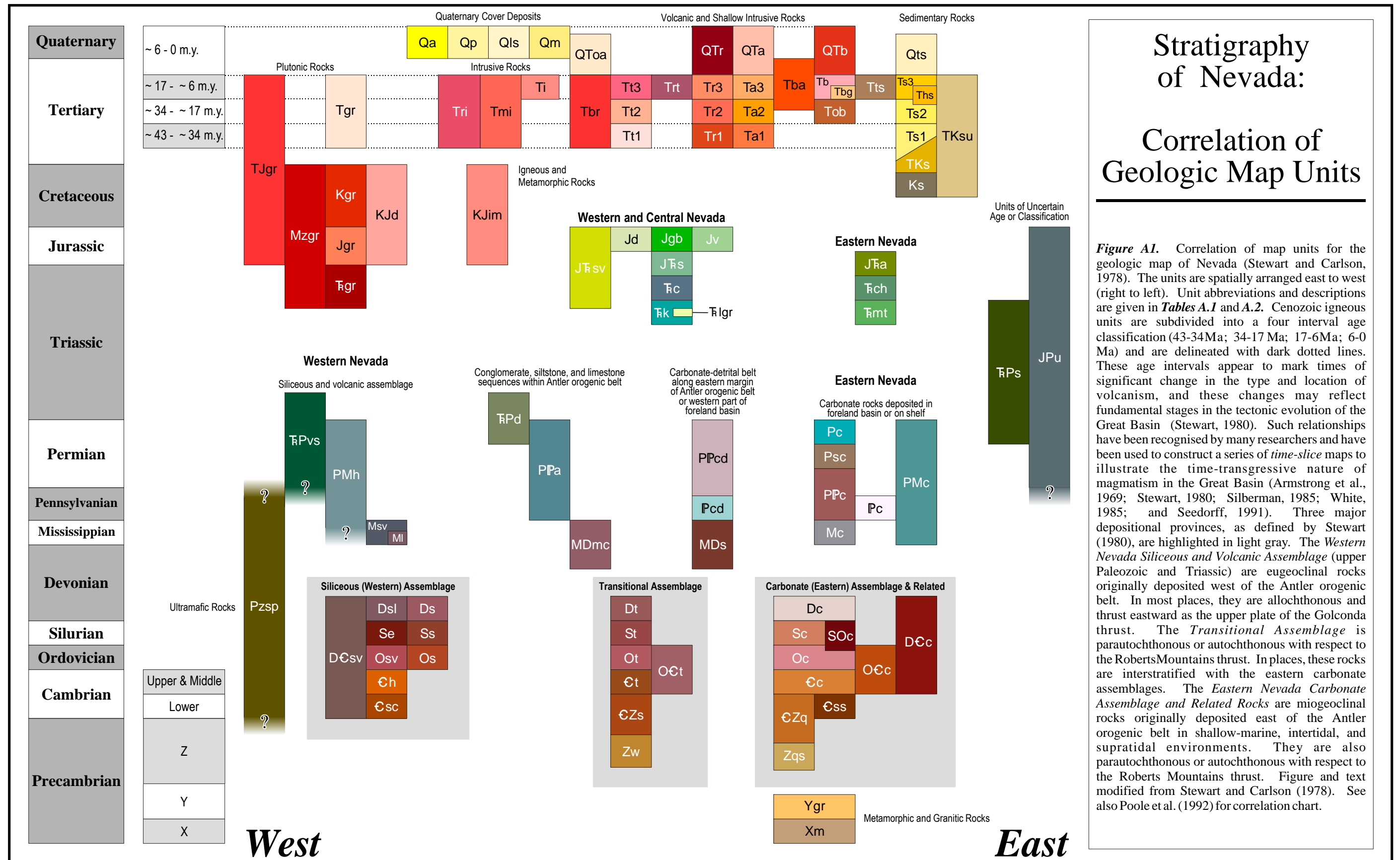
*Table A.1* Description of map units for the geologic map of Nevada. This table contains descriptions of the 101 geologic map units making up Stewart and Carlson’s (1978) geologic map of Nevada, and is derived from information contained in the legend of the geologic map.

## A.2 Digital Geologic Map Key

*Table A.2* Key to lithologic unit acronyms. This table contains the abbreviated unit descriptions used on the various digital renderings of the geologic map of Nevada and their correlative unit legend acronyms as they appear on Stewart and Carlson’s (1978) geologic map.

## A.3 Digital Lithologic Assemblage Map Key

*Table A.3* Key to the makeup of the lithologic assemblage map units. This table contains the geologic units, as coded on Stewart and Carlson’s (1978) geologic map of Nevada, that were combined to create the 20 lithologic assemblage units making up the digital lithologic assemblage map.



Unit Abbreviation	Unit Name	Unit Description
<b>Quaternary Cover and Sedimentary, Volcanic, and Shallow Intrusive Rocks</b>		
<b>Qa</b>	Alluvial Deposits	Locally includes lacustrine, shoreline, and eolian sand dune deposits.
<b>Qp</b>	Playa, Marsh, and Alluvial-Flat Deposits, Locally Eroded	Forms widespread alluvial fan, stream terrace flood plain, valley flat, and playa deposits. Grade from coarse gravel near mountains or ranges to fine silt and clay in the valleys and on the playas.
<b>Qls</b>	Landslide Deposits	Occur primarily in the mountainous areas of northern and western Nevada.
<b>Qm</b>	Morainal Deposits	
<b>QToa</b>	Older Alluvial Deposits	Consist largely of dissected gravel and sand.
<b>QTr</b>	Rhyolitic Flows and Shallow Intrusive Rocks	Rhyolite flows and flow domes and andesite flows occur in western Mineral and southern Lyon Counties, and rhyolite domes occur in Storey and southern Washoe Counties.
<b>QTa</b>	Andesite Flows and Breccias	
<b>QTb</b>	Basalt Flows	Locally includes maar deposits and cinder cones.
<b>QTS</b>	Sedimentary Rocks	Mostly lake deposits.
<b>Tri</b>	Rhyolitic Intrusive Rocks	Range in age from about 43 to 6 Ma, across the 43-34 Ma, 34-17 Ma, 17-6 Ma time-slice intervals of Stewart and Carlson (1976).
<b>Tmi</b>	Intrusive Rocks of Mafic and Intermediate Composition	
<b>Ti</b>	Intrusive Rocks	Aphanitic, porphyritic, and coarsely granular rocks ranging in composition from diorite to granite. Clark County.
<b>Tbr</b>	Breccia	Volcanic, thrust, and jasperoid breccia and landslide mega-breccia.
<b>Tt3</b>	Welded and Non-Welded Silicic Ash-Flow Tuffs	Locally includes thin units of air-fall and tuff and sedimentary rock.
<b>Trt</b>	Ash-Flow Tuffs, Rhyolitic Flows, and Shallow Intrusive Rocks	Range in age from 17-6 Ma. Coeval with widespread eruption of mafic lavas and bimodal assemblages of rhyolite and basalt. Rhyolites include high-silica subalkaline, as well as peralkaline varieties.
<b>Tr3</b>	Rhyolitic Flows and Shallow Intrusive Rocks	

**Table A.1.** Description of map units for the Geologic Map of Nevada (Stewart and Carlson, 1978). See Figure A.1 for the stratigraphic correlation of the map units. See also table 1 in Stewart (1980), *Precambrian Z and Lower Paleozoic Assemblages and Provinces in the Great Basin*. Text from Stewart and Carlson (1978), with supplemental material from Stewart (1980). Refer to Stewart and Carlson (1978) for references herein.

Unit Abbreviation	Unit Name	Unit Description
<b>Ta3</b>	Andesite and Related Rocks of Intermediate Composition	Flows and breccias.
<b>Tba</b>	Andesite and Basalt Flows	Mostly in ~17 to ~6 Ma age range. In Humboldt County, locally includes rocks as old as 21 Ma. May include rocks younger than 6 Ma in places.
<b>Tb</b>	Basalt Flows	Includes alkali-olivine and tholeiitic basalts.
<b>Tbg</b>	Banbury Formation	Basalt, gravel, and tuffaceous sediments locally. Northeast Humboldt County and northwest Elko County.
<b>Tts</b>	Ash-Flow Tuffs and Tuffaceous Sedimentary Rocks	Range in age from 17-6 Ma.
<b>Ts3</b>	Tuffaceous Sedimentary Rocks	Locally includes minor amounts of tuff.
<b>Ths</b>	Horse Spring Formation	Tuffaceous sedimentary rocks, southern Nevada.
<b>TKsu</b>	Continental Sedimentary Rocks	Clark County.
<b>Tt2</b>	Welded and Non-Welded Silicic Ash-Flow Tuffs	Locally includes thin units of air-fall tuff and sedimentary rock. In places form thick sequences that constitute virtually entire mountain ranges.
<b>Tr2</b>	Rhyolitic Flows and Shallow Intrusive Rocks	Generally far less voluminous than tuffs (Tt2) during this time period (34-17 Ma), but probably most voluminous in northwestern Nevada.
<b>Ta2</b>	Andesite and Related Rocks of Intermediate Composition	Flows and breccias.
<b>Tob</b>	Older Basalt Rocks	Basaltic lavas are relatively sparse during this time interval (34-17 Ma).
<b>Ts2</b>	Tuffaceous Sedimentary Rocks	Locally includes minor amounts of tuff.
<b>Tt1</b>	Welded and Non-Welded Silicic Ash-Flow Tuffs	Locally includes thin units of air-fall tuff and sedimentary rocks.
<b>Tr1</b>	Rhyolitic Flows and Shallow Intrusive Rocks	Lava flows during this time interval (43-34 Ma) include moderately to highly potassic andesite, latite, quartz latite, and rhyolite. Ta1 is composed of flows and breccias.
<b>Ta1</b>	Andesite and Related Flows rocks of Intermediate Composition	

Table A.1, continued.

<b>Unit Abbreviation</b>	<b>Unit Name</b>	<b>Unit Description</b>
--------------------------	------------------	-------------------------

<b>Ts1</b>	Sedimentary Rocks	Includes Sheep Pass Formation (Eocene) and related units and unnamed tuffaceous sedimentary rocks.
<b>TKs</b>	Continental Sedimentary Rocks	Includes units such as Pansy Lee Conglomerate in Humboldt County, part of Cretaceous(?) and Tertiary rocks of Kleinhampl and Ziony (1967) in northern Nye County, and part of "older clastic rocks" of Tschanz and Pampeyan (1970) in Lincoln County.
<b>Ks</b>	Continental Deposits of Siltstone, Shale, Conglomerate, and Limestone	Includes units such as King Lear Formation in Humboldt County, Newark Canyon Formation in Eureka County, Willow Tank Formation and Baseline Sandstone in Clark County.

<b>Plutonic Rocks</b>		
<b>TJgr</b>	Granitic Rocks, Central and Eastern Nevada	Mostly quartz monzonite and granodiorite. Inconclusively dated or not dated radiometrically.
<b>Tgr</b>	Granitic Rocks	Mostly quartz monzonite and granodiorite.
<b>Mzgr</b>	Granitic Rocks, Western Nevada (Mesozoic)	Mostly quartz monzonite and granodiorite. Inconclusively dated or not dated radiometrically.
<b>Kgr</b>	Granitic Rocks	Mostly quartz monzonite and granodiorite.
<b>KJd</b>	Diorite	
<b>Jgr</b>	Granitic Rocks	Mostly quartz monzonite and granodiorite.
<b>Trgr</b>	Granitic Rocks	Quartz monzonite in northern Esmeralda County.

<b>Igneous and Metamorphic Rocks</b>		
<b>KJim</b>	Igneous and Metamorphic Complex	Pegmatitic granite and other granitic rocks complexly intermixed with metasedimentary rocks. Considered to be Mesozoic igneous complex intruding lower Paleozoic and possibly Precambrian Z sedimentary rocks. Grades into units shown on map as lower Paleozoic. Ruby Mountains and East Humboldt Range, Elko

Table A.1, continued.

Unit Abbreviation	Unit Name	Unit Description
<b>Jurassic and Triassic Rocks in Western and Central Nevada</b>		
<b>JTrsv</b>	Shale, Sandstone, Volcanogenic Clastic Rocks, Andesite, Rhyolite, and Locally Thick Carbonate Units	Undivided sequence locally containing recognizable equivalents of the Luning and Dunlap Formations.
<b>Jd</b>	Dunlap Formation (Lower and Middle Jurassic)	Conglomerate, sandstone, greenstone, felsite, and tuff. Locally contemporaneous with folding and thrusting. Mineral County and adjacent parts of Esmeralda and Nye Counties.
<b>Jgb</b>	Gabbroic Complex (Lower and Middle Jurassic)	Includes gabbro, basalt, and synorogenic quartz sandstone (Boyer Ranch Formation). Churchill and Pershing Counties.
<b>Jv</b>	Volcanic Sandstone, Felsic Ash-Flow Tuffs, Rhyolite, and Rhyodacite Flows (Upper? Jurassic)	Pony Trail Group of Cortez Mountains, Eureka County.
<b>JTrs</b>	Shale, Mudstone, Siltstone, Sandstone, and Carbonate Rock; Sparse Volcanic Rock (Upper Triassic and Lower Jurassic)	Includes Auld Lang Syne Group, Nightingale sequence on Bonham (1969), and Gabbs and Sunrise Formations.
<b>Trc</b>	Limestone, Minor Amounts of Dolomite, Shale, and Sandstone; Locally Thick Conglomerate Units (Lower, Middle, and Upper Triassic)	Includes Tobin, Dixie Valley, Favret, Augusta Mountain, and Cane Spring Formations and Star Peak Group in central Nevada and Grantsville and Luning Formations in west-central Nevada.
<b>Trk</b>	Koipato Group and Related Rocks (Lower Triassic)	Altered andesitic flows, rhyolitic tuffs and flows, and clastic rocks. Includes rocks mapped by Silberling (1959) as Pablo Formation and originally considered to be Permian in the Shoshone Mountains, Nye County. Includes Tallman Fonglomerate (Permian?) in Humboldt County.
<b>Trlgr</b>	Leucogranite and Rhyolite Porphyry	
<b>JTra</b>	Aztec Sandstone (Triassic? and Jurassic)	Friable fine- to medium- grained sandstone with conspicuous large-scale cross strata; considered eolian. Age based on correlation with Navajo Sandstone.

Table A.1, continued.

<b>Unit Abbreviation</b>	<b>Unit Name</b>	<b>Unit Description</b>
<b>Trch</b>	Chinle Formation and Associated Rocks (Upper Triassic)	Continental deposits of variegated bentonitic claystone, siltstone, and clayey sandstone; ledge-forming sandstone; and red siltstone.
<b>Trmt</b>	Moenkopi Formation, Thaynes Formation, and Related Rocks (Lower Triassic)	Marine deposits of siltstone, limestone, and sparse conglomerate.
<b>JPu</b>	Volcanogenic Sedimentary Rocks, Tuff, Andesitic and Felsitic Flows, and Carbonate Rocks	Age uncertain. Mineral, Esmeralda, and northwest Nye Counties.
<b>TrPs</b>	Silty Limestone, Minor Amounts of Shale, and Some Greenstone	Unnamed sequence in Adobe Range, northern Elko County.

<b>Western Nevada Siliceous and Volcanic Assemblage (Upper Paleozoic and Triassic)</b>		
<b>TrPvs</b>	Volcanic Flows and Flow Breccias, Chiefly of Andesitic Composition, Tuffs, Sparse Sandstone and Graywacke	Includes Happy Creek Volcanic Series and related rocks in Humboldt County and similar rocks in Washoe and Pershing Counties; includes andesite breccias and volcanogenic sedimentary rocks in Mineral County.
<b>PMh</b>	Havallah Sequence of Silberling and Roberts (1962)	Chert, argillite, shale, greenstone, and minor amounts of siltstone, sandstone, conglomerate, and limestone. Includes Schoonover Formation of Fagan (1962) and Reservation Hill Formation in Elko County, Farrel Canyon Formation in southwestern Humboldt County, Havallah and Pumpernickel Formations in Pershing, Lander, and parts of Humboldt Counties, and rocks originally considered a part of the Pablo and Excelsior Formations in northern Nye, northern Esmeralda, and southern Mineral Counties. Assignment of some rocks to the Havallah sequence in the East Range, Pershing County, is highly uncertain. Includes rocks ranging in age from Late Mississippian to Early Permian.

*Table A.1*, continued.



<b>Unit Abbreviation</b>	<b>Unit Name</b>	<b>Unit Description</b>
------------------------------	----------------------	-----------------------------

<b>Msv</b>	Siliceous and Volcanic Rocks	In Humboldt County, consists of altered pillow lavas, coarse volcanic breccias, clastic limestone, and minor amounts of sandstone, shale, siliceous shale, and chert of the Goughs Canyon Formation (Lower and Upper Mississippian). In the East Range, Pershing County, consists of quartzite, conglomerate, slate, limestone, chert, and greenstone of the Inskip Formation (Mississippian?).
<b>MI</b>	Massive Limestone	In the San Antonio Mountains, western Nye County.

<b>Conglomerate, Siltstone, and Limestone Sequences within Antler Orogenic Belt (each sequence rests unconformably on folded Paleozoic rocks in its respective area of distribution)</b>		
<b>TrPd</b>	Conglomerate, Sandstone, Shale, and Dolomite of Diablo Formation Below and Shale, Sandstone, and Conglomerate of Candelaria Formation Above (Lower or Upper Permian to Lower Triassic)	Mineral, Esmeralda, and northwestern Nye Counties.
<b>PPa</b>	Antler Sequence of Silberling and Roberts (1962) (Middle Pennsylvanian to Early or Late Permian) (Guadalupian)	Conglomerate, sandy to conglomeratic limestone, limestone, sandstone, and calcareous shale. Thin detrital and carbonate sequence within main part of Antler orogenic belt. Includes units such as Sunflower Formation of Bushnell (1967) in Elko County, Battle Formation, Antler Peak Limestone, and Edna Mountain Formation in Lander and western Eureka Counties, and Wildcat Peak Formation in northern Nye County.
<b>MDmc</b>	Conglomerate, Limestone, Meta-Andesite, Phyllite, and Shale	Includes Grossman, Banner, Nelson, and Mountain City Formations. Northern Elko County.

*Table A.1, continued.*

<b>Unit Abbreviation</b>	<b>Unit Name</b>	<b>Unit Description</b>
--------------------------	------------------	-------------------------

<b>Carbonate-Detrital Belt Along Eastern Margin of Antler Orogenic Belt or Western Part of Foreland Basin</b>		
<b>PPcd</b>	Sandy and Silty Limestone, Conglomerate, and Siltstone (Upper Pennsylvanian to Upper Permian)	Includes units such as Strathearn Formation of Dott (1955) and Buckskin Mountain, Beacon Flat, and Carlin Canyon Formations of Fails (1960) in Elko County and Carbon Ridge and Garden Valley Formations in Eureka County.
<b>Pcd</b>	Limestone, Cherty Limestone, Sandy Limestone, and Chert-Pebble Conglomerate (Lower and Middle Pennsylvanian)	Includes units such as Moleen and Tomera Formations of Dott (1955).
<b>MDs</b>	Shale, Siltstone, Sandstone, Chert-Pebble Conglomerate, and Limestone	Includes units such as Pilot Shale, Joana Limestone, Chainman Shale, and Diamond Peak Formation in northern and eastern Nevada and Narrow Canyon Limestone, Mercury Limestone, and Eleana Formation in southern Nevada.

<b>Carbonate Rocks Deposited in Foreland Basin or on Shelf, Eastern Nevada</b>		
<b>Pc</b>	Cherty Limestone and Sparse Dolomite, Shale, and Sandstone (Lower and Upper Permian)	Includes units such as Park City Group and equivalent rocks in northern Nevada and Toroweap Formation and Kaibab Limestone in southern Nevada.
<b>PMc</b>	Limestone, Dolomite, and Shale (Upper Paleozoic)	Includes Van Duzer Limestone of Decker (1962).
<b>Psc</b>	Siltstone, Sandstone, Limestone and Dolomite (Commonly Silty or Sandy), and Gypsum (Lower Permian)	Includes units such as Rib Hill Sandstone and Pequop Formation of Steele (1959) in Elko County, Rib Hill Sandstone and Arcturus Formation in White Pine County, Queantoweap Sandstone of McNair (1951), Hermit Shale, and Coconino Sandstone in Clark and southern Lincoln Counties.

Table A.1, continued.

Unit Abbreviation	Unit Name	Unit Description
<b>PPc</b>	Limestone and Sparse Dolomite, Siltstone, and Sandstone (Lower Pennsylvanian to Lower Permian)	Includes units such as undivided Riepe Spring Limestone of Steele (1960) and Ely Limestone or their equivalent in Elko, White Pine, and northern Lincoln Counties and most of the Bird Spring Formation and Callville Limestone in Clark and southern Lincoln Counties. Includes some stratigraphically higher Permian rocks in Leppy Peak, easternmost Elko County.
<b>Pc</b>	Limestone	Includes Ely Limestone (mostly Lower and Middle Pennsylvanian).
<b>Mc</b>	Limestone and Minor Amounts of Dolomite and Shale	Includes units such as Rogers Spring and Monte Cristo Limestones.
<b>Ultramafic Rocks</b>		
<b>Pzsp</b>	Serpentinite (Paleozoic)	Mineral, northwestern Nye, and eastern Humboldt Counties.
<b>Siliceous (Western) Assemblage (Lower Paleozoic)</b>		
<b>DCsv</b>	Chert, Shale, Argillite, Siltstone, Quartzite, and Greenstone	Undivided siliceous assemblage. Mostly Ordovician.
<b>Dsl</b>	Slaven Chert	Chert and sparse limy sandstone, siltstone, and limestone. Lander County.
<b>Ds</b>	Shale, Siliceous Siltstone, Chert, and Minor Amounts of Limestone	Includes Cockalorum Wash Formation on northern Nye County and Woodruff Formation and unnamed rocks in Elko County.
<b>Se</b>	Elder Sandstone	Feldspathic sandstone, siltstone, shale, and chert. Lander County.
<b>Ss</b>	Shale and Chert	Includes Fourmile Canyon Formation in Eureka County and Noh Formation of Riva (1970) and unnamed rocks in Elko County.

Table A.1, continued.

Unit Abbreviation	Unit Name	Unit Description
<b>Osv</b>	Siliceous and Volcanic Rocks	Chert, shale, quartzite, greenstone, and minor amounts of limestone. Includes units such as Valmy Formation of north- central Nevada and some rocks mapped as Palmetto Formation in northern part of Esmeralda County and adjacent parts of Mineral and Nye Counties. Locally includes rocks of Silurian and Devonian age.
<b>Os</b>	Shale, Chert, and Minor Amounts of Quartzite, Greenstone, and Limestone	Includes units such as Vinini Formation of north- central Nevada, Palmetto Formation in southern and central parts of Esmeralda County, and Comus Formation in Humboldt County. Locally includes rocks of Silurian and Devonian age.
<b>Ch</b>	Harmony Formation (Upper Cambrian)	Feldspathic and arkosic sandstone and minor amounts of shale, limestone, and chert.
<b>Csc</b>	Scott Canyon Formation (Lower or Middle Cambrian)	Chert, shale, greenstone, and (Lower sparse limestone and quartzite. Southeast Humboldt County and Northwest Lander County.

Transitional Assemblage		
<b>Dt</b>	Argillaceous Limestone, Chert, and Shale	Elko and Eureka Counties.
<b>St</b>	Platy Limestone and Limy Siltstone, Chert at Base	Includes units such as Roberts Mountains Formation, and Storff Formation and Chellis Limestone of Decker (1962). Locally includes rocks of Early Devonian age at top.
<b>Ot</b>	Shale, Chert, and Limestone	Includes Aura Formation of Decker (1962) in north- west Elko County and Perkins Canyon Formation of Kay and Crawford (1964) in northern Nye County.
<b>OCt</b>	Phyllite, Shale, and Limestone	Locally includes chert and quartzite. Includes Tennessee Mountain Formation of Bushnell (1967) in western Elko County, Broad Canyon sequence of Means (1962) in Lander County, and rocks originally mapped as Palmetto Formation in Toiyabe and Toquima Ranges, northern Nye County.

Table A.1, continued.

<b>Unit Abbreviation</b>	<b>Unit Name</b>	<b>Unit Description</b>
--------------------------	------------------	-------------------------

<b>Ct</b>	Shale and Thin-Bedded or Laminated Limestone; Also Thinly Interbedded Limestone and Chert	Includes units such as Preble and Emigrant Formations.
<b>CZs</b>	Phyllitic Siltstone, Quartzite, and Lesser Amounts of Limestone and Dolomite	Includes Reed Dolomite; Deep Sprint, Campito, Poleta, Harkless, and Saline Valley Formations; and Mule Spring Limestone.
<b>Zw</b>	Wyman Formation	Phyllite and phyllitic siltstone and minor amounts of limestone, dolomite, and sandstone.

<b>Carbonate (Eastern) Assemblage and Related Rocks</b>		
<b>Dc</b>	Dolomite, Limestone, and Minor Amounts of Sandstone and Quartzite	Includes units such as Sevy and Simonson Dolomites, Guilmette and Nevada Formations, and Devils Gate Limestone.
<b>DCc</b>	Dolomite and Limestone (Lower Paleozoic)	
<b>Sc</b>	Dolomite	Includes units such as Laketown and Lone Mountain Dolomites. Locally includes rocks of Early Devonian age at top.
<b>SOc</b>	Dolomite	Includes uppermost part of Ordovician System (Ely Springs Dolomite and equivalent rocks) and all of Silurian System.
<b>Oc</b>	Limestone, Dolomite, Shale, and Quartzite	Includes units such as Pogonip Group, Eureka Quartzite, and Ely Springs Dolomite. Where Ely Springs Dolomite or equivalent rocks are included in SOc unit, this unit includes only the Pogonip Group and Eureka Quartzite or their equivalents.
<b>OCc</b>	Dolomite and Limestone	Undivided Cambrian and Ordovician rocks in part of Clark County; mostly Cambrian.
<b>Cc</b>	Limestone and Dolomite, Locally Thick Sequences of Shale and Siltstone	Includes units such as Pioche Shale, Eldorado Dolomite, Geddes Limestone Secret Canyon Shale, Hamburg Dolomite, Dunderberg Shale, and Windfall Formation of northern Nevada and Carrara, Bonanza King, and Nopah Formations of southern Nevada.

Table A.1, continued.

Unit Abbreviation	Unit Name	Unit Description
<b>CZq</b>	Quartzite and Minor Amounts of Conglomerate, Phyllitic Siltstone, Limestone, and Dolomite	Includes Prospect Mountain Quartzite, Osgood Mountain Quartzite, and Gold Hill Formation in northern Nevada and Stirling Quartzite, Wood Canyon Formation, and Zabriskie Quartzite in southern Nevada..
<b>Css</b>	Sandstone and Quartzite	Includes Tapeats Sandstone and related rocks. Rests on Precambrian metamorphic rocks.
<b>Zqs</b>	Quartzite, Phyllitic Siltstone, Conglomerate, Limestone, and Dolomite	Includes McCoy Creek Group (excluding Stella Lake Quartzite) of Misch and Hazzard (1962) in east- central Nevada and Johnnie Formation in southern Nevada.
Metamorphic and Granitic Rocks		
<b>Ygr</b>	Granitic Rocks	Porphyritic rapakivi granite; 1,450 plus or minus 25 Ma (L. T. Silver, oral communication., 1973).
<b>Xm</b>	Metamorphic Rocks	Gneiss and schist and lesser amounts of gneissic granite, pyroxenite, hornblendite, migmatite, pegmatite, and marble. Includes highly folded granite lenses 1,740 plus or minus 25 m. y. old (L. T. Silver, oral communication., 1973). In southern Nye County, may be Precambrian Z rocks metamorphosed during the Mesozoic.

Table A.1, continued.

#	Legend Description	Unit	#	Legend Description	Unit
1	Alluvium	<b>Qa</b>	51	Leucogranite & Ryo. Porphyry	<b>Trlgr</b>
2	Playa, Marsh, Alluvial-Flat	<b>Qp</b>	52	Aztec sandstone	<b>JTra</b>
3	Landslide	<b>Qls</b>	53	Chinle Fm.-Clays & Clastics	<b>Trch</b>
4	Moraine	<b>Qm</b>	54	Moenkopi & Thaynes Fm.-Sed.	<b>Trmt</b>
5	Older Alluvium	<b>QToa</b>	55	Epiclastic, Tuffs, Flows, Carb.	<b>JPu</b>
6	Ryo. Flows, Shallow Intrusives	<b>QTr</b>	56	Limestone, Clastic, Greenstone	<b>TrPs</b>
7	Andesite Flows, Breccias	<b>Qta</b>	57	Andesite Flows, Tuff, Clastics	<b>TrPvs</b>
8	Basalt Flows	<b>Qtb</b>	58	Havallah Seq.-Clastics & Carb.	<b>PMh</b>
9	Lacustrine Sedimentary Rocks	<b>QTs</b>	59	Siliceous & Volcanic Rocks	<b>Msv</b>
10	Rhyolitic Intrusive Rocks	<b>Tri</b>	60	Massive Limestone	<b>MI</b>
11	Mafic-Intermediate Intrusives	<b>Tmi</b>	61	Diablo & Candelaria Fm.-Sed	<b>TrPd</b>
12	Dioritic-Granitic Intrusives	<b>Ti</b>	62	Antler Seq.-Clastics & Carb.	<b>PPa</b>
13	Breccia	<b>Tbr</b>	63	Clastics, Carb., Meta-Andesite	<b>MDmc</b>
14	Silicic Ash-Flow Tuffs	<b>Tt3</b>	64	Limestone, Clastics	<b>PPcd</b>
15	Tuffs, Ryo. Flows, Intrusives	<b>Trt</b>	65	Limestone, Cherty Clastics	<b>Pcd</b>
16	Ryo. Flows, Shallow Intrusives	<b>Tr3</b>	66	Clastics & Limestone	<b>MDs</b>
17	Andesite, Intermediate Rocks	<b>Ta3</b>	67	Cherty Carbonates, Clastics	<b>Pc</b>
18	Andesite & Basalt Flows	<b>Tba</b>	68	Carbonates & Shale	<b>PMc</b>
19	Basalt Flows	<b>Tb</b>	69	Clastics, Carbonates, Gypsum	<b>Psc</b>
20	Banbury Formation	<b>Tbg</b>	70	Carbonates, Clastics	<b>PPc</b>
21	Ash-Flow Tfs, Tfs Sed. Rocks	<b>Tts</b>	71	Limestone	<b>Pc</b>
22	Tuffaceous Sedimentary Rocks	<b>Ts3</b>	72	Limestone, Dolomite, Shale	<b>Mc</b>
23	Horse Spring Formation	<b>Ths</b>	73	Serpentine	<b>Pzsp</b>
24	Continental Sedimentary Rocks	<b>TKsu</b>	74	Clastics, Metamorphic Rocks	<b>DCsv</b>
25	Silicic Ash-Flow Tuffs	<b>Tt2</b>	75	Slaven Chert	<b>Dsl</b>
26	Ryo. Flows, Shallow Intrusives	<b>Tr2</b>	76	Clastics, Chert, Limestone	<b>Ds</b>

**Table A.2.** Key to lithologic units. "#"—map class ID number assigned to lithologic unit in maps; *Legend Name*—brief unit description appearing in the map legends; *Unit*—unit abbreviation. From Stewart and Carlson (1978).



#	Legend Description	Unit	#	Legend Description	Unit
27	Andesite, Intermediate Rocks	<b>Ta2</b>	77	Elder Sandstone	<b>Se</b>
28	Older Basalt Rocks	<b>Tob</b>	78	Shale & Chert	<b>Ss</b>
29	Tuffaceous Sedimentary Rocks	<b>Ts2</b>	79	Siliceous & Volcanic Rocks	<b>Osv</b>
30	Silicic Ash-Flow Tuffs	<b>Tt1</b>	80	Clastics, Metamorphics, Carb.	<b>Os</b>
31	Ryo. Flows, Shallow Intrusives	<b>Tr1</b>	81	Harmony Fm.-Clastics	<b>Ch</b>
32	Andesite, Intermediate Rocks	<b>Ta1</b>	82	Scott Canyon Fm.-Sed & Meta.	<b>Csc</b>
33	Sedimentary Rocks	<b>Ts1</b>	83	Argillaceous Carb., Chert, Sed.	<b>Dt</b>
34	Continental Sedimentary Rocks	<b>TKs</b>	84	Limestone, LimyClastic, Chert	<b>St</b>
35	Continent Clastics, Limestone	<b>Ks</b>	85	Shale, Chert, Limestone	<b>Ot</b>
36	Granitic Rocks, Central & East	<b>TJgr</b>	86	Phyllite, Shale, Limestone	<b>OCt</b>
37	Monzonite & Granodiorite	<b>Tgr</b>	87	Shale, Limestone, Chert	<b>Ct</b>
38	Granitic Rocks, West	<b>Mzgr</b>	88	Clastics, Meta., Carbonates	<b>CZs</b>
39	Qtz-Monzonite & Granodiorite	<b>Kgr</b>	89	Wyman Fm.-Phyllite & Sed.	<b>Zw</b>
40	Diorite	<b>KJd</b>	90	Carbonate, Clastics, Quartzite	<b>Dc</b>
41	Qtz-Monzonite & Granodiorite	<b>Jgr</b>	91	Dolomite & Limestone	<b>DCc</b>
42	Quartz Monzonite	<b>Trgr</b>	92	Dolomite	<b>Sc</b>
43	Igneous & Metamorphic Complex	<b>KJim</b>	93	Dolomite	<b>SOc</b>
44	Volcano- & Clastics, Carbonate	<b>JTrsv</b>	94	Carbonates, Shale, Quartzite	<b>Oc</b>
45	Dunlap Fm.-Clastics & Tuffs	<b>Jd</b>	95	Dolomite & Limestone	<b>OCc</b>
46	Gabbroic Complex	<b>Jgb</b>	96	Dolomite & Limestone, Clastics	<b>Cc</b>
47	Volcaniclastic, Tuff, Ryo. Flow	<b>Jv</b>	97	Quartzite, Clastic, Carbonates	<b>CZq</b>
48	Clastics, Carbonate, Volcanics	<b>JTrs</b>	98	Sandstone & Quartzite	<b>Css</b>
49	Limestone, Minor Clastics	<b>Trc</b>	99	Quartzite, Clastic, Carbonates	<b>Zqs</b>
50	Koipato Group - Volc. & Clastic	<b>Trk</b>	100	Granitic Rocks	<b>Ygr</b>
			101	Metamorphic Rocks	<b>Xm</b>

Table A.2, continued.

#	<b><i>Lithologic Assemblage Map Unit</i></b>	<b><i>Geologic Map of Nevada Lithologic Units Composing the Assemblage Unit</i></b>
1	Quaternary Cover	<i>Qa, Qp, Qls, Qm, QToa, QTs</i>
2	Continental Clastics- CZ-MZ	<i>TKsu, TKs, Ks</i>
3	Continental Clastics- Mid MZ	<i>JTra, Trch</i>
4	Marine & Shelf- Early-Mid MZ	<i>JTrsv, Jd, JTrs, Trc, Trmt</i>
5	Marine & Shelf- Late PZ	<i>TrPs, MI, TrPd, PPa, MDmc, PPcd, Pcd, MDs, Pc, PMc, Psc, PPc, Pc, Mc</i>
6	Marine & Shelf- Early-Mid PZ	<i>Dt, St, Ot, OCt, Ct, Dc, DCc, Sc, SOc, Oc, OCc, Cc</i>
7	Shelf & Marine- Early PZ-PC	<i>CZs, Zw, CZq, Css, Zqs</i>
8	Silicious Rocks- Late PZ	<i>TrPvs, PMh, Msv</i>
9	Silicious Rocks- Mid PZ-PC	<i>DCsv, Dsl, Ds, Se, Ss, Osv, Os, Ch, Csc</i>
10	Tuff & Sed Rocks- Late CZ	<i>Tts, Ts3, Ths, Ts2, Ts1</i>
11	Breccia & Tuffs- Late CZ	<i>Tbr, Tt3, Tt2, Tt1</i>
12	Fel-Int Ex- & Intrus- Late CZ	<i>QTr, QTa, Tri, Ti, Trt, Tr3, Ta3, Tr2, Ta2, Tr1, Ta1</i>
13	Fel-Int Extrus- Early-Mid MZ	<i>Jv, Trk, JPu</i>
14	Int-Maf Ex- & Intrus- Late CZ	<i>QTb, Tmi, Tba, Tb, Tbg, Tob</i>
15	Granitic Pluton- Late MZ-CZ	<i>TJgr, Tgr, Mzgr, Kgr, KJd, Jgr, Trgr, Trlgr</i>
16	Granitic Pluton- PC	<i>Ygr</i>
17	Gabbroic Pluton- Early-Mid MZ	<i>Jgb</i>
18	Ultramafic Rocks- Late PZ	<i>Pzsp</i>
19	Ign/Meta Complex- Early-Mid MZ	<i>KJim</i>
20	Ign/Meta Complex- PC	<i>Xm</i>

**Table A.3.** Key to the makeup of the lithologic assemblage map units. "#"—map class ID number assigned to assemblage unit in maps; *Lithologic Assemblage Map Unit*—brief unit description appearing in the map legends; *Geologic Map of Nevada Lithologic Units Composing the Assemblage Unit*—the lithologic units from Stewart and Carlson's (1978) geologic map of Nevada that were grouped together to create the lithologic assemblage unit.

# APPENDIX B

## Weights of Evidence Mineral Potential Modelling Theory, Implementation, and FORTRAN Utilities:

### Section Contents:

#### Listing of FORTRAN Utilities

#### **B.1** GIS Software and Workstation

##### **B.1.1** Introduction

##### **B.1.2** Software Specifications

##### **B.1.3** Hardware Specifications

#### **B.2** Data Analysis and Modelling Methodology

##### **B.2.1** Introduction

##### **B.2.2** Preliminary Spatial Data Analysis

##### **B.2.3** Weights of Evidence Mineral Potential Modelling—An Overview

##### **B.2.4** Weights of Evidence Mineral Potential Modelling—Theory

##### **B.2.4.1** *Procedure i*—Calculation of Weights of Spatial Association

##### **B.2.4.2** *Procedure ii*—Multi-map overlay and weights combination using Bayes' Rule

#### **B.3** Conditional Independence

##### **B.3.1** Introduction

##### **B.3.2** Pairwise Test and the Chi-Square Statistic

##### **B.3.3** Overall Test and the Kolmogorov-Smirnov Statistic

#### **B.4** Posterior Probability Uncertainty

##### **B.4.1** Introduction

##### **B.4.2** Source and Types of Uncertainty

#### **B.5** Practical Implementation of the Modelling Procedures

##### **B.5.1** Introduction

##### **B.5.2** Estimation of the Spatial Weights of Association

##### **B.5.3** Generation of Binary-Class Mineral Predictor Maps

##### **B.5.4** Bayesian Map Overlay, and Generation of Mineral Potential and Posterior Probability Uncertainty Maps

##### **B.5.5** Conditional Independence Testing

### **Listing of FORTRAN Utilities:**

---

<b>CI</b>	Conditional Independence Contingency Table Utility.
<b>CONTRAST</b>	Individual Case Weights of Spatial Association Estimation.
<b>DLM2VEC</b>	Convert Delimited List of Longitude and Latitude Coordinates to Spans Vec./Veh. Has a bug: longitude must be in column one, latitude in two.
<b>DELIMIT</b>	Example Input File for DLM2VEC.
<b>KOLMOG</b>	Kolmogorov-Smirnov Calculation Utility.
<b>PREDICT</b>	Weights and Various Uncertainty Estimation Utility. Also Does Direct Bayesian, Logistic Regression, Etc.
<b>THINOUT</b>	Utility for Deleting Points Nearer to One Another Than Some User Specified Threshold.
<b>WEIGHTS</b>	Modified Weights Calculation Utility. Cosmetic Modifications to the Output Tables, and Input Tables Can Be Wider.
<b>WTS</b>	Original Weights Calculation Utility.

For additional information about these utilities, consult the comments in the .for source code files. These programs are written to run with output from SPANS 5.2.

## B.1 GIS Software and Workstation

### B.1.1 Introduction

A GIS is a database management system that links data items by geographical position as the primary means by which to organize spatial information. It provides the functionality for integrating, analysing, and displaying large volumes of data from many sources. Most geoscience data can be readily managed and analysed by geographical criteria. Traditionally, geoscientists have integrated data on paper and stable base maps using manual techniques. Whereas conventional maps are not quickly or easily modified and manipulated, digital data can readily be edited, manipulated, transformed, and processed in dynamic environments which permit exploratory data analysis and modelling.

### B.1.2 Software Specifications

SPANS (*SP*atial *AN*alysis *S*ystem) version 5.4 by TYDAC Technologies Inc. is a *quadtree-based* GIS which uses a raster data structure with a variable pixel size ([Fig. B.1](#)). The maximum raster image resolution is  $2^{15}$  by  $2^{15}$  (32,768 by 32,768) pixels. The quadtree is a hierarchical data structure which differs from a conventional raster structure in that the pixel size is not fixed, and that the data items are spatially addressed using the Morton coordinate system rather than the standard Cartesian coordinate system [x,y]. SPANS quadtrees allow a range of class (intensity) values of  $0-2^{26}$  as compared to  $0-2^8$  or  $0-2^{16}$  for standard raster images. In addition, the quadtree equivalent of a raster image requires considerably less storage space. SPANS also employs a topological vector structure, with vertices defined in precise Morton coordinates, and a variety of table structures for handling attribute data. Excellent reviews of GIS data structures may be found in Aronoff (1989), Star and Estes (1990), Maguire et al. (1991), and Bonham-Carter (1994a).

SPANS is structured to facilitate the integration of data from various sources and accommodates numerous spatial and non-spatial data structures. Data may be readily exchanged between many external statistical applications, database managers, spreadsheets, word processors, and drawing packages using ASCII and other popular file formats. SPANS also provides a comprehensive and powerful array of analytical and modelling tools which permits the user to perform customized operations on multiple map layers. Up to 15 quadtree maps can be combined in one step using a modelling language. A complementary digitizing package, TYDIG, allows analog data to be directly captured in a vector or point format.

FORTTRAN command-line utilities used for implementing some of the mineral potential modelling procedures carried out in this study are discussed separately in [section B.5](#).

### B.1.3 Hardware Specifications

This research was carried out on two IBM-compatible PC workstations. Most of the data compilation and integration of data into the GIS environment was carried out on an 80486 IBM PC/AT compatible computer operating at a clock speed of 33 MHZ with ISA-16 bit bus internal architecture and 16 Mb of total system memory. This system is equipped with a SCSI disk drive

controller, a 220 Mb hard disk drive, two high density floppy disk drives (5¼ and 3½ inch), a Sony CDU-7101W external CD-ROM drive unit operating on MS-DOS CD-ROM Extensions version 2.10, a 3.5 by 2.5 foot Gentian Thinline digitizing tablet, a non-interlaced SVGA 17 inch color monitor powered by an ATI Technologies Inc. Graphics Vantage graphics accelerator video card which provides 256 colors at a monitor resolution of 1024 by 768 pixels. The workstation is run under the OS/2 operating system (version 2.1) in Presentation Manager mode with a bus mouse, networked to a Novell 3.11 file server with 1 Gb storage capacity. Analysis and modelling of the spatial data were completed on a similar computer operating at a clock speed of 100 MHZ with ISA-32 bit local-bus internal architecture, 48 Mb of total system memory, and a 2.7 Gb SCSI hard disk drive operating under OS/2 2.11. SPANS will also operate under DOS and on a variety of UNIX platforms.

The data listed in Table 5.1 occupy almost 600 Mb of hard disk space. The vector datasets which represent the geological map of Nevada, for instance, are nearly 38 Mb in size. After these datasets were processed and converted into quadtree maps, the total storage space required for vector and raster structures approached 85 Mb (this is for the highest resolution quadtree structure at a *quadlevel* of  $2^{15}$  which is equivalent to an ordinary raster of 32,768 by 32,768 cells). A high capacity hard disk is necessary. Computer processing of these data are memory intensive, particularly for efficient spatial interpolation of large point datasets. Slight modification of the default OS/2 CONFIG.SYS system file was necessary to successfully process some of the data. System performance was enhanced by increasing the buffers and disk cache size.

## **B.2 Data Analysis and Modelling Methodology**

### **B.2.1 Introduction**

Spatial data analysis can be preliminary in nature, involving non-statistical or summary statistical approaches (e.g.—visual pattern recognition and simple map reclassification, or, histogram generation and area analysis, respectively), or it can be more sophisticated, involving statistical approaches with probabilistic components (e.g.—regression analysis, weights of evidence).

Both preliminary and more sophisticated analysis methods were used to identify and measure the spatial associations between gold-silver-bearing occurrences and various geoscientific datasets. [Section B.2](#) reviews these techniques. The error and uncertainty associated with mineral potential modelling are considered in sections [B.3](#) and [B.4](#). Practical implementation of mineral potential modelling and error analysis is reviewed in section [B.5](#). For a thorough and detailed treatment of spatial modelling and GIS in general, see Bonham-Carter (1994a).

### **B.2.2 Preliminary Spatial Data Analysis**

This research was carried out using many spatial data manipulation and analysis tools available in a standard GIS environment. A comprehensive examination of these tools is beyond the scope of this study, however, a general overview of the techniques useful for implementing weights of evidence mineral potential modelling is presented. For detailed reviews of basic spatial data

manipulation and analysis methods, consult Antenucci et al. (1991), Aronoff (1989), Bonham-Carter (1994a), and ESRI (1994).

The preliminary spatial data manipulation and analysis techniques used here include: (1) map reclassification/generalization; (2) map overlay/combination; (3) spatial and topological modelling; and (4) visual pattern recognition and spatial query. All of these methods assist in clarifying and defining trends and patterns.

Map reclassification is one of the most elementary, yet most powerful techniques of analysis in a GIS. This technique is applicable to nominal, ordinal, interval, or ratio scale data. Map units may be grouped and displayed to generalize and emphasize spatial relationships and highlight various attributes. Reclassification may be accomplished using a variety of interactive and semi-automated techniques. One of the most common methods is table reclassification. This method makes use of polygon or map class attributes that are arranged in a table by rows and columns—a row (representing a map class) is composed of fields (the columns) which contain spatial or non-spatial attribute information relating to the map class (Table B.1). Each unique class of a map is keyed to the table by the map class or polygon number. For a geological map, a typical reclassification table might contain attribute information which categorizes the geologic units by rock type, lithology, age, or by any characteristic that is desired. In the reclassification operation, the geological map units that do not satisfy the reclassification conditions are reclassified to “0”, a null class. Those units that do satisfy these conditions either retain their original map class values, or are re-coded to new values, and are incorporated into the new map. In many instances, histograms were produced from the numeric data associated with the map classes to determine breakpoints for map reclassification schemes.

The process of overlaying or combining two or more maps into a single map is fundamental to weights of evidence modelling, and to GIS modelling and analysis in general. This is a powerful technique for examining the spatial patterns caused by the interaction of one or more maps (Bonham-Carter, 1994a). Maps are typically overlain or combined using a set of rules defined by various arithmetic and Boolean operators in a variety of combinations (a “map model”). The main map overlay operations are illustrated in Figure B.2, and include:

- Ⓒ *Impose*—Portions of one map are cut away based on the boundaries of a second (the second is typically a map consisting of one class). This technique is useful for creating a “mask” to cover or remove parts of a map (Fig. B.2a).
- Ⓒ *Stamp*—A map is overlain (placed on top) of a second. The map placed on top is reclassified by adding the maximum class value of the bottom map to the class values of the top map. This technique is useful for constructing complex maps from several simpler (or binary-class) maps (Fig. B.2b).
- Ⓒ *Join*—The classes of one map are merged with those of a second. This operation is useful for joining two or more overlapping map sheets together (Fig. B.2c).
- Ⓒ *Compare*—Two maps are combined so as to highlight where the maps are the same, different, or where map classes show spatial coincidence. In more sophisticated applications of this technique, the output map class values can be interactively assigned to each combination of classes of the two input maps (Fig. B.2d).
- Ⓒ *Map/Class-Weighted*—Two or more maps are combined using a user-specified relative weighting scheme which ranks the importance of a map and/or map class unit. This technique is useful for assessing the relative suitability or risk associated with some factor (e.g.—“Given the relative importance of various geological factors, is this a good place to prospect for gold?”) (Fig. B.2e).
- Ⓒ *Unique Conditions*—Multiple maps are combined to create a single map composed of unequal-area polygons that are assigned the same class value if they consist of the same overlap combination or characteristic of input



maps (Fig. B.3). This operation produces an associated (linked) attribute table that contains the unique overlay combinations of input map classes that compose a particular unique conditions map class (Table B.2). This is a very powerful map combination method that allows modelling or data analysis to be performed on the table (“table modelling”), rather than using the input maps directly (“map modelling”). The unique conditions map can be reclassified according to the modelling or analysis results, which are directly linked to the unique conditions map via the unique conditions table. This technique plays an especially important role in implementing weights of evidence mineral potential modelling (for additional details on unique conditions maps, see Bonham-Carter, 1994a, p. 235-238; Bonham-Carter, 1991, p. 172).

The spatial and topological modelling techniques used for this analysis include geometric, coincidence, and adjacency analysis. These techniques are applicable to point, line, and polygon spatial objects. Geometric modelling involves calculating polygon areas and perimeters, the generation of point and line buffers, and calculating the distance between objects. Coincidence modelling includes polygon overlay operations and point-in-polygon analysis. Adjacency modelling deals with spatial interpolation (e.g.—surface contouring or generation) and neighbourhood operations, as well as network analysis and similar types of operations. Coincidence and adjacency modelling use spatial and topological information, whereas geometric analysis does not necessarily require such information (e.g.—map unit area analysis and vector/point buffering). Most vector and point datasets were transformed to quadtree raster maps by distance buffering the vector datasets and by surface interpolation of values associated with the point datasets. Some quadtree maps were further processed using spatial neighbourhood analysis to determine map complexity (e.g.—diversity of geology) and to examine the “grain” of geographic/geologic features (e.g.—angle of incidence illumination of topography). Area and point-in-polygon analyses were performed on most maps to delineate the spatial extent occupied by each map class, and to determine the number of points, in this case gold-silver-bearing occurrences, associated with each class.

In addition to the quantitative analysis techniques described above, each map was also visually inspected. A number of the datasets were also viewed in shaded-relief and as 3-dimensional renderings to enhance textural, shape, and directional features. The human eye has an extraordinary ability to distinguish subtle patterns within otherwise complex spatial arrangements. Visual examination of the maps facilitated recognition and interpretation of regional-scale tectonomagmatic trends and patterns which might have otherwise be hidden from area, point, or polygon-based analysis methods. A technique complementary to visual appraisal is spatial query. Simple interactive spatial query techniques were used to examine concurrently the relationships between multiple map layers and an individual or group of mineral occurrences. In this manner, any number of evidence maps were simultaneously queried so as to determine their collective or unique properties and characteristics at specific occurrence locations.

### **B.2.3 Weights of Evidence Mineral Potential Modelling—An Overview**

*Weights of evidence* (WOE) provides a measure of spatial association (a “weight”) between multi- and/or binary-class map patterns and known point or polygon objects, and uses Bayes’ probability theorem to combine the map patterns to predict the distribution of the point or polygon objects. As applied to mineral potential modelling, the point objects represent known mineral deposits. The multi-class map patterns are typically maps of particular geologic phenomena, such as geology, geochemistry, geophysics, etc., which are likely to be useful as mineral deposit predictors. These maps are referred to as “*evidence maps*”, representing geo-

spatial evidence for the occurrence of mineralization. In order to facilitate combination, the evidence maps are usually reduced to deposit-indicator or mineral “*predictor maps*” of a few discrete states (typically binary) where the spatial association between mineralization-favorable evidence and the occurrences is optimized. The mineral predictor maps collectively constitute the “*layers of evidence*” for the mineral potential model.

A layer of evidence need not completely cover the study area, as the WOE modelling method can easily accommodate missing data (incomplete coverage). This is an important and distinct advantage of this method. Other advantages include uncomplicated calculations, an objective procedure for weighting the evidence layers, relatively straightforward interpretation of the weights, direct user involvement with optimization of the evidence maps, which is an important inductive process that provides insight into the spatial data relationships, and the ability to model the uncertainty of the mineral potential map (Bonham-Carter, 1994a, 199b).

The techniques employed by WOE were developed to model spatial data, and depart from classical (non-spatial) statistical theory. The measure of spatial association and the combining of spatial data must therefore be performed and evaluated with care because they are sensitive to choice of the measurement domain, and because their statistical significance is normally not possible to estimate by conventional means (Bonham-Carter, 1994a). The following paragraphs describe and illustrate WOE, and are excerpted largely from Agterberg (1989a), Agterberg et al. (1990), Bonham-Carter (1994a, 1994b), Bonham-Carter (1991), Bonham-Carter et al. (1988), and Bonham-Carter et al. (1989).

Weights of evidence (WOE) is a discrete, multivariate statistical method based on a technique originally developed in a non-spatial context for medical diagnosis (Spiegelhalter and Knill-Jones, 1984) and has been modified by Bonham-Carter et al. (1989) to deal with spatial prediction—“diagnosing” mineral deposits using the “symptoms” of various geologic phenomena (Bonham-Carter, 1994b). WOE evaluates the spatial distribution of known mineral deposits (the *response variable*) relative to multi- or binary-class map patterns (the *predictor variables*), calculates weights of spatial association ( $W^+$  and  $W^-$ ) for each pattern, and produces a multi-map signature for mineralization (Bonham-Carter et al., 1989). The evidence layers are combined using Bayes' Rule in a multi-map overlay operation where the *prior probability* of an occurrence—the probability of an occurrence given no information (random), equal to the average density of known occurrences in the study area, and held constant over the whole area—is updated by the addition of predictor variables and their weights to produce a single *posterior probability* map of occurrence (Bonham-Carter et al., 1989; Bonham-Carter, 1991). In this case, the posterior probability map is a map of mineral potential which reflects the distribution of known occurrences and predicts the distribution of yet unidentified occurrences (Bonham-Carter et al., 1988). The whole process is similar to that of an exploration geologist manually integrating information and combining maps in order to delineate favourable areas of mineralization (Agterberg et al., 1990).

Weights of evidence is a *data-driven* method, requiring data about the distribution of known mineral deposits to estimate weights of spatial association for the mineralization evidence layers. WOE is similar in some ways to logistic regression in that the distribution of mineral deposits over the study area must be known, however, in regression modelling, calculation is complex, the weighting factors are not so readily interpreted, and there is no accommodation for missing

data (Agterberg et al., 1990; Bonham-Carter, 1994b). Weights of evidence differs from *knowledge-driven* methods which do not require deposit distribution data and where the weights are estimated by an expert, such as in the fuzzy logic method (An et al., 1991; Bonham-Carter, 1994a; Wright and Bonham-Carter, 1996), Dempster-Shafer method (Moon, 1990; Leverington and Duguay, 1994; Wright and Bonham-Carter, 1996), or in the PROSPECTOR expert system (see Bonham-Carter, 1994a, chapter 9).

In WOE modelling, no “training area<sup>1</sup>” is used to select the geo-spatial mineralization evidence or to calculate “initial baseline” weights (i.e.—to establish the “initial conditions”). The selection of mineralization evidence maps is largely guided by a conceptual model (this is the normal mode of implementation; see Bonham-Carter et al., 1989; Bonham-Carter, 1994a; Wright, 1996; Wright and Bonham-Carter, 1996). The conceptual model is usually a synopsis that may contain elements of deposit models, which typically focus on characteristics at the deposit scale, and/or exploration models, which include deposit model components that apply to regional-scale exploration, in addition to geophysical, geochemical, remotely-sensed, and other data useful for delimiting regions that may warrant further detailed investigation<sup>2</sup>. The choice of evidence should reflect current understanding on the genesis of the particular deposit type being modelled as well as the geologic features believed to control its spatial distribution. An evidence map should ideally provide either universal coverage or coverage over the majority of the study area (Bonham-Carter et al., 1989).

The “initial conditions” of the mineral potential model are established using the optimized mineralization evidence maps (the mineral predictor maps), where the weighting of each individual layer of evidence is determined automatically using the locations of known mineral deposits over the entire study region for training (Wright and Bonham-Carter, 1996). A model may be further calibrated using other factors such as mineral deposit size, where different schemes for weighting the layers of evidence are calculated for each deposit size subset (Wright and Bonham-Carter, 1996). For Nevada, numerous maps of various geologic phenomena and the distribution of known mineral occurrence types and sizes were used to design, train, and calibrate the models used in this study. The selection of mineralization evidence maps and the subdivision of the mineral occurrences considered in this study are detailed in Chapter 5. Spatial optimization of the evidence maps with respect to the mineral occurrences is covered in Chapter 6.

An important assumption made in WOE modelling is that the mineralization evidence layers included in a model be conditionally independent (CI) of one another with respect to the mineral

---

<sup>1</sup> As used here, the term “training area” is defined as a sub-region of, or a region outside of, the study area which is designated an experimental control, where (1) the geologic conditions are similar to the prospecting region, (2) all the mineral deposits are known, *and no more are expected to be discovered*, (3) all of the geo-spatial mineralization evidence is present (i.e.—full evidence map coverage), and (4) the quantitative relationships (the spatial weights of association) between the mineral deposits and the evidence are established (Chung and Moon, 1990; Chung, 1995).

<sup>2</sup> Deposit models and modelling will not be discussed here, as this topic is the focus of numerous authors, including Babcock (1984), Barton (1986), Berger and Jefferson (1986), Bliss (1992), Bliss and Menzie (1990), Cox and Singer (1986), Eckstrand (1984), Kirkham et al. (1993), Singer and Cox (1988), and Singer (1993).

deposits (see Bonham-Carter, 1994a, pp. 312-317). In practice, CI is probably always violated to some degree, and the possibility of the occurrence of CI generally increases with an increase in the number of evidence layers included in a model (Bonham-Carter, 1991; Bonham-Carter, 1994a). Because of the CI assumption, calculation of the spatial weights of association are carried out independently between the mineral deposits and each evidence layer, and as a result, WOE has the opportunity to examine bivariate relationships in some depth (Bonham-Carter, 1994b). The assumption of CI leads to a model that, like most models, does not fit the data perfectly, but provides a simplification that, when applied carefully, is useful for prediction and gives insight into the relative contributions of the separate sources of evidence (Bonham-Carter, 1994a). Conditional independence can be checked visually and with statistical tests (*pairwise* or *overall* tests) to isolate the layers that clearly violate the assumption. The offending map layers can then either be rejected from the analysis altogether or modified in some manner as to lessen their affect, such as by combining maps using Boolean operators to form a new single joint map (Bonham-Carter, 1991; Bonham-Carter, 1994b).

As applied in this study, the methodological framework for producing mineral potential maps using the WOE modelling method consists of four main steps:

1. Determination of the deposit-type characteristics and development of a conceptual model. The characteristics of the deposit types examined in this study are detailed in Chapter 3 and summarized as synoptic models. Further geological and statistical evaluation of certain features which may be related to the regional-scale distribution of the mineral occurrences is reviewed in Chapter 6.
2. Development of the mineral potential spatial database. This step involved the compilation, preparation, and integration of numerous data sets from a variety of sources, and is reviewed in Chapter 5.
3. Development, design, and training of the model, where information critical to mineral occurrence prediction was extracted from the mineralization evidence maps. This involved the selection of promising multi-class evidence maps, the measurement of spatial association between the evidence maps and the mineral occurrences, determination of the significance of these associations, and, based upon the strength and importance of the spatial associations, the reclassification of the multi-class evidence maps to binary-class mineral predictor maps (layers of evidence). This process is the subject of Chapter 6.
4. Application of the model. This step involved the combination of the mineral predictor maps to generate the mineral potential maps and the examination and evaluation of uncertainty and error. This process is covered in Chapter 7 and Appendices C and D. Interpretation of the model output with respect to geology and metallogeny is discussed in Chapter 8.

The theoretical aspects of these steps follows immediately below. Practical implementation is discussed in [section B.5](#).

## B.2.4 Weights of Evidence Mineral Potential Modelling—Theory

The weights of evidence method is illustrated in [Figure B.4](#) and can be subdivided into two main procedures:

- i. Calculation of  $W^+$  and  $W^-$  weights of spatial association between the response variable and the predictor variable(s), in this case point objects representing mineral deposits and multi-class map patterns representing various geologic phenomena. Generation of the mineral predictor maps (the layers of evidence) by reclassification of the multi-class predictor variables to binary-class predictor variables, using the weights of spatial association for each predictor-response variable set as a guide, where: binary pattern present

represents mineralization-favorable areas, and binary pattern absent represents mineralization-unfavorable areas.

- ii.* Integration of predictor variables in a multi-map overlay operation where a loglinear version of Bayes' Rule is used to sum and update the weights associated with each of the map classes that come into coincidence, producing a compound map which closely exhibits the distribution of known deposits and indicates areas where more deposits are expected than are observed.

The goal of weights of evidence modelling is to estimate the posterior probability of the occurrence of a mineral deposit, given the presence or absence of mineralization-favorable evidence, which, depending on the evidence, may be larger or smaller than the prior probability. Procedure *ii* typically involves conditional independence testing. This issue is addressed under a separate heading below ([section B.3](#)).

#### **B.2.4.1 Procedure *i*—Calculation of Weights of Spatial Association**

In the first procedure, [Figure B.4i](#), area analysis is performed on each of the predictor variable map layers and point-in-polygon analysis is performed on each response/predictor variable set. The output of the area analysis is a table that contains: (1) the percent of the total area occupied by each map class, (2) a running total of area by map class, and (3) area in km<sup>2</sup> occupied by each map class ([Table B.3](#)). The point-in-polygon analysis appends the map class of the predictor variable to the response variable point dataset. The output is a table containing the coordinates of the response variable points and the predictor variable map classes into which the points fall ([Table B.4](#)).

The area analysis ([Table B.3](#)) and point-in-polygon analysis ([Table B.4](#)) data characterize the spatial attributes of the response and predictor variables, and are used to calculate a pair of weights,  $W^+$  and  $W^-$ , for each predictor variable map class (see [section B.5.2](#) for implementation procedure). The value of the weights represent a ratio of area proportions, and is dependent upon the ratio of the number of deposits that fall within a particular map class to the total number of deposits, against, the ratio of the particular map class area to the total map area (Bonham-Carter, 1991). In the case of a multi-class predictor variable, each map class is treated individually as a binary-class map pattern (map class present or absent), and is composed of the area of the particular map class being evaluated and the combined total area of the remaining map classes. A mineral deposit is assumed to occupy a small unit area and is likewise regarded as a present or absent binary pattern. There is no provision for modelling deposit size, grade, or tonnage in WOE. All area values are expressed in unit cells, where  $N$  is the number of unit cells and an area is denoted as  $N()$ . For the analyses carried out here, a 1 km<sup>2</sup> unit cell was used to represent a mineral deposit.

The coincidence between two binary patterns, a deposit distribution pattern (D) and a mineral predictor pattern (B), yields four possible spatial overlap relationships:

1. Both patterns are present.
2. Pattern D is present, pattern B is absent.
3. Pattern D is absent, pattern B is present.
4. Both patterns are absent.

The four overlap states are illustrated in [Figure B.5](#). From these four mutually exclusive response-predictor variable overlap states, four conditional probabilities can be estimated using area ratios:

$$P(D|B) = \frac{N(B\_D)}{N(B)}, \quad P(D|\bar{B}) = \frac{N(\bar{B}\_D)}{N(\bar{B})}, \quad P(\bar{D}|B) = \frac{N(B\_\bar{D})}{N(B)}, \quad \text{and} \quad P(\bar{D}|\bar{B}) = \frac{N(\bar{B}\_\bar{D})}{N(\bar{B})} \quad \mathbf{B.1}$$

Using the conditional probabilities defined in equation B.1, the weights  $W^+$  and  $W^-$  for each predictor variable map class are calculated as log ratios in the following manner:

$$W^+ = \ln \frac{P(B|D)}{P(B|\bar{D})}, \quad \text{and} \quad W^- = \ln \frac{P(\bar{B}|D)}{P(\bar{B}|\bar{D})} \quad \mathbf{B.2}$$

Detailed discussion and the derivation of these equations are found in Bonham-Carter et al. (1989) and Bonham-Carter (1994a), as well as Agterberg (1989a), Agterberg et al. (1988), Bonham-Carter (1994b), Bonham-Carter (1991), Bonham-Carter et al. (1988).

$W^+$  is a measure of the presence of a map class relative to the total number of deposits, whereas  $W^-$  is a measure of absence of the map class (as distinct from unknown).  $W^+$  and  $W^-$  are always opposite in sign, except when the proportion of deposits falling in a map class to the total number of deposits is the same as the proportion of the map class area to the total study area, then:

$$W^+ = W^- = 0 \quad \mathbf{B.3}$$

and no spatial association between the map class and the points exists. If more deposits are spatially associated with a map class than would be expected due to chance,  $W^+$  is positive and  $W^-$  is negative, indicating a positive correlation. Where the presence of a map class “inhibits deposits”,  $W^+$  is negative and  $W^-$  is positive, indicating a negative or inverse correlation. Where information is missing (i.e.—incomplete predictor variable coverage),  $W^+$  and  $W^-$  are set to zero (Bonham-Carter, 1994a).

The weights can be combined into a single coefficient called the contrast (C), where:

$$C = |W^+ \& W^-| \quad \mathbf{B.4}$$

and  $||$  denotes absolute values. The contrast provides a useful measure of the strength of the spatial association between the mineral deposit pattern (response variable) and the mineral predictor pattern (predictor variable).

### B.2.4.2 Procedure ii—Multi-map overlay and weights combination using Bayes' Rule

In the second procedure, [Figure B.4ii](#), Bayes' Rule is used to combine the evidence represented by the predictor variables (multiple binary- and/or multi-class predictor maps) to determine the probability that the response variable is present (i.e.—the probability that a mineral deposit is present at a given location based upon the evidence). One of the main concepts of Bayes' probability law is that of *prior* and *posterior* probabilities. Bayes' Rule gives the probability that some particular phenomena (*B*) is “*the cause among many causes*” of a known end effect (*D*) (Mendenhall and Reinmuth, 1974). In the case of mineral potential modelling, the preceding “*cause*” phrase might be better replaced with “*the most highly correlated geologic phenomena, among many phenomena, that are spatially associated to known mineral deposits*”.

From Bayes' Rule, the conditional probability that a unit cell contains a deposit, given the presence of a binary mineral predictor pattern, is given as:

<p style="text-align: center;"><i>Deposit (D), given presence of binary mineral predictor pattern (B):</i></p> $P(D B) = P(D) \frac{P(B D)}{P(B)}$	
<p style="text-align: center;"><i>Deposit, given <b>two</b> binary mineral predictor patterns:</i></p> $P(D B_1 \text{--} B_2) = \frac{P(B_1 \text{--} B_2 D) P(D)}{P(B_1 \text{--} B_2 D) P(D) + P(B_1 \text{--} B_2 \bar{D}) P(\bar{D})} \quad \textbf{B.5}$	
<p style="text-align: center;"><i>The effects of interaction between <math>B_1</math> and <math>B_2</math> can be ignored by making an assumption of conditional independence, thus, the conditional probability of a deposit, given <b>two</b> mineral predictor patterns:</i></p> $P(D B_1 \text{--} B_2) = P(D) \frac{P(B_1 D)}{P(B_1)} \frac{P(B_2 D)}{P(B_2)}$	

The key to combining binary mineral predictor maps in WOE is the third expression, which permits multiplication of each predictor map's effect, independent of one another. The computed probability  $P(D|B)$  is the *posterior probability* of known end effect (*D*) given the information contained in phenomena (*B*).  $P(D)$  is the simple, or *prior probability* of (*D*), and does not take into account the information contained in (*B*). The value of the prior probability is assumed to be the average density of known deposits in the region of interest and is constant throughout. This can be calculated as:

$P(D) = N(D)/N(A)$	<b>B.6</b>
--------------------	------------

where the area of deposits, *D*, and total area of the study area, *A*, are expressed as the count of unit cells, *N*( ). The posterior probability reflects both the prior and current information, and



provides a more efficient model for prediction. Bayes' Rule effectively updates or revises the prior probability by incorporating the observed information contained within (B) into the model (Mendenhall and Reinmuth, 1974). In this instance, the particular phenomena (B) is some predictor variable, such as geology or a geochemistry anomaly, and the known end effect (D) is the response variable (mineral deposits).

The weights for each predictor variable map class are used to update the prior probability of the occurrence of a deposit, producing a revised posterior probability with the introduction of each subsequent layer of evidence (a binary- or multi-class mineral predictor map). As new evidence is introduced, the prior probability surface is modified, either increasing or decreasing according to the evidence, to produce a posterior probability surface (Bonham-Carter et al., 1991). Where the predictor variable map class is present, the value of  $W^+$  is added. Where the predictor variable map class is absent,  $W^-$  is added. Where a map pattern is unknown or incomplete,  $W=0$ , so that the predictor variable map class neither causes an increase nor a decrease from the prior probability (Agterberg, 1989a). Thus, given the presence of a favourable predictor variable (i.e.—a map class with a high  $W^+$ , such as an associated geochemical anomaly), the posterior probability of the occurrence is higher than the prior probability (Bonham-Carter, 1994a). The posterior probability surface is output as a map which represents the incorporation of all layers of evidence and predicts the distribution of the response variable.

In practice, WOE uses the natural logarithm of odds, also known as log odds or *logits*, formulation of Bayes' Rule, which may possibly be more familiar in terms of probabilities and multiplicative terms. In this form, probabilities are expressed as logits, which make the model linear and additive, and is expressed as:

$$\ln O(D|B_1^{k(1)} B_2^{k(2)} \dots B_n^{k(n)}) = \ln O(D) + \sum_{j=1}^n W_j^{k(j)} \quad B.7$$

where:  $O$  are odds, defined as  $O=P/(1-P)$ ;  $D$  is the number of unit cells containing a mineral deposit;  $j = 1,2,3\dots n$  binary-class predictor map patterns;  $B_j$  is the area of the  $j$ -th predictor variable map pattern;  $k(j)$  is (+) for presence or (-) for absence of the  $j$ -th predictor variable map pattern;  $W_j$  is the spatial weight of association for the presence and absence of the  $j$ -th predictor variable map pattern.

The posterior logit of a cell containing a mineral deposit is obtained by the adding appropriate weights ( $W^+$  or  $W^-$ ) for presence or absence of the binary-class predictor maps to the prior logit. The order of the calculations are as follows:

1. Calculation prior logit from prior probability, using  $O = P / (1-P)$ .
2. Addition of the prior logit to the sum of the weights to derive the posterior logit.
3. Conversion of the posterior logits to posterior odds.
4. Conversion of posterior odds to posterior probability.

As the final step, a user-defined classification scheme is applied to the calculated posterior probabilities to produce a thematic map of mineral potential. Each mineral potential map class

represents a unique overlap condition between binary- and/or multi-class predictor maps (which may consist of a single polygon, or most often, a number of polygons that collectively compose a mineral potential map class; see [section B.2.2](#)). In practice, this procedure can be carried out on a unique conditions table associated with a unique conditions map. The implementation of this procedure is described below in [section B.5.4](#).

## B.3 Conditional Independence

### B.3.1 Introduction

The robustness of a posterior probability map is in part dependent on the *conditional independence* (CI) of the predictor variable map patterns to one another (binary-class mineral predictor map patterns), with respect to the response variable (mineral deposit point occurrences). The posterior probability map is adversely affected if, at the locations of the known mineral occurrences, the presence of a mineralization-favorable map pattern in one layer of evidence is dependent on the presence of a mineralization-favorable map pattern in another layer of evidence. Conditional independence (CI) is assumed to exist, and is necessary if the calculated posterior probabilities are to be strictly accurate (Agterberg, 1989b; Bonham-Carter, 1994a). The degree to which this assumption is satisfied can be tested for, and the purpose of such a test is to determine the magnitude of any binary-class predictor map pattern dependencies and to identify the map(s) that are responsible for the dependency. If a map is found to be in serious violation of the assumption of CI, it can then be (1) rejected from the model, (2) combined with another map in order to minimize the dependency, or (3) modified in some way as to reduce the problem (for more information, see Agterberg et al., 1990; Bonham-Carter, 1994a). Violation of CI results in either the over-estimation or under-estimation of posterior probabilities during the Bayesian map overlay procedure, and the expected mineral deposit frequencies either notably exceed or fall short of the observed deposit frequencies in the most and least favorable areas of the mineral potential map (Agterberg et al., 1990). In essence, the most and least favorable binary-class predictor map overlap areas are “artificially” strengthened or weakened in the posterior probability mineral potential map. In practice, CI is always violated to some degree (Bonham-Carter, 1994a), but it is important to understand how serious the violation is so that the appropriate action can be taken to minimize the problem and so that proper judgments can be made when evaluating areas of high mineral potential.

Two tests are applied to determine whether the assumption of conditional independence is satisfied: a *pairwise* test and an *overall* goodness-of-fit test, both of which make use of the observed versus the expected number of observations (mineral deposits). The pairwise method determines CI between all possible pairings of the binary-class predictor maps by calculating a  $\chi^2$  (chi-square) statistic for each map pair, and comparing the calculated value of  $\chi^2$  to the tabled value of  $\chi^2$  having one degree of freedom (Bonham-Carter, 1994a). The overall method is a simple procedure involving the relative comparison of predicted versus observed deposits—if the total predicted number of deposits is much larger than the total observed number (greater than ~10-15%), it suggests that CI is being violated (Bonham-Carter, 1994a).

The overall goodness-of-fit can be evaluated using the Kolmogorov-Smirnov (K-S) statistic. The K-S statistic is based on the maximum deviation of the observed number of deposits from the

predicted number. The K-S statistic makes as few assumptions about the distribution of the data as possible (i.e.—it is non-parametric: it does not depend upon any assumptions regarding the normality or the distribution of the data), and generally has satisfactory efficiency and robustness properties (Davis, 1973; Chatfield, 1988). Non-parametric tests of model-fitting are usually used for ordinal scale data or data from a skewed or otherwise non-normal distribution, which therefore makes the K-S statistic particularly well suited for this mineral potential modelling application. The implementation of the pairwise and overall tests is given in [section B.5.5](#).

### B.3.2 Pairwise Test and the Chi-Square Statistic

The pairwise goodness-of-fit test measures conditional independence (CI) between all possible pairings of binary-class predictor maps (with respect to the mineral deposits) by calculating the  $\chi^2$  (chi-square) statistic for each map pair. CI may be present due to three-way or multi-way interactions, and testing for these cases is also possible, but for practical purposes, pairwise testing reveals the most serious CI violations (Bonham-Carter, 1994a).

Normally, the pairwise test is conducted *before* the binary-class predictor maps are combined in the Bayesian multi-map overlay procedure (*procedure ii*, [Fig. B.4ii](#)), so that problematic maps can be eliminated, combined, or modified as necessary. The test is performed using normal 2-by-2 contingency tables of observed and expected values (i.e.—number of deposits), and tests the null hypothesis ( $H_0$ ) that “*rows and columns are independent*” (the assumption of CI)—that is, that the probability of an observation falling in any particular column does not depend on which row the observation is in, and vice versa (Chatfield, 1988; the application of this test to mineral potential modelling is explained in detail in Bonham-Carter, 1994a, p. 313). [Table B.5](#) shows the algebraic layout of the contingency table, and represents four overlap conditions between two binary-class map patterns.

	B <sub>1</sub> Present	B <sub>1</sub> Absent	Totals:
B <sub>2</sub> Present	$N(B_1 \_ B_2 \_ D)$	$N(\&_1 \_ B_2 \_ D)$	$N(B_2 \_ D)$
B <sub>2</sub> Absent	$N(B_1 \_ \&_2 \_ D)$	$N(\&_1 \_ \&_2 \_ D)$	$N(\&_2 \_ D)$
Totals:	$N(B_1 \_ D)$	$N(\&_1 \_ D)$	$N(D)$

**Table B.5.** Contingency table for testing conditional independence, based on cells containing deposits only. **N** is the count of unit cells; **B** refers to the presence or absence of a binary pattern, which is numerically represented in unit cells (subscript 1 or 2 denoting two different binary patterns); **D** refers to the presence of a deposit (a point occurrence), which is numerically represented in unit cells. The four values within the table are either the expected values assuming independence, calculated from the margin totals, or the observed values measured from the maps. There is 1 degree of freedom. From Bonham-Carter (1994a).

The  $\chi^2$  statistic is applied only where the mineral deposit binary pattern is present and determines if two binary-class predictor map patterns are conditionally dependent or independent. To calculate the  $\chi^2$  statistic, the observed and expected areas are required (i.e.—the number of deposits, represented in unit cells, where each deposit equals 1 if a 1 km<sup>2</sup> unit cell was selected for the analysis). The term  $N(B_1 \_ B_2 \_ D)$  in the contingency table represents the observed number of deposits occurring in the overlap region where both  $B_1$  and  $B_2$  are present, and is counted directly from a map or the deposit dataset (Bonham-Carter, 1994a). The predicted or

expected number of deposits in the overlap region is calculated by multiplying the number of deposits on  $B_1$  times the number on  $B_2$  divided by the total number of deposits, or as expressed algebraically in terms of the contingency table,  $N(B_1 \cap D) \cdot N(B_2 \cap D) / N(D)$  (multiplying the marginal frequencies and dividing by the total).

Once the observed and expected values have been determined,  $\chi^2$  is calculated using the expression:

$$\chi^2 = \sum_{i=1}^N \frac{(Observed_i - Expected_i)^2}{Expected_i} \quad \text{B.8}$$

which, for this example using the contingency table shown in Table B.5,  $N=4$  and  $i$  refers to the  $i$ -th binary-class predictor map pattern.

If conditional *dependency* exists, the predicted number of deposits in the overlap region of the two predictor binary map patterns will be higher or lower than the observed number; if conditional *independency* exists, the expected number of deposits should be equal to the number of observed deposits.

The results of the pairwise test are typically presented in the form of cross-tabulation tables consisting of a matrix-layout of  $\chi^2$  values for all pairings of binary-class predictor maps. The value of  $\chi^2$  indicates the degree of independency or dependency between predictor binary map pairs—the larger the values, the greater the dependency. The values of  $\chi^2$  are compared to a “tabled” value of  $\chi^2$  with one degree of freedom (DF—number of rows minus one, times, number of columns minus one, therefore  $DF = 1$ ) to determine if  $H_0$  (the null hypothesis that the binary-class predictor map patterns are conditionally independent) is to be rejected or accepted, and at what level of probability  $H_0$  should be rejected. For weights of evidence modelling, a probability level threshold of 98% ( $\chi^2_{0.98,1} = 5.41$ ) or 95% ( $\chi^2_{0.95,1} = 3.84$ ) is sufficient (usually one cutoff is chosen). Test values of  $\chi^2$  that are greater than either of these two tabled cutoff values indicate that the null hypothesis (CI) should be rejected.

### B.3.3 Overall Test and the Kolmogorov-Smirnov Statistic

The overall goodness-of-fit test is a measure of the conditional independence (CI) between all of the layers of evidence in a model as a whole. It is normally performed *after* the binary-class predictor maps are combined in the Bayesian multi-map overlay procedure, where the posterior probabilities are calculated for each unique overlap condition between binary-class predictor maps (which collectively make up the mineral potential map).

The overall test is very simple, consisting of a comparison of the predicted number of deposits to the observed number of deposits. In weights of evidence modelling, the prior probability is assumed to be the average known mineral deposit point density, therefore, the predicted number

of deposits occurring within a unique overlap condition between binary-class predictor maps is determined by summing the areas of the polygons composing each unique overlap condition map class (i.e.—the total area for a particular unique condition map class), multiplied by the posterior probability of that map class (see Bonham-Carter, 1994a, p. 317).

The calculation may be expressed as:

$$N(D)_{calc} = \sum_{k=1}^m P_k N(A)_k \quad B.9$$

where:  $N(D)_{calc}$  is the predicted (calculated) number of deposits, which is determined by adding together the product of the area in unit cells,  $N(A)$ , times the posterior probability,  $P$ , for all unique condition map classes ( $k=1,2,...m$ ) derived from the overlapped binary-class predictor maps that compose the mineral potential map.

A 10% to 15% difference in the number of predicted deposits over the number of observed deposits indicates that some degree of redundancy exists in the predictor variables (the layers of evidence), suggesting that CI is being violated, and may warrant a check of the pairwise tests and some sort of remedial action (Bonham-Carter, 1994a). Unlike the pairwise goodness-of-fit test, the overall test is not a formal test, and in practice, the predicted number of deposits for the weights of evidence modelling method is always higher than the observed (Bonham-Carter, 1994a).

The overall goodness-of-fit can also be assessed using the Kolmogorov-Smirnov (K-S) statistic (non-parametric). Normally, K-S test statistics is used when the expected model can be completely specified (i.e.—the total number of discrete events, or mineral deposits, is correctly predicted), and loses its validity when the expected relative frequency is not approximately equal to 1 at the largest value (Agterberg et al., 1993). For this study, an approximate K-S test is applied, where the relative cumulative predicted and observed mineral deposit frequencies (i.e.—the cumulative occurrence proportions) are constrained to reach a maximum of 1.0 (see Agterberg et al., 1993; Bonham-Carter et al., 1989). Agterberg et al. (1993) pointed out that this has the advantage of satisfying the assumptions for the K-S test (that the expected roughly equals the observed number of deposits), but the disadvantage of failing to recognize predicted frequencies that may be too large. Another advantage is that, because it is not necessary to group observations into arbitrary categories (binning the data), the K-S test is more sensitive to the tails of the distribution, as compared with tests that require binning, such as with the pairwise test which uses the  $\chi^2$  statistic (Davis, 1986).

The K-S statistic is based on the maximum deviation of the observed frequencies from the expected frequencies, and is expressed in Davis (1973, p. 276) as:

$$KS = \text{maximum } |O - E| \quad B.10$$

where O and E are the observed and expected frequency of occurrences and  $||$  denotes absolute

values. In this instance, the K-S statistic is being applied to the observed and expected distributions, not a theoretical Poisson distribution as given in Davis (1973). A more detailed treatment is given by Davis (1986, p. 99) and Wright (1996, p. 114).

The null hypothesis ( $H_0$ ) for the K-S statistic states that there is no significant difference between the observed and predicted distributions. The null hypothesis is rejected if the absolute difference between the relative cumulative predicted and the relative cumulative observed frequency distributions (the “*K-S statistic*”) is larger than the tabled K-S statistic critical value at a specified level of significance. The null hypothesis is “two-tailed”, because it is rejected if the observed series is either significantly too high or too low, as compared to the predicted distribution (Davis, 1973). Where the total number of observations is greater than 40, the critical K-S value for the 5% ( $\alpha = 0.05$ ) level of significance can be computed as  $1.36' / \sqrt{n}$ , where  $n$  is the total number of observed series of events (Davis, 1973), which in this case is the total number of unique condition map classes for a given mineral potential model, not the total number of mineral deposits. If one or more of the binary-class predictor map patterns were conditionally *dependent* with respect to the mineral deposits pattern (i.e.—CI is violated), the expected frequencies would overestimate the observed frequencies where the posterior probabilities are relatively large and would underestimate the observed frequencies where the posterior probabilities are small (Agterberg, 1989b).

## B.4 Posterior Probability Uncertainty

### B.4.1 Introduction

The posterior probability mineral potential map may optionally be augmented with a map of the posterior probability uncertainty. Agterberg et al. (1990) and Bonham-Carter et al. (1989) pointed out that if one or more binary-class predictor map patterns is unknown or incomplete in a given area of the study region, the calculated posterior probability for that area has less certainty than those based on more, or all, of the binary-class predictor map patterns. A map of posterior probability uncertainty can be separately compared to a posterior probability map, or the two can be combined so that the uncertainty map masks out regions of the posterior probability map that have a high uncertainty factor.

### B.4.2 Source and Types of Uncertainty

An important aspect to interpreting a mineral potential map is recognizing and quantifying the uncertainty inherent to the posterior probabilities. The two primary sources of uncertainty are: (1) the uncertainty due to variances in weight estimates ( $W^+$  and  $W^-$ ); and (2) the uncertainty due to one or more of the binary-class predictor maps having incomplete coverage (i.e.—missing data) (Bonham-Carter et al., 1989).

Agterberg et al. (1990) showed that the variance of the weights ( $W^+$  and  $W^-$ ) for each map can be calculated as:

$$s^2(W_j^+) = \frac{1}{N(B_j - D)} \% \frac{1}{N(B_j - \bar{D})}, \text{ and } s^2(W_j^-) = \frac{1}{N(\bar{B}_j - D)} \% \frac{1}{N(\bar{B}_j - \bar{D})} \quad \text{B.11}$$

where  $N(B_j - D)$  is the number of unit cells where both deposits and the  $j$ -th binary-class predictor map pattern are present, and the remaining terms are defined similarly. In most cases, the second term in both expressions is very small, and approaches zero as the unit cell becomes infinitely small. The first term in both expressions, which involve the count of unit cells with deposits, are unaffected by unit cell size. Bonham-Carter et al. (1989) noted that these expressions use an asymptotic result which assumes that the number of deposits is large. For cases with a small number of deposits, the variances of the weights become large (Wright, 1996).

The summed effect of uncertainty due to the variances of the weights for each unique overlap condition of binary-class predictor maps was shown by Agterberg et al. (1990) to be:

$$s^2_{(P_{post})} = \left[ \frac{1}{N(D)} \sum_{j=1}^n s^2(W_j^k) \right] C P_{post}^2 \quad B.12$$

where the superscript  $k$  is (+) for presence and (−) for absence of the  $j$ -th binary-class predictor map pattern, and the other terms are defined as before.

Agterberg et al. (1990) and Bonham-Carter et al. (1989) pointed out that if one or more of the binary-class predictor map patterns is unknown or incomplete in a given region, the estimated posterior probability for areas with missing data are more uncertain than those based on more, or all, of the predictor variable map patterns. Bonham-Carter et al. (1989) indicated that, in order to estimate the uncertainty in posterior probability due to incomplete or missing data in the  $j$ -th binary-class predictor map, the following variance component can be calculated:

$$s_j^2(P_{post}) = \{P(D^*B_j) \& P(D)\}^2 P(B_j) + \{P(D^*\overline{B_j}) \& P(D)\}^2 P(\overline{B_j}) \quad B.13$$

where, for any unique overlap condition between binary-class predictor maps,  $P(D)$  is the posterior probability calculated from the non-missing binary-class predictor maps. The terms  $P(D^*B_j)$  and  $P(D^*\overline{B_j})$  are the updated posterior probabilities assuming that the  $j$ -th binary-class predictor map pattern is present and absent, respectively (Bonham-Carter et al., 1989).

The uncertainties due to weights and due to missing data may be examined separately, or combined to produce a *total* uncertainty for a given unique overlap combination of binary-class predictor maps, which is calculated as the variance due to weights, plus, the sum of variances due to missing data (Bonham-Carter et al., 1989), and is expressed as:

$$s^2_{(total)} = s^2_{(weights)} + \sum_{j=1}^n s_j^2_{(missing)} \quad B.14$$

where the terms are defined as before.



The uncertainty due to the weights, which includes the uncertainty of the prior probability, is in general correlated to the posterior probability, and therefore maps of variance of weights have the same trends as the posterior probability maps (Bonham-Carter et al., 1989).

In addition to the uncertainties due to weights variances and missing data, a *relative certainty* (variance) of the posterior probability can be determined by dividing the posterior probability by its standard deviation (i.e.—a “studentized” posterior probability), which, in effect, applies a student t-test (based on a normal distribution) to determine whether the posterior probability is greater than zero for a given level of statistical significance (i.e.—compared to a tabled t-value) (Bonham-Carter et al., 1989; Agterberg et al., 1993). The larger the t-value over the critical tabled t-value cut-off, 1.645 for a significance of 95% for example, the greater the certainty of the posterior probability. The relative certainty is often more useful than the weights variances or missing data uncertainties because it indicates the degree of confidence to which the posterior probabilities are “real”, as opposed to being an artifact of “chance” effects (or due to chance). As compared to the uncertainty due to the weights variances or missing data, relative certainty is generally not as highly correlated to the posterior probability.

Ideally, the four uncertainty factors (weight variances, missing data, total, and relative) may be used to create classified uncertainty maps for comparison to the posterior probability mineral potential map, or the uncertainty factors may be combined in various ways and reclassified to a binary-class map which can be used to “mask-out” areas of the mineral potential map that are deemed to be too uncertain (Bonham-Carter et al., 1989; Bonham-Carter, 1994a). This procedure is discussed below in [section B.5.4](#).

## **B.5 Practical Implementation of the Modelling Procedures**

### **B.5.1 Introduction**

Weights of evidence modelling may be implemented (1) internal to the GIS, using map and “unique conditions” modelling techniques, or (2) external to the GIS environment, using unique conditions modelling in tandem with DOS and OS/2 FORTRAN utilities to expedite the various statistical procedures described in the preceding sections. The modelling carried out in this study used a combination of internal and external implementations. The FORTRAN utilities used to calculate the spatial weights of association ( $W^+$  and  $W^-$ ), the posterior probabilities, and the uncertainty factors for weights of evidence modelling were provided by G.F. Bonham-Carter (1996, personal communication) of the Geological Survey of Canada. Wright (1996) contains detailed procedures for implementing weights of evidence both internally and externally to the GIS (see Wright's appendix B-2), and gives a detailed history and summary of the FORTRAN utilities (see Wright's appendix B-2, and p. 138). The FORTRAN utilities are included here in Appendix B.

### **B.5.2 Estimation of the Spatial Weights of Association**

The information presented under this heading represents weights of evidence procedure *i*, as discussed in sections [B.2.3](#) and [B.2.4](#), and illustrated in [Figure B.4](#).

In order to generate binary-class mineral predictor maps, spatial weights of association ( $W^+$  and  $W^-$ ) must be calculated between the deposits and each class of each multi-class evidence map to determine which class(es) of an evidence map has the strongest correlation to the deposit distribution. This is done in part internally and externally to the GIS.

The calculation of the weights is done externally using a the FORTRAN utility WTS.EXE (or any of its various incarnations). WTS.EXE requires two files as input: (1) an area analysis of the multi-class evidence map to be processed (Table B.3), and (2) a point-in-polygon analysis between the evidence map and the mineral deposits, where the evidence map class is appended to the deposit point dataset (Table B.4). These two input files are generated within the GIS first, then input into WTS.EXE. WTS.EXE outputs a file containing two area-cumulative and one non-area-cumulative tabulation of the spatial weights of association and contrast (C) between each multi-class evidence map unit with respect to the deposit distribution (Table B.6).

The non-area cumulative table is normally applied to nominal (or categorical) scale evidence datasets, such as a geological map, to determine which map units have higher spatial associations with the deposits (which are more “favorable”). The two area-cumulative tables, one ascending and the other descending, are normally applied to ordinal (or ranked) or higher-scale evidence datasets, such as distance from faults or geomagnetic anomaly, and are used to determine optimum thresholds or cut-offs between successive favorable and not-so-favorable evidence map units (i.e.—a boundary between “background” and “anomalous”; this is further discussed in the following section). The weight values ( $W^+$  and  $W^-$ ) should be evaluated in a relative sense, and augmented with the contrast (C; strength of the spatial association) and with the variances of the weights factors (standard deviations of  $W^+$ ,  $W^-$ , and C, and “studentized” C) when determining the favorability of a particular evidence map unit.

### B.5.3 Generation of Binary-Class Mineral Predictor Maps

The multi-class maps analysed above are reclassified to binary maps that serve as layers of evidence to predict the pattern of mineral deposits. Multi-class maps can be used as layers of evidence in weights of evidence modelling, but the number of possible overlap conditions becomes increasingly large and unwieldy (see Bonham-Carter, 1994a, 1994b). The usage of binary maps also yields more stable and meaningful weights of spatial association, and facilitates interpretation of the mineral potential map (Bonham-Carter, 1994a). The reclassification of multi-class maps into binary maps involves both objective and subjective methods. The spatial weights of association ( $W^+$  and  $W^-$ ) are calculated in order to quantify the spatial relationship between the mineral deposit pattern and the pattern of a map that is used for prediction. The weight estimates, the contrast between the weights ( $C = W^+ - W^-$ , which gives a useful measure of the strength of the spatial association), and the variances of the weights and the contrast, are fundamental to isolating favorable units from the unfavorable or “background” units, and hence for determining which map units are optimal for predicting the mineral deposit pattern. In many cases, however, an optimum threshold between the favorable and not-so-favorable unit(s) is not always clearly defined, and subjective techniques, tempered with a good amount of geologic and other practical considerations, are necessary to determine the best cutoff(s).

Nominal (or categorical) scale multi-class maps, such as geological maps, are reclassified to binary-class maps by combining individual favorable units, constrained only by what seems both

geologically reasonable and numerically advantageous (Bonham-Carter, 1994b). The spatial weights of association are recalculated to determine new values for  $W^+$  and  $W^-$  for the binary-class predictor map. Weight estimates may even be recalculated on various groupings of favorable units to determine which reclassification combination optimises the spatial association between the deposits and the map pattern.

For maps with an ordinal (or ranked), interval, or ratio level of measurement, such as geophysical or geochemical anomaly maps, or distance buffer maps, weights are calculated using successive cumulative map unit areas—weights are calculated for each successive map class using the area of the map class being evaluated plus the area of the previously evaluated map classes. Reclassification to a binary-class map respects the map class sequence, where the threshold cutoff for the optimum number of units to include in the binary-class predictor map is determined by the number of successively combined units which collectively demonstrate the strongest spatial association (Bonham-Carter, 1994a, 1994b).

In practice, a graph is constructed which plots area-cumulative  $C$  along the y-axis and distance buffers or anomaly intensities along the x-axis, as shown in [Figure B.6](#). In this example, the area-cumulative  $C$  peaks at the 3rd interval on the x-axis. For buffer zone distances, which are

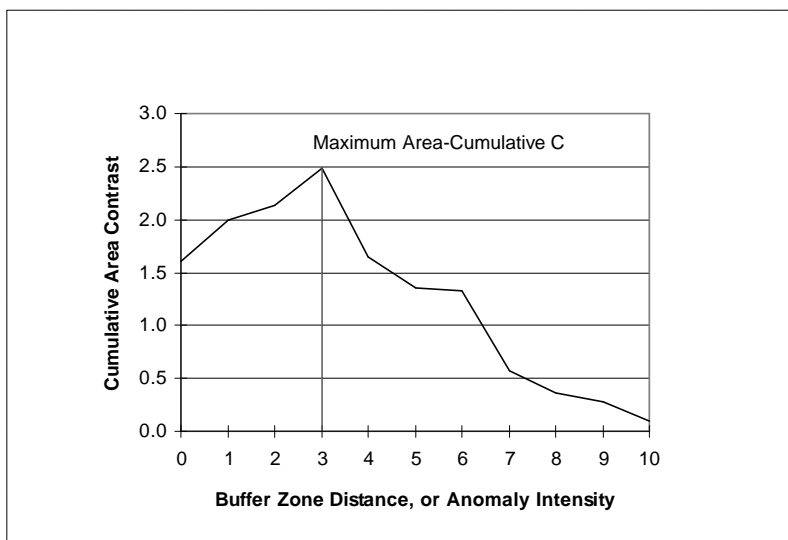


**Figure B.6.** Graph of area-cumulative contrast versus buffer zone distances or anomaly intensity values.

area cumulative from the closest to the farthest distance interval from the buffered object (0 to 10), the combined map classes 0 to 3 show the highest strength of spatial association. For a geophysical or geochemical anomaly, area cumulative from the highest anomaly value to lowest (10 to 0), the combined map classes 10 to 3 show the highest strength of spatial association.

All binary-class mineral predictor maps were coded as:

- 0 class—Predictor pattern missing (no data).
- 1 class—Predictor pattern absent (pattern not favorable).
- 2 class—Predictor pattern present (pattern favorable).

For additional information, see Bonham-Carter (1994a, p. 319-325), and Wright (1996, appendix B-1).

#### **B.5.4 Bayesian Map Overlay, and Generation of Mineral Potential and Posterior Probability Uncertainty Maps**

Once the binary-class predictor maps (layers of evidence) have been generated, the Bayesian multi-map overlay procedure may be performed. Of all the weights of evidence modelling procedures, the Bayesian map combination procedure is the most flexible in terms of implementation. It may be carried out purely within the GIS using a map modelling technique, or external to the GIS using a unique conditions map and table modelling technique in conjunction with a FORTRAN utility to calculate the posterior probabilities. Both the internal and external implementation methods of the Bayesian multi-map overlay procedure were performed in this study.

In the map modelling approach, internal to the GIS, the binary-class predictor maps are combined using an equation which specifies the weights associated with each layer of evidence and evaluates the model at each pixel. Using a predetermined classification scheme, the posterior probability values are grouped into numbered intervals which are assigned to the pixel (or in other words, assigned as the output map class). A “quantiles” approach to creating a classification scheme is often used. This is an “area-based” percentiles scheme where the posterior probability class intervals (the breakpoints) are determined so that each of the posterior probability classes is roughly equal in area (see TYDAC Technologies Inc., 1993, *Reference Manual*, p. 5-56, for more information). An example of a GIS map modelling equation used to combine the layers of evidence is shown in [Table B.7](#). A detailed review of the implementation of this technique is given by Wright (1996, appendix B-2(a)).

A more powerful technique is unique conditions map and table modelling, which is implemented both internal and external to the GIS. The approach involves: (1) the generation of a unique conditions map and associated (linked) attribute table; (2) the execution of an external FORTRAN utility (PREDICT.EXE) which calculates probabilities and uncertainty factors for various map combination methods, including weights of evidence, Bayesian (direct), ordinary regression, logistic regression, and Dempster-Shafer; and (3) the reclassification of the unique conditions map using the posterior probabilities and uncertainty factors calculated by PREDICT.EXE. The main advantage of this method is calculation of the various posterior probability uncertainty factors by PREDICT.EXE, which for each overlay operation includes uncertainty due to weights variances, uncertainty due to missing data, the total uncertainty (weight variances plus missing data), and relative certainty (t-values). PREDICT.EXE also calculates the total number of expected deposits which are predicted by the model, as well as generating a table of spatial weights of association ( $W^+$  and  $W^-$ ) similar to WTS.EXE. Other advantages of this method over the internal map modelling approach is that it minimizes the

number of times the model has to be evaluated, and PREDICT.EXE outputs all the data to an ASCII table, which can be imported into any number of applications for further analysis (x-y plots, etc.).

In the first step, a unique conditions overlay map is generated within the GIS from the binary-class predictor maps which make up the “spatial framework” of mineral potential model. A unique conditions overlay is a multi-map combination technique that produces: (1) a single map composed of unequal-area polygons which are assigned the same class value if they consist of the same overlap combination or characteristic of input maps, and (2) an associated (linked) attribute table that contains the unique overlay combinations of map classes which compose a particular unique conditions map class (see [Fig. B.3](#); for additional details, see Bonham-Carter, 1994a, p. 235-238; Bonham-Carter, 1991, p. 172). The objective is to perform the modelling or data analysis on the table, rather than using the input maps directly, and to reclassify the unique conditions map according to the results, which are directly linked to the unique conditions map via the unique conditions table (see [Table B.2](#)).

In the second step, two tables are exported from the GIS and input into PREDICT.EXE: (1) the unique conditions attribute table ([Table B.2](#)), generated as a result of the unique conditions overlay operation between the various binary-class mineral predictor maps ([Fig. B.3](#)); and (2) a table containing the unique conditions map class value appended to the deposit point locations (i.e.—generated by a point-in-polygon analysis between the deposits and the unique conditions map; see [Table B.4](#) for an example). PREDICT.EXE performs the overlay operation using the information contained in the unique conditions and point-in-polygon attribute tables, and for each unique conditions map class, it calculates a prior probability and the various uncertainty factors ([Table B.8](#)).

In the third step, the output table from PREDICT.EXE ([Table B.8](#)) is imported into the GIS and used to reclassify the unique conditions map by posterior probability or any of the uncertainty factors. The map reclassification scheme is created as indicated for the map modelling method above. In this manner, a posterior probability mineral potential map, an uncertainty due to weights variances map, an uncertainty due to missing data map, a total uncertainty map, and a relative certainty map may be easily generated for a particular mineral potential model.

### **B.5.5 Conditional Independence Testing**

Conditional independence testing, both the pairwise and overall tests, was implemented external to the GIS. The FORTRAN utility CI.EXE was used to conduct the pairwise test, whereas a spreadsheet program was used to carry out a graphical solution (x-y plot) for the overall test.

For the pairwise test, the same tables that were input into PREDICT.EXE (see [section B.5.4](#) above) were input into CI.EXE (a unique conditions attribute table containing the area and a listing of overlain map class combinations that compose each unique conditions map class, and a table containing the unique conditions map class associated with every mineral deposit). Example output is shown in [Table B.9](#).

The overall test was performed using data contained in the output table generated by PREDICT.EXE (see Table B.8). The data were imported into the spreadsheet program and processed as follows:

1. The expected number of deposits for each unique conditions map class was calculated by multiplying the map class area by its respective posterior probability.
2. *Relative* frequencies for the number of expected and the number of observed deposits were calculated by normalizing the observed and predicted number of deposits to 1, respectively (i.e.—for the observed deposit frequency, the number of observed deposits associated with each unique condition map class is divided by the total number of observed deposits; for the expected deposit frequency, the number of expected deposits predicted for each unique condition map class is divided by the total number of expected deposits).
3. The observed and predicted relative frequencies were sorted in ascending order by the posterior probability value. Note that the observed and/or predicted frequencies may also be sorted on a second or third sort key, but whether sorted or not, the absolute maximum difference between the two frequencies will not be affected (e.g.—*1st sort key*: posterior probability; *2nd sort key*: observed relative frequency; *3rd sort key*: predicted relative frequency).
4. The observed and predicted relative frequencies were cumulatively summed from lowest posterior probability to highest (i.e.—in ascending order).
5. The cumulative relative predicted frequency was subtracted from the cumulative relative observed frequency (observed minus predicted) to determine the absolute maximum difference between the observed and predicted distributions.
6. The observed and expected cumulative relative frequencies were plotted against their common (shared) posterior probabilities (the observed and expected cumulative relative frequencies are plotted as two separate data series on the y-axis; the posterior probabilities are plotted as one data series on the x-axis).
7. The differences between the cumulative relative predicted frequency and the cumulative relative observed frequency were plotted against their common (shared) posterior probabilities (the differences are plotted as one data series on the y-axis; the posterior probabilities are plotted as one data series on the x-axis). The absolute maximum datum point on this curve is the K-S statistic used for comparison to the critical tabled K-S value.

An example of the graphical output for the overall test is shown in Agterberg (1989b, p. 81; 1993, p. 28), Davis (1986, p. 101), and Bonham-Carter et al. (1989, p. 180), as well as in Chapter 7. Interpretation of the output for both conditional independence tests is discussed in [section B.3](#) above.

```

ID geo-rc1
TITLE GEOLOGY.MAP Reclassification Table
TABTYPE 4
FTYPE free
KEYFIELD 0
1 3 3.000000 0 geoclass GEOLOGY.MAP map unit class
2 50 30.000000 0 name Map unit name
3 25 5.000000 0 code Map unit abbreviation code
4 1 3.200000 0 area_% Area map unit covers in relative %
5 3 6.000000 0 area_km Area map unit covers in Km2
6 3 1.000000 0 0-6ma Igneous units 0-6 Ma in age
7 3 2.000000 0 6-17ma Igneous units 0-6 Ma in age
8 3 2.000000 0 17-34ma Igneous units 17-34 Ma in age
9 3 2.000000 0 34-43ma Igneous units 34-43 Ma in age
10 3 3.000000 0 felsic Igneous units felsic in composition
11 3 2.000000 0 inter Igneous units intermediate in composition
12 3 2.000000 0 mafic Igneous units mafic in composition
13 3 3.000000 0 igneous Igneous rock units only
14 3 1.000000 0 rx_type Rock type reclass.--sed, ign, meta.
15 3 2.000000 0 cmp/age Rock compositions/packages primary, age secondary
16 3 2.000000 0 age/cmp Age primary, rock compositions/packages secondary
17 3 2.000000 0 simple Simplified according to major rock packages
DATA
1 "Alluvium" " " "Qa" " 43.22 122395 0 0 0 0 0 0 0 0 0 1 1 1 1
2 "Playa, Marsh, Alluvial-Flat" " " "Qp" " 4.61 13064 0 0 0 0 0 0 0 0 0 1 1 1 1
3 "Landslide" " " "Qls" " 0.17 487 0 0 0 0 0 0 0 0 0 1 1 1 1
4 "Moraine" " " "Qm" " 0.09 250 0 0 0 0 0 0 0 0 0 1 1 1 1
5 "Older Alluvium" " " "Qtoa" 1.03 2907 0 0 0 0 0 0 0 0 0 1 1 1 1
6 "Ryo Flows, Shallow Intrusives" " " "Qtr" " 0.00 5 6 0 0 0 6 0 0 6 2 12 5 6
7 "Andesite Flows, Breccias" " " "Qta" " 0.09 265 7 0 0 0 0 7 0 7 2 12 5 6
8 "Basalt Flows" " " "Qtb" " 0.58 1648 8 0 0 0 0 0 8 8 2 14 6 7
9 "Lacustrine Sedimentary Rocks" " " "Qts" " 0.22 623 0 0 0 0 0 0 0 0 1 1 1 1
10 "Rhyolitic Intrusive Rocks" " " "Tri" " 0.10 275 0 0 0 0 10 0 0 10 2 12 5 6
11 "Mafic-Intermediate Intrusives" " " "Tmi" " 0.05 134 0 0 0 0 0 0 11 11 2 14 6 7
12 "Dioritic-Granitic Intrusives" " " "Ti" " 0.17 490 0 12 12 12 0 12 0 12 2 12 5 6
13 "Breccia" " " "Tbr" " 0.03 89 0 0 0 0 0 0 0 0 1 11 4 5
14 "Silicic Ash-Flow Tuffs" " " "Tt3" " 3.42 9675 0 14 0 0 14 0 0 14 2 11 4 5
15 "Tuffs, Ryo Flows, Intrusives" " " "Trt" " 0.14 387 0 0 0 0 15 0 0 15 2 12 5 6
16 "Ryo Flows, Shallow Intrusives" " " "Tr3" " 3.28 9301 0 16 0 0 16 0 0 16 2 12 5 6
17 "Andesite, Intermediate Rocks" " " "Ta3" " 1.59 4508 0 17 0 0 0 17 0 17 2 12 5 6
18 "Andesite & Basalt Flows" " " "Tba" " 2.54 7180 0 18 0 0 0 18 0 18 2 14 6 7
19 "Basalt Flows" " " "Tb" " 1.74 4925 0 0 0 0 0 0 19 19 2 14 6 7
20 "Banbury Formation" " " "Tbg" " 1.33 3779 0 0 0 0 0 0 20 20 2 14 6 7
...
...
...

```

**Table B.1.** Example of an attribute table used for map reclassification. In SPANS GIS, a table consists of a header section (above and including the line “DATA”), which describes the contents and format of a table, and a data section (below the line “DATA”). Polygon or map class attributes are arranged by row, one row for each polygon or map class. Each row is composed of fields (columns) containing spatial or non-spatial attribute information for a particular polygon or map class. This example shows part of a table used to reclassify the digital representation of the Stewart and Carlson’s (1978) geologic map of Nevada (Turner and Bawiec, 1991).



```

ID uqpr7
TITLE uqpr7
MAPID uqpr7
WINDOW nv 0 0 0 0
TABTYPE 5
FTYPE fixed
KEYFIELD 2
KEYBASE 0
NRECORD 154
  1  0 15.400000 0      area area
  2  4  7.000000 0      uqpr7 uqpr7
  3  4  7.000000 0 bfftbipr bfftbipr
  4  4  7.000000 0 bfplbipr bfplbipr
  5  4  7.000000 0 geobihi geobihi
  6  4  7.000000 0 geobilow geobilow
  7  4  7.000000 0 gisobipr gisobipr
  8  4  7.000000 0 knabipr knabipr
  9  4  7.000000 0 magbipr magbipr
DATA
  35810.4492      1      1      1      1      1      1      1      1
  35414.3555      2      1      1      1      1      2      0      1
  32857.1758      3      1      1      1      1      1      0      1
  28826.8594      4      1      1      1      1      2      1      1
  17017.4883      5      2      1      1      1      2      0      1
  15845.0723      6      1      1      1      1      2      0      2
  12352.0596      7      1      1      1      1      2      1      2
  11994.0527      8      1      1      1      1      1      1      2
  11739.1426      9      2      1      1      1      2      1      1
  11134.8115     10      1      1      1      1      1      0      2
  9268.6045      11      2      1      1      1      1      1      1
  9218.2227      12      2      1      1      1      1      0      1
  5113.7158      13      2      1      1      1      2      0      2
  4804.6558      14      2      1      1      1      2      1      2
  4047.9116      15      2      1      1      1      1      0      2
  3502.2903      16      2      1      1      1      1      1      2
  2172.3958      17      1      2      1      1      2      1      1
  1687.9227      18      1      2      1      1      2      1      2
  1501.7610      19      1      2      1      1      2      0      2
  1417.7291      20      1      2      1      1      2      0      1
  1397.7980      21      1      2      1      1      1      1      1
  1376.5876      22      1      1      1      1      2      2      1
  1198.1527      23      2      2      1      1      2      1      1
  997.4451       24      1      1      1      2      2      1      1
  899.9293       25      2      2      1      1      1      1      1
  876.3833       26      2      2      1      1      2      0      2
  842.8678       27      1      2      1      1      1      0      1
  821.7247       28      1      2      1      1      1      1      2
  ...
  ...
  ...

```

**Table B.2.** Example of a unique conditions map attribute table output from SPANS GIS. The table consists of a header section (above and including the line “DATA”), which describes the contents and format of the table, and a data section (below the line “DATA”). The data section shows the area of a unique conditions map class (column 1), the unique conditions map class ID number (column 2; the link to the map), and the unique combination of input map classes that compose the unique conditions map class (columns 3-9; corresponding to the map names listed in lines 3-9 of the header section). This table was created by a unique conditions overlay of seven binary-class maps, where 1 and 2 represent a map class and 0 indicates no map classes present.

## SINGLE MAP ANALYSIS

Map : geology - geology

Window : nv - Whole of Nevada - Full Screen

Class	Legend	Area % (%)	Cumm % Area	Area (km <sup>2</sup> ) (km <sup>2</sup> )
-----				
1	Alluvium	43.22	43.22	122395
2	Playa, Marsh, Alluvial-Flat	4.61	47.83	13064
3	Landslide	0.17	48.00	487
4	Moraine	0.09	48.09	250
5	Older Alluvium	1.03	49.12	2907
6	Ryo Flows, Shallow Intrusives	0.00	49.12	5
7	Andesite Flows, Breccias	0.09	49.21	265
8	Basalt Flows	0.58	49.79	1648
9	Lacustrine Sedimentary Rocks	0.22	50.01	623
10	Rhyolitic Intrusive Rocks	0.10	50.11	275
11	Mafic-Intermediate Intrusives	0.05	50.16	134
12	Dioritic-Granitic Intrusives	0.17	50.33	490
13	Breccia	0.03	50.36	89
14	Silicic Ash-Flow Tuffs	3.42	53.78	9675
15	Tuffs, Ryo Flows, Intrusives	0.14	53.91	387
16	Ryo Flows, Shallow Intrusives	3.28	57.20	9301
17	Andesite, Intermediate Rocks	1.59	58.79	4508
18	Andesite & Basalt Flows	2.54	61.32	7180
19	Basalt Flows	1.74	63.06	4925
20	Banbury Formation	1.33	64.40	3779
21	Ash-Flow Tfs, Tfs Sed Rocks	0.96	65.36	2713
22	Tuffaceous Sedimentary Rocks	5.19	70.55	14701
23	Horse Spring Formation	0.09	70.63	246
24	Continental Sedimentary Rocks	0.14	70.77	399
25	Silicic Ash-Flow Tuffs	6.72	77.49	19026
26	Ryo Flows, Shallow Intrusives	0.45	77.94	1278
27	Andesite, Intermediate Rocks	1.18	79.12	3347
28	Older Basalt Rocks	0.03	79.15	85
29	Tuffaceous Sedimentary Rocks	0.11	79.26	298
30	Silicic Ash-Flow Tuffs	0.56	79.82	1586
31	Ryo Flows, Shallow Intrusives	0.58	80.40	1649
32	Andesite, Intermediate Rocks	0.75	81.16	2137
33	Sedimentary Rocks	0.19	81.35	547
34	Continental Sedimentary Rocks	0.09	81.44	254
35	Continent Clastics, Limestone	0.05	81.49	143
36	Granitic Rocks, Central & East	0.11	81.60	309
37	Monzonite & Granodiorite	0.15	81.75	416
38	Granitic Rocks, West	0.82	82.56	2312
39	Qtz-Monzonite & Granodiorite	1.13	83.70	3211
40	Diorite	0.07	83.76	185
...				
...				
...				
99	Quartzite, Clastic, Carbonates	0.13	99.57	374
100	Granitic Rocks	0.08	99.65	233
101	Metamorphic Rocks	0.35	100.00	992
-----				
Total of 101 classes		100.00	100.00	283219

**Table B.3.** Map area analysis table output from SPANS GIS. Percent of total area, cumulative percent area, and area in km<sup>2</sup> are given for each map class. This example shows part of the area analysis table for the digital representation of the Stewart and Carlson's (1978) geologic map of Nevada (Turner and Bawiec, 1991).

```

ID geoarea
TITLE All MRDS Au and Ag Containing Deposits
MAPID geology
TABTYPE 2
FTYPE free
NRECORD 2690
  1  5 15.000000 0 morton Morton Coordinate
  2  3 1.000000 0 size Size of Occurrence (0-Unkn, 1-Large, 2-Medium, 3-Small)
  3  4 6.000000 0 geology GEOLOGY.MAP Map Class Number
DATA
    17ae6b8      1    101
    17b0ec3      1      1
    17b32ef      1    101
    17b8057      1      1
    17b85ae      1    101
    17b88a2      1    101
    17b8ad2      1    101
    17b9391      1    101
    17b9898      1    101
    17ba27a      1    101
    17ba880      1    101
    17bd561      1     17
    17c5a15      1    100
    17c7ed6      1    100
    17cd78b      1    100
    17cd78b      1    100
    17cfc4f      1    101
    17d4873      1    100
    17d48b1      1     17
    17d8928      1    101
    17e20b4      0      1
    17e25f8      0      1
    17e29c7      1      5
    17e2b94      0      5
    17e2bd1      1      5
    17e2c3c      2     17
    17e2c8f      1     17
    17e2e11      1     17
    17e2ec1      3     17
    17e3e1d      1    101
    17e3ec9      1    101
    17e6a8e      1    101
    17e8155      1      5
    17e833d      0     17
    17e8612      0     17
    17e8683      1     17
    17e8c09      1     17
    17e8c5b      1     17
    17e906d      1     12
    ...
    ...
    ...

```

**Table B.4.** Point-in-polygon analysis table output from SPANS GIS. The table consists of a header section (above and including the line “DATA”), which describes the contents and format of a table, and a data section (below the line “DATA”). The geographic position (column 1), the size (column 2), and the coincident map class (column 3) are given for each gold-silver occurrence. This example shows part of the point-in-polygon analysis table for the digital representation of the Stewart and Carlson’s (1978) geologic map of Nevada (Turner and Bawiec, 1991). The geographic positions of the gold-silver occurrences are given in Morton coordinates (for more information, see TYDAC Technologies Inc., 1993). Gold-silver occurrence size classification scheme is from the *Metallogenic Map of North America* (Guild, 1968).

Name of file: geolpr.WTS  
 Total no of points: 2690  
 Area of unit cell: 1.000000 sq. kms  
 Total area: 283219.000000 unit cells  
 283219.000000 sq. kms.

The following table is non-cumulative.  
 Areas in unit cells.

Class	Area	Points	W+	Sdt (W+)	W-	Sdt (W-)	C	Sdt (C)	Stud (C)
1	122395	198	-1.7776	.0711	.4955	.0202	-2.2731	.0739	-30.7446
2	13064	4	-3.4435	.5001	.0462	.0194	-3.4897	.5005	-6.9731
3	487	2	-.8435	.7086	.0010	.0194	-.8445	.7088	-1.1914
4	250	6	.9421	.4132	-.0014	.0194	.9435	.4137	2.2806
5	2907	16	-.5493	.2507	.0044	.0194	-.5537	.2514	-2.2019
6	5	0							
7	265	0							
8	1648	26	.5142	.1977	-.0039	.0195	.5181	.1986	2.6083
9	623	0							
10	275	12	1.5603	.2952	-.0035	.0194	1.5638	.2958	5.2862
11	134	14	2.4991	.2824	-.0048	.0194	2.5039	.2831	8.8448
12	490	12	.9628	.2923	-.0028	.0194	.9656	.2929	3.2964
13	89	0							
14	9675	44	-.7410	.1511	.0184	.0195	-.7595	.1524	-4.9849
15	387	2	-.6126	.7089	.0006	.0194	-.6132	.7092	-.8647
16	9301	113	.2492	.0946	-.0096	.0198	.2589	.0967	2.6772
17	4508	128	1.1147	.0897	-.0330	.0199	1.1478	.0918	12.4972
18	7180	47	-.3748	.1463	.0081	.0195	-.3830	.1476	-2.5938
19	4925	3	-2.7554	.5775	.0166	.0194	-2.7719	.5779	-4.7970
20	3779	0							
21	2713	30	.1540	.1836	-.0016	.0195	.1556	.1846	.8429
22	14701	28	-1.6141	.1892	.0433	.0195	-1.6573	.1902	-8.7152
23	246	0							
24	399	0							
25	19026	300	.5136	.0582	-.0492	.0206	.5628	.0617	9.1194
26	1278	30	.9194	.1848	-.0068	.0195	.9262	.1858	4.9853
27	3347	77	.8988	.1153	-.0173	.0197	.9161	.1170	7.8327
28	85	0							
29	298	1	-1.0462	1.0017	.0007	.0194	-1.0469	1.0019	-1.0450
30	1586	15	-.0039	.2594	.0000	.0194	-.0039	.2602	-.0151
31	1649	1	-2.7598	1.0003	.0055	.0194	-2.7653	1.0005	-2.7640
32	2137	26	.2507	.1973	-.0022	.0195	.2528	.1983	1.2752
33	547	4	-.2633	.5018	.0004	.0194	-.2638	.5022	-.5252
34	254	1	-.8859	1.0020	.0005	.0194	-.8864	1.0022	-.8845
35	143	0							
...									
...									
...									

**Table B.6.** Output from the FORTRAN utility WTS.EXE for the weights of spatial association estimation component of weights of evidence mineral potential modelling. The table consists of a header, which summarizes the map and point dataset analysed, and a data section. The data section contains the following for each map class: the map class number (columns 1 and 2); area in unit cells (column 3); total number of coincident points (mineral deposits, column 4); positive weight of association ( $W^+$ , column 5); standard deviation of  $W^+$  (column 6); negative weight of association ( $W^-$ , column 7); standard deviation of  $W^-$  (column 8); contrast or  $W^+$  and  $W^-$  ( $C$ , column 9); standard deviation of  $C$  (column 10); and studentized  $C$  (column 11). This example shows part of the weights of spatial association measurements between the gold-silver-bearing occurrences and the digital representation of the Stewart and Carlson's (1978) geologic map of Nevada (Turner and Bawiec, 1991). See text for discussion of spatial association coefficients.

```

:Weights of evidence modelling Bayesian multi-map overlay procedure.
:Response variable (point dataset) is the Nevada MRDS gold-silver occurrences.
:Builds a posterior probability map based upon 11 layers of evidence.
:
:Begin calculations...
:
:Define the prior probability...
:
:Prior probability = total # of points / total area of study region
:
:      (if a unit cell is defined as 1km2)
:      ...or, also considered as...
:
:      # of unit cells with occurrences / total area in unit cells
:
:Number of occurrences = 2,690 (all gold-silver occurrences)
:Total area of analysis = 283,219 km2
:Prior probability = 2690/283219 = 0.009498
:
:      priorp = 0.009498
:
:Calculation of log of prior odds from prior probability...
:
:      lprioro = log(priorp / (1.0 - priorp)) ;
:
:Assign the weights to binary-class mineral prediction maps m1 to m11.
:The maps (names in quotes) are coded as:
: 0 class - predictor pattern missing (no data)
: 1 class - predictor pattern absent (pattern not favorable)
: 2 class - predictor pattern present (pattern favorable)
:The weights were determined using WTS.EXE and are hard-wired into the equation.
:
:      W+ (predictor pattern present)      W- (predictor pattern absent)
:
:m1 = { 0.4560 if class('banabipr') == 2, -0.1110 if class('banabipr') == 1, 0 };
:m2 = { 0.6264 if class('bfftbiipr') == 2, -0.3898 if class('bfftbiipr') == 1, 0 };
:m3 = { 1.4221 if class('bfplbiipr') == 2, -0.2829 if class('bfplbiipr') == 1, 0 };
:m4 = { 2.6252 if class('geobihi') == 2, -0.1267 if class('geobihi') == 1, 0 };
:m5 = { 1.1853 if class('geobilow') == 2, -0.0985 if class('geobilow') == 1, 0 };
:m6 = { 1.8140 if class('geobimed') == 2, -0.2620 if class('geobimed') == 1, 0 };
:m7 = { 0.9598 if class('gedvbiipr') == 2, -0.3418 if class('gedvbiipr') == 1, 0 };
:m8 = { 0.2139 if class('gisobiipr') == 2, -0.3252 if class('gisobiipr') == 1, 0 };
:m9 = { 1.0010 if class('knabiipr') == 2, -0.0560 if class('knabiipr') == 1, 0 };
:m10 = { 0.3904 if class('magbiipr') == 2, -0.2147 if class('magbiipr') == 1, 0 };
:m11 = { 0.4816 if class('trrnbiipr') == 2, -0.2565 if class('trrnbiipr') == 1, 0 };
:
:Total the weights...
:
:      wtot = m1 + m2 + m3 + m4 + m5 + m6 + m7 + m9 + m10 + m11;
:
:Add the log prior odds to the totalled weights to get log of posterior odds...
:
:      lposto = lprioro + wtot;
:
:Convert log odds to odds, but make 0 if all the weights are zero...
:
:      posto = {exp(lposto) if wtot <> 0 , 0};
:
:Convert posterior odds to posterior probability...
:
:      postp = posto / (1.0 + posto);
:
:Build the posterior probability map...
:
:      postp;

```

**Table B.7.** Example of weights of evidence Bayesian map overlay modelling equation implemented in SPANS GIS. Colons ":" indicate comment lines.

```

ID uqpr11
TITLE Weights of Evidence
MAPID uqpr11 (unique conditions overlay map of 11 binary-class mineral predictor maps)
TABTYPE 5
FTYPE free
KEYFIELD 2
NRECORD 1144
  1  0  15.400000  0      area area
  2  4   7.000000  0      uniq unique conditions map class
  3  4   7.000000  0      depos number of deposits
  4  0  10.400000  0      postp posterior probability
  5  0  10.400000  0      tpost Studentized post prob
  6  0  10.400000  0      sdevw Uncertainty (weights)
  7  0  10.400000  0      sdevm Uncertainty (missing)
  8  0  10.400000  0      stot Total uncertainty
DATA
28205.3300      1      32      .0010      3.1488      .0001      .0003      .0003
25433.8100      2      36      .0016      3.1630      .0001      .0005      .0005
18652.4200      3      41      .0008      11.6187      .0001      .0000      .0001
13665.1100      4      34      .0014      12.0878      .0001      .0000      .0001
12665.0000      5      14      .0030      3.1705      .0002      .0009      .0010
11266.3000      6      27      .0017      11.4680      .0001      .0000      .0001
 9648.6680      7      33      .0018      3.1516      .0001      .0005      .0006
 8824.1040      8      23      .0045      3.1868      .0003      .0014      .0014
 7443.1330      9      23      .0015      11.4479      .0001      .0000      .0001
 7103.5460     10      59      .0026      11.9010      .0002      .0000      .0002
 6235.7220     11      18      .0029      11.9252      .0002      .0000      .0002
 5949.4050     12       8      .0027      3.1626      .0002      .0008      .0008
 5257.2710     13      45      .0165      3.2798      .0012      .0049      .0050
 4657.6000     14      39      .0022      11.6428      .0002      .0000      .0002
 4400.3140     15      29      .0038      12.1258      .0003      .0000      .0003
 4067.2670     16      19      .0060      3.1934      .0005      .0018      .0019
 3665.3160     17      16      .0034      3.1743      .0003      .0011      .0011
 3191.0030     18       8      .0031      11.3124      .0003      .0000      .0003
 2965.6220     19       8      .0048      3.1767      .0004      .0015      .0015
 2938.4030     20       6      .0083      3.2137      .0006      .0025      .0026
 2816.4610     21       3      .0030      10.4588      .0003      .0000      .0003
 2541.2050     22       4      .0051      10.8136      .0005      .0000      .0005
 2317.4540     23       8      .0020      3.1539      .0002      .0006      .0006
 2086.0970     24       5      .0047      11.5095      .0004      .0000      .0004
 2043.0330     25       2      .0080      11.9945      .0007      .0000      .0007
 2023.4960     26      50      .0070      11.9625      .0006      .0000      .0006
 1953.3160     27      13      .0041      11.4850      .0004      .0000      .0004
  ...
  ...
  ...

```

**Table B.8.** Output from the FORTRAN utility PREDICT.EXE for the Bayesian multi-map overlay component of weights of evidence mineral potential modelling. The output table is formatted for direct import into SPANS GIS, and consists of a header section (above and including the line “DATA”), which describes the contents and format of a table, and a data section (below the line “DATA”). For each unique conditions map class, the following is given: area (column 1); unique conditions map class ID number (column 2); total number of coincident points (mineral deposits, column 3); posterior probability (column 4); studentized posterior probability (relative uncertainty, column 5); uncertainty due to variances in the weights (column 6); uncertainty due to missing data (column 7); and total uncertainty (column 8). Any of these attributes may be used to reclassify the unique conditions map generated for this particular model (in this instance, all 2690 gold-silver-bearing occurrences and 11 binary-class mineral predictor maps). See text for discussion.

```

map number 1      banabipr.map (Ba/Na geochemical anomaly)
map number 2      bfftbipr.map (buffer zones around faults)
map number 3      bfplbipr.map (buffer zones around plutons)
map number 4      geobihi.map  (lithology)
map number 5      geobilow.map (lithology)
map number 6      geobimed.map (lithology)
map number 7      gedvbipr.map (diversity of lithology)
map number 8      gisobipr.map (isostatic gravity anomaly)
map number 9      knabipr.map  (K/Na geochemical anomaly)
map number 10     magbipr.map  (geomagnetic anomaly)
map number 11     trrnbiipr.map (lithotectonic terranes)

```

Chi-squared summary table:

Upper triangle -- conditional independence (deposits only)

Lower triangle -- conditional independence (non-deposits only)

	1	2	3	4	5	6	7	8	9	10	11
1	<b>0.00</b>	<b>35.73</b>	<b>32.57</b>	<b>15.05</b>	<b>0.03</b>	<b>0.85</b>	<b>93.47</b>	<b>95.73</b>	<b>486.34</b>	<b>6.60</b>	<b>78.37</b>
2		<b>0.00</b>	<b>21.71</b>	<b>0.66</b>	<b>0.39</b>	<b>0.64</b>	<b>124.92</b>	<b>8.46</b>	<b>31.21</b>	<b>14.80</b>	<b>2.93</b>
3			<b>0.00</b>	<b>31.13</b>	<b>44.13</b>	<b>1.19</b>	<b>39.81</b>	<b>45.46</b>	<b>29.91</b>	<b>4.50</b>	<b>29.93</b>
4				<b>0.00</b>	<b>57.30</b>	<b>139.23</b>	<b>12.67</b>	<b>8.04</b>	<b>0.78</b>	<b>1.25</b>	<b>95.93</b>
5					<b>0.00</b>	<b>142.54</b>	<b>0.00</b>	<b>5.70</b>	<b>12.39</b>	<b>21.01</b>	<b>49.60</b>
6						<b>0.00</b>	<b>4.32</b>	<b>18.25</b>	<b>0.11</b>	<b>5.82</b>	<b>0.58</b>
7							<b>0.00</b>	<b>23.44</b>	<b>43.94</b>	<b>1.56</b>	<b>0.19</b>
8								<b>0.00</b>	<b>5.71</b>	<b>20.37</b>	<b>1.81</b>
9									<b>0.00</b>	<b>17.21</b>	<b>6.14</b>
10										<b>0.00</b>	<b>4.51</b>
11											<b>0.00</b>

**Table B.9.** Output from FORTRAN utility CLEXE for the error analysis component of weight of evidence mineral potential modelling. Pairwise conditional independence test  $\chi^2$  scores for 11 binary-class predictor map pair combinations. The predictor maps are denoted as numbers 1-11 along the left-hand and top margin of the lower table, and are keyed to map names shown in a legend which appears over the table of  $\chi^2$  scores. Note that only the upper right-hand triangular block of  $\chi^2$  scores (bold italic numbers) shows the conditional independence between the 11 binary-class predictor map pairs with respect to the deposits. See text for discussion.



# Standard and Quadtree Raster Data Structures

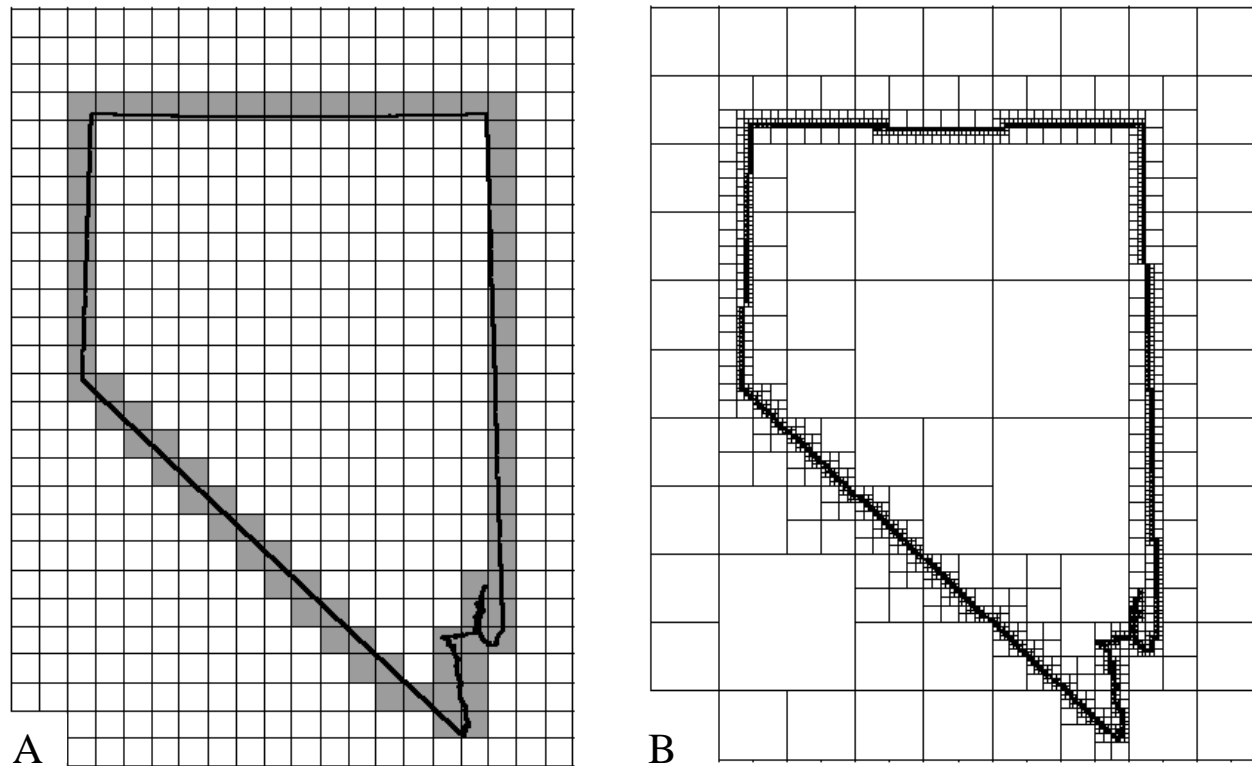


**Figure B.1.** A full expanded uniform-sized pixel raster structure (**A**) and a hierarchical variable sized pixel quadtree data structure (**B**). The vector outline of Nevada is superimposed on a grid which represents the pixel configuration of the data structures. The gray highlight indicates the raster equivalent of the vector data structure (cell sizes are exaggerated).

# Two- and Multi-Map Overlay and Combination Methods

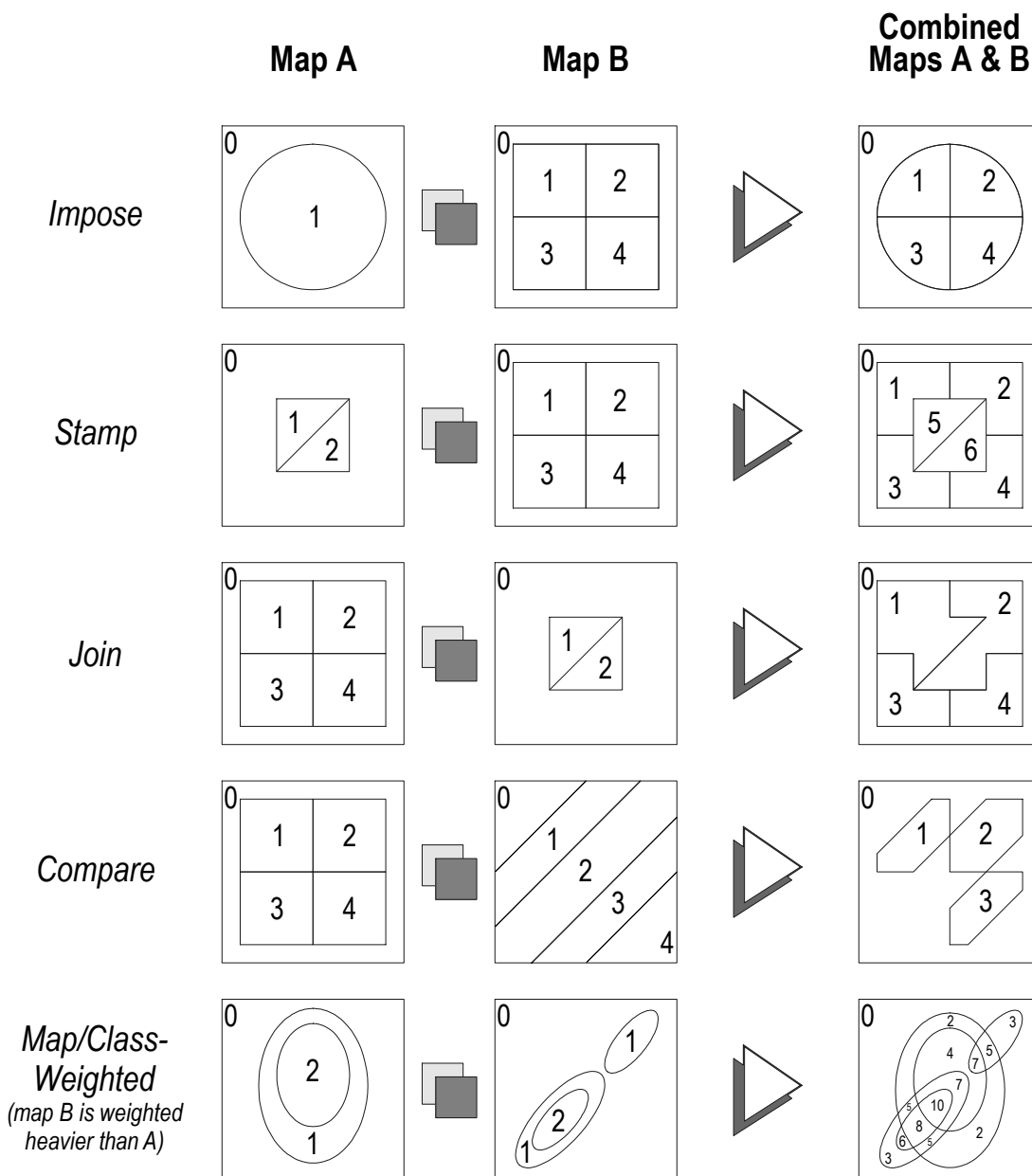


**Figure B.2.** Two-map and multi-map overlay and combination methods. Figure adopted from Bonham-Carter (1994a, p. 223, 225, 226, 229, and 230). See text for discussion.

# Entity and Unique Conditions Map Overlays and Linked Attribute Tables

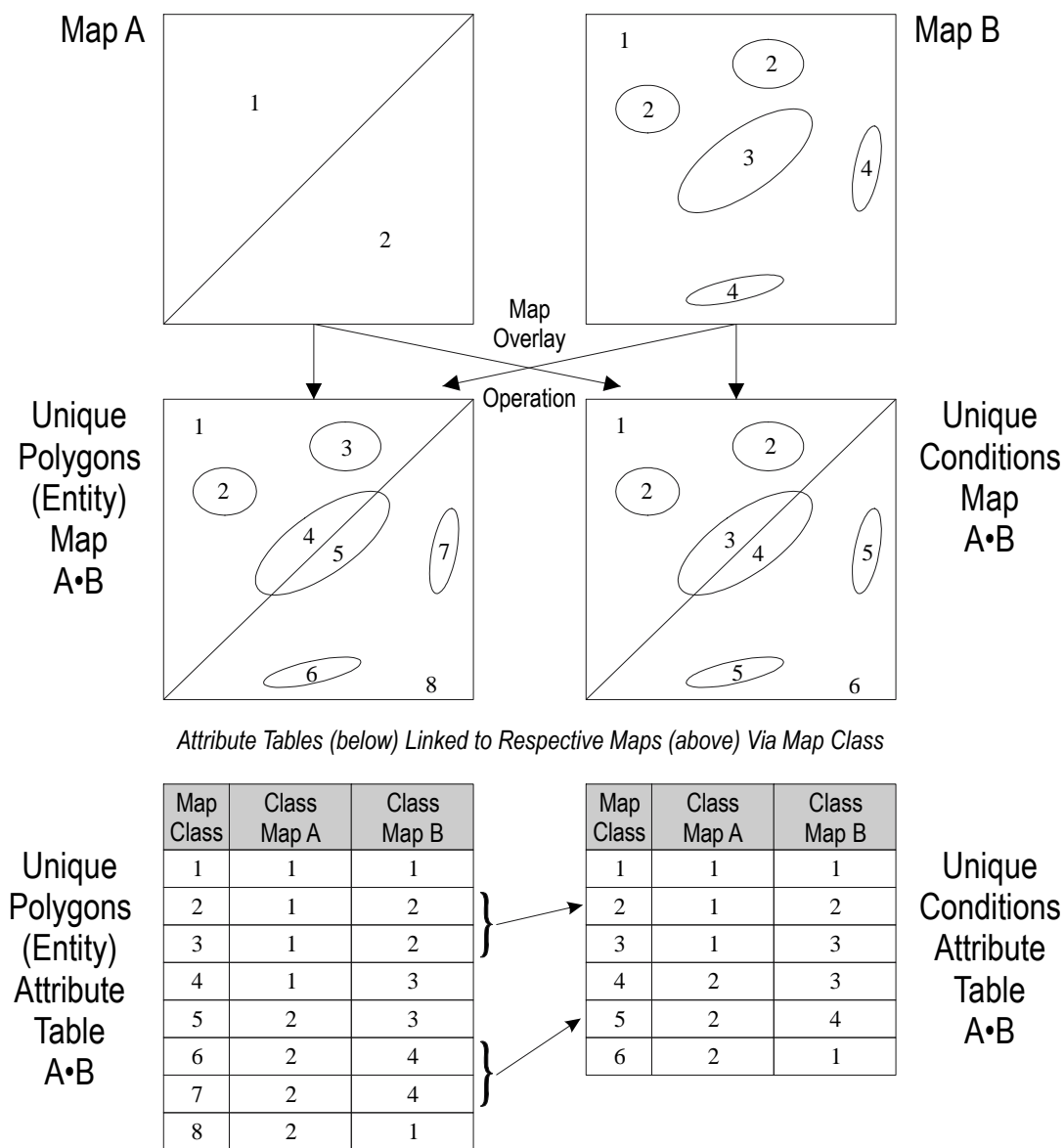


**Figure B.3.** The generation of a single map from overlaying multiple maps. There are two basic types of map overlay operations: (1) an entities overlay, where each new polygon created by the intersection of polygons composing the input maps is assigned a unique class value, or entity number (left side of diagram); and (2) a unique conditions overlay, where the new polygons are assigned the same class value (grouped) if they consist of the same overlap combination or characteristic of input maps (a "unique condition" intersection of input map classes; right side of diagram). The map overlay operation also produces an associated (linked) attribute table that contains information detailing the overlay combinations of input maps which constitute each overlay map class. Figure and text modified from Bonham-Carter (1994a, p. 236). See text for discussion.

## Weights of Evidence Multi-Map Overlay Modelling Method

---

**Figure B.4.** The weights of evidence (WOE) mineral potential modelling method is illustrated by the flow chart on the opposite page. WOE may be subdivided into two main procedures:

- i.* Calculation of  $W^+$  and  $W^-$  weights of spatial association between the response variable and the predictor variable(s), which in this instance are point objects representing gold-silver-bearing occurrences, and multi-class map patterns representing various geologic phenomena.  $W^+$  and  $W^-$  are calculated for each of the predictor variable map classes. The weights are then used as a guide to reclassify a multi-class predictor variable to a binary-class predictor variable (a binary-class deposit predictor map), where binary-class map pattern present represents mineralization-favorable conditions, and binary-class map pattern absent represents mineralization-unfavorable conditions.
- ii.* Combination of predictor variables (the "*layers of evidence*") in a multi-map overlay operation where a loglinear version of *Bayes' Rule* is used to sum and update the weights associated with each of the map classes that come into coincidence, producing a compound posterior probability mineral potential map which closely exhibits the distribution of known occurrences and indicates areas where more occurrences are expected than are observed.

See the text for a more detailed discussion.

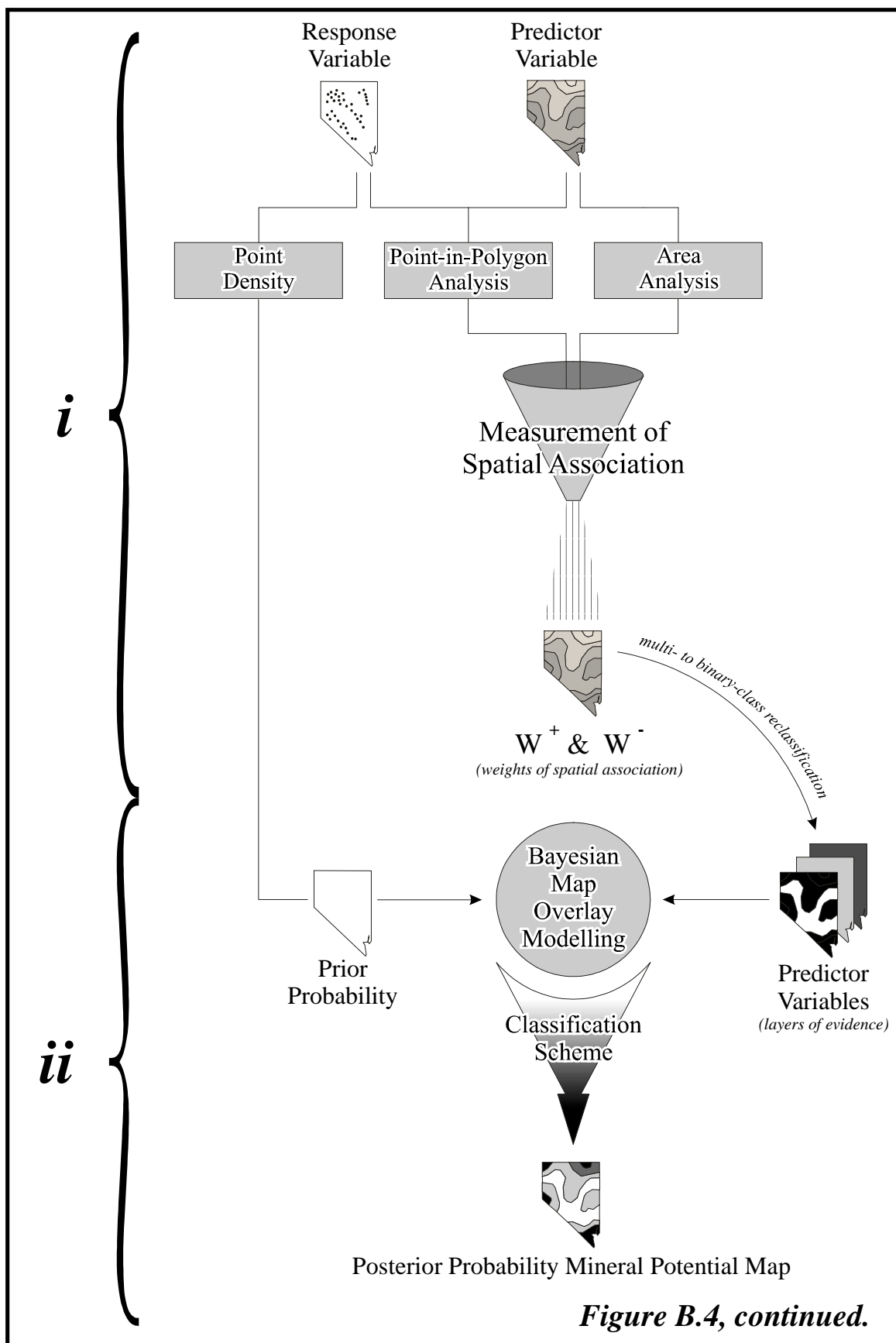
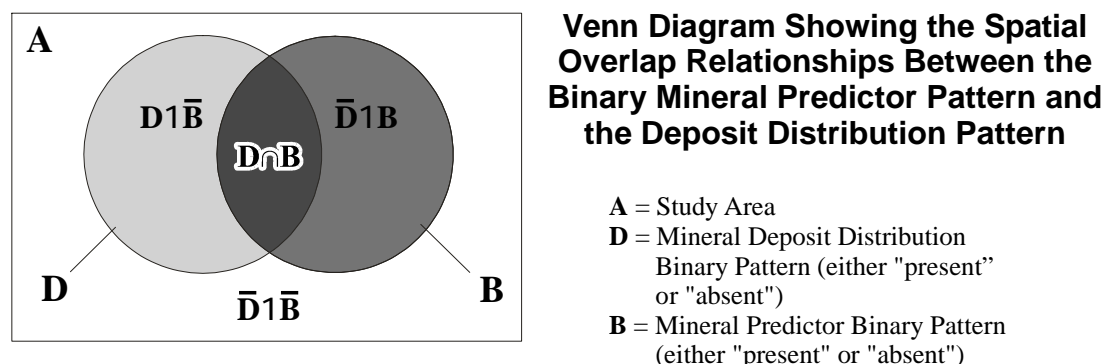
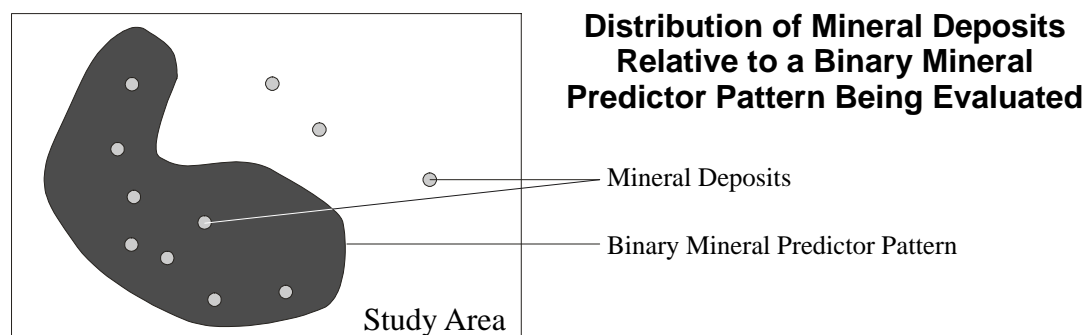


**Figure B.4, continued.**

# Spatial Overlap Relationships



## Four Spatial Overlap Combinations:

- D1B**—regions where both deposit and predictor patterns present.
- D1B̄**—regions where deposit pattern present, predictor pattern absent.
- ̄D1B**—regions where deposit pattern absent, predictor pattern present.
- ̄D1B̄**—regions where neither deposit nor predictor patterns present.

**Figure B.5.** Diagrams illustrating the spatial overlap relationships on which the weights of spatial association ( $W^+$  and  $W^-$ ) are measured. The value of the weights depend on the ratio of deposits that fall on the binary mineral predictor pattern to the total number of deposits, against, the ratio of the binary mineral predictor pattern area to the total study region area. See text for discussion. Modified from Bonham-Carter (1994a, p. 305, 311, and 316).

# APPENDIX C

## Mineral Potential Map Generation, Conditional Independence, and Uncertainty:

### Section Contents:

- C.1** General Introduction (organization of materials presented)
- C.2** Mineral Potential Maps Generated
- C.3** Conditional Independence
  - C.3.1** Introduction
  - C.3.2** Results of the Pairwise Test
  - C.3.3** Results of the Overall Test
  - C.3.4** Mitigation of Conditional Dependence
  - C.3.5** Interpretation of Conditional Dependence
  - C.3.6** Comparison Between CI-Mitigated and Unmitigated Mineral Potential Maps
  - C.3.7** Comparison Between Mineral Potential Maps Generated by the Weights of Evidence and Weighted Logistic Regression Methods
- C.4** Uncertainty of the Mineral Potential Maps
  - C.4.1** Introduction
  - C.4.2** Maps of Mineral Potential Uncertainty



## C.1 General Introduction

Much of the material covered in here is organized in a 2-fold manner: for each of the three occurrence-types (primary, sedimentary and volcanic rock-hosted), two mineral potential models, composed of a differing number of evidence layers, are examined (making a total of six models). The first model is based on *all* of the binary-class mineral predictor maps, while the second model is based on a *fewer number* of predictor maps, where one or more maps have been rejected in order to make the model more statistically sound and/or geologically robust. As such, a pair of tables, graphs, figures, or maps is presented for each of the three occurrence-types (primary, sedimentary and volcanic rock-hosted), resulting in a total number of six tables, graphs, figures, or maps necessary to characterize or illustrate any one point.

## C.2 Mineral Potential Maps Generated

A total of six weights of evidence (WOE) mineral potential maps were produced—two for each of the primary, sedimentary and volcanic rock-hosted occurrence-types. The first map is based on all evidence layers (Figs. [C.1a](#), [C.2a](#), and [C.3a](#)). The second map is based on a fewer number of evidence layers, where predictor maps were removed from the model in an attempt to mitigate conditional dependency violations (Figs. [C.1b](#), [C.2b](#), and [C.3b](#)). Conditional independence and its mitigation are discussed below in [section C.3](#).

In addition, three more mineral potential maps, generated using the weighted logistic regression (WLR) method of predictor map combination, are presented for comparison with the “all-evidence-layers” WOE-derived mineral potential maps for each occurrence-types (Figs. [C.1c](#), [C.2c](#), and [C.3c](#)). Weighted logistic regression is covered below in [section C.3.7](#).

All binary-class mineral predictor maps were coded as:

- 0 class—Predictor pattern missing (no data).
- 1 class—Predictor pattern absent (pattern not favorable).
- 2 class—Predictor pattern present (pattern favorable).

Where data coverage was not complete for an predictor map (e.g.—K/Na and Ba/Na geochemical anomaly maps), the area was assigned “*pattern unknown*” and weighted as “0” for the WOE-derived posterior probability mineral potential maps. For the WLR-derived maps, where no way for representing missing data is possible, areas of incomplete data coverage were reclassified to “*pattern not present*”, and was done so in order to facilitate the comparison between the WOE and WLR map combination methods.

The WOE-derived mineral potential maps were classified using a “quantiles” approach—an “area-based” percentiles scheme where the posterior probability class intervals (the break points) are determined so that each of the posterior probability classes is roughly equal in area (see section B.5.4; also see TYDAC Technologies Inc., 1993, *Reference Manual*, p. 5-56, for more information). The WLR-derived mineral potential maps were also classified using the *same* WOE-derived map classification schemes, so that an absolute-scale comparison could be made between the WOE-derived and WLR-derived maps.

## C.3 Conditional Independence

### C.3.1 Introduction

Conditional independence (CI) between the binary-class mineral predictor map patterns, with respect to the gold-silver-bearing occurrences, is assumed to exist and is necessary when adding the weights of various types of evidence. For a mineral potential model and its resultant posterior probability map to be robust, the presence of a mineralization-favorable map pattern in one layer of evidence (a predictor map) should not be dependent on the presence of a mineralization-favorable map pattern in another layer of evidence. Conditional independence is tested for using *pairwise* and *overall* goodness-of-fit methods. If a predictor map is found to be in serious violation of the assumption of CI, it can then be (1) rejected from the model, (2) combined with another map in order to minimize the dependency, or (3) modified in some way to reduce the problem (for more information, see Agterberg et al., 1990; Bonham-Carter, 1994a).

Both the pairwise and overall CI tests make use of the observed versus the expected number of observations (gold-silver-bearing occurrences). The expected number of occurrences in this instance is calculated by multiplying the total area of the predictor map pattern (in km<sup>2</sup>) by its associated posterior probability (this assumes that the total region of the study area is represented in 1 km<sup>2</sup> size unit cells, where an occurrence is represented by one unit cell, or is 1 km<sup>2</sup> in size) (see Bonham-Carter, 1994a, p. 317). The theoretical aspects and the implementation of these tests are described in the sections B.3 and B.5.

The principal points made in this section are: (1) conditional *dependency* between the layers of evidence for the mineral potential models does exist, however, the “predictive” quality of the mineral potential maps is not seriously affected; and (2) the posterior probability maps generated from the mineral potential models should be considered as “favorability” rather than “probabilistic” mineral potential maps. The results of the pairwise and overall goodness-of-fit tests are presented below in sections C.3.2 and C.3.3. Corrections made to the mineral potential models to mitigate CI problems are reviewed in section C.3.4. Interpretation of the pairwise and overall goodness-of-fit test results is reviewed in section C.3.5 and an evaluation of results is presented in sections C.3.6 and C.3.7.

### C.3.2 Results of the Pairwise Test

The pairwise goodness-of-fit test measures conditional independence (CI) between all possible pairings of the binary-class predictor maps by calculating the  $\chi^2$  (chi-square) statistic for each map pair, and comparing the calculated value of  $\chi^2$  to the tabled value of  $\chi^2$  having one degree of freedom (Bonham-Carter, 1994a). The results of the test are typically presented in the form of pairwise cross-tabulation tables (see sections B.3.2 and B.5.5).

The results of the pairwise  $\chi^2$  test for the primary, sedimentary and volcanic rock-hosted occurrence-type mineral potential models are presented in summary form in Tables C.1, C.2, and C.3. A probability level threshold of 98% ( $\chi^2_{0.98,1} = 5.41$ ) was chosen as the null hypothesis (that CI exists) rejection-acceptance cutoff. Two tables of  $\chi^2$  test results are given for each of the three

occurrence-types. Each table represents a mineral potential model that is identified with a label consisting of the occurrence-type (*primary*, *sed-hosted*, or *vol-hosted*) and the number of layers of evidence composing the particular model (11, 9, etc.). Tables C.1a, C.2a, and C.3a show  $\chi^2$  scores for mineral potential models that combine *all* of the predictor maps for a given mineral potential model. Tables C.1b, C.2b, and C.3b show  $\chi^2$  scores for mineral potential models that combine a fewer number of predictor maps, where some maps have been rejected from the mineral potential model in an attempt to mitigate serious CI violations that appear in Tables C.1a, C.2a, and C.3a. The respective mineral potential models represented by Tables C.1b, C.2b, and C.3b are not fully optimized with respect to the  $\chi^2$  test—all map combinations that yield high rejection-level  $\chi^2$  values ( $> 5.41$ ) have not been eliminated. Instead, these tables represent mineral potential models that are a geologically-sensible compromise between two end-member models. One end member mineral potential model is the combination of all predictor maps, which yields many high  $\chi^2$  scores. The other end member model is a combination of fewer maps, which yields  $\chi^2$  scores all below 5.41, but consists of relatively few predictor maps (e.g.—to eliminate all conditional dependency for the *primary 11-layer mineral potential model*, 8 of the 11 maps would have to be rejected from the model).

### C.3.3 Results of the Overall Test

The overall goodness-of-fit test is a measure of the conditional independence (CI) among all of the layers of evidence in a model as a whole. The overall method is a simple procedure involving the relative comparison of predicted versus observed occurrences—if the total predicted number of occurrences is much larger than the total observed number (greater than ~10-15%), it suggests that CI is being violated, and may warrant a check of the pairwise tests and some sort of remedial action (Bonham-Carter, 1994a). The overall goodness-of-fit can also be evaluated using the Kolmogorov-Smirnov (K-S) statistic. The K-S test is based on the maximum deviation of the observed number of occurrences from the predicted number, and the results are typically presented in graphic form (see sections B.3.3 and B.5.5).

The total expected versus total observed number of occurrences for the various occurrence-type mineral potential models and other overall CI test result data are given in Table C.4. The graphical results of the K-S test are shown in Figures C.4, C.5, and C.6. For each of the three occurrence-types, two mineral potential models were tested (as was performed with the pairwise  $\chi^2$  test). Figures C.4a, C.5a, and C.6a show the K-S test results for the various mineral potential models using all of the available layers of evidence. Figures C.4b, C.5b, and C.6b show the results for mineral potential models that are composed of fewer layers of evidence, where an attempt has been made to mitigate serious CI violations (the “a” and “b” series K-S test figures are complementary to the “a” and “b” series  $\chi^2$  test tables). The figures also show the critical K-S statistic cut-off values and the K-S values calculated for each of the models.

### C.3.4 Mitigation of Conditional Dependence

Both the  $\chi^2$  pairwise tests and the overall tests indicate that a high degree of conditional *dependency* exists between the various layers of evidence, with respect to the occurrences, for all of the occurrence-type mineral potential models. The lack of CI occurs most notably in the mineral potential models where all of the available binary-class predictor maps were combined (the “a” series of Tables C.1, C.2, and C.3, and Figs. C.4, C.5, and C.6).

The primary occurrences mineral potential models showed the greatest violations of pairwise CI of any of the gold-silver-bearing occurrence-types. The highest  $x^2$  scores are found in the primary occurrences 11-layer model (Table C.1a), between the lithologic diversity and fault buffers predictor maps, the medium-potential lithology with the high- and low-potential lithology predictor maps, and most notably, between the K/Na and Ba/Na geochemical anomaly predictor maps ( $x^2 = 486.34$ ). Many of these  $x^2$  scores are an order of magnitude or two higher than most of the other scores for any of the other sedimentary or volcanic rock-hosted mineral potential models. The most severe instances of CI violation in the primary 11-layer model were rectified by removing the Ba/Na, lithology (medium  $W^+$ ), lithologic diversity, and lithotectonic terranes predictor maps (Table C.1b). This modification, while clearly not solving all of the pairwise CI violations, did result in a marked decrease in the number of gold-silver-bearing occurrences of all types and sizes predicted in the overall test (Fig. C.4b; also see Table C.4, the “% expected over observed”, “K-S critical value”, and “K-S statistic for model” values).

The sedimentary rock-hosted occurrence mineral potential models have less pairwise CI violations than the primary occurrence models, and relative to the primary 11-layer model, have substantially lower  $x^2$  scores (Tables C.2a and C.2b). The overall test, however, indicates the highest discrepancy between the number of observed and predicted occurrences for any of the occurrence-types (Table C.4). In order to correct all of the CI violations observed in the pairwise test, the pluton buffers, lithologic diversity, and isostatic gravity predictor maps would have had to been removed from the mineral potential model (leaving only 6 predictor maps). Even with such a modification, the overall test still predicts 452.57 occurrences to the observed 98—from a relative standpoint, not much of an improvement (it is also interesting to note that the number of unique conditions from the 9-layer to the 6-layer mineral potential model decreases from 598 to only 96). Therefore, only the pluton buffers map was removed from the model (Table C.2b and Fig. C.5b), as the geologic factors represented in the other predictor maps were deemed to be more important to the formation of sedimentary rock-hosted occurrences. The removal of the pluton buffers predictor map from the mineral potential model, while perhaps being logical from a geologic perspective, resulted in a slight increase in the number of sedimentary rock-hosted occurrences predicted in the overall test (Table C.4). Irrespective of combination or number of predictor maps included, there is a large degree of conditional dependence in the sedimentary rock-hosted mineral potential models.

The volcanic rock-hosted occurrences mineral potential models, in comparison to the other gold-silver-bearing occurrence-types, showed the least (yet still noticeable) amount of pairwise and overall CI violations, when considered together (Table C.4 and Fig. C.6). The Ba/Na geochemical anomaly and lithotectonic terranes predictor maps were the source of the greatest number and most severe pairwise CI violations. Removal of these two maps from the mineral potential model (Table C.3b and Fig. C.6b), while not remedying all of the pairwise CI violations, resulted in significantly closer agreement between observed and predicted occurrences (see Table C.4).

### C.3.5 Interpretation of Conditional Dependence

The violation of conditional independence in the mineral potential models is not unexpected. Conditional independence in WOE modelling is always violated to some degree (Bonham-Carter, 1994a; see section B.3). The greater the number of evidence maps used in a model,

especially if those maps have similar distribution patterns and represent similar types of evidence, the greater the possibility is that conditional *dependency* will exist (that CI will be violated). For example, the Ka/Na and Ba/Na geochemical anomaly maps are nearly coincident in their spatial distribution, are derived from the same dataset, represent broadly similar information, and are highly correlated spatially with gold-silver-bearing occurrences (sedimentary rock-hosted occurrences in particular). It is not surprising, therefore, that these two layers of evidence show very high  $\chi^2$  scores in the pairwise goodness-of-fit tests. In addition, because these predictor maps have high  $W^+$  values that are essentially compounded during the Bayesian overlay procedure, the dependence between their predictor map patterns results in inflated posterior probabilities, and the overestimation of predicted occurrences. The same is probably true for some of the other dataset pairs, such as the geomagnetic anomaly and lithology datasets, and the fault buffers and lithologic diversity datasets. The failure of the overall goodness-of-fit test also indicates a large degree of interdependency that is probably due to the multiple interactions of many similar and highly mineral-occurrence-correlated predictor maps.

The high degree of CI violation exhibited by these mineral potential models may also be in part related to:

1. Modelling the distribution of a relatively large number of mineral occurrences (response variables).
2. Compounding effects of mineral occurrence point clustering, where more than one point may fall within the 1 km<sup>2</sup> unit cell size assigned to represent a mineral occurrence.

To investigate these possibilities, two simple and non-rigorous empirical tests were performed using the primary occurrences 11-layer mineral potential model datasets. These datasets were chosen because they contain the greatest number of occurrence points (2690), the largest number of predictor maps (11), and therefore, the highest number of mineral potential map unique condition classes.

In the case of possibility #1, six pairwise CI test trials were performed on the primary 11-layer model using six different “dummy” mineral occurrence datasets—consisting of various numbers (139, 277, 565, 1127, 1565, and 2856) of gridded points—in place of the primary occurrences point dataset. The results of the trials show a roughly proportional increase in the magnitude of the highest  $\chi^2$  scores with an increase in the number of dummy occurrence points (smaller  $\chi^2$  scores also showed a general increase in magnitude, but not necessarily in proportion to the number of dummy occurrence points). Given the increases in the magnitude of the CI violations, increases in the number of violations also occur (the increase in the number of violations, however, does not appear to be proportional to the number of dummy occurrence points). These findings indicate that increasingly large response variable datasets (i.e.—greater numbers of mineral occurrences, or points) have increasingly larger magnitude and a greater number of CI violations (this is intuitively what would be expected).

With regard to possibility #2, pairwise and overall CI tests were performed on the primary 11-layer model using a version of the primary occurrences point dataset that was “weeded” so as to remove any points that lay less than 1 km from a neighbouring point. In this manner, the primary occurrences point dataset was reduced from 2690 to 1625 points (it is interesting to note that nearly 40% of gold-silver-bearing occurrences lie within 1 km of another). The results of the pairwise CI test indicate that the magnitudes of the higher  $\chi^2$  scores for the weeded occurrence

point dataset are proportionally just as large as the  $x^2$  scores for the non-weeded occurrence point dataset (proportional relative to the total number of occurrence points, similar to the results demonstrated above with the gridded dummy occurrence datasets). The number of total CI violations also decreased slightly, but this was directly attributable to the decrease in  $x^2$  score magnitudes “across the board”, where borderline scores dropped below the tabled critical  $x^2$  value. The overall test results also indicate negligible differences between the weeded and non-weeded datasets. Using the weeded occurrence point dataset, the overall test predicts proportionately the same number of occurrences as is predicted using the non-weeded occurrence point dataset—for the non-weeded occurrence point dataset, 2690 occurrences observed and 4525.45 occurrences expected (predicted over observed by ~68%, see [Table C.4](#)); for the weeded occurrence point dataset, 1625 occurrences observed and 2770.50 expected (predicted over observed by ~70%).

In summary, the results of this investigation into the influence of large response variable datasets on conditional independence in the WOE modelling method suggest: (1) mineral occurrence point clustering (in this case where occurrence points are assigned a unit cell size of 1 km<sup>2</sup>) has no causal effect on whether or not CI between predictor maps, with respect to mineral occurrences, exists; and (2) large occurrence point datasets influence the calculated  $x^2$  scores in the pairwise goodness-of-fit test, producing larger magnitude  $x^2$  scores with greater numbers of occurrence points.

The fundamental point to be made here is that the layers of evidence composing these mineral potential models are not conditionally independent with respect to the mineral occurrences, and that this lack of CI is real, in both the statistical and the geological sense. Bonham-Carter (1994a) pointed out that the assumption of CI in weights of evidence results in a model that, like most models, does not perfectly represent the data, but does provide a working simplification, which, when applied with care, can be useful for prediction and provides insight into the relative contributions of the separate sources of evidence. It is therefore important to be aware of, as well as understand, the degree and causes for the lack of CI in the models. Given the CI violations discussed in the preceding paragraphs, it is best to consider the mineral potential maps derived from these models as relative “*favorability*” maps, rather than as “*probabilistic*” maps in the strict sense.

### C.3.6 Comparison Between CI-Mitigated and Unmitigated Mineral Potential Maps

The differences between the first and second mineral potential maps—the “all-evidence-layers” WOE-derived mineral potential maps and the maps based on fewer evidence layers—are shown as maps of absolute difference in posterior probability in [Figure C.7](#). These maps indicate that the differences in the posterior probabilities are generally small (relative to the maximum posterior probability for the two models compared for a given occurrence-type group). Where the difference is larger, the corresponding map areas are negligible in size (e.g.—less than 0.5% of the total area for the primary and sedimentary rock-hosted occurrence mineral potential maps, and less than 2.3% for volcanic rock-hosted, accounts for the top two red-and-yellow map-difference classes shown in [Fig. C.7](#)).



### C.3.7 Comparison Between Mineral Potential Maps Generated by the Weights of Evidence and Weighted Logistic Regression Methods

In order to help evaluate and measure the effects of conditional *dependence* in the mineral potential models, a comparison was made between the Bayesian statistical method for combining layers of evidence used in weights of evidence (WOE) modelling and a weighted logistic regression (WLR) method. This comparison was chiefly made because the WLR method does not require statistical independence between the predictor variables (the layers of evidence) with respect to the response variable (the mineral occurrences). Logistic regression analysis techniques for estimating mineral resource potential have been applied by Agterberg (1974, 1992a, 1992b, 1993), Chung and Agterberg (1980), Reddy et al. (1991), and Wright (1996). A detailed review of the WLR method and its theoretical aspects is given in Agterberg (1992a) and an overview given in Wright (1996). The WLR map combination procedure was carried out in a similar manner to WOE (see section B.5.4).

The WLR method usually produces posterior probabilities that are smaller in magnitude than those generated by the WOE method, which results in a fewer number of predicted occurrences. The simple overall goodness-of-fit test, when conducted with the WLR posterior probabilities, results in a predicted number of occurrences that is very close to the observed. Table C.5 shows that WLR expected frequencies generally fall a few percentage points or less short of the observed frequencies, whereas the WOE expected frequencies over-shoot the expected frequencies by 10's to 100's of percent. An examination of the posterior probabilities generated by each method (Figs. C.8, C.9, and C.10) suggests that the large overestimation of predicted occurrences based on the WOE method may, to a certain degree, be the result of anomalously high posterior probability values associated with a small number of unique overlap conditions between the predictor maps for a particular mineral potential model. This is especially apparent for the volcanic rock-hosted 9-layer and sedimentary rock-hosted 9-layer mineral potential models (Figs. C.9a and C.10a, respectively).

In addition, side-by-side visual comparisons were made between mineral potential maps generated from WLR-derived and WOE-derived posterior probabilities. This was done in order to determine if spatial distribution of the WOE-derived mineral potential map patterns were significantly affected by CI violation. These comparisons show only minor differences in the distribution of favorable mineral potential areas at the local-scale, and at the regional scale, no significant differences are visible in the overall map patterns, although the WOE mineral potential maps appear to be somewhat “warmer”(Figs. C.1c, C.2c, and C.3c). In general, the results of the WLR method appear to be consistent with those of the WOE method, and suggest that, for this study, the results of the WOE method are within acceptable and expected bounds.

## C.4 Uncertainty of the Mineral Potential Maps

### C.4.1 Introduction

It is important to recognize and understand the uncertainty inherent to the posterior probabilities when examining a mineral potential map. Uncertainty may be due to the variances in weight estimates ( $W^+$  and  $W^-$ ) and/or to one or more of the predictor maps having incomplete coverage



(i.e.—missing data) (Bonham-Carter et al., 1989). As an aid for interpretation, a posterior probability uncertainty map may be compared separately or combined with a mineral potential map to “mask-out” regions of high posterior probability uncertainty (see section B.4 for additional information).

## C.4.2 Maps of Mineral Potential Uncertainty

The mineral potential uncertainty maps are presented in Figures C.11, C.12, C.13, and C.14. The first series of uncertainty maps (Fig. C.11) illustrates all four types of uncertainties (weights variance, missing data, total, and relative), and was generated using the primary occurrence-type 11-layer mineral potential model. The three remaining series of uncertainty maps (Figs. C.12, C.13, and C.14) show only the total and relative uncertainties for the “CI-optimized” primary, sedimentary and volcanic rock-hosted occurrence-type mineral potential models. The maps were classified using a quantiles technique, as described in section B.5.4, and edited so as to emphasize the upper portion of the uncertainty values.

The maps of uncertainty due to variance in the weights estimates include the uncertainty of the *prior* probability, and in general, are correlated to the posterior probabilities. Hence, the weights variance uncertainty maps tend to have a pattern similar to those of the posterior probability maps. The maps of uncertainty due to missing data are (as is expected) strongly controlled by the incomplete evidence map coverage, which in this case is clearly related to the K/Na and Ba/Na geochemical anomaly evidence (note the “blocky” uncertainty map patterns, particularly in Fig. C11b). The relative certainty maps indicate the degree of confidence to which the posterior probability mineral potential map patterns are “real”, as opposed to being an artifact of “chance” effects (or due to chance). The larger the t-value over the critical tabled t-value cut-off (e.g.—1.645 for a significance of 95%) the greater the certainty of the mineral potential map pattern, although the high t-values in some of these relative certainty maps may be related to violations of CI. In general, the maps of uncertainty due to variance in weights estimates and due to missing data reflect the large overall variation in the data (i.e.—“noise in the system”). However, the relative certainty maps suggest that, despite this high degree of variability, the mineral potential map favorability patterns are reliable.

The uncertainties discussed above are presented in the form of single-theme maps (only uncertainty), however, the uncertainties may alternatively be presented in the form of 3-dimensional illustrations that more discernably relate the degree of certainty to areas of high mineral potential (i.e.—to areas having high posterior probabilities). For example, Fig. C.15 shows a 3-dimensional rendering of relative certainty draped over a pseudo-DEM wire-frame of posterior probabilities for the sedimentary rock-hosted 8-layer mineral potential model. In this illustration, height represents posterior probability values that are greater than the prior, and the color represents the degree of relative certainty of the values, as indicated by t-value. Note that the regions of higher certainty (yellow and red) are spatially coincident to the “V”-shaped relief of high mineral potential, suggesting that this favorability pattern has a high degree of certainty, and is therefore probably not due to chance.

**A.**

<b>Map</b>	<b>Primary (Occurrences of all Sizes and Types) 11-Layer Mineral Potential Model</b>										
	<b>Ba/Na</b>	<b>fault buffers</b>	<b>pluton buffers</b>	<b>lithology (high W+)</b>	<b>lithology (low W+)</b>	<b>lithology (med. W+)</b>	<b>lithologic diversity</b>	<b>isostatic gravity</b>	<b>K/Na</b>	<b>geo-magnetics</b>	<b>litho-tectonic</b>
<b>Ba/Na</b>	0.00	35.73	32.57	15.05	0.03	0.85	93.47	95.73	486.34	6.60	78.37
<b>fault buffers</b>		0.00	21.71	0.66	0.39	0.64	124.92	8.46	31.21	14.80	2.93
<b>pluton buffers</b>			0.00	31.13	44.13	1.19	39.81	45.46	29.91	4.50	29.93
<b>lithology (high W+)</b>				0.00	57.30	139.23	12.67	8.04	0.78	1.25	95.93
<b>lithology (low W+)</b>					0.00	142.54	0.00	5.70	12.39	21.01	49.60
<b>lithology (med. W+)</b>						0.00	4.32	18.25	0.11	5.82	0.58
<b>lithologic diversity</b>							0.00	23.44	43.94	1.56	0.19
<b>isostatic gravity</b>								0.00	5.71	20.37	1.81
<b>K/Na</b>									0.00	17.21	6.14
<b>geomagnetics</b>										0.00	4.51
<b>lithotectonic terranes</b>											0.00

**B.**

<b>Map</b>	<b>Primary (Occurrences of all Sizes and Types) 7-Layer Mineral Potential Model</b>						
	<b>fault buffers</b>	<b>pluton buffers</b>	<b>lithology (high W+)</b>	<b>lithology (low W+)</b>	<b>isostatic gravity</b>	<b>K/Na</b>	<b>geo-magnetics</b>
<b>fault buffers</b>	0.00	21.71	0.66	0.39	8.46	31.21	14.80
<b>pluton buffers</b>		0.00	31.13	44.13	45.46	29.91	4.50
<b>lithology (high W+)</b>			0.00	57.30	8.04	0.78	1.25
<b>lithology (low W+)</b>				0.00	5.70	12.39	21.01
<b>isostatic gravity</b>					0.00	5.71	20.37
<b>K/Na</b>						0.00	17.21
<b>magnetics</b>							0.00

**Table C.1.** Pairwise conditional independence (CI) test  $\chi^2$  scores for primary occurrence-type model. Table **A.** (upper) shows scores for the combination of all (11) binary-class predictor maps. Table **B.** (lower) shows scores for the combination of those maps that have ~10th percentile and lower  $\chi^2$  values relative to the scores shown in the upper table. With 1 degree of freedom and a probability level of 98% ( $\chi^2_{0.98,1} = 5.41$ ), many  $\chi^2$  values in table A exceed the acceptance cutoff of the null hypothesis (that CI exists) by one or two orders of magnitude, therefore indicating a severe violation of conditional independence in those cases. In table B, the most severe cases of conditional dependence have been mitigated by removing the Ba/Na, lithology (medium  $W^+$ ), lithologic diversity, and lithotectonic terranes maps from the model.

A.

Map

	Ba/Na	fault buffers	pluton buffers	lithologic diversity	lithology	isostatic gravity	K/Na	geo-magnetics	litho-tectonic
Ba/Na	0.00	0.84	0.53	1.08	0.82	0.80	6.11	1.99	0.14
fault buffers	0.00		0.28	0.03	1.58	1.20	0.07	0.24	0.04
pluton buffers	0.00			15.30	0.58	0.13	0.54	4.47	0.05
lithologic diversity	0.00				3.84	1.60	2.90	15.54	2.77
lithology	0.00					10.15	2.79	2.21	2.21
isostatic gravity	0.00						6.98	0.46	11.97
K/Na	0.00							0.92	1.33
geomagnetics	0.00								1.09
lithotectonic terranes	0.00								

B.

Map

	Ba/Na	fault buffers	lithologic diversity	lithology	isostatic gravity	K/Na	geo-magnetics	litho-tectonic
Ba/Na	0.00	0.84	1.08	0.82	0.80	6.11	1.99	0.14
fault buffers	0.00		0.03	1.58	1.20	0.07	0.24	0.04
lithologic diversity	0.00			3.84	1.60	2.90	15.54	2.77
lithology	0.00				10.15	2.79	2.21	2.21
isostatic gravity	0.00					6.98	0.46	11.97
K/Na	0.00						0.92	1.33
geomagnetics	0.00							1.09
lithotectonic terranes	0.00							

**Table C.2.** Pairwise conditional independence (CI) test  $\chi^2$  scores for the sedimentary rock-hosted occurrence-type model. Table **A.** (upper) shows scores for the combination of all (9) binary-class predictor maps. Table **B.** (lower) shows scores for the combination of eight maps after removal of the pluton buffers map from the model. With 1 degree of freedom and a probability level of 99% ( $\chi^2_{0.99,1} = 6.63$ ), over 85% of the map pattern pairs in table B approximately satisfy the assumption of conditional independence. Only the pluton buffer map was removed from the model because of its high degree of spatial correlation with the distribution pattern of volcanic rock-hosted occurrences. The isostatic gravity, geomagnetics, and lithotectonic terranes maps, although responsible for a significant amount of conditional dependency, were not eliminated from the model because of their spatial coincidence to the distribution pattern of the sedimentary rock-hosted occurrences.

A.

Map

Volcanic Rock-Hosted 9-Layer Mineral Potential Model									
	Ba/Na	fault buffers	pluton buffers	lithologic diversity	lithology	isostatic gravity	K/Na	geo-magnetics	litho-tectonic
Ba/Na	0.00	0.18	0.17	12.34	10.12	7.08	123.09	7.78	15.94
fault buffers	0.00		2.58	6.17	9.51	2.35	3.96	1.24	0.00
pluton buffers	0.00			13.37	5.72	6.47	0.78	13.56	1.10
lithologic diversity	0.00				0.83	6.21	12.50	3.20	0.85
lithology	0.00					1.70	2.16	11.14	9.02
isostatic gravity	0.00						3.05	0.02	15.40
K/Na	0.00							3.32	7.23
geomagnetics	0.00								0.05
lithotectonic terranes	0.00								

B.

Map

Volcanic Rock-Hosted 7-Layer Mineral Potential Model							
	fault buffers	pluton buffers	lithologic diversity	lithology	isostatic gravity	K/Na	geo-magnetics
fault buffers	0.00	2.58	6.17	9.51	2.35	3.96	1.24
pluton buffers	0.00		13.37	5.72	6.47	0.78	13.56
lithologic diversity	0.00			0.83	6.21	12.50	3.20
lithology	0.00				1.70	2.16	11.14
isostatic gravity	0.00					3.05	0.02
K/Na	0.00						3.32
geomagnetics	0.00						

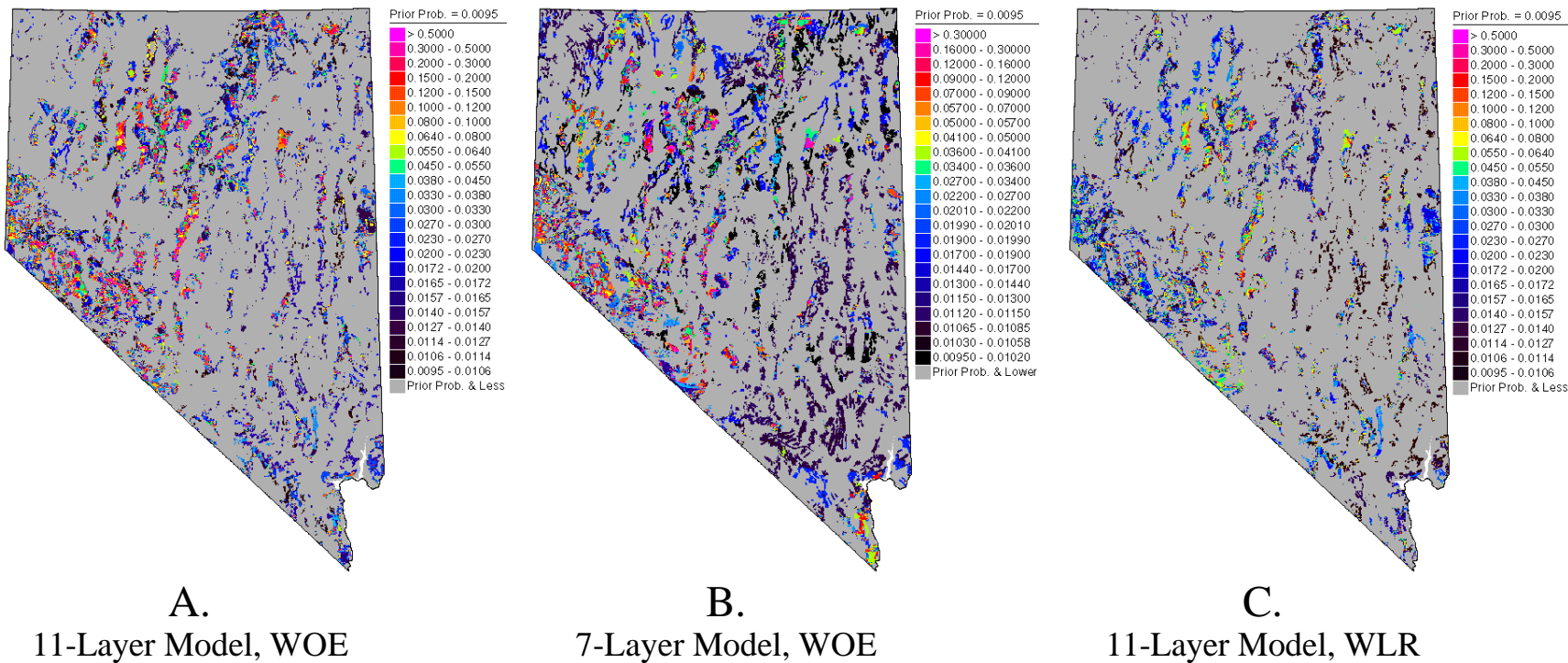
**Table C.3.** Pairwise conditional independence (CI) test  $\chi^2$  scores for the volcanic rock-hosted occurrence-type model. Table **A.** (upper) shows scores for the combination of all (9) binary-class predictor maps. Table **B.** (lower) shows scores for the combination of seven maps after removal of the Ba/Na and lithotectonic terranes maps from the model. With 1 degree of freedom and a probability level of 99% ( $\chi^2_{0.99,1} = 6.63$ ), over 76% of the map pattern pairs in table B approximately satisfy the assumption of conditional independence. The Ba/Na geochemical anomaly map was removed from the model because of the high degree of association of Ba-bearing mineralization (primarily barite) with sedimentary rock-hosted occurrences. The lithotectonic terranes map was removed from the model to eliminate the greatest number of conditional dependencies while rejecting the least number of maps from the model. Other map pair combinations responsible for a significant degree of conditional dependency were not removed from the model because of the relative importance of these features to mineralization (e.g.—fault buffers).

<i>Mineral Potential Model</i>	<b>Occurrence-Type Model</b>					
	<i>Primary (all sizes and types)</i>		<i>Sedimentary Rock-Hosted</i>		<i>Volcanic Rock-Hosted</i>	
	11-Layer	7-Layer	9-Layer	8-Layer	9-Layer	7-Layer
<i>Observed Occurrences</i>	2690	2690	98	98	415	415
<i>Expected Occurrences</i>	4525.45	3261.11	721.99	733.36	654.31	507.21
<i>% Expected &gt; Observed</i>	68.23	21.23	636.72	648.33	57.67	22.22
<i>Number of Unique Conditions</i>	1144	154	598	382	658	198
<i>K-S Critical Value (% = 0.05)</i>	0.0402	0.1096	0.0556	0.0696	0.0530	0.0966
<i>K-S Statistic for the Model</i>	0.2737	0.1725	0.4254	0.4316	0.2547	0.1599

**Table C.4.** Summary information of the overall conditional independence test for the various mineral potential models.

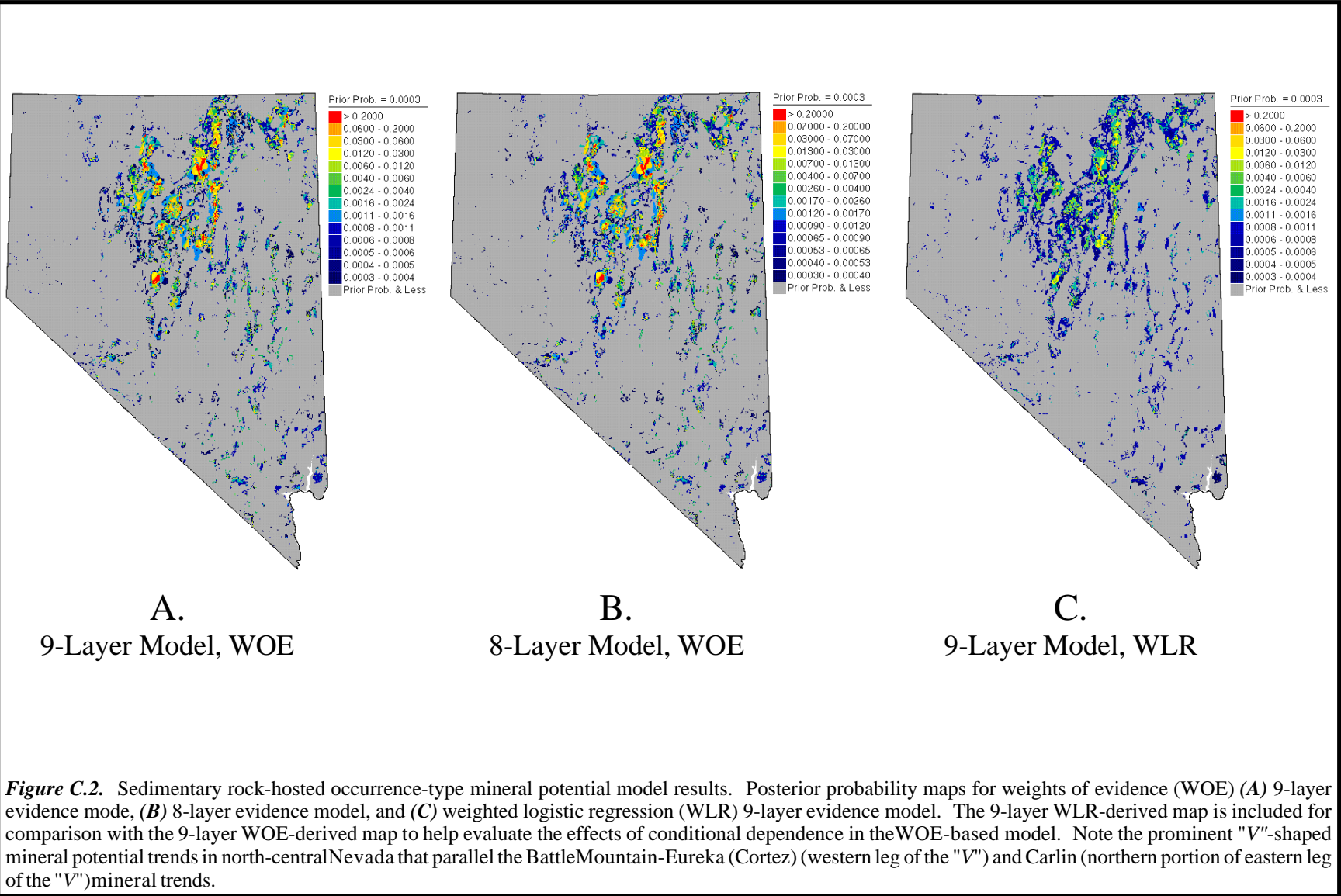
<b>Occurrence-Type Mineral Potential Model</b>						
<i>Mineral Potential Model</i>	<i>Primary (all sizes and types)</i>		<i>Sedimentary Rock-Hosted</i>		<i>Volcanic Rock-Hosted</i>	
	11-Layer	7-Layer	9-Layer	8-Layer	9-Layer	7-Layer
<i>Observed Occurrences</i>	2690	2690	98	98	415	415
<i>WLR Expected Occurrences</i>	2572.94	2606.54	96.42	96.46	411.35	412.07
<i>% WLR Expected Over Observed</i>	-4.35	-3.10	-1.61	-1.57	-0.88	-0.71
<i>WOE Expected Occurrences</i>	4525.45	3261.11	721.99	733.36	654.31	507.21
<i>% WOE Expected Over Observed</i>	68.23	21.23	636.72	648.33	57.67	22.22

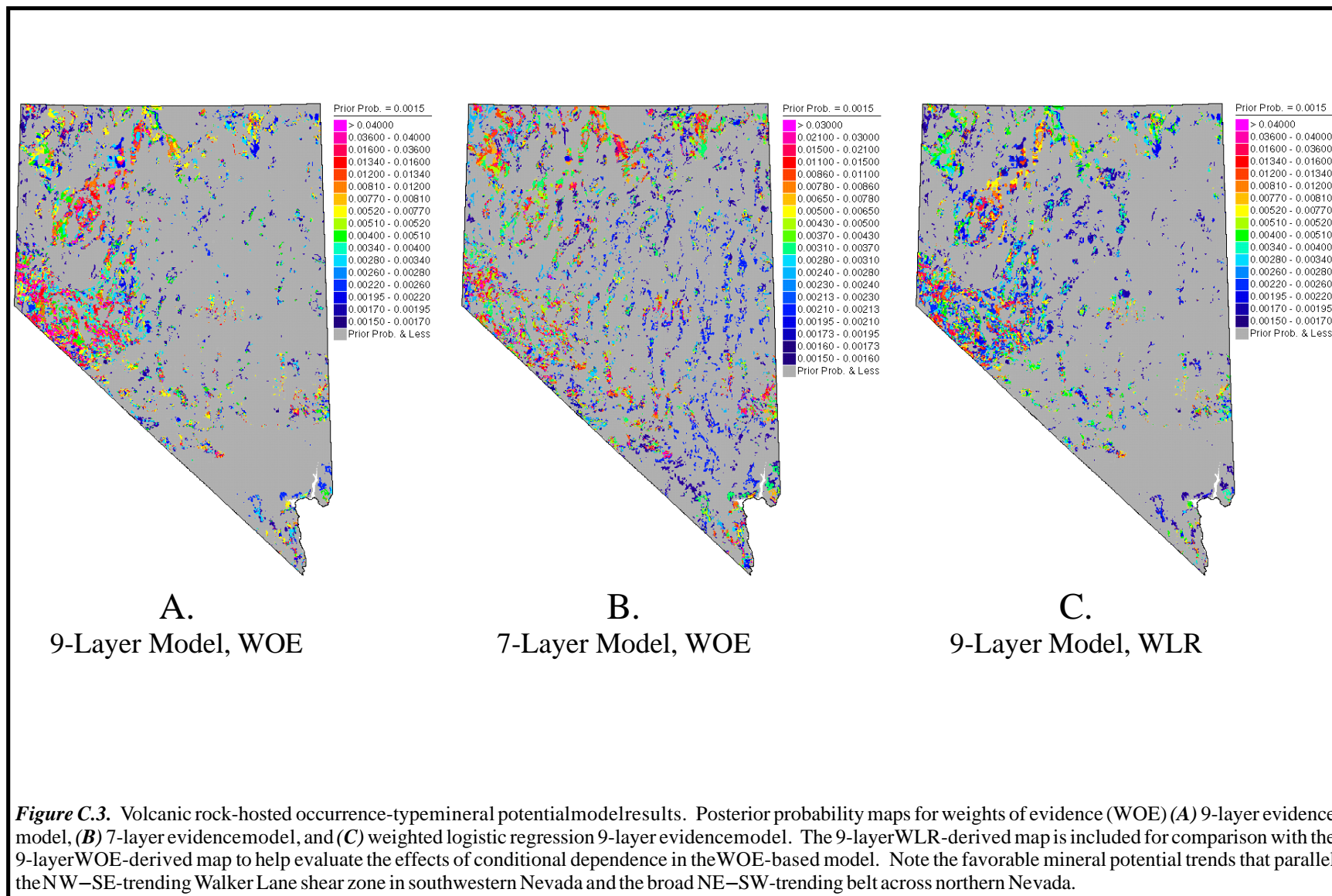
**Table C.5.** Comparison of expected versus observed occurrences for the weights of evidence (WOE) and weighted logistic regression (WLR) methods of evidence combination. In general, the number of occurrences predicted using the WLR method is nearly equal to the number of occurrences observed. Minus percent values indicate the amount that the predicted number of occurrences fall below (short of) the observed (the observed equalling 100%).



**Figure C.1.** Primary occurrence-type mineral potential model results. Posterior probability maps for weights of evidence (WOE) (A) 11-layer evidence model, (B) 7-layer evidence model, and (C) weighted logistic regression (WLR) 11-layer evidence model. The 11-layer WLR-derived map is included for comparison with the 11-layer WOE-derived map to help evaluate the effects of conditional dependence in the WOE-based model. Note the regions of favorable mineral potential along the NW-SE Walker Lane shear zone in southwestern Nevada, the Battle Mountain heat high in north-central Nevada, and the weak pattern along the Battle Mountain-Eureka (Cortez) mineral trend. In general, the WOE- and WLR-derived maps show the same overall map patterns, except that the WOE-derived maps appear to be "warmer" and better highlight favorable mineral potential areas. The WLR map combination method generally produces lower posterior probabilities than does the WOE method. The WLR-derived posterior probability map was generated using the WOE-derived posterior probability classification scheme (to facilitate comparison between the two methods), and is the reason for the overall "less-favorable" appearance ("cooler colors") of the WLR-derived map. If the WLR-derived map was reclassified using a classification scheme based on the range of WLR-derived posterior probabilities, the resultant map would be very similar in appearance to the WOE-derived map.







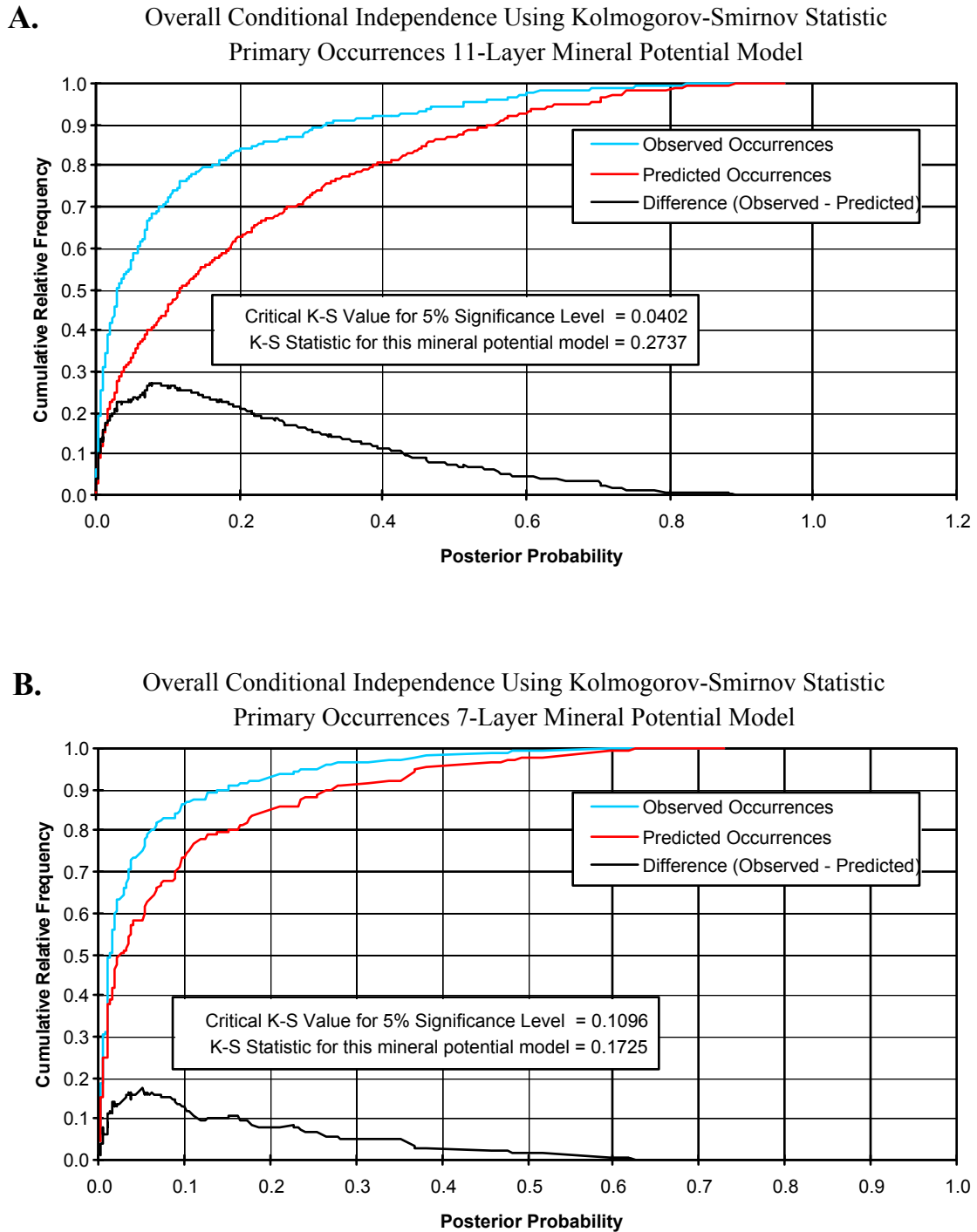
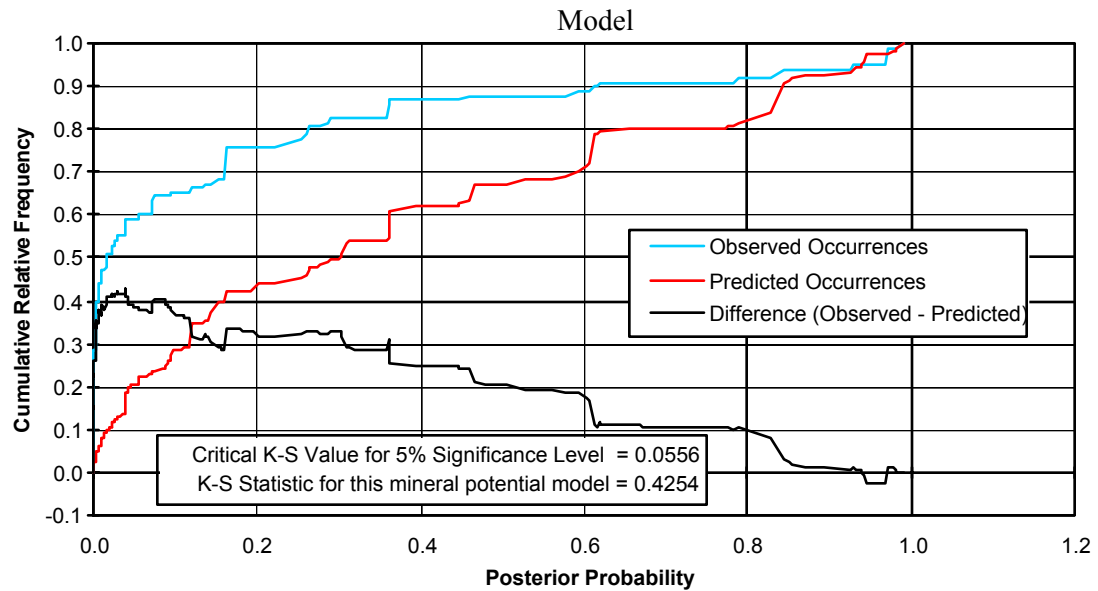


**Figure C.4.** Overall goodness-of-fit test for all size and type occurrences, using the K-S statistic: (A) primary 11-layer model; (B) primary 7-layer model.

**A.** Overall Conditional Independence Using Kolmogorov-Smirnov Statistic  
Sedimentary Rock-Hosted Occurrences 9-Layer Mineral Potential



**B.** Overall Conditional Independence Using Kolmogorov-Smirnov Statistic  
Sedimentary Rock-Hosted Occurrences 8-Layer Mineral Potential

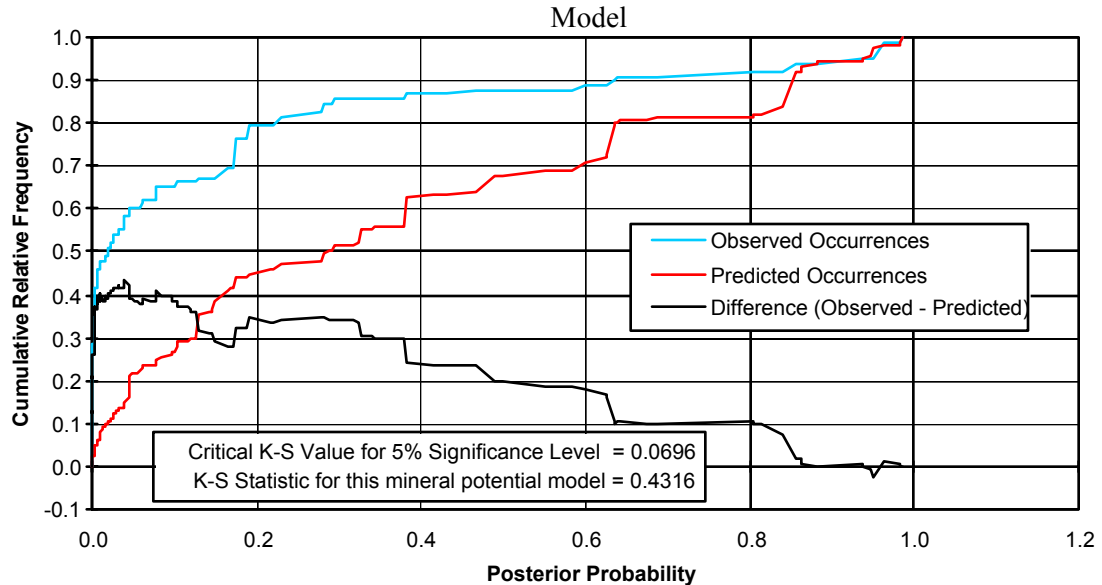
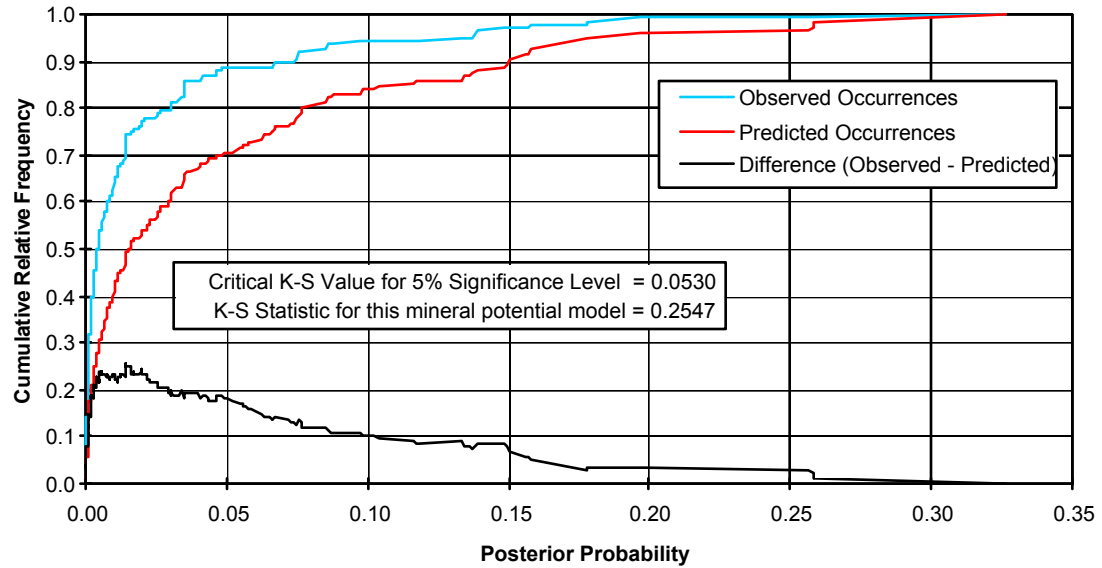


**Figure C.5.** Overall goodness-of-fit test for sed. rock-hosted occurrences, using the K-S statistic: (A) sed-host. 9-layer model; (B) sed-host. 8-layer model.

**A.** Overall Conditional Independence Using Kolmogorov-Smirnov Statistic  
Volcanic Rock-Hosted Occurrences 9-Layer Mineral Potential Model



**B.** Overall Conditional Independence Using Kolmogorov-Smirnov Statistic  
Volcanic Rock-Hosted Occurrences 7-Layer Mineral Potential Model

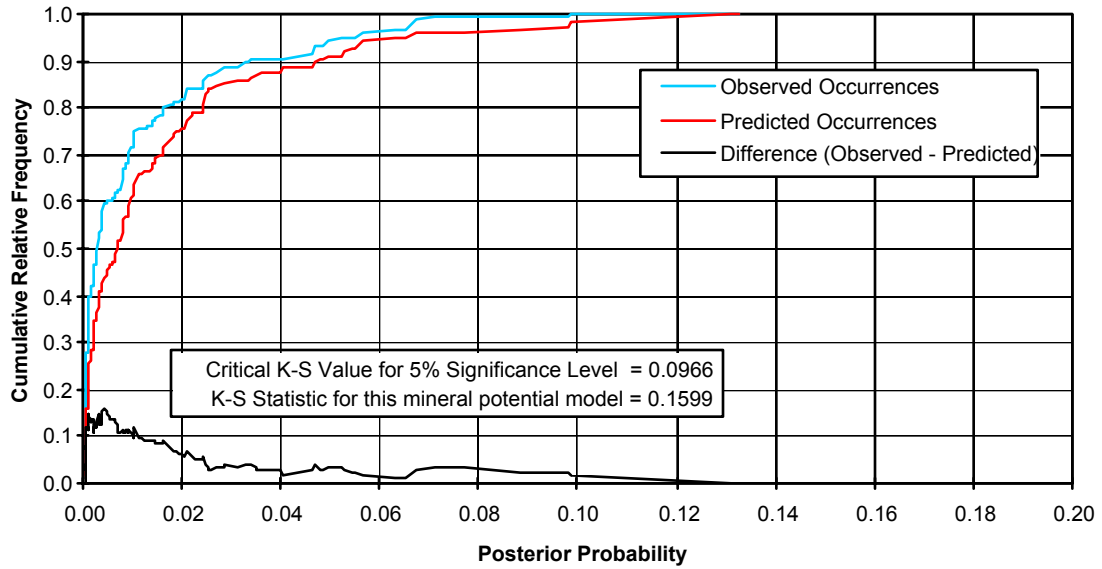
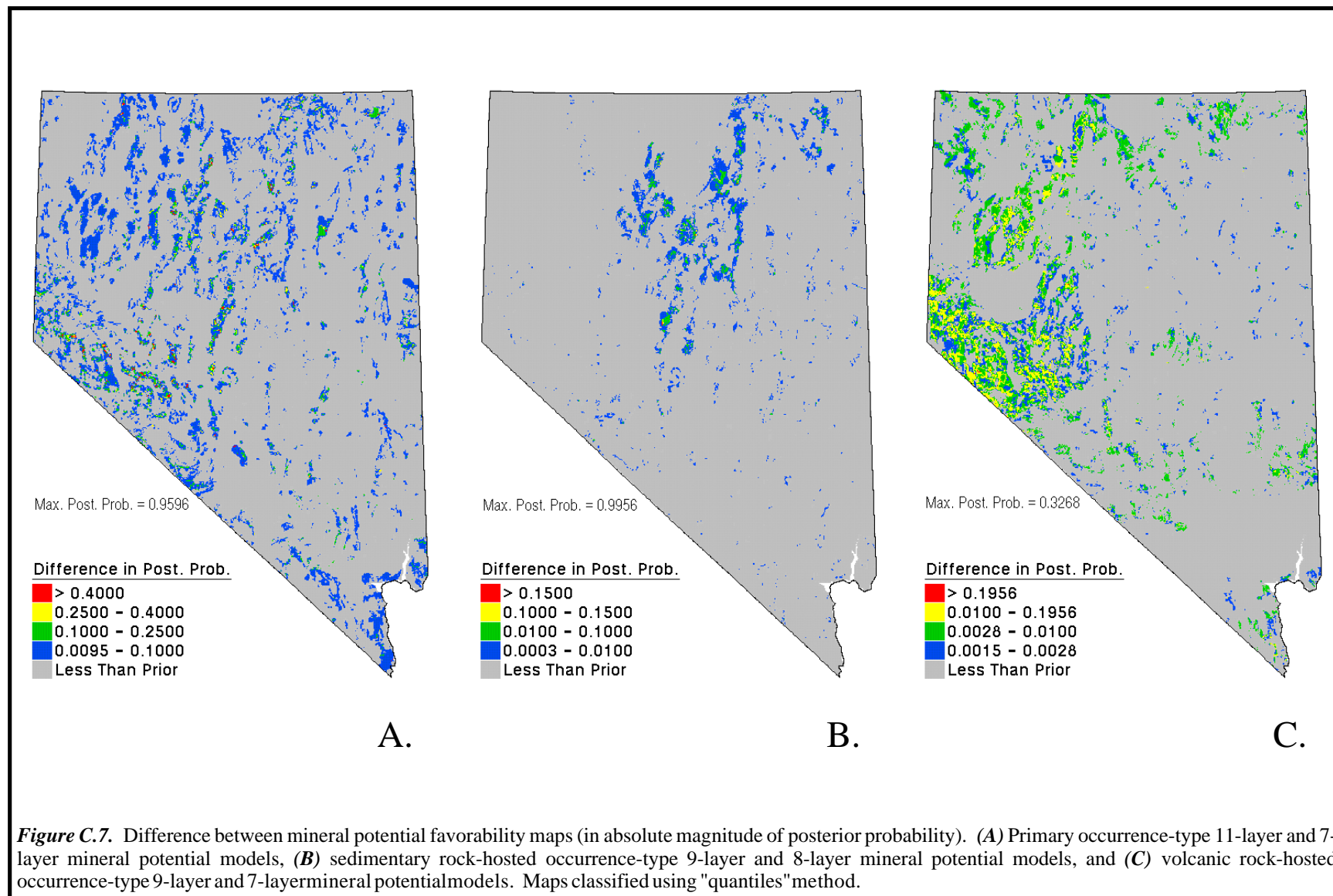
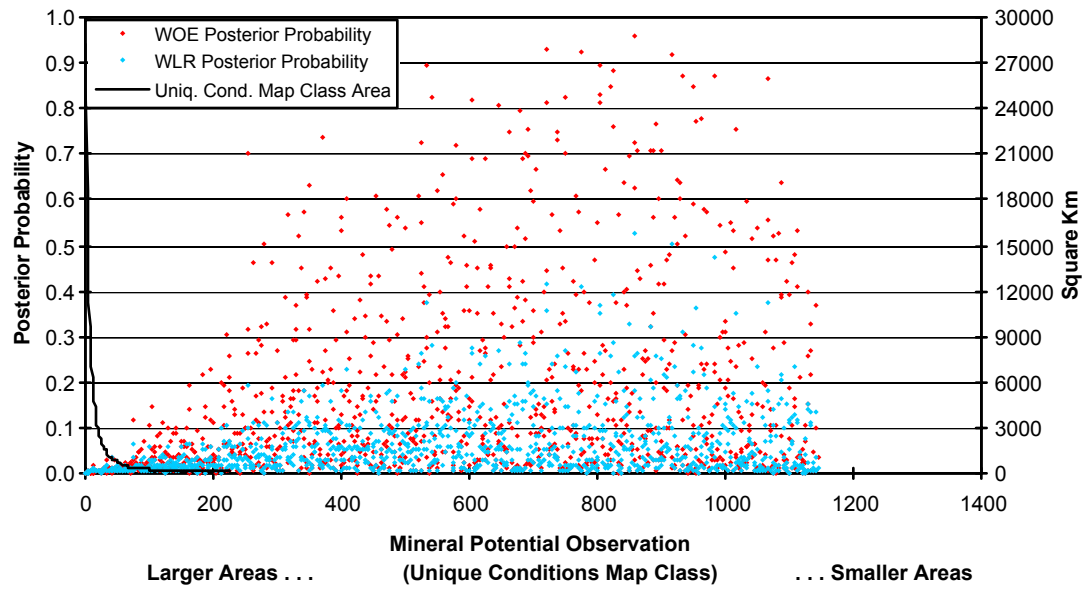


**Figure C.6.** Overall goodness-of-fit test for vol. rock-hosted occurrences, using the K-S statistic: (A) vol-host. 9-layer model; (B) vol-host. 7-layer model.



**A.** Comparison of WOE versus WLR Derived Posterior Probabilities  
Primary Occurrences 11-Layer Mineral Potential Model



**B.** WOE Poster Probability Plotted Against WLR Posterier Probability  
Primary Occurrences 11-Layer Mineral Potential Model

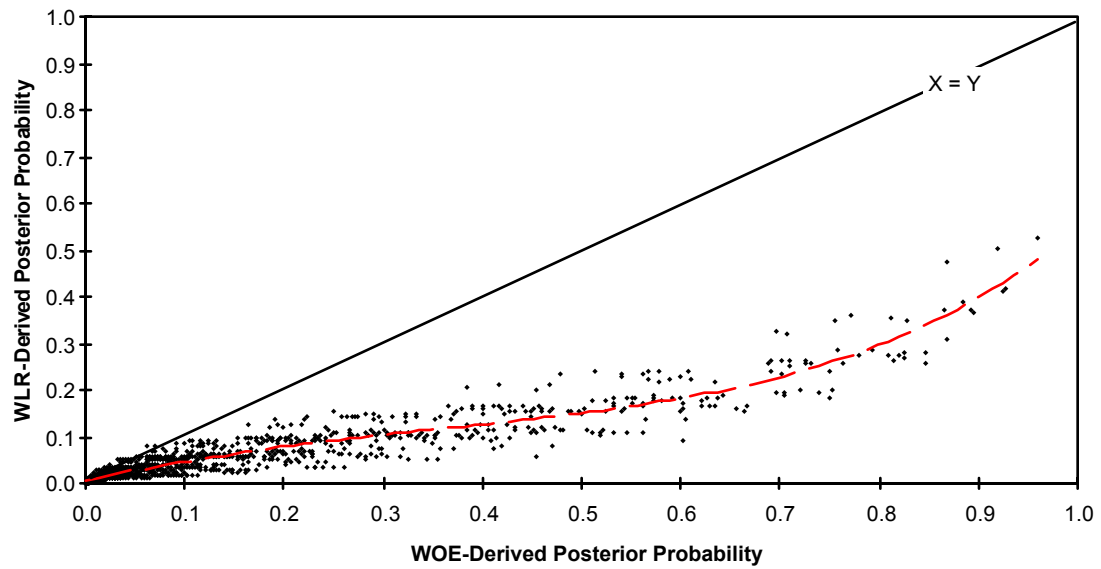


**Figure C.8** Posterior probability estimates derived from WOE and WLR methods for the primary 11-layer mineral potential model. WOE estimates tend to be higher than WLR.



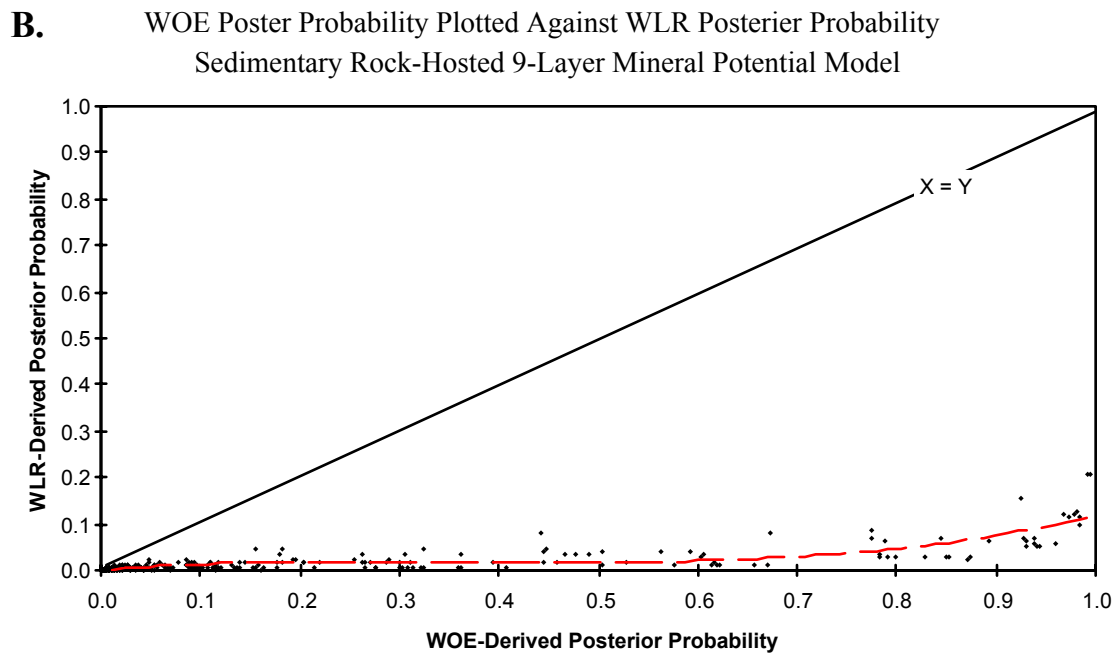
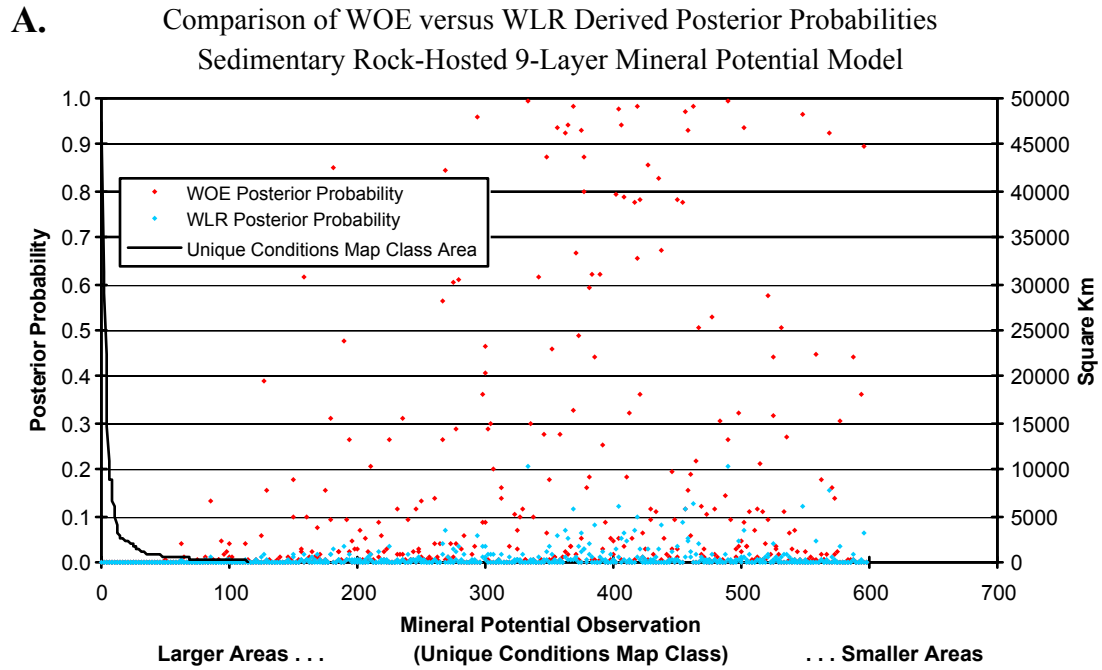


**Figure C.9** Posterior probability estimates derived from WOE and WLR methods for sed. host. 9-layer mineral potential model. WOE estimates tend to be higher than WLR estimates.

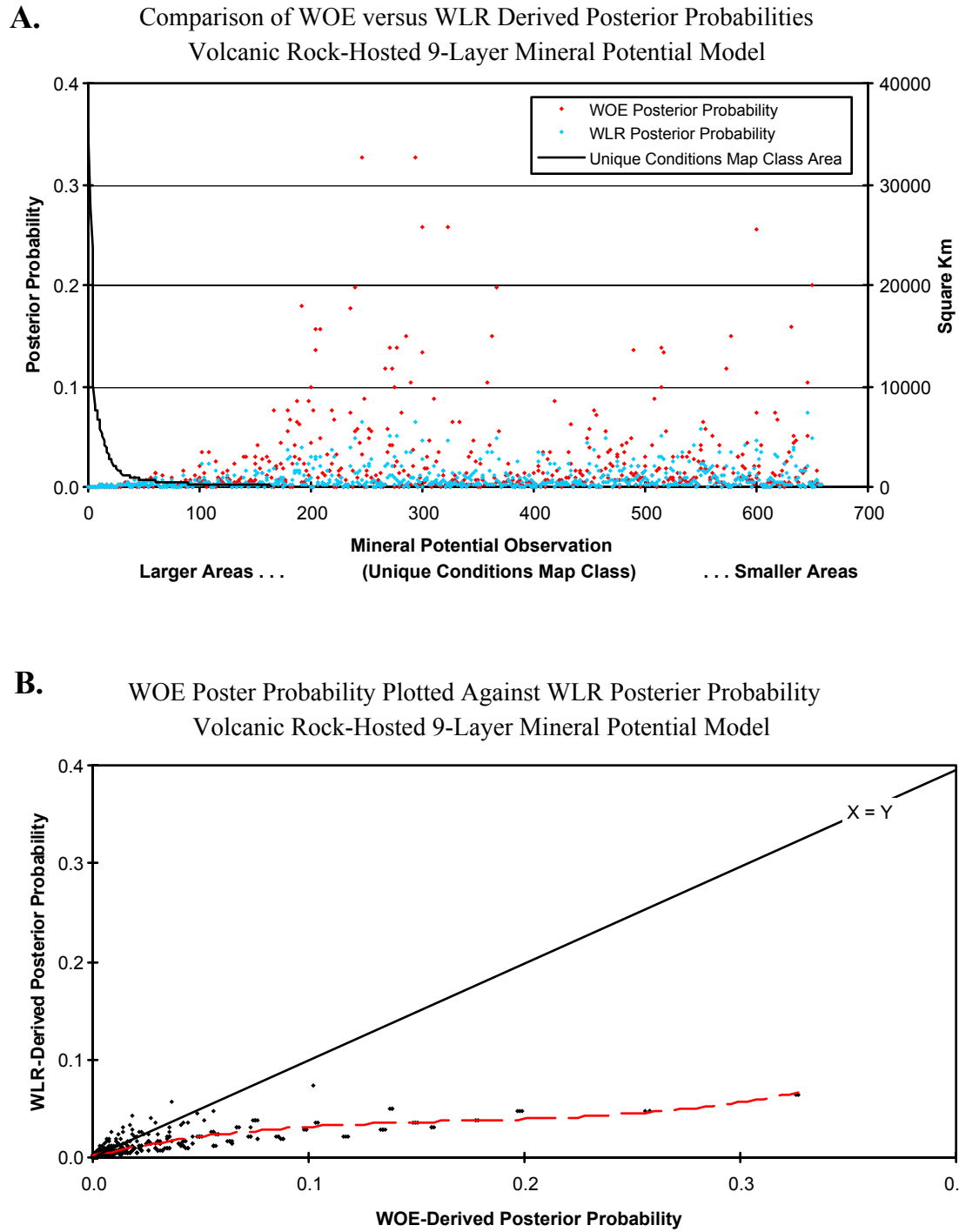


**Figure C.10** Posterior probability estimates derived from WOE and WLR methods for vol. host. 9-layer mineral potential model. WOE estimates tend to be higher than WLR estimates.

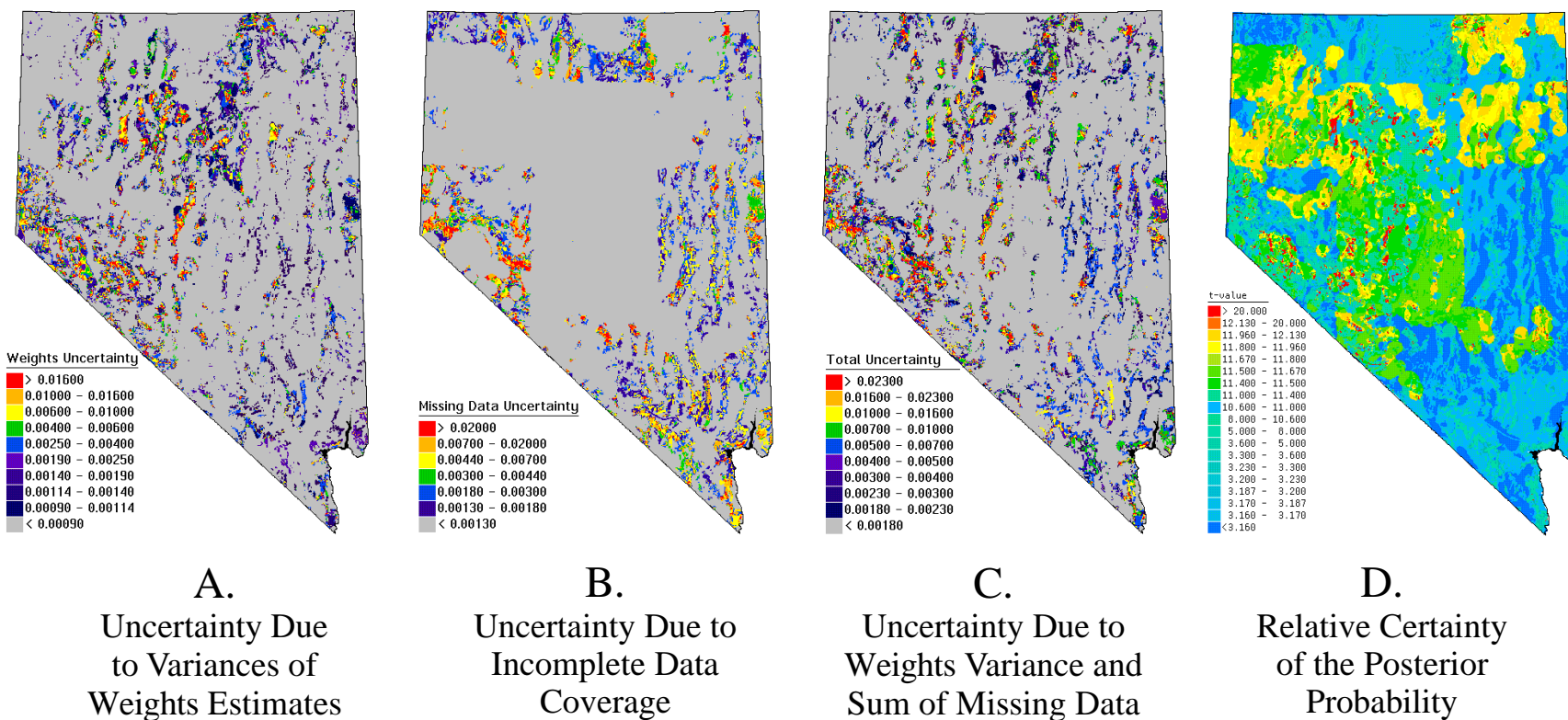
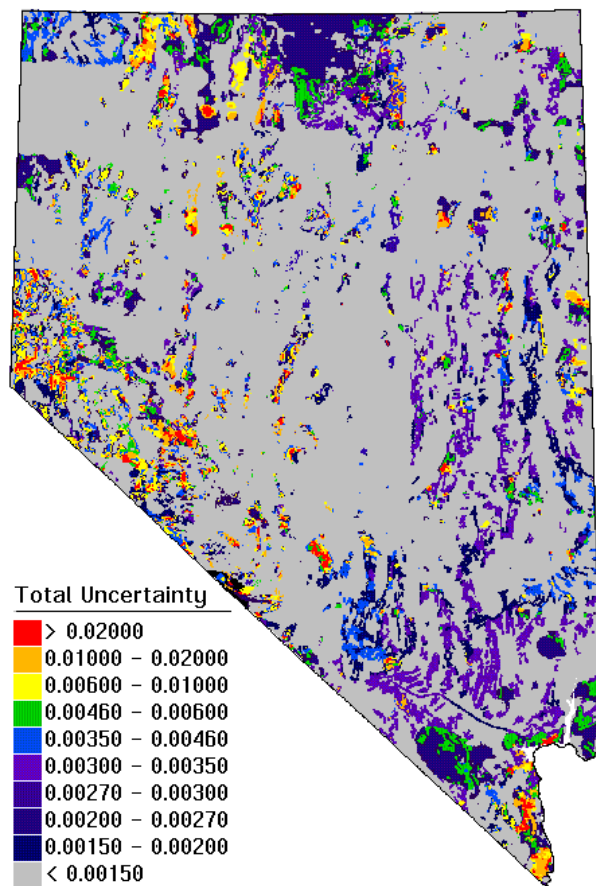


**Figure C.11.** Examples of various sources and types of uncertainty in the posterior probability estimates used to generate the primary occurrence-type 11-layer mineral potential map. (A) Uncertainty due to variances in the estimate of spatial weights of association, (B) uncertainty due to missing data (primarily incomplete coverage of K/Na and Ba/Na geochemical anomaly maps), (C) total uncertainty (uncertainty due to variances of weights, plus, sum of uncertainty due to missing data), and (D) relative certainty of the posterior probability (posterior probability divided by its standard deviation; in effect, the application of an approximate t-test). All maps were classified using a quantiles approach. With the exception of the relative certainty map, the maps have been classified so as to accentuate the 50th percentile of area associated with the higher magnitude uncertainty values. Maps A, B, and C have dimensionless units. Map D units represent t-values (at a significance level of 95%, t-values great than 1.645 indicate that the posterior probabilities are greater than 0). In map D, the mineral potential favorability estimates are relatively more certain in regions that appear yellow-orange-red.

A.



B.

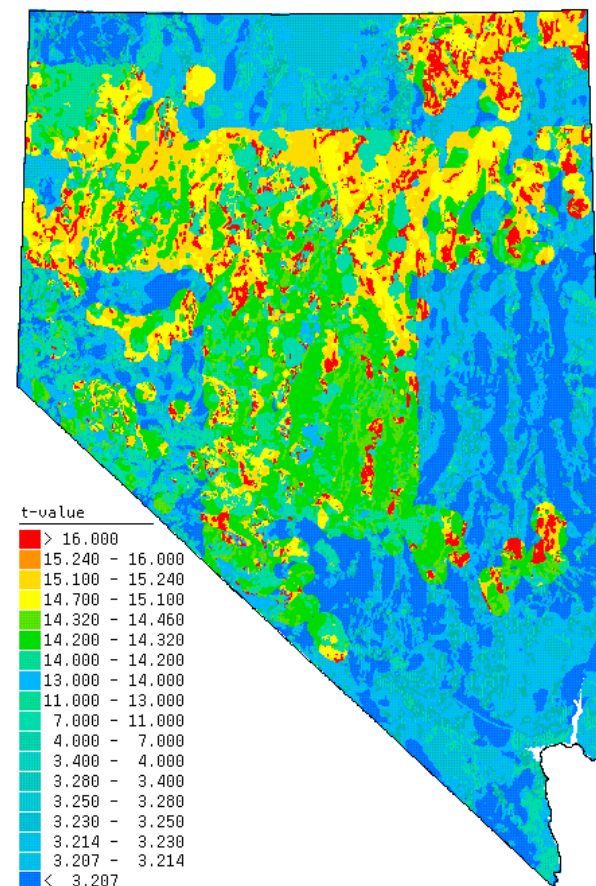
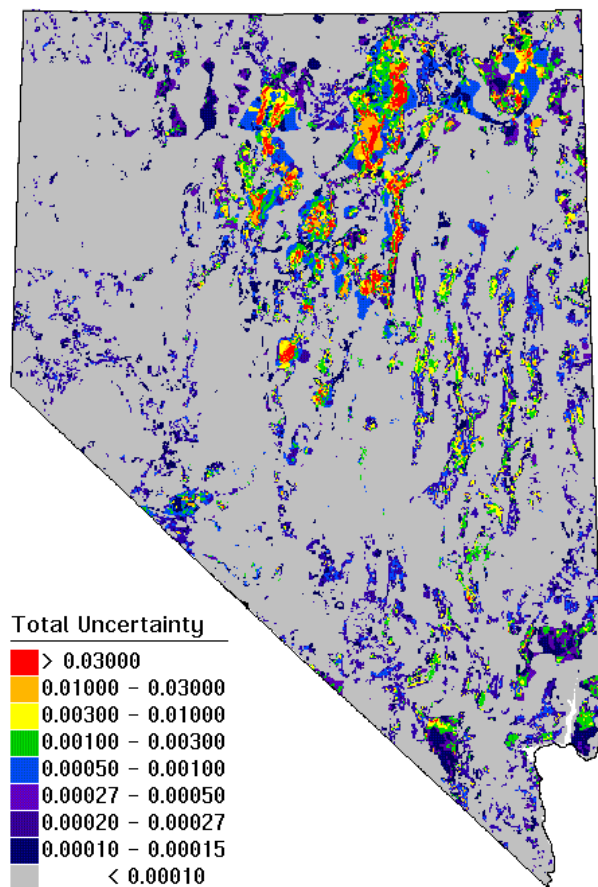


**Figure C.12.** Uncertainty of posterior probabilities used to generate primary occurrence-type 7-layer mineral potential map. (A) Total uncertainty (uncertainty due to variances of weights, plus, sum of uncertainty due to missing data) and (B) relative certainty of the posterior probability (posterior probability divided by its standard deviation, in effect, the application of an approximate t-test). See [Figure C.11](#) caption for additional information.

A.



B.

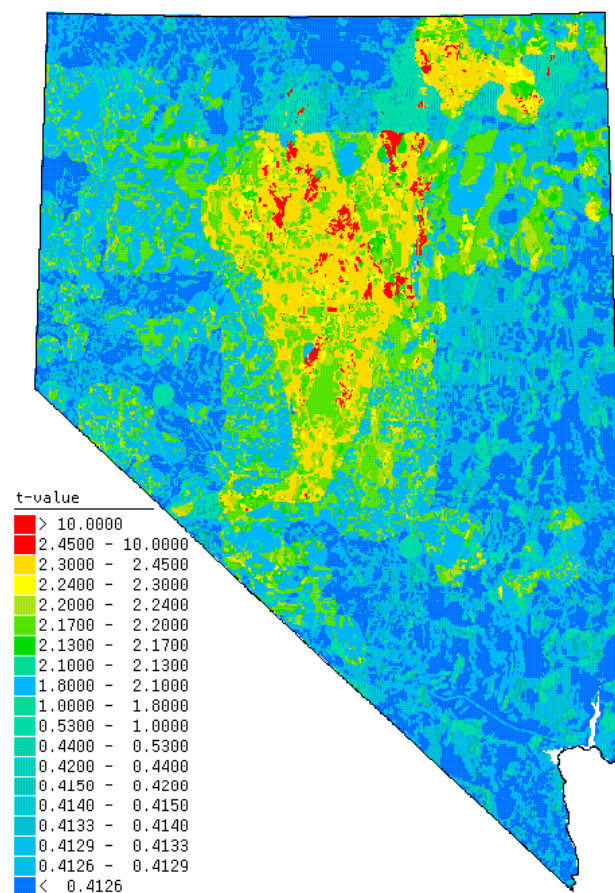
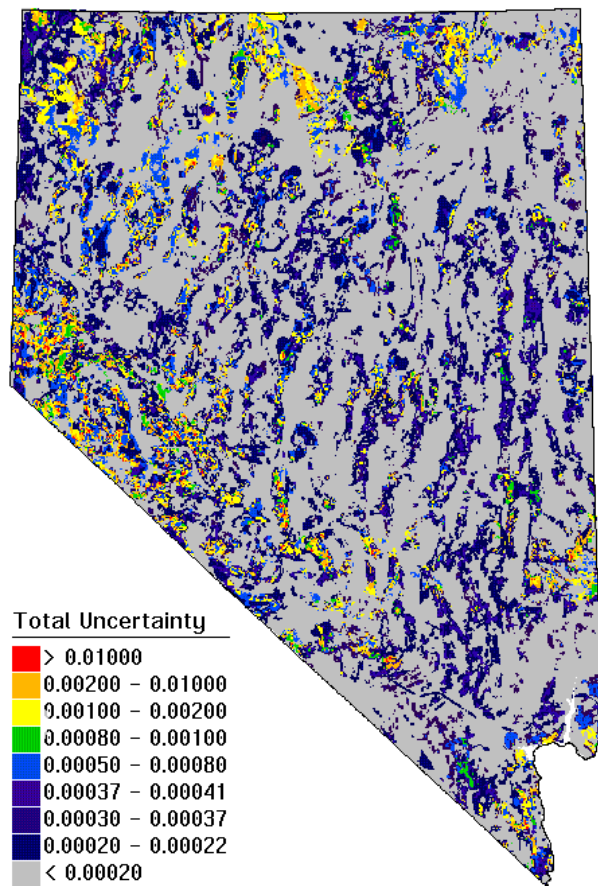


**Figure C.13.** Uncertainty of posterior probabilities used to generate sedimentary rock-hosted occurrence-type 8-layer mineral potential map. (A) Total uncertainty (uncertainty due to variances of weights, plus, sum of uncertainty due to missing data) and (B) relative certainty of the posterior probability (posterior probability divided by its standard deviation, in effect, the application of an approximate t-test). See [Figure C.11](#) caption for additional information.



A.



B.

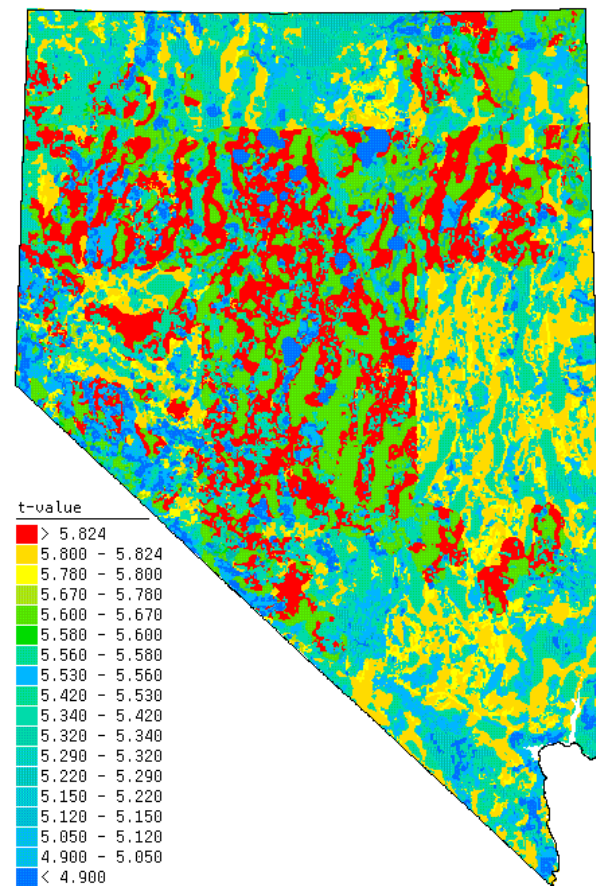
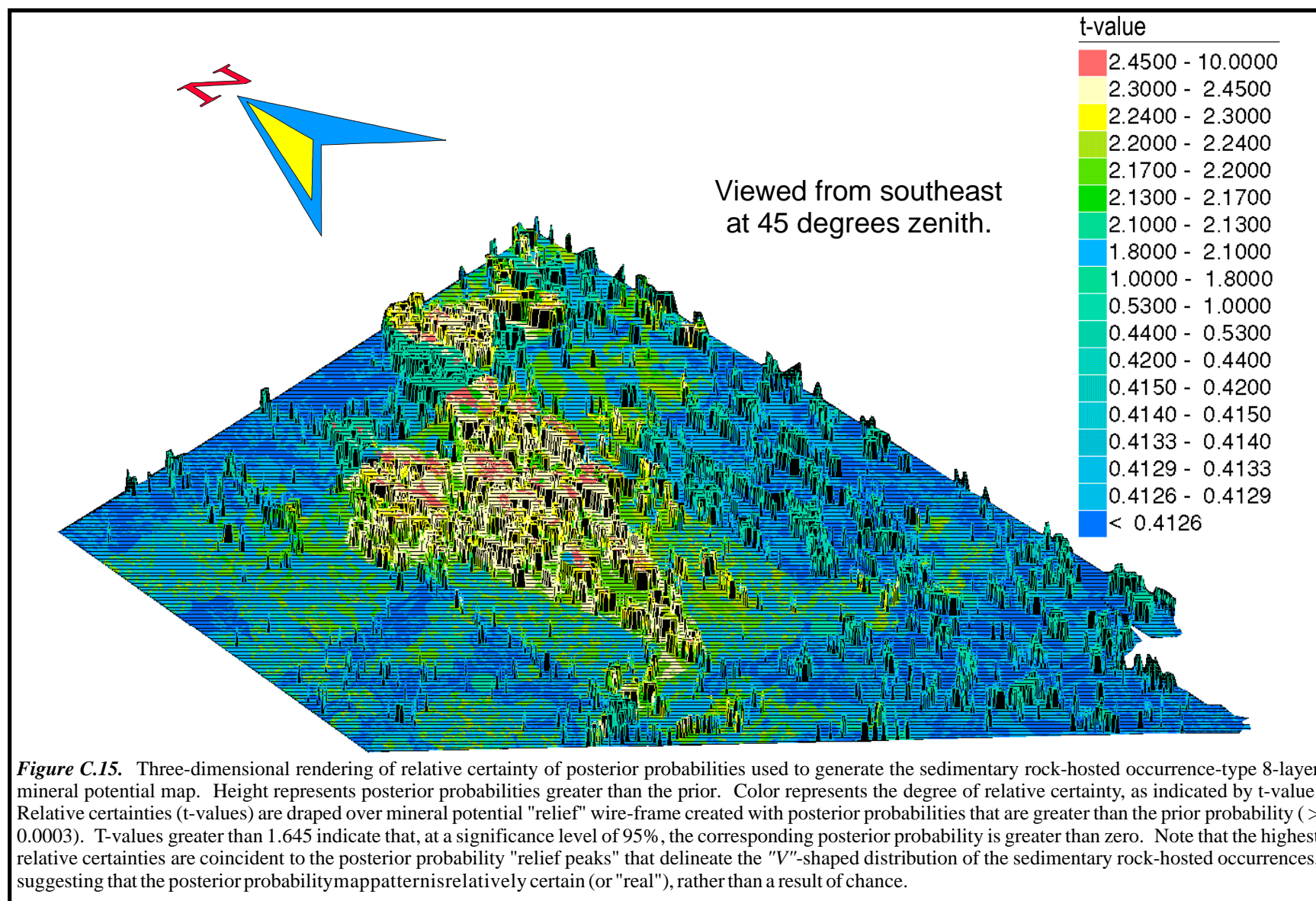


**Figure C.14.** Uncertainty of posterior probabilities used to generate volcanic rock-hosted occurrence-type 7-layer mineral potential map. (A) Total uncertainty (uncertainty due to variances of weights, plus, sum of uncertainty due to missing data) and (B) relative certainty of the posterior probability (posterior probability divided by its standard deviation, in effect, the application of an approximate t-test). See [Figure C. 11](#) caption for additional information.





# APPENDIX D

## Mineral Potential at Known Mineral Occurrence Areas:

### Section Contents:

- D.1** Summary Statement
- D.2** Primary Gold-Silver-Bearing Occurrences
- D.3** Sedimentary Rock-Hosted Gold-Silver-Bearing Occurrences
- D.4** Volcanic Rock-Hosted Gold-Silver-Bearing Occurrences

## D.1 Summary Statement

Approximately  $\frac{2}{3}$  to  $\frac{3}{4}$  of all occurrences, for any given occurrence-type sample, have posterior probabilities greater than the prior probability.

## D.2 Primary Gold-Silver-Bearing Occurrences

*Figure D.1* Approximately 76% of the big (large and medium size) and ~69% of the small size occurrences have posterior probabilities larger than the prior probability, with a total of ~69% of all of the primary occurrences having a higher posterior probability.

*Figure D.2* The spatial distribution of the primary gold-silver-bearing occurrences with elevated posterior probability values is coincident with areas of elevated mineral potential favorability, as predicted by the primary occurrence posterior probability map. In this figure, a conspicuous pattern of occurrences is highlighted with a dashed line (map “B”), and is shown to have a spatially associated and corresponding pattern of areas of elevated posterior probability (map “A”). The dashed line merely delineates the spatial distribution of the occurrences, and does not necessarily reflect any geologic, structural, or other genetic-related trends (particularly in the case of the primary occurrences).

*Table D.1* Primary gold-silver-bearing occurrences of all sizes and types having posterior probabilities  $\geq 0.1000$ , as determined with the primary 7-layer mineral potential model (see table C.1b).

## D.3 Sedimentary Rock-Hosted Gold-Silver-Bearing Occurrences

*Figure D.3* Approximately 84% of the big and ~82% of the small size occurrences have posterior probabilities larger than the prior probability, with a total of ~83% of all of the sedimentary rock-hosted occurrences having a higher posterior probability.

*Figure D.4* The spatial distribution of the sedimentary rock-hosted gold-silver-bearing occurrences with elevated posterior probability values is coincident with areas of elevated mineral potential favorability, as predicted by the sedimentary rock-hosted occurrence posterior probability map. In this figure, a conspicuous pattern of occurrences is highlighted with a dashed line (map “B”), and is shown to have a spatially associated and corresponding pattern of areas of elevated posterior probability (map “A”). The dashed line merely delineates the spatial distribution of the occurrences, and does not necessarily reflect any geologic, structural, or other genetic-related trends, although one may exist..

*Table D.2* Posterior probabilities associated with gold-silver-bearing sedimentary rock-hosted occurrences of all sizes, as determined with the sedimentary rock-hosted 8-layer mineral potential model (see table C.2b).

## **D.4 Volcanic Rock-Hosted Gold-Silver-Bearing Occurrences**

*Figure D.5* Approximately 72% of the big and ~60% of the small size occurrences have posterior probabilities larger than the prior probability, with a total of ~60% of all of the volcanic rock-hosted occurrences having a higher posterior probability.

*Figure D.6* The spatial distribution of the volcanic rock-hosted gold-silver-bearing occurrences with elevated posterior probability values is coincident with areas of elevated mineral potential favorability, as predicted by the volcanic rock-hosted occurrence posterior probability map. In this figure, a conspicuous pattern of occurrences is highlighted with a dashed lines (map “B”), and is shown to have a spatially associated and corresponding pattern of areas of elevated posterior probability (map “A”). The dashed lines merely delineate the spatial distribution of the occurrences, and does not necessarily reflect any geologic, structural, or other genetic-related trends, although one may exist.

*Table D.3* Posterior probabilities associated with gold-silver-bearing volcanic rock-hosted occurrences of all sizes, as determined with the volcanic rock-hosted 7-layer mineral potential model (see table C.3b).

County	Site Name	Size	Post. Prob.	Commodities				Deposit Type
ELKO	HUNTER PROSPECT	S	0.6300	AG	PB	SB	--	---
ELKO	PROSPECT NO. 4	S	0.6199	AU	--	--	--	---
ESMERALDA	DUTCHESS PROSPECT	S	0.6199	AU	CU	AG	F	---
ESMERALDA	ENTERPRISE PROSPECT	S	0.6199	AU	AG	CU	PB	COPPER SKARN
LANDER	GOLD TOP MINE	?	0.6199	AU	AG	CU	ZN	---
LANDER	BENTLEY MINE	S	0.6199	AG	PB	CU	AU	POLYMETALLIC VEINS
LANDER	BIG FOUR MINE	S	0.6199	AG	AU	PB	--	---
LANDER	BUZZARD MINE	S	0.6199	AU	CU	PB	AG	POLYMETALLIC VEINS
LANDER	FAIRVIEW PROPERTY	S	0.6199	AU	AG	PB	CU	---
LANDER	FULLER GROUP	S	0.6199	AU	AG	FE	SB	---
LANDER	INDEPENDENCE MINE	S	0.6199	AG	AU	CU	ZN	---
LANDER	LITTLE GIANT MINE	S	0.6199	AU	AG	CU	PB	POLYMETALLIC VEINS
LANDER	MONITOR CLAIM	S	0.6199	AU	AG	ZN	FE	---
LANDER	PEGGY GROUP MINE	S	0.6199	AG	CU	AU	--	POLYMETALLIC VEINS
LANDER	SILVER KING MINE	S	0.6199	AU	AG	--	--	GOLD SKARN
NYE	NBMG SAMPLE SITE. 3174	S	0.6199	AU	--	--	--	---
NYE	PHILLIPS MINE	S	0.6199	AG	--	--	--	---
NYE	SHAMROCK DIGGINGS	S	0.6199	AG	--	--	--	---
NYE	SHAMROCK MINE	S	0.6199	AG	AU	--	--	---
NYE	UNNAMED PROSPECT (ELLSWORTH DISTRICT)	S	0.6199	AU	AG	--	--	---
PERSHING	AGAMEMNON MINE	?	0.5378	AU	AG	SB	--	LOW-SULFIDE AU-QUARTZ VEINS
PERSHING	BLACK WARRIOR MINE	S	0.5378	SB	AG	CU	ZN	LOW-SULFIDE AU-QUARTZ VEINS
PERSHING	ENTERPRISE MINE	S	0.5378	AU	CU	--	--	LOW-SULFIDE AU-QUARTZ VEINS
PERSHING	PACIFIC MATCHLESS MINE	S	0.5378	AG	PB	--	--	LOW-SULFIDE AU-QUARTZ VEINS
PERSHING	WHEELER MINE	S	0.5378	AG	AU	CU	ZN	LOW-SULFIDE AU-QUARTZ VEINS
CHURCHILL	BLUFF MINE	S	0.4983	AG	AU	--	--	COMSTOCK EPITHERMAL VEINS
CHURCHILL	BUFF CLAIMS	S	0.4983	AU	AG	--	--	COMSTOCK EPITHERMAL VEINS
ESMERALDA	MAUD CLAIMS	S	0.4875	AU	--	--	--	---
ESMERALDA	SILVER KING CLAIMS (TOKOP DISTRICT)	S	0.4875	AU	AG	W	AS	---
NYE	BAXTER SPRINGS PROSPECT	?	0.4875	AU	--	--	--	---
CHURCHILL	DROMEDARY HUMP MINE	S	0.4818	AG	AU	--	--	COMSTOCK EPITHERMAL VEINS
ELKO	HUMBOLDT MINE	S	0.4818	AU	PB	CU	--	POLYMETALLIC VEINS
ELKO	JACKPOT	S	0.4818	AU	AG	--	--	---
NYE	LOCKE MINE	S	0.4818	AU	AG	--	--	---
NYE	SHOE - SHOE MINE	S	0.4818	AU	AG	PB	ZN	---
ELKO	EDGAR TURQUOISE MINE	?	0.4710	GEM	AU	--	--	---
ESMERALDA	APRIL MINE	S	0.4710	AU	--	--	--	---
ESMERALDA	BLACK BEAUTY GROUP	S	0.4710	AU	AG	PB	ZN	---
ESMERALDA	GOLD LEDGE CLAIM GROUP	S	0.4710	AG	AU	PB	--	---
ESMERALDA	LAST CHANCE MINE	S	0.4710	AU	AG	PB	--	---
ESMERALDA	MARY MINE	S	0.4710	AU	AG	PB	--	LOW-SULFIDE AU-QUARTZ VEINS
ESMERALDA	MISSOURI PROSPECT	S	0.4710	AU	--	--	--	---
ESMERALDA	NEW YORK AND SILVER PEAK MINING CO. MINES	S	0.4710	AG	AU	--	--	---
ESMERALDA	POCATELLO MINE	S	0.4710	AG	AU	CU	--	LOW-SULFIDE AU-QUARTZ VEINS
ESMERALDA	SHIPPER GROUP	S	0.4710	AG	AU	CU	--	---
ESMERALDA	TREASURE CLAIM	S	0.4710	AU	?	--	--	---
ESMERALDA	VANDERBILT MINE	S	0.4710	AG	AU	CU	--	---
LANDER	CARISSA MINE	S	0.4710	AU	CU	AG	W	GOLD SKARN

**Table D1.** Primary gold-silver-bearing occurrences of all sizes and types having posterior probabilities \$ 0.1000, as determined with the primary 7-layer mineral potential model (practical space limitations restrict the listing of all 2960 occurrences; sorted in order of descending posterior probability). All data, with the exception of posterior probabilities, from the MRDS mineral occurrences database. Occurrences size from Guild (1968), and deposit types from Cox and Singer (1986). Prior probability = 0.0095.

County	Site Name	Size	Post. Prob.	Commodities				Deposit Type
LANDER	EAGLE MINE	S	0.4710	AU	AG	--	--	---
LANDER	GOLD DYKE MINE	S	0.4710	AU	AG	--	--	---
LANDER	GOLD ROD	S	0.4710	AU	AG	--	--	---
LANDER	LABRADOR DEPOSIT	S	0.4710	AU	AG	--	--	COPPER SKARN
LANDER	NORTHERN LIGHTS DEPOSIT	S	0.4710	AU	AG	CU	--	SEDIMENT-HOSTED AU-AG
NYE	GRIZZLY CLAIM	S	0.4710	AU	--	--	--	---
NYE	KORF PROPERTY	S	0.4710	AU	--	--	--	---
NYE	WHITE HORSE CLAIM	S	0.4710	AU	W	--	--	---
WHITE PINE	ESSEX TUNNEL	?	0.4710	AU	FE	--	--	---
WHITE PINE	GOLD KING GROUP	?	0.4710	AU	SB	--	--	---
NYE	HALLER PROPERTY	S	0.3813	AG	PB	ZN	--	---
ELKO	MOHAWK	S	0.3712	AU	AG	FE	--	---
ELKO	PITTSBURG SILVER	S	0.3712	AU	AG	FE	CU	---
ESMERALDA	JACKSON/ELECTRIC CLAIMS	S	0.3712	AU	CU	AG	--	---
ESMERALDA	NBMG SAMPLE SITE 1377	S	0.3712	AU	AG	CU	--	---
ESMERALDA	NORTHERN ALPINE PROSPECT	S	0.3712	AG	AU	PB	--	---
ESMERALDA	SILVER TOP #2 CLAIM	S	0.3712	AG	?	--	--	---
ESMERALDA	TREASURE HILL CLAIMS	S	0.3712	AU	?	--	--	---
ESMERALDA	WEE CLAIM	S	0.3712	AU	--	--	--	---
ESMERALDA	WEEPAH MINE	S	0.3712	AU	AG	PB	CU	LOW-SULFIDE AU-QUARTZ VEINS
LANDER	BLUE BIRD MINE	S	0.3712	AU	AG	PB	CU	POLYMETALLIC VEINS
NYE	KRAMER-OSGOOD PROPERTY	S	0.3712	AG	AU	CU	PB	---
NYE	RAY RICKETTS GROUP	S	0.3712	AU	--	--	--	---
NYE	RAY RICKETTS MINE	S	0.3712	AU	W	--	--	---
NYE	SERGEANT PROPERTY	S	0.3712	AG	AU	PB	ZN	---
NYE	VALLEY GROUP	S	0.3712	AG	PB	ZN	CU	POLYMETALLIC VEINS
PERSHING	IMPERIAL GROUP	S	0.3712	AU	AG	CU	PB	POLYMETALLIC VEINS
PERSHING	KENNEDY CANYON PROSPECT	S	0.3712	AU	AG	CU	--	PORPHYRY CU
PERSHING	RUSTY PICK PROSPECT	S	0.3712	AU	AG	--	--	LOW-SULFIDE AU-QUARTZ VEINS
PERSHING	SUNNYSIDE MINE	S	0.3712	AU	AG	--	--	POLYMETALLIC VEINS
CHURCHILL	FAIRVIEW EAGLE	L	0.3516	AG	AU	MN	HG	COMSTOCK EPITHERMAL VEINS
CHURCHILL	NEVADA HILLS MINE	L	0.3516	AU	AG	CU	PB	COMSTOCK EPITHERMAL VEINS
CHURCHILL	HAILSTONE GROUP	S	0.3516	AG	AU	--	--	COMSTOCK EPITHERMAL VEINS
CHURCHILL	LENA GROUP	S	0.3516	AG	AU	--	--	---
CHURCHILL	NBMG SAMPLE SITE 3847	S	0.3516	AG	PB	AU	?	---
CHURCHILL	NBMG SAMPLE SITE 3849	S	0.3516	AG	--	--	--	---
CHURCHILL	NBMG SAMPLE SITE 3850	S	0.3516	AG	CU	PB	--	---
CHURCHILL	SEYMOUR FRACTION	S	0.3516	AG	AU	--	--	---
ESMERALDA	GRAND CENTRAL MINE	S	0.3516	AU	AG	--	--	---
ESMERALDA	GREAT WESTERN MINE	S	0.3516	AU	AG	--	--	---
ESMERALDA	JABONRIA CLAIMS	S	0.3516	AU	--	--	--	---
ESMERALDA	OHIO MINES CORP. DUNFEE GROUP	S	0.3516	AU	AG	--	--	---
ESMERALDA	BIG WEDGE CLAIMS	S	0.3418	AG	PB	CU	--	POLYMETALLIC VEINS
ESMERALDA	GYPSY CLAIMS	S	0.3418	AG	?	AU	?	---
ESMERALDA	MABLE MINE	S	0.3418	AU	U	--	--	---
ESMERALDA	OLD INGALLS MINE	S	0.3418	AG	PB	AU	U	---
NYE	BARCELONA MINE	S	0.3418	AG	AU	CU	PB	POLYMETALLIC VEINS
NYE	BEL CLAIMS	S	0.3418	AG	PB	SB	CU	---
NYE	ED WELCH PROPERTY	S	0.3418	AU	--	--	--	---
NYE	NBMG SAMPLE SITES 2076, 2077, 3183.	S	0.3418	AG	AU	PB	CU	---
PERSHING	ROCHESTER	L	0.2964	AG	AU	PB	ZN	LOW-SULFIDE AU-QUARTZ VEINS
PERSHING	LIMERICK GOLD MINE	S	0.2964	AU	AG	--	--	LOW-SULFIDE AU-QUARTZ VEINS

Table D1, continued.

County	Site Name	Size	Post. Prob.	Commodities				Deposit Type
PERSHING	NENZEL CROWN POINT MINES	S	0.2964	AU	AG	ZN	--	LOW-SULFIDE AU-QUARTZ VEINS
PERSHING	PLAINVIEW GROUP MINES	S	0.2964	AU	--	--	--	LOW-SULFIDE AU-QUARTZ VEINS
ELKO	LAST CHANCE	?	0.2900	AG	AU	--	--	POLYMETALLIC REPLACEMENT
ELKO	HELEN M GROUP	S	0.2900	AG	CU	PB	--	---
ELKO	LEE	S	0.2900	AG	AU	CU	PB	---
ELKO	SYLVANIA MINE	S	0.2900	AU	AG	CU	PB	---
ELKO	WEB FOOT	S	0.2900	AG	CU	PB	AU	COPPER SKARN
CLARK	WALL STREET MINE	M	0.2818	AU	AG	--	--	GOLD ON FLAT FAULTS
CLARK	ELDORADO EMPIRE MINING CO.	S	0.2818	AU	--	--	--	---
ESMERALDA	NBMG SAMPLE SITE 1952	S	0.2818	AU	?	AG	?	---
HUMBOLDT	HALL MINE	S	0.2818	AU	AG	FE	CU	LOW-SULFIDE AU-QUARTZ VEINS
HUMBOLDT	NBMG SAMPLE SITE 2966, 2967	S	0.2818	AU	AG	PB	CU	LOW-SULFIDE AU-QUARTZ VEINS
MINERAL	LUNING GOLD CONSOLIDATED	?	0.2818	AU	AG	PB	CU	---
MINERAL	SILVER CHIEF WORKINGS	?	0.2818	AG	--	--	--	---
MINERAL	DISPOZITCH MINE	S	0.2818	AG	PB	CU	AU	---
NYE	SYLVANITE GROUP (HORN SILVER MINE)	S	0.2818	AG	AU	--	--	---
WHITE PINE	MARY ANNE	?	0.2818	AU	AG	PB	CU	POLYMETALLIC VEINS
ELKO	MEMPHIS	S	0.2731	AU	AG	CU	--	---
HUMBOLDT	GOLD RUN NO. 23 CLAIM	S	0.2731	AG	CU	MO	W	POLYMETALLIC VEINS
HUMBOLDT	RED BUTTE MINE	S	0.2731	AU	CU	AG	PB	POLYMETALLIC VEINS
LANDER	BATTLE MOUNTAIN DISTRICT	L	0.2731	AG	AU	CU	PB	POLY MET VEIN;PORP CU;SKARN
LANDER	FORTITUDE MINE	M	0.2731	AU	AG	AS	CU	COPPER SKARN
LANDER	DEAD HORSE MINE	S	0.2731	AU	AG	--	--	---
LANDER	JULIE SHAFT	S	0.2731	AU	AG	ZN	PB	ZINC-LEAD SKARN
LANDER	TRENTON MINE	S	0.2731	AG	CU	PB	ZN	PORPHYRY CU-MO
LANDER	WILSON-INDEPENDENCE MINE	S	0.2731	AU	AG	AS	MO	---
LYON	SECTION 30 PROSPECTS	?	0.2731	AU	AG	--	--	---
LYON	CAMBRIDGE MINE	S	0.2731	AU	AG	U	--	---
NYE	LIBERTY MINE (REPRESENTING SAN ANTONIO DIST.)	S	0.2731	AG	AU	CU	--	COMSTOCK EPITHERMAL VEINS
NYE	MILLETT MINE	S	0.2731	AU	--	--	--	---
NYE	VIKEN CLAIM	S	0.2731	AU	AG	CU	--	---
NYE	YELLOW GOLD CLAIM AND HOLE IN THE WALL GRP.	S	0.2731	AU	AG	--	--	---
PERSHING	EXCALIBUR MINE	?	0.2731	AU	--	--	--	POLYMETALLIC VEINS
STOREY	BEST & BELCHER MINE	?	0.2731	AG	AU	--	--	COMSTOCK EPITHERMAL VEINS
STOREY	C & C SHAFT	L	0.2731	AU	AG	CU	PB	COMSTOCK EPITHERMAL VEINS
STOREY	CONSOLIDATED VIRGINIA MINE	L	0.2731	AG	AU	CU	PB	COMSTOCK EPITHERMAL VEINS
STOREY	SAVAGE MINE	L	0.2731	AG	AU	MN	FE	COMSTOCK EPITHERMAL VEINS
STOREY	CALIFORNIA MINE	M	0.2731	AG	AU	CU	PB	COMSTOCK EPITHERMAL VEINS
STOREY	HALE & NORCROSS MINE	M	0.2731	AG	AU	CU	PB	COMSTOCK EPITHERMAL VEINS
STOREY	MONTE CRISTO MINE	M	0.2731	AU	AG	CU	PB	COMSTOCK EPITHERMAL VEINS
STOREY	ANDES MINE	S	0.2731	AG	AU	PB	ZN	COMSTOCK EPITHERMAL VEINS
LANDER	KINGSTON MINE	?	0.2704	AU	AG	--	--	---
CHURCHILL	NEVADA FAIRVIEW MINE	M	0.2645	AU	AG	--	--	COMSTOCK EPITHERMAL VEINS
ESMERALDA	BIG BLOSSOM MINE	S	0.2561	AU	W	--	--	---
NYE	BIG SPRINGS MINE	S	0.2561	AU	--	--	--	---
NYE	BLAKER-SLOANE PROPERTY	S	0.2561	AG	AU	--	--	---
NYE	JUMBO MINE.	S	0.2561	AU	--	--	--	---
NYE	KEYSTONE MINE	S	0.2561	AU	F	AG	--	COMSTOCK EPITHERMAL VEINS
MINERAL	WAMSLEY MINE	S	0.2518	AG	--	--	--	---
NYE	VANDERHOEF CLAIMS	S	0.2518	AG	PB	ZN	--	POLYMETALLIC VEINS
CHURCHILL	MOTTINI MINE	S	0.2437	AU	AG	PB	CU	COPPER SKARN
ELKO	GOLDEN EAGLE MINE	S	0.2437	AU	PB	--	--	---

Table D1, continued.

County	Site Name	Size	Post. Prob.	Commodities				Deposit Type
ESMERALDA	MINERAL RIDGE DISTRICT	L	0.2437	AU	AG	--	--	---
ESMERALDA	CROWNING GLORY MINE	S	0.2437	AU	AG	--	--	---
ESMERALDA	DRINKWATER MINE	S	0.2437	AU	AG	PB	--	---
ESMERALDA	ESMERALDA PROSPECT	S	0.2437	AU	AG	PB	--	---
ESMERALDA	GOLDEN EAGLE MINE	S	0.2437	AU	AG	PB	--	LOW-SULFIDE AU-QUARTZ VEINS
ESMERALDA	HOMESTAKE MINE	S	0.2437	AU	--	--	--	---
ESMERALDA	SODA MINE	S	0.2437	AU	--	--	--	---
ESMERALDA	W.S. NO. 97 CLAIMS	S	0.2437	AU	?	AG	?	---
ESMERALDA	WESTERN SOLDIER MINE	S	0.2437	AU	AG	PB	--	---
LANDER	GREY EAGLE MINE	M	0.2437	AG	AU	CU	PB	POLYMETALLIC VEINS
LANDER	MUD SPRINGS MINE AND ADJACENT-PROSPECTS.	S	0.2437	AG	PB	CU	AU	---
LANDER	PHOENIX	S	0.2437	AG	PB	AU	CU	POLYMETALLIC VEINS
LANDER	TRIPLET GULCH PROJECT	S	0.2437	AU	--	--	--	SEDIMENT-HOSTED AU-AG
LANDER	TWO WIDOWS CLAIM	S	0.2437	AG	AU	--	--	---
NYE	GREEN TOP CLAIM	S	0.2437	AG	CU	U	--	---
NYE	LAST CHANCE GROUP	S	0.2437	AU	AG	--	--	---
WHITE PINE	ANNA TUNNEL	S	0.2437	AU	--	--	--	---
ESMERALDA	THREE METALS PROSPECT	S	0.2287	AG	PB	CU	--	---
LANDER	ACE OF DIAMONDS CLAIM	S	0.2287	AG	AU	PB	--	---
LANDER	ANNIE BLAINE CLAIM	S	0.2287	AG	PB	FE	--	---
LANDER	AVALANCHE PROSPECT	S	0.2287	AG	PB	AU	--	POLYMETALLIC REPLACEMENT
LANDER	BRYAN MINE	S	0.2287	AU	AG	CU	--	---
LANDER	CLEVELAND CLAIM	S	0.2287	AU	AG	--	--	---
LANDER	DRISCOL PROPERTY	S	0.2287	AG	PB	AU	CU	POLYMETALLIC VEINS
LANDER	EAGLE MINE (BLUE EAGLE, BLACK EAGLE...)	S	0.2287	AU	AG	PB	CU	---
LANDER	GALENA MINE	S	0.2287	AG	PB	AU	CU	---
LANDER	GOLD CASH MINE	S	0.2287	AU	CU	AG	PB	---
LANDER	HARD TIMES CLAIM	S	0.2287	AU	AG	CU	PB	---
LANDER	HUMBUG-LUCKY CHANCE MINE	S	0.2287	AU	AG	CU	PB	---
LANDER	IRISH ROSE MINE	S	0.2287	AG	CU	AU	PB	POLYMETALLIC VEINS
LANDER	MERCURY CLAIM	S	0.2287	AU	AG	FE	--	---
LANDER	MINNIE MINE	S	0.2287	AU	AG	CU	PB	COPPER SKARN
LANDER	MOONLIGHT MINE	S	0.2287	AG	PB	AU	CU	---
LANDER	NEPTUNE CLAIM	S	0.2287	AU	AG	--	--	---
LANDER	PLUMAS MINE	S	0.2287	AG	PB	CU	AU	---
LANDER	SPANISH VEIN PROSPECT	S	0.2287	AG	PB	AU	ZN	---
LANDER	TOMBOY MINE	S	0.2287	AU	AG	CU	PB	COPPER SKARN
LANDER	TRINITY-ARMOR MINE	S	0.2287	AG	CU	PB	AU	POLYMETALLIC VEINS
MINERAL	HECLA MINE	?	0.2287	AG	--	--	--	---
MINERAL	UNKNOWN ADITS AND OPEN STOPES	?	0.2287	AG	--	--	--	---
MINERAL	UNKNOWN SHAFTS AND PROSPECTS	?	0.2287	AG	--	--	--	---
MINERAL	RIP VAN WINKLE MINE	S	0.2287	AG	PB	--	--	---
MINERAL	SILVER GULCH MINE	S	0.2287	AG	PB	--	--	---
NYE	LIME DYKE CLAIMS	S	0.2287	AG	PB	ZN	AU	---
NYE	THELMA MINE	S	0.2287	AG	F	MO	--	---
NYE	UNNAMED GOLD PROPERTY	S	0.2287	AU	--	--	--	---
NYE	UNNAMED PROSPECT B.	S	0.2287	AU	--	--	--	---
PERSHING	ALLIED TUNGSTEN PROSPECT	?	0.2287	AG	W	PB	?	LOW-SULFIDE AU-QUARTZ VEINS
PERSHING	NEVADA HUMBOLDT GROUP	?	0.2287	AU	AG	PB	ZN	LOW-SULFIDE AU-QUARTZ VEINS
PERSHING	SHEBA MINE	M	0.2287	AG	PB	SB	AU	LOW-SULFIDE AU-QUARTZ VEINS
PERSHING	AMERICAN CANYON DIVIDE PROSPECT	S	0.2287	AG	PB	--	--	LOW-SULFIDE AU-QUARTZ VEINS

Table D1, continued.



County	Site Name	Size	Post. Prob.	Commodities				Deposit Type
PERSHING	BLOODY CANYON MINE	S	0.2287	SB	AG	FE	PB	LOW-SULFIDE AU-QUARTZ VEINS
PERSHING	FOUR SISTERS MINE	S	0.2287	AU	AG	CU	PB	LOW-SULFIDE AU-QUARTZ VEINS
PERSHING	HUMBOLDT QUEEN	S	0.2287	AG	PB	AU	CU	LOW-SULFIDE AU-QUARTZ VEINS
PERSHING	LUCKY DOG MINE	S	0.2287	AG	PB	ZN	CU	LOW-SULFIDE AU-QUARTZ VEINS
PERSHING	MARIGOLD MINE	S	0.2287	AU	AG	ZN	PB	LOW-SULFIDE AU-QUARTZ VEINS
PERSHING	MCGEE PROPERTY	S	0.2287	AU	--	--	--	LOW-SULFIDE AU-QUARTZ VEINS
PERSHING	NBMG SAMPLE SITE 2516	S	0.2287	AU	--	--	--	LOW-SULFIDE AU-QUARTZ VEINS
PERSHING	NBMG SAMPLE SITE 2517	S	0.2287	AU	?	--	--	LOW-SULFIDE AU-QUARTZ VEINS
PERSHING	PQX CLAIMS	S	0.2287	AG	AU	PB	ZN	LOW-SULFIDE AU-QUARTZ VEINS
PERSHING	TEHAMA MINE	S	0.2287	AU	AG	CU	--	LOW-SULFIDE AU-QUARTZ VEINS
PERSHING	TROY CANYON PROSPECT	S	0.2287	AU	--	--	--	LOW-SULFIDE AU-QUARTZ VEINS
PERSHING	WABASH MINE	S	0.2287	AG	PB	AU	CU	LOW-SULFIDE AU-QUARTZ VEINS
ESMERALDA	BROUGHER-DIVIDE MINING CO. PROPERTY	S	0.1924	AG	?	AU	--	---
ESMERALDA	DIVIDE EXTENSION MINE	S	0.1924	AG	AU	--	--	HOT-SPRING AU-AG (?)
ESMERALDA	GOLD ZONE DIVIDE MINING CO. PROPERTY	S	0.1924	AU	AG	CU	PB	COMSTOCK EPITHERMAL VEINS
ESMERALDA	HARMILL DIVIDE MINE	S	0.1924	AG	?	AU	?	---
ESMERALDA	KNOX DIVIDE MINE	S	0.1924	AG	--	--	--	---
ESMERALDA	NEW ALTO DIVIDE MINING COMPANY PROPERTY.	S	0.1924	AG	AU	--	--	---
ESMERALDA	TONOPAH DIVIDE MINE	S	0.1924	AU	AG	MO	CU	COMSTOCK EPITHERMAL VEINS
ESMERALDA	TONOPAH-DIVIDEND MINING COMPANY PROPERTY	S	0.1924	AG	?	AU	--	---
PERSHING	ABE LINCOLN MINE	S	0.1870	AG	AU	--	--	LOW-SULFIDE AU-QUARTZ VEINS
PERSHING	BUCK AND CHARLEY MINE	S	0.1870	AG	PB	ZN	AU	LOW-SULFIDE AU-QUARTZ VEINS
PERSHING	FORVILLY MINE	S	0.1870	AU	AG	--	--	LOW-SULFIDE AU-QUARTZ VEINS
PERSHING	LINCOLN HILL MINE	S	0.1870	AU	AG	U	ZN	LOW-SULFIDE AU-QUARTZ VEINS
PERSHING	LOONEY MINE	S	0.1870	AU	AG	PB	ZN	LOW-SULFIDE AU-QUARTZ VEINS
PERSHING	NEVADA PACKARD MINES	S	0.1870	AG	AU	CU	SB	LOW-SULFIDE AU-QUARTZ VEINS
PERSHING	OCTOPUS MINE	S	0.1870	AG	AU	PB	--	LOW-SULFIDE AU-QUARTZ VEINS
PERSHING	RAVEN PROSPECT	S	0.1870	AG	AU	--	--	LOW-SULFIDE AU-QUARTZ VEINS
PERSHING	SUMMIT MINE	S	0.1870	AU	--	--	--	LOW-SULFIDE AU-QUARTZ VEINS
PERSHING	WEAVER CANYON MINE	S	0.1870	AU	--	--	--	LOW-SULFIDE AU-QUARTZ VEINS
CLARK	SEARCHLIGHT DISTRICT	L	0.1862	AU	AG	CU	W	---
MINERAL	JAIME'S RIDGE	S	0.1862	AU	AG	HG	--	HOT-SPRING AU-AG
ESMERALDA	ORIENTAL MINE	S	0.1797	AU	--	--	--	---
LYON	BUCKEY MINE	S	0.1797	AG	AU	--	--	COMSTOCK EPITHERMAL VEINS
STOREY	KENTUCK MINE	?	0.1797	AG	AU	CU	PB	COMSTOCK EPITHERMAL VEINS
STOREY	MERI'S CON VIRGINIA #1 MINE	?	0.1797	AU	AG	--	--	---
STOREY	CHOLLAR MINE	L	0.1797	AG	AU	CU	PB	COMSTOCK EPITHERMAL VEINS
STOREY	CROWN POINT MINE	L	0.1797	AG	AU	CU	PB	COMSTOCK EPITHERMAL VEINS
STOREY	POTOSI MINE	L	0.1797	AG	AU	CU	PB	COMSTOCK EPITHERMAL VEINS
STOREY	YELLOW JACKET MINE	L	0.1797	AG	AU	CU	PB	COMSTOCK EPITHERMAL VEINS
STOREY	CHALLENGE AND CONFIDENCE	M	0.1797	AU	AG	--	--	COMSTOCK EPITHERMAL VEINS
STOREY	ALPHA CLAIM	S	0.1797	AG	AU	--	--	COMSTOCK EPITHERMAL VEINS
STOREY	EXCHEQUER CLAIM	S	0.1797	AG	AU	--	--	COMSTOCK EPITHERMAL VEINS
CLARK	SOUTHERN NEVADA MINE	?	0.1764	AU	AG	--	--	---
CLARK	BLOSSOM MINE	S	0.1764	AU	AG	--	--	---
CLARK	J. E. T.	S	0.1764	AU	--	--	--	---
CLARK	POMPEII MINE	S	0.1764	AU	AG	--	--	---
WASHOE	BLACK WARRIOR PEAK	S	0.1764	AU	AG	--	--	COMSTOCK EPITHERMAL VEINS
DOUGLAS	WINTERS MINE	S	0.1702	AG	AU	FE	CU	POLYMETALLIC VEINS
ESMERALDA	RED LIGHT MINE	S	0.1702	AU	CU	--	--	---
ESMERALDA	SOLBERRY MINE	S	0.1702	AU	AG	PB	--	---
ESMERALDA	VEGA MINE	S	0.1702	AU	AG	PB	--	---

Table D1, continued.

County	Site Name	Size	Post. Prob.	Commodities				Deposit Type
LANDER	GOLD QUARTZ	M	0.1702	AU	AG	PB	ZN	---
LANDER	PAYMASTER & CHRISTOPER	S	0.1702	AU	AG	CU	PB	---
MINERAL	GOLDEN MILE GROUP	S	0.1702	AU	AG	CU	--	---
CHURCHILL	GOLD COIN #2 MINE	S	0.1641	AG	AU	--	--	COMSTOCK EPITHERMAL VEINS
ESMERALDA	ALBERT MINE	S	0.1641	AG	AU	PB	--	---
ESMERALDA	HORNSILVER MAY CO. SHAFT	S	0.1641	AG	AU	--	--	---
ESMERALDA	NBMG SAMPLE SITE	S	0.1641	AG	PB	AU	CU	---
MINERAL	ROCK CABIN MINE	?	0.1641	AU	BA	--	--	---
ESMERALDA	BUCK BOARD CLAIM GROUP	S	0.1582	AG	AU	--	--	---
ESMERALDA	CALLISON PROPERTY	S	0.1582	AU	AG	PB	--	---
ESMERALDA	ENTERPRISE MINE	S	0.1582	AU	--	--	--	---
ESMERALDA	FESLER PROSPECT	S	0.1582	AG	AU	CU	PB	---
ESMERALDA	GOLD CREST CLAIMS	S	0.1582	AU	AG	PB	CU	---
ESMERALDA	GOOD HOPE MINE	S	0.1582	AG	PB	CU	--	---
ESMERALDA	HART SILVER MINE	S	0.1582	AG	PB	AU	?	---
ESMERALDA	NORTH STAR CLAIMS	S	0.1582	AU	AG	?	--	---
ESMERALDA	RUBY D CLAIMS	S	0.1582	AU	AG	--	--	---
ESMERALDA	SNAKE PIT	S	0.1582	AU	?	--	--	---
ESMERALDA	SUNRISE CLAIMS	S	0.1582	AU	AG	CU	--	---
ESMERALDA	VICTORIA PROSPECT	S	0.1582	AU	AG	PB	CU	---
NYE	ARIZONA CLAIM	S	0.1582	AG	CU	SB	AU	---
NYE	COMBINATION MINE	S	0.1582	AG	SB	--	--	POLYMETALLIC VEINS
NYE	EL DORADO SOUTH MINE	S	0.1582	AG	CU	PB	SB	POLYMETALLIC VEINS
NYE	HIGHBRIDGE MINE	S	0.1582	AG	CU	--	--	---
NYE	HOOPER MINE	S	0.1582	AG	--	--	--	---
NYE	MOORE AND MARTIN PROPERTY	S	0.1582	AG	--	--	--	---
NYE	NBMG SAMPLE SITE 2039	S	0.1582	AG	PB	CU	MO	---
NYE	NBMG SAMPLE SITE 2040	S	0.1582	AG	PB	CU	SB	---
NYE	NBMG SAMPLE SITE 2079	S	0.1582	AG	PB	CU	ZN	---
NYE	SAN PEDRO MINE	S	0.1582	AG	HG	ZN	PB	---
NYE	WAR EAGLE MINE (BARCELONA DISTRICT)	S	0.1582	AU	AG	PB	CU	POLYMETALLIC VEINS
MINERAL	UNKNOWN PROSPECTS	?	0.1529	AG	?	--	--	---
MINERAL	UNNAMED PROSPECT (CANDELARIA DISTRICT)	?	0.1474	AG	?	--	--	---
MINERAL	BIRDSONG MINE	S	0.1474	AU	AG	PB	--	---
MINERAL	RIP VAN WINKLE PROSPECT	S	0.1474	AG	PB	--	--	---
MINERAL	GRASSI MINE	S	0.1446	AU	AG	--	--	---
ESMERALDA	B. D. CLAIMS	S	0.1393	AU	AG	PB	--	---
ESMERALDA	COYOTE MINE	S	0.1393	AG	PB	?	--	---
ESMERALDA	CRESCENT MINE	S	0.1393	AU	AG	PB	--	---
ESMERALDA	GOLD COIN MINE (TOKOP DIST.)	S	0.1393	AU	?	--	--	---
ESMERALDA	GOOD BUDDY CLAIMS	S	0.1393	AG	PB	CU	--	---
ESMERALDA	GREAT GULCH MINE	S	0.1393	AU	--	--	--	---
ESMERALDA	MONTEZUMA CAMP	S	0.1393	AG	AU	CU	PB	POLYMETALLIC REPLACEMENT
ESMERALDA	MR LODE CLAIMS	S	0.1393	AU	AG	PB	--	---
ESMERALDA	NBMG SAMPLE SITES 1287, 1288	S	0.1393	AG	PB	CU	--	---
ESMERALDA	OLDT CLAIM	S	0.1393	AG	CU	PB	--	---
ESMERALDA	RADIO TOWER SHAFT	S	0.1393	AU	AG	?	--	---
ESMERALDA	RED MONSTER MINE	S	0.1393	AU	AG	--	--	---
ESMERALDA	SILVER MOON MINE	S	0.1393	AU	?	AG	?	---
ESMERALDA	TOMMY KNODAN CLAIMS	S	0.1393	AU	--	--	--	---
LANDER	BULL DOG JACK MINE	?	0.1393	AG	AU	--	--	---
LANDER	BLUE DICK ANTIMONY MINE	S	0.1393	SB	AU	AG	SE	SIMPLE ANTIMONY

Table D1, continued.

County	Site Name	Size	Post. Prob.	Commodities				Deposit Type
LANDER	LIMELIGHT MINE	S	0.1393	AG	AU	--	--	---
LANDER	PITTSBURG MINE	S	0.1393	AU	AG	CU	PB	POLYMETALLIC VEINS
MINERAL	LUCKY HILL MINE	?	0.1393	AG	AU	PB	FE	DISTAL DISSEMINATED AG-AU
MINERAL	MT. DIABLO MINE	?	0.1393	AG	AU	PB	FE	---
MINERAL	PRINCESS SHAFT	?	0.1393	AG	--	--	--	---
MINERAL	UNKNOWN PROSPECTS	?	0.1393	AG	--	--	--	---
MINERAL	UNKNOWN PROSPECTS	?	0.1393	AG	?	--	--	---
MINERAL	CANDELARIA MINE	M	0.1393	AG	AU	PB	SB	DISTAL DISSEMINATED AG-AU
MINERAL	MOUNT DIABLO MINE	M	0.1393	AG	--	--	--	---
MINERAL	1905 MINE	S	0.1393	AU	AG	--	--	---
MINERAL	ACKERMAN MINE	S	0.1393	AU	AG	--	--	---
MINERAL	BLUE DUMP MINE	S	0.1393	AU	AG	--	--	---
MINERAL	BOUNCE MINE	S	0.1393	AU	AG	--	--	---
MINERAL	BROWN MINE	S	0.1393	AU	AG	--	--	---
MINERAL	CHIEF MINE	S	0.1393	AU	AG	--	--	---
MINERAL	FORTUNA MINE	S	0.1393	AU	AG	--	--	---
MINERAL	FOTTLER MINE	S	0.1393	AU	AG	--	--	---
MINERAL	LUCKY HILLMINE	S	0.1393	AG	--	--	--	---
MINERAL	MARY MINE	S	0.1393	AU	AG	--	--	---
MINERAL	NEW PARTY MINE	S	0.1393	AU	AG	--	--	---
MINERAL	ORPHAN BOY MINE	S	0.1393	AU	AG	--	--	---
MINERAL	SNOWBALL MINE	S	0.1393	AU	AG	--	--	---
MINERAL	SWASTIKA MINE	S	0.1393	AG	--	--	--	---
NYE	BERLIN MINE	S	0.1393	AG	AU	CU	PB	POLYMETALLIC VEINS
NYE	DOONAN PROPERTY	S	0.1393	AU	--	--	--	---
NYE	LUCKY STRIKE MINE	S	0.1393	AU	--	--	--	---
NYE	MURPHY MINE	S	0.1393	AG	AU	CU	SB	POLYMETALLIC VEINS
NYE	SULLIVAN MINE	S	0.1393	AU	--	--	--	---
PERSHING	ALDRICH MINE	S	0.1393	AG	PB	AU	CU	POLYMETALLIC VEINS
NYE	MONTANA - TONOPAH MINING CO.	L	0.1352	AG	AU	--	--	COMSTOCK EPITHERMAL VEINS
NYE	TONOPAH MINING CO.	L	0.1352	AG	AU	CU	PB	COMSTOCK EPITHERMAL VEINS
NYE	RESCUE EULA MINING CO.	M	0.1352	AG	--	--	--	---
HUMBOLDT	QUICK GOLD CLAIMS	S	0.1277	AG	?	AU	?	POLYMETALLIC VEINS
HUMBOLDT	HUNTINGTON-WHITMAN GROUP	S	0.1243	AU	--	--	--	LOW-SULFIDE AU-QUARTZ VEINS
HUMBOLDT	PICK HANDLE MINE	S	0.1243	AU	CU	PB	--	LOW-SULFIDE AU-QUARTZ VEINS
HUMBOLDT	SILVER STATE MINE	S	0.1243	AU	AG	CU	--	LOW-SULFIDE AU-QUARTZ VEINS
MINERAL	TODD MINE	S	0.1243	AU	AG	PB	--	---
WHITE PINE	VICTORIE CLAIMS	S	0.1243	AU	AG	--	--	---
CHURCHILL	NBMG SAMPLE SITE 3944	S	0.1197	AG	CU	MO	PB	---
CHURCHILL	NBMG SAMPLE SITE 3945	S	0.1197	AG	CU	BI	SB	---
ESMERALDA	BLUE DAISY CLAIM	S	0.1197	AU	?	--	--	---
HUMBOLDT	NBMG SAMPLE SITE 2423	S	0.1197	AU	CU	SB	AG	LOW-SULFIDE AU-QUARTZ VEINS
HUMBOLDT	SNOWDRIFT MINE	S	0.1197	SB	AG	AS	FE	SIMPLE ANTIMONY
MINERAL	BELLEVUE MINE	S	0.1197	AU	HG	ZN	--	---
NYE	GRUSS MINE	S	0.1197	AG	PB	CU	--	---
NYE	OPHIR CLAIMS (BLOCK)	S	0.1197	AU	AG	--	--	---
NYE	SUMMIT GROUP	S	0.1197	AU	--	--	--	---
PERSHING	JERSEY VALLEY-REX GROUP	S	0.1197	AG	PB	AU	CU	---
PERSHING	NBMG SAMPLE SITE 1483	S	0.1197	AG	AU	--	--	COMSTOCK EPITHERMAL VEINS
PERSHING	NBMG SAMPLE SITE 2356	S	0.1197	AU	?	AG	PB	LOW-SULFIDE AU-QUARTZ VEINS
PERSHING	STONE HOUSE CANYON MINE	S	0.1197	AU	AG	--	--	COMSTOCK EPITHERMAL VEINS
PERSHING	UNNAMED GOLD MINES	S	0.1197	AU	--	--	--	LOW-SULFIDE AU-QUARTZ VEINS

Table D1, continued.

<i>County</i>	<i>Site Name</i>	<i>Size</i>	<i>Post. Prob.</i>	<i>Commodities</i>				<i>Deposit Type</i>
NYE	NORTHUMBERLAND MINE	M	0.1151	AU	AG	AS	FE	SEDIMENT-HOSTED AU-AG
NYE	GOODING MINE	S	0.1151	AG	AU	AS	SB	---
ESMERALDA	TIP TOP CLAIMS	S	0.1111	AU	AG	HG	--	COMSTOCK EPITHERMAL VEINS
STOREY	GOOSEBERRY MINE	S	0.1111	AU	AG	CU	--	COMSTOCK EPITHERMAL VEINS
MINERAL	NORTH SECTION 31 PROSPECTS	?	0.1069	AU	?	--	--	---

*Table D1, continued.*

County	Site Name	Size	Post. Prob.	Commodities				Deposit Type
EUREKA	LANTERN DEPOSIT	S	0.9972	AU	---	---	---	SEDIMENT-HOSTED AU-AG
EUREKA	BAZZA DEPOSIT	?	0.9881	AU	---	---	---	SEDIMENT-HOSTED AU-AG
EUREKA	BLUE STAR MINE	M	0.9881	AU	AG	GEM	CU	SEDIMENT-HOSTED AU-AG
EUREKA	BOBCAT DEPOSIT	S	0.9881	AU	---	---	---	SEDIMENT-HOSTED AU-AG
EUREKA	LONG LAC DEPOSIT	?	0.9881	AU	---	---	---	SEDIMENT-HOSTED AU-AG
EUREKA	DEEP STAR DEPOSIT	S	0.9588	AU	---	---	---	SEDIMENT-HOSTED AU-AG
EUREKA	CARLIN GOLD MINE	M	0.9073	AU	HG	AG	ZN	SEDIMENT-HOSTED AU-AG
EUREKA	GENESIS MINE	M	0.9073	AU	---	---	---	SEDIMENT-HOSTED AU-AG
EUREKA	NORTH STAR DEPOSIT	S	0.8662	AU	---	---	---	SEDIMENT-HOSTED AU-AG
EUREKA	BULLION-MONARCH OPEN PIT MINE	S	0.7376	AU	AG	---	---	SEDIMENT-HOSTED AU-AG
EUREKA	PETE DEPOSIT	S	0.7335	AU	---	---	---	SEDIMENT-HOSTED AU-AG
EUREKA	TUSC DEPOSIT	M	0.695	AU	AG	AS	SB	SEDIMENT-HOSTED AU-AG
HUMBOLDT	PREBLE MINE	S	0.6293	AU	BA	CU	---	SEDIMENT-HOSTED AU-AG
LANDER	GOLD ACRES DEPOSIT	M	0.4921	AU	W	CU	SB	SEDIMENT-HOSTED AU-AG
EUREKA	GOLD QUARRY MINE	L	0.3904	AU	AG	AS	SB	SEDIMENT-HOSTED AU-AG
ELKO	MAC RIDGE DEPOSIT (BIG SPRINGS)	S	0.3741	AU	---	---	---	SEDIMENT-HOSTED AU-AG
ELKO	SOUTH SAMMY CREEK DEPOSIT (BIG SPRINGS)	S	0.3741	AU	---	---	---	SEDIMENT-HOSTED AU-AG
EUREKA	GOLDSTRIKE MINE	L	0.3498	AU	---	---	---	SEDIMENT-HOSTED AU-AG
EUREKA	SCREAMER DEPOSIT	S	0.3498	AU	---	---	---	SEDIMENT-HOSTED AU-AG
EUREKA	MAGGIE CREEK OPEN PIT GOLD MINE	M	0.3477	AU	AG	BA	AS	SEDIMENT-HOSTED AU-AG
HUMBOLDT	FELIX CANYON	S	0.2179	AU	AG	AS	HG	SEDIMENT-HOSTED AU-AG
HUMBOLDT	GETCHELL MINE	M	0.2179	AU	AG	AS	W	SEDIMENT-HOSTED AU-AG
HUMBOLDT	PINSON MINE	S	0.2179	AU	W	---	---	SEDIMENT-HOSTED AU-AG
HUMBOLDT	MARIGOLD MINE (BATTLE MT. DIST.)	M	0.214	AU	AG	AS	SB	SEDIMENT-HOSTED AU-AG
LANDER	TRIPLET GULCH PROJECT	S	0.214	AU	---	---	---	SEDIMENT-HOSTED AU-AG
ELKO	ALCHEM DEPOSIT	M	0.1897	AU	---	---	---	SEDIMENT-HOSTED AU-AG
ELKO	GENERATOR HILL DEPOSIT	M	0.1897	AU	AG	HG	SB	SEDIMENT-HOSTED AU-AG
ELKO	MARLBORO CANYON DEPOSIT	M	0.1897	AU	---	---	---	SEDIMENT-HOSTED AU-AG
ELKO	NEW DEEP DEPOSIT	M	0.1897	AU	---	---	---	SEDIMENT-HOSTED AU-AG
ELKO	NORTH GENERATOR HILL DEPOSIT	M	0.1897	AU	---	---	---	SEDIMENT-HOSTED AU-AG
ELKO	SAVAL CANYON DEPOSIT (JERRITT CANYON)	S	0.1897	AU	---	---	---	SEDIMENT-HOSTED AU-AG
ELKO	WEST GENERATOR HILL DEPOSIT	M	0.1897	AU	---	---	---	SEDIMENT-HOSTED AU-AG
LANDER	BUFFALO VALLEY MINE	S	0.1847	AU	AG	CU	AS	SEDIMENT-HOSTED AU-AG (?)
ELKO	EMIGRANT SPRINGS	S	0.1368	AU	AS	SB	BA	SEDIMENT-HOSTED AU-AG
ELKO	NORTH SAMMY CREEK DEPOSIT (BIG SPRINGS)	S	0.1226	AU	---	---	---	SEDIMENT-HOSTED AU-AG
EUREKA	GOLD RIDGE DEPOSIT	S	0.1226	AU	---	---	---	SEDIMENT-HOSTED AU-AG
EUREKA	GOLDSTONE DEPOSIT	S	0.1226	AU	---	---	---	SEDIMENT-HOSTED AU-AG
HUMBOLDT	C-ZONE	S	0.0726	AU	AG	AS	HG	SEDIMENT-HOSTED AU-AG
LANDER	NORTHERN LIGHTS DEPOSIT	S	0.0661	AU	AG	CU	---	SEDIMENT-HOSTED AU-AG
MINERAL	CANDELARIA MINE	M	0.0661	AG	AU	PB	SB	DISTAL DISSEMINATED AG-AU
MINERAL	LUCKY HILL MINE	?	0.0661	AG	AU	PB	FE	DISTAL DISSEMINATED AG-AU
ELKO	PATTANI SPRINGS DEPOSIT	S	0.0617	AU	---	---	---	SEDIMENT-HOSTED AU-AG
ELKO	DEE GOLD MINE	S	0.0599	AU	AG	SB	AS	SEDIMENT-HOSTED AU-AG
LANDER	ELDER CREEK MINE	S	0.0599	AU	---	---	---	SEDIMENT-HOSTED AU-AG
EUREKA	HORSE CANYON MINE	S	0.0447	AU	BA	---	---	SEDIMENT-HOSTED AU-AG
ELKO	RAIN MINE	M	0.0426	AU	BA	AS	HG	SEDIMENT-HOSTED AU-AG
EUREKA	GOLD PICK DEPOSIT	M	0.0375	AU	---	---	---	SEDIMENT-HOSTED AU-AG
ELKO	STEER CANYON DEPOSIT	S	0.0269	AU	SB	---	---	SEDIMENT-HOSTED AU-AG

**Table D2.** Posterior probabilities associated with gold-silver-bearing sedimentary rock-hosted occurrences of all sizes, as determined with the sedimentary rock-hosted 8-layer mineral potential model (sorted in order of descending posterior probability). All data, with the exception of posterior probabilities, from the MRDS mineral occurrences database. Occurrences size from Guild (1968), and deposit types from Cox and Singer (1986). Prior probability = 0.0003.

County	Site Name	Size	Post. Prob.	Commodities				Deposit Type
ELKO	BOOTSTRAP MINE	M	0.0267	AU	AG	CU	PB	SEDIMENT-HOSTED AU-AG
ELKO	CAPSTONE DEPOSIT	S	0.0267	AU	---	---	---	SEDIMENT-HOSTED AU-AG
ELKO	TROUT CREEK DEPOSIT	S	0.022	AU	AG	AS	SB	SEDIMENT-HOSTED AU-AG
ELKO	WOOD GULCH MINE	S	0.0163	AU	AG	---	---	SEDIMENT-HOSTED AU-AG
LANDER	CORTEZ GOLD MINE	L	0.0163	AU	HG	AS	SB	SEDIMENT-HOSTED AU-AG
HUMBOLDT	CX DEPOSIT	S	0.0078	AU	AS	HG	SB	SEDIMENT-HOSTED AU-AG
ELKO	BURNS BASIN GOLD DEPOSIT	M	0.0077	AU	---	---	---	SEDIMENT-HOSTED AU-AG
EUREKA	POST DEPOSIT	L	0.0076	AU	AG	AS	---	SEDIMENT-HOSTED AU-AG
NYE	NORTHUMBERLAND MINE	M	0.0076	AU	AG	AS	FE	SEDIMENT-HOSTED AU-AG
LANDER	AUSTIN GOLD VENTURES GOLD MINE (QUITO MINE)	S	0.0055	AU	AS	SB	---	SEDIMENT-HOSTED AU-AG
ELKO	SOUTH BULLION DEPOSIT	M	0.0052	AU	AG	AS	SB	SEDIMENT-HOSTED AU-AG
LANDER	HILLTOP MINE	S	0.0046	AU	AG	CU	PB	DISTAL DISSEMINATED AG-AU
CHURCHILL	REED DEPOSIT (FONDAWAY CANYON MINE)	S	0.0027	AU	---	---	---	SEDIMENT-HOSTED AU-AG
WHITE PINE	BULL TERRIER PATENTED MINES(HAMILTON MINE?)	S	0.0027	AU	PB	---	---	SEDIMENT-HOSTED AU-AG
WHITE PINE	NORTH SELOX CLAIMS.	S	0.0027	AU	BA	---	---	SEDIMENT-HOSTED AU-AG
WHITE PINE	TAYLOR MINE (ARGUS PIT, BISHOP PIT)	M	0.0027	AG	AU	SB	CU	DISTAL DISSEMINATED AG-AU
WHITE PINE	WINROCK MINE	S	0.0027	AU	---	---	---	SEDIMENT-HOSTED AU-AG
WHITE PINE	GREEN SPRINGS MINE	S	0.0023	AU	AG	---	---	SEDIMENT-HOSTED AU-AG
WHITE PINE	ILLIPAH MINE	S	0.0023	AU	AG	---	---	SEDIMENT-HOSTED AU-AG
HUMBOLDT	MAG DEPOSIT	S	0.0022	AU	HG	AS	SB	SEDIMENT-HOSTED AU-AG
HUMBOLDT	CHIMNEY CREEK MINE	M	0.0019	AU	AG	SDG	AS	SEDIMENT-HOSTED AU-AG
HUMBOLDT	RABBIT CREEK MINE	L	0.0019	AU	AG	PB	ZN	SEDIMENT-HOSTED AU-AG
ELKO	MEIKLE MINE	L	0.0018	AU	AG	HG	ZN	SEDIMENT-HOSTED AU-AG
EUREKA	GOLD BAR MINE	M	0.0018	AU	AG	SB	AS	SEDIMENT-HOSTED AU-AG
HUMBOLDT	LONE TREE MINE	M	0.0018	AU	AG	AS	SB	SEDIMENT-HOSTED AU-AG
HUMBOLDT	STONEHOUSE DEPOSIT	M	0.0018	AU	AG	AS	SB	SEDIMENT-HOSTED AU-AG
WHITE PINE	CASINO MINE	S	0.0014	AU	---	---	---	SEDIMENT-HOSTED AU-AG
ELKO	MILL CREEK DEPOSIT	S	0.0008	AU	---	---	---	SEDIMENT-HOSTED AU-AG
CHURCHILL	COLORADO DEPOSIT (FONDAWAY CANYON MINE)	S	0.0007	AU	AG	AS	SB	SEDIMENT-HOSTED AU-AG
EUREKA	TONKIN SPRINGS MINE	S	0.0006	AU	AG	AS	HG	SEDIMENT-HOSTED AU-AG
NYE	STEIGMEYER PROPERTY (SHALE PIT MINE)	S	0.0006	AU	AG	AS	SB	SEDIMENT-HOSTED AU-AG
WHITE PINE	NIGHTHAWK RIDGE MINE (EASY JUNIOR)	S	0.0006	AU	AG	HG	TL	SEDIMENT-HOSTED AU-AG
WHITE PINE	YANKEE MINE	S	0.0006	AU	---	---	---	SEDIMENT-HOSTED AU-AG
PERSHING	STANDARD MINE (GOLD STANDARD)	S	0.0005	AU	AG	AS	BA	SEDIMENT-HOSTED AU-AG
MINERAL	SANTA FE GOLD MINE	S	0.0003	AU	AG	AS	SB	SEDIMENT-HOSTED AU-AG
NYE	STERLING MINE	S	0.0003	AU	AG	F	---	SEDIMENT-HOSTED AU-AG
WHITE PINE	LITTLE BALD MOUNTAIN MINE (LBM)	S	0.0003	AU	HG	---	---	SEDIMENT-HOSTED AU-AG
PERSHING	RELIEF CANYON MINE	S	0.0002	AU	AG	F	AS	SEDIMENT-HOSTED AU-AG
CHURCHILL	S. MOUTH DEPOSIT (FONDAWAY CANYON MINE)	S	0.0001	AU	---	---	---	SEDIMENT-HOSTED AU-AG
EUREKA	NEW WINDFALL SHAFT	L	0.0001	AU	AG	PB	CU	DISTAL DISSEMINATED AG-AU
EUREKA	RATTO CANYON DEPOSIT	S	0.0001	AU	---	---	---	SEDIMENT-HOSTED AU-AG
EUREKA	WINDFALL MINE	M	0.0001	AU	AG	PB	ZN	DISTAL DISSEMINATED AG-AU
HUMBOLDT	KRAMER HILL MINE	S	0.0001	AU	AG	---	---	DISTAL DISSEMINATED AG-AU
LANDER	COVE MINE	M	0.0001	AU	AG	MN	AS	DISTAL DISSEMINATED AG-AU
LINCOLN	ATLANTA MINE	L	0.0001	AU	AG	U	---	SEDIMENT-HOSTED AU-AG
PERSHING	FLORIDA CANYON MINE	M	0.0001	AU	AG	HG	CLY	SEDIMENT-HOSTED AU-AG
WHITE PINE	ALLIGATOR RIDGE MINE	S	0.0001	AU	AG	SB	HG	SEDIMENT-HOSTED AU-AG
WHITE PINE	BALD MOUNTAIN MINE	M	0.0001	AU	AG	CU	ZN	DISTAL DISSEMINATED AG-AU
WHITE PINE	DECKER FLATS DEPOSIT	S	0.0001	AU	AG	---	---	SEDIMENT-HOSTED AU-AG
WHITE PINE	STAR POINTER MINE (INCLUDES ROBINSON MINE CU PORPHYRY)	S	0.0001	AU	AG	---	---	SEDIMENT-HOSTED AU-AG (?)

Table D2, continued.

County	Site Name	Size	Post. Prob.	Commodities				Deposit Type
LYON	BUCKEYE MINE	S	0.1316	AG	AU	---	---	COMSTOCK EPITHERMAL VEINS
STOREY	KENTUCK MINE	?	0.1316	AG	AU	CU	PB	COMSTOCK EPITHERMAL VEINS
STOREY	YELLOW JACKET MINE	L	0.1316	AG	AU	CU	PB	COMSTOCK EPITHERMAL VEINS
CHURCHILL	BLUFF MINE	S	0.0720	AG	AU	---	---	COMSTOCK EPITHERMAL VEINS
CHURCHILL	BUFF CLAIMS	S	0.0720	AU	AG	---	---	COMSTOCK EPITHERMAL VEINS
STOREY	ALPHA CLAIM	S	0.0713	AG	AU	---	---	COMSTOCK EPITHERMAL VEINS
STOREY	ANDES MINE	S	0.0713	AG	AU	PB	ZN	COMSTOCK EPITHERMAL VEINS
STOREY	CHALLENGE AND CONFIDENCE	M	0.0713	AU	AG	---	---	COMSTOCK EPITHERMAL VEINS
STOREY	CHOLLAR MINE	L	0.0713	AG	AU	CU	PB	COMSTOCK EPITHERMAL VEINS
STOREY	CROWN POINT MINE	L	0.0713	AG	AU	CU	PB	COMSTOCK EPITHERMAL VEINS
STOREY	EXCHEQUER CLAIM	S	0.0713	AG	AU	---	---	COMSTOCK EPITHERMAL VEINS
STOREY	HALE & NORCROSS MINE	M	0.0713	AG	AU	CU	PB	COMSTOCK EPITHERMAL VEINS
STOREY	MONTE CRISTO MINE	M	0.0713	AU	AG	CU	PB	COMSTOCK EPITHERMAL VEINS
STOREY	POTOSI MINE	L	0.0713	AG	AU	CU	PB	COMSTOCK EPITHERMAL VEINS
STOREY	SAVAGE MINE	L	0.0713	AG	AU	MN	FE	COMSTOCK EPITHERMAL VEINS
CHURCHILL	DROMEDARY HUMP MINE	S	0.0640	AG	AU	---	---	COMSTOCK EPITHERMAL VEINS
CHURCHILL	KINNEY PROSPECT	S	0.0640	AU	AG	---	---	COMSTOCK EPITHERMAL VEINS
ESMERALDA	GOLDFIELD DEEP MINES CO.	S	0.0634	AU	AG	CU	SN	EPITHERMAL QTZ-ALUNITE AU
ESMERALDA	JUMBO EXTENSION MINING CO. (JUMBO GROUP)	S	0.0634	AU	AG	CU	SN	EPITHERMAL QTZ-ALUNITE AU
ESMERALDA	LAGUNA GROUP	S	0.0634	AU	AG	ZN	PB	EPITHERMAL QTZ-ALUNITE AU
ESMERALDA	RED TOP MINE	S	0.0634	AU	AG	PB	ZN	EPITHERMAL QTZ-ALUNITE AU
HUMBOLDT	RASER AND REEDER MINES	S	0.0549	AU	AG	---	---	HOT-SPRING AU-AG
CLARK	WALL STREET MINE	M	0.0523	AU	AG	---	---	GOLD ON FLAT FAULTS
MINERAL	JAIME'S RIDGE	S	0.0523	AU	AG	HG	---	HOT-SPRING AU-AG
STOREY	BEST & BELCHER MINE	?	0.0518	AG	AU	---	---	COMSTOCK EPITHERMAL VEINS
STOREY	C & C SHAFT	L	0.0518	AU	AG	CU	PB	COMSTOCK EPITHERMAL VEINS
STOREY	CALIFORNIA MINE	M	0.0518	AG	AU	CU	PB	COMSTOCK EPITHERMAL VEINS
STOREY	CONSOLIDATED VIRGINIA MINE	L	0.0518	AG	AU	CU	PB	COMSTOCK EPITHERMAL VEINS
PERSHING	WOMENS RIGHT GROUP	?	0.0480	AU	AG	---	---	COMSTOCK EPITHERMAL VEINS
STOREY	ALTA SHAFT	S	0.0480	AG	AU	PB	ZN	COMSTOCK EPITHERMAL VEINS
STOREY	JUSTICE SHAFT	L	0.0480	AG	AU	PB	CU	COMSTOCK EPITHERMAL VEINS
STOREY	KEYSTONE SHAFT	?	0.0480	AU	---	---	---	COMSTOCK EPITHERMAL VEINS
STOREY	KNICKERBOCKER MINE	S	0.0480	AU	AG	---	---	COMSTOCK EPITHERMAL VEINS
STOREY	LADY WASHINGTON MINE.	S	0.0480	AG	AU	---	---	COMSTOCK EPITHERMAL VEINS
STOREY	NEW YORK MINE	S	0.0480	AU	---	---	---	COMSTOCK EPITHERMAL VEINS
STOREY	OVERMAN 2 MINE	S	0.0480	AU	AG	---	---	COMSTOCK EPITHERMAL VEINS
ESMERALDA	TIP TOP CLAIMS	S	0.0464	AU	AG	HG	---	COMSTOCK EPITHERMAL VEINS
HUMBOLDT	G U B CLAIMS	S	0.0464	AG	AS	CU	---	COMSTOCK EPITHERMAL VEINS
HUMBOLDT	SILVER BUTTE MINE	S	0.0464	AG	AU	ZN	FE	COMSTOCK EPITHERMAL VEINS
HUMBOLDT	WILD GOOSE VEIN	S	0.0464	AG	AS	---	---	COMSTOCK EPITHERMAL VEINS
NYE	JIM BUTLER TONOPAH MINING CO.	L	0.0410	AG	---	---	---	COMSTOCK EPITHERMAL VEINS
NYE	MAC NAMARA MINING CO.	L	0.0410	AG	---	---	---	COMSTOCK EPITHERMAL VEINS
HUMBOLDT	HERMIT GROUP	S	0.0397	AU	AG	---	---	HOT-SPRING AU-AG
WASHOE	LEADVILLE MINE	S	0.0346	AG	PB	ZN	CU	COMSTOCK EPITHERMAL VEINS
CHURCHILL	FAIRVIEW EAGLE	L	0.0335	AG	AU	MN	HG	COMSTOCK EPITHERMAL VEINS
CHURCHILL	HAILSTONE GROUP	S	0.0335	AG	AU	---	---	COMSTOCK EPITHERMAL VEINS
CHURCHILL	NEVADA HILLS MINE	L	0.0335	AU	AG	CU	PB	COMSTOCK EPITHERMAL VEINS
STOREY	GOOSEBERRY MINE	S	0.0335	AU	AG	CU	---	COMSTOCK EPITHERMAL VEINS

**Table D3.** Posterior probabilities associated with gold-silver-bearing volcanic rock-hosted occurrences of all sizes, as determined with the volcanic rock-hosted 7-layer mineral potential model (sorted in order of descending posterior probability). All data, with the exception of posterior probabilities, from the MRDS mineral occurrences database. Occurrences size from Guild (1968), and deposit types from Cox and Singer (1986). Prior probability = 0.0015.



County	Site Name	Size	Post. Prob.	Commodities				Deposit Type
CHURCHILL	NEVADA FAIRVIEW MINE	M	0.0289	AU	AG	---	---	COMSTOCK EPITHERMAL VEINS
MINERAL	SUNNYSIDE CLAIMS	S	0.0289	AU	AG	CU	---	COMSTOCK EPITHERMAL VEINS
WASHOE	PEAVINE PEAK GOLD MINE	S	0.0289	AU	---	---	---	COMSTOCK OR HOT-SPRING EPITHERMAL (?)
PERSHING	AMERICAN FLAT CANYON MINE	S	0.0286	AU	AG	---	---	COMSTOCK EPITHERMAL VEINS
PERSHING	WILDCAT MINE	S	0.0286	AU	AG	---	---	COMSTOCK EPITHERMAL VEINS
STOREY	COMSTOCK LODGE DISTRICT, (SILVER CITY DIST.)	M	0.0286	AG	AU	CU	---	COMSTOCK EPITHERMAL VEINS
STOREY	KEYES MINE	S	0.0286	AG	AU	---	---	COMSTOCK EPITHERMAL VEINS
PERSHING	UNNAMED SILVER PROSPECT (GOLD BUTTE DIST.)	S	0.0253	AU	AG	W	---	COMSTOCK EPITHERMAL VEINS
WASHOE	GOLDEN FLEECE	S	0.0251	AU	AG	CU	PB	EPITHERMAL QTZ-ALUNITE AU
WASHOE	PAYMASTER	S	0.0251	AU	AG	CU	PB	EPITHERMAL QTZ-ALUNITE AU
STOREY	BELCHER CLAIM	M	0.0249	AG	AU	PB	ZN	COMSTOCK EPITHERMAL VEINS
STOREY	BULLION MINE	S	0.0249	AG	AU	CU	PB	COMSTOCK EPITHERMAL VEINS
STOREY	CALEDONIA MINE	S	0.0249	AG	AU	---	---	COMSTOCK EPITHERMAL VEINS
STOREY	IMPERIAL MINE	M	0.0249	AG	AU	---	---	COMSTOCK EPITHERMAL VEINS
STOREY	OVERLAND MINE	M	0.0249	AG	AU	---	---	COMSTOCK EPITHERMAL VEINS
STOREY	OVERMAN CLAIM	M	0.0249	AG	AU	---	---	COMSTOCK EPITHERMAL VEINS
STOREY	SCARPION SHAFT	S	0.0249	AU	AG	---	---	COMSTOCK EPITHERMAL VEINS
CHURCHILL	SUMMIT KING-DAN TUCKER MINE	L	0.0222	AU	AG	---	---	COMSTOCK EPITHERMAL VEINS
ESMERALDA	COMBINATION MINE	M	0.0220	AU	AG	TE	CU	EPITHERMAL QTZ-ALUNITE AU
ESMERALDA	FLORENCE MINE	M	0.0220	AU	AG	CU	BI	EPITHERMAL QTZ-ALUNITE AU
ESMERALDA	JANUARY MINE (JANUARY & FEBRUARY CLAIMS)	S	0.0220	AU	AG	CU	BI	EPITHERMAL QTZ-ALUNITE AU
ESMERALDA	MOHAWK MINE	M	0.0220	AU	AG	CU	SB	EPITHERMAL QTZ-ALUNITE AU
ESMERALDA	SANGER MINE	S	0.0220	AG	AU	CU	PB	COMSTOCK EPITHERMAL VEINS
LYON	SOUTH COMSTOCK MINE	S	0.0220	AU	AG	---	---	COMSTOCK EPITHERMAL VEINS
MINERAL	DOUGLAS GROUP (CAMP DOUGLAS ?)	S	0.0220	AU	AG	PB	---	COMSTOCK EPITHERMAL VEINS
STOREY	BILLY THE KID PIT	M	0.0220	AG	AU	---	---	COMSTOCK EPITHERMAL VEINS
STOREY	DRYSDALE MINE	S	0.0220	AG	AU	---	---	COMSTOCK EPITHERMAL VEINS
STOREY	LUCERNE PIT	M	0.0220	AU	AG	---	---	COMSTOCK EPITHERMAL VEINS
PERSHING	ROSE-DALE MINE	S	0.0205	AU	---	---	---	HOT-SPRING AU-AG
ESMERALDA	GOLDFIELD-BELMONT MINE	S	0.0190	AU	ZN	CU	TE	EPITHERMAL QTZ-ALUNITE AU
ESMERALDA	GREAT BEND MINE	S	0.0190	AU	AG	CU	ZN	EPITHERMAL QTZ-ALUNITE AU
ESMERALDA	LONE STAR GROUP (PATRICK CLAIM)	S	0.0190	AU	---	---	---	EPITHERMAL QTZ-ALUNITE AU
CHURCHILL	NBMG SAMPLE SITE 2882 (TRUCKEE, FIREBALL)	S	0.0180	AU	?	AG	?	COMSTOCK EPITHERMAL VEINS
CLARK	HOMESTAKE GROUP	S	0.0180	AU	AG	---	---	GOLD ON FLAT FAULTS
ELKO	ALPHA MINE	S	0.0178	AU	AG	---	---	COMSTOCK EPITHERMAL VEINS
ELKO	BOURNE MINE	S	0.0178	AU	AG	---	---	COMSTOCK EPITHERMAL VEINS
ELKO	BUSTER G.M. CO.	S	0.0178	AU	AG	---	---	COMSTOCK EPITHERMAL VEINS
ELKO	LONG HIKE	S	0.0178	AU	AG	SE	---	COMSTOCK EPITHERMAL VEINS
ELKO	RIDDLE LEASE	S	0.0178	AU	---	---	---	COMSTOCK EPITHERMAL VEINS
STOREY	OPHIR CLAIM	L	0.0178	AG	AU	PB	ZN	COMSTOCK EPITHERMAL VEINS
STOREY	SIERRA NEVADA MINE	L	0.0178	AG	AU	CU	PB	COMSTOCK EPITHERMAL VEINS
STOREY	UNION MINE	M	0.0178	AG	AU	PB	CU	COMSTOCK EPITHERMAL VEINS
CHURCHILL	NEZELDA MINE	S	0.0159	AU	AG	PB	---	COMSTOCK EPITHERMAL VEINS
CHURCHILL	UNNAMED PROSPECT (TRUCKEE DISTRICT)	S	0.0159	AU	---	---	---	COMSTOCK EPITHERMAL VEINS
HUMBOLDT	NBMG SAMPLE SITE 2605	S	0.0159	AG	CU	AU	PB	COMSTOCK EPITHERMAL VEINS
PERSHING	FENCEMAKER MINE	S	0.0158	SB	AG	HG	AU	HOT-SPRING AU-AG
WASHOE	S.E.D. CLAIMS	S	0.0158	AU	?	---	---	HOT-SPRING HG
CLARK	QUO VADIS	S	0.0143	AU	AG	PB	---	EPITHERMAL QTZ-ALUNITE AU
ESMERALDA	SILVER KING CLAIMS (SPECULATOR, SILVER KNIGHT...)	S	0.0143	AG	PB	---	---	COMSTOCK EPITHERMAL VEINS
NYE	HORN SILVER MINE	S	0.0143	AG	AU	HG	---	COMSTOCK EPITHERMAL VEINS
NYE	LIBERTY MINE (REPRESENTING SAN ANTONIO DIST.)	S	0.0142	AG	AU	CU	---	COMSTOCK EPITHERMAL VEINS

Table D3, continued.

County	Site Name	Size	Post. Prob.	Commodities				Deposit Type
HUMBOLDT	LUCKY JIM NOS. 1-8 AND APEX CLAIMS	S	0.0137	AU	AG	U	---	HOT-SPRING AU-AG
CHURCHILL	GOLD ORE CLAIMS	S	0.0135	AU	AG	---	---	COMSTOCK EPITHERMAL VEINS
CHURCHILL	GOLD COIN #2 MINE	S	0.0131	AG	AU	---	---	COMSTOCK EPITHERMAL VEINS
ESMERALDA	DIVIDE EXTENSION MINE	S	0.0121	AG	AU	---	---	HOT-SPRING AU-AG (?)
ESMERALDA	GOLD ZONE DIVIDE MINING CO. PROPERTY	S	0.0121	AU	AG	CU	PB	COMSTOCK EPITHERMAL VEINS
ESMERALDA	TONOPAH DIVIDE MINE	S	0.0121	AU	AG	MO	CU	COMSTOCK EPITHERMAL VEINS
LYON	TALAPOOSA DEPOSIT	S	0.0114	AU	AG	HG	CU	COMSTOCK EPITHERMAL VEINS
ELKO	ALTITUDE MINE	S	0.0113	AU	AG	---	---	COMSTOCK EPITHERMAL VEINS
ELKO	NEW HOPE GROUP	S	0.0113	AU	AG	---	---	COMSTOCK EPITHERMAL VEINS
ESMERALDA	ATLANTA MINES CO. CLAIMS	S	0.0113	AU	AG	CU	SN	EPITHERMAL QTZ-ALUNITE AU
LYON	SILVER HILL MINE	L	0.0113	AG	AU	FE	MN	COMSTOCK EPITHERMAL VEINS
LYON	VOLCANO MINE	S	0.0113	AG	AU	---	---	COMSTOCK EPITHERMAL VEINS
PERSHING	FAIRVIEW MINE	S	0.0113	AU	AG	---	---	COMSTOCK EPITHERMAL VEINS
PERSHING	J AND B MINE	S	0.0113	AU	AG	---	---	COMSTOCK EPITHERMAL VEINS
PERSHING	KINDERGARTEN AND WIHUA MINES	S	0.0113	AU	AG	PB	CU	COMSTOCK EPITHERMAL VEINS
PERSHING	MAZUMA HILLS MINE	S	0.0113	AU	AG	CU	PB	COMSTOCK EPITHERMAL VEINS
PERSHING	NBMG SAMPLE SITE 2820	S	0.0113	AG	AU	---	---	COMSTOCK EPITHERMAL VEINS
STOREY	DONOUAN PROPERTY	M	0.0113	AU	AG	---	---	COMSTOCK EPITHERMAL VEINS
STOREY	SUCCOR MINE	M	0.0113	AG	AU	---	---	COMSTOCK EPITHERMAL VEINS
STOREY	UTAH SHAFT	S	0.0113	AU	AG	---	---	COMSTOCK EPITHERMAL VEINS
STOREY	WOODVILLE SHAFT	M	0.0113	AG	AU	CU	PB	COMSTOCK EPITHERMAL VEINS
WASHOE	MAHONEY MINE	S	0.0113	AU	AG	---	---	COMSTOCK EPITHERMAL VEINS
WASHOE	PANDORA	S	0.0113	AU	AG	---	---	COMSTOCK EPITHERMAL VEINS
LINCOLN	HOMESTAKE MINE	S	0.0098	AU	AG	HG	CU	COMSTOCK EPITHERMAL VEINS
LINCOLN	IRIS84 09 84 09	S	0.0098	AU	AG	CU	---	COMSTOCK EPITHERMAL VEINS
LINCOLN	KENO CLAIMS	S	0.0098	AU	?	AG	BA	COMSTOCK EPITHERMAL VEINS
LYON	COMO-EUREKA	M	0.0098	AG	AU	CU	---	COMSTOCK EPITHERMAL VEINS
ESMERALDA	JMP CLAIMS	S	0.0097	AU	AG	---	---	EPITHERMAL QTZ-ALUNITE AU
ESMERALDA	QUARTZITE AND BLACK BUTTE MINES	S	0.0097	AU	CU	SB	TE	EPITHERMAL QTZ-ALUNITE AU
PERSHING	DEVANEY PROPERTY	S	0.0097	AU	AG	F	---	COMSTOCK EPITHERMAL VEINS
PERSHING	GOLD CROWN GROUP	S	0.0097	AU	AG	---	---	COMSTOCK EPITHERMAL VEINS
PERSHING	NBMG SAMPLE SITE 1491	S	0.0097	AU	AG	---	---	COMSTOCK EPITHERMAL VEINS
PERSHING	NBMG SAMPLE SITE 2815	S	0.0097	AU	AG	---	---	COMSTOCK EPITHERMAL VEINS
PERSHING	SANTA MARIA PROSPECT	S	0.0097	AU	AG	---	---	COMSTOCK EPITHERMAL VEINS
PERSHING	SNOW SQUALL MINE	S	0.0097	AU	AG	F	---	COMSTOCK EPITHERMAL VEINS
PERSHING	STONE CLAIM SHAFT	S	0.0097	AU	?	---	---	COMSTOCK EPITHERMAL VEINS
HUMBOLDT	BUCKSKIN NATIONAL MINE	S	0.0094	AU	AG	SB	FE	COMSTOCK EPITHERMAL VEINS
ESMERALDA	BLUE BULL MINE	S	0.0086	AU	AG	CU	---	EPITHERMAL QTZ-ALUNITE AU
NYE	LAND MARK MINE	S	0.0086	AU	AG	---	---	COMSTOCK EPITHERMAL VEINS
PERSHING	ANTIMONY IKE MINE	S	0.0086	SB	AU	AG	AS	HOT-SPRING AU-AG
PERSHING	BLACK BOY MINE	S	0.0086	AG	PB	SB	ZN	COMSTOCK EPITHERMAL VEINS
PERSHING	VELVET GOLD MINES	S	0.0086	AU	AG	---	---	COMSTOCK EPITHERMAL VEINS
CLARK	JETCO CLAIMS	S	0.0081	AU	CU	---	---	GOLD ON FLAT FAULTS
ELKO	CORNUCOPIA	S	0.0081	AU	AG	CU	ZN	COMSTOCK EPITHERMAL VEINS
ESMERALDA	TIP TOP MINE	S	0.0081	AU	AG	---	---	COMSTOCK EPITHERMAL VEINS
HUMBOLDT	LUCKY HORSESHOE GROUP	S	0.0081	AU	AG	U	---	HOT-SPRING AU-AG
WASHOE	MAZY MINE	S	0.0081	AU	AG	PB	ZN	COMSTOCK EPITHERMAL VEINS
WASHOE	RENO MAY	S	0.0081	AU	AG	ZN	PB	COMSTOCK EPITHERMAL VEINS
ELKO	AJAX PROSPECT	S	0.0080	AU	AG	---	---	COMSTOCK EPITHERMAL VEINS
ELKO	BEN HUR PROSPECT	S	0.0080	AU	AG	---	---	COMSTOCK EPITHERMAL VEINS
ELKO	PAVLAK MINE JARBIDGE-PAVLAK G.M.CO.PROPERTIES	S	0.0080	AU	AG	---	---	COMSTOCK EPITHERMAL VEINS

Table D3, continued.

County	Site Name	Size	Post. Prob.	Commodities				Deposit Type
ELKO	STARLIGHT GROUP	S	0.0080	AU	AG	CU	---	COMSTOCK EPITHERMAL VEINS
ESMERALDA	MOHAWK MINE (ARGENTITE MINE)	S	0.0080	AG	AU	PB	ZN	COMSTOCK EPITHERMAL VEINS
MINERAL	AURORA DISTRICT (AURORA MINE AREA)	L	0.0080	AU	AG	PB	SE	COMSTOCK EPITHERMAL VEINS
PERSHING	PERSHING MINE	?	0.0080	AU	---	---	---	HOT-SPRING AU-AG
PERSHING	WONDER METAL MINE	S	0.0080	SB	AG	FE	TI	HOT-SPRING AU-AG
LINCOLN	HORSESHOE MINE MINE	S	0.0070	AU	AG	CU	---	COMSTOCK EPITHERMAL VEINS
PERSHING	HOLLYWOOD MINE	M	0.0069	SB	AG	AU	---	HOT-SPRING AU-AG
WASHOE	WESTERN HOG RANCH MINE	M	0.0069	AU	AG	HG	U	HOT-SPRING AU-AG
CHURCHILL	CYCLONE GROUP	S	0.0065	AG	---	---	---	COMSTOCK EPITHERMAL VEINS
CHURCHILL	NEVADA HILLS FLORENCE MINE	S	0.0065	AU	AG	---	---	COMSTOCK EPITHERMAL VEINS
CHURCHILL	OHIO GROUP	S	0.0065	AU	AG	---	---	COMSTOCK EPITHERMAL VEINS
WASHOE	BLACK WARRIOR PEAK	S	0.0065	AU	AG	---	---	COMSTOCK EPITHERMAL VEINS
HUMBOLDT	SLEEPER MINE	M	0.0062	AU	AG	K	S	COMSTOCK EPITHERMAL VEINS
CHURCHILL	UNNAMED PROPERTY	S	0.0061	AU	AG	---	---	COMSTOCK EPITHERMAL VEINS
PERSHING	TRINITY SILVER MINE	S	0.0061	AG	PB	SB	AU	COMSTOCK EPITHERMAL VEINS
ELKO	GOOD HOPE	?	0.0048	AG	AU	SB	---	COMSTOCK EPITHERMAL VEINS
STOREY	BALTIMORE SHAFT	S	0.0048	AG	AU	---	---	COMSTOCK EPITHERMAL VEINS
ESMERALDA	C.O.D. CONSOLIDATED MINING CO CLAIMS	S	0.0044	AU	AG	CU	SB	EPITHERMAL QTZ-ALUNITE AU
HUMBOLDT	KIM BLAIMS, NO.S 1-9	S	0.0044	AU	AG	U	---	HOT-SPRING AU-AG
HUMBOLDT	LUCKY STRIKE PROSPECT	S	0.0044	AU	AG	---	---	HOT-SPRING AU-AG
LINCOLN	FORTUNA AND HELEN CLAIMS	S	0.0044	AU	AG	PB	?	COMSTOCK EPITHERMAL VEINS
LINCOLN	NBMG SAMPLE SITE 788 UNNAMED PROSPECT	S	0.0044	AU	?	BA	?	EPITHERMAL MANGANESE
LYON	HULLEY-LOGAN	S	0.0044	AG	AU	CU	---	COMSTOCK EPITHERMAL VEINS
LYON	RAMSEY COMSTOCK MINE	S	0.0044	AU	AG	---	---	COMSTOCK EPITHERMAL VEINS
LYON	RAPIDAN	M	0.0044	AG	AU	---	---	COMSTOCK EPITHERMAL VEINS
LYON	THE STONE CABIN CLAIMS	S	0.0044	AG	AU	---	---	COMSTOCK EPITHERMAL VEINS
MINERAL	NEVADA RAND	?	0.0044	AU	AG	MN	ZN	COMSTOCK EPITHERMAL VEINS
MINERAL	RANDALL PROPERTY	S	0.0044	AU	AG	CU	---	COMSTOCK EPITHERMAL VEINS
NYE	KEY FLOWER MINE	S	0.0044	AU	AG	CU	PB	COMSTOCK EPITHERMAL VEINS
NYE	PARADISE PEAK MINE	M	0.0044	AU	AG	HG	BA	EPITHERMAL QTZ-ALUNITE AU
PERSHING	NBMG SAMPLE SITE 2809	S	0.0044	AU	?	---	---	COMSTOCK EPITHERMAL VEINS
PERSHING	NBMG SAMPLE SITE 1480	S	0.0044	AU	AG	---	---	COMSTOCK EPITHERMAL VEINS
PERSHING	NBMG SAMPLE SITE 1481	S	0.0044	AG	AU	---	---	COMSTOCK EPITHERMAL VEINS
PERSHING	NBMG SAMPLE SITE 2836	S	0.0044	AG	PB	AU	CU	COMSTOCK EPITHERMAL VEINS
PERSHING	PORTLAND MINE	S	0.0044	AU	AG	PB	ZN	COMSTOCK EPITHERMAL VEINS
PERSHING	SEVEN TROUGHS DISTRICT	S	0.0044	AU	AG	---	---	COMSTOCK EPITHERMAL VEINS
PERSHING	TRINITY SILVER PROSPECT	M	0.0044	AG	---	---	---	COMSTOCK EPITHERMAL VEINS
PERSHING	TRINITY JOINT VENTURE	S	0.0044	AG	PB	CU	W	COMSTOCK EPITHERMAL VEINS
STOREY	FLOWERY MINE	M	0.0044	AU	AG	PB	ZN	COMSTOCK EPITHERMAL VEINS
STOREY	LODY BRYAN MINE	?	0.0044	AU	AG	---	---	COMSTOCK EPITHERMAL VEINS
STOREY	NORTH BONANZA MINE	S	0.0044	AU	AG	PB	---	COMSTOCK EPITHERMAL VEINS
STOREY	PET CLAIM	S	0.0044	AG	---	---	---	COMSTOCK EPITHERMAL VEINS
NYE	MIZPAH EXTENSION MINING CO.	M	0.0040	AG	AU	---	---	COMSTOCK EPITHERMAL VEINS
NYE	MONTANA - TONOPAH MINING CO.	L	0.0040	AG	AU	---	---	COMSTOCK EPITHERMAL VEINS
NYE	TONOPAH MINING CO.	L	0.0040	AG	AU	CU	PB	COMSTOCK EPITHERMAL VEINS
LANDER	ASPEN GROUP	S	0.0039	AU	MN	---	---	COMSTOCK EPITHERMAL VEINS
NYE	MONTGOMERY-SHOSHONE MINE	S	0.0034	AG	AU	---	---	COMSTOCK EPITHERMAL VEINS
WASHOE	GREEN HILL MINES	S	0.0033	AU	AG	CU	---	COMSTOCK EPITHERMAL VEINS
CHURCHILL	GOLD KING CLAIM AND VALLEY KING CLAIMS	S	0.0031	AU	AG	W	---	COMSTOCK EPITHERMAL VEINS
CHURCHILL	UNNAMED PROSPECT (JESSUP DISTRICT)	S	0.0031	AU	AG	---	---	COMSTOCK EPITHERMAL VEINS
ELKO	BLUSTER MINE	S	0.0031	AU	AG	---	---	COMSTOCK EPITHERMAL VEINS
ELKO	FLAXIE MINE	S	0.0031	AU	AG	---	---	COMSTOCK EPITHERMAL VEINS

Table D3, continued.

County	Site Name	Size	Post. Prob.	Commodities				Deposit Type
ELKO	JARBIDGE DISTRICT	L	0.0031	AU	AG	---	---	HOT-SPRING AU-AG (?)
ELKO	NEW STAR GROUP	S	0.0031	AU	AG	---	---	COMSTOCK EPITHERMAL VEINS
ELKO	PAN CLAIM	S	0.0031	AU	AG	---	---	COMSTOCK EPITHERMAL VEINS
ELKO	PICK AND SHOVEL MINE	S	0.0031	AU	AG	---	---	COMSTOCK EPITHERMAL VEINS
HUMBOLDT	GOLDEN CASH; JACKPOT, BURIED TREASURE, AND GOLDEN	?	0.0031	AU	AG	U	---	HOT-SPRING AU-AG
HUMBOLDT	NBMG SAMPLE SITE 2609	S	0.0031	AG	AS	---	---	COMSTOCK EPITHERMAL VEINS
HUMBOLDT	SISKIYOU MINE	S	0.0031	AU	---	---	---	COMSTOCK EPITHERMAL VEINS
PERSHING	BROWN PALACE GROUP	?	0.0031	AU	AG	CU	PB	COMSTOCK EPITHERMAL VEINS
PERSHING	DREAMLAND MINE	S	0.0031	AU	AG	CU	PB	COMSTOCK EPITHERMAL VEINS
PERSHING	ROSEBUD MINE	S	0.0031	AU	AG	CU	PB	COMSTOCK EPITHERMAL VEINS
PERSHING	WILLARD GROUP (NORTH)	S	0.0031	AU	AG	CU	PB	COMSTOCK EPITHERMAL VEINS
LINCOLN	DELAMAR MINE (MAGNOLIA MINE)	L	0.0028	AU	AG	CU	FE	COMSTOCK EPITHERMAL VEINS
PERSHING	NBMG SAMPLE SITE 1483	S	0.0028	AG	AU	---	---	COMSTOCK EPITHERMAL VEINS
PERSHING	STONE HOUSE CANYON MINE	S	0.0028	AU	AG	---	---	COMSTOCK EPITHERMAL VEINS
NYE	FAIRVIEW MINE	S	0.0025	AU	---	---	---	COMSTOCK EPITHERMAL VEINS
NYE	FRANZ HAMMEL MINE	S	0.0025	AU	AG	---	---	COMSTOCK EPITHERMAL VEINS
NYE	TROY MINE	S	0.0025	AG	CU	MN	---	EPITHERMAL MANGANESE
NYE	UNNAMED PROSPECTS #5	S	0.0025	AG	AU	CU	MN	COMSTOCK EPITHERMAL VEINS
PERSHING	BELLE ETC. CLAIMS	?	0.0025	AU	---	---	---	COMSTOCK EPITHERMAL VEINS
CHURCHILL	NEVADA CROWN MINE (GOLD CROWN; PORT AND SAMPSON)	S	0.0024	AG	AU	PB	ZN	COMSTOCK EPITHERMAL VEINS
ELKO	ARGENTA	S	0.0024	AG	AU	---	---	COMSTOCK EPITHERMAL VEINS
ELKO	DEFREES	M	0.0024	AG	AU	---	---	COMSTOCK EPITHERMAL VEINS
ESMERALDA	HASBROUCK MOUNTAIN	S	0.0024	AG	AU	AS	HG	HOT-SPRING AU-AG
LINCOLN	CULVERWELL MINE	S	0.0024	AU	AG	---	---	COMSTOCK EPITHERMAL VEINS
NYE	KING TONOPAH MINE	S	0.0024	AG	AU	---	---	COMSTOCK EPITHERMAL VEINS
WASHOE	ARKELL MINE	S	0.0024	AG	AU	PB	ZN	EPITHERMAL QTZ-ALUNITE AU
WASHOE	BIG MOUTH	S	0.0024	AU	AG	---	---	COMSTOCK EPITHERMAL VEINS
WASHOE	DESERT KING MINE	S	0.0024	AG	AU	PB	ZN	EPITHERMAL QTZ-ALUNITE AU
WASHOE	SECRET CANYON PROSPECT	S	0.0024	AU	AG	---	---	COMSTOCK EPITHERMAL VEINS
WASHOE	WEDEKIND MINE	S	0.0024	AG	AU	PB	ZN	EPITHERMAL QTZ-ALUNITE AU
WASHOE	BUSTER MINES	M	0.0022	AU	AG	CU	PB	COMSTOCK EPITHERMAL VEINS
ESMERALDA	GOLDFIELD DISTRICT	L	0.0021	AU	AG	BI	K	EPITHERMAL QTZ-ALUNITE AU
ESMERALDA	NIVLOC MINE	S	0.0021	AG	AU	PB	---	COMSTOCK EPITHERMAL VEINS
HUMBOLDT	SILVER HILLS MINE	?	0.0021	AU	AG	---	---	HOT-SPRING AU-AG
LYON	DAYTON MINE	?	0.0021	AU	AG	---	---	COMSTOCK EPITHERMAL VEINS
LYON	KOSSUTH MINE	S	0.0021	AU	AG	---	---	COMSTOCK EPITHERMAL VEINS
NYE	WARRIOR MINE	S	0.0021	AU	AG	CU	PB	COMSTOCK EPITHERMAL VEINS
CHURCHILL	FRED BRANCH PROPERTY	S	0.0020	AU	AG	CU	MN	COMSTOCK EPITHERMAL VEINS
PERSHING	STEINER MINE	S	0.0020	AU	AG	PB	SB	COMSTOCK EPITHERMAL VEINS
CLARK	CAMP DUPONT GROUP	S	0.0018	AU	---	---	---	GOLD ON FLAT FAULTS
PERSHING	BLACK STAR CLAIM GROUP	S	0.0018	AU	AG	SB	CU	COMSTOCK EPITHERMAL VEINS
ELKO	COMMON WEALTH	M	0.0017	AG	AU	---	---	COMSTOCK EPITHERMAL VEINS
ELKO	NORTH COMMONWEALTH	M	0.0017	AG	AU	---	---	COMSTOCK EPITHERMAL VEINS
ELKO	OZARK GROUP	?	0.0017	AU	AG	---	---	COMSTOCK EPITHERMAL VEINS
EUREKA	BUCKHORN	S	0.0017	AU	AG	AS	HG	COMSTOCK EPITHERMAL VEINS
HUMBOLDT	BIGHORN GROUP	S	0.0017	AG	U	---	---	HOT-SPRING AU-AG
HUMBOLDT	BLUE DRAGON NOS. 1-3 PROSPECT	S	0.0017	AG	AU	---	---	HOT-SPRING AU-AG
CHURCHILL	M. H. CLAIMS	?	0.0015	AU	CU	---	---	COMSTOCK EPITHERMAL VEINS
ELKO	GOLD CIRCLE DISTRICT (MIDAS)	L	0.0015	AU	AG	---	---	COMSTOCK EPITHERMAL VEINS
CHURCHILL	BIG LEDGE MINE	S	0.0013	AG	AU	---	---	COMSTOCK EPITHERMAL VEINS
CHURCHILL	JELINEK MINE	S	0.0013	AG	AU	---	---	COMSTOCK EPITHERMAL VEINS

Table D3, continued.

County	Site Name	Size	Post. Prob.	Commodities				Deposit Type
CHURCHILL	MIZPAH MINE	S	0.0013	AG	AU	---	---	COMSTOCK EPITHERMAL VEINS
PERSHING	YELLOWSTONE MINE	S	0.0013	AG	AU	?	---	HOT-SPRING AU-AG
WASHOE	TIGER GROUP	S	0.0013	AU	AG	CU	---	COMSTOCK EPITHERMAL VEINS
NYE	KEYSTONE MINE	S	0.0012	AU	F	AG	---	COMSTOCK EPITHERMAL VEINS
NYE	ROUND MOUNTAIN GOLD MINE	M	0.0012	AU	AG	AS	SB	HOT-SPRING AU-AG
CHURCHILL	BLACK BUTTE MINE	S	0.0011	AU	AG	PB	FE	COMSTOCK EPITHERMAL VEINS
CHURCHILL	CENTURION PROSPECT	S	0.0011	AG	AU	CU	---	COMSTOCK EPITHERMAL VEINS
CHURCHILL	CIRAN PROSPECT	S	0.0011	AU	AG	---	---	COMSTOCK EPITHERMAL VEINS
CHURCHILL	CRIPPLE QUEEN MINE	S	0.0011	AG	AU	---	---	COMSTOCK EPITHERMAL VEINS
CHURCHILL	LANSING PROSPECT	S	0.0011	AU	AG	---	---	COMSTOCK EPITHERMAL VEINS
CHURCHILL	NBMG SAMPLE SITE 3941	S	0.0011	AG	CU	PB	---	COMSTOCK EPITHERMAL VEINS
CHURCHILL	PYRAMID MINE	S	0.0011	AG	PB	MN	---	COMSTOCK EPITHERMAL VEINS
CHURCHILL	REX CLAIM #6	S	0.0011	AG	AU	---	---	COMSTOCK EPITHERMAL VEINS
CHURCHILL	SCOTIA MINE	S	0.0011	AG	---	---	---	COMSTOCK EPITHERMAL VEINS
CHURCHILL	WATER SHAFT MINE	S	0.0011	AG	AU	---	---	COMSTOCK EPITHERMAL VEINS
CHURCHILL	WOLVERTON PROSPECT	S	0.0011	AU	AG	---	---	COMSTOCK EPITHERMAL VEINS
ELKO	APRIL FOOL GROUP	S	0.0011	AG	AU	---	---	COMSTOCK EPITHERMAL VEINS
ELKO	GRAND PRIZE	L	0.0011	AG	---	---	---	COMSTOCK EPITHERMAL VEINS
ELKO	TUSCARORA MINE	S	0.0011	AU	AG	---	---	COMSTOCK EPITHERMAL VEINS
HUMBOLDT	ECHO GROUP	S	0.0011	AG	U	---	---	HOT-SPRING AU-AG
LYON	PONY MEADOWS CLAIMS	S	0.0011	AU	AG	---	---	COMSTOCK EPITHERMAL VEINS
MINERAL	OMCO MINE (OLYMPIC MINE; ROYAL GEORGE GRP.)	M	0.0011	AU	AG	---	---	COMSTOCK EPITHERMAL VEINS
NYE	AMALGAMATED MINE	S	0.0011	AU	F	---	---	COMSTOCK EPITHERMAL VEINS
NYE	ARROWHEAD MINE (ARROWHEAD SYNDICATE MINES, INC.)	S	0.0011	AG	AU	SB	---	COMSTOCK EPITHERMAL VEINS
NYE	BULLFROG DISTRICT	L	0.0011	AU	AG	CU	PB	COMSTOCK EPITHERMAL VEINS
NYE	ELLEDALE MINE	S	0.0011	AU	AG	---	---	COMSTOCK EPITHERMAL VEINS
NYE	GOLD BAR GROUP (GOLDEN ARROW DISTRICT)	S	0.0011	AU	AG	CU	---	COMSTOCK EPITHERMAL VEINS
NYE	MANHATTAN CONSOLIDATED MINE	S	0.0011	AG	AU	SB	AS	COMSTOCK EPITHERMAL VEINS
NYE	PIONEER MINE	S	0.0011	AU	---	---	---	COMSTOCK OR HOT-SPRING EPITHERMAL (?)
NYE	SILVER GLANCE GROUP (SILVER BOW DIST.)	S	0.0011	AG	AU	---	---	COMSTOCK EPITHERMAL VEINS
PERSHING	CROFOOT PROJECT	?	0.0011	AU	---	---	---	HOT-SPRING AU-AG
STOREY	GLOBE CONSOLIDATED MINE	S	0.0011	AU	AG	---	---	COMSTOCK EPITHERMAL VEINS
WASHOE	TMB ASSOCIATES CLAIMS	S	0.0011	AU	?	CL Y	---	HOT-SPRING AU-AG
WASHOE	WIND MOUNTAIN MINE	S	0.0011	AU	AG	CL Y	AS	HOT-SPRING AU-AG
CHURCHILL	GRAND CENTRAL MINE	S	0.0009	AG	AU	---	---	COMSTOCK EPITHERMAL VEINS
CHURCHILL	LAST HOPE MINE	S	0.0009	AG	AU	PB	ZN	COMSTOCK EPITHERMAL VEINS
CHURCHILL	NBMG SAMPLE SITE 3935	S	0.0009	AG	AU	---	---	COMSTOCK EPITHERMAL VEINS
CHURCHILL	TERRELL MINE	S	0.0009	AG	PB	---	---	COMSTOCK EPITHERMAL VEINS
CHURCHILL	WINGFIELD MINE	S	0.0009	AG	AU	---	---	COMSTOCK EPITHERMAL VEINS
ELKO	BUCKEYE AND OHIO	L	0.0009	AG	SB	AS	---	COMSTOCK EPITHERMAL VEINS
LINCOLN	POPE MINE	S	0.0009	AU	AG	CU	?	COMSTOCK EPITHERMAL VEINS
LINCOLN	REDLITE CLAIMS	S	0.0009	AU	AG	---	---	COMSTOCK EPITHERMAL VEINS
NYE	GOLDEN CROWN GROUP	?	0.0009	AG	---	---	---	COMSTOCK EPITHERMAL VEINS
NYE	OKEY DAVIS MINE	S	0.0009	AU	---	---	---	COMSTOCK EPITHERMAL VEINS
PERSHING	NBMG SAMPLE SITE 2927	S	0.0009	AU	AG	CU	---	COMSTOCK EPITHERMAL VEINS
WASHOE	WILD ROSE PROSPECT	S	0.0009	AU	U	---	---	HOT-SPRING AU-AG
CHURCHILL	DIXIE COMSTOCK MINE	S	0.0008	AU	AG	CU	PB	COMSTOCK EPITHERMAL VEINS
CHURCHILL	GOLCONDA-GOLD WEDGE GROUP	S	0.0008	AG	AU	CU	MO	COMSTOCK EPITHERMAL VEINS
CHURCHILL	LAST CHANCE AND TONY PAN PATENTED CLAIMS	S	0.0008	AG	AU	---	---	COMSTOCK EPITHERMAL VEINS

Table D3, continued.

County	Site Name	Size	Post. Prob.	Commodities				Deposit Type
CHURCHILL	RUBY-JUNE ROSE GROUP	S	0.0008	AG	AU	---	---	COMSTOCK EPITHERMAL VEINS
CHURCHILL	SPIDER AND WASP PROSPECT	S	0.0008	AG	AU	---	---	COMSTOCK EPITHERMAL VEINS
CHURCHILL	TREASURE HILL CLAIM #1417	S	0.0008	AG	AU	---	---	COMSTOCK EPITHERMAL VEINS
CHURCHILL	WEST JOB CANYON-NORTH	?	0.0008	AU	AG	CU	PB	COMSTOCK EPITHERMAL VEINS
CHURCHILL	WINDLASS MINE	S	0.0008	AU	AG	---	---	COMSTOCK EPITHERMAL VEINS
ELKO	BANNER	S	0.0008	AU	AG	---	---	COMSTOCK EPITHERMAL VEINS
ELKO	DEXTER	L	0.0008	AU	AG	TI	---	COMSTOCK EPITHERMAL VEINS
ELKO	EIRA	M	0.0008	AU	AG	---	---	COMSTOCK EPITHERMAL VEINS
ELKO	ELKO PRINCE	S	0.0008	AU	AG	---	---	COMSTOCK EPITHERMAL VEINS
ELKO	HOLLISTER (IVANHOE)	M	0.0008	AU	AG	HG	CU	HOT-SPRING AU-AG
ELKO	WATER WITCH MINE	S	0.0008	AU	AG	---	---	COMSTOCK EPITHERMAL VEINS
ESMERALDA	GILBERT MINE	S	0.0008	AU	---	---	---	COMSTOCK OR HOT-SPRING EPITHERMAL (?)
ESMERALDA	MAMMOTH PROSPECT	S	0.0008	AG	AU	SB	---	COMSTOCK EPITHERMAL VEINS
ESMERALDA	RED CLOUD CLAIMS	S	0.0008	AU	AG	?	---	COMSTOCK EPITHERMAL VEINS
NYE	AMERICAN EAGLE AND CEDAR VEIN	S	0.0008	AG	AU	CU	---	EPITHERMAL MANGANESE
NYE	BIG PINE MINE	S	0.0008	AU	---	---	---	COMSTOCK EPITHERMAL VEINS
NYE	BIG FOUR MINE	S	0.0008	AU	---	---	---	COMSTOCK EPITHERMAL VEINS
NYE	BOND GOLD BULLFROG MINE	M	0.0008	AU	AG	CU	PB	COMSTOCK EPITHERMAL VEINS
NYE	BRUNER MINE	S	0.0008	AU	---	---	---	SADO EPITHERMAL VEINS
NYE	LONGSTREET MINE	S	0.0008	AU	AG	---	---	COMSTOCK EPITHERMAL VEINS
NYE	MAMMOTH 1-5 CLAIMS	S	0.0008	AU	AG	HG	---	HOT-SPRING HG
NYE	MOTHER LODE MINE	S	0.0008	AU	AG	---	---	COMSTOCK EPITHERMAL VEINS
NYE	MUSTANG MINE	S	0.0008	AU	---	---	---	COMSTOCK EPITHERMAL VEINS
NYE	NATIONAL BANK MINE	S	0.0008	AU	AG	---	---	COMSTOCK EPITHERMAL VEINS
NYE	UNION NO. 9 MINE	S	0.0008	AU	---	---	---	COMSTOCK EPITHERMAL VEINS
PERSHING	BUNCE PROSPECT	S	0.0008	AU	---	---	---	COMSTOCK EPITHERMAL VEINS
PERSHING	GOLDBANKS MERGER MINES	S	0.0008	AU	AG	PB	HG	HOT-SPRING AU-AG
PERSHING	QUEENSTAKE'S NORTH STRUCTURE	S	0.0008	AG	PB	ZN	---	HOT-SPRING AU-AG
PERSHING	TRINITY MINE	?	0.0008	AG	---	---	---	COMSTOCK EPITHERMAL VEINS
STOREY	OCCIDENTAL MINE	S	0.0008	AG	AU	---	---	COMSTOCK EPITHERMAL VEINS
CHURCHILL	WEST JOB CANYON-SOUTH	?	0.0007	AU	AG	CU	PB	COMSTOCK EPITHERMAL VEINS
ELKO	BELLE ISLE	S	0.0007	AG	AU	CU	ZN	COMSTOCK EPITHERMAL VEINS
ELKO	INDEPENDENCE	M	0.0007	AG	CU	PB	---	COMSTOCK EPITHERMAL VEINS
EUREKA	WEST SINTER DEPOSIT	S	0.0007	AU	AG	---	---	COMSTOCK EPITHERMAL VEINS
LANDER	DMB MINING PROPERTIES.	S	0.0007	AG	AU	---	---	HOT-SPRING AU-AG
LANDER	FIRE CREEK MINE	S	0.0007	AU	---	---	---	COMSTOCK OR HOT-SPRING EPITHERMAL (?)
LINCOLN	CHARLEY ROSS MINE	S	0.0007	AU	AG	---	---	COMSTOCK EPITHERMAL VEINS
LINCOLN	CONFIDENCE MINE	S	0.0007	AU	AG	---	---	COMSTOCK EPITHERMAL VEINS
LINCOLN	JENNIE MINE	S	0.0007	AU	AG	PB	CU	COMSTOCK EPITHERMAL VEINS
LINCOLN	SNOWFLAKE MINE	S	0.0007	AG	AU	CU	FE	COMSTOCK EPITHERMAL VEINS
LINCOLN	THOR MINE	S	0.0007	AU	AG	---	---	COMSTOCK EPITHERMAL VEINS
MINERAL	BOREALIS MINE	M	0.0007	AU	AG	ZN	CU	HOT-SPRING AU-AG
MINERAL	FREEDOM FLATS DEPOSIT	S	0.0007	AU	AG	AS	SB	EPITHERMAL QTZ-ALUNITE AU
PERSHING	SILVER PROSPECT (RAGGED TOP DISTRICT)	?	0.0007	AG	---	---	---	COMSTOCK EPITHERMAL VEINS
PERSHING	WILDHORSE GROUP	S	0.0007	AU	AG	---	---	COMSTOCK EPITHERMAL VEINS
CHURCHILL	BUFFALO HUMP MINE	S	0.0006	AG	AU	CU	PB	COMSTOCK EPITHERMAL VEINS
ESMERALDA	16 TO 1 MINE (OLD SILVER PEAK DIST.)	S	0.0006	AG	AU	PB	ZN	COMSTOCK EPITHERMAL VEINS
ESMERALDA	B.C.H. MINERALS CO. PROPERTY	S	0.0006	AU	AG	PT	?	COMSTOCK EPITHERMAL VEINS
HUMBOLDT	CROFOOT/LEWIS MINE	S	0.0006	AU	AG	HG	S	COMSTOCK EPITHERMAL VEINS
HUMBOLDT	LEWIS MINE (AND CROWFOOT?)	S	0.0006	AU	AG	SB	---	COMSTOCK EPITHERMAL VEINS
HUMBOLDT	YELLOW ROCK GROUP	S	0.0006	AU	AG	U	---	HOT-SPRING AU-AG

Table D3, continued.

County	Site Name	Size	Post. Prob.	Commodities				Deposit Type
NYE	ORIGINAL BULLFROG MINE	S	0.0006	AG	AU	CU	---	COMSTOCK EPITHERMAL VEINS
CHURCHILL	GOLD BASIN MINE	S	0.0004	AU	AG	---	---	COMSTOCK EPITHERMAL VEINS
CHURCHILL	GOLD BUG MINE	S	0.0004	AU	AG	---	---	COMSTOCK EPITHERMAL VEINS
CHURCHILL	JACK POT MINE	M	0.0004	AU	AG	---	---	COMSTOCK EPITHERMAL VEINS
CHURCHILL	NEVADA WONDER MINE	L	0.0004	AU	AG	MO	CU	COMSTOCK EPITHERMAL VEINS
CHURCHILL	SILVER CENTER MINE	S	0.0004	AG	AU	?	BA	COMSTOCK EPITHERMAL VEINS
CHURCHILL	VULTURE MINE	S	0.0004	AU	AG	---	---	COMSTOCK EPITHERMAL VEINS
CHURCHILL	WONDER MINE	S	0.0004	AU	AG	---	---	COMSTOCK EPITHERMAL VEINS
ELKO	BULLION PROSPECT	S	0.0004	AU	AG	CU	---	COMSTOCK EPITHERMAL VEINS
ELKO	COEUR D'ALENE-JARBIDGE G.M.CO.	S	0.0004	AU	AG	---	---	COMSTOCK EPITHERMAL VEINS
ELKO	EASTERN STAR MINE	S	0.0004	AU	AG	CU	---	COMSTOCK EPITHERMAL VEINS
ELKO	MODOC	S	0.0004	AU	AG	---	---	COMSTOCK EPITHERMAL VEINS
ELKO	RED DIKE PROSPECT	S	0.0004	AU	---	---	---	COMSTOCK EPITHERMAL VEINS
LANDER	GOLD BASIN GOLD MINING CO.	S	0.0004	AU	AG	CU	PB	COMSTOCK EPITHERMAL VEINS
LINCOLN	SOLO JOKER CLAIM CLAIM	S	0.0004	AG	AU	BA	---	COMSTOCK EPITHERMAL VEINS
LINCOLN	UTAH SPUR MINE	S	0.0004	AU	AG	---	---	COMSTOCK EPITHERMAL VEINS
MINERAL	BOVARD - RAND DISTRICT	S	0.0004	AU	AG	CU	PB	COMSTOCK OR HOT-SPRING EPITHERMAL (?)
MINERAL	BROKEN HILLS MINE	S	0.0004	AG	PB	ZN	AU	COMSTOCK EPITHERMAL VEINS
MINERAL	RAWHIDE DEPOSIT	L	0.0004	AU	AG	CU	PB	COMSTOCK EPITHERMAL VEINS
NYE	AJAX MINE	S	0.0004	AU	AG	---	---	COMSTOCK EPITHERMAL VEINS
NYE	APRIL FOOL MINE	S	0.0004	AU	F	---	---	COMSTOCK EPITHERMAL VEINS
NYE	CLIFFORD MINE	S	0.0004	AG	AU	---	---	COMSTOCK EPITHERMAL VEINS
NYE	GOLD HILL MINE	M	0.0004	AU	---	---	---	COMSTOCK EPITHERMAL VEINS
NYE	GOLDEN KING MINE	S	0.0004	AU	AS	BE	---	COMSTOCK EPITHERMAL VEINS
NYE	HANNAPAH MINE	S	0.0004	AG	---	---	---	COMSTOCK EPITHERMAL VEINS
NYE	JEEP GROUP	S	0.0004	AG	AU	---	---	COMSTOCK EPITHERMAL VEINS
NYE	SAM JACK GROUP	S	0.0004	AU	AG	---	---	COMSTOCK EPITHERMAL VEINS
PERSHING	AMONETT-FRANK CLAIMS	S	0.0004	AU	AG	---	---	HOT-SPRING AU-AG
PERSHING	DEER PROSPECT	S	0.0004	AU	AS	SB	HG	HOT-SPRING AU-AG
PERSHING	VENT CLAIM PROSPECT	S	0.0004	AU	AG	---	---	COMSTOCK EPITHERMAL VEINS
WASHOE	KEYSTONE NEVADA MINE	S	0.0004	AU	AG	---	---	COMSTOCK EPITHERMAL VEINS
WASHOE	PRETTY ROCK GROUP	S	0.0004	AU	AG	U	---	HOT-SPRING AU-AG
CHURCHILL	BELL MOUNTAIN MINE	S	0.0003	AU	AG	---	---	COMSTOCK EPITHERMAL VEINS
CHURCHILL	GEIGER SHAFT	S	0.0003	AG	AU	---	---	COMSTOCK EPITHERMAL VEINS
CHURCHILL	GOLD LEDGE MINE	S	0.0003	AU	AG	PB	CU	COMSTOCK EPITHERMAL VEINS
CHURCHILL	NBMG SAMPLE SITES 3927, 3928	S	0.0003	AG	AU	---	---	COMSTOCK EPITHERMAL VEINS
CHURCHILL	NBMG SAMPLE SITES 3890, 3926	S	0.0003	AG	AU	PB	SB	COMSTOCK EPITHERMAL VEINS
CHURCHILL	NBMG SAMPLE SITE 3925	S	0.0003	AG	AU	---	---	COMSTOCK EPITHERMAL VEINS
CHURCHILL	WILLIAMS MINE	S	0.0003	AG	AU	---	---	COMSTOCK EPITHERMAL VEINS
ELKO	NAVAJO	L	0.0003	AG	AU	---	---	COMSTOCK EPITHERMAL VEINS
ELKO	NORTH BELLE ISLE	L	0.0003	AG	AU	---	---	COMSTOCK EPITHERMAL VEINS
ELKO	REX MINE (GOLD CIRCLE DIST.)	M	0.0003	AU	AG	---	---	COMSTOCK EPITHERMAL VEINS
ELKO	ST. PAUL	S	0.0003	AU	AG	---	---	COMSTOCK EPITHERMAL VEINS
HUMBOLDT	AUTO HILL PROSPECTS	S	0.0003	AG	AU	SB	CU	COMSTOCK EPITHERMAL VEINS
HUMBOLDT	BIRTHDAY MINE	S	0.0003	AU	AG	PB	CU	COMSTOCK EPITHERMAL VEINS
HUMBOLDT	BLUM SHAFT	S	0.0003	AG	AU	HG	PB	COMSTOCK EPITHERMAL VEINS
HUMBOLDT	CAUSTIN MINE	S	0.0003	AG	FE	SB	AU	HOT-SPRING AU-AG
HUMBOLDT	CHEFOO TUNNEL	S	0.0003	AU	AG	CU	ZN	COMSTOCK EPITHERMAL VEINS
HUMBOLDT	CRAWFORD MINE	S	0.0003	AU	?	AG	?	COMSTOCK EPITHERMAL VEINS
HUMBOLDT	HATCH MINE	S	0.0003	AU	AG	---	---	HOT-SPRING AU-AG
HUMBOLDT	INDIAN VALLEY MINE	S	0.0003	SB	AU	AG	---	HOT-SPRING AU-AG

Table D3, continued.



<b>County</b>	<b>Site Name</b>	<b>Size</b>	<b>Post. Prob.</b>	<b>Commodities</b>				<b>Deposit Type</b>
HUMBOLDT	MAMMOTH MINE	S	0.0003	AU	AG	---	---	HOT-SPRING HG
HUMBOLDT	NATIONAL MINE	L	0.0003	AU	AG	CU	PB	COMSTOCK EPITHERMAL VEINS
HUMBOLDT	RADIATOR HILL	S	0.0003	AU	AG	SB	---	COMSTOCK EPITHERMAL VEINS
HUMBOLDT	SULPHUR DISTRICT	S	0.0003	S	AG	HG	AL3	HOT-SPRING HG
NYE	BALD MOUNTAIN PROSPECT	S	0.0003	AU	---	---	---	COMSTOCK EPITHERMAL VEINS
NYE	DULUTH MINE	S	0.0003	AU	AG	---	---	SADO EPITHERMAL VEINS
NYE	MANHATTAN DISTRICT	L	0.0003	AU	AG	SB	AS	COMSTOCK EPITHERMAL VEINS
PERSHING	COYOTE PROSPECT	S	0.0003	AG	AU	---	---	HOT-SPRING AU-AG
PERSHING	D.J. CLAIMS	S	0.0003	AG	AU	---	---	HOT-SPRING AU-AG
WASHOE	OBSIDIAN GROUP	S	0.0003	AU	AG	U	---	HOT-SPRING AU-AG
WASHOE	UNNAMED PROSPECT #2	?	0.0003	AU	AG	U	---	HOT-SPRING AU-AG

Table D3, continued.

Posterior Probabilities Appended to Primary Gold-Silver-Bearing Occurrences:  
Calculated Using Primary 7-Layer Mineral Potential Model

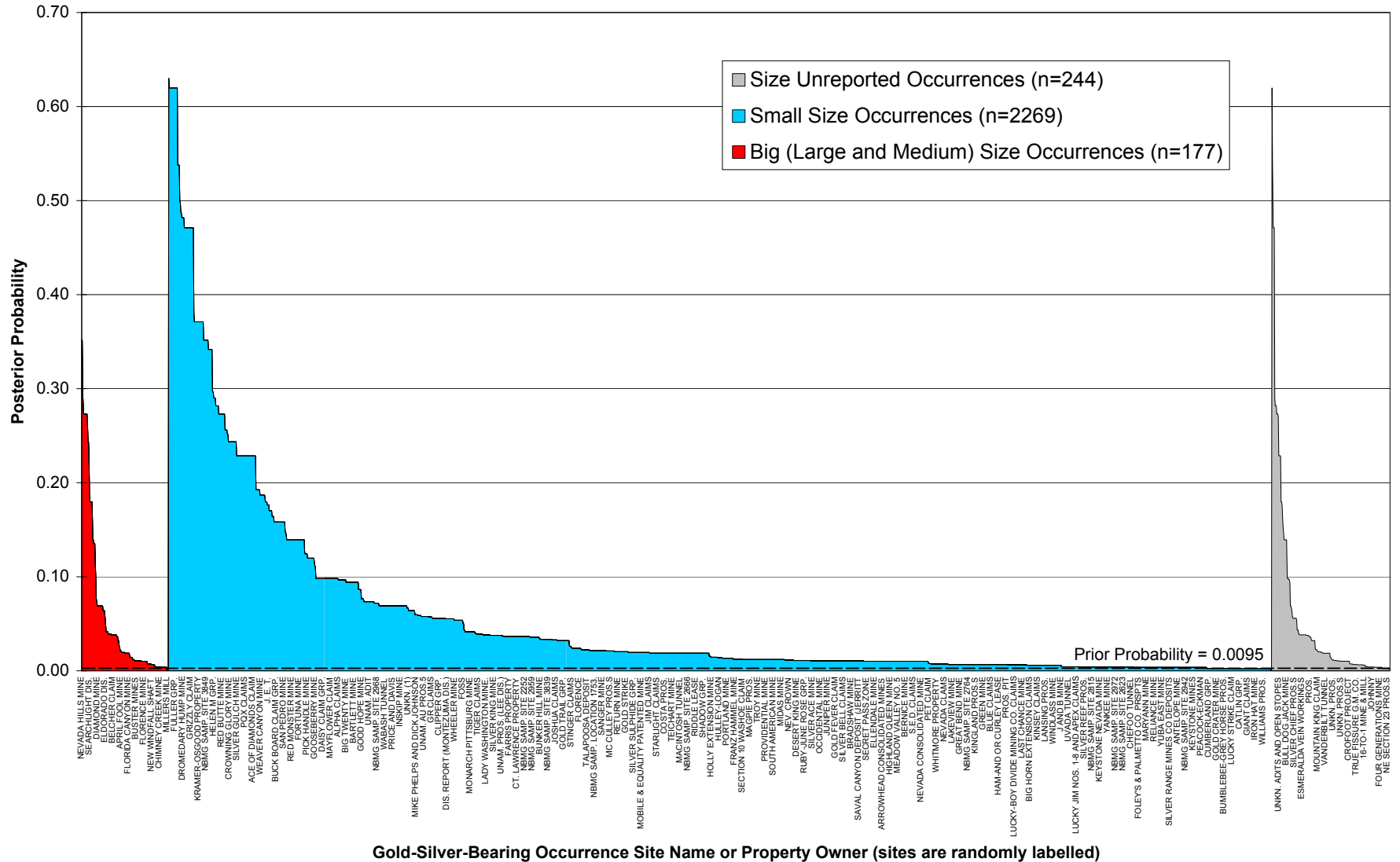
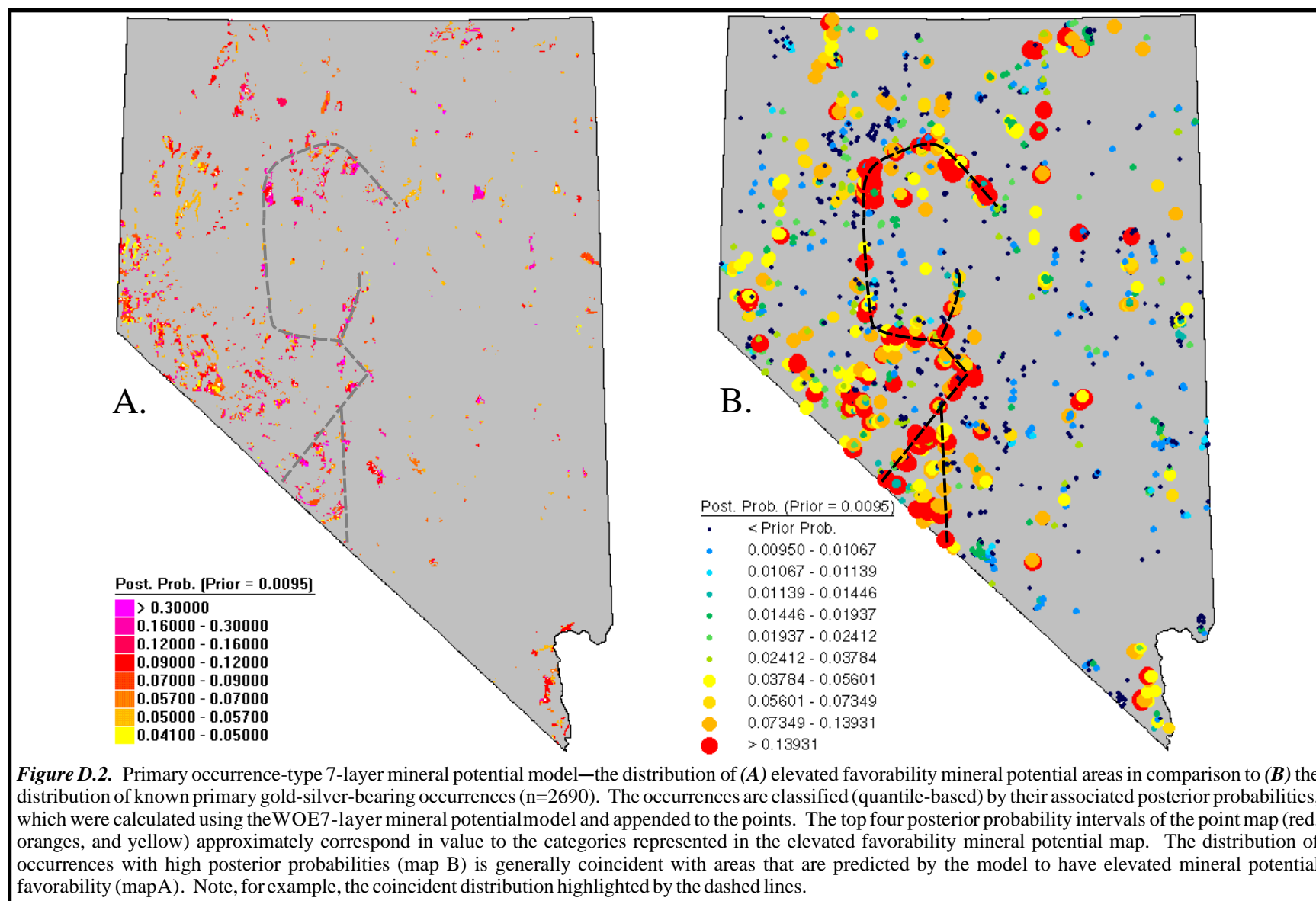
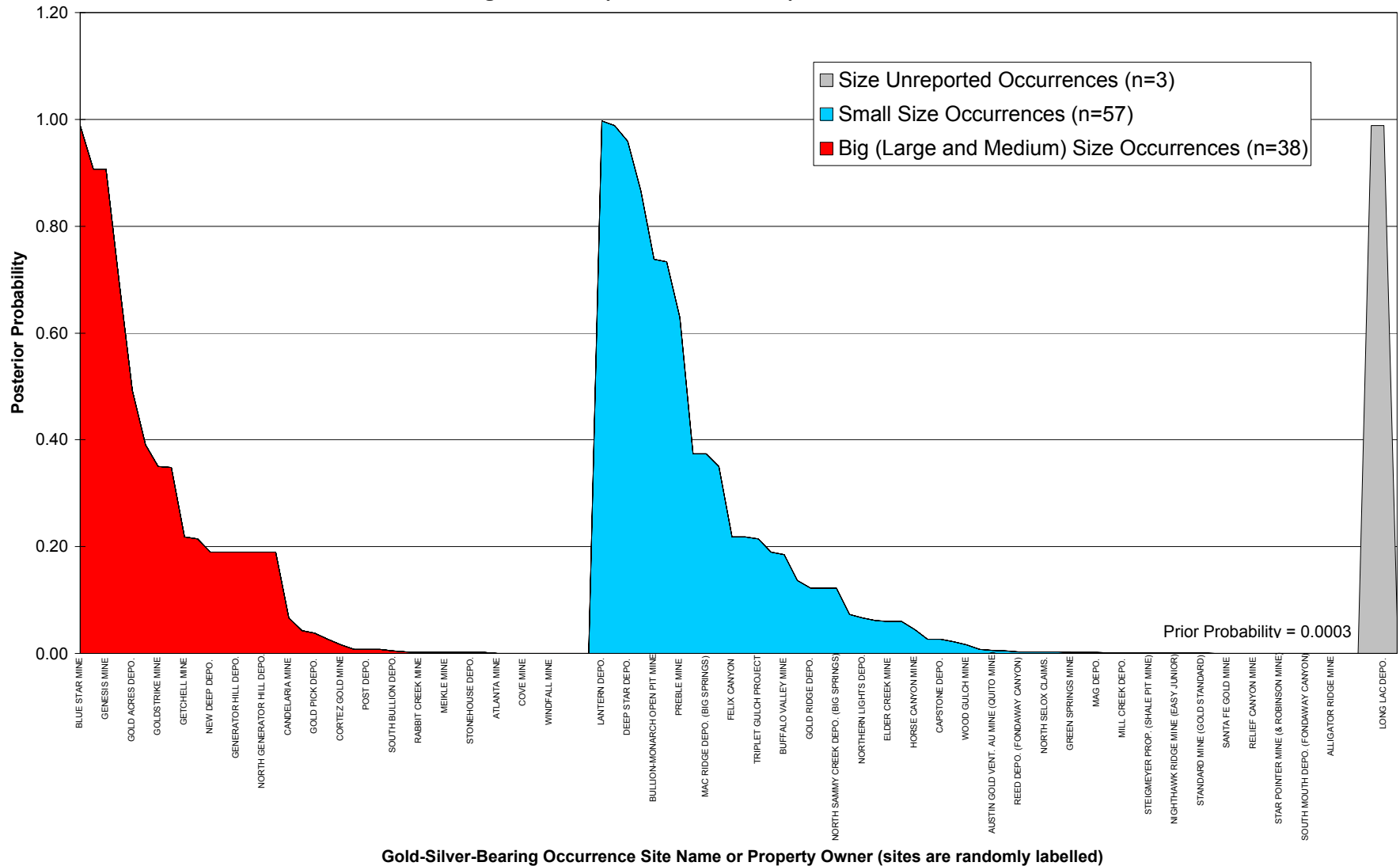


Figure D.1 Distribution of posterior probabilities associated with big (large and medium), small, and unknown size primary occurrences.



**Posterior Probabilities Appended to Sedimentary Rock-Hosted Gold-Silver-Bearing Occurrences:  
Calculated Using Sedimentary Rock-Hosted 8-Layer Mineral Potential Model**



**Figure D3.** Distribution of posterior probabilities associated with big (large, medium), small, and unknown size sedimentary rock-hosted occurrences.

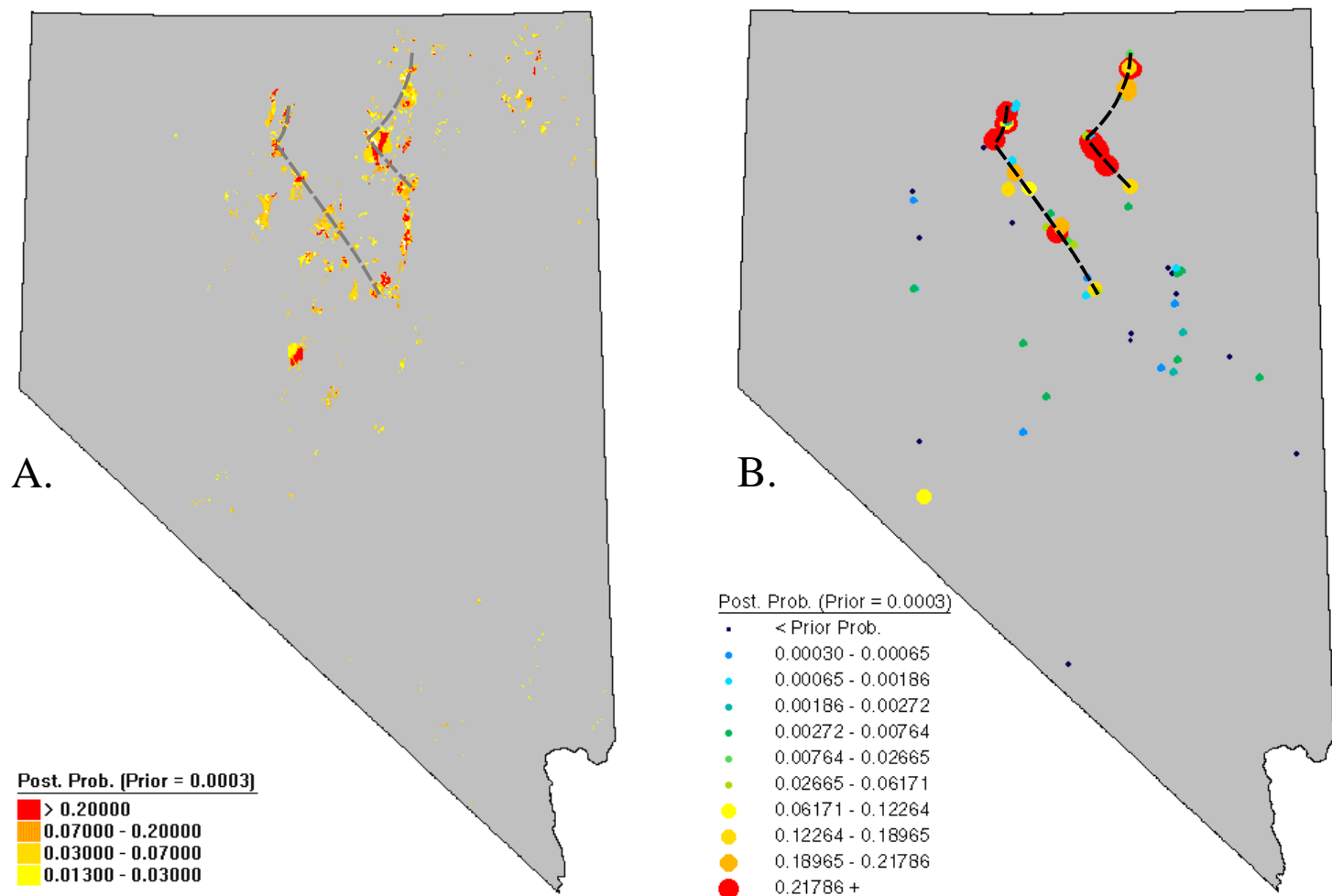


**Figure D.4.** Sedimentary rock-hosted occurrence-type 8-layer mineral potential model—the distribution of (A) elevated favorability mineral potential areas in comparison to the distribution of (B) known sedimentary rock-hosted occurrences (n=98). In general, the distribution of occurrences with high posterior probabilities (map B) is coincident with areas that are predicted by the model to have elevated mineral potential favorability (map A). Note, for example, the coincident distribution highlighted by the dashed lines. See [Figure D.2](#) caption for additional information.

**Posterior Probabilities Appended to Volcanic Rock-Hosted Gold-Silver-Bearing Occurrences:  
Calculated Using Volcanic Rock-Hosted 7-Layer Mineral Potential Model**

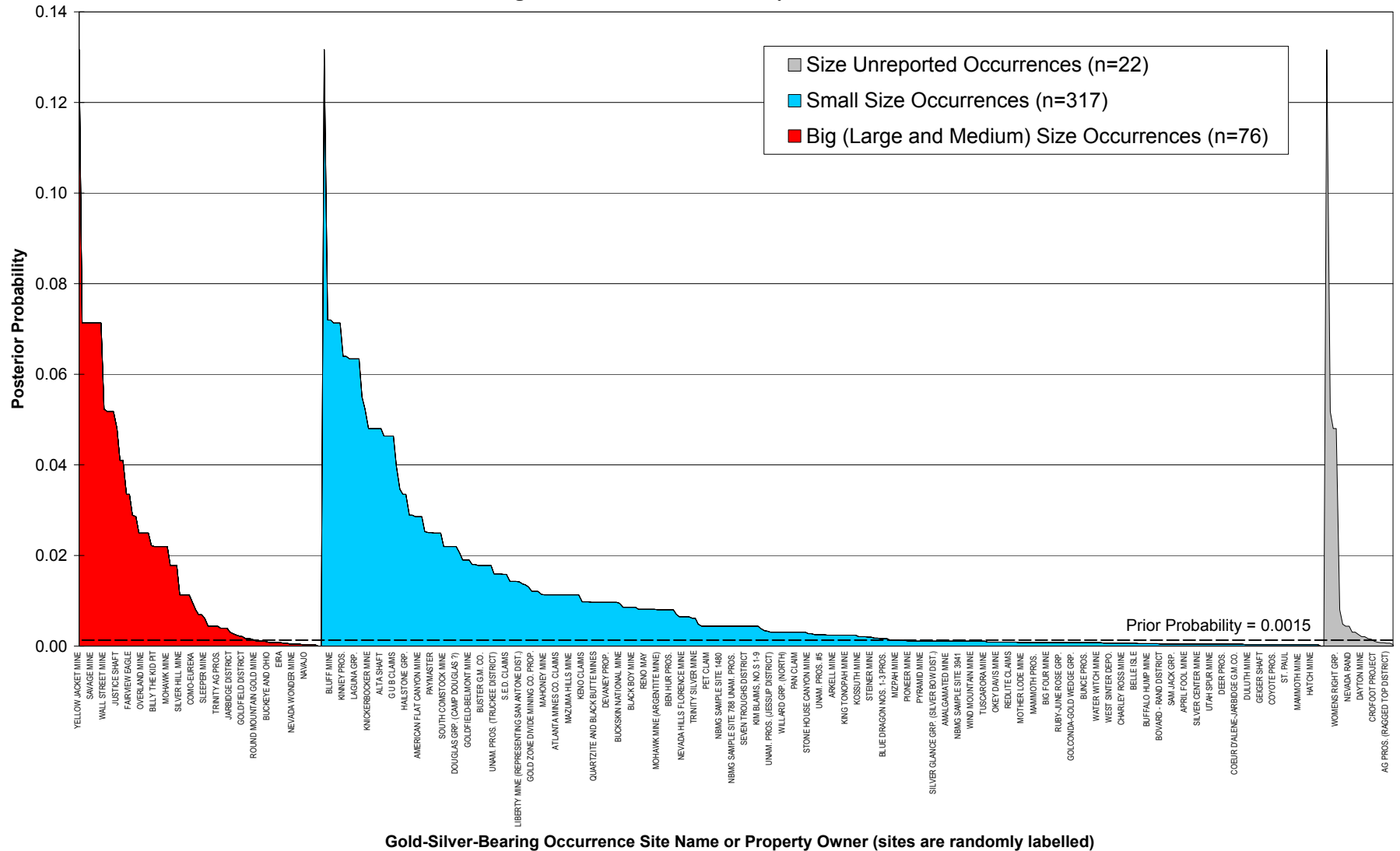


**Figure D.5.** Distribution of posterior probabilities associated with big (large and medium), small, and unknown size volcanic rock-hosted occurrences. D27

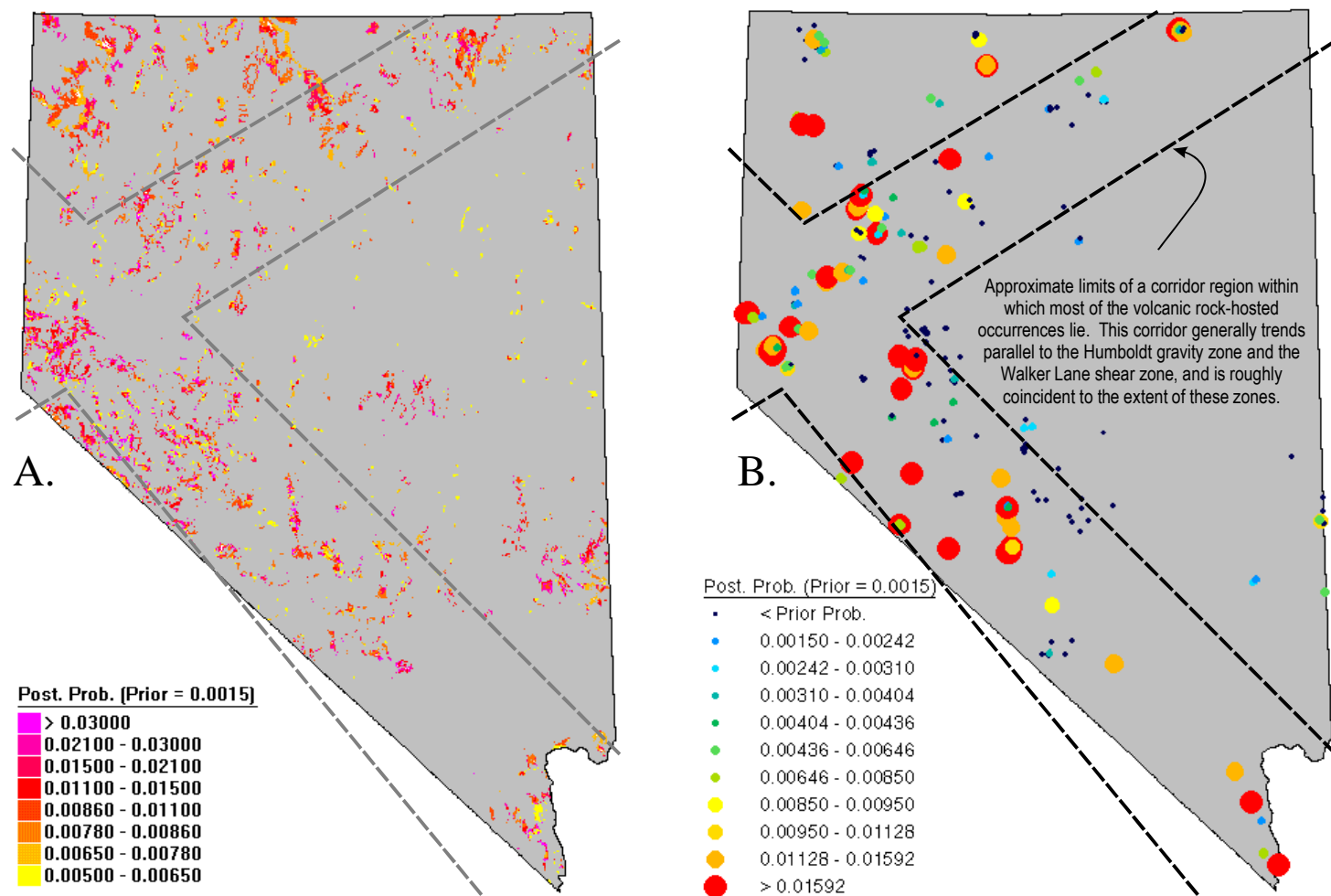


**Figure D.6.** Volcanic rock-hosted occurrence-type 7-layer mineral potential model—the distribution of (A) elevated favorability mineral potential areas in comparison to (B) the distribution of known volcanic rock-hosted occurrences (n=415). In general, the distribution of occurrences with high posterior probabilities (map B) is coincident with areas that are predicted by the model to have elevated mineral potential favorability (map A). Note, for example, the coincident distribution highlighted by the dashed lines. See [Figure D.2](#) caption for additional information.